UNIVERSITY OF ADELAIDE LIBRARY 6/11/84

VARIATIONS IN LOW LATITUDE CIRCULATION AND RAINFALL OVER AUSTRALASIA DURING THE SOUTHERN HEMISPHERE SUMMER MONSOON REGIME

Robert J. Allan
B.A. (Hons)

A thesis submitted for the degree of
Doctor of Philosophy
in
Department of Geography
University of Adelaide
June, 1983

ve consent to this copy of my thesis, when deposited in the University
ary, being available for loan and photocopying.

: ...6/7/83.....Signed :

TABLE OF CONTENTS

Page

TITLE PAGE i

TABLE OF CONTENTS ii

LIST OF FIGURES vi

LIST OF TABLES xxv

ABSTRACT xxvi

DECLARATION xxvii

ACKNOWLEDGMENTS xxviii

CHAPTER I - INTRODUCTION 1

1.1 MONSOON DYNAMICS 5

1.1.1 Historical and Theoretical Considerations ... 5

1.1.2 Teleconnections and the Monsoon System 12

1.2 THE SOUTHERN HEMISPHERE SUMMER MONSOON OF AUSTRALASIA 25

1.2.1 Historical Background 25

1.2.2 Mean Circulation Conditions 28

1.2.3 Monsoonal Extremes and Moisture Characteristics 32

1.2.4 Long Term Variability 35

CHAPTER II - DATA AND COMPUTATIONAL PROCEDURES 45

2.1 DATA SOURCES 45

2.1.1 Regional and Indo-Pacific Domains 45

2.1.2 Local Domain 47

2.1.3 Data Station Changes in the Domains 47

2.1.4 Data Problems 48

2.2 COMPUTATIONAL PROCEDURES 49

2.2.1 Sequence for Divergence and Relative Vorticity Calculations in the Regional and Indo-Pacific Domains 50

2.2.2 Methods and Sequence for Velocity Potential and Streamfunction Calculation in the Regional and Indo-Pacific Domains 50

2.2.3 Sequence for Moisture Characteristics Calculations in the Local Domain 51

2.2.4 Sequence for Kinetic Energy Generation Calculations in the Regional Domain 52

2.2.5 Determination and Interpretation of the Velocity Potential Cross Sections 53

2.2.6 Computational Problems 53

CHAPTER III - RESULTS AND DISCUSSION 55

3.1 INTERANNUAL AND INTRASEASONAL VARIABILITY - UPPER AIR DYNAMICS OF 1973-77 SUMMERS; THE REGIONAL DOMAIN (35°N-35°S; 85°E-175°E) 55

3.1.1 Major Period : January, February and March 1973-77 57

(i) Monthly Mean 850 mb Streamfunction ($\bar{\psi}_{850}$) and Velocity Potential ($\bar{\chi}_{850}$) Fields 57

(ii) Monthly Mean 200 mb Streamfunction ($\bar{\psi}_{200}$) and Velocity Potential ($\bar{\chi}_{200}$) Fields 68

3.1.2 Sub-Period : January and February 1973-75 ... 74

(i) Vertical Cross Sections (Surface to 200 mb) of Monthly Mean Velocity Potential ($\bar{\chi}_{sfc-200}$) 75

(ii) Monthly Mean Surface Streamfunction Fields ($\bar{\psi}_{sfc}$) 90

(iii) Monthly Mean Geopotential Height, Streamfunction and Kinetic Energy Generation (Surface/1000, 850, 700 and 200 mb) Fields 95

3.2 INTERANNUAL AND INTRASEASONAL VARIABILITY - MOISTURE CHARACTERISTICS AND COLD SURGES IN THE 1973-77 SUMMERS OVER THE LOCAL DOMAIN (5°S-30°S; 95°E-155°E) 129

3.2.1 Major Period : January, February and March 1973-77 131

(i) Low-level Monthly Mean (Surface - 700 mb) Moisture Characteristics over Northern Australia : A Comparison between Major Period and 19 year (1957-75) Average Fields 131

(ii) Monthly Mean 850 mb Transient Eddy Moisture Characteristics 154

(iii) Vertical Cross Sections (Surface - 700 mb) of Monthly Mean Advective Water Vapour Flux Divergence over Australia along 20°S during Monsoon extremes : A Comparison between Major Period and 19 year Average Fields 166

(iv) Aerological Traces and Precipitable Water Content over Australia during Monsoon Extremes 179

3.2.2 Sub-Period : Cold Surges - January 1973-75 190

(i) Development 191

(ii) Evolution and Equatorial Penetration . 193

(iii) Influence on Northern Australia 198

3.3 LONG-TERM INTERANNUAL AND INTRASEASONAL VARIABILITY - MONSOON AND SOUTHERN OSCILLATION/ WALKER CIRCULATION DYNAMICS, INDICES AND CORRELATIONS OVER THE INDO-PACIFIC (35°N-35°S; 30°E-60°W) AND REGIONAL (35°N-35°S; 85°E-175°E) DOMAINS 202

3.3.1 Indo-Pacific Circulation and Teleconnection Variability 202

(i) Monthly Mean 850 mb and 200 mb Divergence and Wind Vectors : January 1973 El Niño and January 1974 anti-El Niño Periods 203

(ii) Monthly Mean 850 mb and 200 mb Divergence and Wind Vectors : Composites of January and February Southern Oscillation Index Extremes from 1957-81 209

3.3.2 Upper Air Data over Australia : January 1965-78 216

(i) Monthly Mean Streamfunction and Velocity Potential Sequences (850, 700 and 200 mb) : January 1965-78 217

(ii) Divergence Overlays (850, 700 and 200 mb) and Rainfall over Australia : January 1965-76 227

3.3.3 Longer-Term Monsoon and Teleconnection Variability 232

(i) Southern Oscillation Indices (SOIs) and the Southern Hemisphere Summer Monsoon 233

(ii) *The Southern Oscillation, Australian Rainfall and Lake Eyre Floodings* 240

CHAPTER IV - CONCLUSION 252

APPENDIX 1 Upper Air and Upper Wind Stations : Regional Domain. 258

Upper Air/Radiosonde Stations : Local Domain 262

Upper Air and Upper Wind Stations : Indo-Pacific Domain 263

APPENDIX 2 Theory of Time, Space and Space-Time Component Decomposition 269

APPENDIX 3 Determination of Divergence and Relative Vorticity via Finite Difference Approximation 271

APPENDIX 4 Theory of Velocity Potential and Streamfunction Evaluation 272

APPENDIX 5 Iteration Procedure for Streamfunction and Velocity Potential Determination 274

APPENDIX 6 Theory of Moisture Characteristics 281

APPENDIX 7 Determination of Kinetic Energy Generation Parameter 287

APPENDIX 8 Determination and Interpretation of Velocity Potential Cross Sections 288

APPENDIX 9 *Monthly Weather Review* article on aspects of Section 3.1 290

BIBLIOGRAPHY 320

LIST OF FIGURES

Figure		Page
1	The monsoon region, as defined by Ramage (1971), is bounded by the rectangle. Shadings define the areas seen to be monsoonal by Russian researchers (hatched) and where low frequencies of surface cyclone-anticyclone alternations occur in summer and winter (stippled) (from Ramage, 1971)	8
2	115 year (1860-1975) power spectrum of Wright's 'old' Southern Oscillation Index (data from Lamb, 1977)	15
3	Power Spectra of Wright's 'old' Southern Oscillation Index for the four 32 year intervals; 1851-1882, 1881-1912, 1911-1942, 1941-1972 (from Wright, 1977)	15
4	Climatological classification of mean wind regimes over Australia in January (from Gentilli, 1972)	29
5	January mean surface pressure and geopotential fields at 850, 700 and 200 mb levels over the Australasian segment of the Southern Hemisphere. Geopotential heights are in decametres (from Taljaard *et. al.*, 1969)	31
6	Distribution of upper wind and upper air stations in the regional domain. Solid symbols (circle/triangle, circle) denote upper wind and upper air stations from which data were available for this study. Stations known to have been operating during all or part of the 1973-77 core period, but from which no data were available, are designated by corresponding open symbols. A combination of solid symbols (square/diamond) indicates upper air stations from which data were only available to supplement the data set for monthly mean divergence cross sections and surface streamfunction fields	56
7	Monthly mean 850 mb streamfunction fields in units of 10^5 m^2 s^{-1} at intervals of 5 units over the regional domain during January from 1973-77. Heavy dashed lines indicate the positions of the NET_{NH} and NET_{SH}	58
8	Monthly mean 850 mb streamfunction fields in units of 10^5 m^2 s^{-1} at intervals of 5 units over the regional domain during February from 1973-77. Heavy dashed lines indicate the positions of the NET_{NH} and NET_{SH}	58
9	Monthly mean 850 mb streamfunction fields in units of 10^5 m^2 s^{-1} at intervals of 5 units over the regional domain during March from 1973-77. Heavy dashed lines indicate the positions of the NET_{NH} and NET_{SH}	58
10	Decile rainfall distributions over Australia during January, February and March 1973 (from Bureau of Meteorology, 1973-77)	61
11	Decile rainfall distributions over Australia during January, February and March 1974 (from Bureau of Meteorology, 1973-77)	61

Figure Page

12 Decile rainfall distributions over Australia during January, February and March 1975 (from Bureau of Meteorology, 1973-77) 61

13 Decile rainfall distributions over Australia during January, February and March 1976 (from Bureau of Meteorology, 1973-77) 61

14 Decile rainfall distributions over Australia during January, February and March 1977 (from Bureau of Meteorology, 1973-77) 61

15 Monthly mean 850 mb velocity potential fields in units of 10^6 m^2 s^{-1} at intervals of 2 units over the regional domain during January from 1973-77. The symbols / indicate the direction and magnitude of the divergent part of the wind, where a length of one grid interval equals 9.5 m s^{-1} 66

16 Monthly mean 850 mb velocity potential fields in units of 10^6 m^2 s^{-1} at intervals of 2 units over the regional domain during February from 1973-77. The symbols / indicate the direction and magnitude of the divergent part of the wind, where a length of one grid interval equals 9.5 m s^{-1} 66

17 Monthly mean 850 mb velocity potential fields in units of 10^6 m^2 s^{-1} at intervals of 2 units over the regional domain during March from 1973-77. The symbols / indicate the direction and magnitude of the divergent part of the wind, where a length of one grid interval equals 9.5 m s^{-1} 66

18 Monthly mean 200 mb streamfunction fields in units of 10^6 m^2 s^{-1} at intervals of 5 units over the regional domain during January from 1973-77. Heavy dashed lines indicate monthly mean zonal wind isotachs in m s^{-1} 69

19 Monthly mean 200 mb streamfunction fields in units of 10^6 m^2 s^{-1} at intervals of 5 units over the regional domain during February from 1973-77. Heavy dashed lines indicate monthly mean zonal wind isotachs in m s^{-1} 69

20 Monthly mean 200 mb streamfunction fields in units of 10^6 m^2 s^{-1} at intervals of 5 units over the regional domain during March from 1973-77. Heavy dashed lines indicate monthly mean zonal wind isotachs in m s^{-1} 69

21 Monthly mean 200 mb velocity potential fields in units of 10^6 m^2 s^{-1} at intervals of 1 unit over the regional domain during January from 1973-77. The symbols / indicate the direction and magnitude of the divergent part of the wind, where a length of one grid interval equals 9.5 m s^{-1} 72

Figure Page

22 Monthly mean 200 mb velocity potential fields in units of 10^6 m^2 s^{-1} at intervals of 1 unit over the regional domain during February from 1973-77. The symbols / indicate the direction and magnitude of the divergent part of the wind, where a length of one grid interval equals 9.5 m s^{-1} 72

23 Monthly mean 200 mb velocity potential fields in units of 10^6 m^2 s^{-1} at intervals of 1 unit over the regional domain during March from 1973-77. The symbols / indicate the direction and magnitude of the divergent part of the wind, where a length of one grid interval equals 9.5 m s^{-1} 72

24 Satellite-derived oceanic rainfall rates (mm hr^{-1}) during January from 1973-75 (adapted from Rao *et. al.*, 1976) 76

25 Satellite-derived oceanic rainfall rates (mm hr^{-1}) during February from 1973-75 (adapted from Rao *et. al.*, 1976) 76

26 Latitude and longitude cross sections of monthly mean velocity potential in units of 10^6 m^2 s^{-1} at intervals of 2 units in the regional domain for January 1973. Schematic arrows show strong and weak vertical motions, using large and small arrows, respectively 78

27 Latitude and longitude cross sections of monthly mean velocity potential in units of 10^6 m^2 s^{-1} at intervals of 2 units in the regional domain for February 1973. Schematic arrows show strong and weak vertical motions, using large and small arrows, respectively 80

28 Latitude and longitude cross sections of monthly mean velocity potential in units of 10^6 m^2 s^{-1} at intervals of 2 units in the regional domain for January 1974. Schematic arrows show strong and weak vertical motions, using large and small arrows, respectively 82

29 Latitude and longitude cross sections of monthly mean velocity potential in units of 10^6 m^2 s^{-1} at intervals of 2 units in the regional domain for February 1974. Schematic arrows show strong and weak vertical motions, using large and small arrows, respectively 84

30 Latitude and longitude cross sections of monthly mean velocity potential in units of 10^6 m^2 s^{-1} at intervals of 2 units in the regional domain for January 1975. Schematic arrows show strong and weak vertical motions, using large and small arrows, respectively 87

31 Latitude and longitude cross sections of monthly mean velocity potential in units of 10^6 m^2 s^{-1} at intervals of 2 units in the regional domain for February 1975. Schematic arrows show strong and weak vertical motions, using large and small arrows, respectively 89

Figure Page

32 Distributions of upper cloud in January 1973, 74 and 75. Dark area is greater than 60 per cent frequency of cloud cover, diagonal lines greater than 40 per cent, horizontal lines greater than 20 per cent, clear areas less than 20 per cent, shaded areas have no observations (from Barton, 1983) 91

33 Distribution of outgoing longwave radiation in units of W m^{-2} at intervals of 25 units in January, February and March 1975. Shaded areas denote regions with outgoing longwave radiation values less than 250 W m^{-2} (from Winston *et. al.*, 1979) 91

34 Distribution of outgoing longwave radiation in units of W m^{-2} at intervals of 25 units in January, February and March 1976. Shaded areas denote regions with outgoing longwave radiation values less than 250 W m^{-2} (from Winston *et. al.*, 1979) 91

35 Distribution of outgoing longwave radiation in units of W m^{-2} at intervals of 25 units in January, February and March 1977. Shaded areas denote regions with outgoing longwave radiation values less than 250 W m^{-2} (from Winston *et. al.*, 1979) 91

36 Monthly mean surface streamfunction fields in units of 10^5 m^2 s^{-1} at intervals of 5 units over the regional domain during January and February 1973-75. Heavy dashed lines indicate the positions of the NET_{NH} and NET_{SH} 93

37 Monthly mean surface/1000, 850, 700 and 200 mb streamfunction (light lines), geopotential height (heavy lines) (in the left-hand column) and kinetic energy generation (in the right-hand column) fields over the regional domain in January 1973. Streamfunction field is in units of 10^5 m^2 s^{-1} (surface/1000 to 700 mb) and 10^6 m^2 s^{-1} (200 mb) at intervals of 5 units, geopotential height is in m at intervals of 10 units (surface/1000 to 700 mb) and 50 units (200 mb), and kinetic energy generation in units of 10^{-4} W gm^{-1} at intervals of 5 units (surface/1000 to 700 mb) and in units of 10^{-3} W gm^{-1} at intervals of 10 units (200 mb). Dashed lines at 200 mb (in the left-hand column) indicate monthly mean zonal isotachs in m s^{-1}. Shading (in the right-hand column) indicates areas of negative kinetic energy generation 98

Figure Page

38 Monthly mean surface/1000, 850, 700 and 200 mb streamfunction (light lines), geopotential height (heavy lines) (in the left-hand column) and kinetic energy generation (in the right-hand column) fields over the regional domain in February 1973. Streamfunction field is in units of 10^5 m^2 s^{-1} (surface/1000 to 700 mb) and 10^6 m^2 s^{-1} (200 mb) at intervals of 5 units, geopotential height is in m at intervals of 10 units (surface/1000 to 700 mb) and 50 units (200 mb), and kinetic energy generation in units of 10^{-4} W gm^{-1} at intervals of 5 units (surface/1000 to 700 mb) and in units of 10^{-3} W gm^{-1} at intervals of 10 units (200 mb). Dashed lines at 200 mb (in the left-hand column) indicate monthly mean zonal isotachs in m s^{-1}. Shading (in the right-hand column) indicates areas of negative kinetic energy generation 102

39 Monthly mean surface/1000, 850, 700 and 200 mb streamfunction (light lines), geopotential height (heavy lines) (in the left-hand column) and kinetic energy generation (in the right-hand column) fields over the regional domain in January 1974. Streamfunction field is in units of 10^5 m^2 s^{-1} (surface/1000 to 700 mb) and 10^6 m^2 s^{-1} (200 mb) at intervals of 5 units, geopotential height is in m at intervals of 10 units (surface/1000 to 700 mb) and 50 units (200 mb), and kinetic energy generation in units of 10^{-4} W gm^{-1} at intervals of 5 units (surface/1000 to 700 mb) and in units of 10^{-3} W gm^{-1} at intervals of 10 units (200 mb). Dashed lines at 200 mb (in the left-hand column) indicate monthly mean zonal isotachs in m s^{-1}. Shading (in the right-hand column) indicates areas of negative kinetic energy generation 106

40 Monthly mean surface/1000, 850, 700 and 200 mb streamfunction (light lines), geopotential height (heavy lines) (in the left-hand column) and kinetic energy generation (in the right-hand column) fields over the regional domain in February 1974. Streamfunction field is in units of 10^5 m^2 s^{-1} (surface/1000 to 700 mb) and 10^6 m^2 s^{-1} (200 mb) at intervals of 5 units, geopotential height is in m at intervals of 10 units (surface/1000 to 700 mb) and 50 units (200 mb), and kinetic energy generation in units of 10^{-4} W gm^{-1} at intervals of 5 units (surface/1000 to 700 mb) and in units of 10^{-3} W gm^{-1} at intervals of 10 units (200 mb). Dashed lines at 200 mb (in the left-hand column) indicate monthly mean zonal isotachs in m s^{-1}. Shading (in the right-hand column) indicates areas of negative kinetic energy generation 111

Figure Page

41 Monthly mean surface/1000, 850, 700 and 200 mb streamfunction (light lines), geopotential height (heavy lines) (in the left-hand column) and kinetic energy generation (in the right-hand column) fields over the regional domain in January 1975. Streamfunction is in units of 10^5 m^2 s^{-1} (surface/1000 to 700 mb) and 10^6 m^2 s^{-1} (200 mb) at intervals of 5 units, geopotential height is in m at intervals of 10 units (surface/1000 to 700 mb) and 50 units (200 mb), and kinetic energy generation in units of 10^{-4} W gm^{-1} at intervals of 5 units (surface/1000 to 700 mb) and in units of 10^{-3} W gm^{-1} at intervals of 10 units (200 mb). Dashed lines at 200 mb (in the left-hand column) indicate monthly mean zonal isotachs in m s^{-1}. Shading (in the right-hand column) indicates areas of negative kinetic energy generation 118

42 Monthly mean surface/1000, 850, 700 and 200 mb streamfunction (light lines), geopotential height (heavy lines) (in the left-hand column) and kinetic energy generation (in the right-hand column) fields over the regional domain in February 1975. Streamfunction is in units of 10^5 m^2 s^{-1} (surface/1000 to 700 mb) and 10^6 m^2 s^{-1} (200 mb) at intervals of 5 units, geopotential height is in m at intervals of 10 units (surface/1000 to 700 mb) and 50 units (200 mb), and kinetic energy generation in units of 10^{-4} W gm^{-1} at intervals of 5 units (surface/1000 to 700 mb) and in units of 10^{-3} W gm^{-1} at intervals of 10 units (200 mb). Dashed lines at 200 mb (in the left-hand column) indicate monthly mean zonal isotachs in m s^{-1}. Shading (in the right-hand column) indicates areas of negative kinetic energy generation 123

43 Distribution of radiosonde stations in the local domain. These stations provided both upper air and upper wind data 130

44 Hypsometric map of Australia. Height above sea level in m. (from Department of Minerals and Energy, 1973) 130

45 January mean advective water vapour flux divergence (light lines, convergence shaded) and the streamfunction of the advective water vapour flux (heavy dashed lines) at surface, 900, 850 and 700 mb levels over the local domain for the period from 1957-75 (data from Maher and Lee, 1977). Advective water vapour flux divergence is in units of 10^{-6} gm cm^{-2} mb^{-1} s^{-1} at intervals of 2 units and the streamfunction of the advective water vapour flux is in units of 10^5 gm mb^{-1} s^{-1} at intervals of 5 units. Vertically integrated (surface - 700 mb) advective water vapour flux divergence is in units of 10^{-4} gm cm^{-2} s^{-1} at intervals of 4 units and the vertically integrated streamfunction of the advective water vapour flux is in units of 10^7 gm cm^{-1} mb^{-1} s^{-1} at intervals of 10 units 132

Figure Page

46 February mean advective water vapour flux divergence (light lines, convergence shaded) and the streamfunction of the advective water vapour flux (heavy dashed lines) at surface, 900, 850 and 700 mb levels over the local domain for the period from 1957-75 (data from Maher and Lee, 1977). Advective water vapour flux divergence is in units of 10^{-6} gm cm^{-2} mb^{-1} s^{-1} at intervals of 2 units and the streamfunction of the advective water vapour flux is in units of 10^{5} gm mb^{-1} s^{-1} at intervals of 5 units. Vertically integrated (surface - 700 mb) advective water vapour flux divergence is in units of 10^{-4} gm cm^{-2} s^{-1} at intervals of 4 units and the vertically integrated streamfunction of the advective water vapour flux is in units of 10^{7} gm cm^{-1} mb^{-1} s^{-1} at intervals of 10 units 132

47 March mean advective water vapour flux divergence (light lines, convergence shaded) and the streamfunction of the advective water vapour flux (heavy dashed lines) at surface, 900, 850 and 700 mb levels over the local domain for the period from 1957-75 (data from Maher and Lee, 1977). Advective water vapour flux divergence is in units of 10^{-6} gm cm^{-2} mb^{-1} s^{-1} at intervals of 2 units and the streamfunction of the advective water vapour flux is in units of 10^{5} gm mb^{-1} s^{-1} at intervals of 5 units. Vertically integrated (surface - 700 mb) advective water vapour flux divergence is in units of 10^{-4} gm cm^{-2} s^{-1} at intervals of 4 units and the vertically integrated streamfunction of the advective water vapour flux is in units of 10^{7} gm cm^{-1} mb^{-1} s^{-1} at intervals of 10 units 132

48 January mean standard deviations of zonal (u) and meridional (v) wind components and mixing ratio (mr) for the period from 1958-81. Cross-sections are along 10-12°S and 25°S with all standard deviations at intervals of 0.5. Stations used were Cocos Island (CI), Christmas Island (CH), Darwin (D), Thursday Island (TI), Port Moresby (PM), Honiara (H), Carnarvon (CA), Meekatharra (M), Giles (G), Alice Springs (A), Longreach (L), Charleville (CV) and Gladstone (GL) 135

Figure Page

49 Monthly mean advective water vapour flux divergence (light lines, convergence shaded) and the streamfunction of the advective water vapour flux (heavy dashed lines) at surface, 900, 850 and 700 mb levels over the local domain in January 1973. Advective water vapour flux divergence is in units of 10^{-6} gm cm^{-2} mb^{-1} s^{-1} at intervals of 2 units and the streamfunction of the advective water vapour flux is in units of 10^{5} gm mb^{-1} s^{-1} at intervals of 5 units. Vertically integrated (surface - 700 mb) advective water vapour flux divergence is in units of 10^{-4} gm cm^{-2} s^{-1} at intervals of 4 units and the vertically integrated streamfunction of the advective water vapour flux is in units of 10^{7} gm cm^{-1} mb^{-1} s^{-1} at intervals of 10 units 138

50 Monthly mean advective water vapour flux divergence (light lines, convergence shaded) and the streamfunction of the advective water vapour flux (heavy dashed lines) at surface, 900, 850 and 700 mb levels over the local domain in February 1973. Advective water vapour flux divergence is in units of 10^{-6} gm cm^{-2} mb^{-1} s^{-1} at intervals of 2 units and the streamfunction of the advective water vapour flux is in units of 10^{5} gm mb^{-1} s^{-1} at intervals of 5 units. Vertically integrated (surface - 700 mb) advective water vapour flux divergence is in units of 10^{-4} gm cm^{-2} s^{-1} at intervals of 4 units and the vertically integrated streamfunction of the advective water vapour flux is in units of 10^{7} gm cm^{-1} mb^{-1} s^{-1} at intervals of 10 units 138

51 Monthly mean advective water vapour flux divergence (light lines, convergence shaded) and the streamfunction of the advective water vapour flux (heavy dashed lines) at surface, 900, 850 and 700 mb levels over the local domain in March 1973. Advective water vapour flux divergence is in units of 10^{-6} gm cm^{-2} mb^{-1} s^{-1} at intervals of 2 units and the streamfunction of the advective water vapour flux is in units of 10^{5} gm mb^{-1} s^{-1} at intervals of 5 units. Vertically integrated (surface - 700 mb) advective water vapour flux divergence is in units of 10^{-4} gm cm^{-2} s^{-1} at intervals of 4 units and the vertically integrated streamfunction of the advective water vapour flux is in units of 10^{7} gm cm^{-1} mb^{-1} s^{-1} at intervals of 10 units 138

Figure Page

52 Monthly mean advective water vapour flux divergence (light lines, convergence shaded) and the streamfunction of the advective water vapour flux (heavy dashed lines) at surface, 900, 850 and 700 mb levels over the local domain in January 1974. Advective water vapour flux divergence is in units of 10^{-6} gm cm^{-2} mb^{-1} s^{-1} at intervals of 2 units and the streamfunction of the advective water vapour flux is in units of 10^{5} gm mb^{-1} s^{-1} at intervals of 5 units. Vertically integrated (surface - 700 mb) advective water vapour flux divergence is in units of 10^{-4} gm cm^{-2} s^{-1} at intervals of 4 units and the vertically integrated streamfunction of the advective water vapour flux is in units of 10^{7} gm cm^{-1} mb^{-1} s^{-1} at intervals of 10 units 140

53 Monthly mean advective water vapour flux divergence (light lines, convergence shaded) and the streamfunction of the advective water vapour flux (heavy dashed lines) at surface, 900, 850 and 700 mb levels over the local domain in February 1974. Advective water vapour flux divergence is in units of 10^{-6} gm cm^{-2} mb^{-1} s^{-1} at intervals of 2 units and the streamfunction of the advective water vapour flux is in units of 10^{5} gm mb^{-1} s^{-1} at intervals of 5 units. Vertically integrated (surface - 700 mb) advective water vapour flux divergence is in units of 10^{-4} gm cm^{-2} s^{-1} at intervals of 4 units and the vertically integrated streamfunction of the advective water vapour flux is in units of 10^{7} gm cm^{-1} mb^{-1} s^{-1} at intervals of 10 units 140

54 Monthly mean advective water vapour flux divergence (light lines, convergence shaded) and the streamfunction of the advective water vapour flux (heavy dashed lines) at surface, 900, 850 and 700 mb levels over the local domain in March 1974. Advective water vapour flux divergence is in units of 10^{-6} gm cm^{-2} mb^{-1} s^{-1} at intervals of 2 units and the streamfunction of the advective water vapour flux is in units of 10^{5} gm mb^{-1} s^{-1} at intervals of 5 units. Vertically integrated (surface - 700 mb) advective water vapour flux divergence is in units of 10^{-4} gm cm^{-2} s^{-1} at intervals of 4 units and the vertically integrated streamfunction of the advective water vapour flux is in units of 10^{7} gm cm^{-1} mb^{-1} s^{-1} at intervals of 10 units 140

Figure Page

55 Monthly mean advective water vapour flux divergence (light lines, convergence shaded) and the streamfunction of the advective water vapour flux (heavy dashed lines) at surface, 900, 850 and 700 mb levels over the local domain in January 1975. Advective water vapour flux divergence is in units of 10^{-6} gm cm^{-2} mb^{-1} s^{-1} at intervals of 2 units and the streamfunction of the advective water vapour flux is in units of 10^{5} gm mb^{-1} s^{-1} at intervals of 5 units. Vertically integrated (surface - 700 mb) advective water vapour flux divergence is in units of 10^{-4} gm cm^{-2} s^{-1} at intervals of 4 units and the vertically integrated streamfunction of the advective water vapour flux is in units of 10^{7} gm cm^{-1} mb^{-1} s^{-1} at intervals of 10 units 142

56 Monthly mean advective water vapour flux divergence (light lines, convergence shaded) and the streamfunction of the advective water vapour flux (heavy dashed lines) at surface, 900, 850 and 700 mb levels over the local domain in February 1975. Advective water vapour flux divergence is in units of 10^{-6} gm cm^{-2} mb^{-1} s^{-1} at intervals of 2 units and the streamfunction of the advective water vapour flux is in units of 10^{5} gm mb^{-1} s^{-1} at intervals of 5 units. Vertically integrated (surface - 700 mb) advective water vapour flux divergence is in units of 10^{-4} gm cm^{-2} s^{-1} at intervals of 4 units and the vertically integrated streamfunction of the advective water vapour flux is in units of 10^{7} gm cm^{-1} mb^{-1} s^{-1} at intervals of 10 units 142

57 Monthly mean advective water vapour flux divergence (light lines, convergence shaded) and the streamfunction of the advective water vapour flux (heavy dashed lines) at surface, 900, 850 and 700 mb levels over the local domain in March 1975. Advective water vapour flux divergence is in units of 10^{-6} gm cm^{-2} mb^{-1} s^{-1} at intervals of 2 units and the streamfunction of the advective water vapour flux is in units of 10^{5} gm mb^{-1} s^{-1} at intervals of 5 units. Vertically integrated (surface - 700 mb) advective water vapour flux divergence is in units of 10^{-4} gm cm^{-2} s^{-1} at intervals of 4 units and the vertically integrated streamfunction of the advective water vapour flux is in units of 10^{7} gm cm^{-1} mb^{-1} s^{-1} at intervals of 10 units 142

Figure Page

58 Monthly mean advective water vapour flux divergence (light lines, convergence shaded) and the streamfunction of the advective water vapour flux (heavy dashed lines) at surface, 900, 850 and 700 mb levels over the local domain in January 1976. Advective water vapour flux divergence is in units of 10^{-6} gm cm^{-2} mb^{-1} s^{-1} at intervals of 2 units and the streamfunction of the advective water vapour flux is in units of 10^{5} gm mb^{-1} s^{-1} at intervals of 5 units. Vertically integrated (surface - 700 mb) advective water vapour flux divergence is in units of 10^{-4} gm cm^{-2} s^{-1} at intervals of 4 units and the vertically integrated streamfunction of the advective water vapour flux is in units of 10^{7} gm cm^{-1} mb^{-1} s^{-1} at intervals of 10 units 144

59 Monthly mean advective water vapour flux divergence (light lines, convergence shaded) and the streamfunction of the advective water vapour flux (heavy dashed lines) at surface, 900, 850 and 700 mb levels over the local domain in February 1976. Advective water vapour flux divergence is in units of 10^{-6} gm cm^{-2} mb^{-1} s^{-1} at intervals of 2 units and the streamfunction of the advective water vapour flux is in units of 10^{5} gm mb^{-1} s^{-1} at intervals of 5 units. Vertically integrated (surface - 700 mb) advective water vapour flux divergence is in units of 10^{-4} gm cm^{-2} s^{-1} at intervals of 4 units and the vertically integrated streamfunction of the advective water vapour flux is in units of 10^{7} gm cm^{-1} mb^{-1} s^{-1} at intervals of 10 units 144

60 Monthly mean advective water vapour flux divergence (light lines, convergence shaded) and the streamfunction of the advective water vapour flux (heavy dashed lines) at surface, 900, 850 and 700 mb levels over the local domain in March, 1976. Advective water vapour flux divergence is in units of 10^{-6} gm cm^{-2} mb^{-1} s^{-1} at intervals of 2 units and the streamfunction of the advective water vapour flux is in units of 10^{5} gm mb^{-1} s^{-1} at intervals of 5 units. Vertically integrated (surface - 700 mb) advective water vapour flux divergence is in units of 10^{-4} gm cm^{-2} s^{-1} at intervals of 4 units and the vertically integrated streamfunction of the advective water vapour flux is in units of 10^{7} gm cm^{-1} mb^{-1} s^{-1} at intervals of 10 units 144

Figure Page

61 Monthly mean advective water vapour flux divergence (light lines, convergence shaded) and the streamfunction of the advective water vapour flux (heavy dashed lines) at surface, 900, 850 and 700 mb levels over the local domain in January 1977. Advective water vapour flux divergence is in units of 10^{-6} gm cm^{-2} mb^{-1} s^{-1} at intervals of 2 units and the streamfunction of the advective water vapour flux is in units of 10^{5} gm mb^{-1} s^{-1} at intervals of 5 units. Vertically integrated (surface - 700 mb) advective water vapour flux divergence is in units of 10^{-4} gm cm^{-2} s^{-1} at intervals of 4 units and the vertically integrated streamfunction of the advective water vapour flux is in units of 10^{7} gm cm^{-1} mb^{-1} s^{-1} at intervals of 10 units 146

62 Monthly mean advective water vapour flux divergence (light lines, convergence shaded) and the streamfunction of the advective water vapour flux (heavy dashed lines) at surface, 900, 850 and 700 mb levels over the local domain in February 1977. Advective water vapour flux divergence is in units of 10^{-6} gm cm^{-2} mb^{-1} s^{-1} at intervals of 2 units and the streamfunction of the advective water vapour flux is in units of 10^{5} gm mb^{-1} s^{-1} at intervals of 5 units. Vertically integrated (surface - 700 mb) advective water vapour flux divergence is in units of 10^{-4} gm cm^{-2} s^{-1} at intervals of 4 units and the vertically integrated streamfunction of the advective water vapour flux is in units of 10^{7} gm cm^{-1} mb^{-1} s^{-1} at intervals of 10 units 146

63 Monthly mean advective water vapour flux divergence (light lines, convergence shaded) and the streamfunction of the advective water vapour flux (heavy dashed lines) at surface, 900, 850 and 700 mb levels over the local domain in March 1977. Advective water vapour flux divergence is in units of 10^{-6} gm cm^{-2} mb^{-1} s^{-1} at intervals of 2 units and the streamfunction of the advective water vapour flux is in units of 10^{5} gm mb^{-1} s^{-1} at intervals of 5 units. Vertically integrated (surface - 700 mb) advective water vapour flux divergence is in units of 10^{-4} gm cm^{-2} s^{-1} at intervals of 4 units and the vertically integrated streamfunction of the advective water vapour flux is in units of 10^{7} gm cm^{-1} mb^{-1} s^{-1} at intervals of 10 units 146

Figure Page

64 Monthly mean streamfunction of the advective water vapour flux in cyclonic/NET_{SH} centres over Australia for January, February and March in the period 1957-75 and in the individual years from 1973-77. Vertical traces are in units of 10^5 gm mb^{-1} s^{-1} at the surface, 900, 850 and 700 mb levels. Dashed lines indicate abrupt changes from cyclonic to anticyclonic circulation and VI and AVI designate vertically integrated and average vertically integrated values respectively. The latter are in units of 10^7 gm cm^{-1} mb^{-1} s^{-1} 148

65 Monthly mean advective water vapour flux convergence over north-northeastern (heavy lines) and west-southwestern (light lines) Australia for January, February and March in the period 1957-75 and in individual years from 1973-77. Both vertical traces are in units of 10^{-6} gm cm^{-2} mb^{-1} s^{-1} at the surface, 900, 850 and 700 mb levels 148

66 Monthly mean total precipitable water content at various Australian radiosonde stations for January (J), February (F) and March (M) 1973-77. Total precipitable water content is in units of gm cm^{-2} . Stations used are D (Darwin, large dots), B (Broome, small dots), P (Port Hedland, dashed line), C/M (Cloncurry/Mount Isa, solid line), T (Townsville, smallest dotted line), CI (Cocos Island, open circles), WI (Willis Island, solid diamonds), A (Alice Springs, open diamonds) and CA (Carnarvon, solid squares) 151

67 Monthly mean 850 mb wind steadiness at various Australian upper wind stations. Wind steadiness values are given as a per cent and are the ratio of the speed of the monthly mean vector wind to the monthly mean scalar wind. Stations used are D (Darwin), CI (Cocos Island), T (Townsville), WI (Willis Island), P (Port Hedland), G (Giles), A (Alice Springs), C/M (Cloncurry/Mount Isa), CA (Carnarvon), CV (Charleville) and E (Eagle Farm) 153

68 Monthly mean 850 mb transient eddy water vapour flux divergence (light lines, convergence shaded) and the streamfunction of the transient eddy water vapour flux (heavy dashed lines) over the local domain in January, February and March 1973. Transient eddy water vapour flux divergence is in units of 10^{-6} gm cm^{-2} mb^{-1} s^{-1} at intervals of 2 units and the streamfunction of the transient eddy water vapour flux is in units of 10^5 gm mb^{-1} s^{-1} at intervals of 5 units 155

Figure Page

69 Monthly mean 850 mb transient eddy water vapour flux divergence (light lines, convergence shaded) and the streamfunction of the transient eddy water vapour flux (heavy dashed lines) over the local domain in January, February and March 1974. Transient eddy water vapour flux divergence is in units of 10^{-6} gm cm^{-2} mb^{-1} s^{-1} at intervals of 2 units and the streamfunction of the transient eddy water vapour flux is in units of 10^{5} gm mb^{-1} s^{-1} at intervals of 5 units 157

70 Monthly mean 850 mb transient eddy water vapour flux divergence (light lines, convergence shaded) and the streamfunction of the transient eddy water vapour flux (heavy dashed lines) over the local domain in January, February and March 1975. Transient eddy water vapour flux divergence is in units of 10^{-6} gm cm^{-2} mb^{-1} s^{-1} at intervals of 2 units and the streamfunction of the transient eddy water vapour flux is in units of 10^{5} gm mb^{-1} s^{-1} at intervals of 5 units 159

71 Monthly mean 850 mb transient eddy water vapour flux divergence (light lines, convergence shaded) and the streamfunction of the transient eddy water vapour flux (heavy dashed lines) over the local domain in January, February and March 1976. Transient eddy water vapour flux divergence is in units of 10^{-6} gm cm^{-2} mb^{-1} s^{-1} at intervals of 2 units and the streamfunction of the transient eddy water vapour flux is in units of 10^{5} gm mb^{-1} s^{-1} at intervals of 5 units 161

72 Monthly mean 850 mb transient eddy water vapour flux divergence (light lines, convergence shaded) and the streamfunction of the transient eddy water vapour flux (heavy dashed lines) over the local domain in January, February and March 1977. Transient eddy water vapour flux divergence is in units of 10^{-6} gm cm^{-2} mb^{-1} s^{-1} at intervals of 2 units and the streamfunction of the transient eddy water vapour flux is in units of 10^{5} gm mb^{-1} s^{-1} at intervals of 5 units 163

73 Monthly mean 850 mb total, advective and transient eddy water vapour fluxes in the meridional (Q_v) and zonal (Q_u) planes over the local domain in January, February and March 1973. Water vapour fluxes are in units of gm cm^{-1} mb^{-1} s^{-1} at intervals of 5 units (arrows schematically denote the direction of the flow) 165

74 Monthly mean 850 mb total, advective and transient eddy water vapour fluxes in the meridional (Q_v) and zonal (Q_u) planes over the local domain in January, February and March 1974. Water vapour fluxes are in units of gm cm^{-1} mb^{-1} s^{-1} at intervals of 5 units (arrows schematically denote the direction of the flow) 165

Figure Page

75 Monthly mean 850 mb total, advective and transient eddy water vapour fluxes in the meridional (Q_v) and zonal (Q_u) planes over the local domain in January, February and March 1975. Water vapour fluxes are in units of gm cm^{-1} mb^{-1} s^{-1} at intervals of 5 units (arrows schematically denote the direction of the flow) 165

76 Monthly mean 850 mb total, advective and transient eddy water vapour fluxes in the meridional (Q_v) and zonal (Q_u) planes over the local domain in January, February and March 1976. Water vapour fluxes are in units of gm cm^{-1} mb^{-1} s^{-1} at intervals of 5 units (arrows schematically denote the direction of the flow) 165

77 Monthly mean 850 mb total, advective and transient eddy water vapour fluxes in the meridional (Q_v) and zonal (Q_u) planes over the local domain in January, February and March 1977. Water vapour fluxes are in units of gm cm^{-1} mb^{-1} s^{-1} at intervals of 5 units (arrows schematically denote the direction of the flow) 165

78 Vertical cross sections (surface - 700 mb) of monthly mean advective water vapour flux divergence over Australia along 20°S for January 1957-75 and in the individual January of 1973, 1974 and 1975. Advective water vapour flux divergence is in units of 10^{-6} gm cm^{-2} mb^{-1} s^{-1} at intervals of 2 units (convergence shaded) 168

79 Vertical cross sections (surface - 700 mb) of monthly mean advective water vapour flux divergence over Australia along 20°S for February 1957-75 and in the individual February of 1975, 1976 and 1977. Advective water vapour flux divergence is in units of 10^{-6} gm cm^{-2} mb^{-1} s^{-1} at intervals of 2 units (convergence shaded) 172

80 Vertical cross sections (surface - 700 mb) of monthly mean advective water vapour flux divergence over Australia along 20°S for March 1957-75 and in the individual March of 1974, 1975 and 1977. Advective water vapour flux divergence is in units of 10^{-6} gm cm^{-2} mb^{-1} s^{-1} at intervals of 2 units (convergence shaded) 175

81 Monthly mean aerological traces and precipitable water content over northern Australia in January 1973, 1974 and 1975. Dashed traces indicate dew point temperatures (in °C) and solid traces indicate dry bulb temperatures (in °C). Precipitable water values are indicated for three 100 mb layers (1000-900, 900-800 and 800-700 mb) in units of gm cm^{-2} 180

Figure Page

82 Monthly mean aerological traces and precipitable water content over northern Australia in February 1975, 1976 and 1977. Dashed traces indicate dew point temperatures (in °C) and solid traces indicate dry bulb temperatures (in °C). Precipitable water values are indicated for three 100 mb layers (1000-900, 900-800 and 800-700 mb) in units of gm cm^{-2} 184

83 Monthly mean aerological traces and precipitable water content over northern Australia in March 1974, 1975 and 1977. Dashed traces indicate dew point temperatures (in °C) and solid traces indicate dry bulb temperatures (in °C). Precipitable water values are indicated for three 100 mb layers (1000-900, 900-800 and 800-700 mb) in units of gm cm^{-2} 187

84 Cold surges as dictated by surface pressure and wind data in the cross section from Hong Kong through Ishigakijima to Naha in January 1973. Surge passages are indicated by the schematic arrow marker on the left-hand side of the diagram 192

85 Cold surges as dictated by surface pressure and wind data in the cross section from Hong Kong through Ishigakijima to Naha in January 1974. Surge passages are indicated by the schematic arrow marker on the left-hand side of the diagram 192

86 Cold surges as dictated by surface pressure and wind data in the cross section from Hong Kong through Ishigakijima to Naha in January 1975. Surge passages are indicated by the schematic arrow marker on the left-hand side of the diagram 192

87 Daily streamline charts in the near tropical portion of the regional domain (20°N-20°S; 90°E-175°E) for the January 1973 surge period of 1st-4th (Days 0 to 3). Heavy dashed lines indicate wind isotachs, with areas of 15 knots and above shaded (redrawn from the Bureau of Meteorology's Darwin Regional Office charts) 195

88 Daily streamline charts in the near tropical portion of the regional domain (20°N-20°S; 90°E-175°E) for the January 1973 surge period of 17th-20th (Days 0 to 3). Heavy dashed lines indicate wind isotachs, with areas of 15 knots and above shaded (redrawn from the Bureau of Meteorology's Darwin Regional Office charts) 195

89 Daily streamline charts in the near tropical portion of the regional domain (20°N-20°S; 90°E-175°E) for the January 1973 surge period of 24th-27th (Days 0 to 3). Heavy dashed lines indicate wind isotachs, with areas of 15 knots and above shaded (redrawn from the Bureau of Meteorology's Darwin Regional Office charts) 195

Figure | Page

90 Daily streamline charts in the near tropical portion of the regional domain (20°N-20°S; 90°E-175°E) for the January 1974 surge period of 11th-14th (Days 0 to 3). Heavy dashed lines indicate wind isotachs, with areas of 15 knots and above shaded (redrawn from the Bureau of Meteorology's Darwin Regional Office charts) 197

91 Daily streamline charts in the near tropical portion of the regional domain (20°N-20°S; 90°E-175°E) for the January 1974 surge period of 18th-21st (Days 0 to 3). Heavy dashed lines indicate wind isotachs, with areas of 15 knots and above shaded (redrawn from the Bureau of Meteorology's Darwin Regional Office charts) 197

92 Daily streamline charts in the near tropical portion of the regional domain (20°N-20°S; 90°E-175°E) for the surge period from 30th January to 2nd February 1974 (Days 0 to 3). Heavy dashed lines indicate wind isotachs, with areas of 15 knots and above shaded (redrawn from the Bureau of Meteorology's Darwin Regional Office charts) 197

93 Daily water vapour flux roses for Darwin, Broome, Port Hedland, Carnarvon, Giles, Alice Springs and Cloncurry in January 1973, 1974 and 1975. Water vapour fluxes are in units of gm cm^{-1} mb^{-1} s^{-1} with small arrows denoting water vapour flux in the range of 0-5 gm cm^{-1} mb^{-1} s^{-1}, medium arrows denoting water vapour flux in the range 5-10 gm cm^{-1} mb^{-1} s^{-1} and large arrows denoting water vapour flux in the range of greater than 10 gm cm^{-1} mb^{-1} s^{-1} 199

94 Distribution of upper air and upper wind stations in the Indo-Pacific Domain 204

95 Monthly mean 850 and 200 mb wind vectors and divergence (convergence shaded) over the Indo-Pacific domain in the January 1973 - SOI phase. Wind vectors are in units of m s^{-1} with vectors of 1 cm length equal to 37 m s^{-1} and dashed lines in the 850 mb diagrams indicating the position of the (NET_{NH} and NET_{SH}). Divergence fields are in units of 10^{-6} s^{-1} at intervals of 5 units. Grey areas on the land masses at 850 mb indicate the distribution of relief 206

96 Monthly mean 850 and 200 mb wind vectors and divergence (convergence shaded) over the Indo-Pacific domain in the January 1974 + SOI phase. Wind vectors are in units of m s^{-1} with vectors of 1 cm length equal to 37 m s^{-1} and dashed lines in the 850 mb diagrams indicating the position of the (NET_{NH} and NET_{SH}). Divergence fields are in units of 10^{-6} s^{-1} at intervals of 5 units. Grey areas on the land masses at 850 mb indicate the distribution of relief 206

Figure Page

97 Monthly mean 850 and 200 mb wind vectors and divergence (convergence shaded) over the Indo-Pacific domain in the - SOI composite (January 1958 and 1959 and February 1959, 1970, 1973 and 1978). Wind vectors are in units of m s^{-1} with vectors of 1 cm length equal to 37 m s^{-1} and dashed lines in the 850 mb diagrams indicating the position of the (NET_{NH} and NET_{SH}). Divergence fields are in units of 10^{-6} s^{-1} at intervals of 5 units. Grey areas on the land masses at 850 mb indicate the distribution of relief 211

98 Monthly mean 850 and 200 mb wind vectors and divergence (convergence shaded) over the Indo-Pacific domain in the + SOI composite (January 1962, 1967 and 1974 and February 1971 and 1974). Wind vectors are in units of m s^{-1} with vectors of 1 cm length equal to 37 m s^{-1} and dashed lines in the 850 mb diagrams indicating the position of the (NET_{NH} and NET_{SH}). Divergence fields are in units of 10^{-6} s^{-1} at intervals of 5 units. Grey areas on the land masses at 850 mb indicate the distribution of relief 211

99 Monthly mean streamfunction fields at 850, 700 and 200 mb in January 1965-78. Fields are in units of 10^{5} m^2 s^{-1} (850 and 700 mb) at intervals of 1 unit and in units of 10^{6} m^2 s^{-1} (200 mb) at intervals of 5 units. Dashed lines at 850 and 700 mb levels indicate the position of the (NET_{NH} and NET_{SH}) and the SOI values on the right-hand side of the diagram are those of Troup 218

100 Monthly mean velocity potential overlays (850, 700 and 200 mb) in January 1965-78 and total cloud cover distributions over the Pacific region (Sadler *et. al.*, 1976 and Shidler and Sadler, 1979) in the same period (January 1965 unavailable). Velocity potential overlay features are explained by the symbols and colours on the diagram, while total cloud cover regions of 5 octa and above are shaded blue. Velocity potential fields are in units of 10^{6} m^2 s^{-1} at intervals of 2 units 223

101 Monthly mean divergence overlays (850, 700 and 200 mb) over the Australian continent in January 1965-76. Shading relationships and underlying isohet patterns are shown in the accompanying key. The numbers at some grid point intersections indicate 200 mb divergence/convergence (top) and 850 mb divergence/convergence (bottom) values of significant magnitude. Divergence is in units of 10^{-6} s^{-1} 229

102 Matching of three surface pressure derived SOIs (Wright's 'old' and 'new', and Troup's) with a 200 mb geopotential height (GPH) SOI (Horel and Wallace, 1981) for the Southern Hemisphere summers (December - February) from 1951-78. Stippled areas in the diagram indicate strong, - SOI phases and horizontal shadings indicate strong, + SOI phases when both surface and 200 mb SOIs concur 236

Figure Page

103 Relationships between the Southern Hemisphere summer monsoon of Australasia and SOI intensities. The top diagram from Tanaka (1981) shows the matching and correlation (+ 0.94) between an index of the Asian monsoon (150 mb zonal wind speed at Singapore) and an SOI or Walker Circulation Index (surface pressure difference between Tahiti and Cocos Island) in the Southern Hemisphere summers from 1961-80. The two remaining diagrams illustrate a similar relationship between Troup's SOI and Singapore 150 mb zonal wind speed and Troup's SOI and Darwin 150 mb zonal wind speed in the Southern Hemisphere summer months of January and February from 1961-81. The correlations for the latter are + 0.76 and + 0.50 respectively. In the top diagram, numbers on the right-hand side are of zonal wind speed in m s^{-1} while those on the left-hand side are those of the Walker Circulation Index 238

104 Lake Eyre drainage system (from Department of National Resources Australian Water Resources Council, 1976) 242

105 Pattern of equal correlation coefficients between an annual mean Southern Oscillation Index (Troup's SOI) and district mean annual rainfall (left-hand diagram) and between the annual mean latitude of the surface high pressure belt over eastern Australia and district mean annual rainfall (right-hand diagram) from 1941-70 (from Pittock, 1975) 242

106 Pattern of equal correlation coefficients between a seasonal mean Southern Oscillation Index (Wright's 'old' SOI) and district mean seasonal rainfall from 1933-74. Seasons are defined as summer (December - February), autumn (March - May), winter (June - August) and spring (September - November) (from Nicholls and McBride, 1981 personal communication) 242

107 Relationship between Wright's 'old' SOI, extensive or isolated outbreaks of equatorial PDZ rainfall and major or minor floodings of Lake Eyre in South Australia over the period 1860-1975. PDZ data from a combination of material in Quinn and Burt (1970) and Reiter (1978, 1979) and Lake Eyre flooding data from a combination of material in Bonython and Mason (1953), Mason (1955), Bonython (1960, 1963), Tetzlaff (unpublished) and Graetz (1980) 246

108 Distribution of playa lakes over the Australian continent (from Bowler, 1981) 249

109 Lake Frome pollen diagram over the last 10,000 years. Pollen catch A is the modern annual pollen influx (grains cm^2 yr^{-1}) and charcoal particle influx (numbers greater than 10 µ cm^2 yr^{-1} x 5) from 13th November 1973 to 13th November 1977. Fossil pollen record B shows percentages of total land plant pollen and the charcoal influx record (numbers greater than 10 µ cm^3 yr^{-1}) from the sediments of the lake (from Singh, 1981) 249

LIST OF TABLES

Table		Page
1	List of recent Southern Oscillation Indices (SOIs)	234
2	Histogram of Wright's 'new' SOI values by season 1947-73	244
3	Histogram of Wright's 'old' SOI values by season 1947-73	244

ABSTRACT

Monsoon dynamics in the Indian and West African regions have received increased scientific attention in the last 10-20 years. By comparison, the dynamics of the northern Australian monsoon have received relatively little recognition. It is for this reason that this thesis is undertaken.

In this study, three spatial domains are used to examine the tropospheric dynamics of the Southern Hemisphere summer monsoon regime of Australasia and its large-scale interactions with Indo-Pacific teleconnection patterns. The 1973-77 summer period is of particular interest because it contains several extreme atmospheric and oceanic events (e.g. 1973 - El Niño; 1974 - summer floods in Australia and the filling of Lake Eyre; 1975 - intraseasonal variability from dry January to wet February; 1976 - summer floods in Australia).

Although the analysis focuses primarily on time-average fields during the months of January, February and March 1973-77, evidence from this period provides a basis for the consideration of long-term monsoon and teleconnection variability.

DECLARATION

I hereby declare that none of the material contained in this thesis has been accepted for the award of any other degree or diploma in any institution and that, to the best of my knowledge and belief, the thesis contains no material previously published or written by another person, except where due reference has been made in the text of the thesis.

Robert J. Allan

ACKNOWLEDGMENTS

I would like to acknowledge those persons, organizations and weather services without whose assistance this thesis would not have been possible.

Firstly, I express my gratitude to my supervisors, Dr. Peter Lamb, Mr. Adrian Gordon and Dr. Sandy Taylor.

Dr. Lamb, now with the Illinois State Water Survey in the United States, suggested the basis for this topic and supervised its early stages. I am grateful for his continued interest and assistance and for his constructive criticism of the final draft.

Mr. Gordon, of the Flinders Institute for Atmospheric and Marine Sciences, Flinders University, South Australia, has provided enthusiastic supervision from a wealth of meteorological experience. His encouragement and support is very much appreciated.

Dr. Taylor, of the Department of Geography, University of Adelaide, South Australia, acted as my Departmental supervisor. I am grateful for her advice and thorough appraisal of the text.

I would like to thank the following people and organizations for their constructive advice and assistance during the preparation of this thesis.

Dr. Peter Webster, of the CSIRO Division of Atmospheric Physics, Melbourne, gave expert advice and provided me with the opportunity to present aspects of my research to the wider meteorological community in Australia. I thank him for arranging seminars at the Department of Applied Mathematics, Monash University, Melbourne, and at the CSIRO Division of Atmospheric Physics, Melbourne.

Dr. R.A.D. Byron-Scott, of the Flinders Institute for Atmospheric and Marine Sciences, Flinders University, South Australia, kindly proof read the mathematical appendices and was always available to discuss the research topic. He also organized two seminars for me in the School of Earth Sciences, Flinders University, South Australia.

Drs. John McBride, Neville Nicholls, Bryant McAvaney and Noel Davidson, of the Australian Numerical Meteorology Research Centre (ANMRC), Melbourne, were always prepared to discuss the research and offer advice during my visits to Melbourne. I also thank them, along with Mr. Jim Ginnane of ANMRC, for providing the opportunity to present a seminar on aspects of this research at ANMRC.

Drs. Jim Bowler and Gurdip Singh, of the Department of Biogeography and Geomorphology, Australian National University, Canberra, and Dr. Bob Wasson, of CSIRO Division of Land Use Research, Canberra, gave expert advice on palaeoenvironmental research, particularly in regard to Lake Eyre.

Dr. Bruce Currey, of the Department of Geography, Flinders University, South Australia, was always willing to discuss the general impact of teleconnection extremes in the Indo-Pacific basin.

Dr. John Bye, of Flinders Institute for Atmospheric and Marine Sciences, Flinders University, South Australia, and the Lake Eyre Committee of the Royal Geographical Society of Australasia, South Australian Branch, were valuable sources of information on Lake Eyre floodings. I thank the Royal Geographical Society of Australasia, South Australian Branch, for the opportunity to prepare a monograph on the aspects of Lake Eyre floodings contained in this thesis.

The following people and meteorological services provided data for this thesis.

Dr. David Karoly, of ANMRC, Melbourne, made available a copy of a data tape he had obtained from the National Center for Atmospheric Research in the United States.

Mr. Sandy Troup, of CSIRO Division of Atmospheric Physics, Melbourne, and Dr. Peter Wright from the United Kingdom, kindly provided copies of their Southern Oscillation Indices.

Mr. Rex Falls and staff of the Darwin Regional Office of the Bureau of Meteorology, aided in obtaining upper air data and streamline charts for this thesis. I most grateful for their kindness and co-operation during my brief

visit to their Divisional Office.

Dr. Leslie Potter, of the Department of Geography, University of Adelaide, South Australia, was instrumental in helping me to procure upper air and upper wind data from Indonesia.

Meteorological data from the following services was used in this thesis: Australian Bureau of Meteorology, Malaysian Meteorological Service, Service de la Meteorologie en Nouvelle - Calédonie, Thai Meteorological Department, Japanese Meteorology Agency, Central Weather Bureau of Taiwan, Royal Observatory at Hong Kong, Malawi Government Meteorological Service, Instituto Meteorologico Nacional of Costa Rica, Pakistan Meteorological Department, Meteorologische Dienst of Netherlands Antilles, Meteorological Department of the Republic of Vanuatu, New Zealand Meteorological Service, Republic of Seychelles Directorate of Civil Aviation, Servico Meteorologico de Mocambique, Republika Demokratika Malagasy Service de la Meteorologie, Indonesian Meteorological and Geophysical Institute, Kenyan Meteorological Department, Republic of Maldives Department of Meteorology, Mauritius Meteorological Department, Philippine Atmospheric, Geophysical and Astronomical Services Administration, United Republic of Tanzania Directorate of Meteorology, Republic of Zambia Meteorological Department, Service Météorologique de la Réunion and the Democratic Republic of the Sudan Meteorological Department.

Several services provided data that either duplicated already available material or was outside the period of study. There were: Iraqi Meteorological Organization, Météorologie Nationale of France, Climatological Officer Abu Dhabi International Airport, Bangladesh Meteorological Department, Direccion Meteorologia de Chile, Service Météorologique de la Polynésie Francaise and the Oman National Meteorological Service.

Finally, I am particularly grateful to the following people for providing technical assistance in this thesis.

Mr. Wence Sulda and Mr. Errol Bamford, successive computer programmers in the Department of Geography, University of Adelaide, South Australia, helped in the formulation of programmes and decoding of data tapes. Their assistance is most appreciated.

Mr. Max Foale, Mrs. Chris. Crothers and Ms Debbie Oakley, of the Cartographic Section, Department of Geography, University of Adelaide, South Australia, worked tirelessly on the cartographic aspects of this study. Without their efforts this thesis would certainly not have been completed.

I would like to thank Mrs. Mary Allan for typing the final manuscript.

Financial support for this study was provided by a University of Adelaide research grant. Additional funding for cartography was made available by the Department of Geography, University of Adelaide, South Australia.

UNIVERSITY OF ADELAIDE LIBRARY

CHAPTER I - INTRODUCTION

To date, little research has been directly concerned with large-scale monsoon and teleconnection variations over northern Australia. In this study an attempt is made to redress aspects of this deficiency.

The approach takes the form of a diagnostic analysis of low latitude circulation, moist processes and teleconnection variability over Australasia during Southern Hemisphere summers. Particular emphasis is placed on developing a three dimensional picture of monsoon and teleconnection structures.

This analysis is undertaken in three sections.

1. Regional domain (35°N-35°S; 85°E-175°E)

In the Southern Hemisphere summer, the Australasian region is the focus of the Asian/Australasian monsoon and a major source region of teleconnections. This area, herein designated as the 'regional domain', forms the basis for an analysis of large-scale intraseasonal and interannual circulation and teleconnection variations during the Southern Hemisphere summer monsoon months of January, February and March 1973-77. This period was particularly interesting as it contained several extreme atmospheric and oceanic events which influenced the Indo-Pacific region.

The analysis uses monthly mean upper wind and upper air observations at standard atmospheric levels to develop fields of geopotential height, velocity potential, streamfunction and kinetic energy generation. Such material is presented not only in the horizontal plane but also in the vertical plane, in the form of cross sections of velocity potential. Finally, these dynamic fields are compared to and contrasted with remotely-sensed rainfall rates, cloud cover and outgoing longwave radiation distributions.

2. Local domain (5°S-30°S; 95°E-155°E)

Within this localized area of the regional domain, a specific analysis is undertaken at standard atmospheric levels of the circulation and divergence

of monthly mean total, advective and transient eddy water vapour fluxes during the months of January, February and March 1973-77. This is used as the basis for an evaluation of intraseasonal and interannual changes in the spatial extent and vertical structure of convective processes and moisture characteristics over northern Australia during the summer monsoon. Particular emphasis is placed on an examination of the depth and organisation of moist processes during monsoon and teleconnection extremes. In addition, there are brief attempts to examine heat low/Near Equatorial Trough in the Southern Hemisphere (NET_{SH}) discontinuities over the Australian continent and cold surge penetration into the Australasian region during the study period.

3. Wider spatial and longer temporal variability

In this section, three aspects are involved :

(*i*) investigation over a larger spatial area of those dynamic patterns and signatures identified in the regional domain.

(*ii*) analysis of the relationship between upper air dynamics, physical manifestations, remotely-sensed data and monsoon and teleconnection indices.

(*iii*) evaluation of longer-term observational, historical and proxy data sequences.

Since the regional domain focuses mainly on a major teleconnection source region, it is desirable to investigate wider atmospheric responses (e.g. circulation and divergence) in the larger Indo-Pacific domain (35°N-35°S; 30°E-60°W). Initially, this is undertaken for the two months of January 1973 and January 1974, when, according to the dynamic analysis in the regional domain, two distinct Southern Oscillation/Walker Circulation (SO/WC) modes are operating. However, to gauge whether these two months are truly representative of extreme SO/WC modes, composites of summer months with strong positive and negative Southern Oscillation Indices (SOI's) in the period 1957-81 are also examined dynamically over the Indo-Pacific domain.

From this analysis, it is suggested that discrepancies exist between

those circulation and divergence patterns representing SO/WC extremes deduced from dynamic analysis (as in January 1973 and January 1974) and those deduced from SOI's (positive and negative composites). Moreover, the most pronounced discrepancies appear to be in the Australasian region.

To investigate whether these differences are real or merely a quirk of the data concerned, an extended analysis of streamfunction and velocity potential fields in the regional domain is then undertaken. This evaluation focuses on the month of January for the 1965-78 period inclusive, and attempts to interrelate dynamics, SOI's, physical manifestations and remotely-sensed data, and examine whether major features observed in 1973-77 are representative of longer time periods. This analysis also includes a scale change, in that summer rainfall distributions over the Australian continent are examined in terms of fields of divergence rather than larger-scale velocity potential fields.

The nature of long-term relationships between physical manifestations, SOIs and monsoon dynamics is developed from investigations of the spatial distribution of SOI/rainfall correlations over the Australian continent, the extent of SOI/monsoon indice correlations, and comparisons between several SOIs in the Australasian region. Observed coherence between indices, dynamics and physical manifestations during periods of enhanced persistence of atmospheric modes in contemporary data sets suggests that strong SOI/physical manifestation links during historical periods and strong physical manifestations in longer Holocene and Quaternary periods are indicators of long-term monsoon and teleconnection variations. One physical manifestation that is examined in this context is the flooding/filling of Lake Eyre in South Australia. Its potential as a long-term indicator is evaluated.

Overall, this study highlights the need for a concerted examination of the role of the Asian/Australasian monsoon in the seasonal evolution of teleconnection patterns. Apart from the Global Atmospheric Research Programme (GARP) and observational phases, such as the First GARP Global Experiment (FGGE), the Monsoon Experiment (MONEX) and the West African Monsoon

Experiment (WAMEX), existing low latitude data sets are generally of poor quality and do not allow for more than a very broad-scale appraisal of atmospheric elements. Thus the ability to probe and further verify aspects of the monsoon and SO/WC relationships described in this thesis must await more detailed data collection programmes.

To provide a setting for the current research, the first section in this chapter deals with an historical review of the changing concept of a monsoon and its relationship to large-scale teleconnection patterns. A more specific examination of the historical background and nature of the Southern Hemisphere summer monsoon of Australasia is presented in the second section of Chapter I together with a survey of recent concepts of climatic variability and their implications for long-term monsoon research.

1.1 MONSOON DYNAMICS

1.1.1 Historical and Theoretical Considerations

No single definition of a monsoon has yet been developed that will satisfy all meteorologists and climatologists. The concept of a monsoon has been variously employed to describe major temporal and spatial changes in wind circulation regimes from tropical to polar latitudes (Ramage, 1971). It is only in the last 10-20 years that the definition has come to be associated primarily with tropical and subtropical latitudes and with interactions involving both the lower and upper layers of the atmosphere.

Since the turn of this century, the concept of a monsoon has changed with the increased acquisition of data through improved rawinsonde equipment, satellite technologies and co-ordinated studies. Prior to World War II, most workers regarded a monsoon as a giant, low-level sea breeze effect. This was to be expected since the majority of data were derived from ground-based observations. Yet, recent dictionary and encyclopaedia definitions still describe a monsoon in these terms, thereby failing to take into account the influence that upper-level data analysis has had in shaping the concept of a monsoon.

During this century, not only the definition but also the cause of monsoon circulations has been a point of disagreement. The early premise which equated the monsoon with a giant seasonal sea breeze was derived from a combination of Halley's 17th Century differential heating theory and Hadley's observations of coriolis deflected wind systems in the 18th Century. During and immediately after the Second World War, causality was re-examined because of new findings about upper air flow and an entirely thermal explanation was found wanting. In particular, the seasonal sea breeze concept of trade wind flow was found to be only a shallow, low-level aspect of the total monsoonal process in the troposphere. These findings led to new assessments of the monsoon concept.

As Trewartha (1954:95) states :

> To a greater extent than was formerly thought to be the case the monsoons appear to be in the nature of various kinds and degrees of modification of the general planetary wind system. The thermally induced monsoon winds are always superimposed upon an original planetary system, which is usually the dominant one.

Not all researchers have concurred with a fusion of thermal and planetary scale causes. For example, Gentilli (1958:69) replaced thermal causality with entirely planetary air mass and circulation factors :

> The *seasonal reversal of the direction of air flow at the surface* over south Asia and the surrounding seas is therefore due to the seasonal swing of the planetary wind belts, which move some 40° of latitude south or north according to the time of the year.

As will be shown, resolution of this dilemma has only come about through more detailed research and observations of the monsoon system.

Three recent definitions detail the current understanding and illustrate the nature of the phenomenon examined in this study. Ramage (1971:6) provides a definition of a monsoon based solely on changing surface conditions :

> I define the monsoon area as encompassing regions with January and July surface circulations in which:
>
> 1. The prevailing wind direction shifts by at least 120° between January and July.
> 2. The average frequency of prevailing wind directions in January and July exceeds 40%.
> 3. The mean resultant winds in at least one of the months exceed 3 m/sec, and
> 4. Fewer than one cyclone-anticyclone alternation occurs every two years in either month in a 5° latitude-longitude rectangle.

However, Barry and Chorley's (1976:300) statement, although referring specifically to the Asian monsoon, neatly summarizes the recent findings about monsoon systems in general :

> The Asiatic monsoon regime is a consequence of the interaction of both planetary and regional factors, both at the surface and in the upper troposphere.

Linacre and Hobbs (1977:139) provide another variation of this theme :

> A *monsoon* is a secondary circulation occurring over a wide area, characterised by a seasonal reversal of the steady, prevailing wind directions and by only rare alternations of high and low pressure systems.

From the above, a reasonable approximation of the extent of the monsoonal system is given by Ramage (1971) in Figure 1. Included in this figure is an example of the range of monsoonal regimes that many Russian researchers often claim. Their broad terminology ensures that a monsoon is as equally applicable to polar as to tropical regions (Flöhn, 1955).

Probably one of the most important technological advances to influence meteorology and climatology has been the use of satellite observations (Streten, 1982). Before the early to mid 1960's, global climatological and meteorological research, together with subsequent atlases, were dependent on sparse ground, ship-based and aerological observations. As a result of the particularly poor data coverage in the tropics, the whole relationship of the monsoons to total atmospheric processes was underestimated. Since then, tropical research in particular has profited immensely from the expanded use of satellite observations which allow more detailed investigations of a myriad of spatial and temporal phenomena. A consequence of this development has been a growing acceptance of the concept of a planetary-scale monsoon system in preference to the notion that monsoons only occur in, and influence, very distinct regions.

In fact, it has become clear that it may be restrictive to speak of 'The Indian Monsoon', 'The West African Monsoon', 'The Asian Monsoon' or even 'The Northern Australian Monsoon' in any sharp, regionally binding sense. Hence, it is simplistic to attempt to develop the concept of a monsoon without taking account of the atmospheric circulation as a whole, or to try to analyse monsoon foci in total isolation. What is required, as Barry and Chorley (1976:300) previously noted, is a balance between both regional and planetary-scale factors in which regional factors cannot be wholely neglected.

Figure 1 The monsoon region, as defined by Ramage (1971), is bounded by the rectangle. Shadings define the areas seen to be monsoonal by Russian researchers (hatched) and where low frequencies of surface cyclone-anticyclone alternations occur in summer and winter (stippled) (from Ramage, 1971).

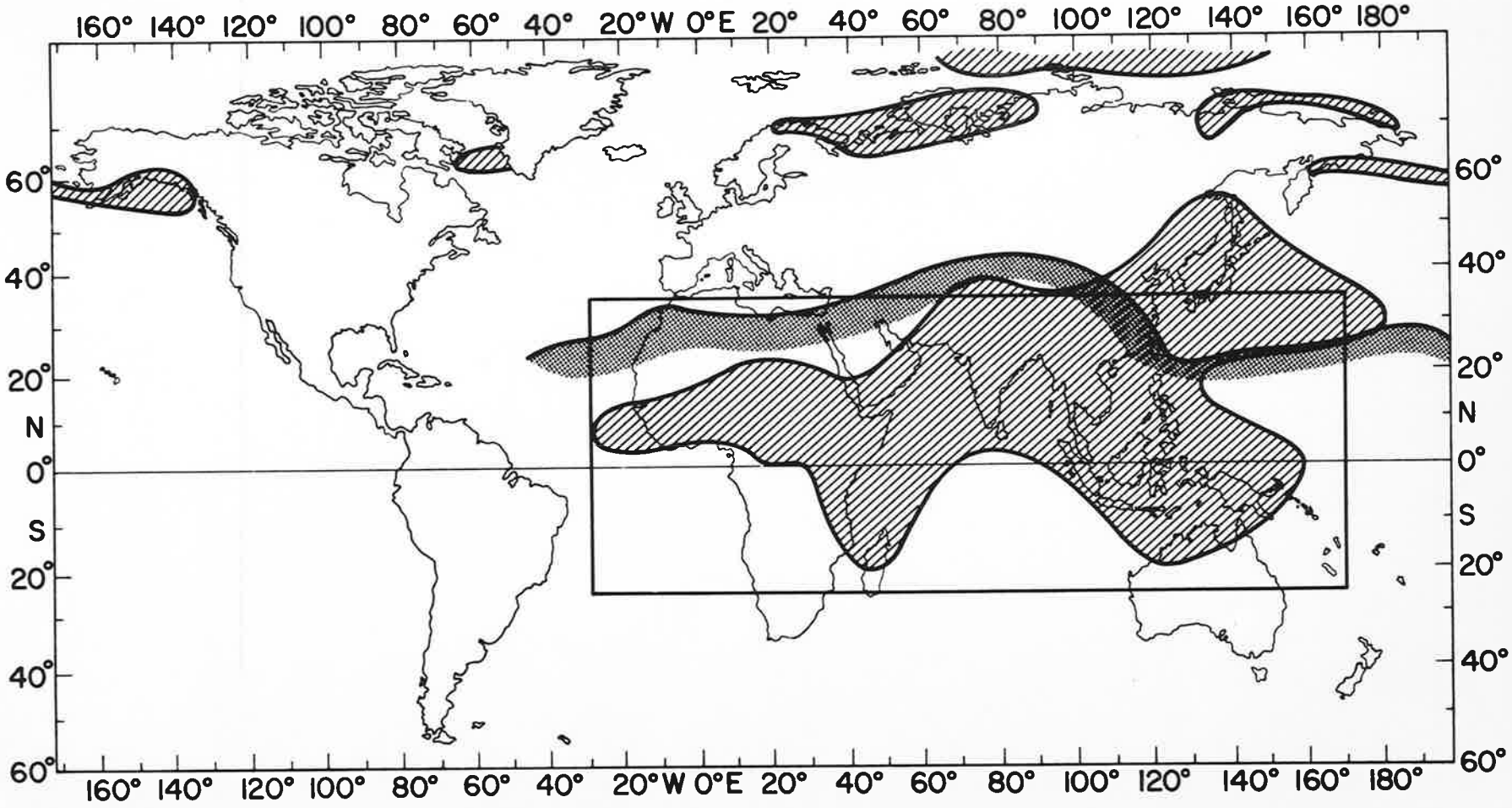
160° 140° 120° 100° 80° 60° 40° 20° W 0° E 20° 40° 60° 80° 100° 120° 140° 160° 180°
60°
40°
20°
N
0°
S
20°
40°
60°

For instance, regionality must still be invoked to explain important aspects of the finer structure and symmetry of the monsoons during summer and winter in each hemisphere. In the Asian portion of the monsoon system, there is little hemispherical symmetry between the northeast and southwest monsoon circulations. As Webster *et. al.* (1977:1468) point out, this lack of symmetry is caused by :

> ...the distribution of mountains in the monsoon region, the relative sizes of the continental land masses of Australia and Asia and the distribution of the large mountainous islands which contribute [to] the 'maritime' continent (Ramage, 1968) made up of Sumatra, Borneo, New Guinea plus numerous other smaller islands characterized by equally high terrain, all of which are surrounded by extremely warm ocean water.

Orography plays a two-fold part in giving a distinctly regional touch to both summer and winter hemisphere monsoon structures. It can act as a simple mechanical barrier generating perturbations in the large-scale winter flow or, more intricately, as an elevated heat source affecting atmospheric mass and heat balance in summer. This two-fold effect is noted by Webster *et. al.* (1977:1469, 1471) in the following statements :

> It was found that the mountains [viz the raised Tibetan Plateau in the Himalayas] were responsible for the formation and maintenance of the warm upper-tropospheric anticyclone via latent heating.
>
> With the mean westerlies considerably poleward of their summer position, the Himalayas act as a strong mechanical perturber of the mean zonal flow.

The sizes and positions of continental masses have further implications for circulation patterns. Australia, a large island continent of relatively low relief, appears to be more or less in a peripheral area of the planetary monsoon system. It therefore produces little in the way of major mechanical perturbations or raised heat sources. Yet, no doubt as a result of interactions between the Australian continent and the atmospheric circulation, some interesting thermal, pressure and hydrological effects do occur (Sumi and Murakami, 1981). As Riehl (1967:3) states :

> The concept of "critical size" must be raised - how important is a continent of Australia's particular size and topography in manufacturing its own general circulation?

However, on a global scale, the consequences of the Australian continent's size and location on monsoon character is generally lost among the more 'spectacular' phenomena. This is evident in the description of the major 200 mb summer and winter features of the planetary monsoon system given by Chang (1977:1089, 1089-90) :

> During summer these features include a strong anticyclone centered over the Tibetan Plateau, a weaker anticyclone over Mexico and elongated troughs oriented northeast-southwest in the mid-Pacific and mid-Atlantic.
>
> During winter a large streamfunction high over the equatorial South China Sea and western Pacific replaces the Tibetan high to become the most pronounced planetary scale feature, with two weaker highs appearing over the equatorial eastern Africa and the northeastern South America and three oceanic troughs extending from the equator to the southern subtropics.

In fact, only Krishnamurti *et. al.* (1973) have examined the importance and significance of upper-level anticyclones to the northeast and northwest of the Australian continent in the Southern Hemisphere winter. Upper-level Southern Hemisphere summer anticyclones are only noted in passing in the works of Krishnamurti *et. al.* (1973), Krueger and Winston (1974, 1975) and Murakami and Unninayar (1977).

In the 1960's-70's, the development of satellite technology and remotely-sensed imagery focused attention on large-scale interactions between the atmosphere and the oceanic regions which cover most of the earth's surface. What was perhaps most illuminating was the apparent interactions, on a hemispherical scale, between the monsoon regions and the adjacent ocean basins. Previously, particularly over the tropical and near-tropical Pacific and Indian Oceans, the only co-ordinated large-scale meteorological and climatological research had taken place during the International Geophysical Year (1957-58), the early stages of the International Indian

Ocean Experiment (1959-65), or had been initiated by workers and organisations from various countries (i.e. U.S.A., U.S.S.R., U.K., Netherlands, Peru, Germany and Australia). However, in more recent times, although some researchers have continued to produce tropical atlases and assemblages from terrestrial, marine and aerial observations (viz. Atkinson and Sadler, 1970; Hastenrath and Lamb, 1977, 1978, 1979 a,b; Romanov and Romanova, 1976), the vast majority have used a remote sensing base (e.g. Raschke and Bandeen, 1967; Taylor and Winston, 1968; Allison *et. al.*, 1969; Bjerknes *et. al.*, 1969; Godshall *et. al.*, 1969; Kreins and Allison, 1969; Sadler, 1969; Atkinson and Sadler, 1970: Vol I and Vol II; Miller, 1971; Rao *et. al.*, 1976; Winston *et. al.*, 1979).

Numerical modelling techniques have also been increasingly employed to probe and test both spatial and temporal aspects of planetary monsoon structure. Comparisons of the results obtained from this work are presented in the overviews of Krishnamurti *et. al.*(1973) and Chang (1977). Basically the modellers have investigated the following areas;

(a) energy exchanges and interactions between various scales of waves and flows (e.g. Colton, 1973; Krishnamurti *et. al.*, 1973)

(b) broad-scale monsoon climatology as dictated by orographic barriers and heat sources and sinks (e.g. Manabe *et. al.*, 1970; Krishnamurti *et. al.*, 1973; Hahn and Manabe, 1975)

(c) variable large-scale heating and equatorial wave patterns (e.g. Murakami, 1973, 1974; Webster and Lau, 1978; Gill, 1980; Geisler, 1981; Lau, 1981; Sasamori, 1982)

(d) forcing on and from tropical latitudes (e.g. Webster, 1972, 1973 a,b, 1978, 1981 b; Chang, 1977; Lau and Lim, 1982; Webster and Holton, 1982)

(e) the oscillations of the monsoon system (e.g. Krishnamurti and Bhalme, 1976).

Other studies (e.g. Krishnamurti, 1971 a,b ; Kanamitsu *et. al.*, 1972; Krishnamurti *et. al.*, 1973; Murakami, 1978) have used real time data to

explore further the intricacies of the monsoon system.

1.1.2 Teleconnections and the Monsoon System

One of the most constructive developments in tropical meteorology research has been the fusion of current concepts of the monsoon system with the often previously maligned evidence for long-range atmospheric-oceanic interactions. Two important steps in establishing such linkages have been the deductions of possible physical mechanisms to account for a coherent phenomenon and the naming of such atmospheric-oceanic interactions as teleconnections (Bjerknes, 1969).

Before the Second World War, the major studies concerned with long-range atmospheric relationships were the statistical works of Walker and Bliss (Walker, 1923, 1924, 1928; Walker and Bliss, 1930, 1932, 1937 - reviewed in Wright, 1977; Julian and Chervin, 1978; Rasmusson and Carpenter, 1982). The most dominant and enduring aspect of their research was the concept that pressure and rainfall oscillations existed across the Indian and Pacific Oceans. In other words, high(low) pressure over Australasia correlated with low(high) pressure over the South Pacific. However, in the following 20-30 years, little further effort was made to verify, explain or monitor this 'Southern Oscillation' phenomenon. Willett and Bodurtha (1952:429) contended that :

> Because the mechanism for the existence of this oscillation is unknown and because Walker's complete southern oscillation is difficult to evaluate, it has not received much attention in the past decade.

Troup (1965:490) also stated that "At present the phenomenon known as the 'southern oscillation' receives little attention".

This phenomenon began to attract renewed attention as remotely-sensed imagery (visible and infra-red) accumulated in favour of interactions between atmospheric variables on hemispherical scales. Ironically, these findings mainly focused attention on existing temporal records. Examples of

this type of study include the various time series approaches used by Kidson (1975) and Trenberth (1975, 1976 a,b) to determine the periodicity, phase associations, and spatial correlations and variances expressed by the Southern Oscillation, and those of Van Loon and Jenne (1969, 1970) and Madden and Julian (1971, 1972) which have been more concerned with particular frequencies and circulations in the atmosphere that may have implications for the Southern Oscillation fluctuation. More directly related to the Australasian region, Kidson (1925), Quayle (1929), Treloar (1934), Treloar and Grant (1953), O'Mahony (1961), Priestley (1962), Troup (1965, 1967), Pittock (1973, 1974, 1975), Pittock *et. al.* (1978), Nicholls and Woodcock (1981), Nicholls *et. al.* (1982) and McBride and Nicholls (1983) have examined both general and specific aspects of circulation changes through correlations between pressure and rainfall distributions.

Only recently have various researchers made exclusive use of satellite-derived data to deduce large-scale patterns in the global distribution of oceanic rainfall rates, total and upper-level cloud decks and radiation balance components (Sadler, 1969; Atkinson and Sadler, 1970: Vol II; Murakami, 1975, 1980 a,b; Rao *et. al.* 1976; Rao and Theon, 1977; Winston *et. al.* 1979; Webster and Stephens, 1980; Heddinghaus and Krueger, 1981; Lyons, 1981; Liebmann and Hartmann, 1982; Barton, 1983). Interestingly, these large-scale patterns show an interannual variability in atmospheric and oceanic features over the Indo-Pacific region which is both spatially and temporally synonymous with the Southern Oscillation. In fact, this evidence has prompted researchers to strive to isolate the mechanism(s) responsible for this teleconnection phenomenon.

Before dealing with the mechanisms directly, it is important to identify the characteristics of this phenomenon. Most early researchers in the field would probably have agreed with Troup's (1965:491) summation that "Walker was therefore considering a standing fluctuation over the Indo-Pacific region, which

need not be at all regular in time" and with the following physical aspects described by Wright (1977:2) :

(1) The strong correlation between SST (sea surface temperature) in the equatorial Pacific and the atmospheric circulation in the Pacific.

(2) The teleconnections (simultaneous positive and negative correlations with atmospheric and oceanic circulation features and weather elsewhere).

(3) The persistence of anomalies for several reasons.

(4) The irregular fluctuations of the feature.

However, works by Trenberth (1976 a,b), Chen (1982 a) and Rasmusson and Carpenter (1982) have indicated that the concept of the Southern Oscillation as a standing fluctuation is not spatially or temporally correct. Rather, the fluctuation displays some important lagged relationships, with surface pressure at stations in the South Pacific leading those in Australasia by up to several months. Nevertheless, it is still useful to examine aspects of the Southern Oscillation as revealed by unlagged data.

The following sets of spectral distributions illustrate some of these features. Figure 2, using 115 years of surface pressure derived Southern Oscillation Indices (SOI's) as formulated by Wright (Lamb, 1977), highlights a peak in the spectral density curve at 46 months or 3.8 years with a lesser peak occurring at 34 months or 2.8 years. However, using the same data but calculating spectral densities over 32 year periods, Figure 3 (Wright, 1977) indicates that the periodicity is not fixed but varies markedly (i.e. it is non-stationary). As Rasmusson and Carpenter (1982:357) indicate, "Spectra of its [i.e. Southern Oscillation's] various components are often quite different from one period to another". A measure of persistence in the 115 year Southern Oscillation sequence can be obtained by comparing the Southern Oscillation spectral density curve with the 'null' continuum of 'white' and/or 'red' noise. In the case of the Southern Oscillation spectral distribution in Figure 2, the 'red' noise significance is more appropriate as a test. The two spectral peaks at 3.8 and 2.8 years are

Figure 2 115 year (1860-1975) power spectrum of Wright's 'old' Southern Oscillation Index (data from Lamb, 1977).

Figure 3 Power Spectra of Wright's 'old' Southern Oscillation Index for the four 32 year intervals; 1851-1882, 1881-1912, 1911-1942, 1941-1972 (from Wright, 1977).

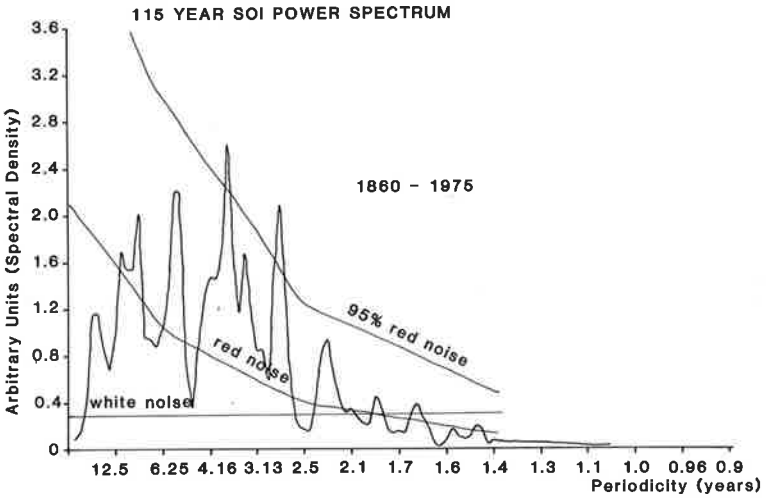
115 YEAR SOI POWER SPECTRUM
Arbitrary Units (Spectral Density)
3.6
3.2
2.8
2.4
2.0
1.6
1.2
0.8
0.4
0
1860 - 1975
95% red noise
red noise
white noise
12.5 6.25 4.16 3.13 2.5 2.1 1.7 1.6 1.4 1.3 1.1 1.0 0.96 0.9
Periodicity (years)

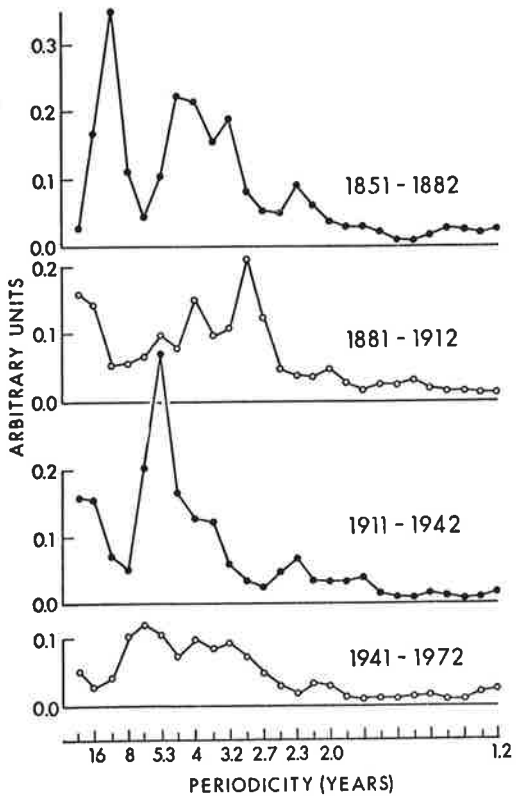
ARBITRARY UNITS
0.3
0.2
0.1
0.0
1851 - 1882
1881 - 1912
1911 - 1942
1941 - 1972
16 8 5.3 4 3.2 2.7 2.3 2.0 1.2
PERIODICITY (YEARS)

both manifestations of Southern Oscillation persistence which is significant at the 95% 'red' noise confidence limit. Thus despite the marked variability of the Southern Oscillation over shorter time periods (Wright, 1977; Van Loon and Madden, 1981; Rasmusson and Carpenter, 1982), the fluctuation generally tends to possess persistence centred around three to six years when using longer-period data.

Until recent times, attempts to evolve a complete and coherent picture of this fluctuation have essentially approached the task via a synthesis of observations and statistics rather than from theoretical and dynamic considerations. As a result, the problem has been one of relating theories to observations.

Using both satellite and conventional terrestrial observations, meteorologists and oceanographers from the Americas have been trying to relate and match an amalgam of atmospheric and oceanic variables with possible mechanisms for the Southern Oscillation phenomenon (most recently in projects such as the Equatorial Pacific Ocean Climate Studies [EPOCS]). The following synopsis provides a brief overview of the major features (namely, Pacific Dry Zone rainfall and the El Niño) and mechanisms thought to be inherent in the phenomenon.

Julian and Chervin (1978) suggested that early works on precipitation and trade wind variability in the equatorial Pacific Ocean were vital in developing the concept of the Southern Oscillation. Such research led to the identification of an area that, although usually experiencing poor rainfall, was occasionally subject to major periods of above average falls. Termed the Pacific Dry Zone (PDZ), it is, according to Quinn and Burt (1970:25), :

> ...a rather extensive feature of the middle and lower latitude eastern South Pacific which slims down to a narrow tongue as it extends westward through the central equatorial Pacific into the western equatorial Pacific.

According to Donguy and Henin (1980), the rainfall pattern in the western Pacific is out of phase between the equatorial region (10°N-10°S;

160°E-130°W) and the subtropics in both hemispheres. The above factors, together with subsequently deduced sea surface temperature (SST) anomalies, provided direct physical evidence for the operation of the Southern Oscillation.

One particular oceanic phenomenon, which has been observed by Peruvian mariners for at least 200 years, is the 'El Niño' current off the coast of South America. Although this term was originally used to designate a regular local warm current (Wyrtki, 1975), it has now come to define more irregular periods when anomalously warm water appears and normal upwelling patterns along the coast are disrupted (Patzert *et. al.* 1978). Furthermore, it has taken on large-scale proportions as it is suspected of being an indirect consequence of Southern Oscillation variability. Hastenrath and Kaczmarczyk (1981) have found a correlation of + 0.42 between sea level pressure in the northern Australian region and sea surface temperature off Ecuador and Peru, with strongest phase relationships in the 3-6 and 17-21 year bands. As Zuta *et. al.* (1980:11) note, "...it [El Niño] involves a transitory irregularity in the ocean-atmosphere system". Rasmusson and Carpenter (1982:354) also suggest that "These warm episodes exhibit a wide spectrum of amplitudes, as well as variations in character and timing", while Caviedes (1973:46) notes that the "...meteorological *El Nino* phenomenon requires the concurrence of oceanographic and climatological factors, which may begin to develop a few years before the event itself....".

Although the amount of recent research on the El Niño is immense and involves the joint input of many meteorologists and oceanographers, these investigations have yet to provide a complete scenario of the ocean-atmosphere interactions involved. One particular missing link is the cause of the weakening of the South Pacific anticyclone. Despite this, particular attention has now been drawn to the ecological and social implications of this feature since the most recent and severe El Niño of 1972-73 caused the Peruvian anchovy industry to all but collapse.

Developments in the search for a complete understanding of the mechanisms of the Southern Oscillation teleconnection owe much to the work of Jacob Bjerknes. As a consequence of his work on ocean-atmosphere coupling mechanisms, Bjerknes (1969) coined a new term for what he saw as a thermally direct circulation that was an integral component of the Southern Oscillation. Like Walker's original concept of the Southern Oscillation, this 'Walker Circulation' developed in a near-zonal direction, but according to Bjerknes (1969:169), responded directly to SST anomalies between the eastern and western hemispheres :

> What distinguishes the Walker Circulation from other tropical east-west exchanges of air is that it operates a large tapping of potential energy by combining the large-scale rise of warm-moist and descent of colder dry air.

Since then, the Walker Circulation has been increasingly suspected of being the phenomenon linking the Pacific region to the Asian foci of the monsoon system (Krueger and Winston, 1975). As Philander (1983:295) points out :

> The westward tradewinds that prevail over most of the tropical Pacific Ocean converge on the North Australian-Indonesian Low Pressure Zone where the air rises and where there is considerable cloudiness and rainfall. The air returns eastwards at greater altitudes and sinks over the cold, dry South-east Pacific High Pressure Zone ... This zonal cell is known as the Walker Circulation.

Although Bjerknes may have identified important components of the Walker Circulation, his conjecture that large-scale SST gradients provide the prime driving mechanism for this circulation has not gone unquestioned. From heat budget analysis, Cornejo-Garrido and Stone (1977:1155) suggested that the driving force for the Walker Circulation was condensational heating via moisture convergence :

> The primary drive for the circulation is the heating due to zonal variations in condensation ... sea surface temperature gradients only play a secondary role in forcing the Walker circulation.

Further support is found in Webster's (1972, 1973 a,b) numerical analyses of tropical atmospheric responses to large-scale forcing mechanisms.

Webster (1973 b :815) states :

> Specifically, then, it appears that the correlations of Walker and others are no more than variations in the magnitude of the response of the ultralong slow-moving waves of low latitudes ... and Walker's correlations may [be] considered to be further deviations (e.g., stronger heating or cooling) superimposed upon ... regular seasonal anomalies.

The above discussion would suggest that complex ocean-atmosphere interactions and feedbacks are hallmarks of Southern Oscillation/Walker Circulation/El Niño sequences. In essence, as Bjerknes observed, these sequences embody responses of the ocean to wind anomalies and of the atmosphere to SST anomalies. Nevertheless, such air-sea relationships are modulated spatially and temporally to the extent that the latitudinal and longitudinal location and the seasonal timing of events can be critical to the outcome of the interaction. This is further compounded by the observation that localized effects need not necessarily produce localized responses. Thus it is suggested that the Walker Circulation " ...is supplied by horizontal convergence of moisture from distant regions of excess surface evaporation" (Cornejo-Garrido and Stone, 1977:1162) rather than by " ...local evaporation associated with warm sea surface temperature" (Geisler, 1981:1390). Yet, most researchers are still uncertain of the intricacies of the prime forcings in the ocean-atmosphere system of complex feedbacks and responses. In fact, the intrinsic nature of this system probably makes such dissection difficult or any results meaningless.

Recent attempts to unravel this puzzle have concentrated on the use of numerical models with variable parameter inputs and connections. Numerous ocean-atmosphere models have been used to investigate this component of large-scale monsoon processes (e.g. Manabe *et. al.*, 1974; Bryan *et. al.*, 1975; Manabe *et. al.*, 1975; Webster and Lau, 1977, 1978; Julian and Chervin, 1978; Lau, 1978, 1981; Wells, 1979; Washington and Chervin, 1980). More specific works have looked at air-sea interactions across the tropical regime (Pike, 1971; Rowntree, 1972, 1976; McWilliams and Gent, 1978; Lau, 1979), in the

Australian region (Nicholls, 1978, 1979 a) or in regards to the Southern Oscillation/El Niño phenomenon itself (Hurlbert *et. al.*, 1976; McCreary, 1976; Barnett, 1977 a,b, 1981; Wright, 1979 b; Geisler, 1981; Philander, 1981; Keshavamurty, 1982; Zebiak, 1982).

However, one of the major problems in this area of modelling is that ocean-atmosphere models are unable to simulate the total interaction between the atmosphere and the ocean. As Julian and Chervin (1978:1433) state, " ...a fully coupled atmosphere-ocean model is presently impractical...." A complete testing of the various interaction theories is therefore still not possible. Resolution of this problem is crucial to the validity of models attempting to simulate mechanisms responsible for long-term climatic changes (e.g. Williams *et. al.*, 1974; Gates, 1976 a,b; Manabe and Hahn, 1977; Williams, 1978; Kutzbach, 1981; Kutzbach and Otto-Bliesner, 1982).

It should be noted that there is still much contention and confusion about terms such as Walker Circulation and Southern Oscillation. Some texts use these terms interchangeably. However, a more prevalent source of ambiguity stems from varying conceptions of the spatial extent of these two features. For example, some researchers relate them specifically to events in the Indo-Pacific region, as Julian and Chervin (1978:1433) suggest :

> The Southern Oscillation - an oscillatory exchange of atmospheric mass between the eastern south Pacific and Indonesia - and the Walker Circulation - its counterpart in wind circulation - have a time-scale of years and are manifestations of a near-global variation in circulation, clouds and precipitation, centered in the equatorial eastern Pacific.

Others assume a global scale, as evidenced by Wright's (1977:1; 1978:184) comments :

> It is increasingly recognized that the phenomenon [Southern Oscillation] is global in scale, and that a knowledge of its global effects may be a prerequisite to a thorough understanding of the mechanisms.
>
> The Walker Circulation may be more accurately regarded not as a simple cell, but as a complex set of vertical motions involving the whole equatorial zone.

In contrast, Bjerknes (1969:169) combines both scales in his definition :

> Whereas the Walker Circulation maintains east-west exchange of air covering a little over an earth quadrant of the equatorial belt from South America to the west Pacific, the concept of the Southern Oscillation refers to the barometrically recorded exchange of mass along the complete circumference of the globe in tropical latitudes.

Compounding this matter still further, the term 'east-west' circulations has been suggested by Krishnamurti (1971 a) to denote the pattern of near-global, zonal thermal overturnings. The Walker Circulation is then seen as " ...merely the southern extension of a much more vigorous east-west circulation ...." (Krishnamurti, 1971 a :1342).

In this study I will use the term Southern Oscillation/Walker Circulation (SO/WC) to describe the teleconnection overturning linking the Asian monsoon focus to the eastern South Pacific. The Southern Oscillation aspect refers to the mass contrast and the Walker Circulation to the vertical circulation in the troposphere.

During the past decade, broad-scale tropical analyses have been increasingly concerned with investigating links between the planetary-scale monsoon system and the pattern, structure, extent, and sources and sinks of global tele-connections. Such relationships have been demonstrated by Bjerknes (1966, 1969, 1972), examined in papers such as Flöhn (1973) and Flöhn and Fleer (1975) and investigated on a seasonal basis by Krishnamurti (1971 a), Krishnamurti *et. al.* (1973), Kanamitsu and Krishnamurti (1978) and Lighthill and Pearce (1981). As a result, teleconnections have been identified with the interacting zonal and meridional exchanges that serve the total atmospheric process linking tropical, subtropical and perhaps extratropical regions. As Krishnamurti (1971 a :1347) suggests, the total South East Asian/Indian monsoon complex is a major source of Hadley, Walker and east-west Circulations :

> The observational evidence of mass "spill-over" from the region of the southwest monsoons ... in both zonal and meridional directions suggests that the southwest monsoons are an intense energy source for the tropical latitudes.

Within the tropical latitudes, three major near-equatorial source regions or foci for these teleconnections have been identified. These are associated with the convective maxima over South America, Africa and South East Asia/'Malesia' (Barry, 1978). The two latter centres are important foci within the planetary monsoon system.

Both Krishnamurti *et. al.* (1973) and Murakami and Unninayar (1977) have shown that the most active region for divergent mass outflow, at 200 mb during the Southern Hemisphere summer, is located in the vicinity of the convective region of low latitude South East Asia. The importance of this maxima, and its Southern Hemisphere winter counterpart, is stressed in Webster *et. al.* (1977:1467) :

> So extensive are the summer and winter maxima that the mean divergent motions emerging from them are of planetary scale. This allows one to construe that the convective regions associated with both the summer and winter monsoons must be dominant over most phenomena in the tropics and perhaps even at higher latitudes.

In the last 10-15 years, important monsoon research has been made possible by the World Meteorological Organisation (WMO) through projects such as the Global Atmospheric Research Programme (GARP) - its history is reviewed in Ashford (1982) - and its sub-programmes GARP Atlantic Tropical Experiment (GATE), Continental Africa Project (CAP), Air Mass Transformation Experiment (AMTEX), Monsoon - 77, Indo-Soviet Monsoon Experiment (ISMEX - 73), West African Monsoon Experiment (WAMEX) and Monsoon Experiment (MONEX). Many of these projects have been directly responsible for increased concern with large-scale dynamics of monsoon systems and have indicated the need for more surface and upper air data recording stations across the tropics. As well as long-range teleconnection research, renewed interest and new developments have occurred in the areas of atmospheric heat and energy balances and interhemispherical interactions.

In the Asian sector there is now more evidence from Cheang (1977 a,b) and Murakami (1977 a,b) of possible interhemispherical/cross-equatorial flows

and periodic surges into the Australian region in summer. The converse has been suggested for the Australian winter (Webster, 1981 a), when surges are directed into the Northern Hemisphere during the southwest monsoon. Nicholls (1977) postulated rapid, simple forcing mechanisms (via latent heat release) governing tropical and subtropical interactions across Australia. Krueger and Winston (1974, 1975) compared cloudiness/convective maxima for two seasonal extremes of the Walker Circulation. Using preliminary winter MONEX data, Webster and Stephens (1980) have analysed the tropical radiation balance of upper- and middle-level tropospheric-extended clouds originating in the Asian convective region. Murakami (1975) looked extensively at cloudiness changes on an annual basis without deriving many conclusive explanations for correlations that seemed to support teleconnection variations. However, his two-part investigation (Murakami, 1980 a,b) of 4-6 day and 15-30 day oscillations in Outgoing Longwave Radiation (OLR) was more encouraging with firm suggestions and support for cross-equatorial surges and interseasonal monsoon variability at both frequency ranges. Lyons (1981) extended this analysis to include 200 mb vorticity (VOR) and investigated non-stationary OLR and VOR patterns on intraseasonal time scales.

Some studies now point to links, at a similar longitude, between the Hadley Circulation and subtropical jetstream maxima in the winter hemisphere, where a sinking arm of this cell is located. It is also suggested that a similar, but weaker, interaction occurs in the summer hemisphere (Murakami and Unninayar, 1977; Seymour, 1981; Webster, 1981 a). The most recent works of Chang *et. al.* (1979) and Chang and Lau (1980) have investigated the phenomenon in finer detail for the Northern Hemisphere winter, and have found that the process may be more complicated for time scales of several days. The study of Murakami and Unninayar (1978) is particularly interesting in that it details possible interactions between regional cloudiness and convective activity over the maritime continent and large-scale circulation and teleconnection changes. Paegle *et. al.* (1979), Yi-hui and Reiter (1981) and Keen (1982) suggest that individual monsoon foci and even synoptic scale

disturbances in the summer hemisphere and near-equatorial latitudes can affect the planetary-scale teleconnection fields.

One of the most intriguing and challenging aspects of these studies concerns the forcings and feedback mechanisms behind the atmospheric teleconnections. Not only is there contention regarding the ocean-atmosphere system but also, disagreement exists as to the direction of the forcings. Much is yet to be resolved between the two basic schools of thought, which either see the tropics as the instigating zone or regard the midlatitudes as the initial forcing domain.

Yet, once again, the present state of numerical models limits the investigations of this dilemma. In fact, much of the polarity that exists can probably be traced back to the very inabilities and limitations of the mathematical theories and basic equations used by both schools. Pittock (1974:720) is perhaps closer to the truth :

> It is perhaps worth adding that arguments, such as, whether the Hadley circulation is primarily driven by tropical air/sea interactions (Bjerknes, 1966, 1969; Rowntree, 1972) or by influences extending from middle latitudes (e.g., Namias, 1972 and Ramage, 1971) may well lose their importance if "forcing functions" and "feedback processes" at and between latitude belts are incorporated into such a model.

This is verified by the more recent numerical studies of Gill (1980), Webster (1978, 1981 b, 1982), Geisler (1981), Lau (1981), Lau and Lim (1982), Sasamori (1982) and Webster and Holton (1982). They suggest that the Walker Circulation, in the form of forced stationary waves (Kelvin and Rossby) generated by the semi-permanent heat and convective sources, is equatorially trapped by longitudinally varying 'critical latitudes' through which even midlatitude Rossby waves cannot generally pass. However, where the above sources may be partially in the subtropical westerlies or where a westerly wind 'duct' occurs in equatorial regions, it is possible for equatorial to midlatitude, midlatitude to equatorial (both hemispheres), or midlatitude to midlatitude responses to occur respectively.

A complete numerical approach should aim to verify and test the current understanding of monsoon processes in the integrated ocean-atmosphere system. So far, "Despite the successful atmospheric modelling of tropical SST anomalies, a complete theory of the Southern Oscillation has not been forthcoming" (Wells, 1982:163). Until this is possible, the present understanding of monsoon structure and processes will be much as Webster *et. al.* (1977:1463) note :

> ...the principal time scale variation or phasing of the *interseasonal* transition is determined by the different response times of the oceans and land areas to variable solar heating. The reaction of the ocean is a strong function of latitude because of its ability to be heated by solar radiation and mixed mechanically by the atmosphere. The return heating distribution imposed on the atmosphere by the ocean strongly affects the circulation. The inclusion of a hydrology cycle adds a further time scale to the monsoon system allowing much more rapid variations to be superimposed on the modulations caused by radiative and sensible heating effects. The inclusion of clouds introduces a further *intra-seasonal* time-scale into the monsoon circulation causing 'break-like' variations of the precipitation pattern and circulation fields during the late summer.

1.2 THE SOUTHERN HEMISPHERE SUMMER MONSOON OF AUSTRALASIA

1.2.1 Historical Background

Some of the earliest research in Australian meteorology which analysed the nature and patterns of the summer monsoon were those of Hunt *et. al.* (1913), Quayle (1918) and Taylor (1918, 1920). These authors developed hypotheses concerning Australian summer rainfall and monsoonal incursions into the continental heat lows of northern Australia. They regarded any depression of tropical origin as monsoonal. Lacking any detailed upper air data, they speculated that Australian summer monsoon flow was of unsteady nature, that two main centres of low surface pressure and high temperature formed from continental heating in summer and that the broad, lower pressure region surrounding them could initiate indraughts from tropical latitudes.

Taylor (1920) devised a concept of 'convection domes' located above the surface heat low pressure centres that develop near Pilbarra (Western Australia) and Cloncurry (Queensland). Although this idea may now seem unrealistic, such works have provided the basis for most monsoon studies in this continent. Climatologically, Hunt *et. al.* (1913) produced one of the earliest attempts to locate monsoon influence within the broad pattern of Australian climatic zones. Apart from some general considerations after World War II (e.g. Fletcher, 1945; Garbell, 1947; Glenn, 1947) major revisions of Australian monsoon climatology have only recently been put forward by Gentilli (1971, 1977), McBoyle (1971) and Boucher (1975).

Since Berson (1961), Berson and Troup (1961), Troup (1961) and Vis (1966) examined aspects of Australian monsoon meteorology, tropical atmospheric circulation and energetics concepts have not, as yet, been evaluated fully during Australian summer monsoon seasons. The majority of Australian tropical meteorological/climatological research has been concerned primarily with case studies of major synoptic-scale features (Newman *et. al.*, 1956; Forecasting Section, 1959 a,b, 1961; Newman and Bath, 1959; Whittingham, 1960; Staff of Divisional Office, 1961, 1962 a,b,c, 1965; Staffs of Regional Offices, 1966, 1968 a,b, 1969, 1970, 1971, 1973 a,b, 1975; Southern, 1964; Falls, 1970; Southern *et. al.*, 1970) or their destructive effects (Bureau of Meteorology Reports, Technical Notes and Meteorological Summaries; Oliver, 1974, 1975, 1980; Lourensz, 1977, 1981; various papers in Heathcote and Thom, 1979; Pickup, 1979). A few studies have dealt with the summer monsoon as part of the general seasonal circulation and rainfall variations over the Australian continent (Gentilli, 1971, 1972, 1977; Wittwer, 1971, 1973; Boucher, 1975; Linacre and Hobbs, 1977). Only recently has the Tropical Meteorology Programme of the Commonwealth Scientific and Industrial Research Organisation (CSIRO) Division of Atmospheric Physics and the Australian Numerical Meteorology Research Centre (ANMRC) begun analysing the data collected during the winter phases of MONEX (WMONEX) from 1st December 1978 to 5th March 1979 (Webster, 1981; personal communication).

Research conducted in New Guinea has been even slower, with monsoon climatology occasionally included in the reports and papers of some Australian Government bodies such as the Bureau of Meteorology and the CSIRO (Commonwealth Year Books, until 1974, and/or Bureau of Meteorology publications 'Climate of Australia and Papua New Guinea'; Brookfield and Hart, 1966; McAlpine, Keig and Short, 1975; McAlpine, Keig and Falls, in press). Increasing meteorological interest in this large island is found in the monsoon studies of Ramage (1968, 1971), Nicholls (1973), Staff Members (1972), Musk (1976) and Barry (1978). This interest dates from the inclusion of New Guinea in the 'maritime continent', a region encompassing Indonesia and the Carolines (Ramage, (1968) and, more recently, in the archipelago of Malesia (Barry, 1978). These works point to the New Guinean region as often being located in, or near, a rainfall transitional zone between South East Asia and the western Pacific.

However, most world attention has focused on Northern Hemisphere monsoon features and patterns within the wider regional framework of the islands and surrounding seas of low latitude South East Asia. Monsoon meteorological/climatological analyses in these regions are summarized in many recent texts such as Nieuwolt (1968, 1977), Arakawa (1969), Ramage (1971), Yoshino (1971), Newton (1972), Lockwood (1974) and Barry and Chorley (1976). These works reflect the fact that only in the last 10-15 years has much of the early research, conducted by British, Dutch and German colonial workers, undergone revision. Although many meteorological studies have discussed meso- and synoptic-scale phenomena (e.g. Mangunredjo, 1964; Ramage, 1964; Sutrisno, 1964; Lim, 1976; Cheang, 1977 a,b; Houze *et. al.*, 1981), the integration of such works into an understanding of aspects of the Southern Hemisphere summer (northeast) monsoon system over South East Asia is also more complete than is the case in the Australian sector (e.g. Ramage, 1968; Murakami, 1977 a,b, 1980 a,b; Barry, 1978; Chang *et. al.*, 1979; Chang and Lau, 1980; Webster and

Stephens, 1980; Johnson and Priegnitz, 1981). In fact, even since the WMONEX period, works such as Murakami and Sumi (1981) and Sumi and Murakami (1981) note problems in developing their findings in the maritime continent region because of a lack of detailed information on the Australian monsoon.

1.2.2 Mean Circulation Conditions

Two questions that have often been asked, but seldom answered, are what type of monsoon does Australia experience and what area of the continent is monsoonal? The answers to such questions seem to rest on one's definition of the term monsoon. The most recent definitions (see Section 1.1.1) seem to suggest that Australia is on the periphery of the planetary monsoon system. Thus it is useful to examine briefly some of the recent concepts concerning the Australian monsoon.

As suggested previously, little specifically climatological analysis of the Australian monsoon has been carried out. Of the recent research undertaken, the most often quoted distribution of monsoonal influence in northern Australia is that derived from Gentilli (1972). Essentially, Gentilli's postulated distribution (Fig.4) indicates that, on average, only a small portion of the northern coast, including the 'top end', Cape York and a strip of the 'gulf country' experiences true monsoonal conditions. Other areas, such as the 'Kimberley Coast' of Western Australia and the northeastern coast of Queensland, are influenced by either 'pseudo' or 'quasi' monsoonal patterns. Similar forms of these patterns appear in Van Loon *et. al.* (1972) and Boucher (1975).

However, given that northern Australia lies in a peripheral region of the planetary monsoon system, the average patterns of Gentilli have only broad climatological validity. They do not reflect the variability of monsoon distribution. Since the research of Berson (1961), Hutchings (1961) and Troup (1961) suggests that eddy terms are significant over

Figure 4 Climatological classification of mean wind regimes over Australia in January (from Gentilli, 1972).

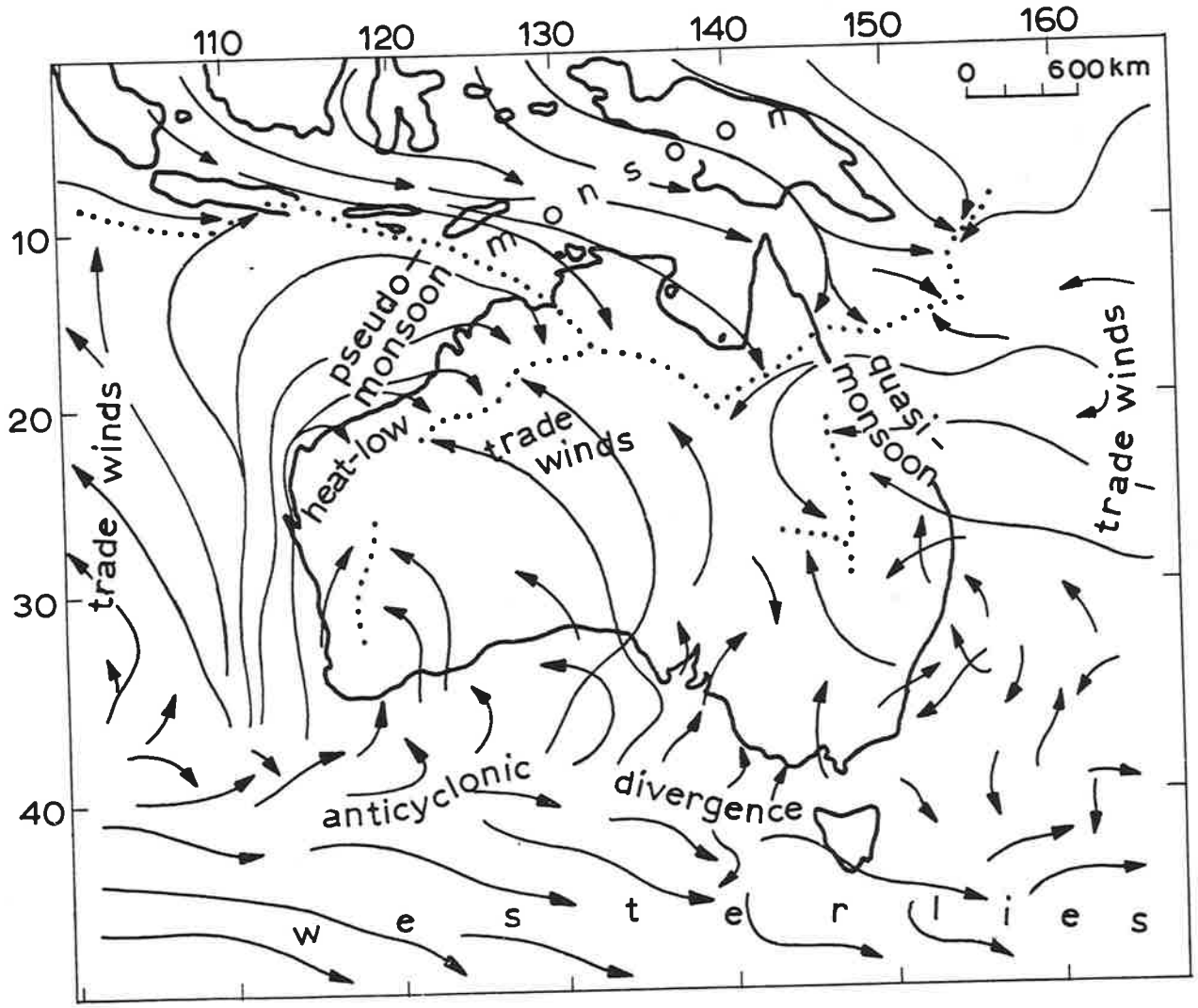
110
120
130
140
150
160
0 600km
10
20
30
40
monsoon
pseudo monsoon
heat-low
trade winds
trade winds
quasi-monsoon
trade winds
anticyclonic
divergence
westerlies

Australia during monsoon seasons, it would seem that any comprehensive definition of monsoonal and non-monsoonal regions must attempt to take such factors into account.

It is probably more useful to view the Australian monsoon as a very variable phenomenon. This variability can been seen in the extremes of monsoon seasons that have been documented, whether from general records, rainfall distributions or atmospheric circulation patterns. Thus although the concept of long period, mean monsoonal patterns cannot be denied as a starting point and an initial descriptive aid, it must been seen to represent time-average conditions that prevail in the context of often dominant and very variable interannual, intraseasonal and eddy fluctuations.

Mean conditions may be illustrated by atmospheric circulation patterns, as shown in Figure 5, derived from Taljaard *et. al.* (1969). These diagrams illustrate the January mean surface pressure field and geopotential fields at the 850, 700 and 200 mb levels over the Australasian section of the Southern Hemisphere. It is evident that several circulation features are prominent during Southern Hemisphere summers. The low pressure cell over northern Australia, between the surface and 850 mb levels, consists of a quasi-permanent heat low complex which is thermally induced in the summer months when insolation is high and the continental interior is dry and relatively cloud free. At approximately 700 mb, this heat low complex is usually capped by a temperature inversion and higher pressure predominates up to the 200 mb level. Any semblance of low pressure in the Australian region at 700 mb is located further north, extending from the Indonesian seas to the Gulf of Carpentaria. Although it is not evident in Figure 5, the low-level, low pressure pattern is often synonymous with the near-equatorial or monsoon trough in the Australian sector of the Southern Hemisphere. Thus the continental heat low appears to act as an anchoring mechanism for the near-equatorial trough in this sector of the Southern Hemisphere and aids in drawing in moist, onshore flow across the northern coasts.

Figure 5 January mean surface pressure and geopotential fields at 850, 700 and 200 mb levels over the Australasian segment of the Southern Hemisphere. Geopotential heights are in decametres (from Taljaard *et. al.*, 1969).

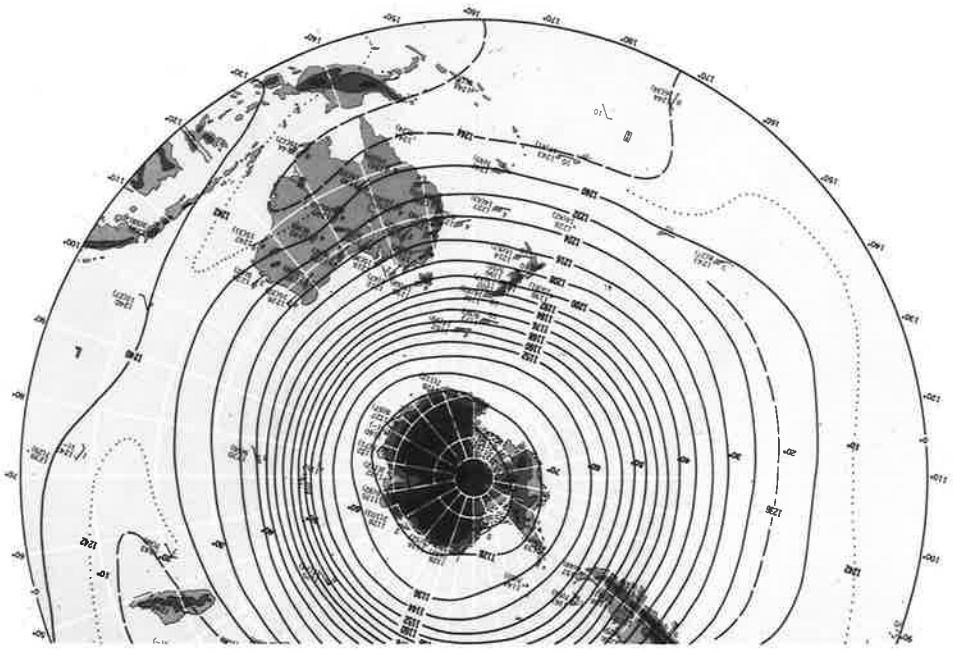

200 mb

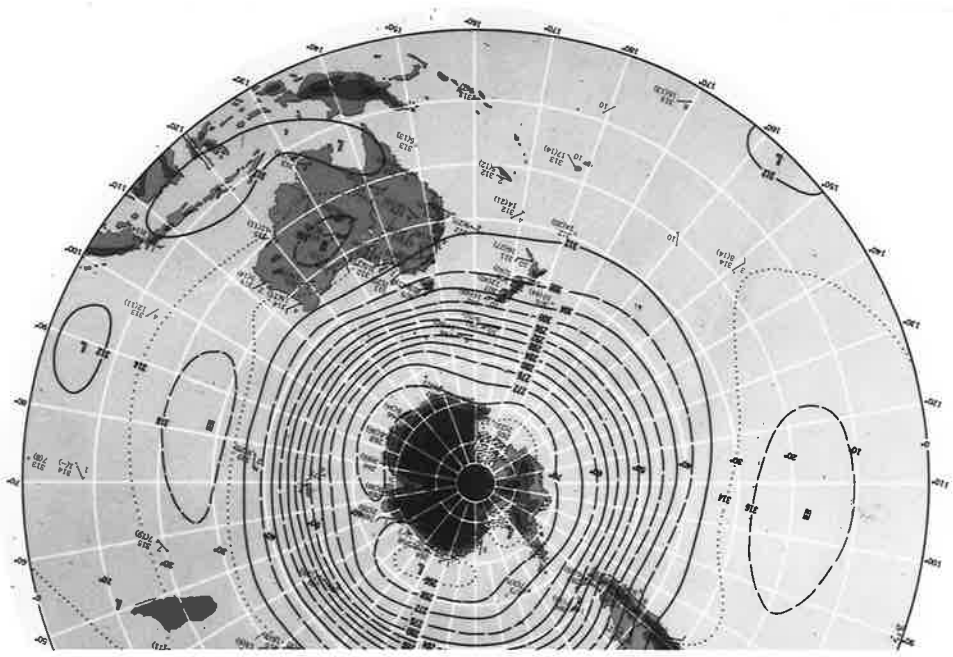

700 mb

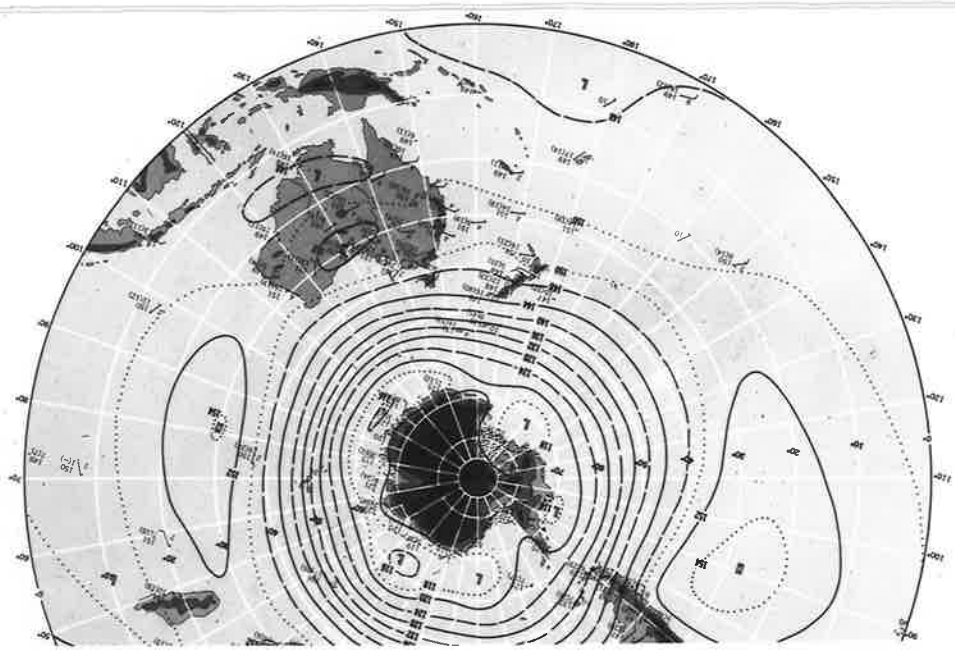

800 mb

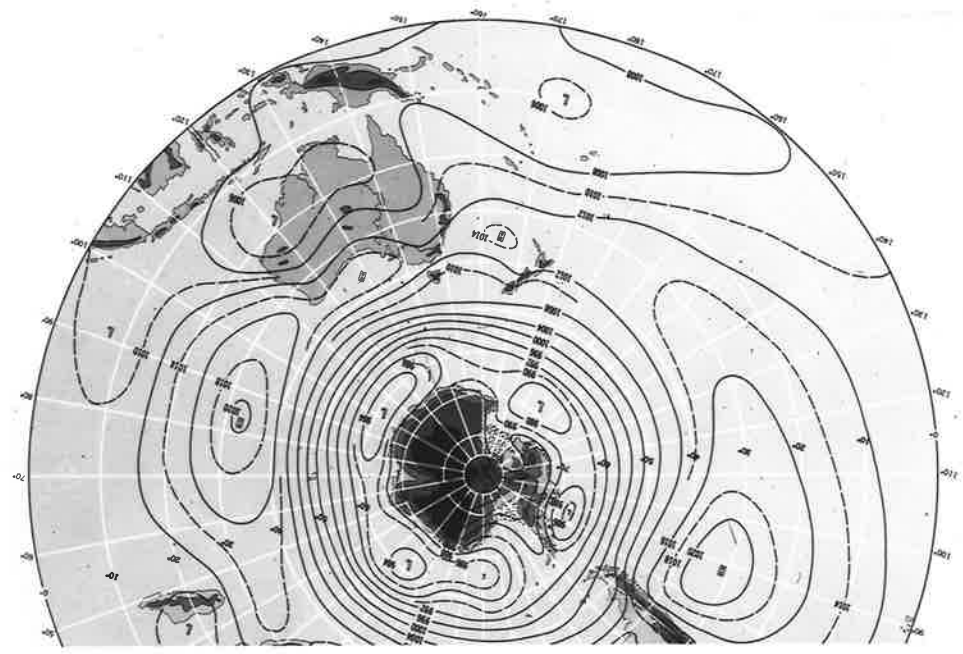

Sfc

To the west and east of the continent, high pressure predominates up to the 700 mb level over the midlatitude Pacific and Indian Oceans. However, at the 200 mb level near the top of the troposphere, higher pressures are found over the continental masses of northern Australia, southern Africa and South America (last not visible in Fig.5). Such a pattern is a direct response to the earth's rotation and the varying heat capacity of land and sea during the Southern Hemisphere summer. It would seem that these anticyclonic regions are analogous with areas of large-scale subsidence, and that local circulations (e.g. heat lows) " ...are of the thermally indirect type, driven, not by local heating contrasts, but by a continual input of kinetic energy from other regions ...." (Wallace and Hobbs, 1977:430).

However, the above considerations do not illustrate the monsoon's influence on the continent's hydrological regime. Australian summer rainfall records throughout this century and earlier suggest that monsoonal incursions into the continent may be as important rainfall instigators as tropical cyclones and related disturbances. In fact, it would seem that such incursions are responsible for prolonged and extensive 'wet spells' that penetrate deep into the 'normally' dry interior.

1.2.3 Monsoonal Extremes and Moisture Characteristics

Atmospheric moisture processes are one of the most important factors influencing the magnitude and transfer of energy in the planetary monsoon system. As Webster (1981 c :75-76) notes :

> Hence one effect of moist processes in the atmosphere is to increase the strength of the monsoon circulation. Without moist processes the circulation would still exist, but it would be weaker.

Although the amount and spatial extent of precipitation induced by monsoonal and other summer convective activity is available in the climatological statistics of 'wet' and 'dry' periods in Australian summers,

few diagnostic studies have focused on the moist processes involved. As a result, little is known about the variability and role that large-scale moisture characteristics play in the dynamics of this monsoon region. Compared with the more specific analyses of moisture fluxes and budgets in the Indian and West African monsoon regimes, most references to the Australasian sector are found in broad, global studies such as Kidson *et. al.* (1969), Taljaard *et. al.* (1969), Newell *et. al.* (1972, 1974) and Van Loon *et. al.* (1972). In fact, apart from the broad moisture and energy budget research of Berson (1961) and Hutchings (1961), this subject has been seriously neglected. More surprisingly, there has been no concise examination of the variability of moisture characteristics over a number of monsoon seasons or months.

The key to understanding many of the mechanisms underlying features of the Australasian monsoon regime may be found in an analysis of moist processes. It is still not clear whether marked variability in the low-level depth and extent of moisture characteristics and/or convective mechanisms accompanies periods of monsoonal extremes in Australasia. Further, there is no certainty about the relative contributions of mean advective and transient eddy moisture terms in a monsoon regime that is strongly influenced by eddy fluctuations in both heat budget (Berson, 1961) and wind circulation regimes (Troup, 1961). It would also seem that moist processes are a vital element in 'break-like' periods during monsoon seasons and may, in turn, be related to a dichotomy between the Australian heat low complex and the Near Equatorial Trough in the Southern Hemisphere (NET_{SH}) (Webster, 1981 c). This situation is compounded by the absence of systematic studies of the nature and dynamics of the two quasi-permanent heat lows. Only recently have attempts been made (Leslie, 1980; Skinner and Leslie, 1982) to numerically model these features. However, data distributions are at present inadequate to resolve fully the heat low phenomenon.

The variable character of the Australian summer monsoon appears to be

expressed, in one sense, by major incursions of the NET_{SH} into the Australian continent. On such occasions one might expect widespread changes in both convective mechanisms and moisture characteristics. Yet, in the majority of seasons, the monsoon is characterized by less defined atmospheric circulations. This situation again highlights the need to investigate fully the finer points of moisture and dynamic effects. However, such investigations should focus also on the relief of northern Australia which provides orographic lifting of moist, onshore flow. In summer, at least some parts of the northern coasts receive moist flow which is directed onshore by either trade wind, cyclonic or anticyclonic circulations. Together with eddy fluctuations (i.e. tropical cyclones and rain depressions) and steady-state conditions, these constitute the bulk of summer rainfall producing mechanisms.

An important consideration that may influence monsoonal extremes is the time of onset of the monsoon. Much of the wind criteria used by Troup (1961) to evaluate dates of onset have been re-examined in conjunction with satellite mosaics by Davidson *et. al.* (1981). The latter work suggests that the monsoon onset is triggered by midlatitude events in the Southern Hemisphere. Certainly the abrupt changes in upper-level flow which lead to strong easterlies in the tropics and a southward displacement of the subtropical jetstream in Australian longitudes, noted by Troup (1961), are evident in the above work.

Another circumstance which warrants further study is the possibility that more steady-state circulation and convective rainfall conditions occur during strong monsoonal periods. It has often been implied that the 'true' monsoon in northern Australia is only manifest during periods of intermittent, cross-equatorial flow or surges from South East Asia (Gentilli, 1972). This has not yet been established; nor has the question been answered as to whether there is increased depth and extent of flow or influence on moisture characteristics during such times.

1.2.4 Long Term Variability

One particularly intriguing aspect of the Australasian monsoon regime is whether it has undergone any marked changes during historical or prehistorical times. To investigate some of these possibilities it is useful to examine briefly the background and current theories of climatic variability.

Recent interest in world-wide climatic variability has primarily resulted from increasing scientific and public concern about the influence of climatic extremes on man-environment systems (Lamb, 1979, 1981). The scope for scientific interests has basically been dictated by the type of evidence available and the technical skills of the researchers involved. Indeed, specialization has seen the growth of expertise in many areas and periods of climatic history. However, efforts have increasingly been made to provide fruitful discourse and engender more multi-disciplinary co-operation among specialists (e.g. conferences and projects such as Climate and Climatic Change (Melbourne) - 1975; CLIMAP - 1976; Climate and History (Norwich) - 1979; World Climate Conference (Geneva) - 1979; CLIMANZ (Howmans Gap, Australia) - 1981).

A similar multi-disciplinary approach to the study of climatic history appears likely to evolve within Australasian monsoonal research. In the first instance, marked variability in monsoonal conditions and related disturbances has occurred in the last decade with often spectacular physical results (e.g. 1974 Lake Eyre floods and Cyclone 'Tracy' in Darwin). However, at this stage, the general lack of expertise in this area has thwarted any major contribution to long-term climatic histories. This is particularly evident in the field of Australian palaeoclimatology, which has been largely left to researchers with a background in the solid earth sciences or the natural sciences (e.g. Williams, 1975; Bowler *et. al.*, 1976; Rognon and Williams, 1977; Henderson and Stephenson, 1980). Such a situation is to be expected, given that extensive evidence for past climatic regimes

comes from geological, faunal and floral material. Yet, there are now some recent studies to suggest that this need no longer be the case (e.g. Gentilli, 1961; Webster and Streten, 1972, 1978; Pittock *et. al.*, 1978; Wyroll, 1979).

One phenomenon which is being increasingly re-emphasized in conjunction with Australasian monsoon studies is the Southern Oscillation. As the physical processes underlying this fluctuation become better understood, the value of its temporal record to historical climate studies in Australia will increase markedly. Already this record has been related to rainfall 'outbreaks' in the Pacific Dry Zone (PDZ) (Quinn and Burt, 1970; Quinn, 1974; Reiter, 1978, 1979) and considered in regard to the El Niño phenomenon over periods of 100 years and more (Quinn *et. al.*, 1978). Since the calculation of Southern Oscillation Indices (SOIs) usually relies on surface pressure observations (from at least one Indian Ocean/Australasian or one Pacific Ocean station as a bare minimum), temporal record lengths of the above order are quite feasible. This is particularly true of sequences which can be supplemented by general historical material (especially primary sources such as diaries, accounts, journals, newspaper articles, etc.) and concurrent meteorological/climatological records (i.e. rainfall, wind and temperature observations).

In the Australasian context, historical Southern Oscillation trends have yet to be examined thoroughly. Furthermore, the nature of their influence on current climatic patterns or their applicability as potential forecasting tools has been uncertain (Quayle, 1929; Rimmer and Hossack, 1939; Priestley, 1962; Angell, 1981; Nicholls *et. al.*, 1982; McBride and Nicholls, 1983). Consequently, there has been little or no research to date that has resolved the possible implications of Southern Oscillation and monsoonal variability for Quaternary climatic histories in the Australian setting (Pittock *et. al.*, 1978). In fact, palaeo-researchers are continually faced with the daunting task of analysing an often confusing

array of climatic change hypotheses over which even specialist climatologists/meteorologists and related experts disagree. As Hecht and Imbrie (1979:2) state :

> In many ways our understanding of climate is at a developmental point similar to the prerevolutionary stage experienced by physics, biology and geology ... this phase is ... characterized by an absence of a comprehensive theory or paradigm that helps unify the research.

Thus much of the climatic reconstruction of historical and Quaternary periods must be viewed with care and, at times, scepticism.

It is important at this stage to provide some review of the current state of climatic change theories. Probably the most basic theoretical division is that based on the hypothesized source of the forcings. In this regard, three major categories, based on external, internal or mixed criteria, are evident. External processes are those which are seen to develop external to the atmosphere-ocean-ice system; that is, forcings originating from terrestrial sources (e.g. earth orbit/rotation perturbations, volcanic activity, continental distributions and man-made activity) and extra-terrestrial sources (e.g. meteorite or comet passages or hits, solar output variability, planetary influence from within the solar system and cosmic dust clouds). Such phenomena can influence the atmosphere but are not necessarily, in turn, influenced by the atmosphere.

It is essentially from an external theory of climatic change that many of the pessimistic and dire forecasts for climatic conditions in the immediate future are derived. This trend has come about following the vast accumulation of climatic statistics over the last 10-15 years. It has led to claims of increased climatic variability in marginal zones, a steady decrease in annual average surface air temperature in the Northern Hemisphere (Mitchell, 1961; Paltridge and Woodruff, 1981) and increased man-made and volcanic-induced dustiness and pollution of the atmosphere (Bryson, 1968, 1973, 1974). Some scientists have noted the potential for a return to the colder conditions of the 'Little Ice Age' of the 17th-19th Centuries, if not

to a full ice age.

Advocates of an externally-induced climatic change theory postulate a physically plausible sequence whereby the cooling of the middle to high latitudes of the Northern Hemisphere causes an expansion of the circumpolar vortex and increased equatorward displacement of circulation features (Bryson, 1974, 1975). Such events have been suggested as the cause of Sahelian droughts and African monsoon failures during contemporary and historical periods (Winstanley, 1973 a,b; Bryson, 1975). Ironically, this reasoning has developed in the Northern Hemisphere in the face of contrary evidence from Southern Hemisphere temperature patterns (Salinger and Gunn, 1975; Tucker, 1975).

In juxtaposition to this is the stand taken by other atmospheric scientists who maintain that such large-scale changes do not represent the entire picture; nor are they as certain as some researchers believe. As Hare (1977:706) notes :

> At the time, these hypotheses were strenuously resisted by orthodox dynamic meteorologists, who believed that short-lived episodes of unusual climate were merely random fluctuations of a highly variable system which itself remained unchanged.

and more significantly :

> ...we should probably not be able to distinguish between a temporary fluctuation of the 1968-73 Sahelian kind and the early stages of a more lasting desiccation.

Proponents of Hare's former statement tend to adhere to a second hypothesis based on internal forcings. This concept implies that because the atmosphere-ocean-ice system is governed by laws expressed as highly non-linear mathematic equations " ...the uniqueness of long-term statistics [climate] is not assured" (Lorenz, 1968:2). The work of Lorenz (1968, 1970, 1976, 1979) has been the focal point for the evolution of this essentially non-deterministic concept which stands somewhat at odds with external theories of climatic variability. Basically, Lorenz examined whether the system in contention was 'transitive', and thus " ...one

whose statistics (i.e. the climate) are uniquely determined by the governing physical laws" (Lamb, 1979:224), or whether it could be 'intransitive', that is, where " ...there are two or more distinct sets of statistics, any one of which could constitute the climate of the system without violating any physical laws" (Lorenz, 1976:499). Hence, an 'intransitive' system would dictate that climatic change " ...would not necessarily be directly forced in the manner proposed by the [external] climatic change hypothesis" (Lamb, 1979:224). The latter premise provides an explanation for the variability within the system and a vital link for more comprehensive models. However, as Lorenz (1976:499) freely admits, intransitivity " ...cannot be a *sole* cause of climatic change". In fact, the only evidence for either transitive or intransitive modes comes from laboratory 'dishpan' experiments and ergodic theory.

What Lorenz has proposed is an 'almost intransitive' atmosphere-ocean-earth system which is distinguishable from the external approach because, as Lamb (1979:224) comments :

> A change in the external conditions from one configuration to another and back, for example, need not produce a re-establishment of the original climate. One of the alternative climates compatible with this set of external conditions may instead prevail.

A further advantage of this theory is that it suggests a modulation of the climate system by the non-linear processes in the atmosphere. Lorenz (1968:2) suggests that in the above system :

> ...statistics [climate] taken over infinitely long time intervals are independent of initial conditions, but statistics [climate] taken over very long but finite intervals depend very much upon initial conditions.

and " ...that a single solution will exhibit different statistical properties within different segments of a long time span" (Lorenz, 1976:499). Thus Lorenz's model foreshadows the possibility that a number of distinct climatic states or modes may exist simultaneously in the atmosphere-ocean-earth system. Over the long, but finite, time scales of climatic change

research, any one of these climatic states may predominate for various periods. However, over an infinite time span, changes of climate would not, by definition, be possible. Hence, the system could appear to be transitive at infinite time scales and intransitive on very long, but finite, scales.

Interestingly, Lorenz has tentatively proposed the basis for a third type of theory which contains a mix of internal and external elements. However, such a model would seem to require a more thorough theoretical background and the use of elaborate numerical models to bring it to complete fruition.

The most useful aspect of the above discussion is whether an almost intransitive atmosphere-ocean-earth system has any role to play in the nature of persistence as well as change. A phenomenon such as the Southern Oscillation, with its relationship to monsoonal and oceanic features, is prone to both distinct modes and changes. It represents the type of phenomena that often accompanies atmosphere-ocean interactions, and may, as Caviedes (1982) suggests, ultimately lend itself to interpretation by topological theories such as the Catastrophe Theory (Thom, 1975).

In analysing aspects of the 1972-73 El Niño and PDZ rainfall outbreaks, Flöhn (1973:136) makes mention of Lorenz's theories, to the extent of suggesting that atmosphere-ocean events in the Pacific " ...may be recognized as a typical example of a regional intransitivity....". Thus Lorenz's concept is an important step towards explaining the nature of atmospheric and oceanic anomalies. Suggested periods for the development and persistence of such anomalies are in the order of months to seasons, and Lorenz (1976:504) has expressed the belief that " ...seasonal variations of the environment need not prevent almost-intransitivity of the complete atmosphere-ocean-earth system, if present, from leading to long period fluctuations".

An answer to the whole dilemma has generally been sought in the field of numerical modelling. The current aim among atmospheric scientists is progressively to improve numerical models for both short- and long-term weather

and climate analyses. However, there is yet to emerge a model which can reproduce a completely coupled atmosphere-ocean-earth system. In fact, total parameterization of the complex feedbacks in such a system is not yet possible because of incomplete knowledge of the processes involved, let alone the system dynamics. As Barry (1979:119) remarks " ...even the sign of some relationships is in doubt".

Thus what has tended to occur is a general modification of external theories, based on the more reasonable assumption of non-uniform expansions and contractions of atmospheric circulation belts and vertical circulations. In addition, the expansion of both land and particularly oceanic data bases has provided researchers in many fields with at least a better initial 'working set'. The net result is that increased numerical research has led to an ever-increasing range of models (Barry, 1975). As Barry (1979:120) notes "There now exists an hierarchy of climate models ranging from simple energy budget models (EBMS) in zero, one, or two dimensions, to three dimensional general circulation models (GCMS)".

Possibly the most encouraging sign for long-term climatic research is that "Despite the overall inadequate data base it is at least possible to devise model synoptic zonal patterns derived from oceanic and continental information" (Bowen, 1979:181). A major global step in this direction was the reconstruction of the climate for January 18,000 years BP (CLIMAP, 1976). Information of particular note came from palaeoecological fields and has allowed the evaluation of sea surface temperatures and salinities. As a consequence, a spate of new reconstructions of Indo-Pacific oceanic and atmospheric circulations has begun to appear in the literature (e.g. Bé and Duplessy, 1976; Prell and Hutson, 1979; Thiede, 1979; Moore *et. al.*, 1980; Prell *et. al.*, 1980; Duplessy, 1982; Van Campo *et. al.*, 1982).

In regard to the Australasian region itself, the most thorough appraisal of atmospheric conditions during the Quaternary glacial maximum is that of Webster and Streten (1978) (presented in an earlier form in Walker, 1972). Like aspects of the recent CLIMANZ Conference (1981), and many of the global

endeavours in this field, this paper focuses on a major geophysical extreme or 'spike'. It uses knowledge of present weather patterns and atmospheric circulation dynamics to provide a basis for deductions about Holocene and Quaternary systems. Of particular interest is the authors' ability to deduce quite convincing Quaternary glacial climates and even upper air circulations based on both known geological and environmental changes and present day circulation analogs. Interwoven within such a framework is an attempted differentiation of regionally anomalous climatic regimes in New Guinea and southern Australia. As Webster and Streten (1978:285) state :

> An important aim of a paleoenvironmental interpretation is an attempt to discern whether or not a local indicator (e.g., anomalously drier conditions in northern Australia) resulted directly from the imposition of planetary scale controls (such as the strengthening of the Hadley Circulation) or as the result of the variation of a local control (such as the increased land area).

Of particular interest is the indication that Australasian monsoon circulation during the last glacial maximum may have been markedly weakened with fewer tropical disturbances affecting the continent (see also Street, 1981). Such a situation would have contributed significantly to continental aridity (i.e. desert dust in marine sediments downwind from the Australian deserts - Thiede, 1979; Street, 1981). Certainly there is supportive evidence from South East Asia (Vestappen, 1975, 1980) for such a view. Other model evidence (Kutzbach, 1981; Kutzbach and Otto-Bliesner, 1982) for 9,000 years BP supports an early Holocene monsoonal optimum, at least in Africa, Arabia and India (see also Street and Grove, 1979; Flöhn and Nicholson, 1980; Sarnthein *et. al.*, 1981; Maley, 1982; Rossignol-Strick *et. al.*, 1982). Both Australian pollen and geomorphological records (Bowler *et. al.*, 1976; Rognon and Williams, 1977) tend to confirm a similar pluvial stage in Australia with the latter inferring a monsoonal optimum around 10,000-8,000 years BP (Rognon and Williams, 1977:315-317) but with a later or perhaps secondary (Singh, 1981) 8,000-5,000 year BP rainfall response in southern Australia (Pittock, 1980).

A full investigation of monsoon variability in Australasia during the Quaternary awaits further detailed continental and oceanic data collection phases. Certainly, a knowledge of SST distributions in both the Indian and Pacific oceans may permit the resolution of El Niño and thus even Southern Oscillation phases. As Pittock, in Pittock *et. al.* (1978:175) states :

> ...the Southern Oscillation is indeed important on longer time scales, and ... this should be taken into account in considering climatic changes throughout the Holocene and perhaps earlier in the Quaternary.

Furthermore, Pittock and Salinger (1982:31) note that "It is thus significant that the palaeoclimatic indicators support the suggestion of a dominant positive Southern Oscillation index during the Hypsithermal".

On the Australian continent the need to expand current research efforts and methods has already been stressed by Walker in Pittock *et. al.* (1978:96) :

> The most obvious and potentially rewarding development would be the extension of sedimentological and pollen-analytical investigations to lake deposits in currently semi-arid areas in eastern and northern Australia.

Street and Grove (1979:103) suggest that "Fluctuations in water level in closed-basin lakes appear to be one of the best indicators of continental paleoclimates during the late Quaternary". Some progress has been made, at least at Lake Frome in South Australia (Singh, 1981). This site promises to provide some important information on pollen type and rainfall seasonality. Furthermore, although the core referred to in Singh (1981) has provided only a record of the last 10,000 years, vegetation in its earliest stage (9,500-8,000 years BP) reflects a period when " ...summer rainfall was higher than at any other time during the rest of the sequence" (Singh, 1981:428).

Although such findings suggest a monsoon optimum, they need further support. It would seem that this could come from a palaeo-analysis of the Lake Eyre region. This salt lake, the biggest in the continent, is the focus of a large and extensive drainage basin which includes the arid regions of

South Australia and the Northern Territory as well as stretching into tropical/sub-tropical Queensland. Historically it has generated several contentious issues ranging from the 'inland sea' claims of early explorers to questions of its genesis, morphology and flooding/filling capabilities. In fact, the latter issue has only been resolved since the observed floodings and fillings of the lake in 1950, 1955 and more recently in 1974-76.

From work such as Bonython and Mason (1953) and Mason (1955) there is the suggestion that the Lake Eyre basin may respond to Australasian monsoon fluctuations. The floodings originate from heavy monsoonal rainfall in the Queensland section of the drainage system. Such findings would provide further support for a co-ordinated study of palaeo-environments at Lake Eyre. In particular, a knowledge of Quaternary lake levels may provide a useful indirect measure of major Australasian monsoon fluctuations.

CHAPTER II - DATA AND COMPUTATIONAL PROCEDURES

The diagnostic analysis of monsoon and teleconnection variations in this study is performed using three spatial domains. These domains, regional (35°N-35°S; 85°E-175°E); local (5°S-30°S; 95°E-155°E) and Indo-Pacific (35°N-35°S; 30°E-60°W), contain grid arrays of 15 by 19, 6 by 13 and 15 by 55, 5° latitude by 5° longitude grid intersection points respectively. The domains are delimited in accordance with various spatial and locational criteria. The regional domain is based on a WMONEX-sized area, since this makes it possible to examine how atmospheric circulation processes over Australia relate to the overall Australasian/South East Asian northeast monsoon. The local domain is determined by the extent of data available to analyse moist processes in the more localized Australian region. Finally, the Indo-Pacific domain is defined as the area under the direct influence of the teleconnections associated with the Asian monsoon system.

2.1 DATA SOURCES

The number, type and distribution of upper air and upper wind stations in the regional, local and Indo-Pacific domains are shown at the beginning of each of the results sections in Figures 6, 43 and 94 respectively. A full list of stations is contained in Appendix 1.

2.1.1 Regional and Indo-Pacific Domains

Individual monthly winds and geopotential heights for standard isobaric levels were obtained from National Oceanic and Atmospheric Administration (NOAA) (1973-77 a) and supplemented by daily and monthly records of the Australian Bureau of Meteorology, NOAA (1973-77 b) Malaysian Meteorological Service, Service de la Meteorologie en Nouvelle - Calédonie (1973-77) and the Thai Meteorological Department. Additional upper wind data from stations at Chichijima (47971; 27°5'N, 142°11'E), Clark (98327; 15°10'N, 120°34'E) and Minamitorishima (47991; 24°18'N, 153°58'E) were obtained

from the Japanese Meteorology Agency (1973-77), while additional geopotential height data were procured from the Central Weather Bureau of Taiwan.

When the regional domain was expanded to create the Indo-Pacific domain, additional upper wind data were acquired from the U.S. Weather Bureau (1958-65), Environmental Science Services Administration (ESSA) (1966-70), NOAA (1971-72), NOAA (1978-81), Japanese Meteorology Agency (1958-72) and from National Center for Atmospheric Research (NCAR) tapes for the 1958-81 period (Karoly, 1982; personal communication). However, to provide a more complete coverage of this domain, data were also sought from individual countries in the Indo-Pacific area. The following meteorological services provided supplementary information; the Malawi Government Meteorological Service, Instituto Meteorologico Nacional of Costa Rica, Pakistan Meteorological Department, Meteorologische Dienst of Netherlands Antilles, Meteorological Department of the Republic of Vanuatu, New Zealand Meteorological Service, Republic of Seychelles Directorate of Civil Aviation, Servico Meteorologico de Mocambique, Republika Demokratika Malagasy Service de la Meteorologie, Indonesian Meteorological and Geophysical Institute, Kenyan Meteorological Department, Republic of Maldives Department of Meteorology, Mauritius Meteorological Department, Philippine Atmospheric, Geophysical and Astronomical Services Administration, the United Republic of Tanzania Directorate of Meteorology, Republic of Zambia Meteorological Department, Service Météorologique de la Réunion and the Democratic Republic of the Sudan Meteorological Department.

In addition to using Wright's seasonal Southern Oscillation indices (SOI's) (Lamb, 1977; Wright, 1981; personal communication), Section 3.3 also used monthly mean SOI values (from 1932-81) provided by A.J. Troup (CSIRO Division of Atmospheric Physics, Melbourne, Australia). Pacific Dry Zone (PDZ) rainfall and Lake Eyre flooding/filling criteria were derived from previously published material (e.g. Bonython and Mason, 1953; Mason, 1955; Bonython, 1960, 1963; Quinn and Burt, 1970;

Tetzlaff, unpublished; Reiter, 1978, 1979; Graetz, 1980).

Monthly mean isohyets for January and February 1960-81 were taken from the map insets in Bureau of Meteorology (1960-81), and monthly mean decile rainfall distributions over Australia were obtained from maps in Bureau of Meteorology (1973-77).

2.1.2 Local Domain

In the local domain, Section 3.2.1, resultant wind vectors and mixing ratios were obtained from the Australian Bureau of Meteorology, while data used to calculate the 19 year mean advective water vapour flux were obtained from Maher and Lee (1977). For the local domain, Section 3.2.2, Hong Kong cold surge dates were obtained from P.J. Webster (CSIRO Division of Atmospheric Physics, Melbourne, Australia) and supplemented with daily surface observations provided by C.W. Kong of the Royal Observatory, Kowloon, Hong Kong. Daily streamline charts were obtained from the Bureau of Meteorology, Melbourne, Australia.

2.1.3 Data Station Changes in the Domains

Major changes in data station operations occurred during the 1973-77 period. In Malaysia, the upper air station at Kuching (96413; 1°29'N, 110°20'E) began operations in 1976, while upper wind data for Kuala Lumpur (48647; 3°6'N, 101°39'E) and Kuantan (48657; 3°47'N, 103°13'E) were not available prior to 1974 and 1975 summer periods respectively. The United States Trust Territories' upper air station at Kwajelein (91366; 8°43'N, 167°44'E) was closed in 1974 and a station at Tarawa (91610; 1°21'N, 172°55'E) came into operation in 1974. All Papua New Guinean stations were transferred from Australian to Papua New Guinean control in 1973 and no data were available after this time due to staff shortages and processing problems. In Vietnam, the upper air stations at Da Nang (48855; 16°4'N, 108°13'E) and Saigon (48900; 10°49'N, 106°40'E) ceased operation in 1974-75 following the fall of the regime in South Vietnam. Data from Chinese mainland stations were available for study only for the month of

March 1977. In the Philippines, the only data available were from the United States Airforce base (upper air station) at Clark (98327; 15°10'N, 120°34'E) during the period from 1973-75.

The following changes in upper air and upper wind operations occurred in Australia. The upper wind station at Onslow (94305; 21°40'S, 115°7'E) was closed in 1975 and a new station at North West Cape (94301; 21°49'S, 114°10'E) opened in the same year. Rockhampton (94374; 23°23'S, 150°29'E) was upgraded to include upper air operations in 1977, and upper air and upper wind operations at Cloncurry (94335; 20°40'S, 140°30'E) were transferred to Mount Isa (94332; 20°40'S, 139°29'E) in 1976. Because of the close proximity of Cloncurry and Mount Isa, only one triangle is used for both stations in Figure 6.

2.1.4 Data Problems

In generating any field within a bounded domain, one factor crucial to the degree of resolution is the distribution of data stations. Every station used in this study was land (continental or island) based. With oceans comprising a major proportion of the regional and, more particularly, the Indo-Pacific domain, data distribution is markedly restricted. As Figure 6 shows, there are added problems when data distribution over land areas in the domain is very sparse.

Not only were there gaps in terms of the number of stations actually recording such data on a continuous basis, but also, significant problems and delays were encountered in obtaining data from stations which did make such recordings. In particular, although upper air and upper wind observations were recorded at various Indonesian, Philippine and eastern Japanese island stations, such data were not obtained in time to be included in those analyses undertaken in Sections 3.1 and 3.2 of this thesis. However, they were finally obtained and included in Section 3.3 analyses.

The 200 mb fields (Figs.18-20), showing monthly mean streamfunction and zonal wind component isotachs, illustrate error terms generated in

sparse data areas during the initial gridding of the wind field and subsequently carried over into the final fields. Error terms were also evident when monthly mean velocity potential fields generated with the additional data from Indonesia, the Philippines and Japan were compared with those presented in this study. Such fields generated with this additional data have not been shown in this thesis because of the large volume of material involved. The most notable change is in the 200 mb fields where the large positive values in the northern Pacific section of the diagrams are reduced. Generally, however, field patterns are not unduly affected by the absence of subsequently obtained data.

In the Indo-Pacific domain (Fig.94), the sparcity of data in the eastern equatorial and southeastern Pacific Ocean and the southern Indian Ocean presents major problems for the determination of streamfunction and velocity potential over this domain. It was found that these parameters were particularly distorted when areas of good data coverage, experiencing rapid wind flow, adjoined sparse data regions. At 200 mb, the Northern Hemisphere winter jetstream over the North Pacific Ocean produced a very marked distortion of the flow pattern well into the southern Pacific region of sparse data coverage.

Given these problems, it was decided to rely on parameters which did not require the extent of data processing necessary to develop streamfunctions and velocity potentials. The least processed of those parameters which could be used for such an approach were gridded wind vectors to depict rotational motion and divergence to depict divergent motion.

2.2 COMPUTATIONAL PROCEDURES

The following sub-sections (2.2.1 - 2.2.4) detail the procedures used to evaluate the final fields in each of the three domains. In sub-section 2.2.1, the gridding sequence (*iii*) details specifically the procedure in regard to zonal (u) and meridional (v) wind components. The same gridding routine was also used for geopotential heights, pressures and mixing ratio

data which, by their very nature, do not require steps (*i*) and (*ii*) outlined in sub-section 2.2.1.

2.2.1 Sequence for Divergence and Relative Vorticity Calculations in the Regional and Indo-Pacific Domains

(*i*) Obtain (or calculate from daily values) monthly mean wind direction (θ) and speed (V) data for stations within the bounds of the domain.

(*ii*) Using equations $u = - V \sin \theta$ and $v = - V \cos \theta$, which relate cartesian and polar coordinates, calculate u and v wind components ($m\ s^{-1}$) from data at the stations in (*i*).

(*iii*) Generate the u and v wind components at grid points on a 5° latitude by 5° longitude grid of the domain using an 'objective' analysis technique developed by Yanai (1964). This technique involves a successive correction procedure, where an initial guess field for the parameter at every grid point is equated with station observations of the parameter and the resulting error is corrected by successive iterations until close approximation between interpolated grid point values and station observations is achieved.

(*iv*) From the u and v fields generated, relative vorticity (ζ_r) and horizontal divergence ($\vec{V}.\nabla$) can be evaluated by centred differencing (a form of finite difference) using adjacent grid points (Appendix 3).

2.2.2 Methods and Sequence for Velocity Potential and Streamfunction Calculation in the Regional and Indo-Pacific Domains

From calculations of divergence and relative vorticity terms, it is possible to determine velocity potential (χ) and streamfunction (ψ) from their Laplacian forms, $\nabla^2\chi$ and $\nabla^2\psi$ (Appendix 4).

This study considered two basic approaches to velocity potential and streamfunction determination - iterative and matrix inversion. Of these two methods, the former was found to be the most practicable, especially when coupled with a boundary correction procedure (Appendix 5.1).

2.2.3 Sequence for Moisture Characteristics Calculations in the Local Domain

Advective and transient eddy moisture characteristics were determined at 1000, 900, 850 and 700 mb levels to augment the investigation of local circulation variations over northern Australia, New Guinea, Indonesia and adjacent seas. The moisture characteristics calculated by grid point approach were water vapour fluxes, water vapour flux divergence, streamfunction of the water vapour flux and precipitable water content. These characteristics were determined at standard isobaric levels between the 1000 and 700 mb pressure levels, with the water vapour flux divergence and streamfunction of the water vapour flux being vertically integrated.

Using daily and monthly mean gridded wind components and specific humidity derived from mixing ratio data (Appendix 6.1) :

(*i*) Calculate horizontal monthly mean advective water vapour fluxes from a combination of the gridded fields of monthly mean u and v wind components and specific humidity for the 1000, 900, 850 and 700 mb levels (Appendix 6.1).

(*ii*) Using the divergence formula in centred difference (finite difference) form (Appendix 3), substitute the monthly mean advective water vapour flux components for u and v wind components to obtain horizontal monthly mean advective water vapour flux divergence (Appendix 6.2), then vertically integrate (Appendix 6.4).

(*iii*) Using the relative vorticity formula in centred difference (finite difference) form (Appendix 3), substitute the monthly mean advective water vapour flux components to obtain the relative vorticity of the horizontal monthly

mean advective water vapour flux and vertically integrate (Appendix 6.5).

(*iv*) Calculate, for various layers or depths, precipitable water content knowing the average specific humidity between standard low-level pressure surfaces (Appendix 6.6).

The transient eddy components of the above parameters (excluding precipitable water content) can then be evaluated in regard to the type of decomposition process outlined in Appendix 2.1 :

(*v*) Calculate total horizontal water vapour flux from the monthly mean of the daily covariance of gridded u and v wind components and specific humidity values for the 1000, 900, 850 and 700 mb levels (Appendix 6.1).

(*vi*) Following equations (32a - f) in Appendix 6.1, evaluate and substitute the monthly mean transient eddy water vapour flux terms for the u and v wind components in the centred difference (finite difference) form of the divergence formula (Appendix 3) to obtain horizontal transient eddy water vapour flux divergence (Appendix 6.2), then vertically integrate (Appendix 6.4).

(*vii*) As in step (*vi*), determine the horizontal transient eddy water vapour flux components and substitute into the centred difference (finite difference) form of the relative vorticity formula (Appendix 3) to obtain the relative vorticity of the horizontal transient eddy water vapour flux, then (using Appendix 6.3), determine the streamfunction of the horizontal transient eddy water vapour flux and vertically integrate (Appendix 6.5).

2.2.4 Sequence for Kinetic Energy Generation Calculations in the Regional Domain

Cross isobaric flow is a response to the ageostrophic component of

atmospheric circulation and an important source of kinetic energy which is reflected in the kinetic energy generation (KEG) parameter. This generation is prevalent particularly in low latitudes where both pressure gradient and coriolis forces are weak and geostrophic imbalance occurs. A measure of this effect can be deduced from the response of the wind field to pressure gradients.

This parameter is calculated in the following manner :

Obtain gridded u and v wind components and geopotential height values (sub-section 2.2.1 - point *iii*) and combine in a centred difference (finite difference) form of the kinetic energy generation (KEG) parameter (Appendix 7).

2.2.5 Determination and Interpretation of the Velocity Potential Cross Sections

Vertical cross sections of velocity potential are determined by the normalization procedure in Appendix 8. Included in this Appendix is a mathematical appraisal of the velocity potential cross sections. In Appendix 9, the *Monthly Weather Review* article (containing the bulk of Section 3.1.1 in this thesis) has divergence cross sections for January 1973-75. A comparison of the cross sections in Section 3.1.1 and Appendix 9 illustrates the 'noisiness' of divergence as opposed to velocity potential in vertical cross sections.

2.2.6 Computational Problems

The iterative approach and the boundary correcting method used in this study produce only one set of solutions to equations (12a) and (12b) in Appendices 4 and 5. As Shukla and Saha (1974:425) point out, solutions to (12a) and (12b) depend on :

a) Type of boundary condition
b) Type of finite difference scheme used to evaluate the differentials
c) Type of synoptic situation which implies the type of distribution of wind, vorticity, and divergence fields
d) Relative magnitudes and distribution of vorticity and divergence

Of the above factors, a) and b) are most commonly considered in investigations and studies using streamfunction and velocity potential fields. An examination of various studies indicates that they have developed boundary schemes in regard to either Dirichlet, Neumann or mixed conditions, and evaluated differentials (Laplacian) by five or nine point finite difference approximations (e.g. Hawkins and Rosenthal, 1965; Shukla and Saha, 1974; Stephens and Johnson, 1978).

The choice of the Shukla and Saha boundary correcting techniques and the five point Laplacian approximation for this study was made in regard to the project at hand, the computing time and programming complexity required, and the theoretical material available. However, considering the comments made in McAvaney (1983), neither the approach of Shukla and Saha (1974) nor that of Stephens and Johnson (1978) is considered satisfactory in solving the boundary conditions for Poisson equations (12a) and (12b) in a limited domain. In fact, McAvaney (1983:34) states 'All methods suggested in the literature are found deficient when strongly divergent features exist close to the boundary'.

Given these comments, it would seem that no technique can claim to be able to solve successfully the boundary problem in a limited domain. Nevertheless, it is felt that the streamfunction and velocity potential fields in this study can depict observed atmospheric features and do concur with patterns in remotely-sensed data sets in the bulk of the domains.

CHAPTER III - RESULTS AND DISCUSSION

This chapter examines Southern Hemisphere monsoon and teleconnection dynamics on regional (35°S-35°N; 85°E-175°E), local (5°S-30°S; 95°E-155°E) and Indo-Pacific (35°N-35°S; 30°E-60°W) scales and suggests possible implications for historical and pre-historical reconstructions. The regional and local domains focus extensively on the months of January, February and March from 1973 to 1977, while the Indo-Pacific domain and the long-term variability sections expand both the spatial and temporal scales in order to evaluate the broader significance of monsoon and teleconnection variability. In examining the latter, questions are raised as to the reliability and precision of indices of the Southern Oscillation teleconnection, the influence of this teleconnection on Australian summer rainfall patterns, and the use of proxy data (such as Lake Eyre floodings/fillings) to determine long-term monsoon and teleconnection variability in the Australian environment.

3.1 INTERANNUAL AND INTRASEASONAL VARIABILITY - UPPER AIR DYNAMICS OF 1973-77 SUMMERS; THE REGIONAL DOMAIN (35°N-35°S; 85°E-175°E)

In this section, streamfunction, velocity potential, geopotential height and kinetic energy generation fields are deduced in order to examine aspects of large-scale monsoon and teleconnection structure and variability over Australasia. The analysis covers two temporal periods. These are the major period of January, February and March 1973-77 and the sub-period of January and February 1973-75. The major period examines the variability and spatial distribution of atmospheric features in streamfunction and velocity potential fields at 850 and 200 mb levels, while the sub-period concentrates on the vertical structure and spatial pattern of these features in surface - 200 mb cross sections, and at surface/1000 mb, 850, 700 and 200 mb levels during the most variable portion of the major period.

Figure 6 shows the distribution of upper air and upper wind stations from which data were obtained in the regional domain. The outer boundary

Figure 6 Distribution of upper wind and upper air stations in the regional domain. Solid symbols (circle/triangle, circle) denote upper wind and upper air stations from which data were available for this study. Stations known to have been operating during all or part of the 1973-77 core period, but from which no data were available, are designated by corresponding open symbols. A combination of solid symbols (square/diamond) indicates upper air stations from which data were only available to supplement the data set for monthly mean divergence cross sections and surface streamfunction fields.

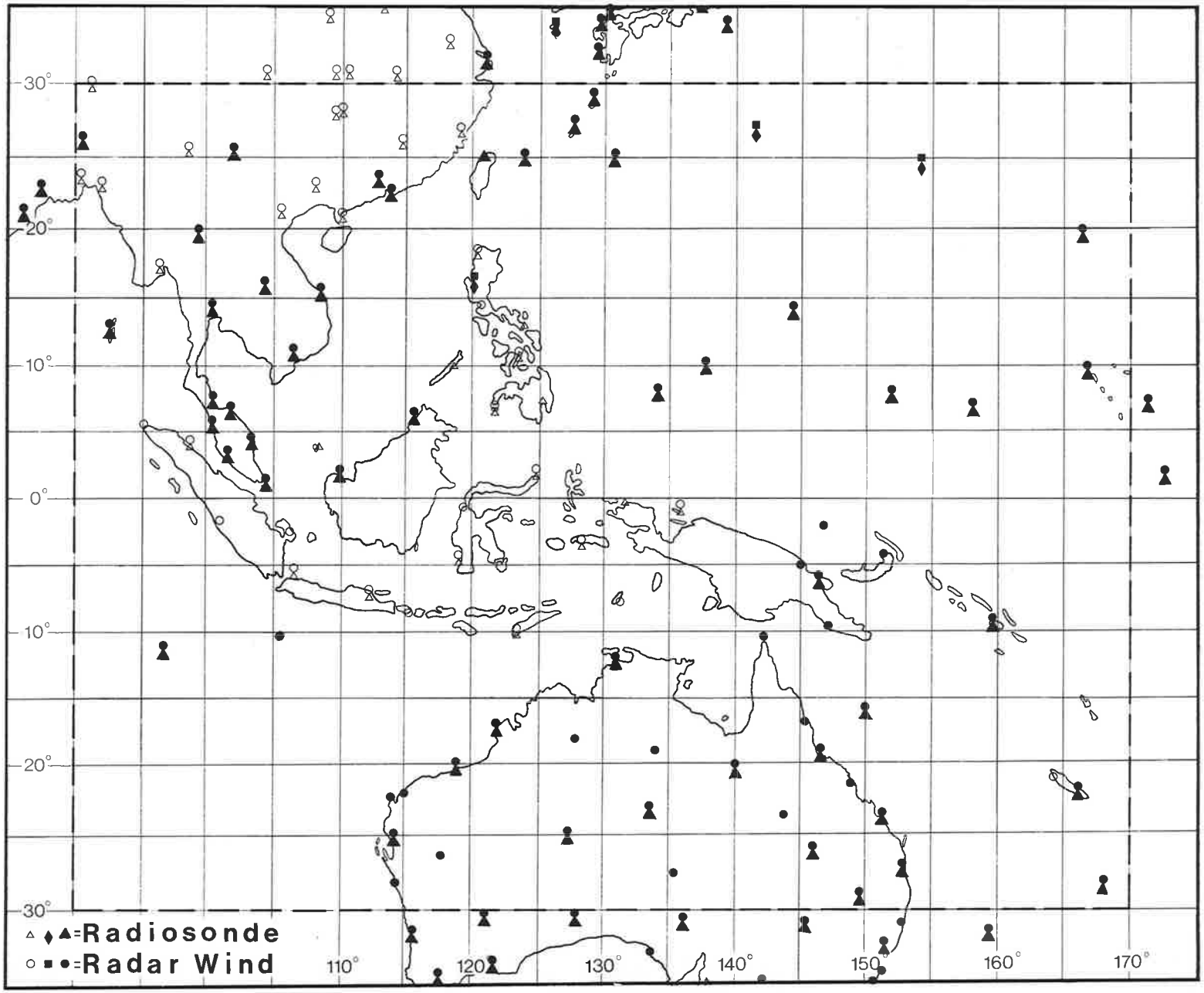
30°
20°
10°
0°
10°
20°
30°
△ ♦ ▲=Radiosonde
○ ■ ●=Radar Wind
110°
120°
130°
140°
150°
160°
170°

of this diagram marks the extent of gridded wind components, while the inner dashed boundary delineates the area for which the final gridded velocity potential and streamfunction fields were obtained.

3.1.1 Major Period : January, February and March 1973-77

(i) Monthly Mean 850 mb Streamfunction ($\bar{\psi}_{850}$) and Velocity Potential ($\bar{\chi}_{850}$) Fields

The 850 mb level was chosen for the initial broad-scale analysis of low-level monsoon flow because it is usually below the 'average' trade wind inversion layer (Riehl, 1969, 1979). The 850 mb level is an intermediate zone between lower levels, which experience progressively larger frictional effects in the planetary boundary layer, and higher levels, where anticyclonic patterns tend to persist (Troup, 1974).

Streamfunction fields are used for the analysis of circulation because the regional domain covers tropical and sub-tropical latitudes. In equatorial and near-equatorial regions pressure gradients and the coriolis parameter are weak, with the result that atmospheric features tend to be poorly represented in pressure analyses. Thus flow is often out of geostrophic balance and circulation is best examined by parameters derived from the wind data.

The map sequences shown in Figures 7, 8 and 9 depict streamfunction fields over the regional domain in the months of January, February and March 1973-77. These illustrate that interannual and intraseasonal variability of circulation are particularly evident over the Australian continent. Interannual changes in circulation patterns and the location of the Near Equatorial Trough in the Southern Hemisphere (NET_{SH}) are most pronounced in odd and even Januarys. During January 1973 and January 1975 the NET_{SH} is weak, with distinct cyclonic centres ($+ \bar{\psi}_{850}$) in the north-eastern and northwestern Australian regions and anticyclonicity ($- \bar{\psi}_{850}$) located over the remainder of the continent. At the other extreme, January 1974 and January 1976 are dominated by a strong and extensive NET_{SH}

Figure 7 Monthly mean 850 mb streamfunction fields in units of 10^5 m^2 s^{-1} at intervals of 5 units over the regional domain during January from 1973-77. Heavy dashed lines indicate the positions of the NET_{NH} and NET_{SH}.

Figure 8 Monthly mean 850 mb streamfunction fields in units of 10^5 m^2 s^{-1} at intervals of 5 units over the regional domain during February from 1973-77. Heavy dashed lines indicate the positions of the NET_{NH} and NET_{SH}.

Figure 9 Monthly mean 850 mb streamfunction fields in units of 10^5 m^2 s^{-1} at intervals of 5 units over the regional domain during March from 1973-77. Heavy dashed lines indicate the positions of the NET_{NH} and NET_{SH}.

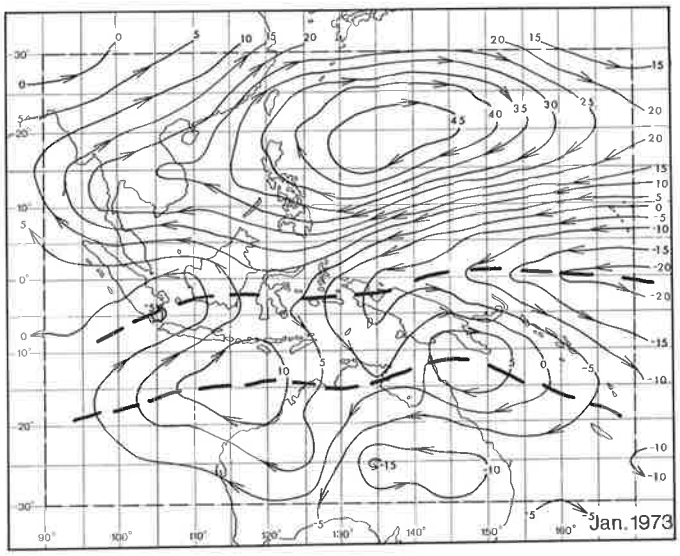

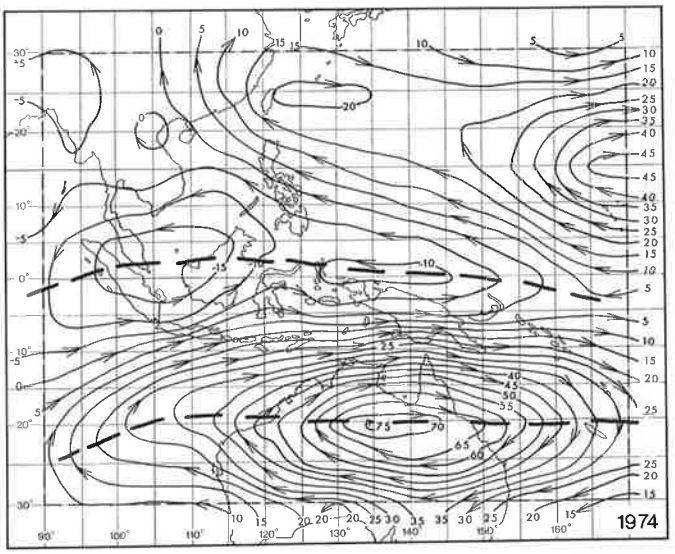

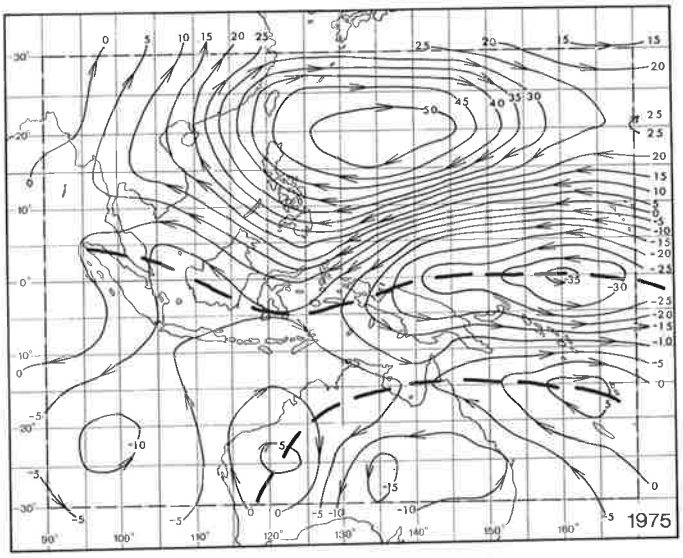

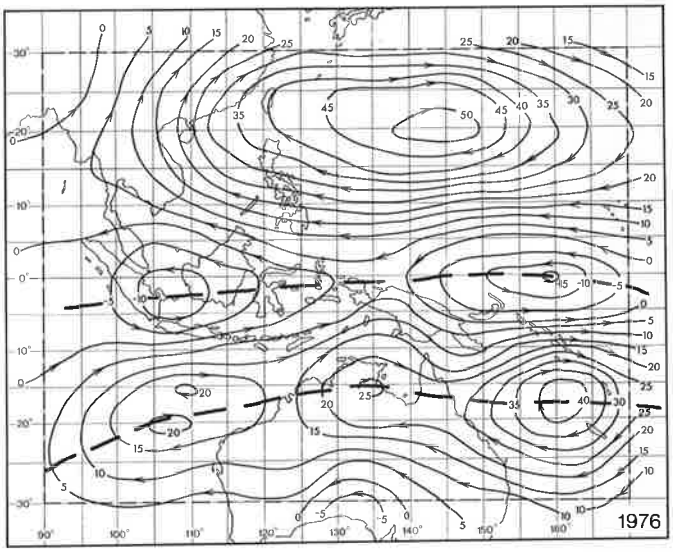

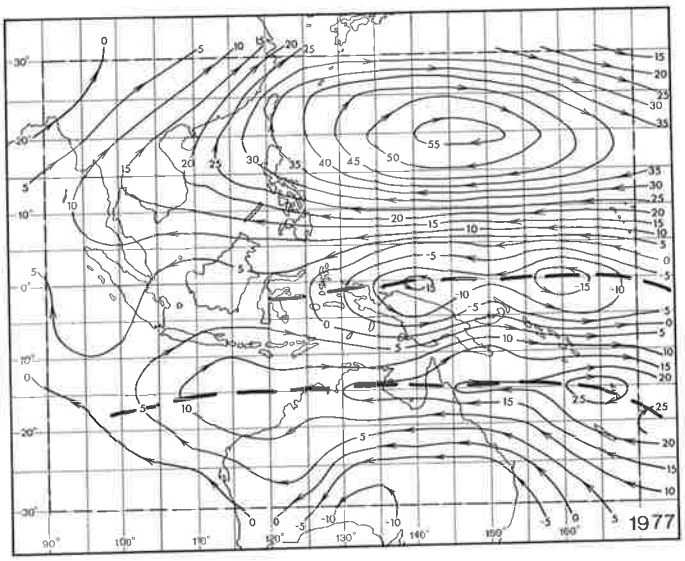

STREAMFUNCTION

x 10^5 m^2/sec

Jan 1973 - 1977

850 mb

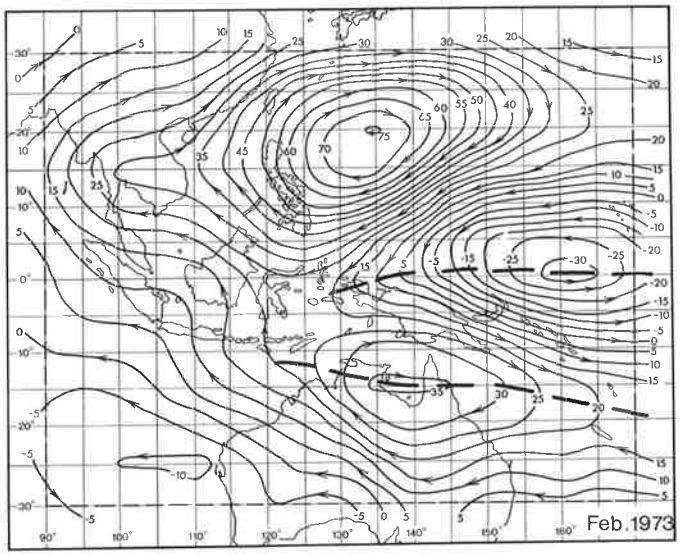

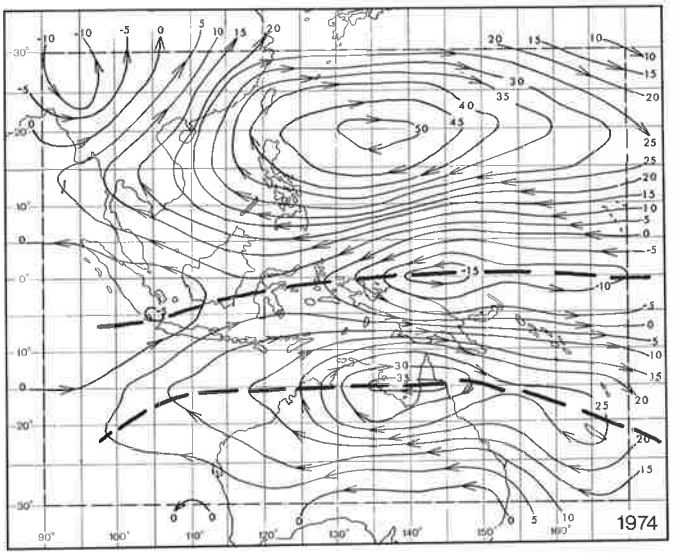

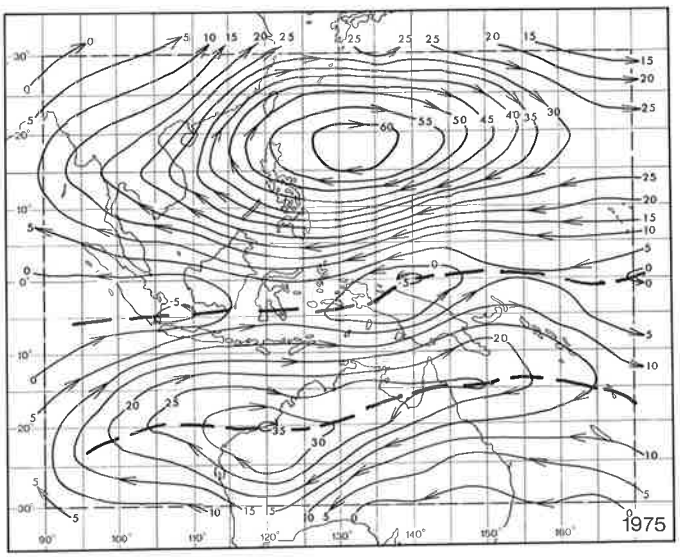

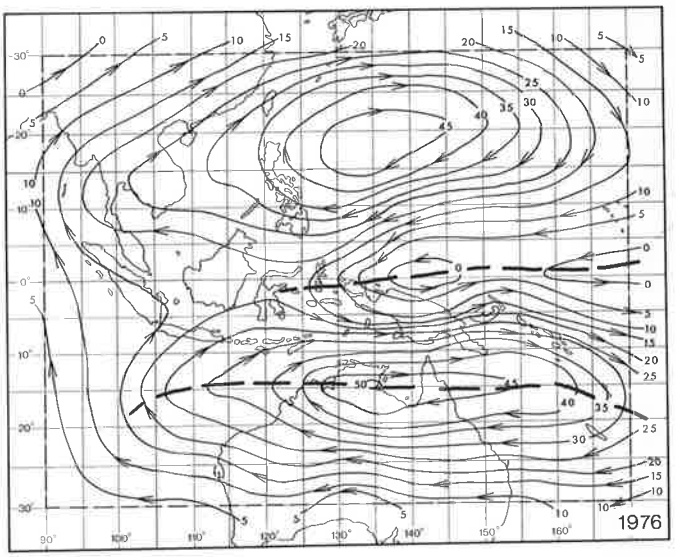

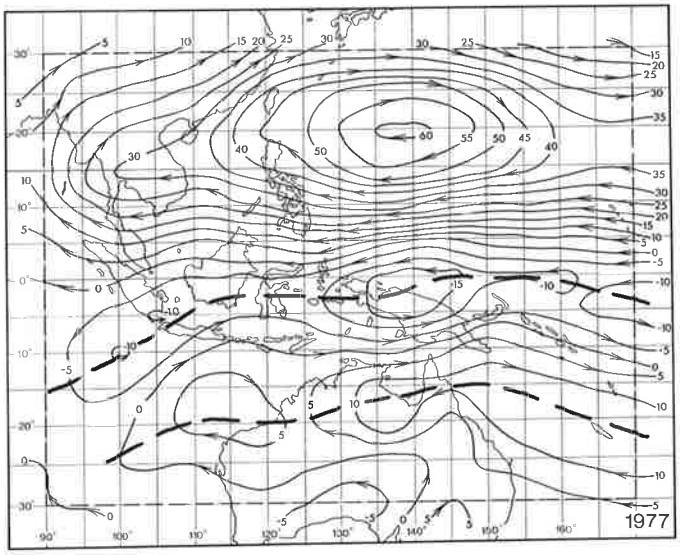

STREAMFUNCTION

$\times 10^5$ m^2/sec

Feb 1973 - 1977

850 mb

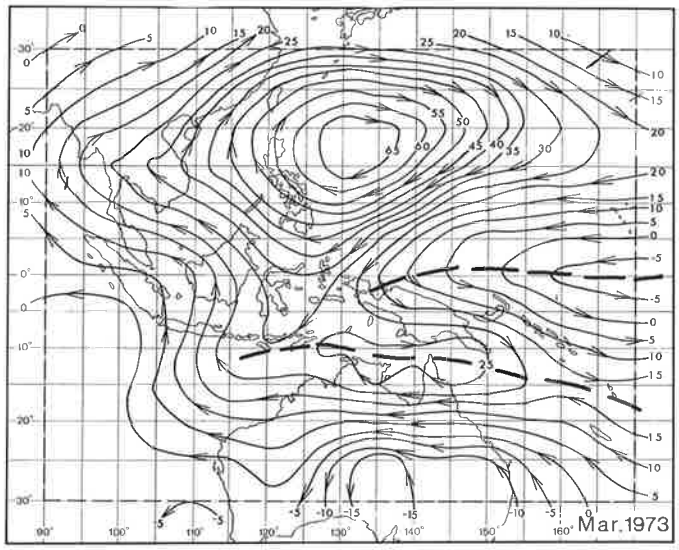

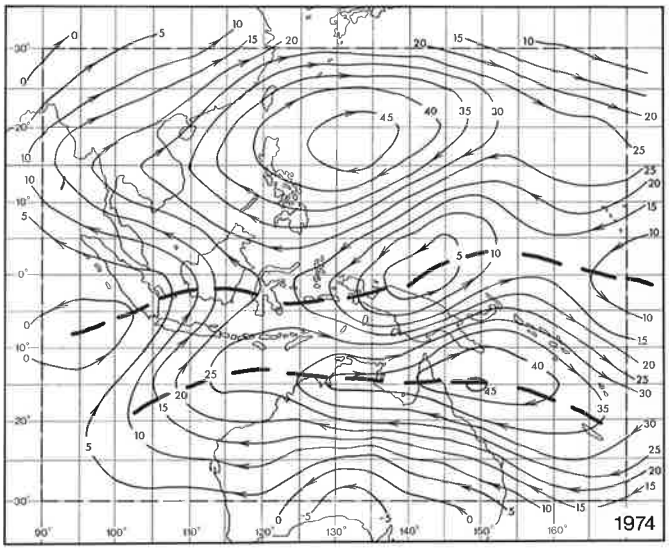

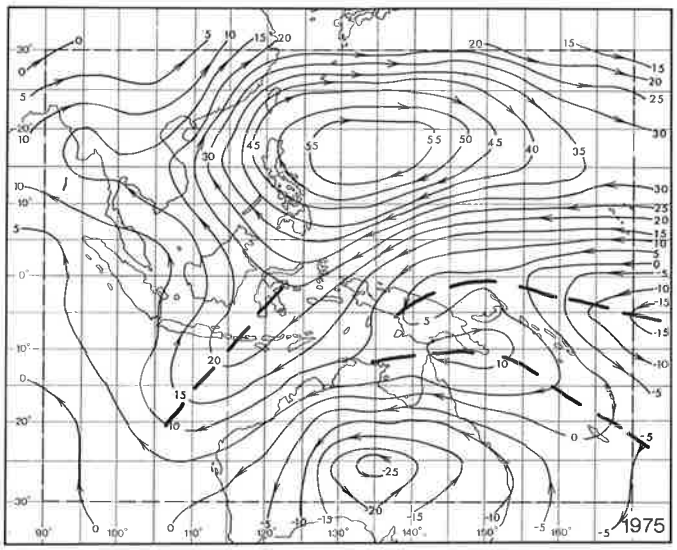

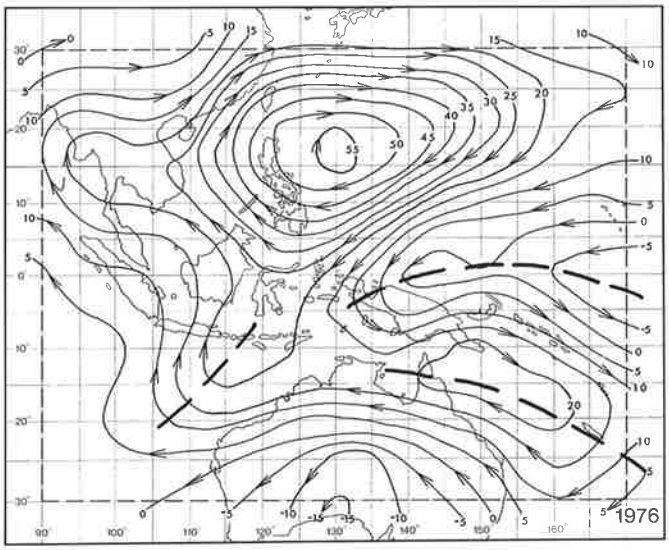

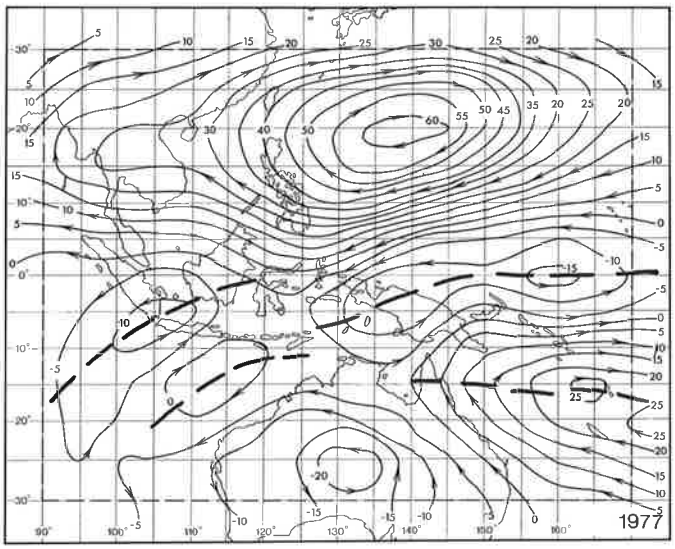

STREAMFUNCTION

x 10^5 m^2/sec

Mar 1973 - 1977

850 mb

across northern Australia. However, only in the months of January does the alternation of monsoon activity (Fig.7) suggest any regular quasi-biennial pattern. Such variability is more likely to be a reflection of the monsoon onset characteristics noted by Troup (1961) and examined in greater detail by Davidson *et. al.* (1981) and McAvaney *et. al.* (1981).

In contrast, the February sequence (Fig.8) exhibits the strongest consistency and organisation of monthly mean monsoon activity, with the NET_{SH} usually being strong and displaced over various parts of the continent. In fact, the most variable aspect of the NET_{SH} in February is its location.

During the March sequence (Fig.9), weaker NETs occur in both hemispheres, with the NET_{SH} rarely displaced more than 10°-15°S. This illustrates the weakening and northward withdrawal of the NET_{SH} as the monsoon season comes to a close. Anticyclonicity ($-\bar{\psi}_{850}$) is markedly evident over the inland of Australia during almost the entire March sequence. Only in March 1974 (Fig.9) is there any indication of the persistence of a pronounced NET_{SH} over Australia.

Intraseasonal variability and persistence of circulation features are evident in the 1973-77 period (Figs.7,8 and 9). Variability is most marked in the 1973 and 1975 summers. In both years, the NET_{SH} is prominent over the northern Australian region in February (Fig.8). These patterns follow the January situations (Fig.7) where the NET_{SH} is weak and centred over northeastern and northwestern Australia. By March, the NET_{SH} has shifted northward (it is somewhat stronger in 1973 than in 1975) as the monsoon season finishes (Fig.9).

In terms of intraseasonal persistence of monsoon activity, 1974, 1976 and 1977 stand out. The 1974 and 1976 seasons display strong and southerly-displaced NET_{SH}'s for most of the monsoon season. In contrast, the 1977 summer is characterized by the persistence of a weak NET_{SH} distribution in northern Australian regions and $-\bar{\psi}_{850}$ centres over southern and central Australia.

Marked rainfall variability is also evident within this five year period,

both within individual seasons and between years (Figs.10-14). In broad terms, the summers of 1974 and 1976 (Figs.11 and 13 respectively) experience above average rainfall distributions, while the 1973, 1975 and 1977 summers (Figs.10,12 and 14 respectively) experience average to markedly below average rainfall patterns. The variability and persistence of circulation features in Figures 7, 8 and 9 tend to coincide with these broad rainfall patterns, being most pronounced in major monsoonal extremes such as 1974 and 1975. During the period of above average monsoon rainfall in January 1974 (Fig.9), the NET_{SH} is extremely strong, displaced to 20°S and centred over the continent. However, in the dry January of 1975 a very weak cyclonic circulation over the western portion of the continent is more in character with typical summer heat low conditions (Ramage, 1971:15).

The intraseasonal nature of rainfall patterns also tends to parallel the observed circulation distributions. In this regard, 1973 and 1975 have distinct February rainfall maxima, while 1974 and 1976 tend to be dominated by January, and January and February maxima respectively. The observed persistence in NET_{SH} strength and location during 1974 is not as strongly reflected in the rainfall patterns, particularly in February. In 1977, the persistence of a weak NET_{SH} distribution is partly reflected in the rainfall deciles, although it is obvious that smaller-scale disturbances play an important part in generating more isolated rainfall maxima. This is probably also true of March 1975 and March 1976.

The above patterns indicate that in very wet Australian summers (e.g. 1974 and 1976) monsoon flow tends to become established early in the season (perhaps even around early to mid December) and is carried over into March. In drier years, monsoon circulation may not only be weak but also of limited duration and spatial extent. Again, the monsoon onset characteristics of Davidson *et. al.* (1981) and McAvaney *et. al.* (1981) may play an important part in determining the nature of the subsequent monsoon season. It is also evident that the month of February usually experiences the peak in monsoonal activity, with cessation and withdrawal of the monsoon

Figure 10 Decile rainfall distributions over Australia during January, February and March 1973 (from Bureau of Meteorology, 1973-77).

Figure 11 Decile rainfall distributions over Australia during January, February and March 1974 (from Bureau of Meteorology, 1973-77).

Figure 12 Decile rainfall distributions over Australia during January, February and March 1975 (from Bureau of Meteorology, 1973-77).

Figure 13 Decile rainfall distributions over Australia during January, February and March 1976 (from Bureau of Meteorology, 1973-77).

Figure 14 Decile rainfall distributions over Australia during January, February and March 1977 (from Bureau of Meteorology, 1973-77).

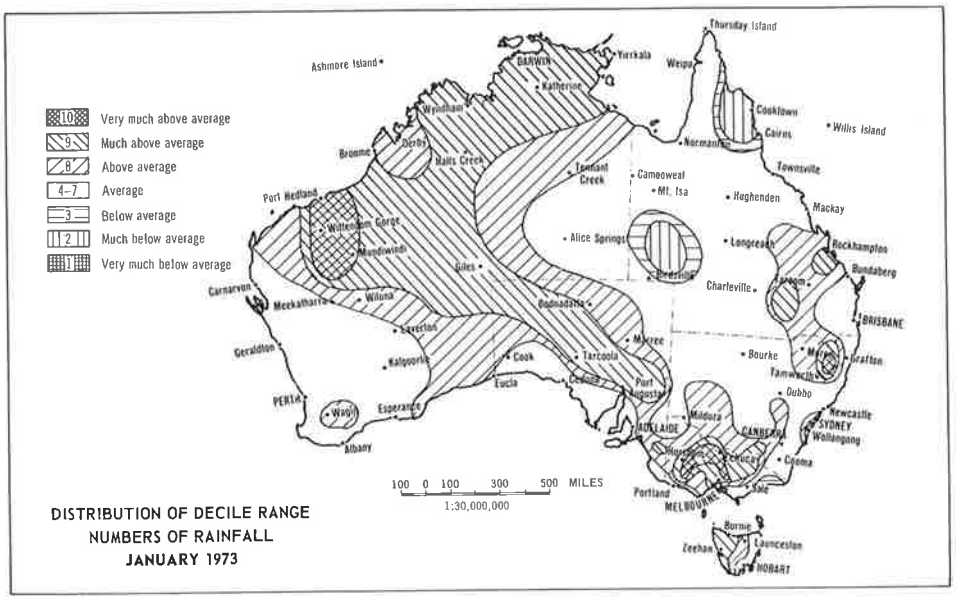

DISTRIBUTION OF DECILE RANGE NUMBERS OF RAINFALL JANUARY 1973

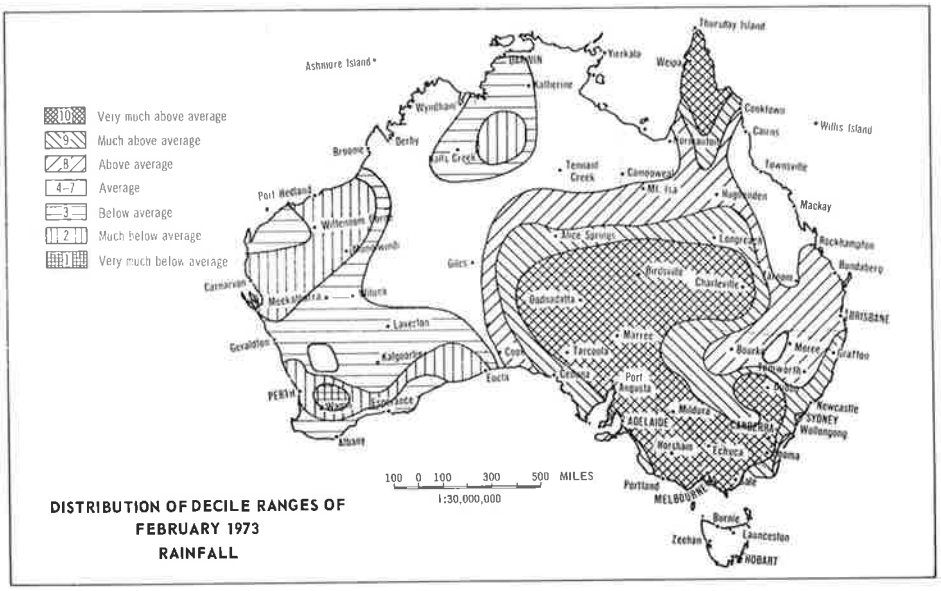

DISTRIBUTION OF DECILE RANGES OF FEBRUARY 1973 RAINFALL

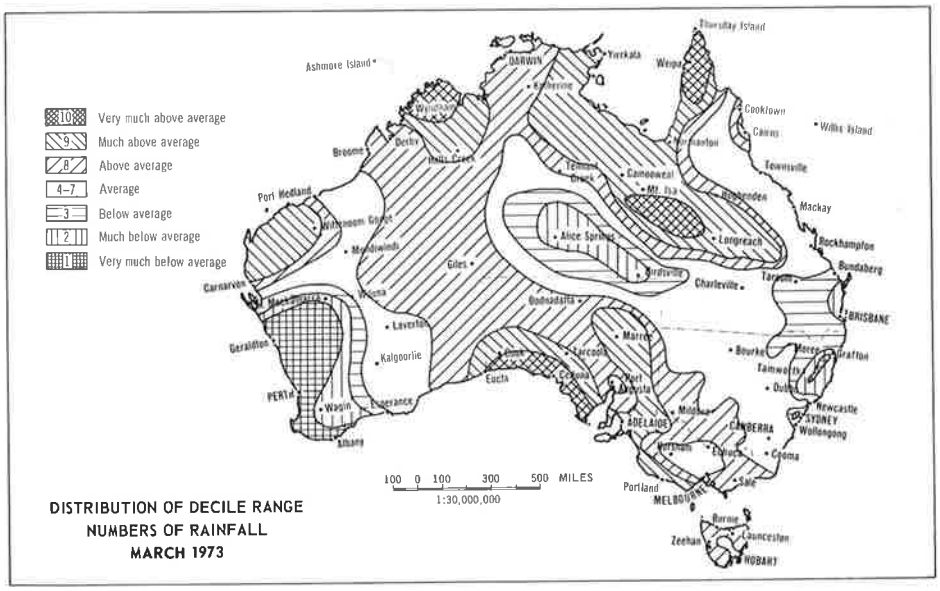

DISTRIBUTION OF DECILE RANGE NUMBERS OF RAINFALL MARCH 1973

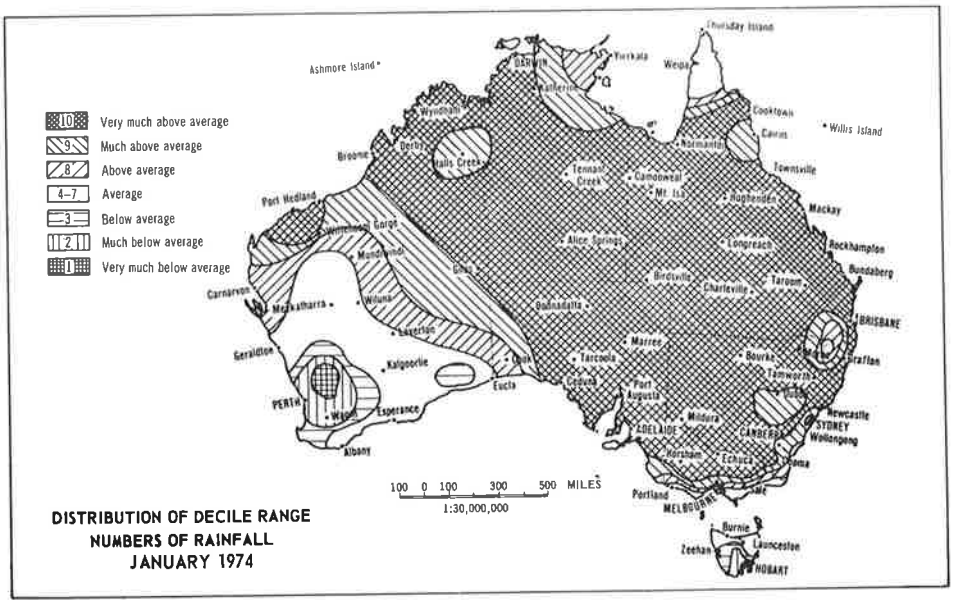

DISTRIBUTION OF DECILE RANGE NUMBERS OF RAINFALL JANUARY 1974

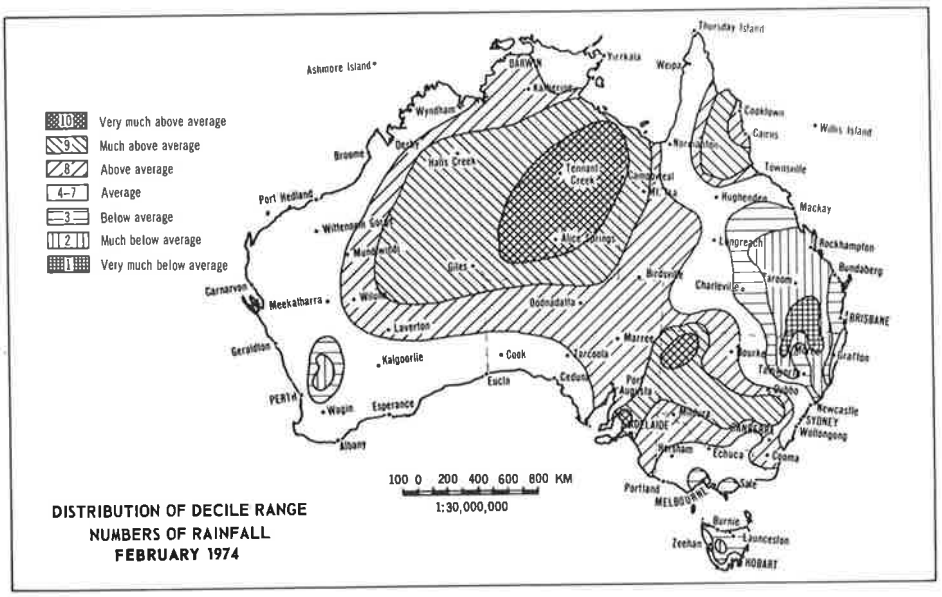

DISTRIBUTION OF DECILE RANGE NUMBERS OF RAINFALL FEBRUARY 1974

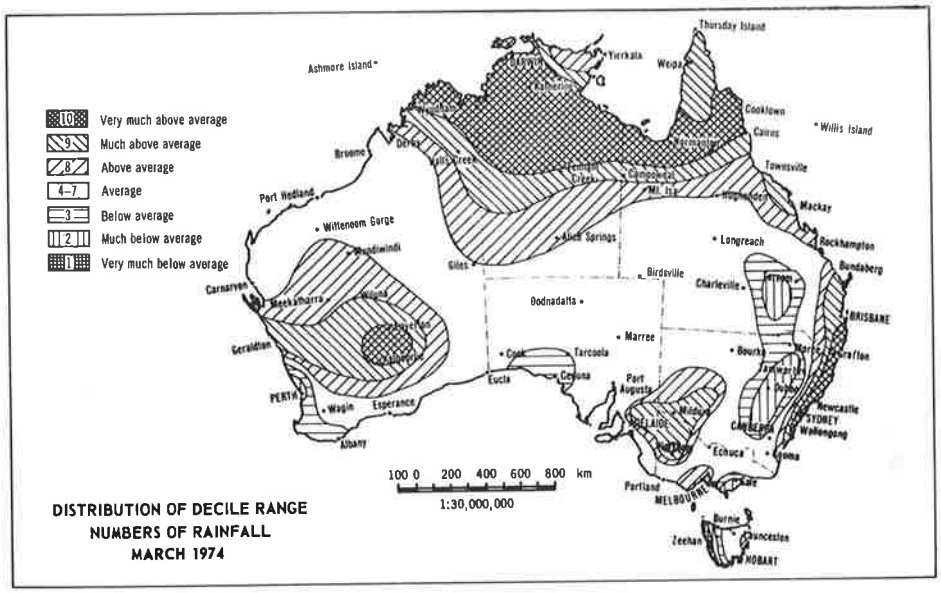

DISTRIBUTION OF DECILE RANGE NUMBERS OF RAINFALL MARCH 1974

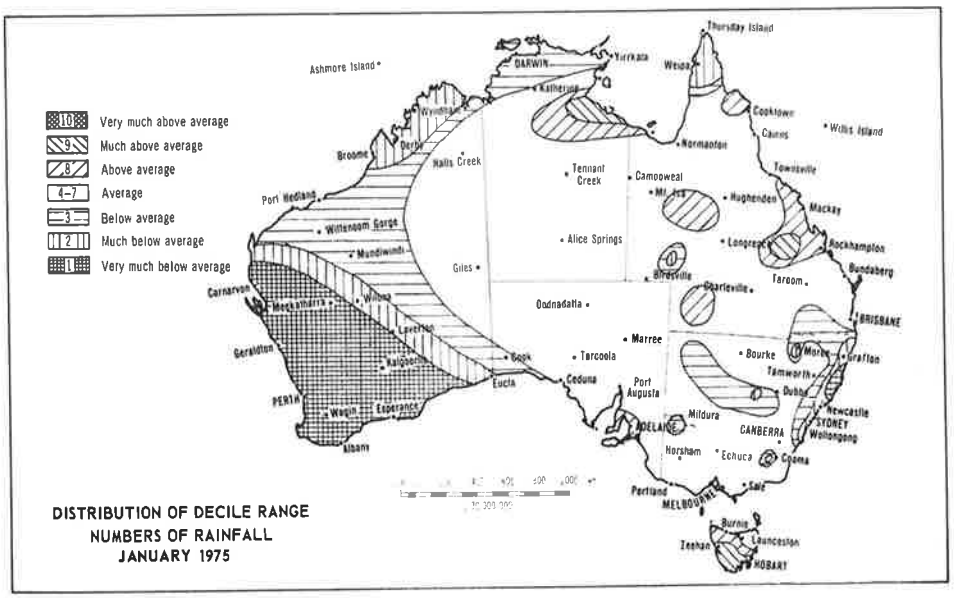
10 Very much above average
9 Much above average
8 Above average
4–7 Average
3 Below average
2 Much below average
1 Very much below average
Thursday Island
Ashmore Island
DARWIN
Tirrkata
Weipa
Katherine
Wyndham
Cooktown
Cairns
Willis Island
Normanton
Broome
Derby
Halls Creek
Townsville
Tennant Creek
Camooweal
Mt Isa
Hughenden
Mackay
Port Hedland
Alice Springs
Longreach
Rockhampton
Wittenoom Gorge
Mundiwindi
Giles
Birdsville
Bundaberg
Carnarvon
Charleville
Taroom
Oodnadatta
BRISBANE
Meekatharra
Wiluna
Laverton
Marree
Geraldton
Kalgoorlie
Cook
Tarcoola
Bourke
Grafton
Tamworth
Eucla
Ceduna
Port Augusta
Dubbo
PERTH
Wagin
Esperance
Mildura
Newcastle
SYDNEY
ADELAIDE
CANBERRA
Wollongong
Albany
Horsham
Echuca
Cooma
Portland
Sale
MELBOURNE
Burnie
Launceston
Zeehan
HOBART
DISTRIBUTION OF DECILE RANGE
NUMBERS OF RAINFALL
JANUARY 1975

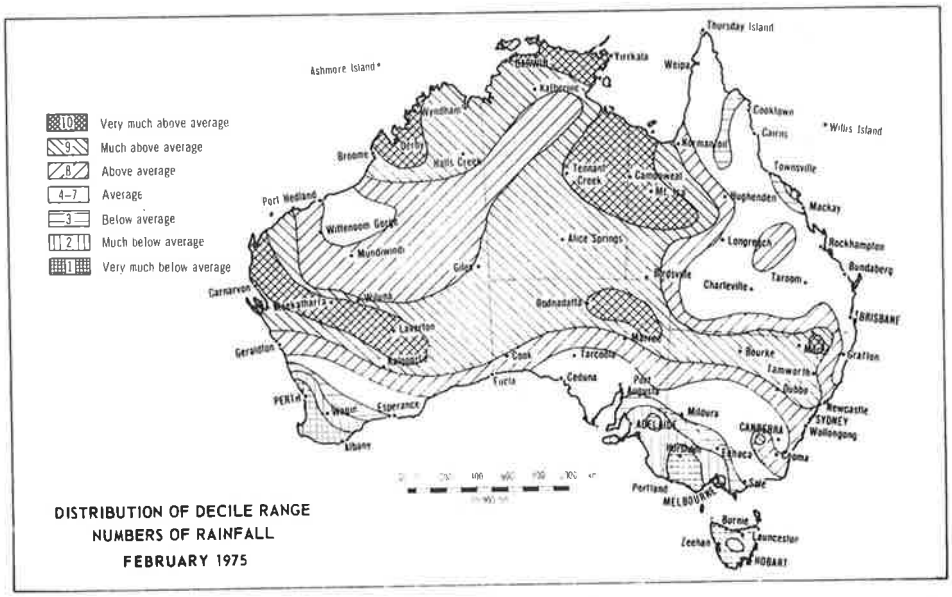
10 Very much above average
9 Much above average
8 Above average
4–7 Average
3 Below average
2 Much below average
1 Very much below average
Thursday Island
Ashmore Island
Tirrkata
Weipa
Cooktown
Cairns
Willis Island
Normanton
Broome
Derby
Halls Creek
Townsville
Tennant Creek
Camooweal
Mt Isa
Hughenden
Mackay
Port Hedland
Alice Springs
Longreach
Rockhampton
Wittenoom Gorge
Mundiwindi
Giles
Birdsville
Bundaberg
Carnarvon
Charleville
Taroom
Oodnadatta
BRISBANE
Meekatharra
Wiluna
Laverton
Marree
Geraldton
Kalgoorlie
Cook
Tarcoola
Bourke
Grafton
Tamworth
Eucla
Ceduna
Port Augusta
Dubbo
PERTH
Wagin
Esperance
Mildura
Newcastle
SYDNEY
ADELAIDE
CANBERRA
Wollongong
Albany
Horsham
Echuca
Cooma
Portland
Sale
MELBOURNE
Burnie
Launceston
Zeehan
HOBART
DISTRIBUTION OF DECILE RANGE
NUMBERS OF RAINFALL
FEBRUARY 1975

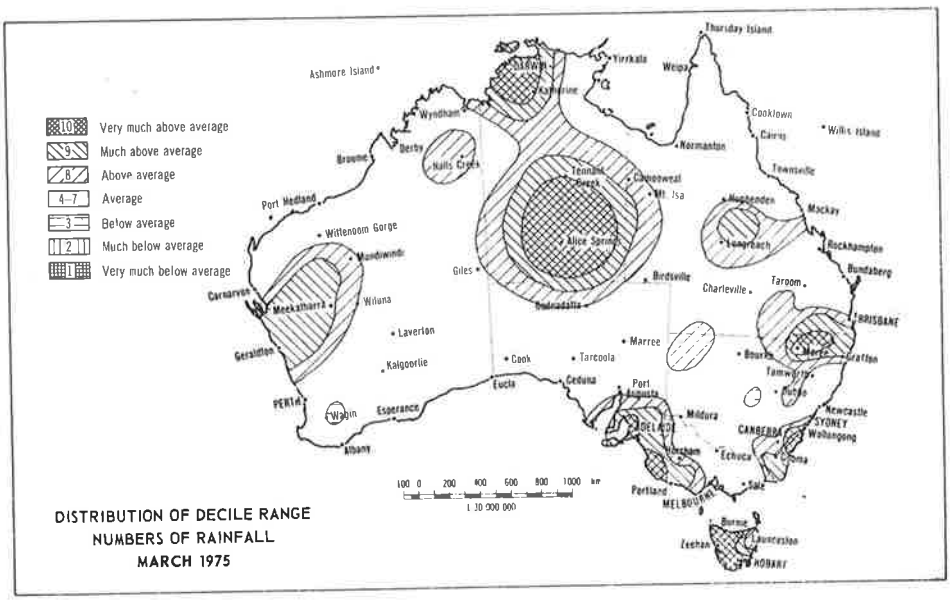
10 Very much above average
9 Much above average
8 Above average
4–7 Average
3 Below average
2 Much below average
1 Very much below average
Thursday Island
Ashmore Island
Tirrkata
Weipa
Cooktown
Cairns
Willis Island
Normanton
Broome
Derby
Halls Creek
Townsville
Tennant Creek
Camooweal
Mt Isa
Hughenden
Mackay
Port Hedland
Alice Springs
Longreach
Rockhampton
Wittenoom Gorge
Mundiwindi
Giles
Birdsville
Bundaberg
Carnarvon
Charleville
Taroom
Oodnadatta
BRISBANE
Meekatharra
Wiluna
Laverton
Marree
Geraldton
Kalgoorlie
Cook
Tarcoola
Bourke
Grafton
Tamworth
Eucla
Ceduna
Port Augusta
Dubbo
PERTH
Wagin
Esperance
Mildura
Newcastle
SYDNEY
ADELAIDE
CANBERRA
Wollongong
Albany
Horsham
Echuca
Cooma
Portland
Sale
MELBOURNE
Burnie
Launceston
Zeehan
HOBART
100 0 200 400 600 800 1000 km
1 : 20 000 000
DISTRIBUTION OF DECILE RANGE
NUMBERS OF RAINFALL
MARCH 1975

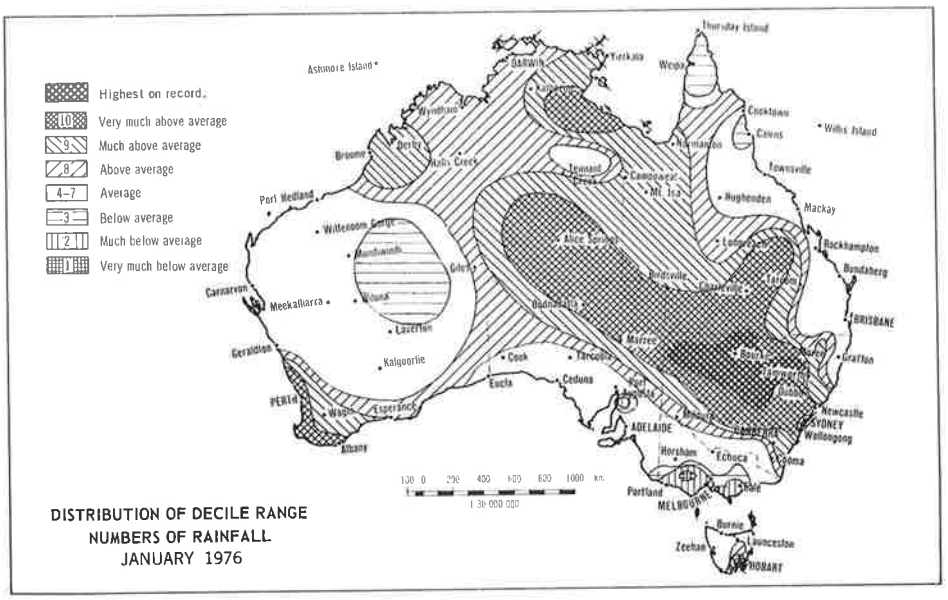

DISTRIBUTION OF DECILE RANGE
NUMBERS OF RAINFALL
JANUARY 1976

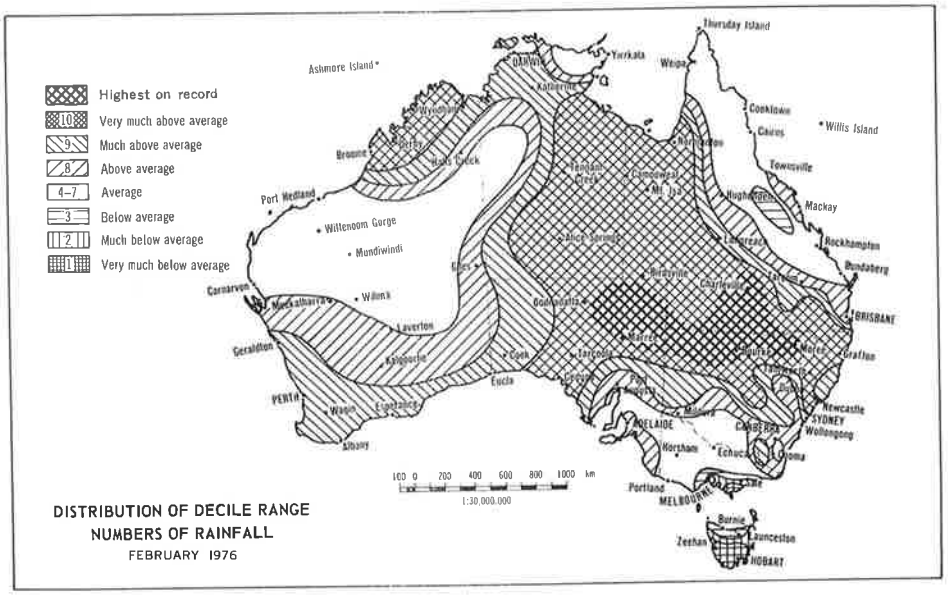

DISTRIBUTION OF DECILE RANGE
NUMBERS OF RAINFALL
FEBRUARY 1976

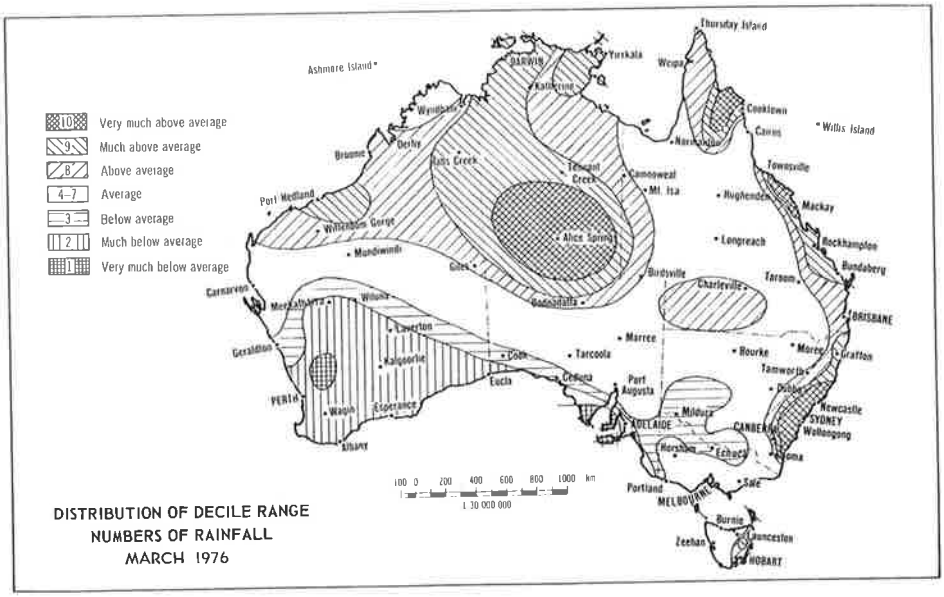

DISTRIBUTION OF DECILE RANGE
NUMBERS OF RAINFALL
MARCH 1976

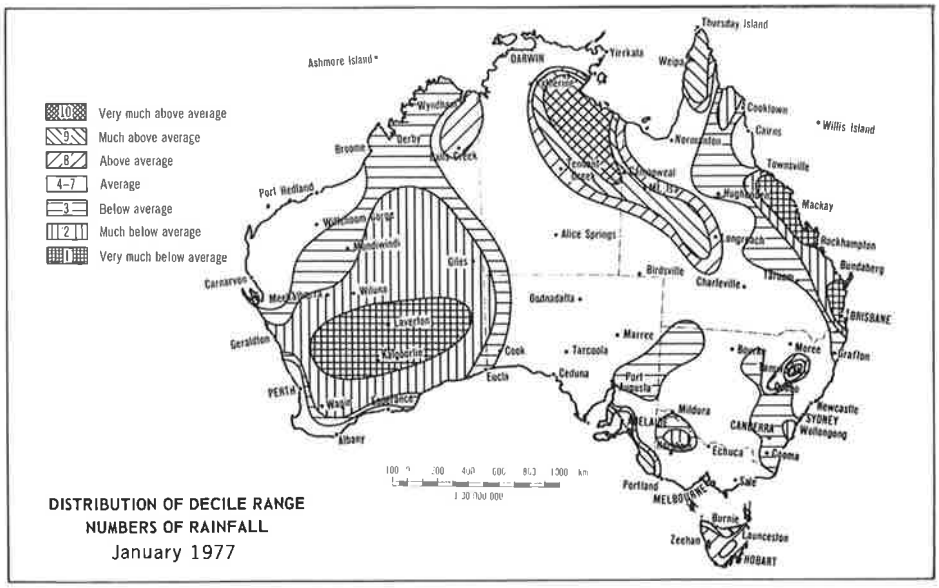
10 Very much above average
9 Much above average
8 Above average
4–7 Average
3 Below average
2 Much below average
1 Very much below average
Thursday Island
Ashmore Island
DARWIN
Yirrkala
Weipa
Wyndham
Derby
Broome
Halls Creek
Port Hedland
Wittenoom Gorge
Mundiwindi
Carnarvon
Meekatharra
Wiluna
Gascoyne Junction
Laverton
Kalgoorlie
Geraldton
PERTH
Wagin
Esperance
Albany
Alice Springs
Giles
Birdsville
Charleville
Oodnadatta
Cook
Tarcoola
Eucla
Ceduna
Port Augusta
Maree
Normanton
Cooktown
Cairns
Willis Island
Townsville
Hughenden
Mackay
Rockhampton
Longreach
Bundaberg
Taroom
BRISBANE
Bourke
Moree
Grafton
Mildura
ADELAIDE
CANBERRA
Newcastle
SYDNEY
Wollongong
Echuca
Portland
MELBOURNE
Sale
Burnie
Launceston
Zeehan
HOBART
DISTRIBUTION OF DECILE RANGE
NUMBERS OF RAINFALL
January 1977

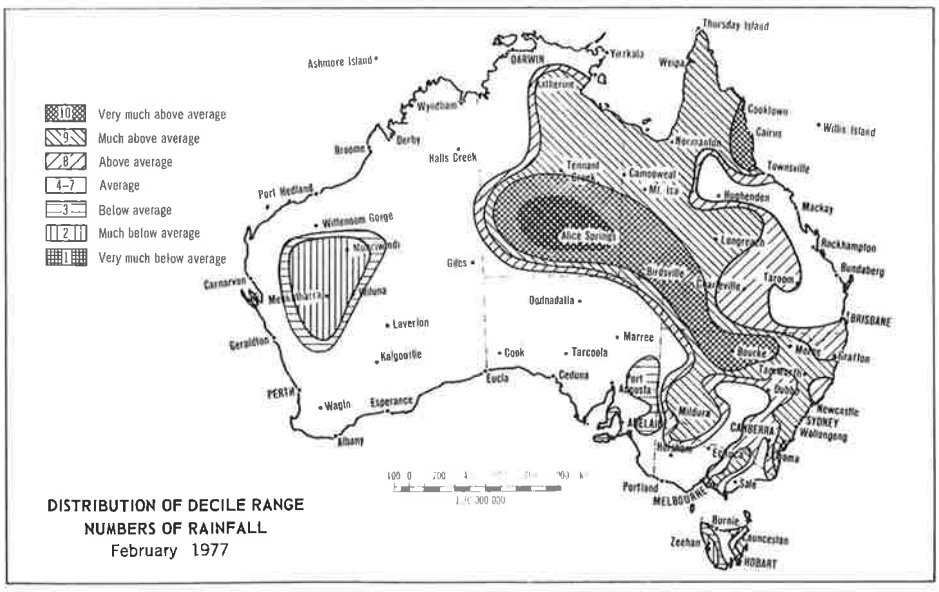
10 Very much above average
9 Much above average
8 Above average
4–7 Average
3 Below average
2 Much below average
1 Very much below average
Thursday Island
Ashmore Island
DARWIN
Yirrkala
Weipa
Wyndham
Derby
Broome
Halls Creek
Port Hedland
Wittenoom Gorge
Mundiwindi
Carnarvon
Meekatharra
Wiluna
Laverton
Kalgoorlie
Geraldton
PERTH
Wagin
Esperance
Albany
Alice Springs
Giles
Birdsville
Charleville
Oodnadatta
Cook
Tarcoola
Eucla
Ceduna
Port Augusta
Marree
Normanton
Cooktown
Cairns
Willis Island
Townsville
Hughenden
Mackay
Rockhampton
Longreach
Bundaberg
Taroom
BRISBANE
Bourke
Moree
Grafton
Mildura
ADELAIDE
CANBERRA
Newcastle
SYDNEY
Wollongong
Portland
MELBOURNE
Sale
Burnie
Launceston
Zeehan
HOBART
DISTRIBUTION OF DECILE RANGE
NUMBERS OF RAINFALL
February 1977

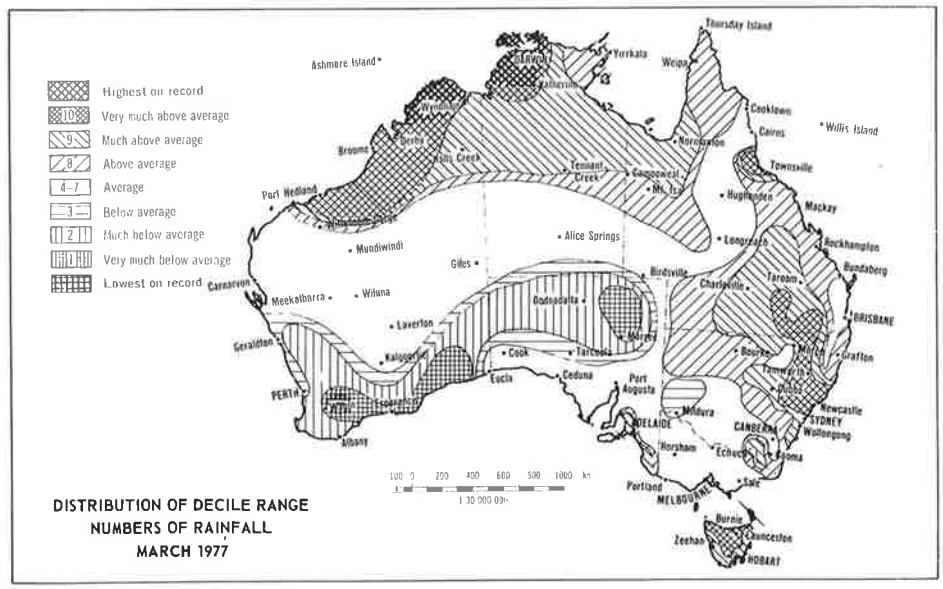
Highest on record
10 Very much above average
9 Much above average
8 Above average
4–7 Average
3 Below average
2 Much below average
1 Very much below average
Lowest on record
Thursday Island
Ashmore Island
DARWIN
Yirrkala
Weipa
Wyndham
Derby
Broome
Halls Creek
Port Hedland
Wittenoom Gorge
Mundiwindi
Carnarvon
Meekatharra
Wiluna
Laverton
Kalgoorlie
Geraldton
PERTH
Esperance
Albany
Alice Springs
Giles
Birdsville
Charleville
Oodnadatta
Cook
Tarcoola
Eucla
Ceduna
Port Augusta
Maree
Normanton
Cooktown
Cairns
Willis Island
Townsville
Hughenden
Mackay
Rockhampton
Longreach
Bundaberg
Taroom
BRISBANE
Bourke
Moree
Grafton
Mildura
ADELAIDE
CANBERRA
Newcastle
SYDNEY
Wollongong
Horsham
Portland
MELBOURNE
Sale
Burnie
Launceston
Zeehan
HOBART
DISTRIBUTION OF DECILE RANGE
NUMBERS OF RAINFALL
MARCH 1977

in March. Even so, the monsoon regime experiences distinctive 'break-like' periods, particularly at temporal scales of less than a month (Troup, 1961; Webster *et. al.*, 1977; McBride, 1981; Webster, 1981 b). Thus the variations and persistence of circulation and rainfall patterns must be seen to represent broad time-average conditions in the 1973-77 period.

This analysis also suggests that extremes in the Australasian monsoon are linked with broad, hemispheric circulation changes and interhemispheric interactions. In this regard, the position and intensity of the quasi-permanent North Pacific anticyclone and the more variable Northern Hemisphere Near Equatorial Trough (NET_{NH}) appear to have some influence on Southern Hemisphere systems.

In response to the equatorially-converging Northern Hemisphere northeast trade winds (as reflected in the high OLR distributions in Heddinghaus and Krueger, 1981), the NET_{NH} in Figures 7, 8 and 9 generally exhibits greater vigour in its eastern section which is located to the northwest of New Guinea. Having recurved into near-equatorial Southern Hemisphere regions, this flow is then westerly and probably contributes to the convergence field under changing coriolis deflection. In the wet summer periods (especially in the Januarys of 1974 and 1976) the western portion of the NET_{NH} (west of 115°E) intensifies, matching that in its eastern extremity. This action, at least at the 850 mb level, probably promotes slow cross-equatorial flow from more Asian sources into the Australasian region. In contrast, during the drier January of 1975 (Fig.12), the moderately wet (at least on the Australian east coast) February of 1973 (Fig.10), and the slightly wet March of 1977 (Fig.14), there is stronger circulation in the eastern section of the NET_{NH}. This is responsible for cross-equatorial flow across New Guinea and those areas immediately to the north-northeast of Australia. Yet, there are some grounds to suggest that, during certain periods of strong northeast monsoon activity, low-level Australian monsoon circulation is maintained by processes located almost entirely within the Southern Hemisphere. Thus despite the relatively

stronger western portion of the NET_{NH} in the Januarys of 1974 and 1976, the massive + $\bar{\psi}_{850}$ centre(s) over Australia draws much of its mass and moisture from Southern Hemisphere sources.

The influence of the North Pacific anticyclone is more difficult to interpret. However, the extremely anomalous flow pattern in January 1974 indicates that this anticyclone may respond to broad-scale interactions. Such interactions are manifested by Hadley and east-west teleconnections which form from vertical cells originating in the monsoon foci of South East Asia. Research which has analysed the Southern Oscillation/Walker Circulation (SO/WC) teleconnection, the El Niño phenomenon, and Pacific Dry Zone (PDZ) rainfall extremes, indicates that variations in the strength of the Pacific trade wind system may be a response to, and/or may initiate changes in, the SO/WC (Quinn and Burt, 1970, 1972; Flöhn, 1973; Quinn, 1974; Flöhn and Fleer, 1975; Wyrtki, 1975, 1977, 1979; Hickey, 1975; Ramage, 1975; Wyrtki and Myers, 1976; Barnett, 1977 a,b, 1981; Quinn *et. al.*, 1978; Julian and Chervin, 1978; Reiter, 1978; Angell, 1981; Enfield, 1981; Ramage and Hori, 1981).

It would seem that the El Niño cycles of 1972-73, 1975 and 1976 are reflected in the strength of circulation in the eastern extremity of the NET_{NH} and perhaps in the North Pacific anticyclone (NPA). Wyrtki (1975, 1977) indicates that the termination of the 1972-73 El Niño was heralded by an increase in equatorial Pacific trade wind activity. This activity also appears to coincide with the very strong circulation about the eastern section of the NET_{NH} and the NPA in February 1973. Ramage and Hori (1981) suggest that this El Niño was at its strongest in December and January, while Ramage (1975) states that the phenomenon had terminated in March 1973 (although Figs.8 and 9 suggest that February is more likely). Evidence of trade wind and NET_{NH} changes, which may have occurred at either the beginning or end of the very weak El Niño of early 1975, are harder to find. In this period, the eastern section of the NET_{NH} shows a marked weakening in February (Fig.8), followed by slight recovery in March (Fig.9), although

coincidence is not found in the NPA which is strong throughout both months. This concurs with Arkin (1982) and Keen (1982) who observe that changes in upper- and lower-level circulation features indicative of El Niño periods were absent or weak in the equatorial Pacific in 1975. Wyrtki *et. al.* (1976) also note that oceanographic cruise observations found evidence for El Niño development in February and March and cessation by April and May of 1975 (also evident in Liebmann and Hartmann, 1982). A moderate El Niño in mid 1976 was heralded by weakening equatorial trade winds in late 1975 and early 1976, while its termination coincided with strengthening trade winds in early 1977 (Wyrtki, 1979). Again, the best evidence for trade wind weakening comes from the $\bar{\psi}_{850}$ fields, with February 1976 showing a marked drop in NET_{NH} strength from January values (Figs.7 and 8). Distinct cloudiness changes indicative of PDZ rainfall do not occur in the western-central Pacific until the Southern Hemisphere winter of 1976 (Heddinghaus and Krueger, 1981; Liebmann and Hartmann, 1982). This cycle was apparently completed by an increase in trade wind strength in the entire 1977 sequence of Southern Hemisphere summer months (Figs.7,8 and 9) (Enfield, 1981).

Although it is not evident in the map sequences (Figs.7,8 and 9) because the analysis is terminated at 180°E, the South Pacific quasi-permanent anticyclone is known to vary in location and strength (Quinn, 1974; Ramage, 1975). It is possible that the western extremity of this cell periodically undergoes expansion into the eastern parts of Australia. Strong anticyclonicity is indicated over this part of the continent in the drier months of the sequence (namely, January 1973 and January 1975 in Fig.7). Such anticyclonic expansion, other than that caused by the seasonal shift beginning around March, could effectively squeeze the monsoon trough out of the continent. In fact, this effect may be the result of variations in South Pacific circulation, Indian Ocean anticyclonicity, and hemispherical changes in teleconnections (Pittock, 1973, 1975; Dyer, 1979).

Although being a dynamically-induced component of horizontal circulation systems, regions of divergent and convergent motion are usually an order of magnitude less than horizontal rotational fields (Haltiner, 1971:57). As shown by Appendix 3, the velocity potential fields used in this study are determined from divergence distributions. Although not entirely coincidental, positive velocity potential maxima approximate regions of convergence while negative velocity potential maxima approximate regions of divergence (Krishnamurti *et. al.*, 1973). Thus velocity potential maxima illustrate the broad-scale pattern of divergent and convergent motion.

The map sequences shown in Figures 15, 16 and 17 depict velocity potential fields over the regional domain in the months of January, February and March 1973-77. Generally, these figures indicate that velocity potential fields at low levels are not distributed about circulation features in the same manner as they are at upper levels (see later discussion of Figs.21,22 and 23). With closed, low-level + $\bar{\psi}_{850}$ there is generally convergence (+ $\bar{\chi}_{850}$) to the east and divergence (- $\bar{\chi}_{850}$) to the west on the equatorward side of these systems. The major $\bar{\chi}_{850}$ maxima tend to occur in the near-equatorial zone, extending on occasions to about 10°N and 10°S latitude. They seem to exhibit a degree of variability which is directly related to large-scale teleconnection fluctuations. These 'centres of action' are the broad-scale, low-level moisture and latent heat sources which, when coupled with upper-level divergent maxima ($\bar{\chi}_{200}$ minima) (Figs.21,22 and 23), fuel the teleconnection extensions. It would seem that these $\bar{\chi}_{850}$ maxima are analogous with the regions of time-averaged moisture convergence and thus condensational heating sources which are considered by Cornejo-Garrido and Stone (1977) and Ramage and Hori (1981) to be the prime driving force for the Walker Circulation.

During the 1973 summer (Figs.15,16 and 17), low-level $\bar{\chi}_{850}$ maxima appear in the near-equatorial region around 160°E. These centres seem to

Figure 15 Monthly mean 850 mb velocity potential fields in units of 10^6 m^2 s^{-1} at intervals of 2 units over the regional domain during January from 1973-77. The symbols / indicate the direction and magnitude of the divergent part of the wind, where a length of one grid interval equals 9.5 m s^{-1}.

Figure 16 Monthly mean 850 mb velocity potential fields in units of 10^6 m^2 s^{-1} at intervals of 2 units over the regional domain during February from 1973-77. The symbols / indicate the direction and magnitude of the divergent part of the wind, where a length of one grid interval equals 9.5 m s^{-1}.

Figure 17 Monthly mean 850 mb velocity potential fields in units of 10^6 m^2 s^{-1} at intervals of 2 units over the regional domain during March from 1973-77. The symbols / indicate the direction and magnitude of the divergent part of the wind, where a length of one grid interval equals 9.5 m s^{-1}.

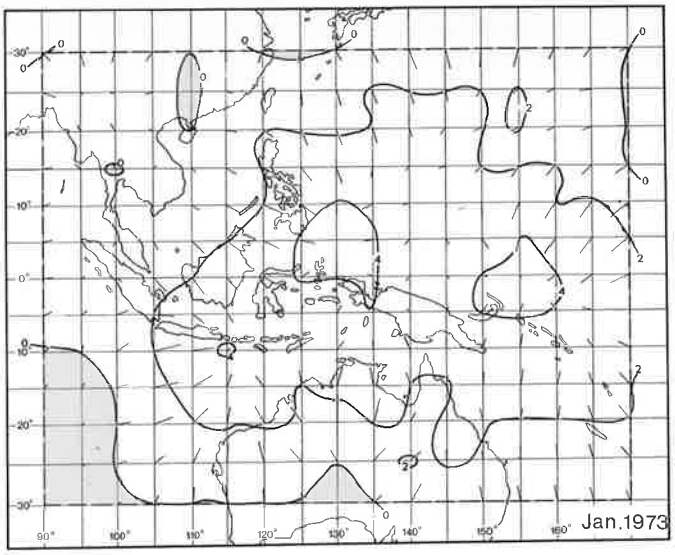

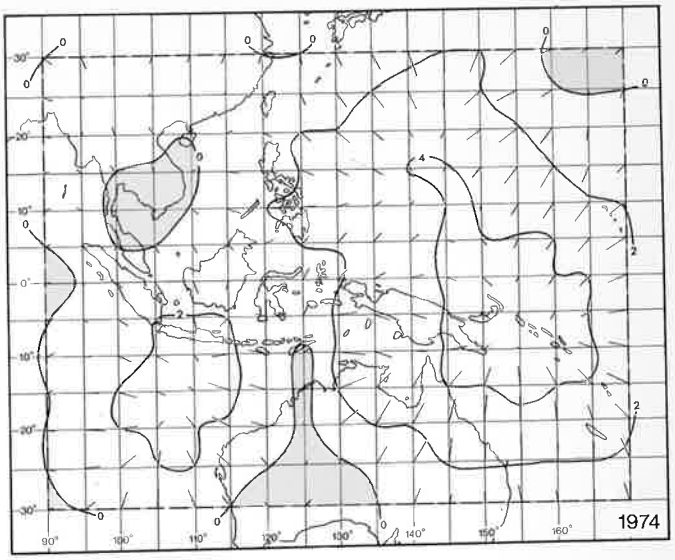

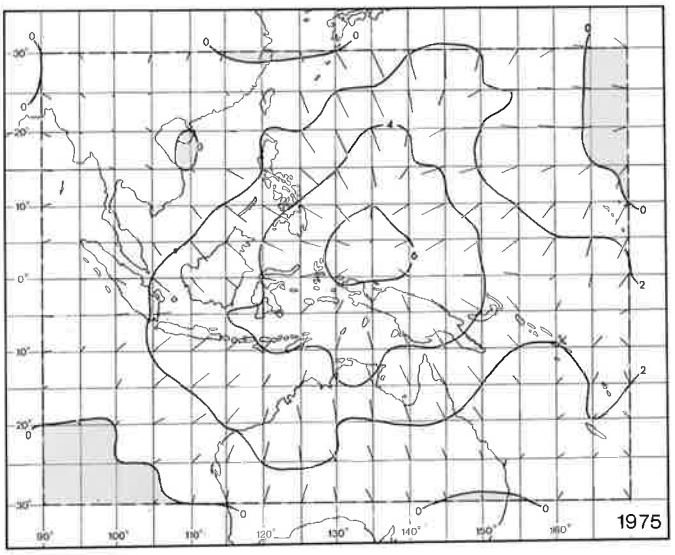

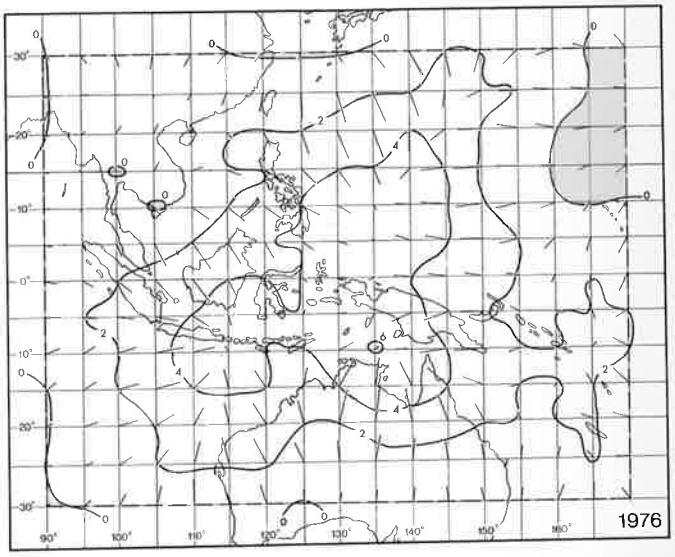

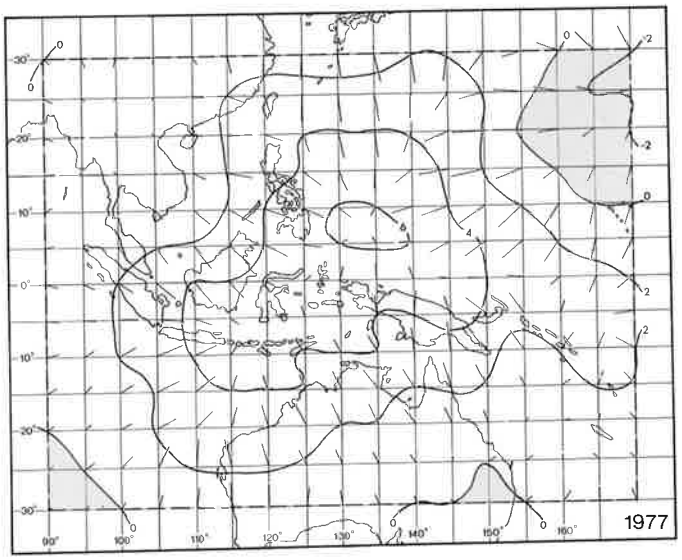

VELOCITY POTENTIAL

$\times 10^6$ m^2/sec

Jan 1973 - 1977

850 mb

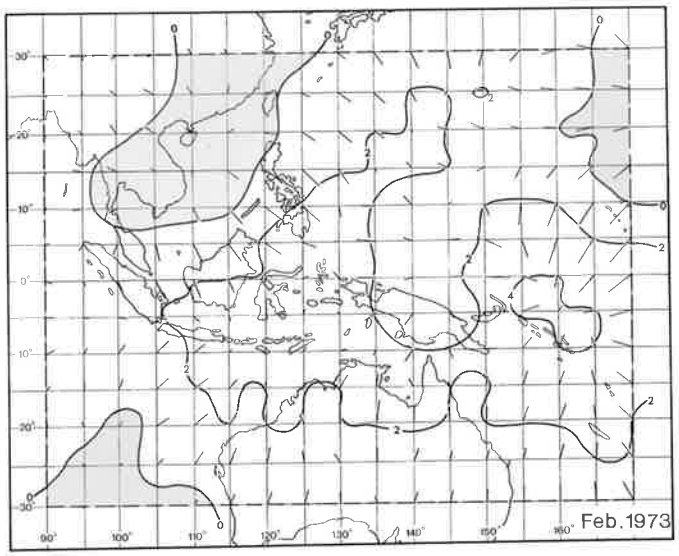

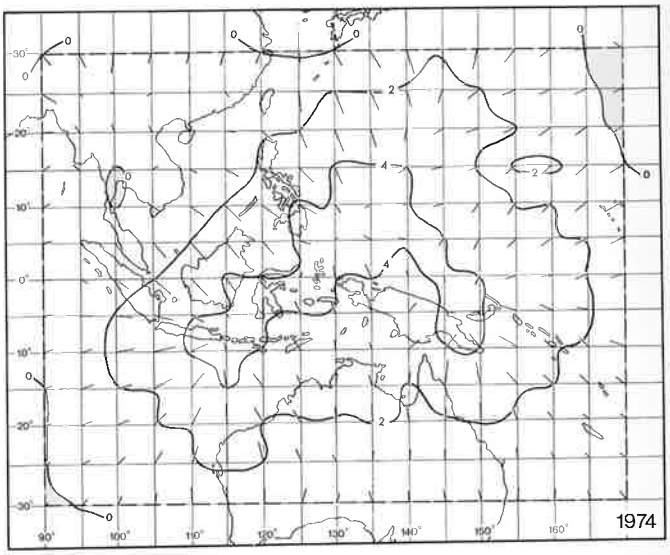

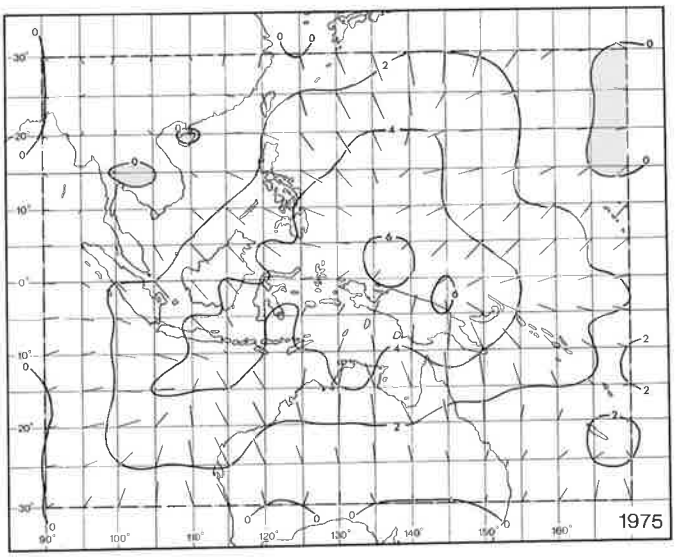

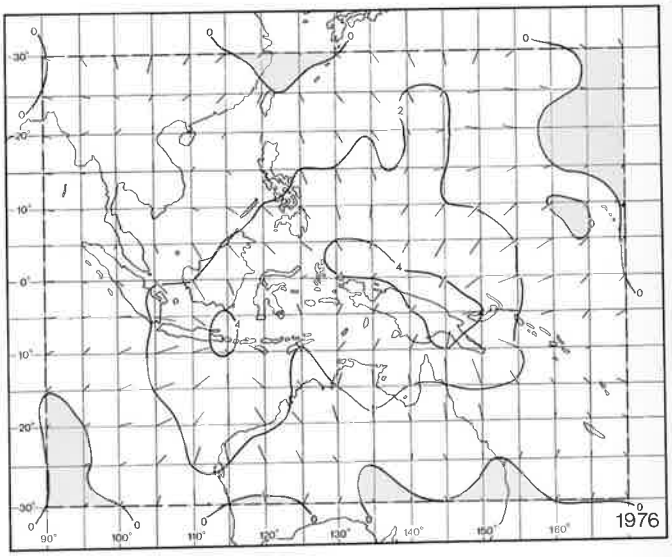

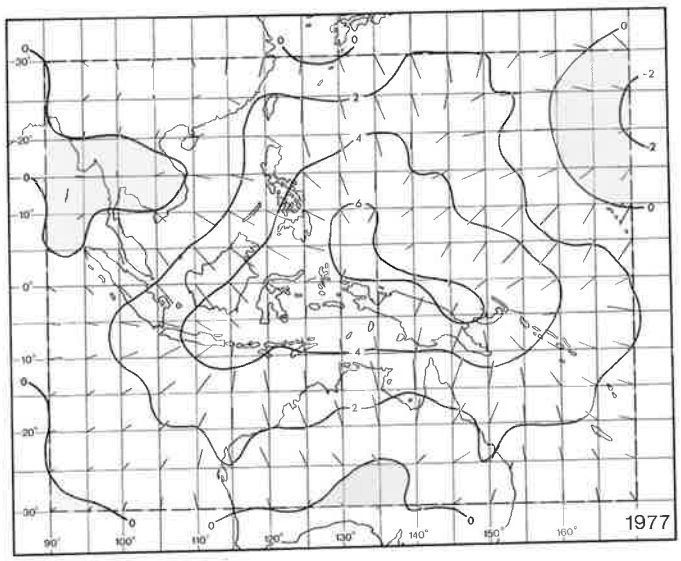

VELOCITY POTENTIAL

$\times 10^6$ m^2/sec

Feb 1973 - 1977

850 mb

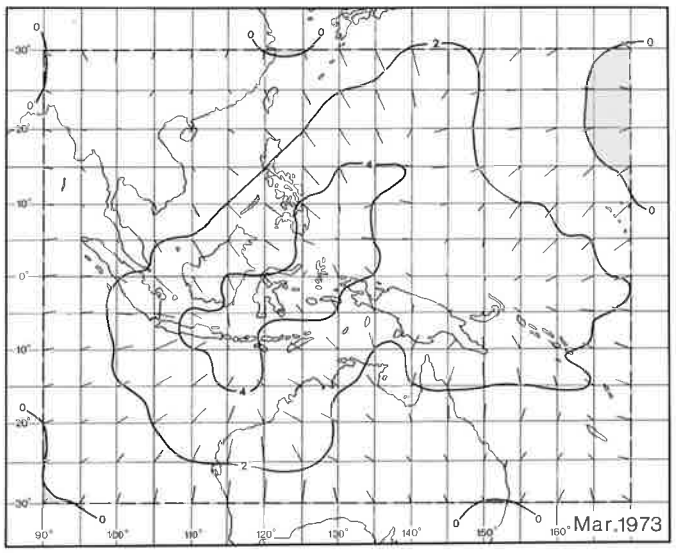

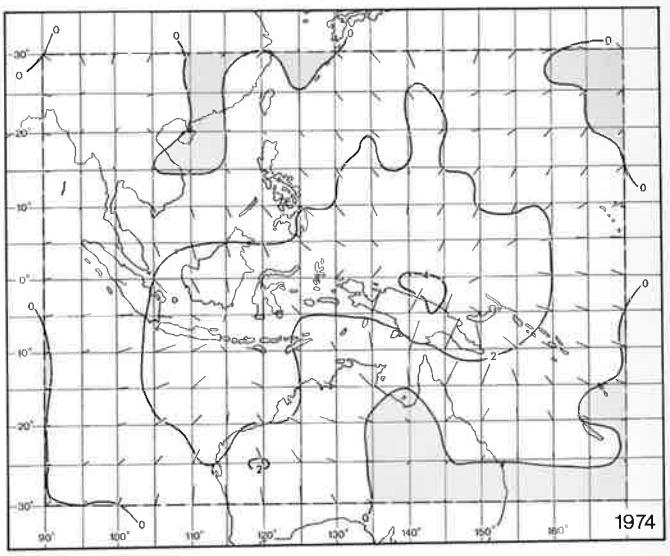

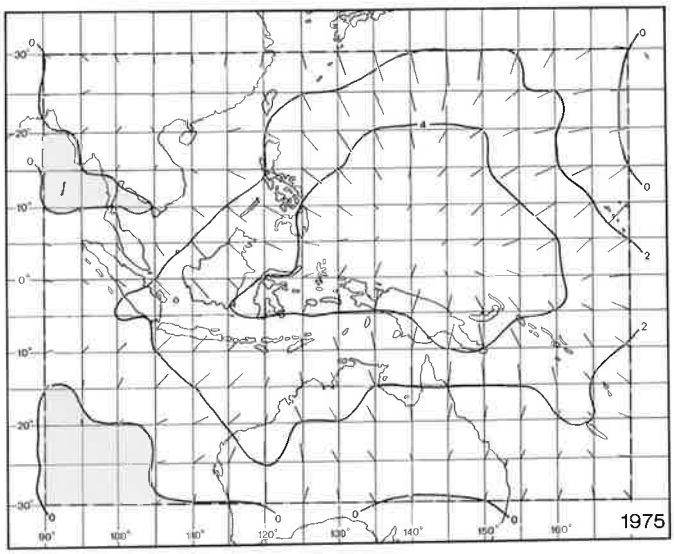

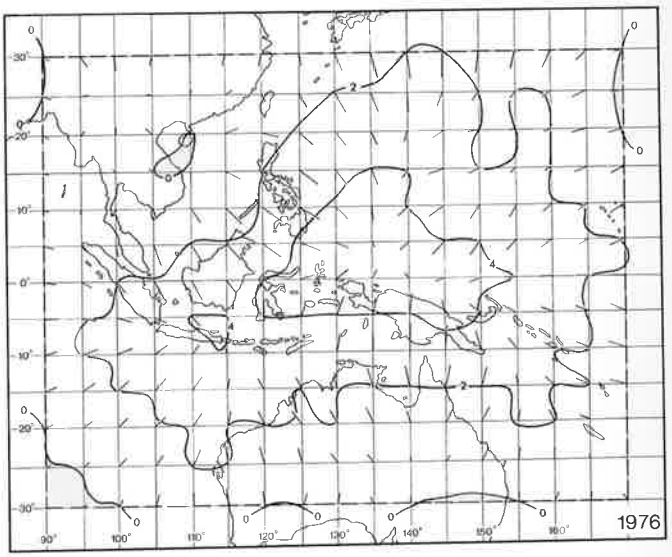

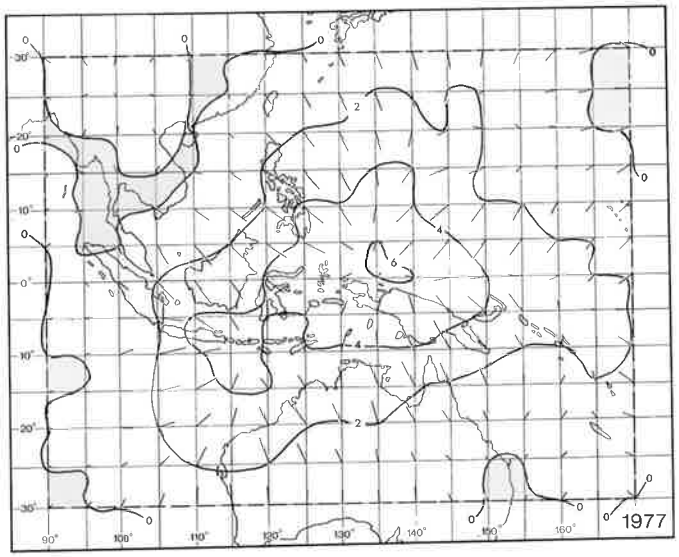

VELOCITY POTENTIAL

$\times 10^6$ m^2/sec

Mar 1973 - 1977

850 mb

result from convergence induced by the strong circulation ($-\bar{\psi}_{850}$) in the eastern section of the NET_{NH} and consequently, from a peak in the Pacific northeast trade wind regime.

In very wet summer periods (e.g. 1974 and 1976) low-level velocity potential maxima with strong ascending motion intrude into the Australian continent. In January 1974 (Fig.15) there are two $\bar{\chi}_{850}$ maxima of opposite sign affecting the Australian continent. The low-level impetus for the extreme rainfall at this time comes from convergence in that section of the $\bar{\chi}_{850}$ maxima (shown by the size and orientation of the symbol (/) in January 1974) encompassing much of Queensland and the Northern Territory. The summer of 1973-74 is notable for above average rainfall across northern Australia (Figs.10 and 11) and subsequently for the most documented flooding of the Lake Eyre salt pan (centred around 28°30'S, 137°15'E) this century.

In the relatively drier summers of 1975 and 1977, $\bar{\chi}_{850}$ maxima appear to be strong and displaced somewhat to the north of the equator. This pattern indicates that the NET_{NH} is enhanced and systems in general are displaced into the Northern Hemisphere. Tanaka (1980, 1981) suggests that periods of strong monsoonal activity are characterized by two low-level Inter-Tropical Convergence Zones (ITCZs), while in weaker periods only one ITCZ forms. Although the notion of two ITCZs is disputed by Hubert *et. al.* (1969) and Gruber (1972), it would appear that major segments of the NET_{SH} weaken in a relatively dry Australian summer month, such as January 1975 (Fig.7), while the converse may be true for some sections of the NET_{NH} in wet Australian summer months (as shown in January 1974 and January 1976 in Fig.7).

The northwest - southeast oriented convergence band dipping out of the diagrams around 160°-170°E and 5°-15°S in January 1975, 1976 and 1977 in Figure 15, and the closely aligned NET_{SH} in Figure 7, may be more related to the South Pacific Convergence Zone (SPCZ) examined by Streten (1970, 1973, 1975), Trenberth (1976 a,b) and Musk (1976).

(ii) Monthly Mean 200 mb Streamfunction ($\bar{\psi}_{200}$) and Velocity Potential ($\bar{\chi}_{200}$) Fields

The 200 mb level is analysed because it highlights the position and magnitude of upper tropospheric features of the large-scale planetary flow.

The streamfunction sequence depicted in Figures 18, 19 and 20 shows the presence of quasi-permanent anticyclonic systems in the regions of Australia, the east Indian Ocean and the northwest Pacific. Zonal wind component isotachs are included to illustrate the location of jetstreams and jet-like flow in Southern Hemisphere summer and Northern Hemisphere winter situations. Strong jet maxima off Japan are a feature of the entire map sequence. However, sub-tropical jet maxima over southern Australia are more variable and since they are evident only in the Januarys of 1973 and 1975, and Marchs of 1973, 1975 and 1977, they may reflect changes in upper-level flow characteristic of monsoon onset (Troup, 1961; McBride, 1981) and cessation.

The major feature of this map sequence is the periodic change in the intensity and pattern of Australian upper-level anticyclonic flow. This is reflected by marked variability in the position and strength of $-\bar{\psi}_{200}$ features during January and February, as opposed to their persistently stronger central Australian locations during March. The latter may again be indicative of the termination of monsoon activity as the season draws to a close. In summer, upper-level $-\bar{\psi}_{200}$ maxima appear to be directly caused by the sensible and latent heat released into the upper atmosphere by strong continental heating and monsoonal convective activity (Ramage, 1971). Although not possessing any elevated heat source to anchor and develop strong, quasi-permanent upper anticyclonic features, the Australian continent seems to produce a distinctive, although variable, upper anticyclonic pattern.

For much of the 1973 summer, the $\bar{\psi}_{200}$ pattern shows a strong, distinctly cellular $-\bar{\psi}_{200}$ centre over the western portion of the Australian continent. January 1973 also contains the northern edge of a sub-tropical jet maximum in this western area (peak at 30°S, 115°E). The month of January 1974,

Figure 18 Monthly mean 200 mb streamfunction fields in units of 10^6 m^2 s^{-1} at intervals of 5 units over the regional domain during January from 1973-77. Heavy dashed lines indicate monthly mean zonal wind isotachs in m s^{-1}.

Figure 19 Monthly mean 200 mb streamfunction fields in units of 10^6 m^2 s^{-1} at intervals of 5 units over the regional domain during February from 1973-77. Heavy dashed lines indicate monthly mean zonal wind isotachs in m s^{-1}.

Figure 20 Monthly mean 200 mb streamfunction fields in units of 10^6 m^2 s^{-1} at intervals of 5 units over the regional domain during March from 1973-77. Heavy dashed lines indicate monthly mean zonal wind isotachs in m s^{-1}.

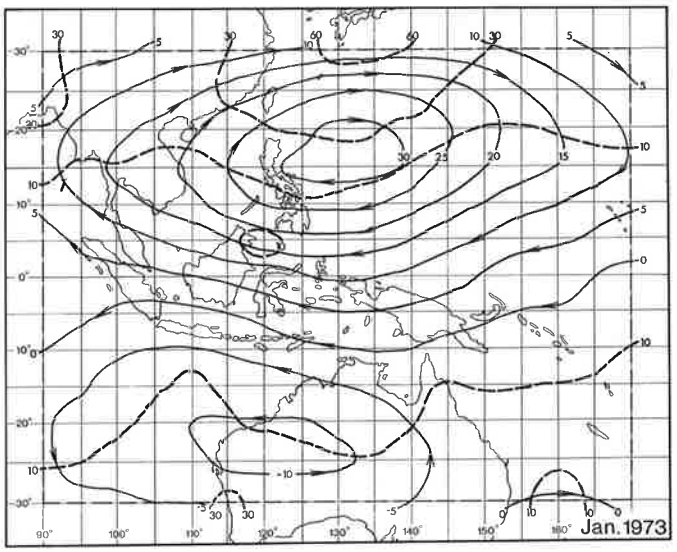

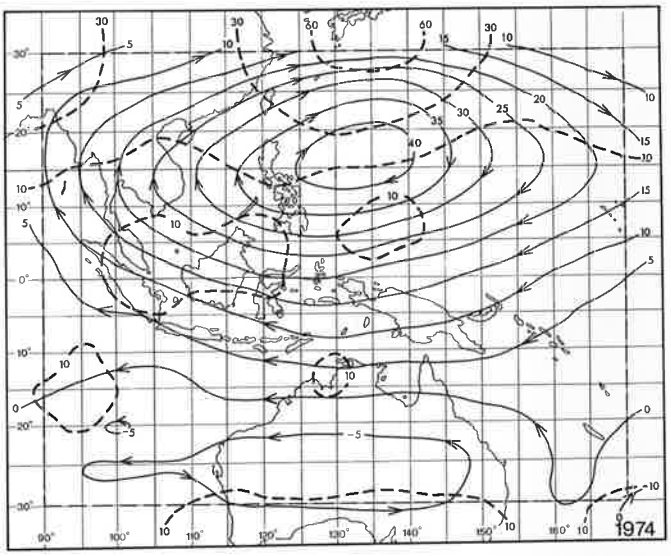

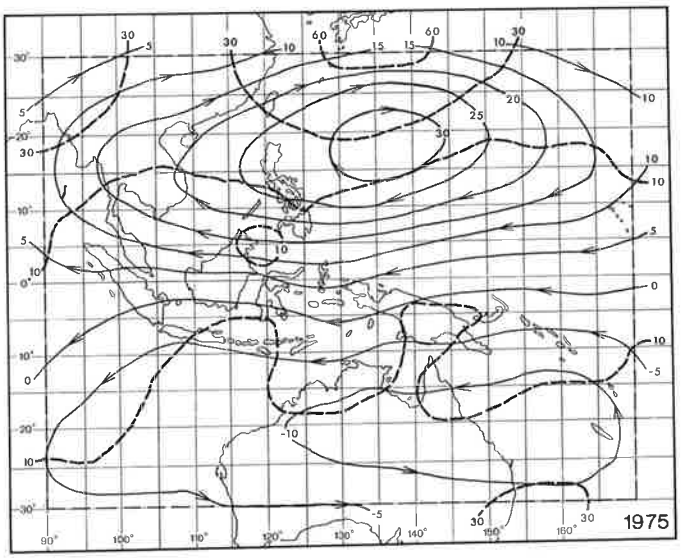

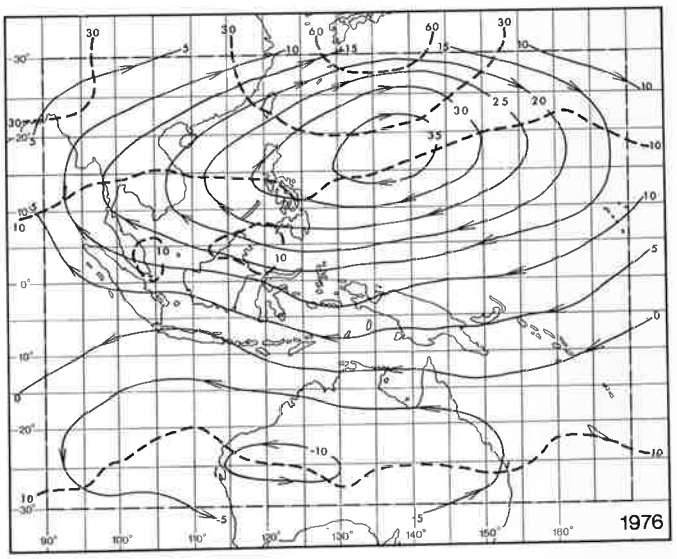

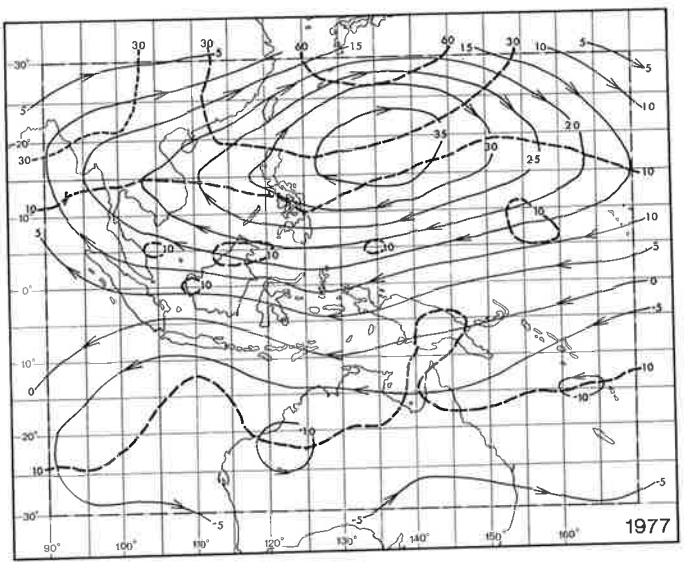

STREAMFUNCTION

$\times 10^6$ m^2/sec

Jan 1973 - 1977

200 mb

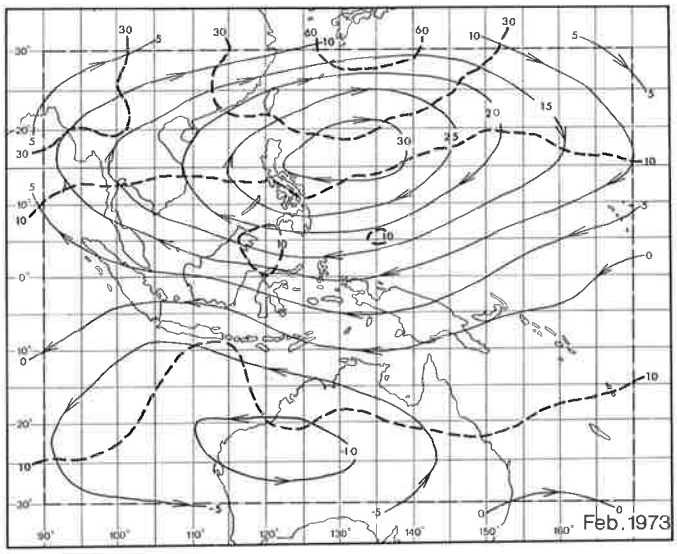

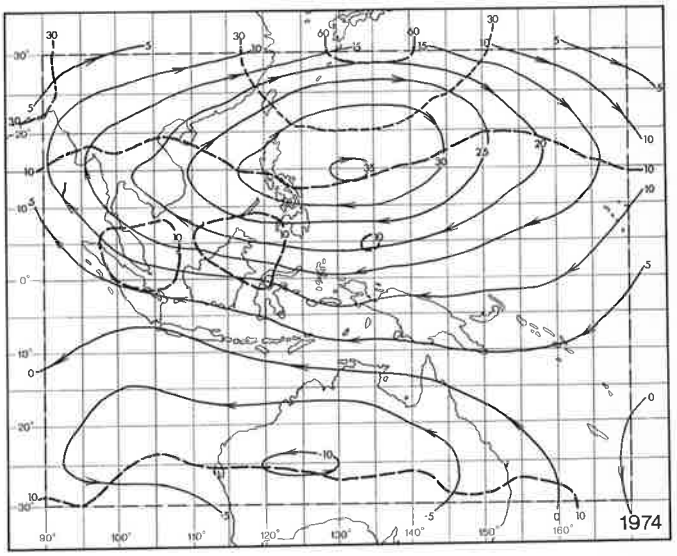

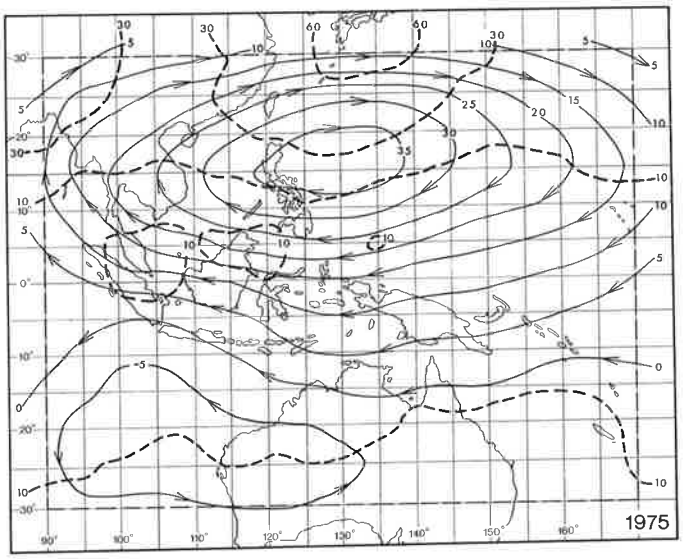

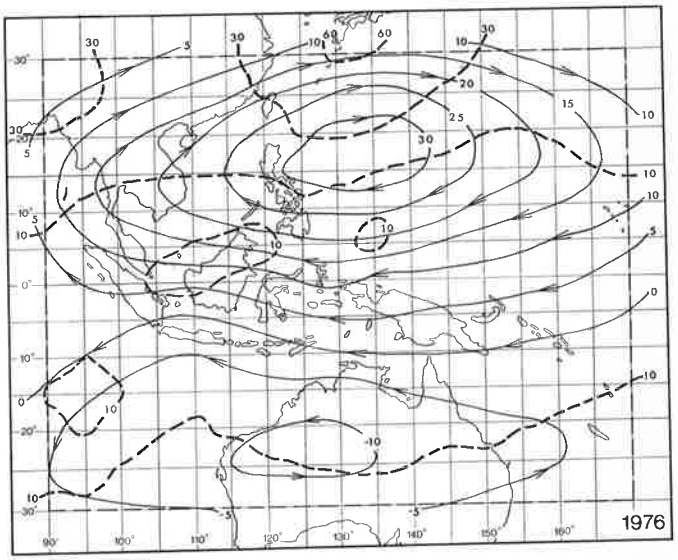

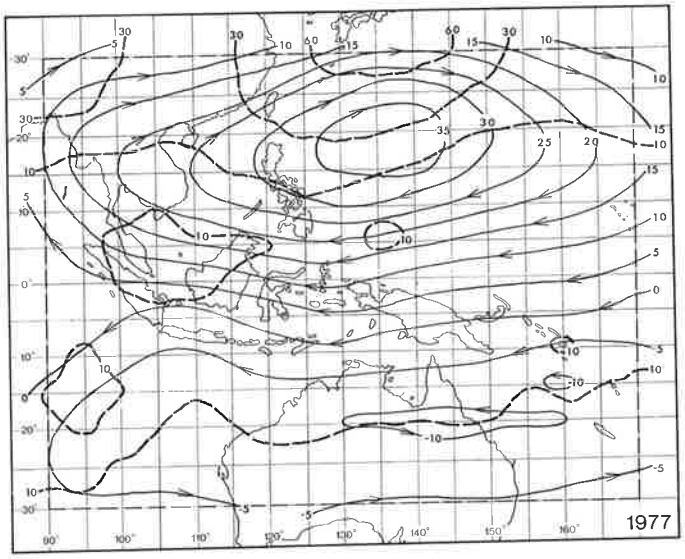

STREAMFUNCTION

$\times 10^6$ m^2/sec

Feb 1973 - 1977

200 mb

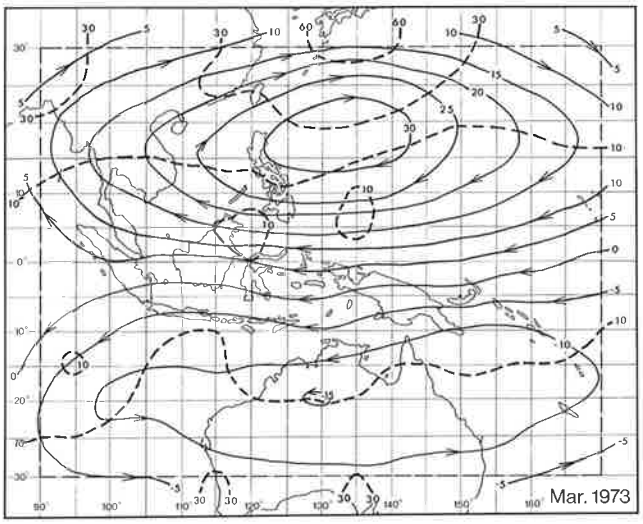

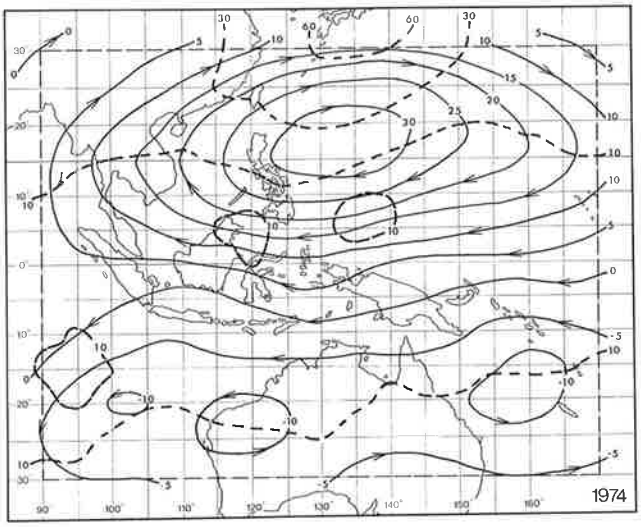

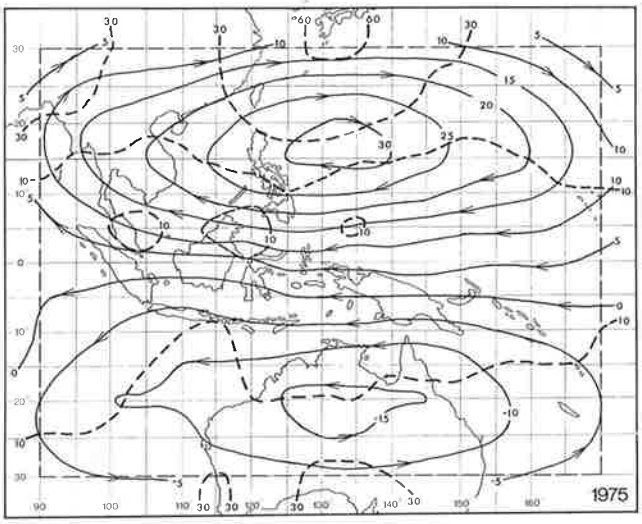

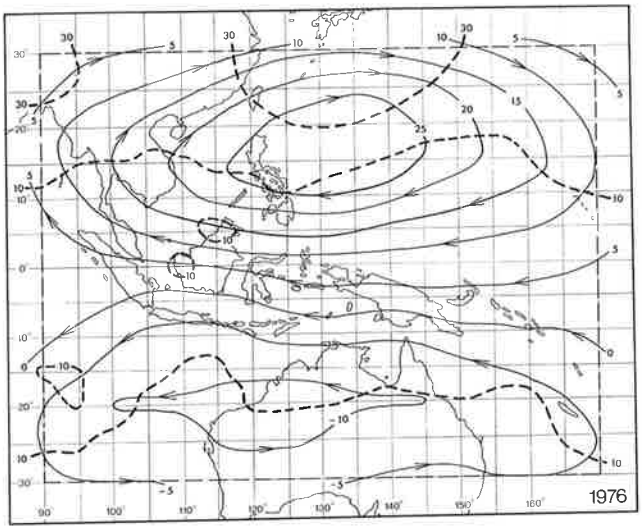

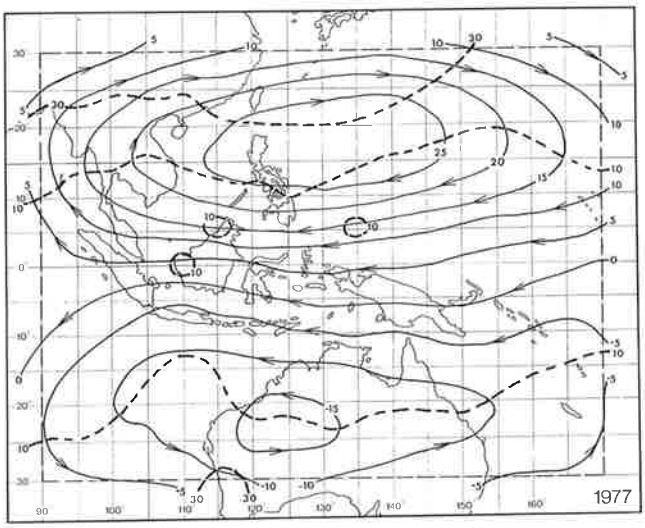

STREAMFUNCTION

$\times 10^6$ m^2/sec

Mar 1973 - 1977

200 mb

coinciding with the extreme Australian summer flooding period, is the most anomalous shown. Australian anticyclonicity is weak, with a cellular arrangement spread out over the broad expanse of the continent. In the 1974 summer months, the isotach field shows no sub-tropical jetstream maxima, while during January, the major jet-like flow has an easterly maximum in the region of Darwin. January 1975 provides another situation where the cell is very strong and broad but displaced to the eastern areas of Australia. This summer period also shows a major intraseasonal swing in the location and strength of the cell, being in a strong easterly position in January, weaker and to the west in February, and strong over the centre of the continent by March. Such variability suggests that changes in continental heat, radiation or convective processes may influence the atmosphere on relatively short time scales.

Although displaced slightly to the west in 1976, the anticyclonic cell still covers much of the continent. However, $-\bar{\psi}_{200}$ is somewhat greater than in the other major wet season of 1974. Thus during the extremely wet months of 1974 and 1976, the anticyclonic pattern is one of relatively weaker, more southerly-displaced centres over the continent than in the other drier months in the 1973-77 period. On the other hand, the relatively dry January of 1977 is dominated by a broad belt of anticyclonicity located across the entire domain south of 10°S and $-\bar{\psi}_{200}$ maxima over the northwest of the continent and out to the northeast over the New Hebrides. There is little change in this pattern during February 1977, with only an eastward shift in $-\bar{\psi}_{200}$ maxima over Australia.

It could be argued that large amounts of latent heat, released into the upper atmosphere by the deep convection in 1974 and 1976, would have contributed to strong $-\bar{\psi}_{200}$. However, this is not evident in the anti-cyclonic circulation regime during the 1974 summer. One possible conclusion is that horizontal processes aloft were acting to remove this liberated heat. Ramage (1971:234) suggests that mechanisms such as strong vertical tele-connection circulations could act rapidly to remove latent heat in these

circumstances. It is suggested that teleconnections, particularly the strong SO/WC in 1974, performed this function. Interestingly, the 200 mb temperature field over inland Australia was 2° to 3°C warmer than average in January 1974 but had returned to near average values by February 1974.

It seems that the position and strength of upper-level - $\bar{\psi}_{200}$ features have an important bearing on atmospheric flow, jetstream location and convective processes. The Northern Hemisphere upper anticyclone seems to be involved in such interactions and probably has a direct effect on the nature of upper-level divergence fields. This is certainly true on an interannual basis when the anticyclone tends to be stronger in January and February than in March. In the wetter months, this anticyclonic cell appears to expand and strengthen (as in January 1974) at the expense of its Southern Hemisphere counterpart. Such a process tends to coincide with the previous observation of a weaker, southerly-displaced anticyclonic circulation over Australia in the wet summer months.

The 200 mb velocity potential fields shown in Figures 21, 22 and 23 provide further evidence of the variability of upper-level circulation. A negative velocity potential (- $\bar{\chi}_{200}$) predominates over the South East Asian/Indonesian sector, and illustrates the strong, divergent mass outflow associated with the vigorous convection during the northeast monsoon regime. The symbols (/) in Figures 21, 22 and 23 testify to the strength, direction and extent of the divergent motion emanating from this region.

The locations of coupled 200 mb divergent and 850 mb convergent maxima during the summers of 1975, 1976 and 1977 closely coincide with regions of remotely-sensed OLR minima during this period (Winston *et. al.*, 1979). According to Heddinghaus and Krueger (1981) this is to be expected since low radiation values are synonymous with low cloud-top temperatures and thus major convective zones. Around the convective maxima, parts of the upper-level divergent outflow may also be related to the large areas of tropical upper tropospheric-extended cloud decks noted by Webster and Stephens (1980)

Figure 21 Monthly mean 200 mb velocity potential fields in units of 10^6 m^2 s^{-1} at intervals of 1 unit over the regional domain during January from 1973-77. The symbols / indicate the direction and magnitude of the divergent part of the wind, where a length of one grid interval equals 9.5 m s^{-1}.

Figure 22 Monthly mean 200 mb velocity potential fields in units of 10^6 m^2 s^{-1} at intervals of 1 unit over the regional domain during February from 1973-77. The symbols / indicate the direction and magnitude of the divergent part of the wind, where a length of one grid interval equals 9.5 m s^{-1}.

Figure 23 Monthly mean 200 mb velocity potential fields in units of 10^6 m^2 s^{-1} at intervals of 1 unit over the regional domain during March from 1973-77. The symbols / indicate the direction and magnitude of the divergent part of the wind, where a length of one grid interval equals 9.5 m s^{-1}.

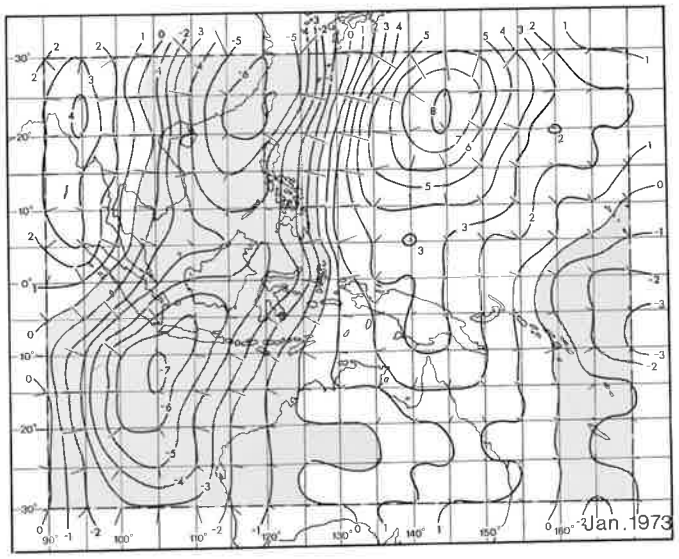

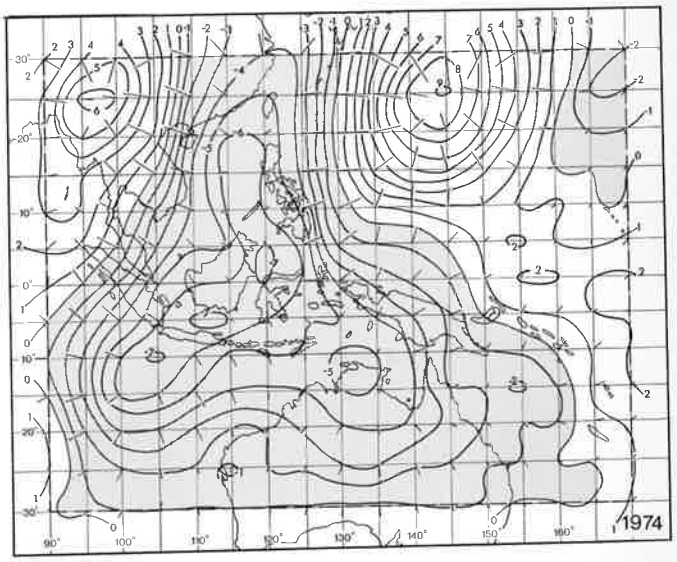

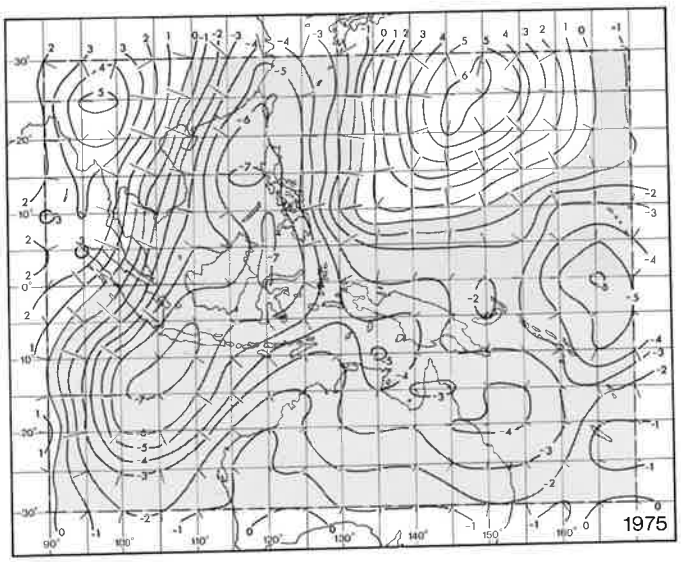

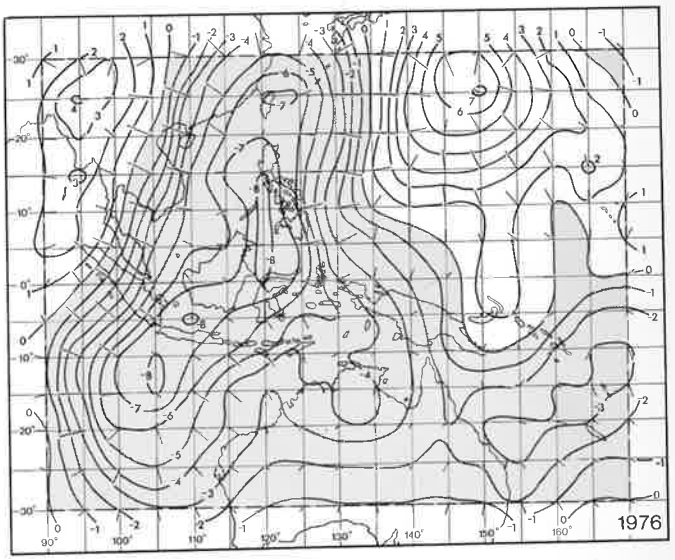

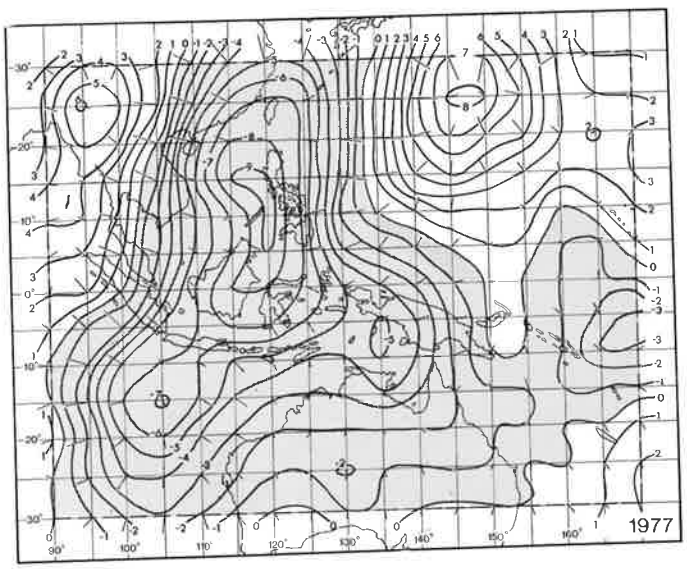

VELOCITY POTENTIAL

$\times 10^6$ m^2/sec

Jan 1973 - 1977

200 mb

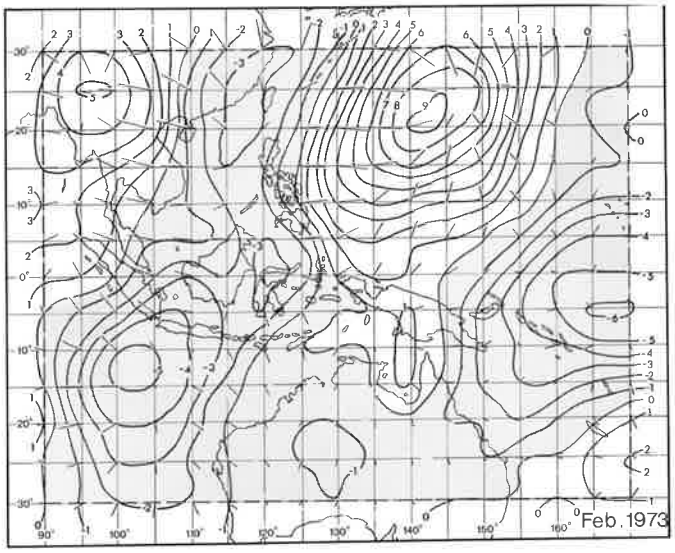

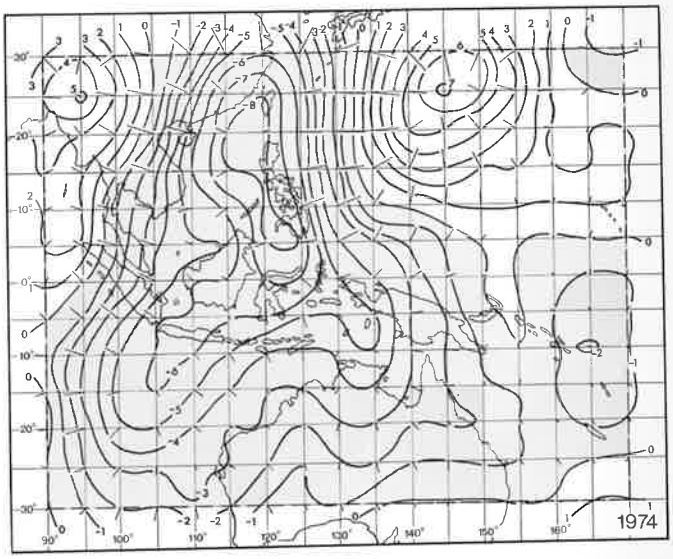

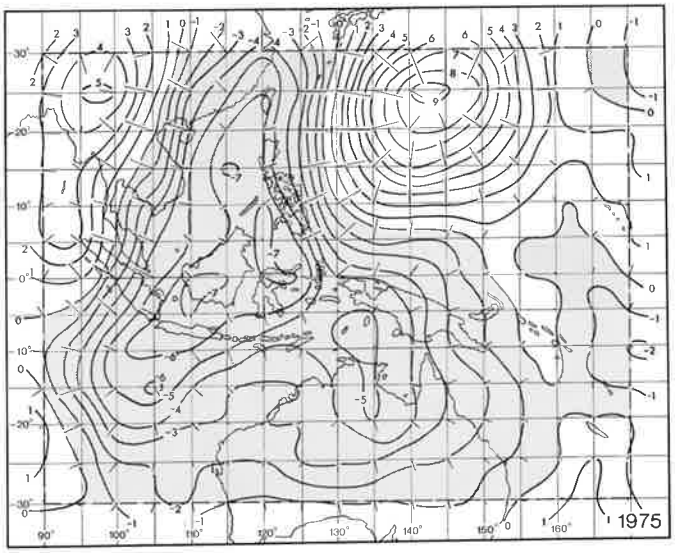

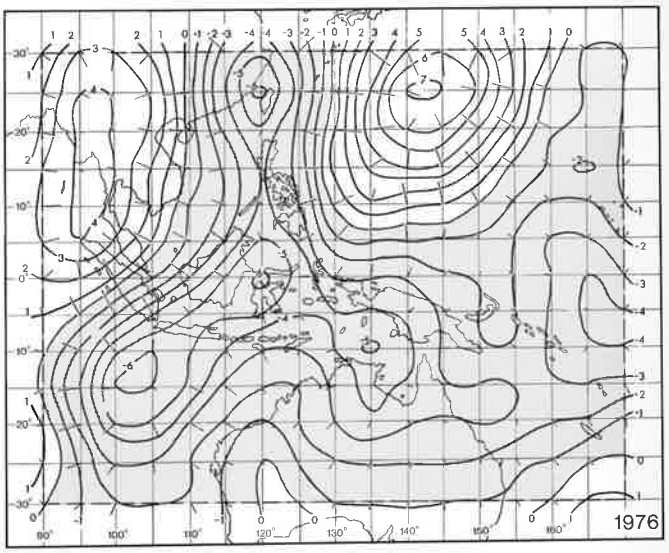

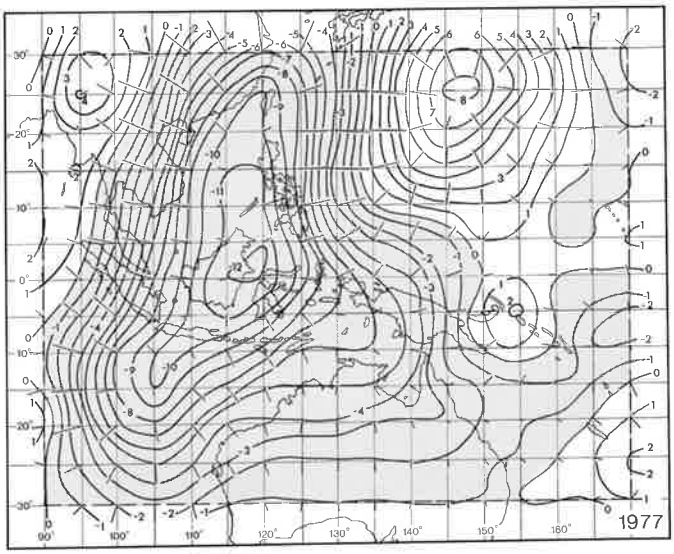

VELOCITY POTENTIAL

x 10^6 m^2/sec

Feb 1973 - 1977

200 mb

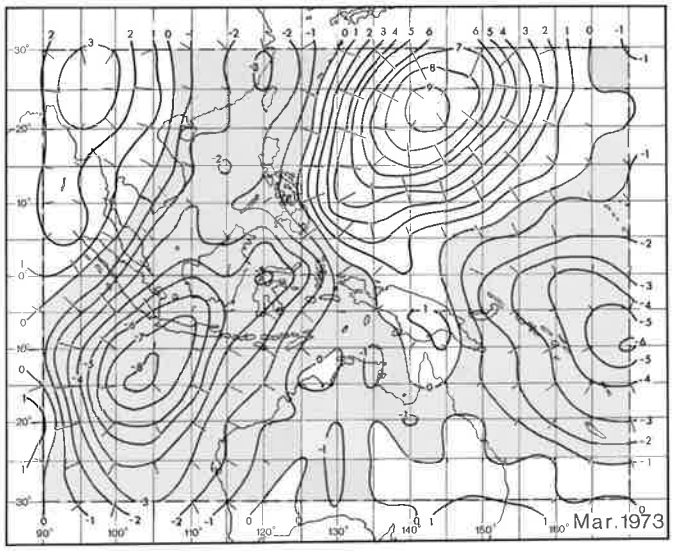

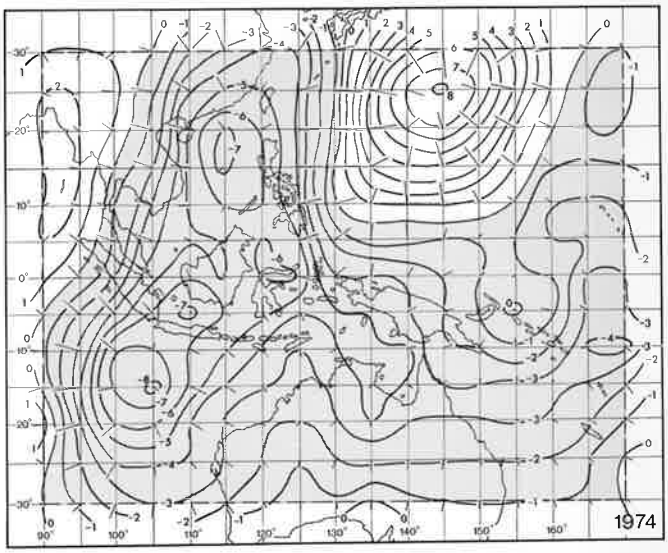

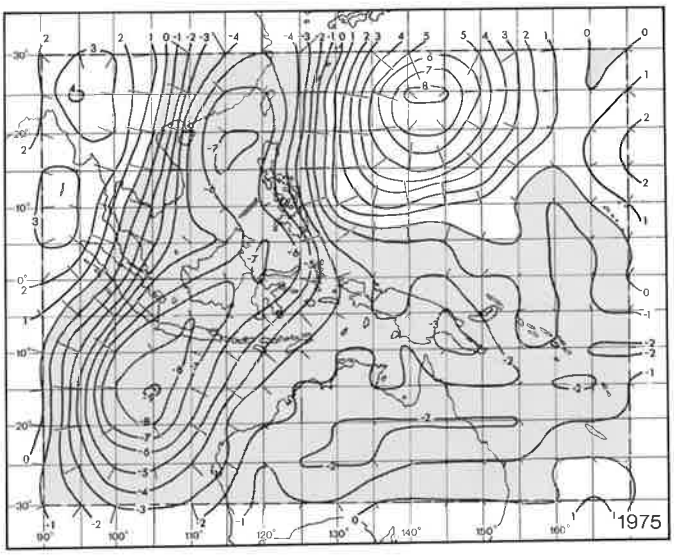

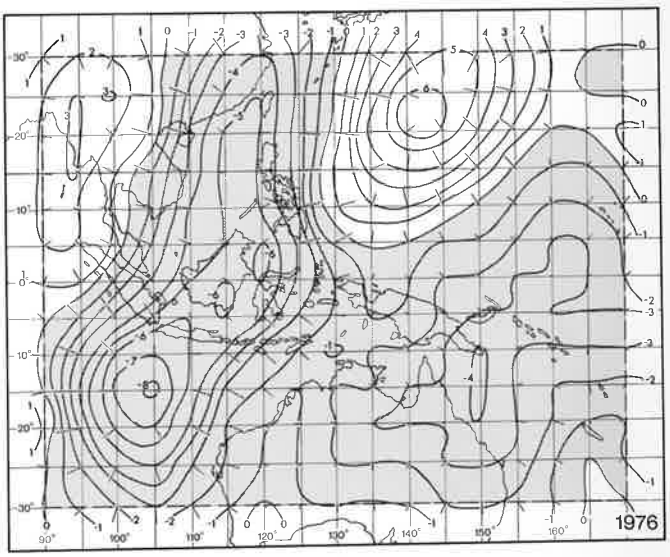

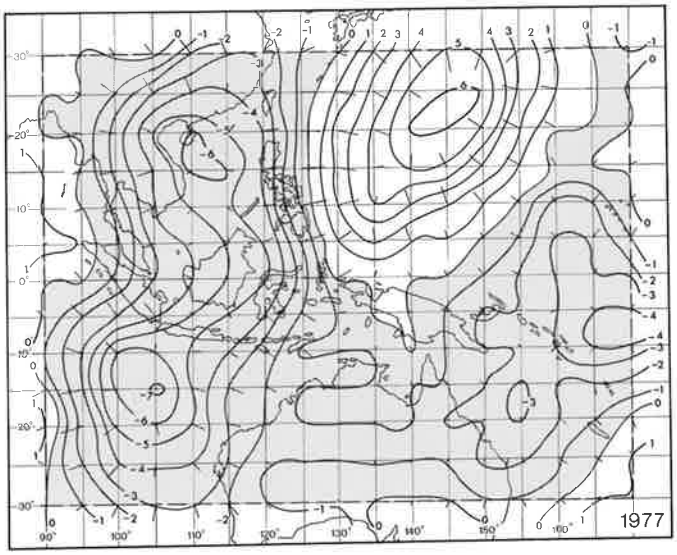

VELOCITY POTENTIAL

$\times 10^6$ m^2/sec

Mar 1973 - 1977

200 mb

and satellite-derived upper-level cloud distributions of Barton (1983).

Predominant elongations of divergent maxima, extending in approximately meridional (Hadley) and zonal (east-west and SO/WC) directions, illustrate the teleconnections emanating from the monsoon foci of South East Asia. However, as Krishnamurti (1971 a) and Krishnamurti *et. al.* (1973) suggest (and Figs.21,22 and 23 show) these divergent arms form a set of radial rather than distinctly orthogonal overturnings.

One feature of most diagrams in Figures 21, 22 and 23 is a divergent lobe or arm which extends across the northeastern section of Australia and out into the South Pacific. It seems that variations in anticyclonic flow in both hemispheres cause this arm to oscillate in strength and extent. In fact, the March weakening of the North Pacific upper anticyclone is reflected in the $-\bar{\chi}_{200}$ fields. The previously noted extreme of a westerly-displaced cell with increased anticyclonicity should result in stronger divergent and convergent maxima about the system. Such a pattern occurs during the 1973 circulations. In fact, coinciding with a weak SO/WC period in January 1973 (Flöhn, 1973; Flöhn and Fleer, 1975; Ramage, 1975; Rao and Theon, 1977; Quinn *et. al.*, 1978; Ramage and Hori, 1981), the divergent arm disappears and is replaced by weak convergent motion over the eastern half of the continent. This trend is a feature of the entire 1973 Southern Hemisphere summer and extends late into the season, only showing signs of a return of divergent motion in March (Fig.23).

Periods when strong anticyclonic cells are displaced to the east of Australia provide further evidence of major changes in $\bar{\chi}_{200}$ fields. January 1975 (Fig.21) is such a case. This month shows a strong divergent arm across Australia, with local divergent maxima along its whole length and in the near-equatorial regions east of 160°E. The $-\bar{\chi}_{200}$ centres in the latter regions strongly coincide with the lower-level convergent maxima (Figs.15,16 and 17) in the summer of 1973 and to a lesser degree in the Januarys of 1975, 1976 and 1977. They apparently represent circulation patterns which constitute a part of SO/WC anomalies. In fact, the $\bar{\chi}_{200}$

pattern in the Southern Hemisphere summers of 1975-77 highlights a range of 'breakdowns' in the divergent arm across northern Australia. The abortive El Niño of early 1975 is perhaps reflected in the weakening of the divergent arm from January to February of that year (Figs.21,22 and 23). However, definite evidence of such direct inter-relatedness is difficult to find in the other two summer sequences. Only the formation of a $\bar{\chi}_{200}$ maximum in the east (around 160°-170°E) during the early months of 1976 seems to be related to a pending weakening of the SO/WC. The 1977 summer pattern fails to support a strengthening of trade winds and the SO/WC.

Strong SO/WC phases in both January 1974 and January 1976 (Troup, 1981; personal communication) are manifested by a pronounced divergent arm across northern Australia and a local divergent maximum over Darwin (Fig.21). Similar, although less well defined, features are prevalent in the Februarys of 1974, 1975 and 1976. In the abnormally wet summers of 1974 and 1976 there would appear to be strong coupling between $-\bar{\chi}_{200}$ and $+\bar{\chi}_{850}$, with January 1974 standing out as a month in which Australian upper-level anticyclonicity was weak, the Northern Hemisphere upper anticyclone and the South East Asian/Malesian divergence field expanded, a northern Australian easterly jet maximum was set up and the SO/WC divergent arm was enhanced.

The Southern Hemisphere sub-tropical jetstream is probably not only affected by variations in the Australian upper anticyclone, but also appears to receive injections of mass and momentum through both Hadley and SO/WC teleconnections. However, this suggestion needs more support from data concerning the summer location and strength of the sub-tropical jetstream in latitudes south of 35°S.

3.1.2 Sub-Period : January and February 1973-75

The January and February 1973-75 sub-period examines the three summers of greatest variability in the major period and also the two months of peak monsoonal activity. It allows an examination of the vertical structure, variability and extent of teleconnection fields in the immediate Australasian

region and attempts to investigate some aspects of surface flow and NET_{NH} and NET_{SH} interaction. Finally, the relationship between flow and the pressure field is exemplified by the superimposition of streamfunction and geopotential height fields.

(i) Vertical Cross Sections (Surface to 200 mb) of Monthly Mean Velocity Potential ($\bar{\chi}_{sfc-200}$)

Unfortunately, the analysis of streamfunction fields for only two levels ($\bar{\chi}_{850}$ and $\bar{\chi}_{200}$) in Section 3.1.1 does not provide a complete picture of the vertical coupling and structure of teleconnection features. Variations in Australasian and western Pacific oceanic rainfall rates (Rao *et. al.*, 1976 - Figs.24 and 25), upper cloud distributions (Barton, 1983 - Fig.32), nephanalyses (Sadler *et. al.*, 1976; Shideler and Sadler, 1979) and OLR (Winston *et. al.*, 1979 - Fig.33) are well related to the vertical circulations shown in the latitudinal and longitudinal cross sections of monthly mean velocity potential ($\bar{\chi}_{sfc-200}$) (Figs.26-31). However, it must be remembered that the nephanalyses refer to total cloud cover and do not resolve the various heights of clouds. Furthermore, cloud cover from satellite brightness distributions includes the effects of non-convective stratus regions (Lyons, 1981).

Four fixed latitudinal (Equator, 5°S, 10°S and 15°S) and four variable longitudinal (between 85°E and 180°E) cross sections are examined in this sub-period. The latitudinal cross sections cover the entire Southern Hemisphere near-equatorial segment of the regional domain, while the longitudinal cross sections were made through the major oceanic rainfall maxima in the regional domain during each month in the 1973-75 sub-period (Figs.24 and 25). Schematic arrows in both cross sections show areas of 'strong' and 'weak' vertical motion based on subjective analyses of velocity potential magnitudes (see captions to Figs.26-31). Velocity potentials rather than divergence are used for the cross sections because they are less 'noisy' and thus provide a better representation of large-scale features (see Appendices 8 and 9).

Figure 24 Satellite-derived oceanic rainfall rates (mm hr^{-1}) during January from 1973-75 (adapted from Rao *et. al.*, 1976).

Figure 25 Satellite-derived oceanic rainfall rates (mm hr^{-1}) during February from 1973-75 (adapted from Rao *et. al.*, 1976).

GLOBAL OCEANIC RAINFALL RATE (AVG MM/HR) JANUARY 1973

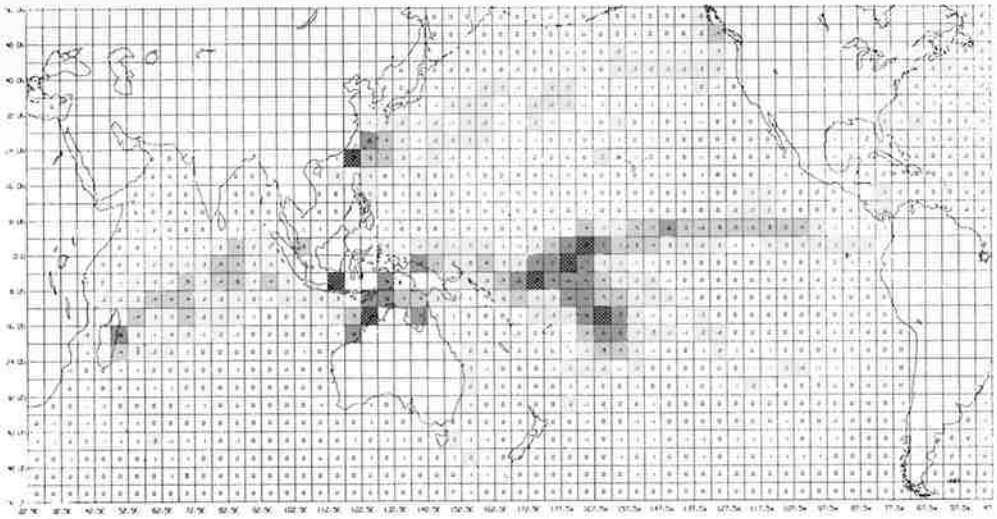

JANUARY 1974

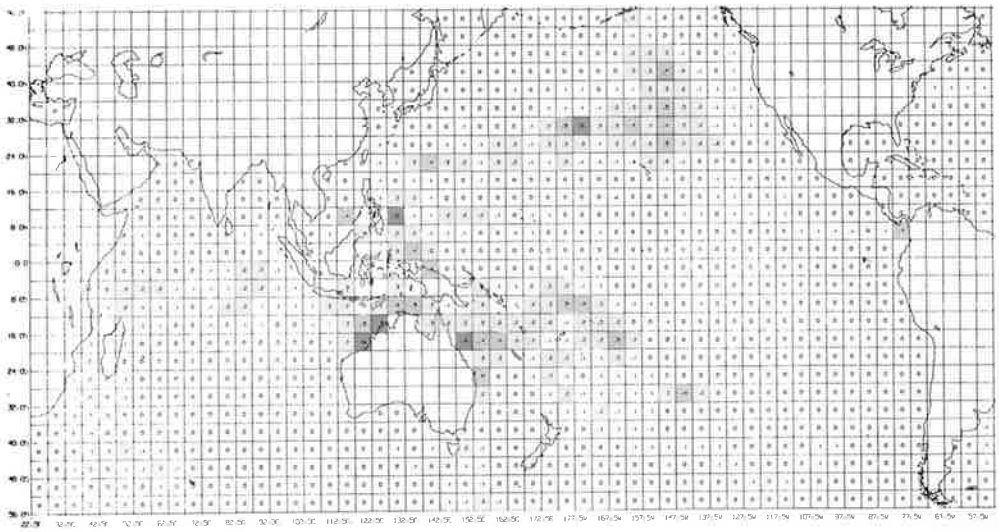

JANUARY 1975

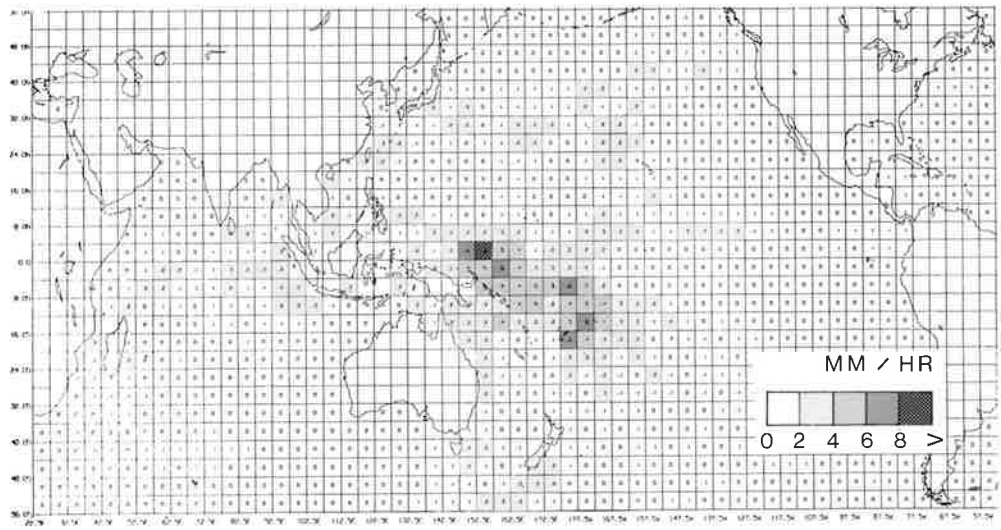

Coinciding with the final stages of the severe El Niño conditions of 1972-73, the rainfall regime in January 1973 (Fig.24 top) shows an area of extensive precipitation in the western to central equatorial region of the Pacific Dry Zone (PDZ)[1]. A second rainfall maximum exists in the Indonesian/Java Sea region. Both areas are closely aligned with the distribution of ascending motion in the latitudinal cross sections of Figure 26 and the upper-level cloud maxima noted by Barton (1983) (Fig.32), although the latter centre is not as distinct in Sadler *et. al.* (1976). A third, but smaller, rainfall maximum around Taiwan and mainland China is also associated with ascending motion in the 115°E and 125°E longitudinal cross sections (Fig.26). Vertical motion appears to be organized along 5°S with strong, low-level convergent and upper-level divergent maxima over Indonesia and, to a lesser degree, over the western Pacific (schematic arrows in Fig.26). Interestingly, the convergent maximum in the 5°S cross section occurs at about 700 mb, indicating a deep convective zone near the equator.

All four latitudinal cross sections show a distinctly bi-cellular mode of zonal circulation. This arrangement agrees well with the previously observed major 'breakdown' in the SO/WC overturning in 1973 ($\bar{\chi}_{200}$ fields in Figs.21 and 22). As Ramage (1975) suggests, such periods are most likely characterized by 'localized' convective maxima over the PDZ, with sinking motion to the east (South America) and the west (Australia). The latter circulation arm is certainly evident in January 1973. However, suppression of convective activity over the entire Indonesian region by the type of large-scale SO/WC reversal, often attributed to Bjerknes (1969), is not observed. On the contrary, broad-scale precipitation is very high over parts of Indonesia in January 1973, with mass removed by both the Hadley Circulation and a reduced SO/WC arm (latitudinal cross sections in Fig.26).

---

1. Following Quinn and Burt (1970:25), the PDZ is described as

> ...a rather extensive feature of the middle and lower latitude eastern south Pacific which slims down to a narrow tongue as it extends westward through the central equatorial Pacific into the western equatorial Pacific.

Figure 26 Latitude and longitude cross sections of monthly mean velocity potential in units of 10^6 m^2 s^{-1} at intervals of 2 units in the regional domain for January 1973. Schematic arrows show strong and weak vertical motions, using large and small arrows, respectively.

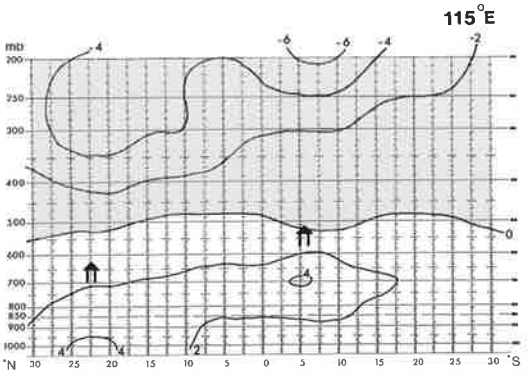
115°E
mb
°N
°S

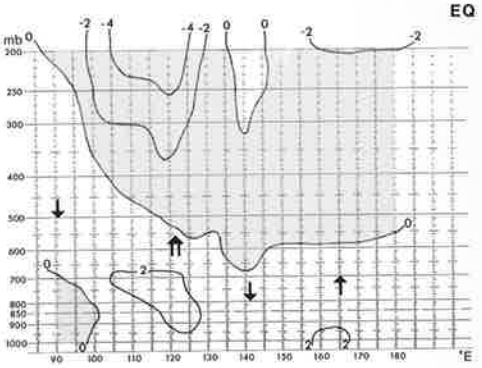
EQ
mb
°E

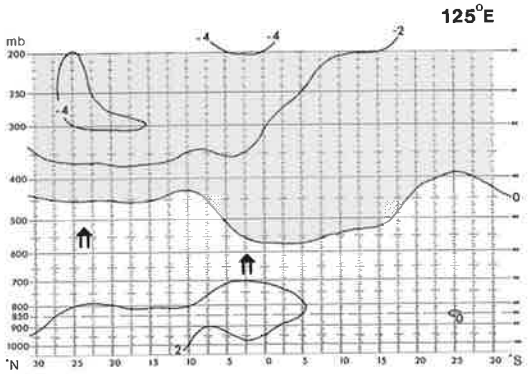
125°E
mb
°N
°S

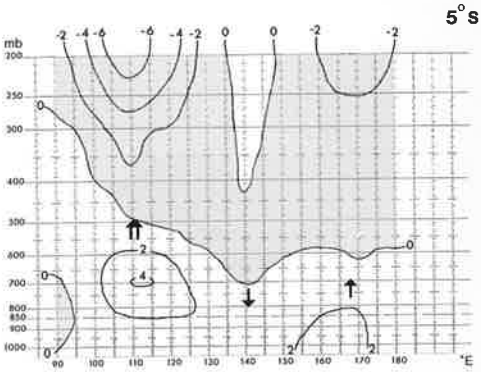
5°S
mb
°E

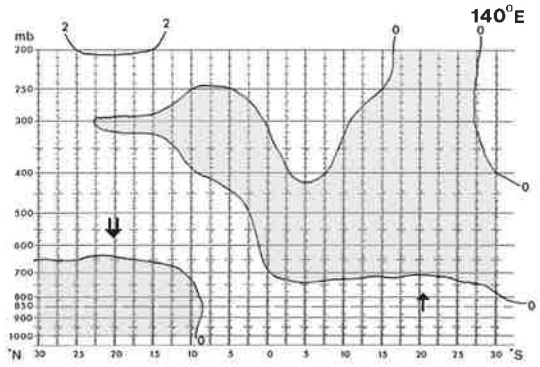
140°E
mb
°N
°S

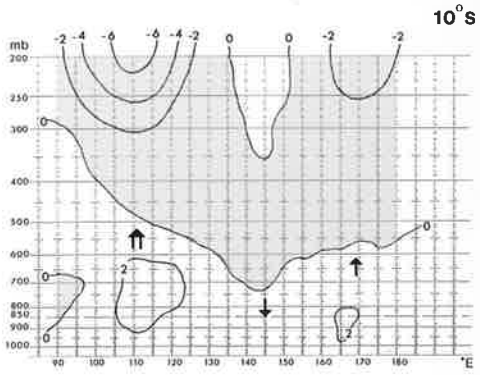
10°S
mb
°E

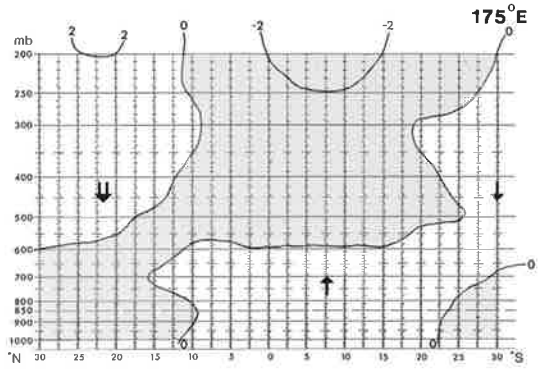
175°E
mb
°N
°S

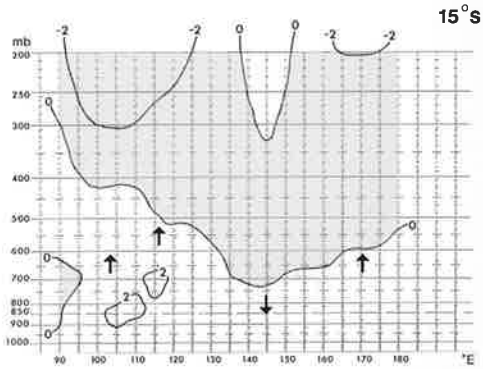
15°S
mb
°E

JAN 1973

Contributions to meridional, Hadley-type Circulation are most evident in the winter hemisphere between 105°-125°E and at 175°E in the January 1973 longitudinal cross sections. Although not on the same scale as the Asian system in the west, the 175°E cell represents a significant anomaly in the meridional field at this longitude. Such enhanced Hadley cell activity in this region (especially in the Northern Hemisphere branch) has been suggested by Bjerknes (1966, 1969, 1972) for the El Niños of 1957-58, 1963-64 and 1965-66.

Although the distribution of near-equatorial rainfall in February 1973 (Fig.25 top) is little different from that in January 1973, there is a noticeable reduction in its intensity over the PDZ. Oceanic rainfall distributions still occur over much of the Indian Ocean between the equator and approximately 20°S, while remnants of the January maximum off Taiwan and mainland China still persist. A marked rainfall maximum is also seen to persist in the Indonesian/Java Sea region.

The bi-cellular mode of zonal circulation is still evident in the February 1973 latitudinal cross sections (Fig.27), although vertical motion in both convective centres is of more even magnitude than in January 1973. In fact, despite the overall reduction in PDZ rainfall intensity in February, the incidence of stronger convective activity (centred on about 165°E) in the equatorial, 5°S and 10°S cross sections relates well to several small rainfall maxima to the west of the dateline (Fig.25 top). An area of subsidence is still located around 140°E but, in keeping with the localized convergent centre noted in the $\bar{\chi}_{200}$ fields (Fig.22), it displays greatest vigour in the equatorial and 5°S cross sections. Certainly, this is to be expected when enhanced convective motion is located only some 25° further east, rather than 50°-55° to the east as would have seemed to be the case in January 1973. Although it persists into February 1973, the Indonesian rainfall maximum is more localized (centred on about 5°S, 115°E) than in January. This may be reflected by a weakening of convective motion over this region in the February latitudinal cross sections.

Figure 27 Latitude and longitude cross sections of monthly mean velocity potential in units of 10^6 m^2 s^{-1} at intervals of 2 units in the regional domain for February 1973. Schematic arrows show strong and weak vertical motions, using large and small arrows, respectively.

115°E

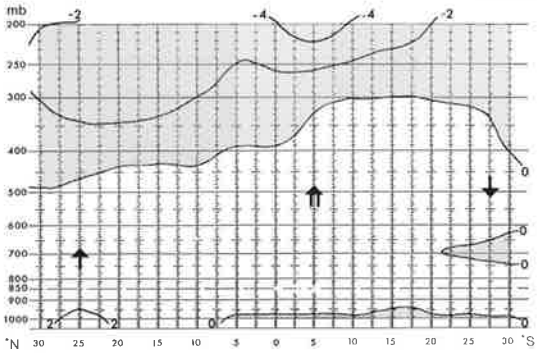

EQ

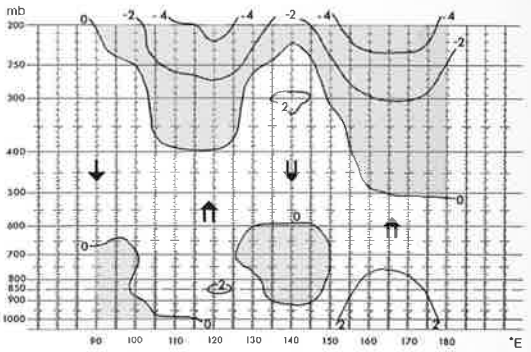

130°E

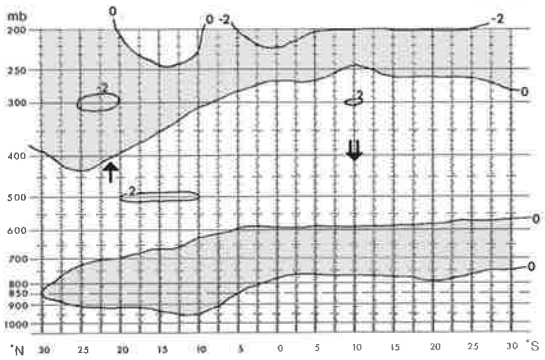

5° S

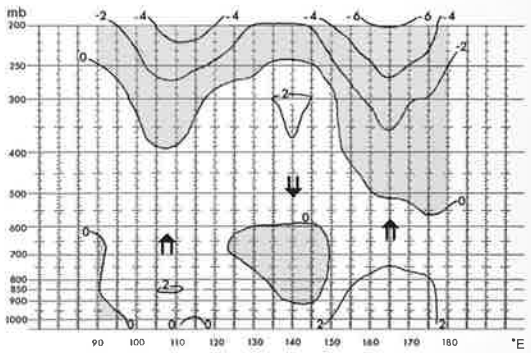

140°E

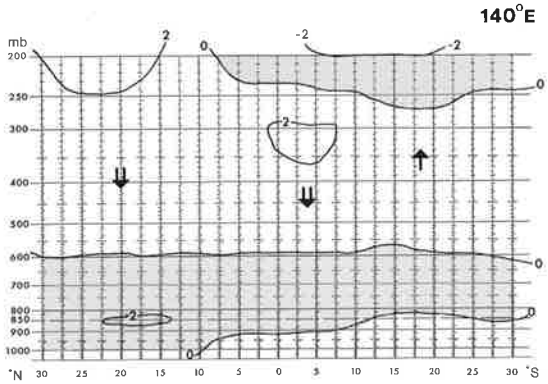

10° S

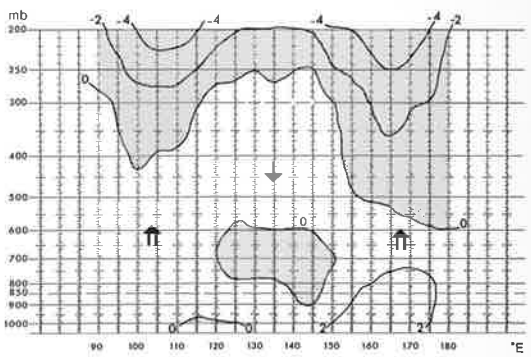

165°E

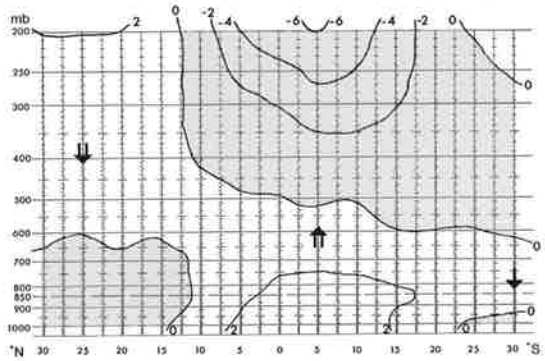

15° S

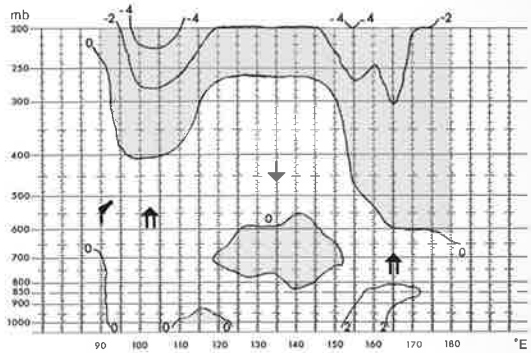

FEB1973

Longitudinal cross sections in February 1973 show further evidence of Hadley Circulation, particularly in the most eastern longitude (165°E). As observed with near-zonal overturnings in the latitudinal sequence, meridional mass outflow from the Indonesian region is less than that from the western portion of the PDZ in February 1973 and greater than that in January 1973. In the longitudes between about 130°-150°E, the strong subsidence, allied with a 'breakdown' of the SO/WC, appears to markedly influence meridional circulation. This is most evident in the 130°E and 140°E longitudinal cross sections where something akin to a reversed Hadley cell appears to be operating. In the 130°E section, this reversal is centred in the Northern Hemisphere, while in the 140°E diagram it has a distinctly Southern Hemisphere focus. However, such features are not distinguishable in January 1973 when the area of 'breakdown' is not as well developed as in February. Interestingly, it could be speculated that the above distributions strongly reflect trends in Troup's monthly mean SOI's (Troup, 1981; personal communication), and thus intraseasonal variations within a weak SO/WC phase. The SOI values for January and February 1973 are - 4 and - 19 respectively. However, this still does not support the longer term SOI, El Niño and Indonesian drought relationships noted in Quinn *et. al.* (1978) and Rasmusson and Carpenter (1982), although their association is very pronounced in the Southern Hemisphere winter monsoon regime and involves a seasonal evolution of such features.

In January 1974, the major oceanic rainfall maxima in the Australian region (Fig.24 centre), upper-level cloud maxima (Barton, 1983) (Fig.32) and cloud octa maxima (Shideler and Sadler, 1979) coincide with a large-scale vertical motion field which is suggestive of a large, strong SO/WC overturning (Fig.28). Such an extensively organized near-zonal circulation seems to be a hallmark of strong SO/WC periods. Regions of subsidence are evident in the extreme east and west of all latitudinal cross sections. As Musk (1976) speculates, the eastern regions are either allied with, or consequences of, processes 'normally' suppressing PDZ rainfall.

Figure 28 Latitude and longitude cross sections of monthly mean velocity potential in units of 10^6 m^2 s^{-1} at intervals of 2 units in the regional domain for January 1974. Schematic arrows show strong and weak vertical motions, using large and small arrows, respectively.

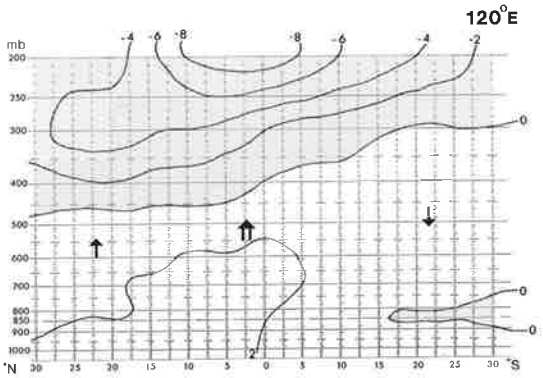
120°E
mb
°N
°S

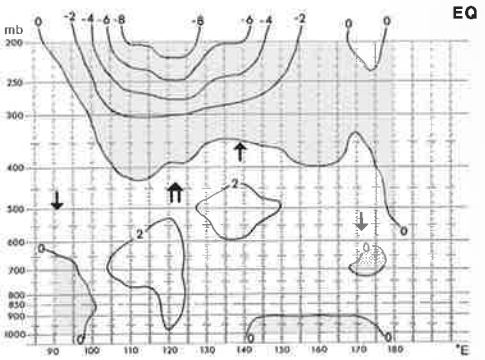
EQ
mb
°E

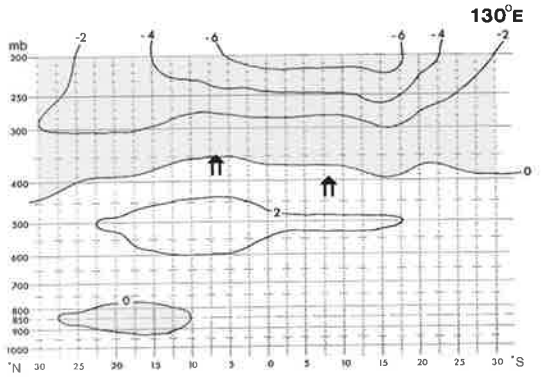
130°E
mb
°N
°S

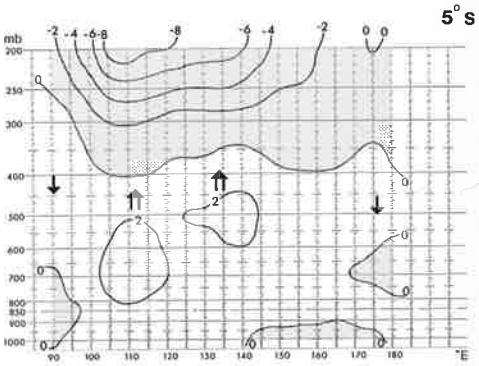
5° S
mb
°E

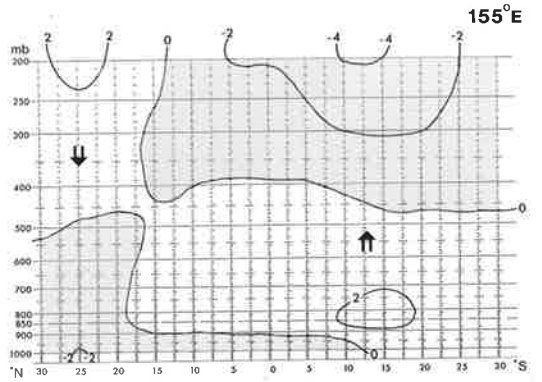
155°E
mb
°N
°S

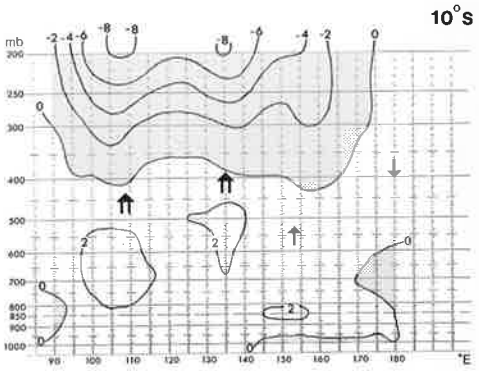
10° S
mb
°E

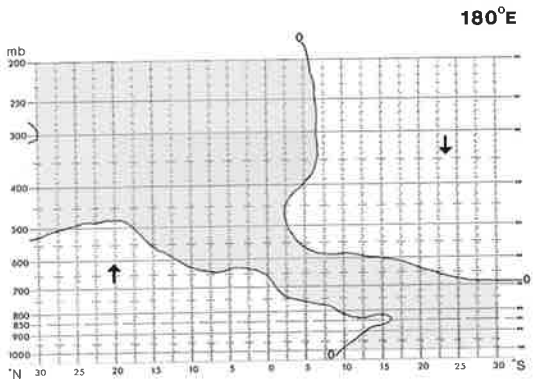
180°E
mb
°N
°S

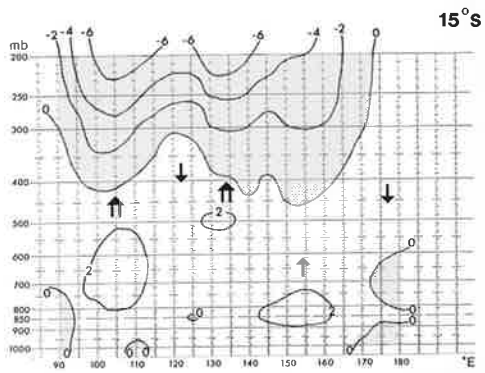
15° S
mb
°E

JAN 1974

Latitudinal cross sections in January 1974 show aspects of the major rainfall features (Fig.24 centre). In particular, they suggest that vertical motion in the Malesian/Australasian region is generally more organized than in January 1973. The extent of such changes over northern Australia is chiefly observed in a comparison of the 10°S and 15°S cross sections in Figures 26 and 28. Another important feature of the January 1974 distribution is the absence of the type of secondary cell in the PDZ vicinity that occurred in January 1973.

The January 1974 longitudinal cross sections suggest that important changes have also occurred in meridional circulation. Within the north-western Pacific bounds of Figure 28, the strong vertical ascending motion from the equator to 10°N in the 120°E cross section is consistent with the moderate to heavy precipitation in the vicinity of the Philippines (Fig.24 centre). The most noticeable facet of the cross sections in regard to the Australian rainfall maximum is the presence of ascending motion around 15°S at 130°E and 155°E. Of particular interest in the final longitudinal cross section, at 180°E, is the absence of the type of meridional anomaly occurring in January and February 1973. In its place is a meridional circulation dominated by strong ascending motion near 30°N. The latter region coincides with an area of high oceanic rainfall rates in the mid North Pacific.

The oceanic rainfall distribution in February 1974 (Fig.25 centre) differs from that in January 1974 in the central North Pacific (approximately 40°N) and Australasian regions. There is no indication of the large area of high rainfall rates that occurred over the central North Pacific in January 1974, while the concentration of high rainfall rates around Australia is not nearly as prevalent in February 1974.

A major cause of the changes in Australasian rainfall regimes can be seen in the February 1974 latitudinal cross sections (Fig.29). Although vertical motion is still relatively strong over this region, it does not appear to have quite the spatial extent, and most certainly not the vertical depth nor lower- and middle-level convergent structure, of the January 1974

Figure 29 Latitude and longitude cross sections of monthly mean velocity potential in units of 10^6 m^2 s^{-1} at intervals of 2 units in the regional domain for February 1974. Schematic arrows show strong and weak vertical motions, using large and small arrows, respectively.

115°E

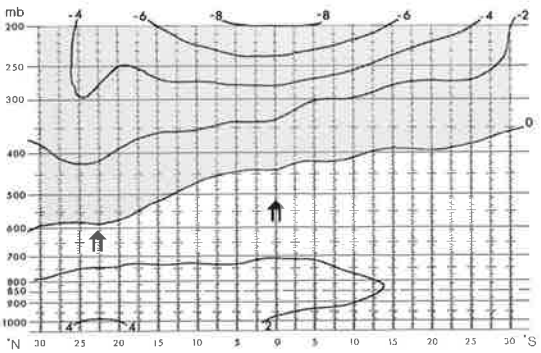

EQ

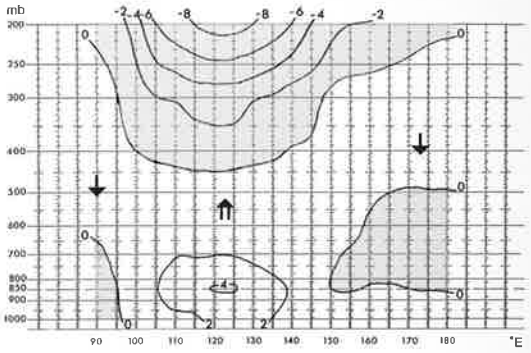

125°E

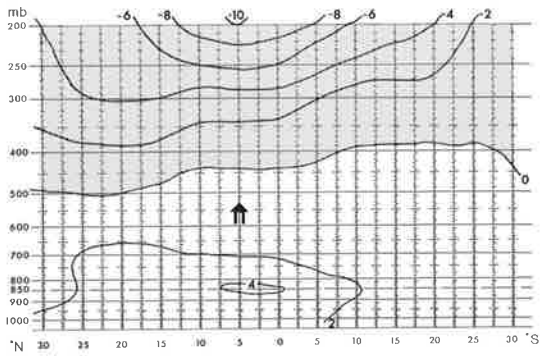

5° S

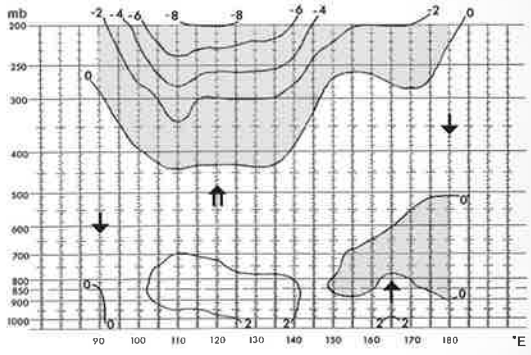

140°E

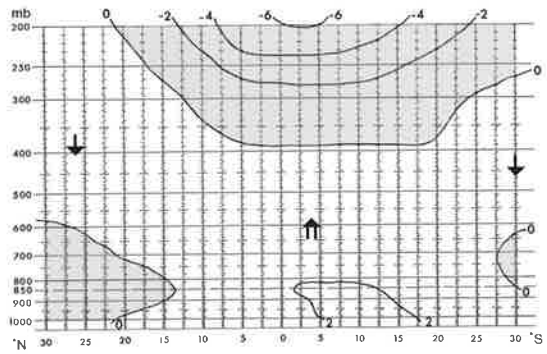

10°S

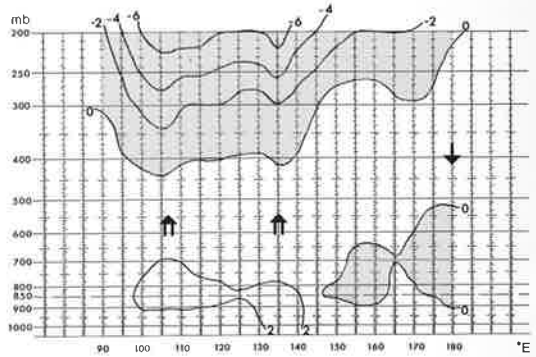

170°E

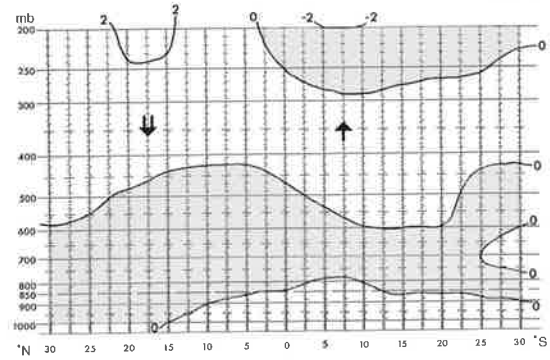

15°S

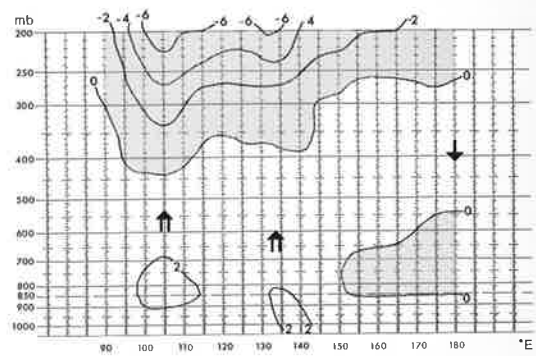

FEB 1974

could be related to the vertical motion area observed in the equatorial and 5°S latitudinal cross sections (Fig.30).

Latitudinal cross sections in January 1975 (Fig.30) tend to show some semblence of bi-cellular, if not multi-cellular, overturnings and SO/WC 'breakdown'. However, this mode seems to differ from that in January 1973 as there is relatively well organized vertical ascent to 145°-150°E with a small subsident area (especially in the 10°S cross section) around 155°-160°E and a second ascending region near 165°-170°E. In fact, the 'breakdown' in January 1975 is centred on 155°-160°E, while that in January 1973 occurred further to the west, near 135°-140°E. This arrangement is evident in the first three latitudinal cross sections and may be related to the occurrence of an abortive El Niño at this time. On the other hand, the sequence does not have the degree of organization of vertical motion that was observed at 10°S and 15°S in January 1974. Even the magnitude of ascending motion at 15°S in Figures 28 and 30 is noticeably different. Further north, the amount of precipitation over Indonesia (Fig.24 bottom) and the extent of upper-level cloud (Barton, 1983) (Fig.32) are below the January 1973 and January 1974 values.

Pronounced meridional overturnings are evident in most of the longitudinal cross sections, with a major change in the pattern occurring around 155°E. Although Hadley Circulation is evident in the winter hemisphere branch between 115°-130°E, the local contribution provided by the ascending motion near 165°E cannot be neglected. However, it is difficult to judge from this analysis whether the latter provides as distinct a mass and momentum source as does the Asian focus to the winter jetstream near Japan (Murakami and Unninayar, 1977; Webster, 1981 a). Certainly, there would appear to be evidence of relationships between Australian sub-tropical jetstream locations in January 1973 (displaced to the north near 115°E) and January 1975 (displaced to the north near 150°-160°E) and the Southern Hemisphere Hadley cell.

Oceanic rainfall rates in January and February 1975 (Figs.24 and 25

Figure 30 Latitude and longitude cross sections of monthly mean velocity potential in units of 10^6 m^2 s^{-1} at intervals of 2 units in the regional domain for January 1975. Schematic arrows show strong and weak vertical motions, using large and small arrows, respectively.

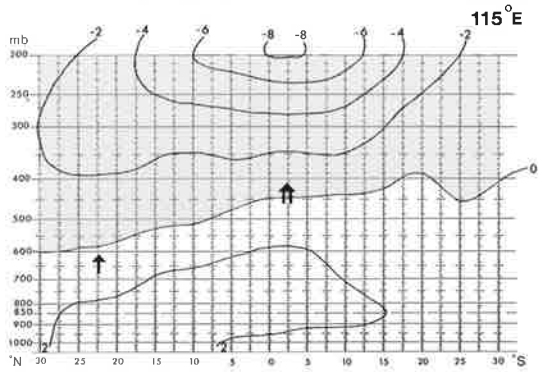
115°E
mb
°N
°S

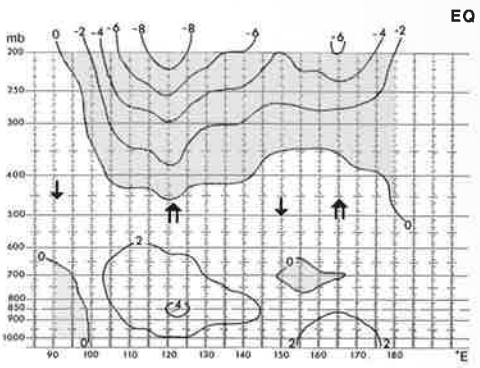
EQ
mb
°E

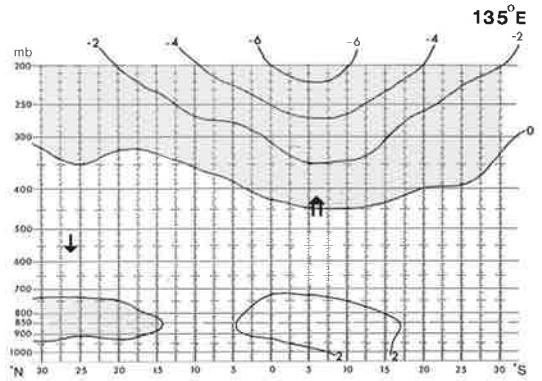
135°E
mb
°N
°S

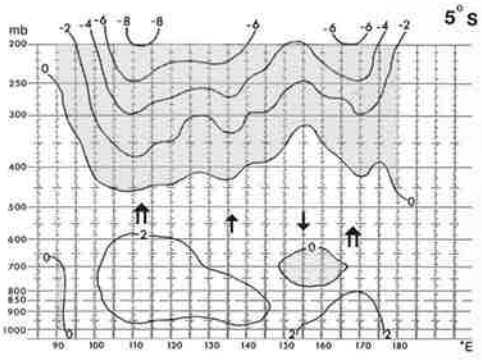
5°S
mb
°E

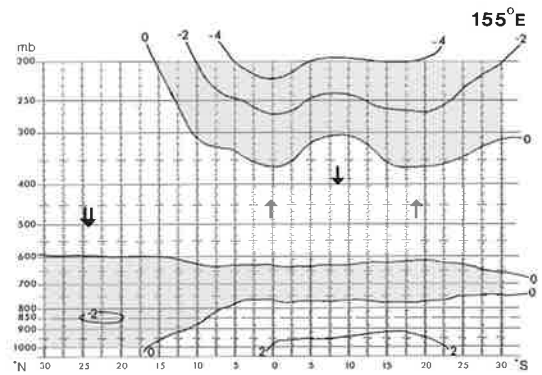
155°E
mb
°N
°S

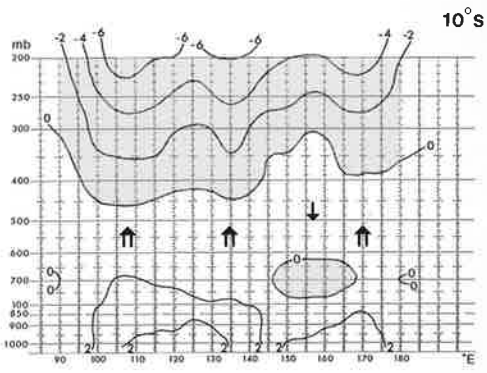
10°S
mb
°E

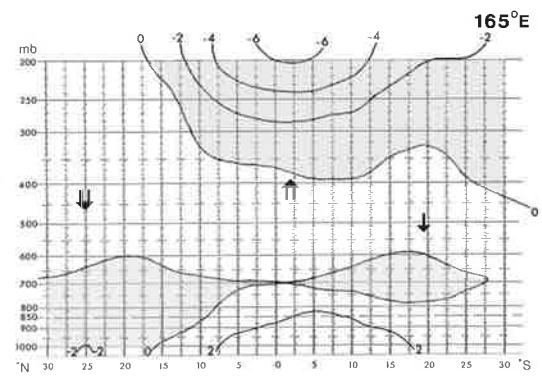
165°E
mb
°N
°S

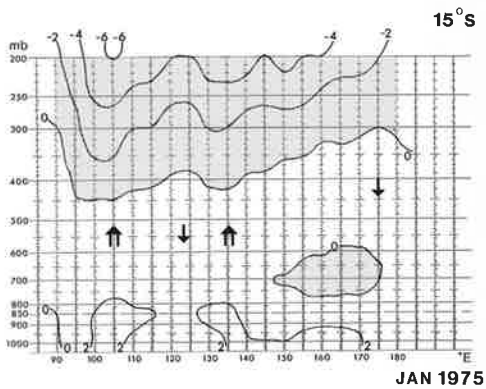
15°S
mb
°E

JAN 1975

bottom) may be indicative of the abortive El Niño at this time (Wyrtki *et. al.*, 1976). Certainly, there is a marked intraseasonal swing in rainfall maxima and OLR minima (Fig.33) between January and February 1975 to match the previously-noted circulation changes at 850 mb and 200 mb (Figs.7,8,18 and 19). In January, there is evidence of high rainfall rates in the PDZ, but the maxima are centred on Australasia by February. In fact, rainfall patterns seem to have been affected as far as the middle and high latitudes of the North Pacific.

As in January 1975, the February 1975 latitudinal cross sections (Fig.31) show evidence of a 'breakdown' in the SO/WC, with subsident motion near 150°-160°E. However, the structure of the February event suggests that the 'breakdown' is very weak and does not support a pronounced bi-cellular overturning. Consequently, it could possibly be interpreted as signalling the restoration of a larger-scale convective system from the more distinct bi-cellular format of January 1975. An examination of Troup's SOI would tend to support this premise, as the index changes sign from a value of - 8 in January to a value of + 4 in February (Troup, 1981; personal communication).

Ascending motion may be a little more widespread in Australian longitudes (especially along 10°S and 15°S) by February (Fig.31), but it certainly has a noticeably different lower-level convergent structure from the January sequence (Fig.30). Whereas convergence becomes shallow and is located at increasingly lower levels by 10°S and 15°S in January, there is a distinctly lower middle-level convergent focus in all the sections in February. Coupled with a marginally stronger upper-level divergent field, vertical overturnings tend to be enhanced along the lines noted in the comparison of January and February 1974 sequences. The resulting precipitation variations are observed in the oceanic rainfall rates (Figs.24 and 25 bottom).

Longitudinally, the cross sections in February 1975 (Fig.31) tend to provide additional support for the arguments put forward above. Hadley overturnings are evident in the 120°, 130° and 140°E cross sections, with

Figure 31 Latitude and longitude cross sections of monthly mean velocity potential in units of 10^6 m^2 s^{-1} at intervals of 2 units in the regional domain for February 1975. Schematic arrows show strong and weak vertical motions, using large and small arrows, respectively.

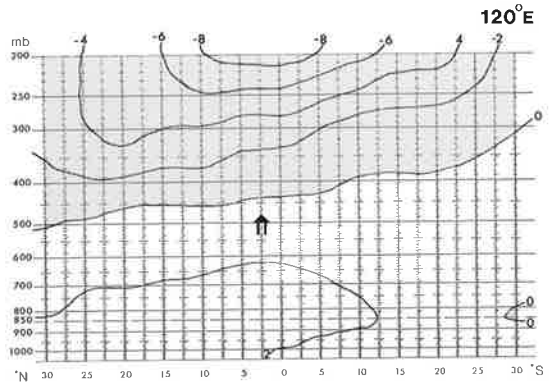
120°E
mb
°N 30 25 20 15 10 5 0 5 10 15 20 25 30 °S

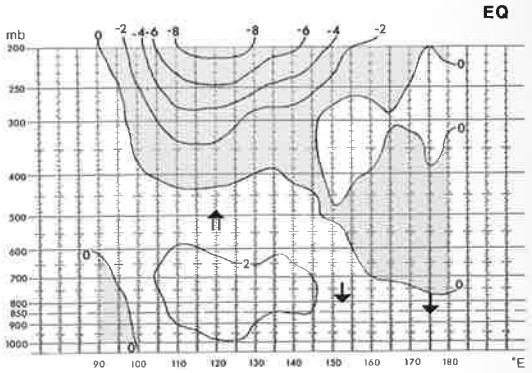
EQ
mb
90 100 110 120 130 140 150 160 170 180 °E

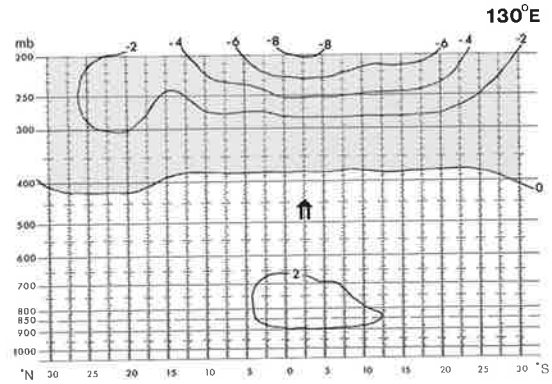
130°E
mb
°N 30 25 20 15 10 5 0 5 10 15 20 25 30 °S

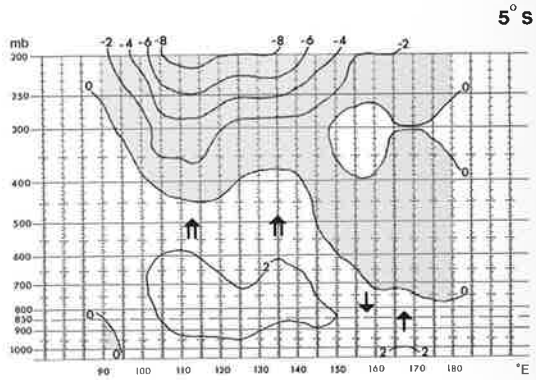
5° S
mb
90 100 110 120 130 140 150 160 170 180 °E

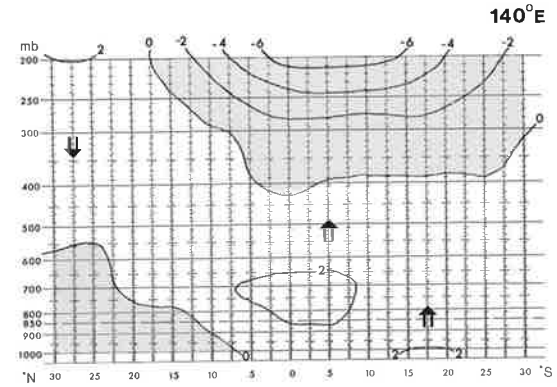
140°E
mb
°N 30 25 20 15 10 5 0 5 10 15 20 25 30 °S

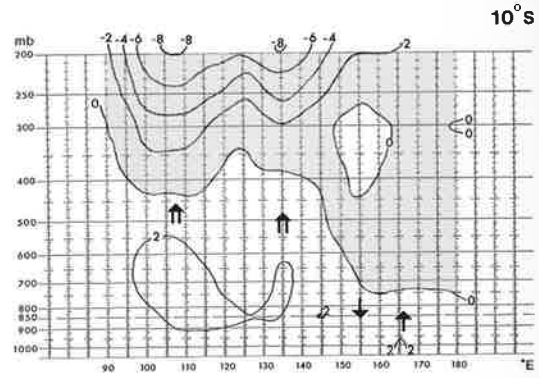
10° S
mb
90 100 110 120 130 140 150 160 170 180 °E

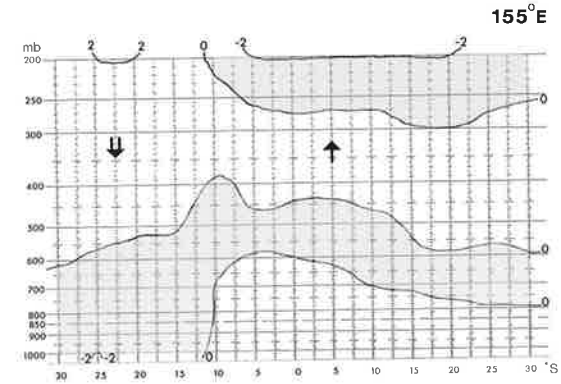
155°E
mb
30 25 20 15 10 5 0 5 10 15 20 25 30 °S

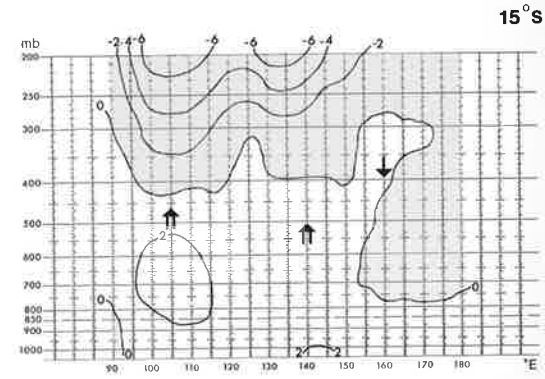
15° S
mb
90 100 110 120 130 140 150 160 170 180 °E

FEB1975

a weaker situation at 155°E. The latter shows a degree of convective organization not much weaker than in January 1975. Although there is no longitudinal cross section shown that is further east than 150°E, the raw data and OLR do not indicate that there was a convective maximum in the PDZ locale at this time. Interestingly, these sections did not resolve any clear convective maximum that could be associated with the more pronounced rainfall rates in the East China Sea/North Pacific region off Taiwan. However, the February 130°E cross section is somewhat more conducive to rainfall processes at 20°-30°N than the January 135°E cross section.

The overall pattern in all of the latitudinal cross sections is one of marked variability in the extent, intensity and organization of the SO/WC phenomenon. It appears that strong SO/WC periods can be partially characterized by the type of large-scale near-zonal overturning that many researchers envisage, although this is a product of the coalescence of a number of smaller overturnings. However, other SO/WC periods reflect a tendency for the overturning to break down into a series of less organized and more isolated local cells. This variability in SO/WC structure may explain some of the inconsistencies in the statistical results of studies aimed at relating Australian and New Guinean rainfall to Southern Oscillation Indices. As Nicholls (1973), Musk (1976) and Barry (1978) note, SO/WC variations form a highly complex spatial and temporal pattern which cannot be explained by simple correlations alone.

(ii) Monthly Mean Surface Streamfunction Fields ($\bar{\psi}_{sfc}$)

Important circulation features are found in the lower levels of the tropical atmosphere. One aspect of such flow is the tendency for winds to blow across the equator, often with a marked ageostrophic component. At such levels, the structure, intensity and location of features such as the NETs and their related convergence zones, trade wind regimes and the continental heat lows are most pronounced.

In the Australasian region, during the Southern Hemisphere summer, the

Figure 32 Distributions of upper cloud in January 1973, 74 and 75. Dark area is greater than 60 per cent frequency of cloud cover, diagonal lines greater than 40 per cent, horizontal lines greater than 20 per cent, clear areas less than 20 per cent, shaded areas have no observations (from Barton, 1983).

Figure 33 Distribution of outgoing longwave radiation in units of W m^{-2} at intervals of 25 units in January, February and March 1975. Shaded areas denote regions with outgoing longwave radiation values less than 250 W m^{-2} (from Winston *et. al.*, 1979).

Figure 34 Distribution of outgoing longwave radiation in units of W m^{-2} at intervals of 25 units in January, February and March 1976. Shaded areas denote regions with outgoing longwave radiation values less than 250 W m^{-2} (from Winston *et. al.*, 1979).

Figure 35 Distribution of outgoing longwave radiation in units of W m^{-2} at intervals of 25 units in January, February and March 1977. Shaded areas denote regions with outgoing longwave radiation values less than 250 W m^{-2} (from Winston *et. al.*, 1979).

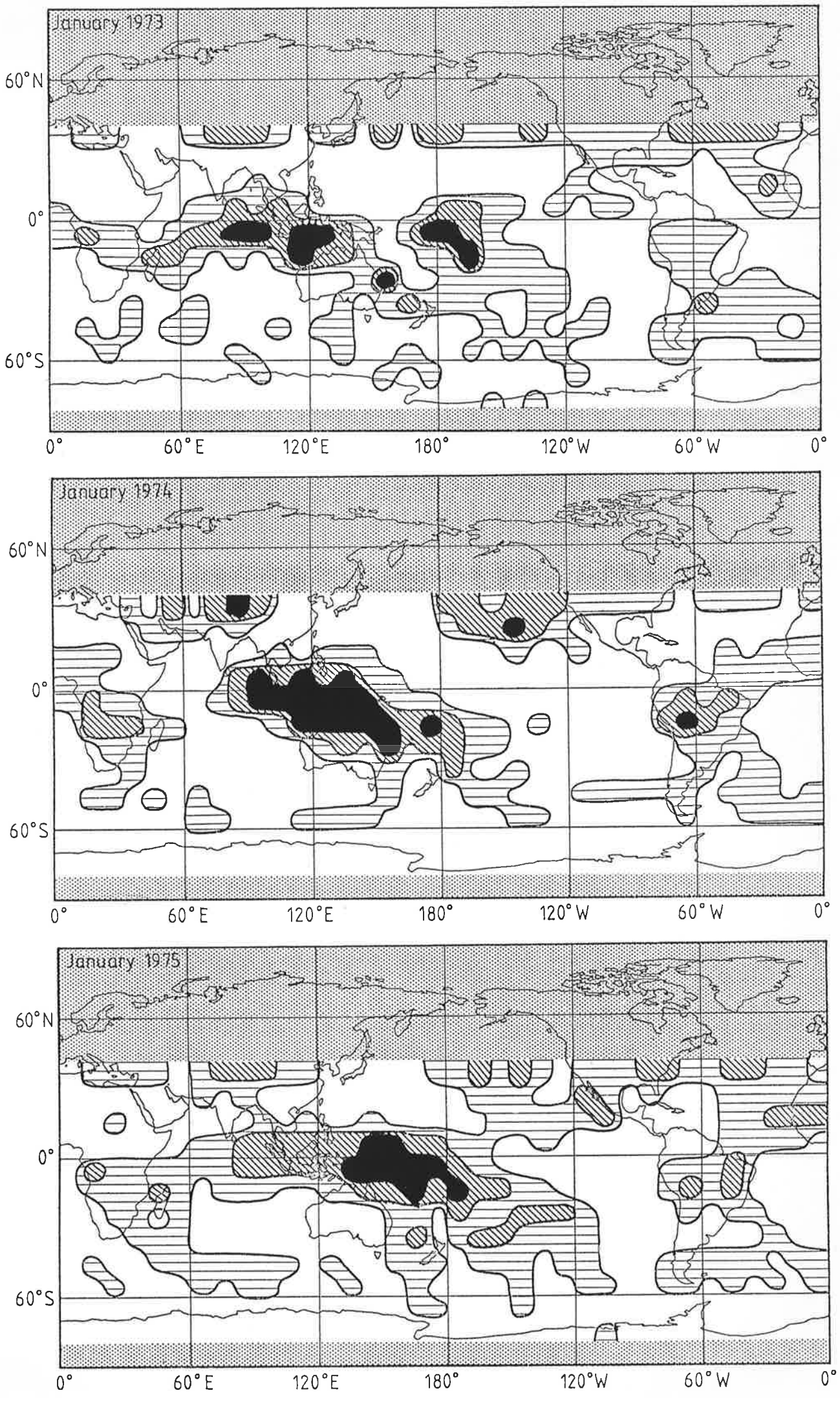
January 1973
60°N
0°
60°S
0°
60°E
120°E
180°
120°W
60°W
0°
January 1974
60°N
0°
60°S
0°
60°E
120°E
180°
120°W
60°W
0°
January 1975
60°N
0°
60°S
0°
60°E
120°E
180°
120°W
60°W
0°

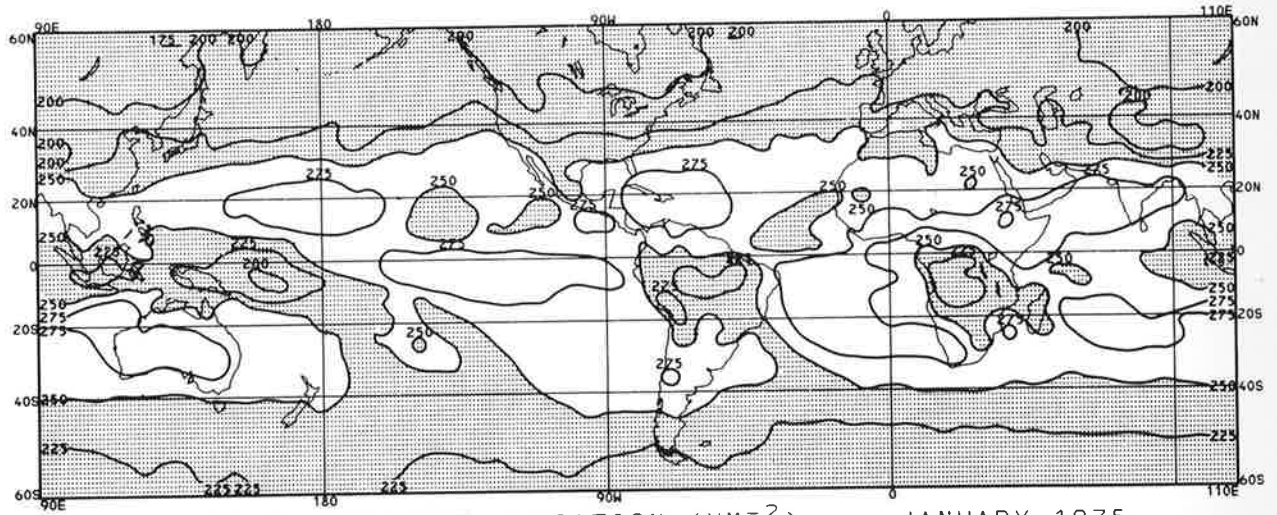

OUTGOING LONGWAVE RADIATION (WM^{-2}) JANUARY 1975

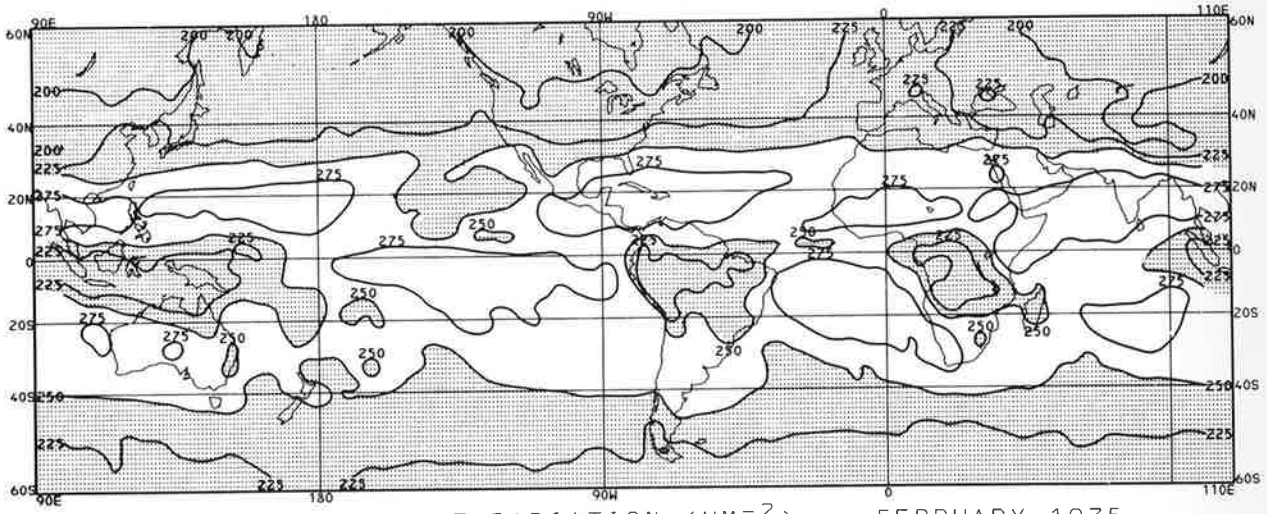

OUTGOING LONGWAVE RADIATION (WM^{-2}) FEBRUARY 1975

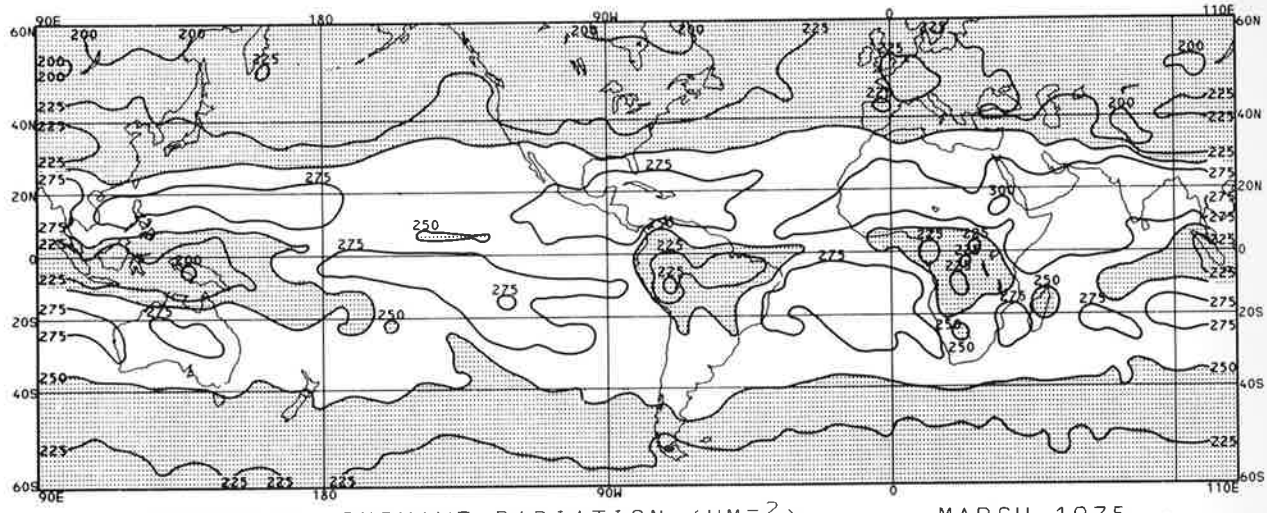

OUTGOING LONGWAVE RADIATION (WM^{-2}) MARCH 1975

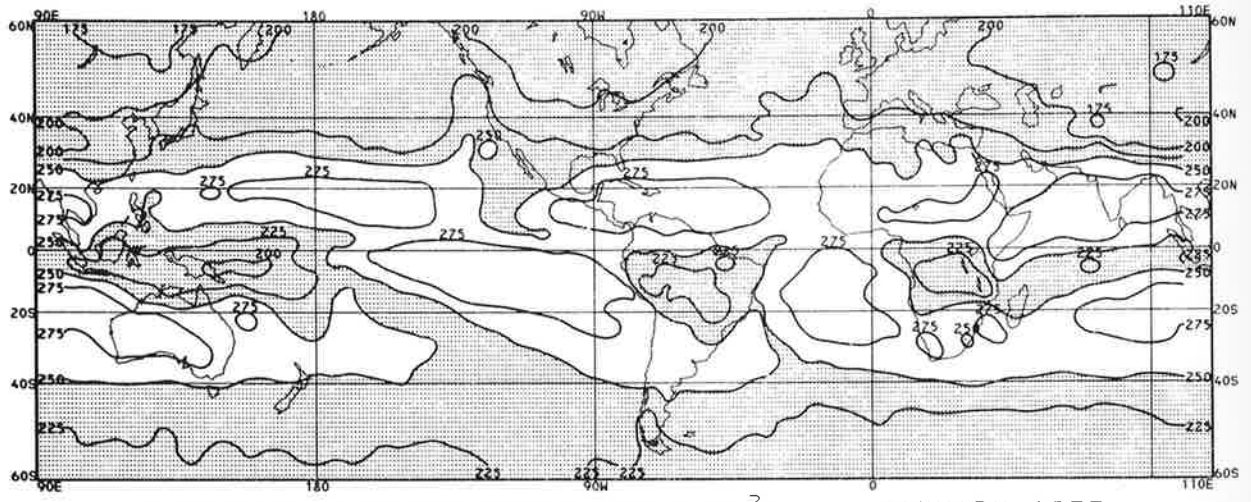

OUTGOING LONGWAVE RADIATION (WM^{-2}) JANUARY 1977

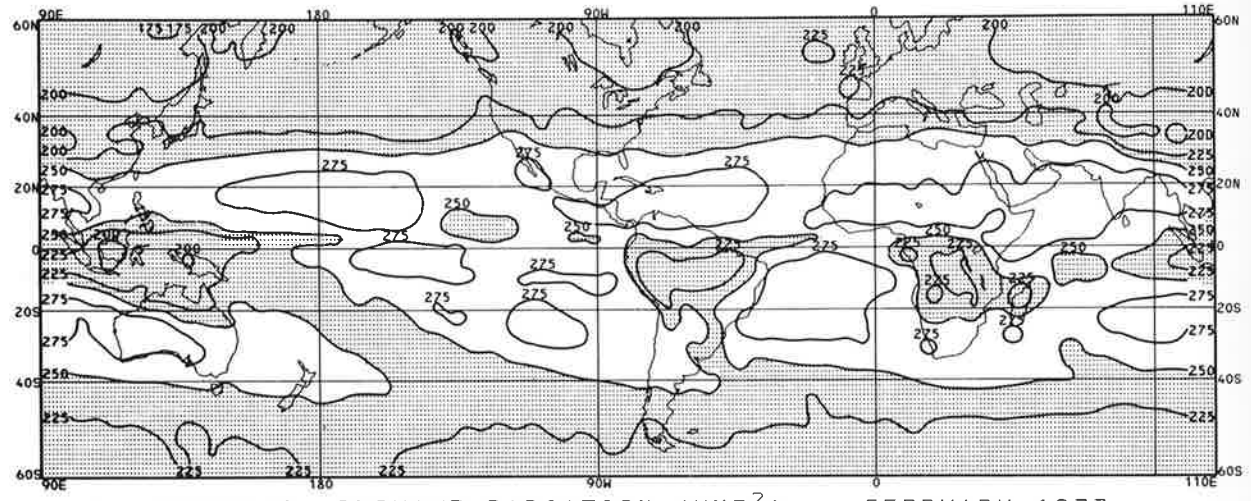

OUTGOING LONGWAVE RADIATION (WM^{-2}) FEBRUARY 1977

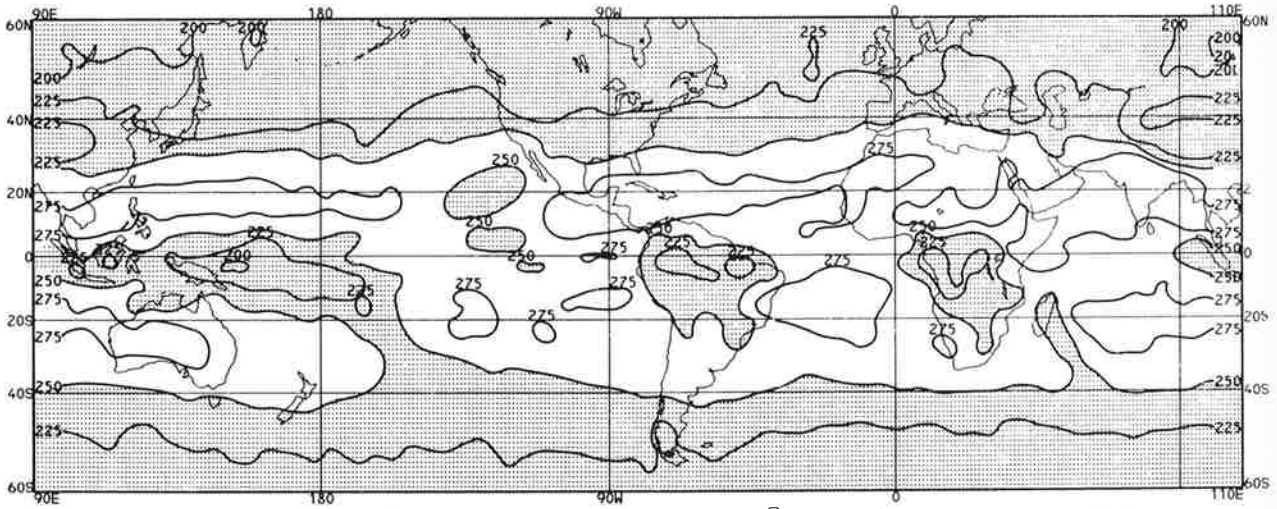

OUTGOING LONGWAVE RADIATION (WM^{-2}) MARCH 1977

Indonesian/north-northwestern Australian and New Guinean/western equatorial Pacific sectors would seem to be influenced by cross-equatorial interactions in the form of surges from Asia and northeast trade wind flow over the North Pacific respectively. Over the Australian continent itself, pressure fields (and sometimes the wind regime) testify to the development of two shallow, low-level heat lows. In an effort to examine further the nature and variability of these features, monthly mean streamfunction fields at the surface are constructed for the January and February 1973-75 sub-period.

The pattern of the cross-equatorial flow from Indonesian longitudes into northern Australia in the monthly mean surface streamfunction ($\bar{\psi}_{sfc}$) fields of January and February 1973-75 (Fig.36) is somewhat at variance with that observed at 850 mb in Section 3.1.1. At the surface, cross-equatorial flow is most evident in January 1973 and 1975 and February 1973, while in the wetter Australian January of 1974 and, to a lesser degree, February of 1975 (Fig.36) this flow is minimal. As was suggested for the 850 mb circulation, the extreme wetness in the Australian region during January 1974 appears to be coincident with a vigorous southerly-displaced NET_{SH}.

It is evident that, in January 1973 and 1975 and February 1973, the eastern section of the NET_{NH} is strong at both the surface and 850 mb levels and directs northeast trade wind flow across the equator into the New Guinean sector. Only in these months does the western section of an extended surface NET_{NH} strongly interact with the northwestern Australian heat low and/or surface NET_{SH} to initiate inflow from across Indonesia into this part of the Southern Hemisphere. As Murakami (1980 a,b) suggests, the Indonesian longitudes are a preferred area for cross-equatorial flows and surges from Asia, although Sumi and Murakami (1981) indicate that such action may not be the genesis of the stronger 850 mb westerlies in Indonesian longitudes at the peak of Southern Hemisphere summers. Rather, they suggest that this boost in westerly intensity results from Southern Hemisphere developments (at least during the WMONEX period). The orientation of the surface NET_{SH} at such times is very much from southwest to northeast, while in the other

Figure 36 Monthly mean surface streamfunction fields in units of 10^5 m^2 s^{-1} at intervals of 5 units over the regional domain during January and February 1973-75. Heavy dashed lines indicate the positions of the NET_{NH} and NET_{SH}.

JAN

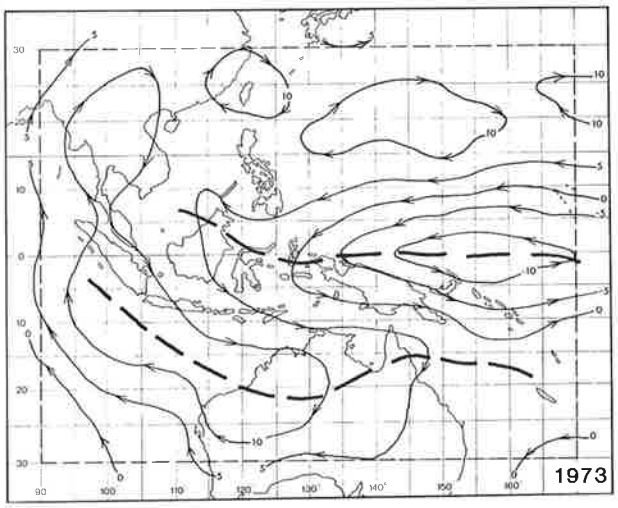

FEB

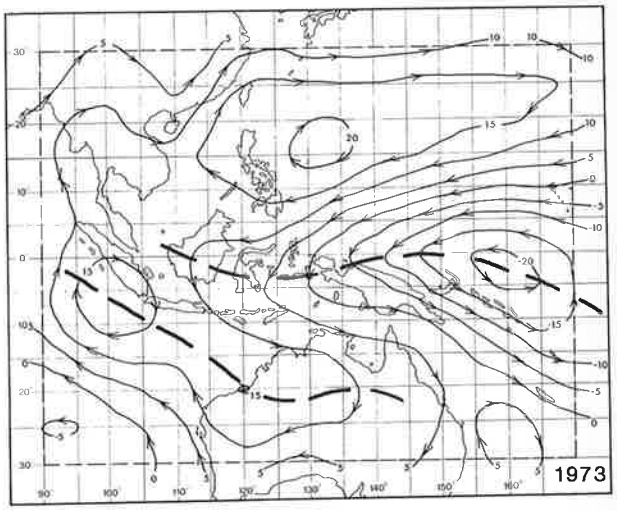

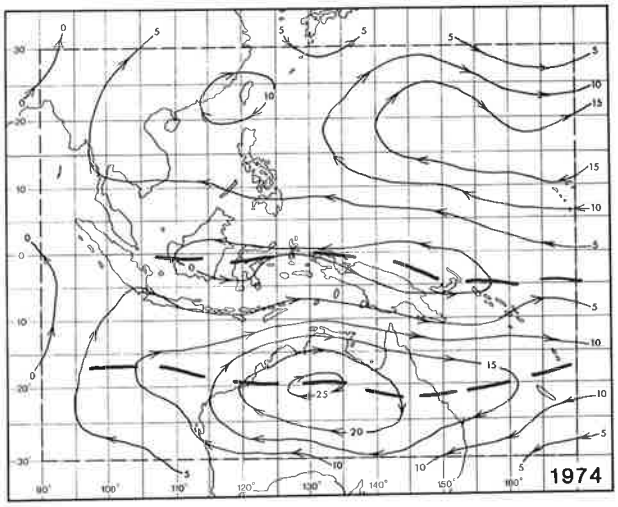

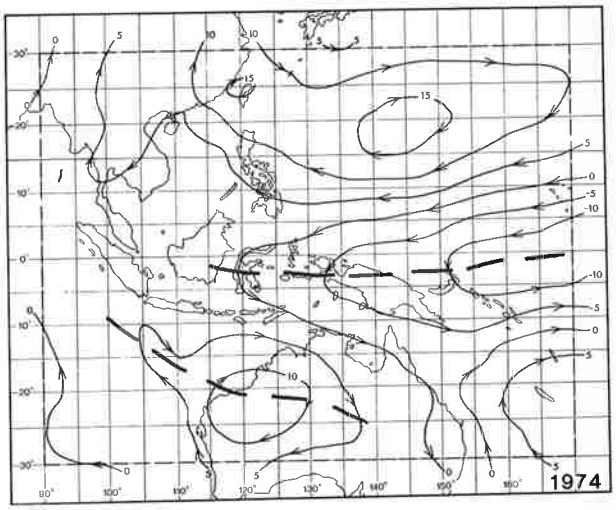

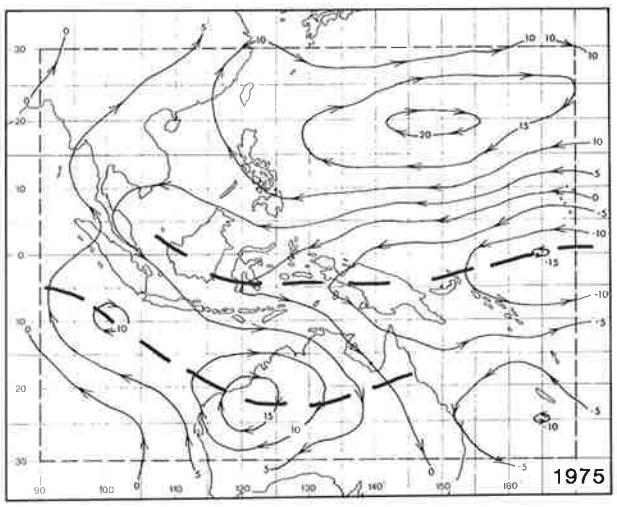

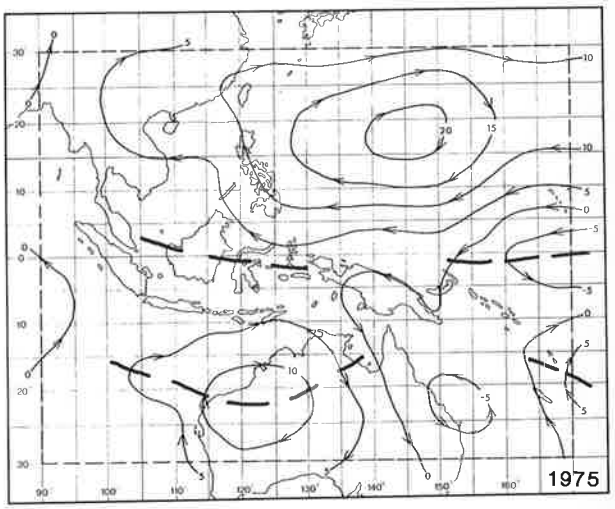

months it takes on a definite east-west inclination.

A feature evident when comparing the surface location (Fig.36) and 850 mb location (Figs.7,8 and 9) of the NET_{SH} over Australia is the marked southwest-northeast vertical tilt of this trough in the Februarys of 1973 and 1974 and a moderate southeast-northwest tilt in January 1973. An aspect of the NET_{SH} at these two levels is the tendency for it to be stronger at 850 mb than at the surface. This is to be expected, as flow nearer the surface is subject to larger frictional effects than that in higher levels above the planetary boundary layer. However, in January 1975 the NET_{SH} is apparently stronger at the surface than at 850 mb, while in January 1973 there is no marked increase in intensity over these two levels. This occurrence in the former month would tend to suggest that cyclonic activity is confined to a shallow layer, perhaps indicative of heat low conditions. Certainly, convective activity in the near-equatorial Indonesian longitudes is quite shallow in January 1975 (Fig.30). It would seem that a better resolution of this discrepancy may result from a more detailed examination of the vertical depth and extent of low-level circulation, moisture and convergence. This is attempted in the local domain section of this thesis.

As a quasi-permanent feature of the low-level Australian summer circulation, the northwest heat low appears to act as an anchoring mechanism for the NET_{SH}. A second continental heat low, centred around Cloncurry (20° 42'S, 140°30'E) in Queensland, is only evident in pressure and geopotential fields (Leslie, 1980). Its function in Australian summer rainfall mechanisms is not discernible in circulation fields alone.

There is a suggestion that on shorter time scales the northwestern heat low and the NET_{SH} may become synonymous, with the heat low's capping inversion being destabilized by periods of strong tropical and near-equatorial moisture infeed into the low (Webster, 1981 c:77-80). In fact, during the month of January 1974, the NET_{SH} totally dominates the Australian circulation pattern. At this time, Australian rainfall is not only high but also widespread (Fig.11), and appears to be associated with a pronounced

monsoon incursion rather than transient features. Such periods reflect the organizing effect which a strong NET_{SH} exerts on low-level circulation over Australia and the Indo-Pacific region as a whole. However, they appear to be distinctly different from periods when low-level flow in the Australian region is marked by the shallow, cyclonic circulation of the heat lows and when monsoon activity is generally weaker. In the latter situations, the northwestern heat low seems to draw in more near-surface cross-equatorial flow from Asian sources. The resolution of this type of dichotomy requires the additional analysis of daily flows and surges before any firm conclusions can be made. Aspects of these flows and surges are examined in the local domain section of this thesis.

(iii) Monthly Mean Geopotential Height, Streamfunction and Kinetic Energy Generation (Surface/1000, 850, 700 and 200 mb) Fields

Having used streamfunction fields to analyse aspects of circulation in the regional domain (Section 3.1.1), it is desirable to see how these patterns relate to geopotential height (GPH) distributions. This is particularly important in view of the fact that tropical circulations can often only be poorly inferred from pressure analysis. Another consequence of the interaction between streamfunction and geopotential height fields is the generation of kinetic energy by cross isobaric motion. Kinetic energy generation (KEG) is readily calculated from a combination of the raw data used to deduce the separate streamfunction and GPH fields (Appendix 7). Where air is flowing up the GPH gradient (that is, from areas of low to high GPH) the KEG field is found to be negative, while, conversely, when it flows down the GPH gradient, positive KEG magnitudes are observed.

Previously, streamfunction fields were calculated for the surface, 850 and 200 mb levels ($\bar{\psi}_{sfc}$, $\bar{\psi}_{850}$, $\bar{\psi}_{200}$). This discussion focuses on the January and February 1973-75 sub-period, but includes additional streamfunction fields for the 700 mb level and GPH fields at the 1000, 850, 700 and 200 mb levels.

Each of Figures 37-42 contains two adjacent sequences, one of streamfunction overlain by GPH (on the left-hand side), the other of KEG (on the right-hand side), at the surface/1000, 850, 700 and 200 mb levels. On the streamfunction/GPH side of these diagrams, the streamfunctions are marked as in Section 3.1.1, while the GPH fields show heights of the 1000 mb level in 20 metre intervals, the 850 mb and 700 mb levels in 10 metre intervals, and the 200 mb level in 50 metre intervals. The right-hand side of the above figures present KEG fields marked in intervals of 5 units for all but the 200 mb surface, where the interval is doubled. Areas of + KEG values (or generation) are unshaded, while areas of - KEG values (or dissipation) are stippled.

One prominent feature in all of the following diagrams (Figs.37-42) is the extent of cross isobaric flow. In fact, areas of geostrophic flow are only readily evident in situations of strong jetstreams (i.e. in the Northern Hemisphere off Japan) or in intense cyclonic or anticyclonic systems. As one would expect, this tends to restrict such conditions to the higher latitudes in both hemispheres. With much of the regional domain taken up by tropical and sub-tropical latitudes, ageostrophic conditions predominate in regions where both pressure and GPH gradients and the coriolis parameter are often weak.

As in the longer 1973-77 sequence (Section 3.1.1), the major variability of atmospheric features is observed over the Southern Hemisphere. In particular, this involves the extent, intensity and depth of cyclonic (both NETs) and anticyclonic circulations and GPH maxima and minima. The Northern Hemisphere situation is more stable throughout the sequence, with the transgressions of January 1974 being the exception. Essentially, the patterns involve a quasi-permanent anticyclone over the northwestern Pacific (NPA) that varies somewhat in intensity but little in position. Overlain with this are GPH fields that are dominated by GPH maxima in the near-equatorial and sub-tropical regions and GPH minima at the northernmost latitudes.

In January 1973 (Fig.37), streamfunction and GPH fields suggest that lower-level circulation associated with the NET_{SH} forms a complex pattern. At each of the 1000, 850 and 700 mb levels, GPH contours locate three major areas of low height in the Australasian region. These centres are situated to the west of Australia around 15°-20°S, near the northwest coast of Australia and to the east of Australia at 5°-10°S near the Solomon Islands. Of these centres, the first two would appear to be slightly stronger than the latter. However, the underlying streamfunction fields only resolve cyclonic circulation associated with two of these areas. The region of low GPH near the northwest coast of Australia displays the most consistent association with adjacent cyclonic circulation. This relationship is evident at the surface/1000 mb and 850 mb levels, while the second association over the Solomon Islands (which may be biased by the Honiara observation) is only evident at the 850 mb level. By 200 mb, the ageostrophic component is dominant in all but the most northerly and southerly midlatitudes of the domain.

At the surface/1000 mb level, a fourth low GPH region (near 20°S, 140°E) seems to be related to the Cloncurry heat low centre over Australia (Leslie, 1980). However, it would appear to be a shallow feature as it is not observed at, or above, 850 mb. Atmospheric flow is directed around the GPH minimum over northwestern Australia, rather than through it as occurs with the GPH minima to the east and west of the continent. Yet, over the regional domain, it seems that geostrophic associations are not generally dominant. This is especially true in the eastern section of the NET_{NH} and even in the higher GPH region associated with anticyclonicity between 20°-30°N.

Strongest + KEG at the surface/1000 mb level (Fig.37) is found in the region of Carnarvon in Western Australia. Here, air from a south-southeasterly direction flows down a marked gradient associated with the northwestern low GPH region. The strongest dissipation of KEG (negative regions) is observed in the far west, over the Indian Ocean, due to pronounced flow being directed up the gradient associated with the local GPH minimum.

Figure 37 Monthly mean surface/1000, 850, 700 and 200 mb streamfunction (light lines), geopotential height (heavy lines) (in the left-hand column) and kinetic energy generation (in the right-hand column) fields over the regional domain in January 1973. Streamfunction field is in units of 10^5 m^2 s^{-1} (surface/1000 to 700 mb) and 10^6 m^2 s^{-1} (200 mb) at intervals of 5 units, geopotential height is in m at intervals of 10 units (surface/1000 to 700 mb) and 50 units (200 mb), and kinetic energy generation in units of 10^{-4} W gm^{-1} at intervals of 5 units (surface/1000 to 700 mb) and in units of 10^{-3} W gm^{-1} at intervals of 10 units (200 mb). Dashed lines at 200 mb (in the left-hand column) indicate monthly mean zonal isotachs in m s^{-1}. Shading (in the right-hand column) indicates areas of negative kinetic energy generation.

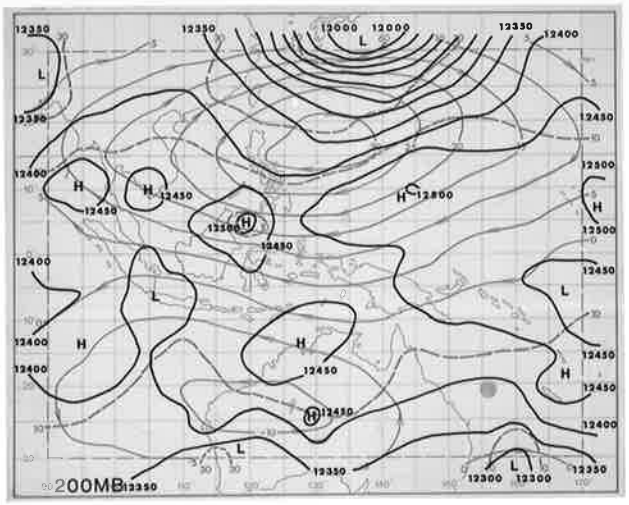

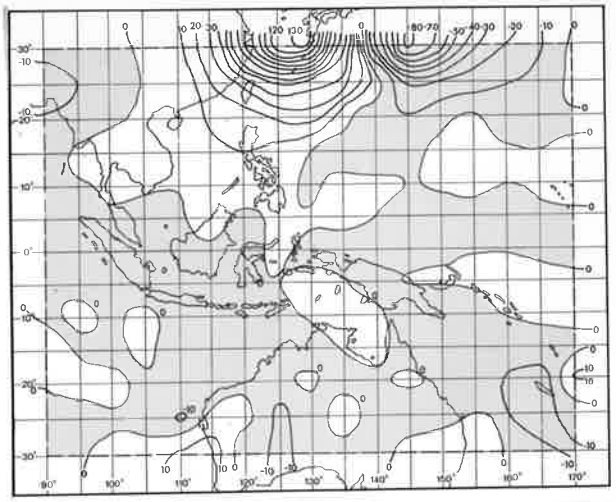

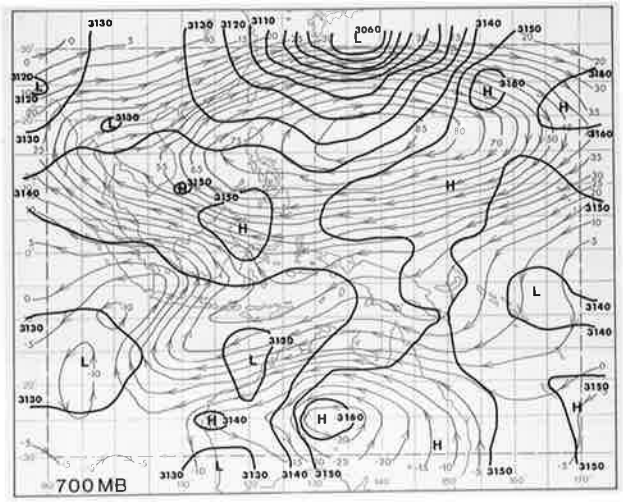

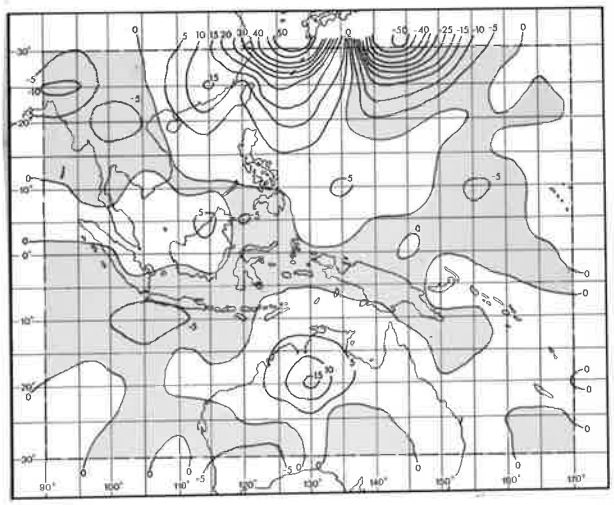

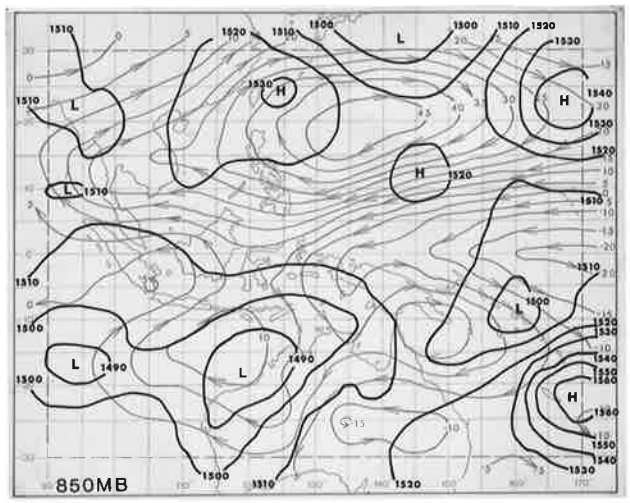

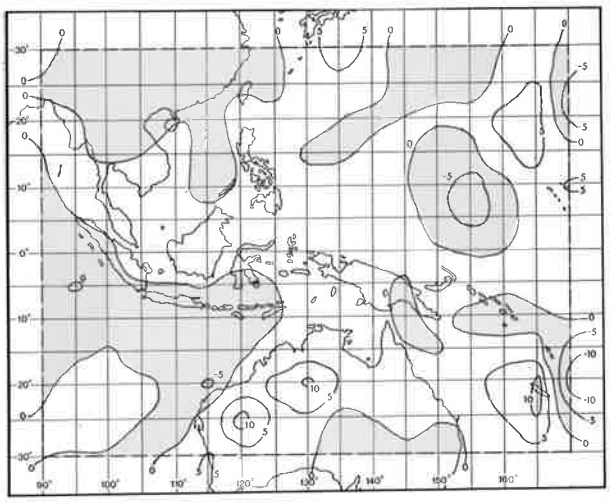

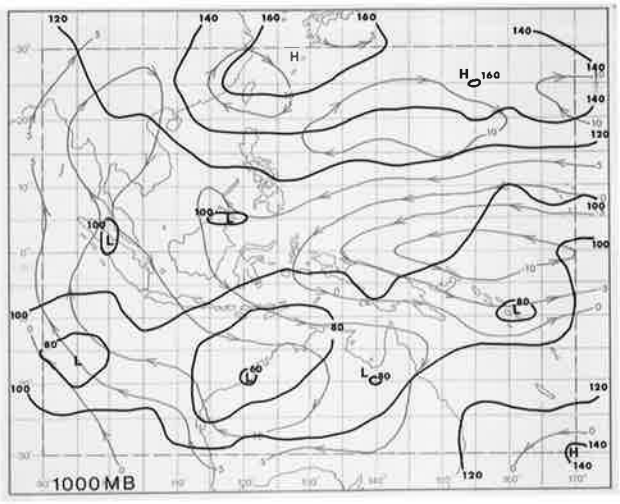

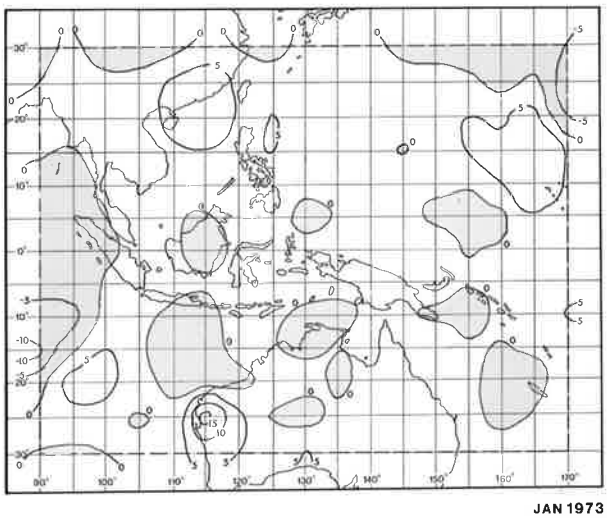

JAN 1973

By 850 mb (Fig.37), streamfunction, GPH and KEG gradients show increased intensity. Over the northwest of Australia the conjunction of streamfunction and GPH fields is slightly reduced, although it is still more noticeable than in regions either to the north-northwest or north-northeast of the continent. Marked anticyclonicity over eastern Australia in the streamfunction field appears to be associated partly with an extension of the pronounced GPH maximum further to the east. Although there is a small anticyclonic maximum to the northwest of Australia, it does not have any apparent relationship to the surrounding GPH field. This may be due to its near-equatorial location and thus the fact that it is influenced by only small coriolis and pressure gradient forces.

In the Northern Hemisphere the large NPA in the streamfunction field is not well aligned with any one distinct GPH maximum. Rather, the flow possesses a marked ageostrophic character with regard to many of the surrounding GPH maxima and minima. Only at higher latitudes in both hemispheres does it appear to maintain some degree of geostrophic balance. This would probably have been even more obvious had GPH and wind data been available from mainland China.

The 850 mb KEG field displays some consequences of the above interactions. Major areas of generation of kinetic energy are evident over west-central and northern Australia and New Calendonia. Again, they are a result of intense flow interacting with sharp GPH gradients. The New Caledonian situation is a prime example of flow moving through a GPH maxima. In fact, a marked gradient from - to + KEG values develops in this region as a result of the abruptness of the above interaction. Similar, but smaller, transitions in KEG sign are evident throughout the regional domain at this level.

The increased intensity of flow and GPH gradients (particularly off Japan) at 700 mb (Fig.37) does not necessarily ensure more geostrophic conditions. Geostrophic balance is most likely in conjunction with flow

at higher latitudes, especially with anticyclonicity over Australia.

Although markedly weakened, three centres of low GPH continue to be associated with the NET_{SH}. Of these, the Indian Ocean and northwestern Australian are still slightly more dominant than the Solomon Islands feature. Moreover, the Indian Ocean GPH centre is aligned with anticyclonic circulation, while the others are located in strong flow associated with adjacent NET_{SH} remnants. In the near-equatorial region of the Northern Hemisphere the flow is also ageostrophic, as it is directed across the high GPH field covering this area.

The resulting KEG distribution shows a marked increase in intensity, especially in the higher latitudes of the Northern Hemisphere. Here, pronounced flow interacts with the strong GPH minimum off Japan to create juxtaposed regions of intense kinetic energy generation and dissipation. However, GPH gradients are not as steep as those in the Northern Hemisphere midlatitudes and, despite the intense flow immediately north of the equator, only small areas of moderate + and - KEG develop.

At the 200 mb level (Fig.37), ageostrophic conditions are still dominant in the domain. However, in the region of the winter jetstream in the Northern Hemisphere and the small northward protrusion of a jet maximum in the Southern Hemisphere, the geostrophic component is more prominent. Throughout the equatorial and near-equatorial regimes, flow is basically easterly and directed across the gradients of GPH maxima and minima alike.

In the Southern Hemisphere, the 200 mb circulation is dominated by a prominent anticyclonic cell over northwestern Australia. However, as in the Northern Hemisphere, there is a poor geostrophic relationship between areas of high GPH and anticyclonic maxima. Although a small region of high GPH is associated with one end of the upper anticyclone over Australia, the major GPH maximum is further north over the northwestern coast of the continent. Once again, this mismatch of circulation and GPH fields appears to be a consequence of weak pressure gradient and coriolis forces in equatorial and near-equatorial latitudes.

UNIVERSITY OF ADELAIDE LIBRARY

The February 1973 sequence (Fig.38) displays many features observed in January 1973. Low-level GPH fields are again dominated by areas of low height in the Southern Hemisphere. However, the January 1973 pattern of three distinct centres is really only evident at 1000 mb. The 850 mb and 700 mb levels reveal that the lowest GPH values are only allied with cyclonic flow over the northeastern Australia/Solomon Islands region. To the west, cyclonic flow at the surface may be a distinct heat low feature, as it is weak at 850 mb (despite the presence of a GPH minimum) and replaced by strong anticyclonicity and high GPH values by 700 mb. In the Northern Hemisphere, GPH distributions are more akin to the January 1973 sequence with a belt of high GPH centres in the tropical to sub-tropical latitudes and markedly lower values in the extreme north. The latter is also prevalent at the 200 mb level.

At the surface/1000 mb level in February 1973 (Fig.38) there is only one distinct centre of low GPH over Australia. Indeed, the heat low/NET_{SH} dichotomy would appear to be manifest in the GPH and streamfunction fields over the northwestern section of the continent. As in January 1973 (Fig.37), the low GPH region takes the form of a band, 15°-20° in width, oriented roughly west-east across the Southern Hemisphere subtropics. As noted above, the central to eastern sections of the low GPH region show a tendency towards slightly lower GPH magnitudes than in the western extreme. Although circulation associated with the eastern section of the NET_{SH} is stronger than in January 1973, a similar pattern of flow across GPH surfaces still occurs. Prime examples of such cross isobaric motion are evident in the most western and eastern centres of low GPH where the flow is directed over or through the GPH minima.

As in January 1973 (Fig.37) the major focus of strong + KEG is in the Carnarvon region, although centres are also associated with the western (Indian Ocean) GPH minimum and mid North Pacific region. Areas of strong - KEG are adjacent to the last two locations and also occur in the region of the South China Sea (20°N, 115°E).

Figure 38 Monthly mean surface/1000, 850, 700 and 200 mb streamfunction (light lines), geopotential height (heavy lines) (in the left-hand column) and kinetic energy generation (in the right-hand column) fields over the regional domain in February 1973. Streamfunction field is in units of 10^5 m^2 s^{-1} (surface/1000 to 700 mb) and 10^6 m^2 s^{-1} (200 mb) at intervals of 5 units, geopotential height is in m at intervals of 10 units (surface/1000 to 700 mb) and 50 units (200 mb), and kinetic energy generation in units of 10^{-4} W gm^{-1} at intervals of 5 units (surface/1000 to 700 mb) and in units of 10^{-3} W gm^{-1} at intervals of 10 units (200 mb). Dashed lines at 200 mb (in the left-hand column) indicate monthly mean zonal isotachs in m s^{-1}. Shading (in the right-hand column) indicates areas of negative kinetic energy generation.

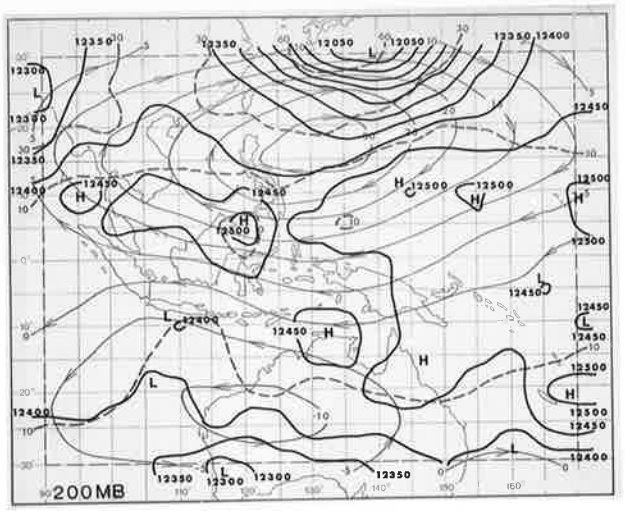

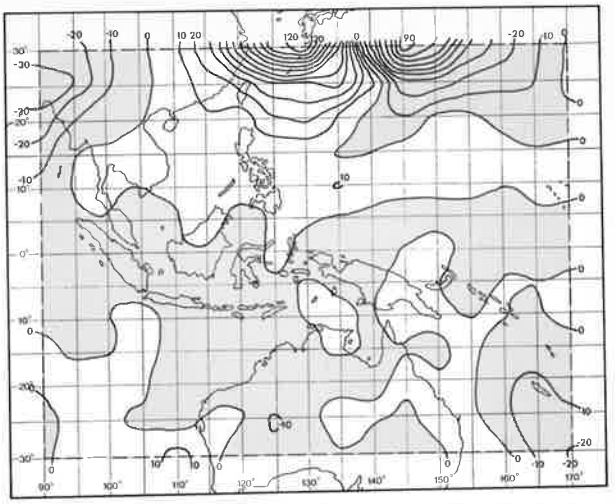

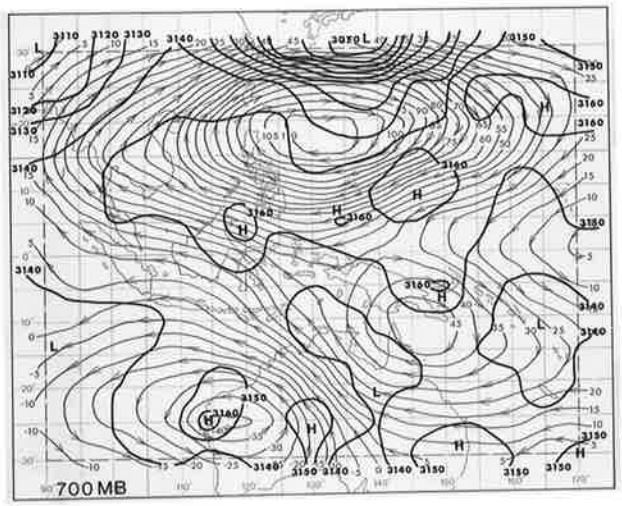

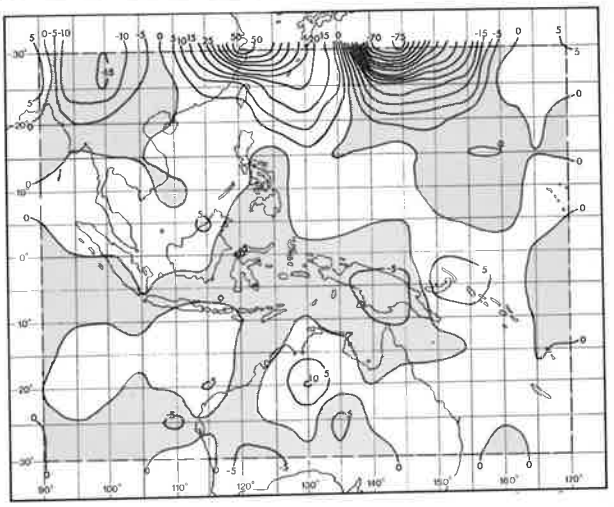

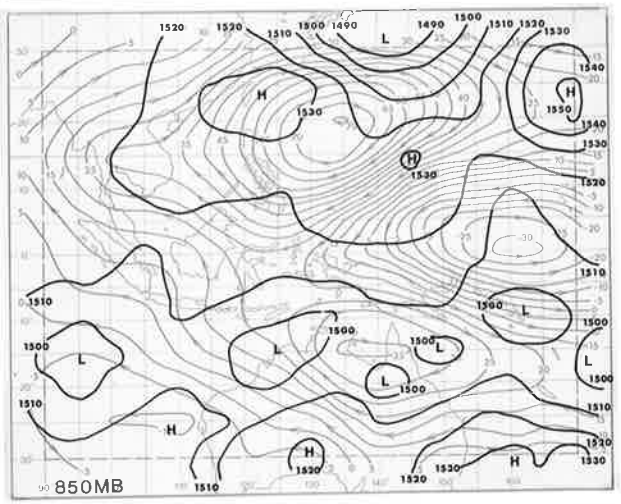

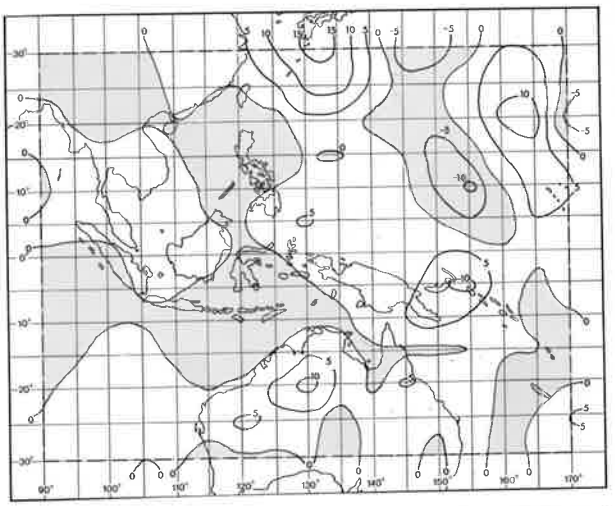

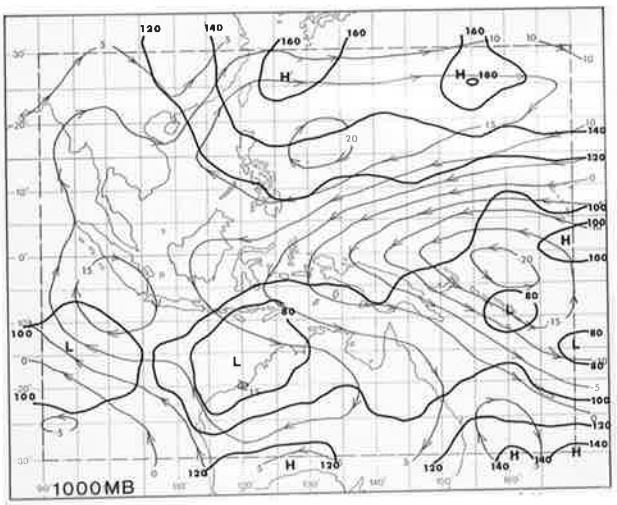

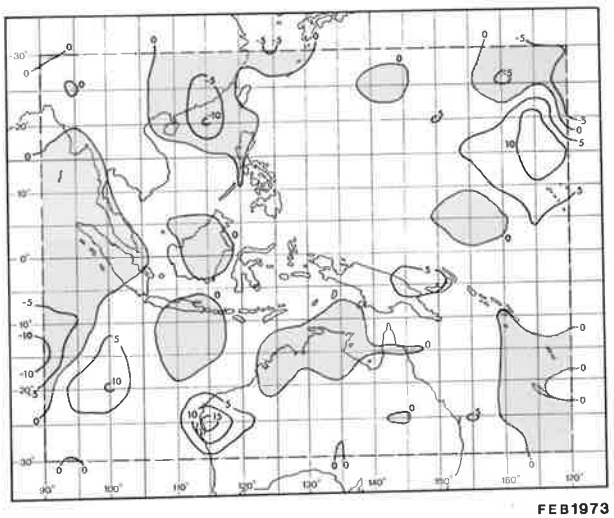

FEB1973

By 850 mb (Fig.38) the low GPH band in the Southern Hemisphere is imbedded with four to five centres below 1500 metres. With streamfunction fields showing that circulation is particularly intense, it is interesting to note that there is some improvement in geostrophic conditions at higher latitudes of the Southern Hemisphere. However, the tropical and sub-tropical regions in both hemispheres continue to display pronounced ageostrophic conditions. Despite the distribution of GPH minima at 850 mb, cyclonic circulation over Australia is now focused on the Gulf of Carpentaria. In fact, the cyclonic circulation maximum in the above region is associated with three areas of low GPH. Of these centres, the two over Australia appear to be related to the heat low complex. In the sub-tropical and middle latitudes of the Northern Hemisphere, the region of high GPH values observed in January 1973 is still prevalent although notably stronger and broader. As in the Southern Hemisphere, circulation and GPH centres do not coincide although they are often closely associated. Like several of the Southern Hemisphere centres of low GPH, flow is also directed across and through some of the prominent areas of high GPH. This chiefly involves the GPH maxima centred near Taiwan and 10°-15°N, 145°E. In fact, it is these areas, together with the Solomon Islands centre of low GPH in the Southern Hemisphere, which display the most persistent cross isobaric action in 1973. This is mainly because of the intense circulation around the NPA and the NET_{SH}.

At 850 mb, KEG is more pronounced in February 1973, probably as a result of the enhanced circulation outweighing any decrease in GPH. Areas of kinetic energy generation and dissipation are more widespread in both hemispheres, with the most marked increase being in the Northern Hemisphere. Once again, the strongest centres occur where pronounced flow traverses steep GPH gradients.

The 700 mb level (Fig.38) is also markedly influenced by an intense streamfunction pattern. However, the accompanying GPH field varies mainly in its distribution, rather than its intensity, of maxima and minima. As at other levels the ageostrophic component is dominant, although strong geostrophic conditions are evident in the higher latitudes of the Northern

Hemisphere and in conjunction with the strong anticyclonic flow over Western Australia.

Cyclonic circulation is still pronounced in the Southern Hemisphere, with the major vortex being centred just off the northeast coast of Australia. Together with the NPA, this centre has an ageostrophic association with nearby GPH maxima and minima. Thus the nature and distribution of cyclonic circulation and low GPH at lower levels in the Southern Hemisphere suggests that the area from the northeastern coast of Australia to the Coral Sea is the seat of the major NET_{SH} circulation in February 1973. Anticyclonicity over Australia is affected, with the focus of the cell being to the west in February 1973 (Fig.38), rather than over the continental interior as in January 1973 (Fig.37).

The distribution of KEG at 700 mb is mainly affected by increased circulation in localized regions. Off Japan, the gradient between the intense + and - KEG centres is enhanced, primarily as a result of stronger flow interacting with the steep GPH gradient. To a lesser degree, this is also observed over mainland China, Papua New Guinea/Solomon Islands, the Timor Sea and central-western Australia.

At the 200 mb level (Fig.38), both cyclonic and anticyclonic flow continue to show a strong tendency towards cross isobaric motion. As a result, the distribution of geostrophic and ageostrophic regions appears to be very similar to that in January 1973 (Fig.37). Any changes in GPH and streamfunction fields between January and February 1973 are small and, at best, appear to be limited in extent. The most notable is an indication that GPH magnitudes at higher latitudes in both hemispheres are affected. In the Northern Hemisphere(Southern Hemisphere), the GPH is 50 metres higher(lower) in February than January 1973 (Figs.37 and 38).

The resulting KEG pattern contains few variations from the January 1973 distribution. Most notable is the increased - KEG magnitude over the Bangaladesh/Thailand region. Otherwise, KEG increases in the order of + or - 10×10^{-3} W gm^{-1} and slight variations in the areas occupied by positive

and negative regions are the only changes. Certainly, this would appear to be a testimony to the intraseasonal persistence of upper-level streamfunction and GPH fields during the peak of the 1973 summer.

During January 1974 (Fig.39) the distribution and intensity of GPH, streamfunction and KEG fields reflect pronounced changes in the Australasian monsoon regime. In the lower levels of the troposphere, strong NET_{SH} activity and low GPH values are concentrated over Northern Australia and the Indian Ocean. In the Northern Hemisphere, it is the streamfunction rather than the GPH that is noticeably affected, with the NPA displaced to the east in all of the lower levels in Figure 39. Of further interest are the dual centres of low GPH in the Southern Hemisphere. Unlike the January and February 1973 sequences (Figs.37 and 38), circulation about the NET_{SH} is more closely associated with an easterly GPH minimum than with the centres over northwestern Australia and the Indian Ocean. However, there is no distinct cyclonic circulation centre or GPH minimum in the region of the Solomon Islands. At 200 mb the situation is marked by a pronounced southerly displacement and closer association of high GPH and anticyclonic circulation in the Southern Hemisphere. Over the remainder of the domain there are noticeable changes in GPH and streamfunction intensity.

At the surface/1000 mb level, GPH minima and cyclonic circulation in the Southern Hemisphere are concentrated over the Australian continent. Once again, these centres are not directly aligned, as the low GPH regions approximate the locations of the dual heat lows, while the cyclonic circulation maximum is over the centre of Australia. Unlike 1973, there are no really distinct centres of low GPH or cyclonic circulation over the Indian Ocean or in the vicinity of the Solomon Islands. As noted in previous discussions, there is little cross-equatorial flow into the Southern Hemisphere, while anticyclonic circulation in the Northern Hemisphere is displaced to the east. Moreover, the GPH maximum in the Northern Hemisphere is centred on 25°-30°N, 125°-130°E, with no secondary maximum further to the east in the middle latitudes of the North Pacific. Thus the intense circulation in

Figure 39 Monthly mean surface/1000, 850, 700 and 200 mb streamfunction (light lines), geopotential height (heavy lines) (in the left-hand column) and kinetic energy generation (in the right-hand column) fields over the regional domain in January 1974. Streamfunction field is in units of 10^5 m^2 s^{-1} (surface/1000 to 700 mb) and 10^6 m^2 s^{-1} (200 mb) at intervals of 5 units, geopotential height is in m at intervals of 10 units (surface/1000 to 700 mb) and 50 units (200 mb), and kinetic energy generation in units of 10^{-4} W gm^{-1} at intervals of 5 units (surface/1000 to 700 mb) and in units of 10^{-3} W gm^{-1} at intervals of 10 units (200 mb). Dashed lines at 200 mb (in the left-hand column) indicate monthly mean zonal isotachs in m s^{-1}. Shading (in the right-hand column) indicates areas of negative kinetic energy generation.

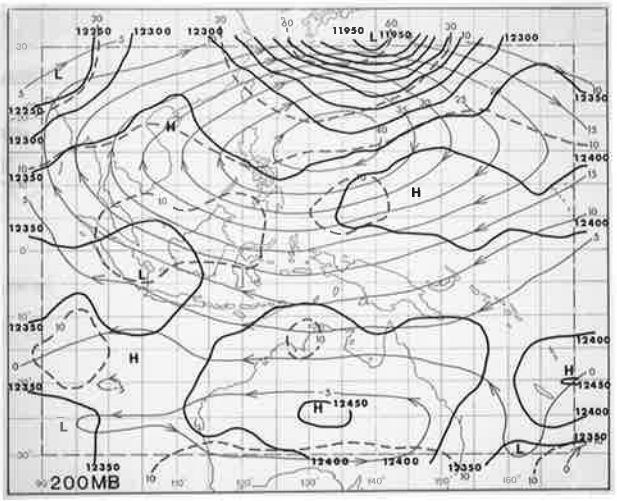

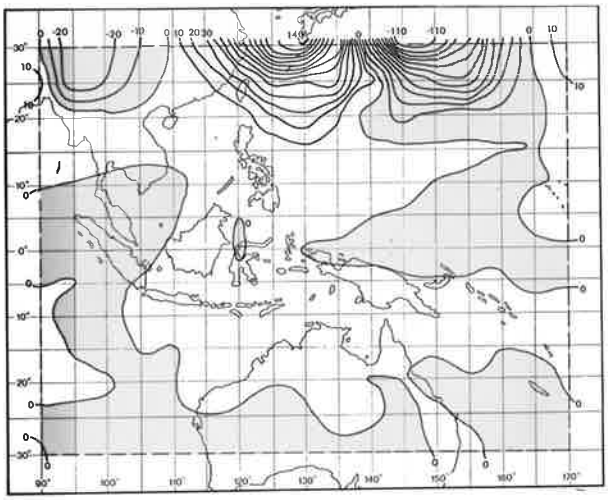

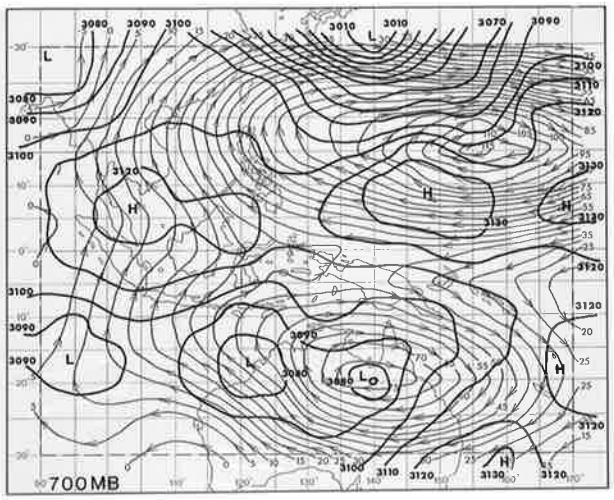

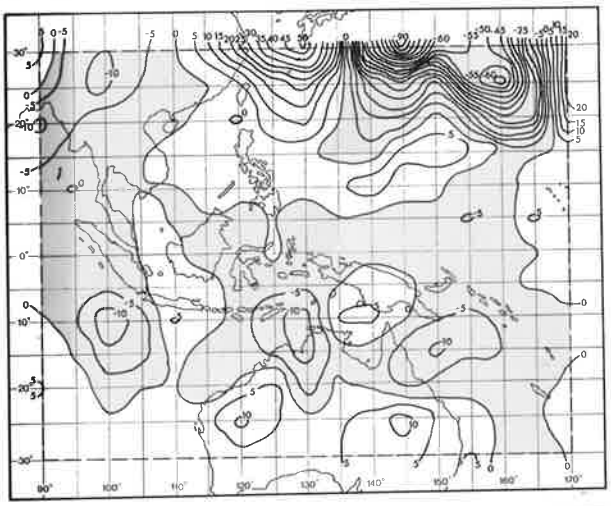

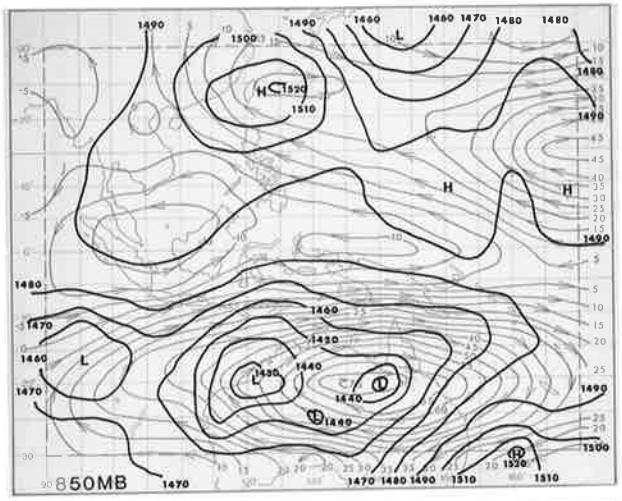

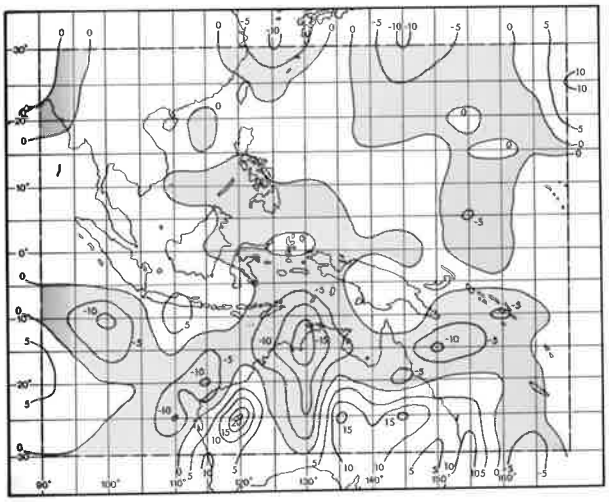

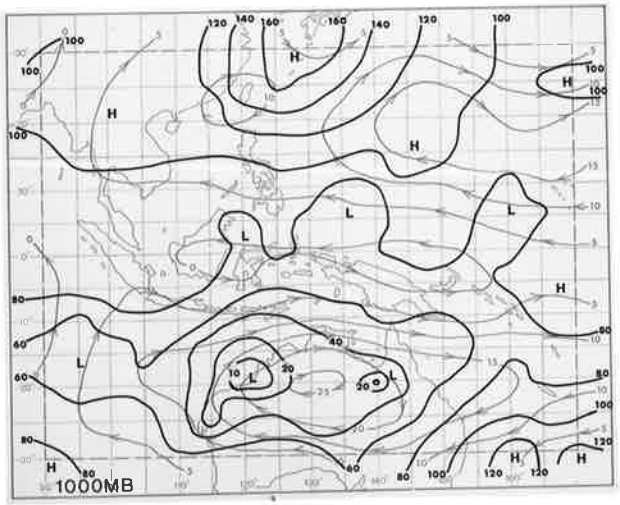

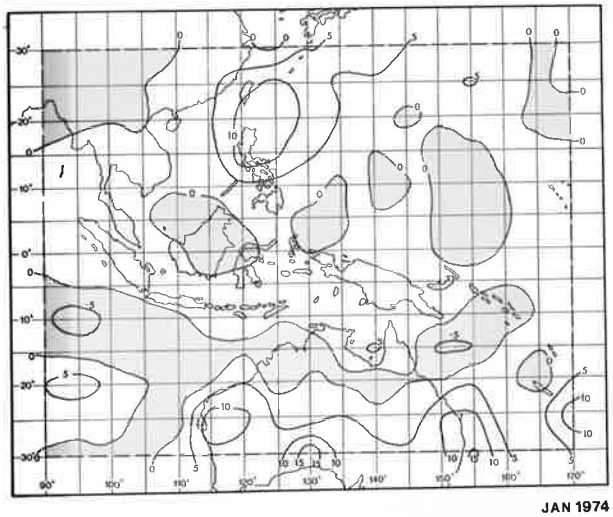

JAN 1974

January 1974 displays little geostrophic balance at this level.

With intense flow often being directed at an angle to sharp GPH gradients, the propensity for enhanced KEG fields is heightened. This is particularly evident over Australia, with centres of + KEG near Carnarvon, over the Nullabor Plain (near 30°S, 130°E) and near the east coast of the continent. To the north, a thin band of - KEG extends from the Indian Ocean in the west to the Coral Sea/Solomon Islands region in the east. The most pronounced minima in the above area are located near its most eastern and western extremities. Over the Northern Hemisphere, an area of + KEG is found in the vicinity of the northern Philippines/South China Sea region. However, there are only isolated + and - KEG regions over the remainder of the hemisphere.

By 850 mb (Fig.39) the intensity and domination of the NET_{SH} over Australia is most evident. As at the surface/1000 mb level, the NET_{SH} is closely associated with several centres of low GPH. However, the more easterly GPH minimum is better allied to the centre of cyclonic circulation near 20°S, 135°E. In the remainder of the Southern Hemisphere, a strong GPH minimum is still evident over northwestern Australia with a weak centre also observed over the Indian Ocean.

Major changes in anticyclonic circulation and GPH in the Northern Hemisphere mirror those at the surface/1000 mb level. The highest GPH centre is associated with a weak anticyclonic remnant to the east of Taiwan. However, the most intense anticyclonic circulation, near 15°N, 170°E, occurs in the absence of a pronounced GPH maximum. NET_{NH} activity is concentrated in more western longitudes, although it continues to be 'ambivalent' to the GPH characteristics.

As at the surface/1000 mb level, the ageostrophic coupling of intense streamfunction and GPH fields results in a marked enhancement of KEG intensity. With a highly active NET_{SH} over Australia at this time, areas of significant + and - KEG engulf the continent. Regions of strong + KEG over western and central-eastern Australia are a result of intense cyclonic

circulation being directed down the steep gradient associated with the lowest GPH centres in the Southern Hemisphere. Further north, several areas of intense - KEG are imbedded in a band of kinetic energy dissipation spanning much of the Southern Hemisphere Indian Ocean, northern Australia and the Coral Sea/Solomon Islands region. These centres result from intense flow ascending the gradient associated with the Australian GPH minima. Over the Northern Hemisphere, areas of strong - KEG tend to predominate. This distribution is probably influenced to a large degree by the displaced anticyclonic circulation pattern.

The 700 mb level (Fig.39) also shows an eastward displacement of anticyclonicity in the Northern Hemisphere and the continued presence of intense cyclonic circulation over Australia. As at the surface/1000 mb and 850 mb levels, the low GPH centres continue to display a persistent association with the NET_{SH}. Likewise, the most geostrophic balance occurs with the GPH minimum and cyclonic circulation over Queensland. However, the low GPH centres over northwestern Australia and the Indian Ocean continue to experience strong ageostrophic flow conditions. Another persistent feature at all three levels is the high GPH centre near 30°S, 160°E. Such continuity is not observed in the 1973 sequences (Figs.37 and 38).

In the Northern Hemisphere, an intense flow gradient is associated with strong anticyclonicity centred over the central North Pacific. This flow is directed through the region of high GPH in the near-equatorial zone of the Northern Hemisphere. However, further north, near the axis of the low GPH region off Japan, it once again shows signs of conforming to more geostrophic conditions. Of some interest is the tendency for basically meridional flow to be directed through the high GPH centre over the Malaysian/Borneo (Kalimantan) sector. As in 1973, the other near-equatorial GPH maxima interact with primarily zonal flow.

The KEG field at 700 mb mirrors such features, with a combination of the sharp + and - KEG gradients observed at 850 mb. This is particularly true of the gradient configuration over Australasia. Centres of strong + KEG

are still evident over western and eastern Australia and result from flow being directed through the northwestern and eastern GPH gradients respectively. Further north, in the Southern Hemisphere near-equatorial and sub-tropical latitudes, centres of + and - KEG are interspersed. A large area of - KEG is still present over the Indian Ocean near 10°S, 100°E and appears to result from strong meridional flow that continues to move normal to GPH gradients well into the Northern Hemisphere. The adjacent area of + KEG centred on Java is much weaker in magnitude, probably because it forms from flow interacting with the GPH gradient at shallower angles. The result could be that the flow in such areas is actually moving slightly down the gradient for short distances and thus contributing to generation rather than dissipation. With intense flow patterns, the angle of interaction with GPH contours is critical in deciding whether + or - KEG areas develop. Over northern Australia and New Guinea, the cause of + and - KEG regions is more obvious. Here, flow crosses the GPH gradient in a sequence from west to east and can clearly be seen to develop the strong - KEG regions over the northwestern and northeastern coasts of Australia and the intermediate + KEG area in the vicinity of Torres Strait.

The Northern Hemisphere pattern is again dominated by regions of extremely intense kinetic energy dissipation and generation over the mid-latitude North Pacific Ocean, from mainland China to the dateline. This is a direct consequence of the intense NPA interacting with a GPH field that is some 50-60 metres lower in height at 30°N than in January and February 1973 (Figs.37 and 38). To the west, a - KEG centre develops over China, but it should be viewed with care, as both raw flow and GPH data are absent over much of this region.

By 200 mb (Fig.39), major changes in flow are centred on a marginal increase in the intensity of circulation associated with the NPA and the southward displacement and weakening of its Australian counterpart. The GPH field reflects some of these changes, particularly in the Northern Hemisphere where the GPH minimum at higher latitudes of the northwestern

Pacific is some 50-100 metres lower in height than in January and February 1973. Coincident with the above is a similar decrease in the height of the GPH maximum in near-equatorial latitudes of the northwestern Pacific. As a result, the GPH gradient in the Northern Hemisphere is little changed from the previous sequences (Figs.37 and 38).

The Southern Hemisphere situation does not seem to reflect the overall decrease in GPH observed in the Northern Hemisphere. However, as with the circulation, there is a noticeable southward shift in the GPH field, with the area of highest values being displaced over the centre of the Australian continent. Yet, this shift in the GPH field is not evident over the southwestern Pacific where high GPHs continue to persist around 20°S. The net result of these changes is that there is a marked increase in the intensity of the flow in the equatorial and near-equatorial latitudes of both hemispheres. Of further interest is the observation that higher latitude flow appears to be markedly displaced to the south across the whole longitudinal belt. As at the lower levels, the increase in flow intensity across GPH gradients results in stronger KEG fields.

Increases in the intensity of + and - KEG centres are most evident across the higher latitudes of the Northern Hemisphere. Such changes amount to some 10-30 per cent of January and February 1973 values. However, in the Southern Hemisphere, the intensity of the KEG field is somewhat less than that observed previously. This may result from the fact that anti-cyclonic circulation conforms to more geostrophic conditions in January 1974. Certainly, this is true of the interaction between southerly-displaced GPH and circulation over Australia. Under such circumstances, one would anticipate that a greater potential for geostrophic alignment would exist.

The February 1974 situation (Fig.40) indicates that some aspects of the previous month's conditions continue to persist. However, there are none of the large-scale displacements of circulation that were evident in the January 1974 sequence (Fig.39). This is exemplified by the more northward location of the NET_{SH} and associated GPH minima through the

Figure 40 Monthly mean surface/1000, 850, 700 and 200 mb streamfunction (light lines), geopotential height (heavy lines) (in the left-hand column) and kinetic energy generation (in the right-hand column) fields over the regional domain in February 1974. Streamfunction field is in units of 10^5 m^2 s^{-1} (surface/1000 to 700 mb) and 10^6 m^2 s^{-1} (200 mb) at intervals of 5 units, geopotential height is in m at intervals of 10 units (surface/1000 to 700 mb) and 50 units (200 mb), and kinetic energy generation in units of 10^{-4} W gm^{-1} at intervals of 5 units (surface/1000 to 700 mb) and in units of 10^{-3} W gm^{-1} at intervals of 10 units (200 mb). Dashed lines at 200 mb (in the left-hand column) indicate monthly mean zonal isotachs in m s^{-1}. Shading (in the right-hand column) indicates areas of negative kinetic energy generation.

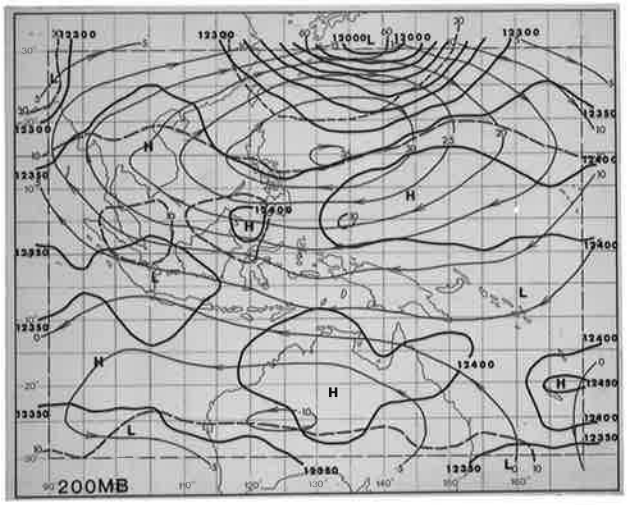

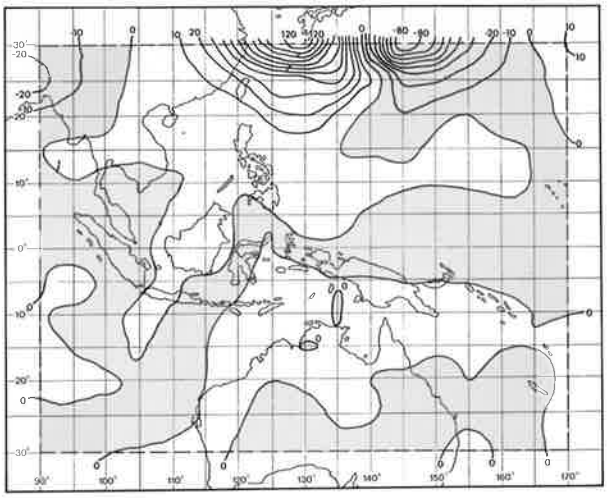

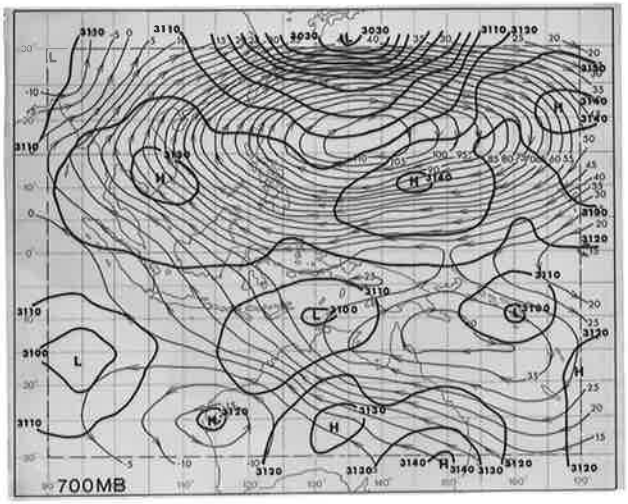

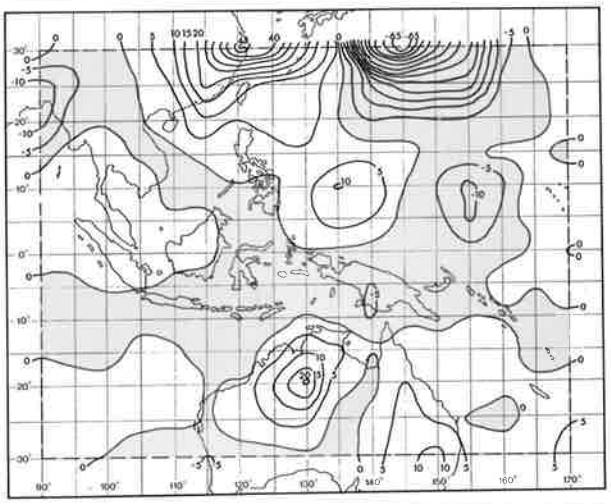

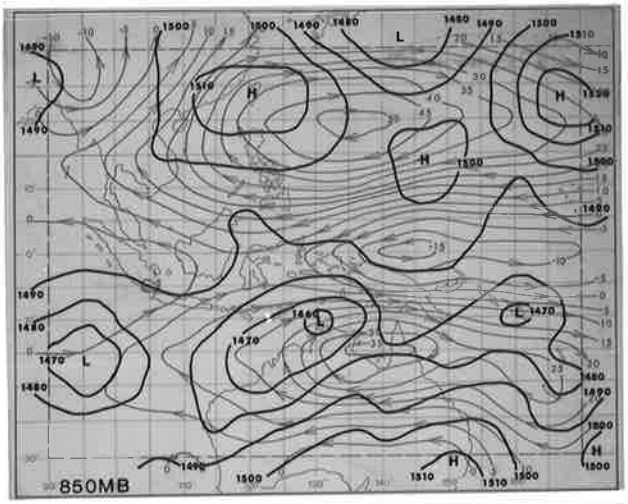

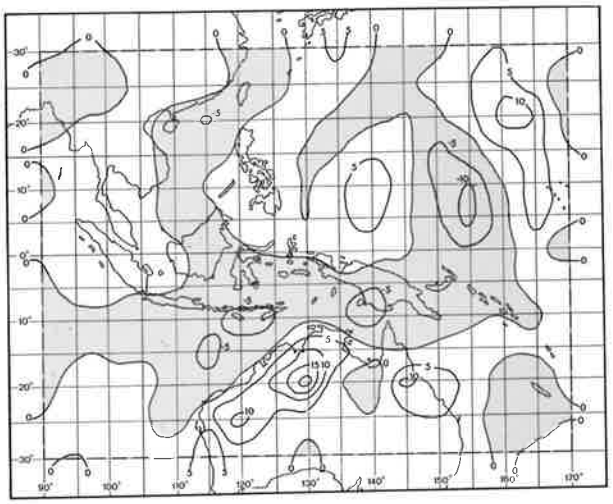

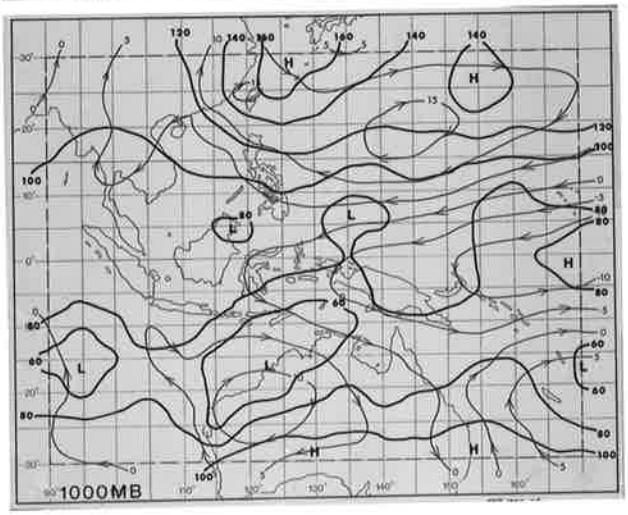

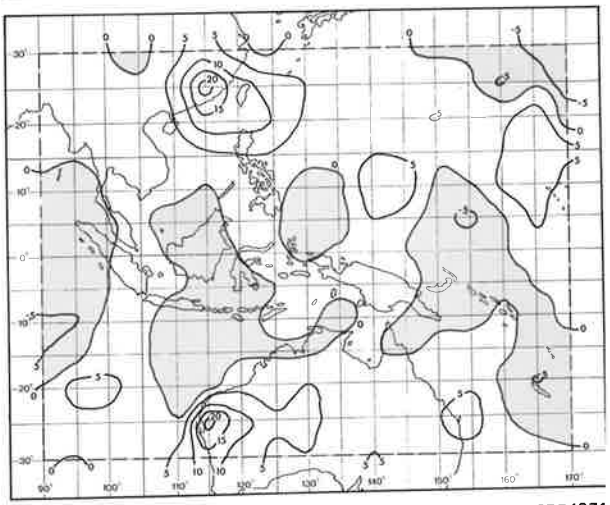

FEB 1974

850 and 700 mb levels, the return of the NPA to a 1973 type location (Figs.37 and 38) and the presence of three distinct low GPH centres across the Southern Hemisphere near-equatorial regions. With the above changes has come a general increase in GPH values at all levels in the domain. Upper-level flow highlights a more northward location of the GPH maximum over Australia, although the area of strongest anticyclonic circulation is still further to the south.

At the surface/1000 mb level, a more elongated zonal band of low GPH is associated with areas of cyclonic circulation in the Southern Hemisphere near-equatorial and sub-tropical regions. The lowest GPH values in the band occur over the Indian Ocean, northwestern Australia and in the extreme eastern longitudes near the New Hebrides. Of these centres, the northwestern Australian and New Hebridean display the most pronounced association with cyclonic circulation. The northwestern Australian situation is particularly prominent, with the circulation perhaps reflecting the influence of the Western Australian heat low. By 30°S, higher GPH values affect most of southern Australia, although values are marginally lower than those in January 1974 (Fig.39) over the Tasman Sea.

In the Northern Hemisphere, anticyclonic flow is once again established over the northwestern Pacific. A smaller cell near Taiwan completes an anticyclonic complex that is closely associated with the high GPH maxima slightly further to the north. In eastern near-equatorial regions, the NET_{NH} is again more prominent in a regime of weak GPH gradients and isolated maxima and minima.

The KEG pattern that results from the above interactions highlights most of the features observed in the previous sequences. Over Australia, the Carnarvon maximum is the most pronounced centre of + KEG, although a small east coast maximum still persists. As observed previously, the northwestern centre results from vigorous offshore flow being directed normal to the low GPH region over the coast. This basically ageostrophic association between cyclonic circulation and low GPH appears to be characteristic of many

northern Australian summer monsoon seasons. In fact, only the January 1974 situation shows any noticeable departure from this type of alignment. Out over the Indian Ocean the flow is directed through the low GPH centre near 15°S, 95°E, and results in areas of + and - KEG developing where the flow descends or ascends the GPH gradient respectively. Throughout the remainder of the near-equatorial regime, weak KEG centres illustrate the nature of GPH and circulation interactions in such regions.

The higher latitudes of the Northern Hemisphere are dominated by stronger KEG extremes, with a centre of pronounced generation located over southern mainland China, and + and - KEG centres over the midlatitude North Pacific, the former centre being a consequence of the interaction between the small anticyclonic maximum over Taiwan and the high GPH area further north.

By 850 mb (Fig.40), the pattern of three low GPH centres within the broad GPH minimum in the Southern Hemisphere low latitudes is again prominent. Although it is focused on a distinct cyclonic centre over Cape York and the Gulf of Carpentaria, the NET_{SH} is still associated with this feature. As the alignment suggests, the area of greatest ageostrophic interaction is still over the north-northwestern coast of Australia. However, further south, higher GPH and stronger anticyclonic circulation are in more geostrophic balance. Associations between the circulation and the GPH minima to the west and northeast of Australia are weaker and basically categorized by flow being directed through the GPH centres. This is most evident in regard to the northeastern (Solomon Islands) centre.

In the Northern Hemisphere tropics, the NET_{NH} is particularly vigorous to the north of New Guinea, but it is not associated with any marked GPH centre or gradient. Over the remainder of the domain, areas of high and low GPH are located around the centre of the NPA. Higher GPH regions are found across the Northern Hemisphere near-equatorial zone, with lower values in the extreme north.

The KEG pattern at this level shows a distribution that is strongly dominated by positive and negative centres formed from the interaction of

low GPH and cyclonic circulation in the vicinity of the northwestern Australian coast and high GPH and pronounced anticyclonic circulation over the sub-tropical North Pacific Ocean. In the former region, a band of strong + KEG lies inland along the northwestern coast, with an abrupt change to - KEG conditions immediately off the coast. This pattern appears to be a consequence of offshore flow moving down the local GPH gradient (associated with the low GPH centre near 10°S, 130°E) while still overland, then veering sharply to move nearly parallel to the coast and slightly up the gradient once out to sea. A similar, although weaker, situation occurs off the north to northeastern coast of Australia. Over the North Pacific Ocean, strong centres of + and - KEG result from the interaction of the high GPH maxima with the NPA. The most prominent interaction occurs near 170°E where the highest GPH maximum in the Northern Hemisphere is centred in a zone of strong horizontal shearing on the eastern flank of the NPA. Other KEG centres develop where the flow is directed through GPH maxima or where GPH maxima are associated with weak shear zones.

At the 700 mb level (Fig.40), anticyclonic circulation in the Northern Hemisphere is of a similar magnitude to that occurring in January 1974 (Fig.39). However, in the Southern Hemisphere, cyclonic circulation is notably weaker and centred further to the northeast over the Coral Sea. In western regions of the hemisphere, anticyclonicity is dominant, with a strong centre located over the Western Australian coast. GPH centres are related to the above circulation in much the same manner as before, but ageostrophic conditions are somewhat more predominant in the vicinity of the NET_{SH} than in January 1974, while greater geostrophic balance is observed in conjunction with the major Australian anticyclonic centre, much like the situation in 1973. Yet, the area of highest GPH over eastern Australia is not associated with anything like the geostrophic conditions over the Western Australian coast. As at 850 mb, the NET_{SH} is associated with a single cyclonic circulation centre and three areas of low GPH, but it is the most eastern of the low GPH areas that seems to be more closely aligned with the NET_{SH}. Unlike the

other sequences, the above GPH minima all share a similar magnitude, despite the fact that the Indian Ocean centre shows no association with the cyclonic circulation of the NET_{SH}.

In the Northern Hemisphere, the NPA is strong, being of similar magnitude to that in January 1974 (Fig.39). Now located in much the same position as it was in 1973, the NPA continues to produce an extremely vigorous ageostrophic component as a result of its interaction with the high GPH centres in near-equatorial regions. Further into the Northern Hemisphere midlatitudes, geostrophic balance becomes more pronounced as flow is dominated by the winter hemisphere jetstream.

The KEG field at 700 mb (Fig.40) exhibits a predominance of strong generation over the Australian continent, off mainland China and in the northwestern Pacific. These regions highlight the areas where flow is moving rapidly down and at a pronounced angle to the GPH gradient. Apart from the + KEG area in the vicinity of China, the Australian maximum is the most obvious example of this effect. As at the 850 mb level, a band of - KEG is found to the north-northwest of the Australian continent. However, it is in the Northern Hemisphere, again in conjunction with the winter jetstream, that the strongest - KEG region develops. In the near-equatorial northwestern Pacific, + and - centres of similar magnitude develop as a result of rapid flow passing through the GPH maximum in this region. Already, it is obvious that the lower levels of the atmosphere over western and northern Australia are often the seat of the major generation of kinetic energy in the Southern Hemisphere. This location appears to be a direct consequence of the ageostrophic relationship between the circulation and low GPH associated with the NET_{SH}.

Generally, the 200 mb level (Fig.40) displays similar interactions between GPH and circulation fields as were observed in January 1974. The most outstanding differences are found over Australia, where the GPH maximum is marginally weaker and further north than in January 1974. Southern Hemisphere anticyclonic circulation is also affected, with the closed

cell over Australia being displaced slightly further north and possessing marginally stronger circulation in February 1974. As the Australian centre of high GPH is now further north than the anticyclonic maximum, ageostrophic interactions increase. Nevertheless, GPH and flow gradients are not overly steep and thus one would expect any increases in the KEG field to be small. The area of highest GPH in the Southern Hemisphere is to be found to the east of Australia in the vicinity of New Caledonia. This centre is on the eastern extremity of the domain making its full spatial extent and possible interaction with the 200 mb circulation difficult to evaluate. As in January 1974 (Fig.39), the location of the Southern Hemisphere 10 m s^{-1} isotach suggests that strong westerly flow is further south than 30°S. Together with the GPH pattern, this would appear to confirm that a gross southerly displacement of systems took place during the peak of the 1974 Australian summer. Northern Hemisphere GPH and circulation fields continue to demonstrate that variations in this hemisphere appear to be relatively small in magnitude yet wide ranging in their consequences for Southern Hemisphere systems.

As indicated above, KEG in February 1974 shows little overall change from that in January 1974. The variations in Australian GPH and circulation features probably only result in minor changes in the broad areas of weak + and - KEG in this region. In the vicinity of the Northern Hemisphere winter jetstream near Japan, centres of intense + and - KEG continue to persist, the magnitudes of each centre being directly related to the speed of air in the jetstream and the interaction with the GPH gradient. With GPH values at least some 50 metres higher over this region in February 1974, it is not surprising that KEG centres are some 20-30 x 10^{-3} W gm^{-1} less in magnitude than January 1974 values. Apart from this, the pattern of KEG in both of the 1974 summer months is very similar.

As has been previously shown in Section 3.1.1, January 1975 circulation stands markedly at odds with that in 1974. Therefore, it is not surprising that there are also some significant differences in the GPH and KEG patterns

between January 1975 and any of the other peak summer months presented in this three year sequence. The most noticeable feature of the January 1975 (Fig.41) situation is that low GPH and cyclonic circulation centres over Australia are extremely shallow in depth to the extent that marked anticyclonicity covers much of the Southern Hemisphere by 700 mb. The NET_{SH} over Australia is thus restricted to the low levels of the atmosphere, being located over the northwest of the continent and seemingly reflecting the dominance of heat low conditions. Up to 850 mb, the Southern Hemisphere GPH field is dominated by three to four centres of low height which occur in similar locations to those in other months of this sequence. Yet, high GPH over central Australia at 850 mb is perhaps a sign that the depth of NET_{SH} activity over the continent is shallow. Higher level conditions indicate that circulation in the Northern Hemisphere may play a part in dictating some Southern Hemisphere trends. However, the location and intensity of the 700 mb and 200 mb Australian anticyclones seem to indicate that the nature of hemispheric interactions is very complex and that the response of GPH and circulation in one month cannot hope to delineate much more than a fraction of the processes involved.

The surface/1000 mb level circulation and GPH fields (Fig.41) typify the pattern discussed for other months, although these fields give no discernible indication of the marked changes that occur in the vertical structure of systems in January 1975. The strongest association between cyclonic circulation and low GPH in the Southern Hemisphere is found over northwestern Australia. Other areas of low GPH are found over the Indian Ocean, in the second Australian heat low position in Queensland and out over the Solomon Islands. Of these centres, only the last reaches GPH values comparable with the northwestern Australian complex. All three GPH centres experience an association with atmospheric circulation that amounts to the flow being directed near normal to them.

The Northern Hemisphere distribution of streamfunction and GPH centres is very similar to that in other months in the sequence, although the GPH

Figure 41 Monthly mean surface/1000, 850, 700 and 200 mb streamfunction (light lines), geopotential height (heavy lines) (in the left-hand column) and kinetic energy generation (in the right-hand column) fields over the regional domain in January 1975. Streamfunction is in units of 10^5 m^2 s^{-1} (surface/1000 to 700 mb) and 10^6 m^2 s^{-1} (200 mb) at intervals of 5 units, geopotential height is in m at intervals of 10 units (surface/1000 to 700 mb) and 50 units (200 mb), and kinetic energy generation in units of 10^{-4} W gm^{-1} at intervals of 5 units (surface/1000 to 700 mb) and in units of 10^{-3} W gm^{-1} at intervals of 10 units (200 mb). Dashed lines at 200 mb (in the left-hand column) indicate monthly mean zonal isotachs in m s^{-1}. Shading (in the right-hand column) indicates areas of negative kinetic energy generation.

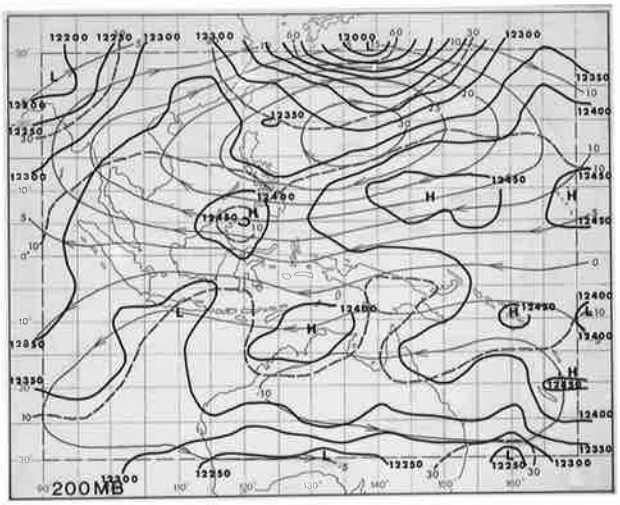

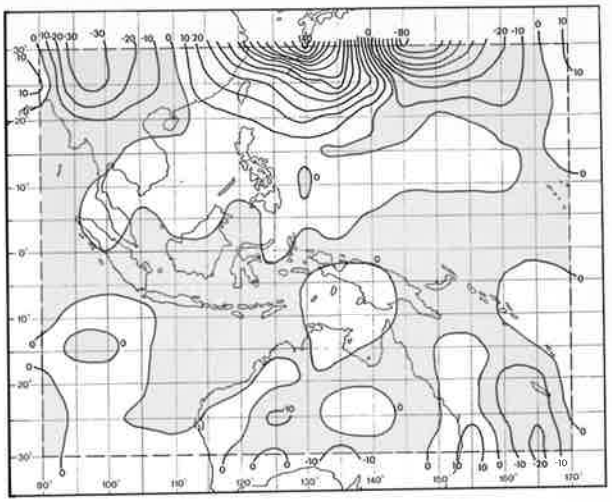

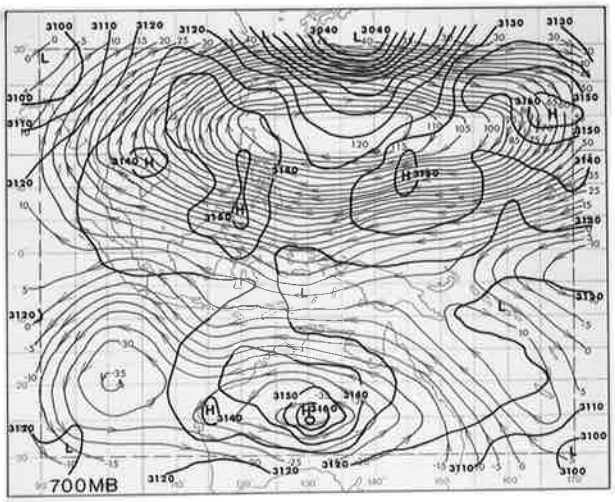

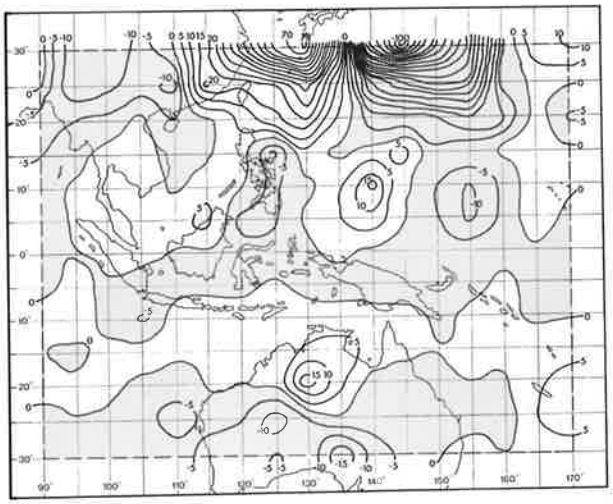

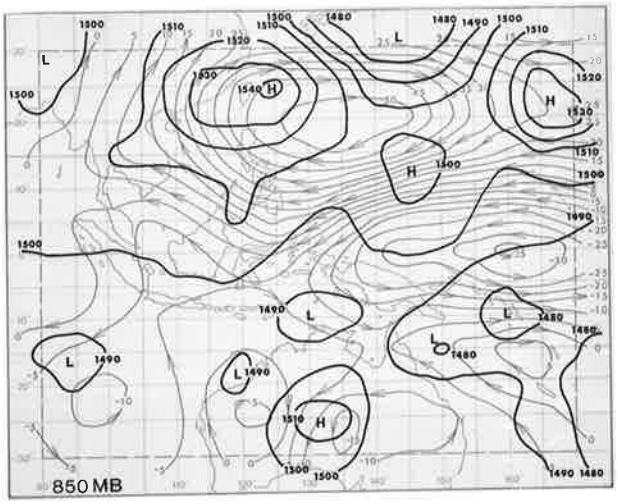

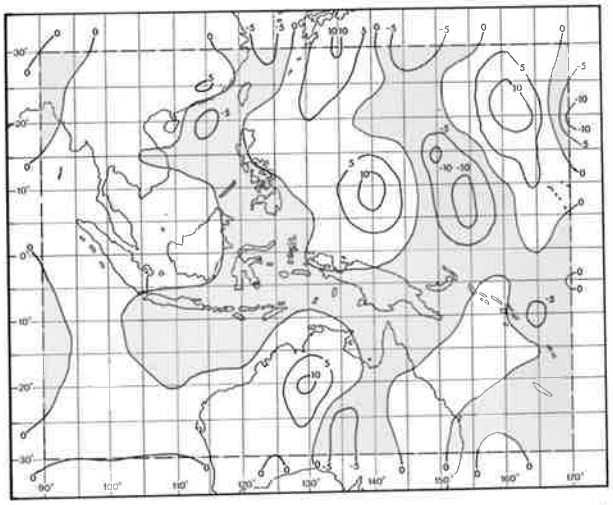

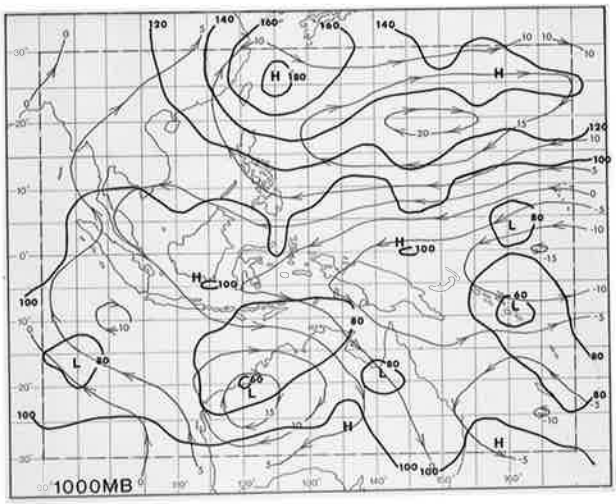

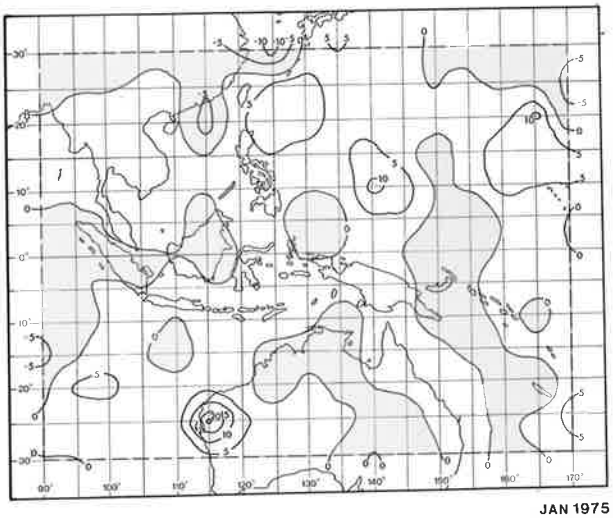

JAN 1975

maximum off Taiwan is marginally deeper than in any of the previous situations. Certainly, there continues to be a poor association between anticyclonic circulation and GPH maxima in the winter hemisphere.

The KEG pattern at the above level continues to show a dominant generation maximum in the region of Carnarvon on the Western Australian coast. With flow forced to ascend the GPH gradient across the middle of the continent in a north to south direction, weak - KEG is observed in this region. A band of weak - KEG also extends south-north from the Tasman Sea to the northwestern Pacific, with some component due to the interaction of the Solomon Islands GPH minimum and the NET_{NH}. Adjacent KEG centres are more apparent over the southern Indian Ocean as a result of the stronger interaction between the low GPH area and flow in this vicinity. More localized KEG maxima and minima are found over the near-equatorial sub-tropical northwestern Pacific, as the basically east to northeasterly flow interacts with minor contortions in the GPH field. Further north, in the higher latitudes of the Northern Hemisphere, + and - KEG regions develop around China and Japan where the western end of the NPA is associated with a pronounced centre of high GPH. Here, the intensity of the GPH field would appear to outweigh that of the circulation field. This is somewhat of a reversal of the situation observed in the vicinity of the Western Australian coast.

By 850 mb (Fig.41), circulation in the regional domain suggests that a major decrease in NET_{SH} activity has occurred over the Australian continent, but the GPH field in this region does not as readily portray the above changes. In fact, GPHs in the Southern Hemisphere are collectively lower than they were in February 1973 when the NET_{SH} was firmly established in the circulation pattern. The only indication that low-level monsoonal structure may be shallow is the presence of an incipient GPH maximum over central Australia. With the lowest GPH centres associated with a strong NET_{NH} and the strongest portion of the NET_{SH} to the northeast of the continent, it is apparent that the most vigorous processes are located in the

vicinity of the tight flow gradient between the Western Australian heat low and an anticyclonic cell to the east.

In the Northern Hemisphere, anticyclonic circulation over the northwestern Pacific is flanked by GPH maxima across the subtropics, with the high GPH centre near Taiwan being the strongest in the total three year period. As in other months, low GPH dominates the higher latitudes of the northern Pacific with flow being mostly geostrophic in its immediate vicinity but becoming rapidly ageostrophic on its eastern and western extremities. On the other hand, most of the interaction between the NPA and its adjacent GPH maxima is distinctly ageostrophic.

The above regions of ageostrophic flow coincide with areas of + and - KEG. In the Southern Hemisphere, this is most evident over central Australia, although a weaker - KEG centre is observed in the vicinity of the Solomon Islands. Further to the north of Australia, the Southern Hemisphere near-equatorial latitudes are covered by a band of weak kinetic energy dissipation which is only punctuated by equally weak KEG over the Indian Ocean.

Northern Hemisphere distributions are more pronounced, with the entire northwestern Pacific sector being populated by an assortment of + and - KEG centres. In the central and northeastern portion of the Pacific Ocean, strong KEG extremes form where the northeast trade winds are directed through local GPH maxima. Flow, interacting with the steep GPH gradient between the GPH maximum near Taiwan and the low GPH areas east of Japan, is responsible for the KEG pattern in the immediate region. The same can be said of the KEG centres in the northeastern corner of the domain.

Circulation and GPH fields at 700 mb (Fig.41) highlight the strong anticyclonic circulation which dominates both hemispheres. The Southern Hemisphere arrangement is particularly interesting in that centres of anticyclonic circulation over the Australian continent and the Indian Ocean differ in their alignment with GPH features. In the former case, there is a marked association of circulation and GPH which conforms more

closely to conditions of geostrophic balance. On the other hand, the Indian Ocean anticyclonic centre is not aligned with any distinct GPH maximum, while the only semblance of the NET_{SH} is also poorly related to the GPH field. Certainly, the intense GPH maximum over the centre of the continent dominates the GPH field in the Southern Hemisphere.

The Northern Hemisphere circulation is dominated by the intense flow pattern of the NPA. No other feature is as prominent. The only semblance of the NET_{NH} is found in the equatorial Pacific. The centres of high GPH that cover the Northern Hemisphere subtropics continue to be overridden by strong atmospheric flow. In fact, as noted in other months of the sequence, the only area of geostrophic or near-geostrophic alignment is found further north, in conjunction with the area of low GPH off Japan.

Despite the prevalence of geostrophic conditions over central Australia, KEG over the continent is most marked in the Southern Hemisphere. Once again, this situation appears to develop because the system in question involves the interaction of intense GPH and streamfunction fields. Any minor misalignment of either field is sufficient to produce large KEG extremes.

The Northern Hemisphere midlatitudes are also the seat of various + and - KEG centres. This is to be expected because of the interaction between the flow circulating about the NPA and local GPH maxima over the region. Further north, ageostrophic and geostrophic conditions alternate abruptly, although (as in Section 3.1.1) this could well be magnified by the sparse data in parts of these regions.

The 200 mb circulation and GPH overlay (Fig.41) illustrate the association of these fields during a period when the upper anticyclone in the Australian region is strong and displaced somewhat to the east of the continent. In this case, GPH centres do not align well with the Southern Hemisphere circulation regime. The major GPH maxima are found in the Solomon Islands/ New Caledonian region, with a weaker area on the north-northwestern Australian coast. Geostrophic conditions are only evident in the extreme southerly latitudes of the domain.

Immediately north of the equator, areas of high GPH are traversed by the southern extremity of the circulation of the NPA. However, gradients of both fields are not nearly as pronounced as those in the extreme north of of the domain, although, for most parts, ageostrophic conditions prevail. Here, the now familiar pattern of low GPH and jetstream flow in an intense association is again evident.

The KEG field at 200 mb suggests that the Southern Hemisphere is dominated by weak + and - centres off the east coast of Australia. Over the remainder of the hemisphere the KEG field is very flat, following much the same amorphous pattern of other months in the sequence. In the Northern Hemisphere, however, the continuation of juxtaposed + and - KEG maxima is the most prominent feature. Any lack of strong KEG extremes in Northern Hemisphere near-equatorial regions is evidently the result of poor circulation and/or GPH gradients.

As noted in Section 3.1.1, January and February 1975 represent a period of marked intraseasonal variability in the monsoonal regime over Australia. In Figures 41 and 42 this may be observed in both circulation and GPH fields at all levels. However, it is most pronounced at the 850 mb and 700 mb levels where circulation and GPH fields associated with the NET_{SH} are noticeably more organized and deeper in the February 1975 sequence (Fig.42). By 200 mb, the most direct consequence of such changes appears to be the position and strength of anticyclonic circulation over the Australian region. As in other months during 1973-77, the association of GPH and circulation fields suggests that ageostrophic conditions tend to prevail at all levels in the domain. This has important ramifications, not only for the structure of monsoonal features in the Australasian region but also for teleconnection dynamics.

There are many similarities between circulation and GPH associations at the surface/1000 mb level in January and February 1975 (Figs.41 and 42). Both months show a northwestern Australian centre of cyclonic circulation in association with a GPH minima that is part of a more extensive band of

Figure 42 Monthly mean surface/1000, 850, 700 and 200 mb streamfunction (light lines), geopotential height (heavy lines) (in the left-hand column) and kinetic energy generation (in the right-hand column) fields over the regional domain in February 1975. Streamfunction is in units of 10^5 m^2 s^{-1} (surface/1000 to 700 mb) and 10^6 m^2 s^{-1} (200 mb) at intervals of 5 units, geopotential height is in m at intervals of 10 units (surface/1000 to 700 mb) and 50 units (200 mb), and kinetic energy generation in units of 10^{-4} W gm^{-1} at intervals of 5 units (surface/1000 to 700 mb) and in units of 10^{-3} W gm^{-1} at intervals of 10 units (200 mb). Dashed lines at 200 mb (in the left-hand column) indicate monthly mean zonal isotachs in m s^{-1}. Shading (in the right-hand column) indicates areas of negative kinetic energy generation.

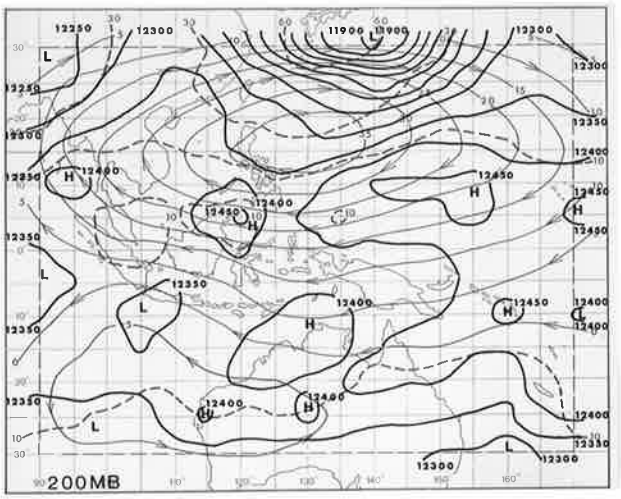

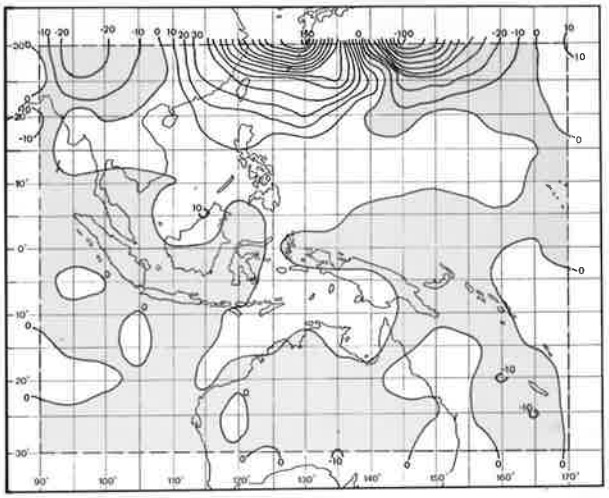

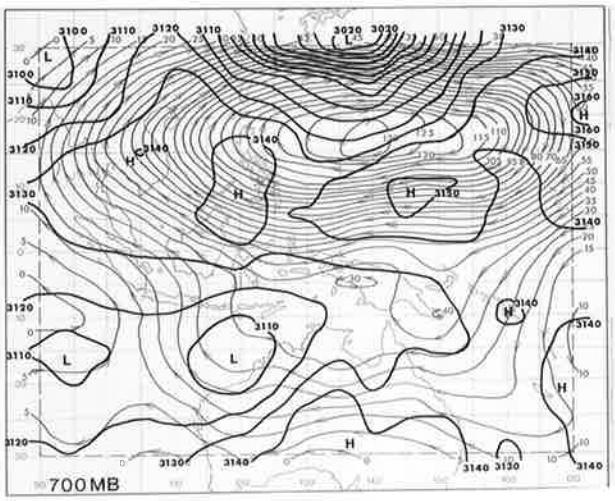

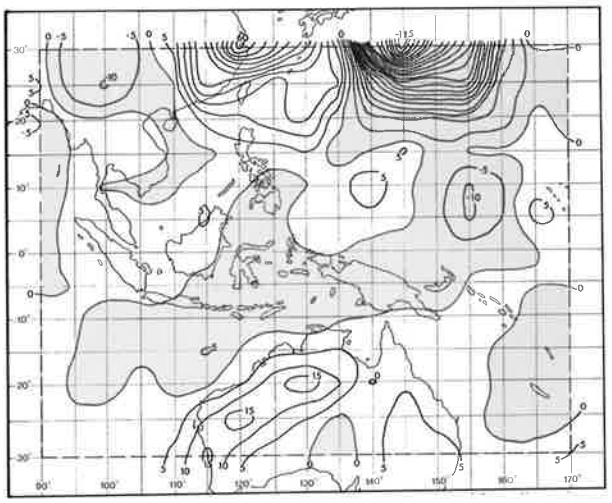

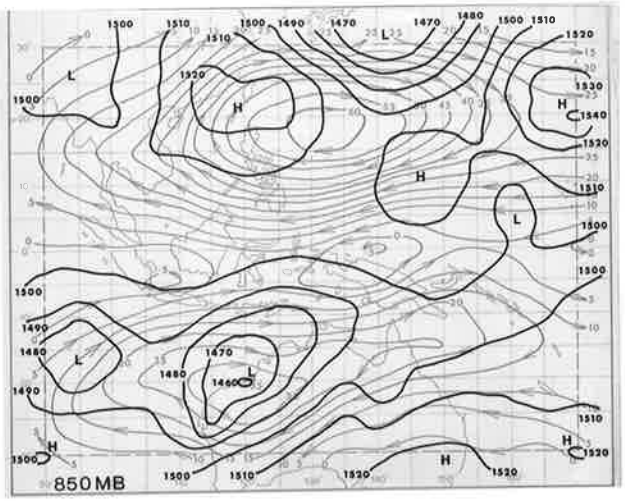

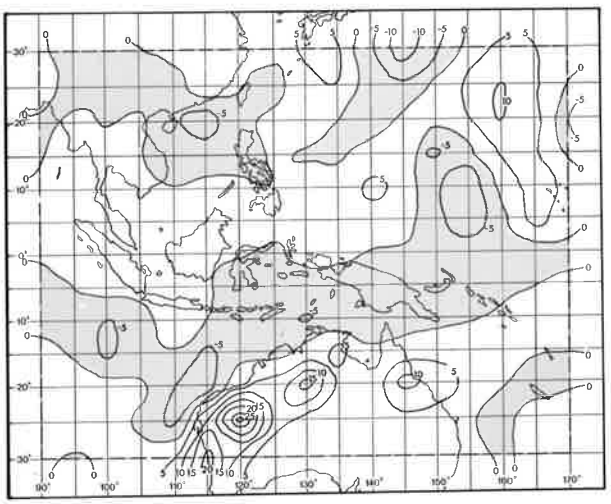

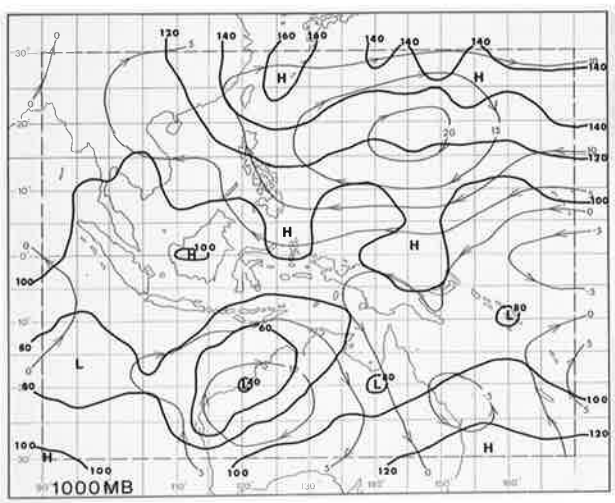

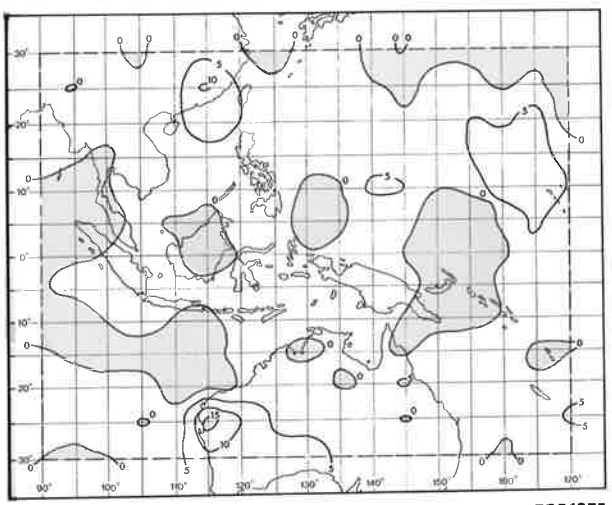

FEB1975

low GPH across the Southern Hemisphere near-equatorial and sub-tropical regions. Similar to other months during 1973-77, the above band is imbedded with three to four areas of particularly low GPH. Over Australia, the northwestern and the smaller northeastern GPH minima appear to constitute the continental summer heat low complex. Interestingly, the intensity of cyclonic circulation over northwestern Australia in January 1975 is slightly stronger than that in February 1975, despite the opposite trend in the associated GPH centres. Further to the west and northeast of the continent the Indian Ocean and Solomon Islands centres continue to show poor associations with the circulation regime.

Northern Hemisphere circulation also displays a poor relationship with the GPH field, as the NPA interacts with a band of high GPH further to the north. Thus atmospheric flow continues to be basically ageostrophic, with a similar configuration of circulation and GPH fields in most of the sequences. Nearer to the equator there is little evidence of NET_{NH} activity in the face of weak flow and GPH gradients.

The KEG distribution reflects the above trends, with the strongest centres being the generation regions near Carnarvon in Australia and southern China. The former centre results from flow rushing down the strong GPH gradient associated with the northwestern Australian cyclonic region. In the Northern Hemisphere, the other strong + KEG area probably results from a localized movement of air slightly along and down the GPH maximum off Taiwan. A number of smaller + and - KEG areas populate the remainder of the domain, with the largest expanses of - KEG being over parts of the Indian Ocean, centred on the eastern edge of the 'maritime continent' and in the midlatitude North Pacific Ocean (Fig.42). Apart from the Carnarvon region, most of Australia is influenced by an amorphous distribution of KEG. A weaker area of + KEG is found in the mid northern Pacific where flow on the southern flank of the NPA is directed across the local GPH gradient.

By 850 mb (Fig.42), Southern Hemisphere cyclonic circulation is particularly strong and GPH low over northwestern Australia. In fact, the

northwest Australian centre of cyclonic circulation dominates the hemisphere and constitutes the NET_{SH}. The low GPH band associated with the above has only two extremely low centres, the major one over Australia and a secondary centre over the Indian Ocean. Although the flow still displays a strong ageostrophic element, it conforms to more geostrophic conditions over the midlatitudes of eastern Australia. Further to the north of the continent, the NET_{NH} is still weak, being sandwiched between the strong circulation of the NET_{SH} and the NPA. The latter feature dominates the Northern Hemisphere circulation regime and is flanked by areas of high GPH in the subtropics and low GPH in the middle to higher latitudes. Only in the low GPH region further north does the flow briefly attain geostrophic balance. However, as noted in other sequences, the sub-tropical GPH maxima experience pronounced ageostrophic conditions as vigorous flow is directed through them.

The 850 mb KEG pattern indicates that there is a fine separation between regions experiencing ageostrophic and geostrophic conditions. The most intense area of + KEG in any of the sequences is found in a band across Western Australia and the Northern Territory. This develops as a result of intense flow on the southeastern flank of the NET_{SH} being out of balance with the adjacent steep GPH gradient. A secondary generation centre develops over the Queensland coast, seemingly as a result of localized interaction between circulation and GPH fields. Similar to other months during 1973-77, the region to the north-northwest of Australia is influenced by a band of - KEG. Several stronger - KEG centres are imbedded in a tract that develops in response to flow on the northern flank of the NET_{SH}, being directed at slight angles up the gradient of the low GPH regions further south.

In Northern Hemisphere near-equatorial latitudes, + and - KEG centres are found to develop where flow moves through the high GPH region in the mid north Pacific. This is also true of areas further north where the flow is directed through or at an angle to GPH surfaces. Apart from the higher latitudes of the Southern Hemisphere, the above region is the only other in

the domain in which flow is in any sort of geostrophic balance for short distances.

At the 700 mb level (Fig.42), only a remnant of the cyclonic circulation associated with the NET_{SH} is over Papua New Guinea. However, the major foci of low GPH in the Southern Hemisphere are in two centres, one off the northwestern coast of Western Australia and the other over the Indian Ocean. As a result, flow is generally oriented at an angle to the GPH gradient, with only a hint of geostrophic conditions where anticyclonic flow and higher GPH values occur over southern Australia. Two areas of high GPH are found in the far eastern longitudes of the domain, although only the larger area appears to be allied with anticyclonic circulation.

Northern Hemisphere near-equatorial and sub-tropical regions are dominated by the intense easterly flow on the southern flank of the massive NPA. This flow is directed through the high GPH centres which occupy much of the above region. Further north, the intense flow and GPH gradient on the northern flank of the NPA come into geostrophic balance in the middle longitudes of the domain. However, they are essentially ageostrophic over the remainder of middle latitudes of the hemisphere.

The Southern Hemisphere KEG distribution at 700 mb is again dominated by strong generation over the western half of the continent. This is expected because the flow is directed at right angles to the steepest GPH gradient in the hemisphere. Areas to the north-northwest of Australia are covered by a broad band of - KEG which does not reach any degree of intensity until it is well into the Northern Hemisphere subtropics. In the latter hemisphere, the strongest KEG centres are in the highest latitudes where both flow and GPH gradients are at a maximum. However, there are several weaker centres in the subtropics where the strong flow interacts with localized GPH maxima.

The pattern of 200 mb anticyclonic circulation over the Southern Hemisphere varies markedly between January and February 1975 (Figs.41 and 42). Although the Australian upper anticyclone shifts from a distinctly easterly

to a marked westerly location during this period, the GPH field displays little change. An area of high GPH is still evident over northwestern Australia, with the Southern Hemisphere extention of a larger GPH maximum covering much of the area to the east-northeast of the continent. Lower GPHs influence the higher latitudes, having the most pronounced minimum off the east coast of Australia. Circulation continues to display a markedly ageostrophic association with the GPH field, although traces of geostrophic balance are found in the most southerly latitudes.

The Northern Hemisphere pattern is similar to that in previous months. An intense NPA dominates the circulation and areas of high and low GPH occur in near-equatorial and sub-tropical latitudes respectively. However, any intraseasonal changes in this hemisphere are restricted to a slight (10 metre) lowering of GPH at higher latitudes and an increase in anticyclonic circulation (5×10^6 m^2 s^{-1}) in the northwestern Pacific.

The 200 mb KEG distribution over the domain continues to be dominated by areas of intense + and - magnitude across the northernmost latitudes. Little vigour is detected in the remainder of the region since intense flow and GPH interactions are very localized.

From this analysis, it is apparent that ageostrophic conditions dominate the tropical and sub-tropical regimes of both hemispheres, and probably encompass the entire vertical extent of flow in the troposphere. The association of streamfunction and GPH fields at all levels provide examples of this phenomena. As in the case of circulation fields, there is a pronounced variability in GPH and KEG fields over the Australian region.

Although streamfunction and GPH centres are generally associated, they are, in the main, not distinctly aligned. In fact, geostrophic balance is most readily evident in situations of strong jetstreams and broad cyclonic or anticyclonic systems. As a result, geostrophic balance is frequently observed at higher latitudes in both hemispheres. Yet, even in the above situations, small variations in either field appear sufficient to trigger

large KEG values as a result of one intense field coming out of alignment with another.

3.2 INTERANNUAL AND INTRASEASONAL VARIABILITY - MOISTURE CHARACTERISTICS AND COLD SURGES IN THE 1973-77 SUMMERS OVER THE LOCAL DOMAIN (5°S-30°S; 95°E-155°E)

In this section, moisture characteristics and cold surges are examined at low levels (surface, 900, 850 and 700 mb levels) in the more local Australian domain (5°S-30°S; 95°E-155°E). As in Section 3.1.1, this analysis covers two temporal periods. These are the major period of January, February and March 1973-77 and the sub-period of January 1973-75. The major period examines the spatial distribution and vertical structure of monthly mean total, advective and eddy moisture characteristics in the surface to 700 mb layer over northern Australia. Moisture characteristics examined include the streamfunction of the water vapour flux, water vapour flux divergence, precipitable water content, wind direction steadiness, water vapour flux, mixing ratio, u and v wind components and aerological traces of dry bulb and dew point temperature. The sub-period investigates the spatial extent and penetration of Northern Hemisphere cold surges over the Australian region.

Figure 43 shows the radiosonde and rawinsonde station distribution in the local domain from which the moisture characteristics fields were calculated (area enclosed by dashed lines). Although the number of stations is much fewer than those available for the same portion of the regional domain (rawinsonde or upper wind stations alone in Fig.6), circulation distributions and intensities at 850 mb in the local domain closely resemble those in the regional domain (Figs.7, 8 and 9 compared with Figs.49-63). Figure 44 is included to illustrate the orography of the Australian continent and to supplement later references to the possible influence of orography on low-level moisture fluxes and convergence. In fact, despite an overall predominance of low relief, areas as high as 600 to 1200 metres exist in northern Australia and can be expected to provide interaction with flow in layers between the surface and 900 mb levels. One important aspect of such interactions may involve the development, location and structure of the low-level heat lows and the Australian continental portion of the NET_{SH}.

Figure 43 Distribution of radiosonde stations in the local domain. These stations provided both upper air and upper wind data.

Figure 44 Hypsometric map of Australia. Height above sea level in m. (from Department of Minerals and Energy, 1973).

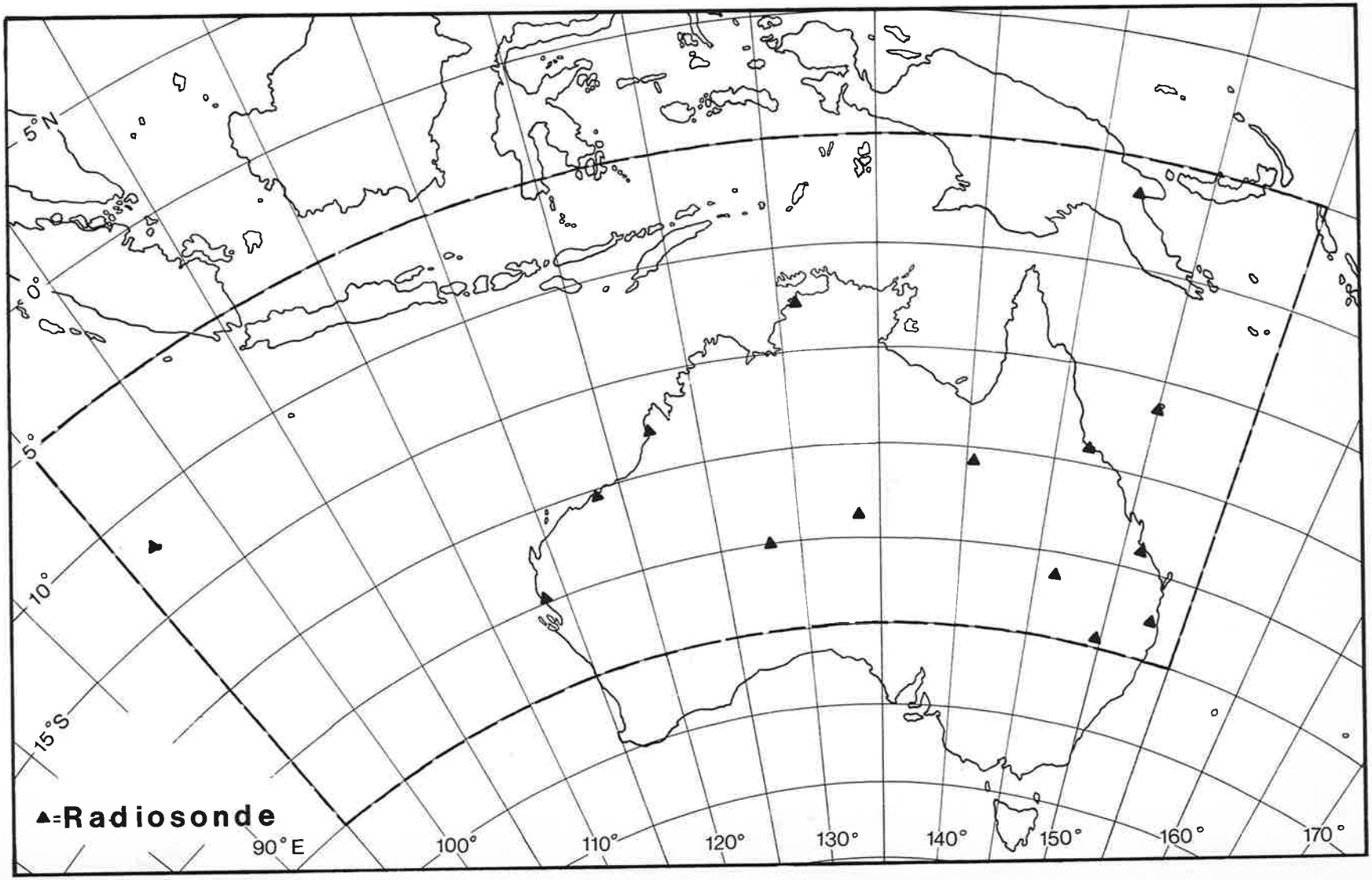
5°N
0°
5°
10°
15°S
▲=Radiosonde
90°E
100°
110°
120°
130°
140°
150°
160°
170°

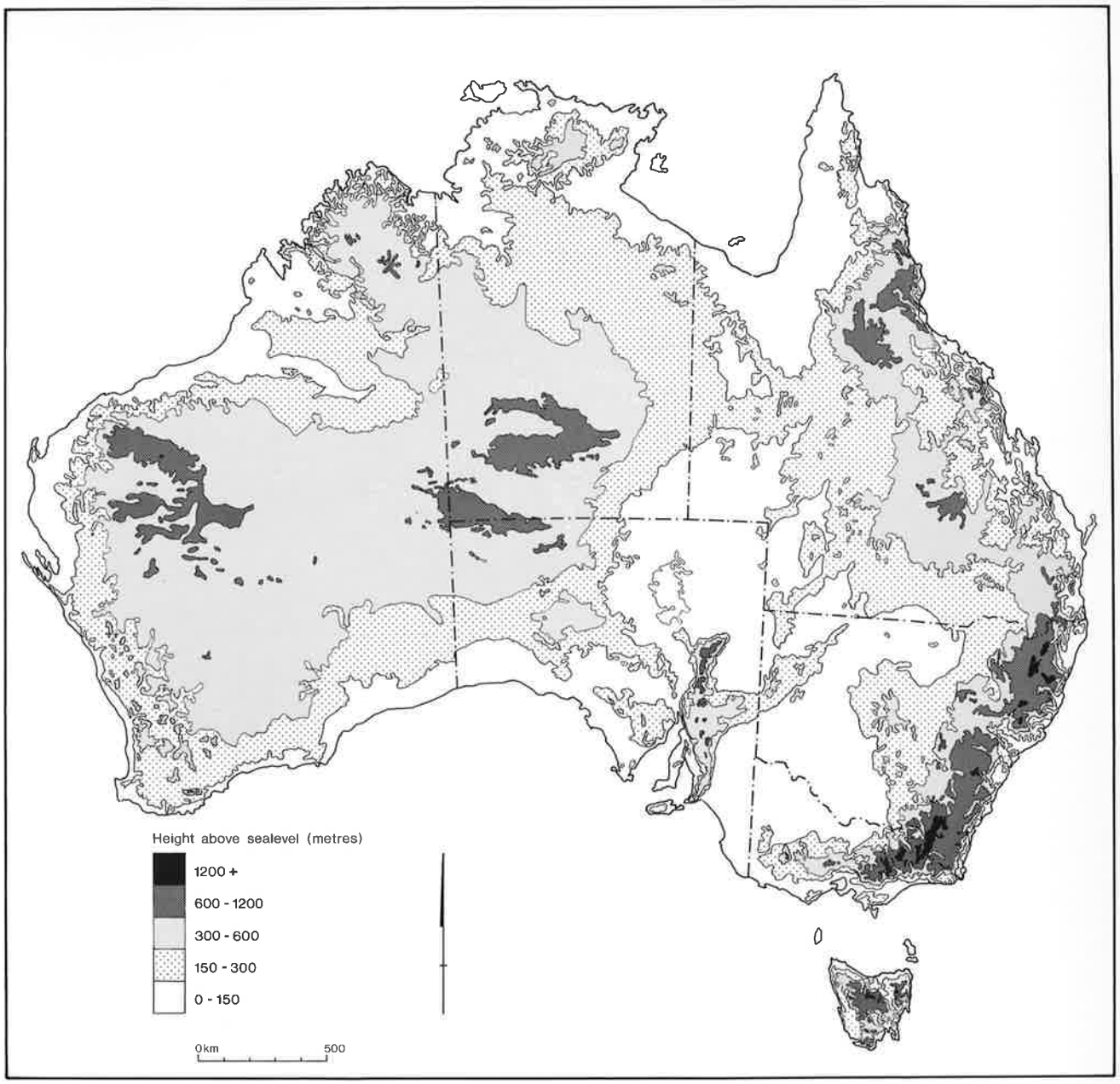
Height above sealevel (metres)
1200 +
600 - 1200
300 - 600
150 - 300
0 - 150
0km
500

3.2.1 Major Period : January, February and March 1973-77

(i) Low-level Monthly Mean (Surface - 700 mb) Moisture Characteristics over Northern Australia : A Comparison between Major Period and 19 year (1957-75) Average Fields

Low-level moisture characteristics analysed at four standard pressure levels (surface, 900, 850 and 700 mb) during January, February and March 1973-77 illustrate both the interannual and intraseasonal variability of moist processes in the Australian sector of the larger Australasian monsoon regime. In this discussion, these characteristics are shown by the fields of the streamfunction of the advective water vapour flux (circulation), advective water vapour flux or moisture divergence/convergence, precipitable water content and wind direction steadiness, and presented in Figures 49-67.

Unlike the regional domain, divergence is used rather than velocity potential because the former parameter, although somewhat noisy, provides finer resolution in the smaller area constituting the local domain. Further, it is more sensitive to the often lower magnitude and smaller-scale features over the continent which are otherwise swamped in velocity potential fields by near-equatorial convective maxima associated with the focus of the monsoon system in areas to the north of Australia.

To put the variability during 1973-77 in perspective, the analysis and discussion focuses initially on the 19 year (1957-75) monthly averages of advective moisture characteristics and the 24 year (1958-81) standard deviations of zonal and meridional wind components and mixing ratio in January (Figs.45-48). Over the 1957-75 period (Figs.45-47), January and February exhibit the strongest cyclonic circulation and advective moisture convergence values in the layer between the surface and 700 mb. All three months show a distinct change in circulation, from cyclonic to anticyclonic, by at least 700 mb (Troup, 1974), with a tendency for marked weakening of the cyclonic circulation at the 850 mb level in March. Concurrent with this change in circulation are the marked changes in advective moisture convergence between 850 mb and 700 mb levels. The generally southwest-northeast oriented

Figure 45 January mean advective water vapour flux divergence (light lines, convergence shaded) and the streamfunction of the advective water vapour flux (heavy dashed lines) at surface, 900, 850 and 700 mb levels over the local domain for the period from 1957-75 (data from Maher and Lee, 1977). Advective water vapour flux divergence is in units of 10^{-6} gm cm^{-2} mb^{-1} s^{-1} at intervals of 2 units and the streamfunction of the advective water vapour flux is in units of 10^{5} gm mb^{-1} s^{-1} at intervals of 5 units. Vertically integrated (surface - 700 mb) advective water vapour flux divergence is in units of 10^{-4} gm cm^{-2} s^{-1} at intervals of 4 units and the vertically integrated streamfunction of the advective water vapour flux is in units of 10^{7} gm cm^{-1} mb^{-1} s^{-1} at intervals of 10 units.

Figure 46 February mean advective water vapour flux divergence (light lines, convergence shaded) and the streamfunction of the advective water vapour flux (heavy dashed lines) at surface, 900, 850 and 700 mb levels over the local domain for the period from 1957-75 (data from Maher and Lee, 1977). Advective water vapour flux divergence is in units of 10^{-6} gm cm^{-2} mb^{-1} s^{-1} at intervals of 2 units and the streamfunction of the advective water vapour flux is in units of 10^{5} gm mb^{-1} s^{-1} at intervals of 5 units. Vertically integrated (surface - 700 mb) advective water vapour flux divergence is in units of 10^{-4} gm cm^{-2} s^{-1} at intervals of 4 units and the vertically integrated streamfunction of the advective water vapour flux is in units of 10^{7} gm cm^{-1} mb^{-1} s^{-1} at intervals of 10 units.

Figure 47 March mean advective water vapour flux divergence (light lines, convergence shaded) and the streamfunction of the advective water vapour flux (heavy dashed lines) at surface, 900, 850 and 700 mb levels over the local domain for the period from 1957-75 (data from Maher and Lee, 1977). Advective water vapour flux divergence is in units of 10^{-6} gm cm^{-2} mb^{-1} s^{-1} at intervals of 2 units and the streamfunction of the advective water vapour flux is in units of 10^{5} gm mb^{-1} s^{-1} at intervals of 5 units. Vertically integrated (surface - 700 mb) advective water vapour flux divergence is in units of 10^{-4} gm cm^{-2} s^{-1} at intervals of 4 units and the vertically integrated streamfunction of the advective water vapour flux is in units of 10^{7} gm cm^{-1} mb^{-1} s^{-1} at intervals of 10 units.

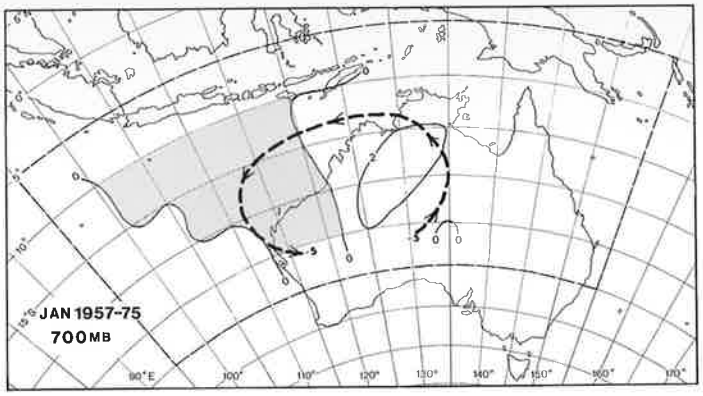
JAN 1957-75
700MB

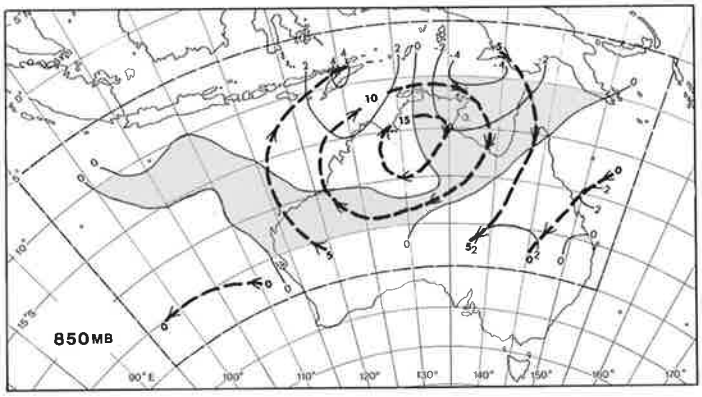
850MB

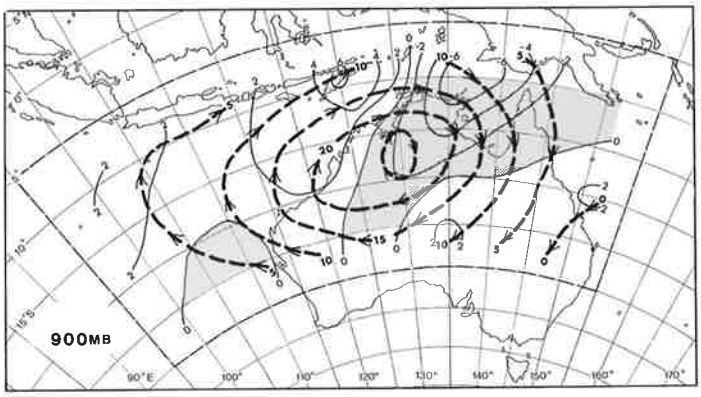
900MB

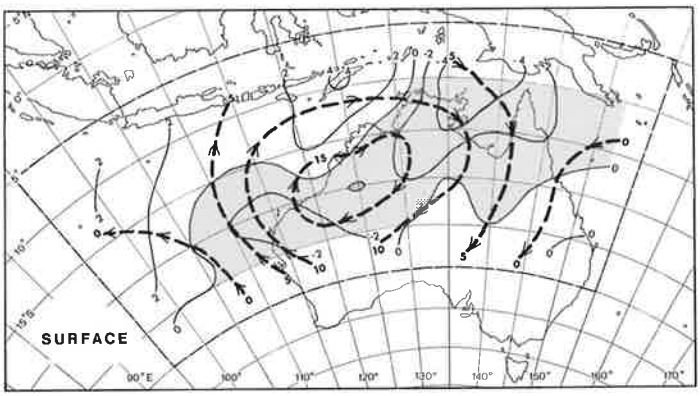
SURFACE

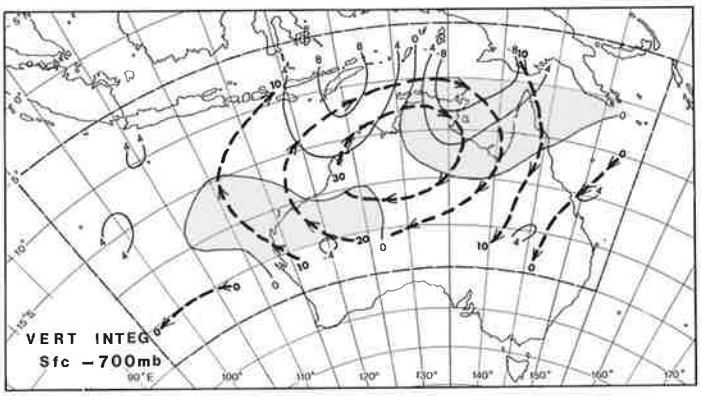
VERT INTEG
Sfc – 700mb

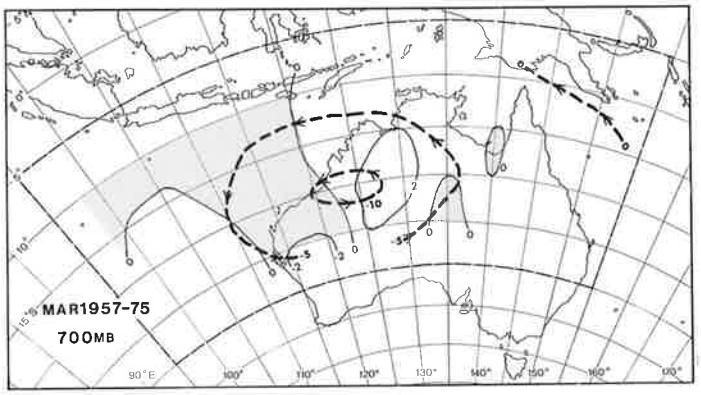
MAR1957-75
700MB

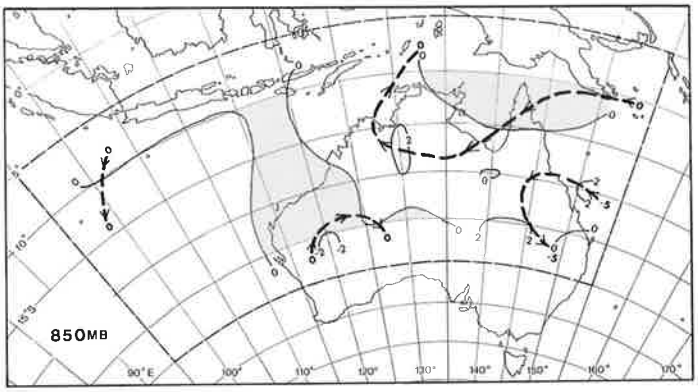
850MB

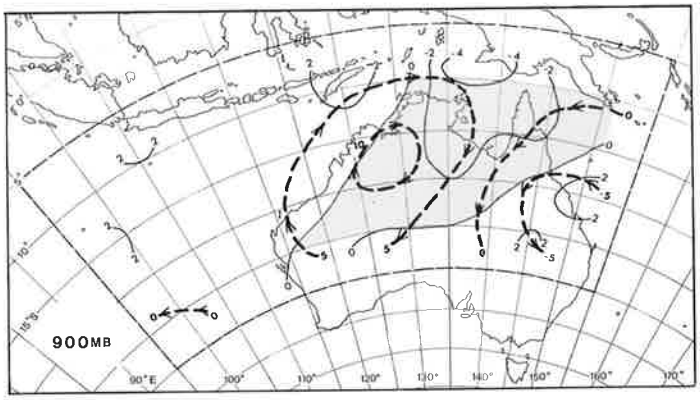
900MB

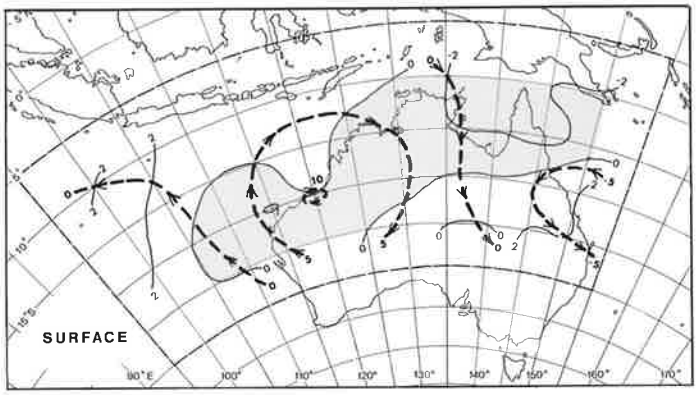
SURFACE

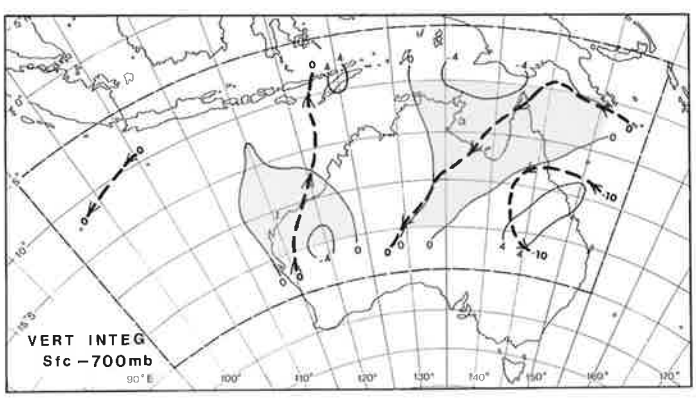
VERT INTEG
Sfc –700mb

convergence band induced by the cyclonic circulation disappears between 850 mb and 700 mb in January and February and between 900 mb and 850 mb by March 1957-75. This would suggest that, on average, January and February (Figs.45 and 46) constitute the peak in the Australian summer monsoon, with March (Fig.47) showing a distinct transition to weaker monsoonal conditions as the season draws to a close. Certainly, the strongest anticyclonic circulation prevails at 700 mb in March (Fig.47) and the anticyclonic influence over eastern Australia up to 850 mb is stronger than in January or February (Figs.45 and 46). Interestingly, both the vertically integrated cyclonic circulation and advective moisture convergence in February are slightly above the January values, perhaps supporting the tendency for a February maximum of monsoon persistence noted in the regional domain (Section 3.1.1). In fact, the latter is also reflected in the surface circulation magnitudes which may, in turn, be a product of heat low characteristics.

The maximum intensity in circulation (streamfunction of the advective water vapour flux) and advective moisture convergence predominates at 900 mb in all three months, although to a lesser degree in March (Fig.47). In general, this would seem to reflect weakening frictional influences near the top of the planetary boundary layer. At such levels, advective moisture convergence reaches a peak, particularly in the north-northeastern section of the convergence band.

Another aspect of the vertical change from cyclonic to anticyclonic flow is the distinct southwest-northeast vertical tilt in the locations of the centres of the cyclonic circulation. Mean geopotential height fields in Figure 5 strongly support this observation, with a general northward shift in the monsoon trough with height. In addition, the tilt could be allied with the loss of a distinct anchor for the trough once it is above the shallow Western Australian heat low. Certainly, the presence of marked cyclonic circulation at the surface is restricted to northwestern Australia in all three months.

Further analysis, involving individual water vapour flux components in

the surface to 700 mb layer, highlights aspects of the standard deviation of features over the local domain. The standard deviation of u and v wind components and mixing ratios along near-equatorial (10°-12°S) and sub-tropical (25°S) cross sections is presented for the Januarys from 1958-81 (Fig.48).

Broadly, it can be seen that standard deviations in near-equatorial wind components (in particular the u component) are greater than those in the sub-tropical section. Conversely, sub-tropical mixing ratios display larger deviations than their near-equatorial counterparts.

In the near-equatorial cross sections (Fig.48 top), areas of large standard deviation are found in the Torres Strait/Papua New Guinea region (in the v component field), in the middle levels of the atmosphere over Darwin (in the u component field) and, to a lesser degree, over Cocos Island (in the mixing ratio field). Weak standard deviation values are evident in the near-surface layers (in the u and v components) and over the greater part of the mixing ratio cross section. The meridional wind component (v) maximum over Port Moresby may be related to longer-term fluctuations in NET_{SH} structure. It is also possible that this maximum may be a consequence of interactions between the flow and the Owen Stanley Ranges in Papua New Guinea, as a large proportion of these Ranges is over 2000 metres in height, with several peaks in the vicinity of 4000 metres. However, near-surface standard deviations are much weaker, probably because the focus of the NET_{SH} is often associated with the northwestern Australian heat low centre, while flow generally tends to reach a peak only once above the planetary boundary layer. Across the near-surface area to the west of Australia, the standard deviation is also very low. This regime would appear to be dominated by a weak, but more steady, southerly flow component.

Zonal flow in the near-equatorial regime is dominated by high standard deviations, especially in the middle levels (around 700 mb) over north-northwestern Australia. This would appear to be a statistical manifestation of spatial fluctuations caused by monsoonal extremes and may thus involve

Figure 48 January mean standard deviations of zonal (u) and meridional (v) wind components and mixing ratio (mr) for the period from 1958-81. Cross-sections are along 10-12°S and 25°S with all standard deviations at intervals of 0.5. Stations used were Cocos Island (CI), Christmas Island (CH), Darwin (D), Thursday Island (TI), Port Moresby (PM), Honiara (H), Carnarvon (CA), Meekatharra (M), Giles (G), Alice Springs (A), Longreach (L), Charleville (CV) and Gladstone (GL).

STANDARD DEVIATION OF U AND V WIND COMPONENTS AND MIXING RATIO

JANUARY 1958-81

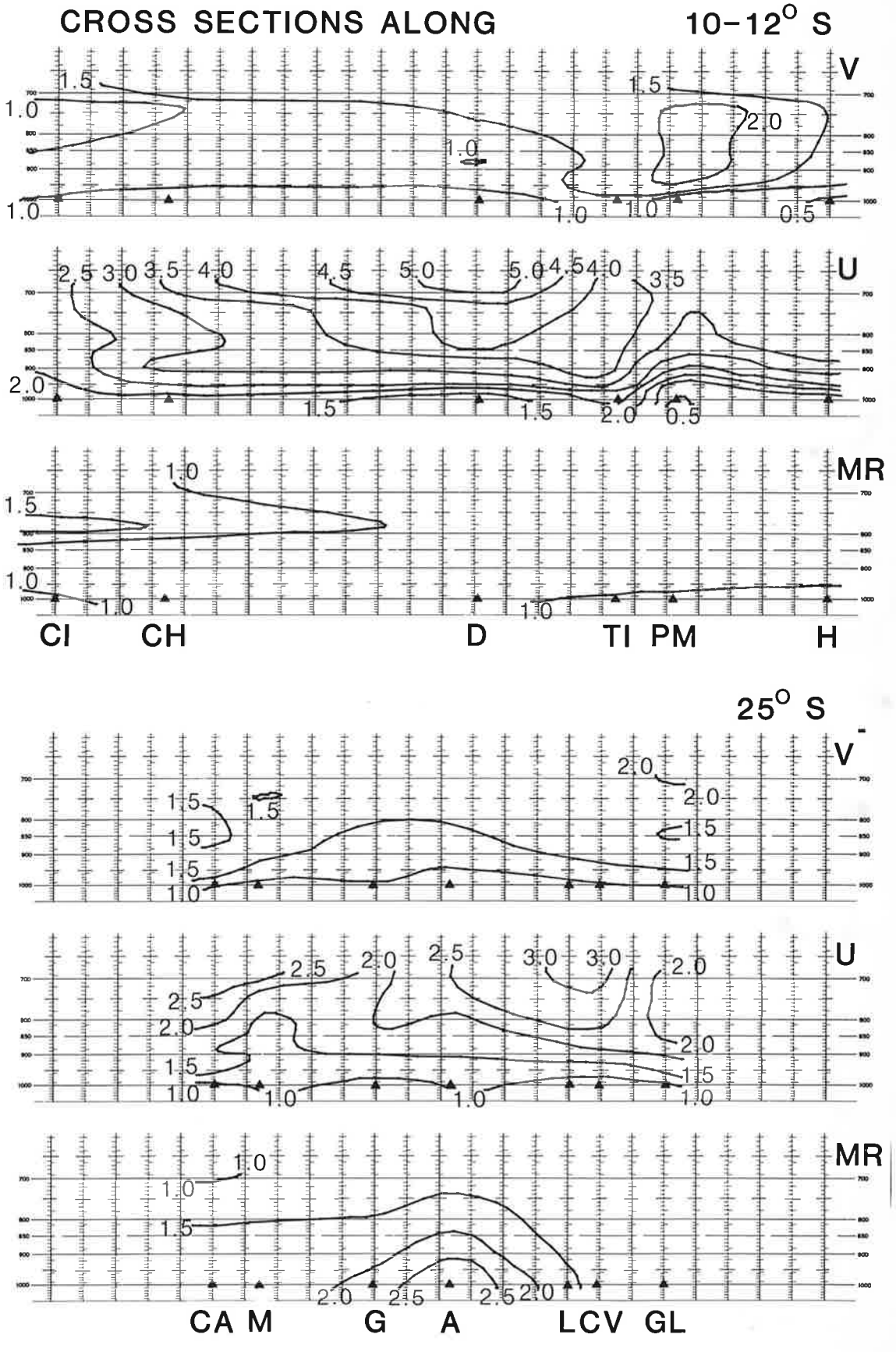

cyclonic and anticyclonic circulation distributions. Yet, the middle-level location of the standard deviation maximum suggests that the situation is more intricate, in that it may also involve variations in the vertical depth, as well as the spatial character, of the NET_{SH}.

As in the meridional section, the lowest standard deviation values are found in the near-surface layers of the transect. Of particular interest are the areas around Darwin and between Port Moresby and Honiara, where values fall below + 1 standard deviation in both u and v wind components. Both regions may reflect vagaries in the NET_{SH}, with the more steady, although weaker, near-surface flow being overlain by stronger, but more variable, circulation aloft. However, the area of the section above Port Moresby shows a dome of weak standard deviation in the zonal wind field that is juxtaposed with the stronger standard deviation maximum in the meridional plane. As the vector form indicates that the above area is usually influenced by strong northwesterly flow, it would appear that greater variability is inherent in the meridional wind component.

Standard deviations in moisture (mixing ratio) are substantially lower than either of the wind component deviations. In fact, mixing ratio averages during the 1958-81 period (Maher and Lee, 1977) show that near-equatorial moisture content is high. Thus near-equatorial water vapour fluxes are more likely to vary as a result of changes in the wind field (particularly the u component) than in the moisture content.

Over the sub-tropical cross sections (Fig.48 bottom), the largest standard deviation values occur in the middle levels of the wind component fields and in a dome over the centre of the continent in the mixing ratio transect. As in near-equatorial sections, the lowest standard deviations occur in the near-surface layers of the wind component fields.

The meridional component shows strongest standard deviation values in the middle levels of the cross section. However, this region is also influenced by a dome of lower standard deviation values over the centre of the continent. This seems to suggest that the continent has an influence

on lower-level flow. Higher aloft, there may be some suggestion of cyclonic/anticyclonic alternations and an indication that large-scale variability of features is common.

An examination of the zonal wind component field provides further support for the above. In this cross section, middle-level standard deviation is more pronounced, with maxima located above Carnarvon and Charleville. These centres are probably another manifestation of the alternation in circulation direction during monsoonal extremes. However, the lower-level regions of weak standard deviation would seem to indicate that the wind regime is very steady across the centre of Australia. This is observed in the long-term wind averages in Maher and Lee (1977) which indicate that strong east-northeasterlies dominate this region. Thus zonal flow does not seem to be overly different during periods of pronounced cyclonic or anticyclonic circulation.

The mixing ratio distribution in the sub-tropical cross section indicates that large standard deviations in moisture occur over central Australia. With average mixing ratio values being low over the continent (Maher and Lee, 1977), it would seem that monsoonal incursions are the source of the large variability in this field.

During the 1973-77 period, many of the basic observations noted in the above discussion are seen to apply, although there are some interesting seasonal differences (Figs.49-63). As observed in the regional domain, the 1973 summer appears to have been under the influence of an El Niño regime and some unusual patterns in the moisture characteristics over Australia. In contrast to this are the 1974 and 1976 summers of extreme monsoonal activity and the intervening summer of 1975 when weak monsoonal conditions prevailed.

Circulation structure over the continent approaches the 1957-75 average in January 1973 (Fig.49), with a change from cyclonic to anticyclonic conditions between 850 mb and 700 mb. However, cyclonic circulation magnitudes are slightly less than average and there is a marked southeast-northwest tilt in

Figure 49 Monthly mean advective water vapour flux divergence (light lines, convergence shaded) and the streamfunction of the advective water vapour flux (heavy dashed lines) at surface, 900, 850 and 700 mb levels over the local domain in January 1973. Advective water vapour flux divergence is in units of 10^{-6} gm cm^{-2} mb^{-1} s^{-1} at intervals of 2 units and the streamfunction of the advective water vapour flux is in units of 10^{5} gm mb^{-1} s^{-1} at intervals of 5 units. Vertically integrated (surface - 700 mb) advective water vapour flux divergence is in units of 10^{-4} gm cm^{-2} s^{-1} at intervals of 4 units and the vertically integrated streamfunction of the advective water vapour flux is in units of 10^{7} gm cm^{-1} mb^{-1} s^{-1} at intervals of 10 units.

Figure 50 Monthly mean advective water vapour flux divergence (light lines, convergence shaded) and the streamfunction of the advective water vapour flux (heavy dashed lines) at surface, 900, 850 and 700 mb levels over the local domain in February 1973. Advective water vapour flux divergence is in units of 10^{-6} gm cm^{-2} mb^{-1} s^{-1} at intervals of 2 units and the streamfunction of the advective water vapour flux is in units of 10^{5} gm mb^{-1} s^{-1} at intervals of 5 units. Vertically integrated (surface - 700 mb) advective water vapour flux divergence is in units of 10^{-4} gm cm^{-2} s^{-1} at intervals of 4 units and the vertically integrated streamfunction of the advective water vapour flux is in units of 10^{7} gm cm^{-1} mb^{-1} s^{-1} at intervals of 10 units.

Figure 51 Monthly mean advective water vapour flux divergence (light lines, convergence shaded) and the streamfunction of the advective water vapour flux (heavy dashed lines) at surface, 900, 850 and 700 mb levels over the local domain in March 1973. Advective water vapour flux divergence is in units of 10^{-6} gm cm^{-2} mb^{-1} s^{-1} at intervals of 2 units and the streamfunction of the advective water vapour flux is in units of 10^{5} gm mb^{-1} s^{-1} at intervals of 5 units. Vertically integrated (surface - 700 mb) advective water vapour flux divergence is in units of 10^{-4} gm cm^{-2} s^{-1} at intervals of 4 units and the vertically integrated streamfunction of the advective water vapour flux is in units of 10^{7} gm cm^{-1} mb^{-1} s^{-1} at intervals of 10 units.

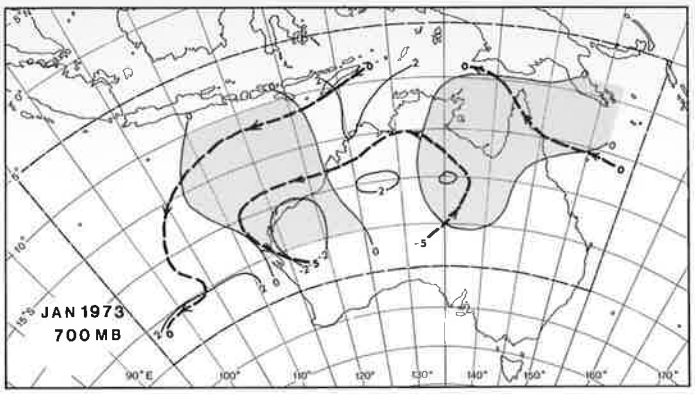
JAN 1973
700 MB
90°E
100°
110°
120°
130°
140°
150°
160°
170°

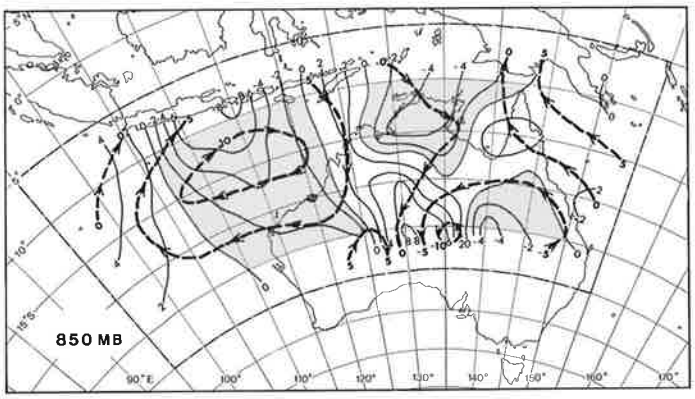
850 MB
90°E
100°
110°
120°
130°
140°
150°
160°
170°

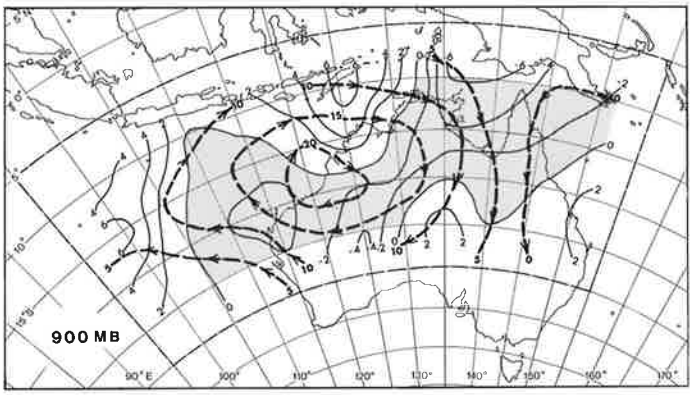
900 MB
90°E
100°
110°
120°
130°
140°
150°
160°
170°

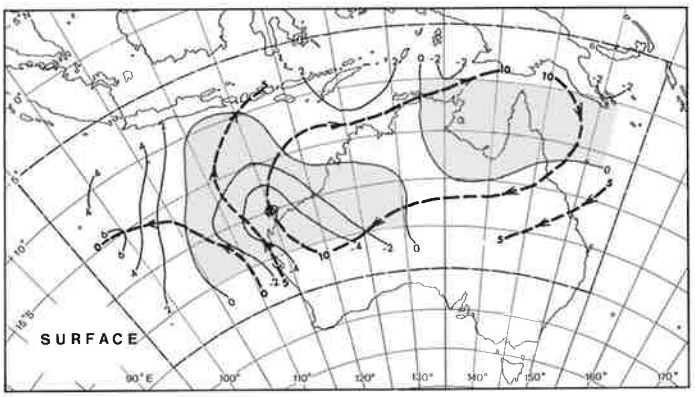
SURFACE
90°E
100°
110°
120°
130°
140°
150°
160°
170°

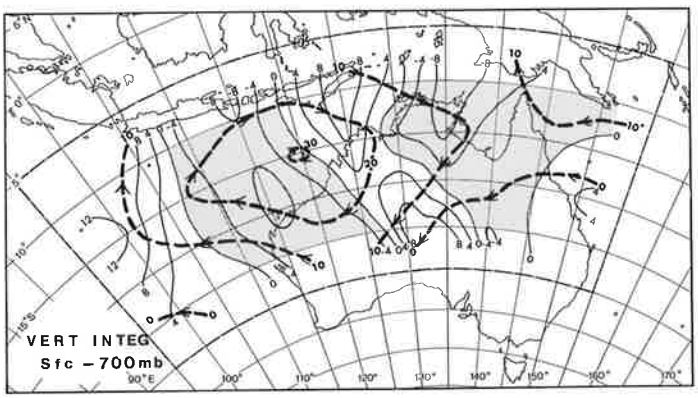
VERT INTEG
Sfc – 700mb
90°E
100°
110°
120°
130°
140°
150°
160°
170°

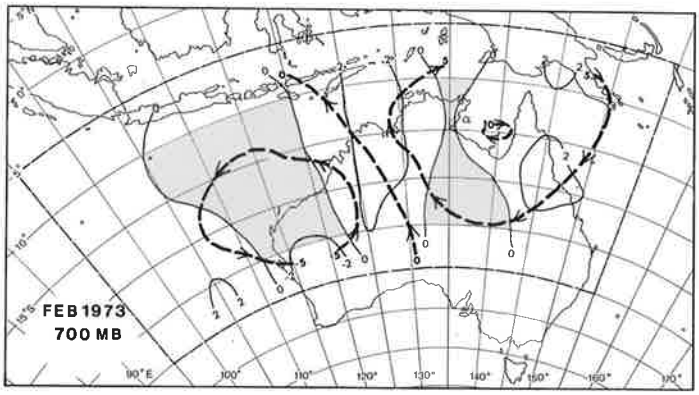
FEB 1973
700 MB

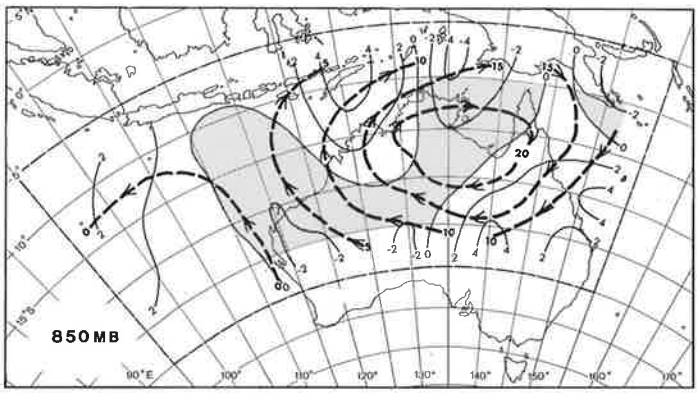
850 MB

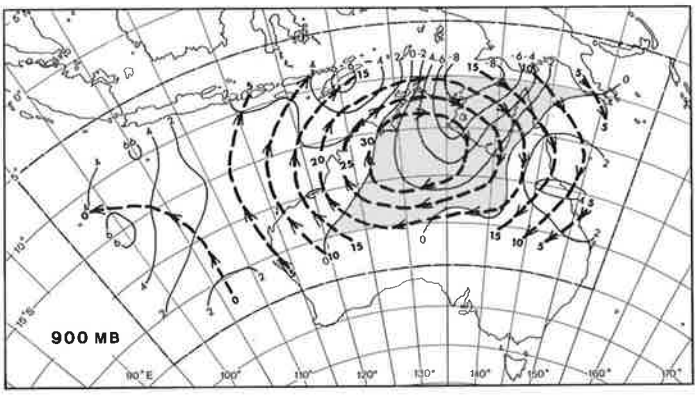
900 MB

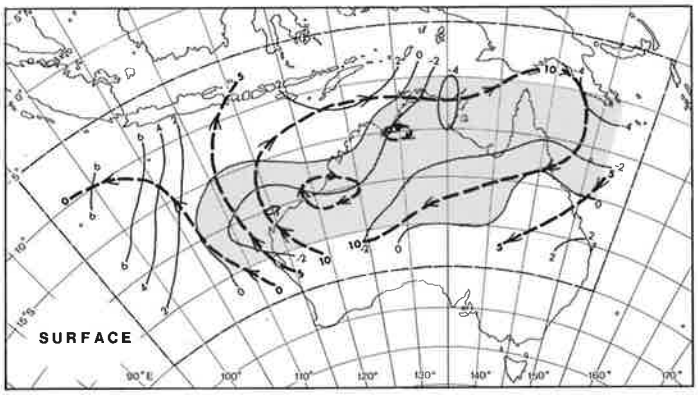
SURFACE

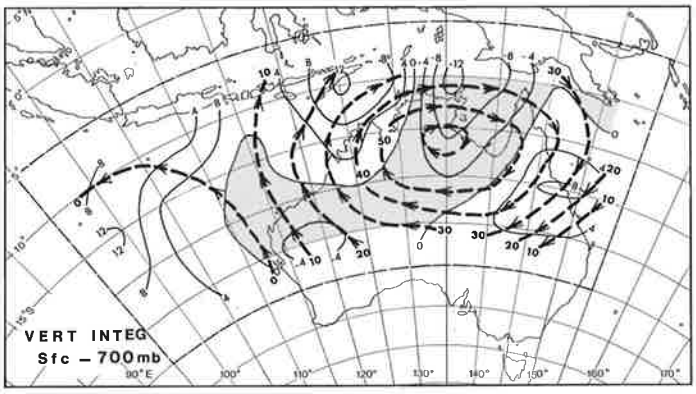
VERT INTEG
Sfc – 700mb

the circulation centres from the surface to 850 mb. As a result, the southwest-northeast orientation of advective moisture convergence weakens above 900 mb and, even at the surface, the most predominant concentration of advective moisture convergence is off Western Australia. An anticyclonic influence is also marked at 850 mb over eastern Australia, to the extent that the NET_{SH} becomes situated to the northwest of Australia.

By February 1973 (Fig.50), the southwest-northeast tilt in the NET_{SH} and the orientation of the convergence band are restored as a stronger monsoon system becomes established over the continent. As with the 1957-75 averages, the strongest cyclonic circulation values occur at 900 mb, with the result that deep convection is concentrated over north-northeastern Australia (Fig.46). However, unlike January 1973 and the 1957-75 averages, cyclonic circulation is not replaced by anticyclonic by 700 mb. Although weak, the trough is still a feature of the circulation at this level.

In March 1973 (Fig.51) the monsoon is at its weakest, with cyclonic circulation restricted to the surface and 900 mb levels and the trough (NET_{SH}) almost out of the continent by 850 mb. Yet, some convective activity is still evident over north-northeastern Australia and in shallow layers over Western Australia. Strong advective moisture divergence is observed at 850 mb and 700 mb levels (over north-northwestern Australia) and is also a noteworthy feature in January 1973 over parts of the continent. Such features are not always supported by the rainfall regimes, but it must be remembered that these are monthly mean advective fields and do not represent eddy fluctuations (e.g. tropical cyclones and rain depressions) which are often the source of extreme rainfall events. Thus the 1973 season would seem to be representative of a degree of intraseasonal variability, with the most pronounced monsoonal activity centering on February.

As noted in the regional domain (Section 3.1.1), the 1974 summer constitutes the major peak in monsoonal activity during the 1973-77 period. The month of January shows the presence of a massive and deep NET_{SH} centred over the Australian continent. Cyclonic circulation and advective moisture

Figure 52 Monthly mean advective water vapour flux divergence (light lines, convergence shaded) and the streamfunction of the advective water vapour flux (heavy dashed lines) at surface, 900, 850 and 700 mb levels over the local domain in January 1974. Advective water vapour flux divergence is in units of 10^{-6} gm cm^{-2} mb^{-1} s^{-1} at intervals of 2 units and the streamfunction of the advective water vapour flux is in units of 10^{5} gm mb^{-1} s^{-1} at intervals of 5 units. Vertically integrated (surface - 700 mb) advective water vapour flux divergence is in units of 10^{-4} gm cm^{-2} s^{-1} at intervals of 4 units and the vertically integrated streamfunction of the advective water vapour flux is in units of 10^{7} gm cm^{-1} mb^{-1} s^{-1} at intervals of 10 units.

Figure 53 Monthly mean advective water vapour flux divergence (light lines, convergence shaded) and the streamfunction of the advective water vapour flux (heavy dashed lines) at surface, 900, 850 and 700 mb levels over the local domain in February 1974. Advective water vapour flux divergence is in units of 10^{-6} gm cm^{-2} mb^{-1} s^{-1} at intervals of 2 units and the streamfunction of the advective water vapour flux is in units of 10^{5} gm mb^{-1} s^{-1} at intervals of 5 units. Vertically integrated (surface - 700 mb) advective water vapour flux divergence is in units of 10^{-4} gm cm^{-2} s^{-1} at intervals of 4 units and the vertically integrated streamfunction of the advective water vapour flux is in units of 10^{7} gm cm^{-1} mb^{-1} s^{-1} at intervals of 10 units.

Figure 54 Monthly mean advective water vapour flux divergence (light lines, convergence shaded) and the streamfunction of the advective water vapour flux (heavy dashed lines) at surface, 900, 850 and 700 mb levels over the local domain in March 1974. Advective water vapour flux divergence is in units of 10^{-6} gm cm^{-2} mb^{-1} s^{-1} at intervals of 2 units and the streamfunction of the advective water vapour flux is in units of 10^{5} gm mb^{-1} s^{-1} at intervals of 5 units. Vertically integrated (surface - 700 mb) advective water vapour flux divergence is in units of 10^{-4} gm cm^{-2} s^{-1} at intervals of 4 units and the vertically integrated streamfunction of the advective water vapour flux is in units of 10^{7} gm cm^{-1} mb^{-1} s^{-1} at intervals of 10 units.

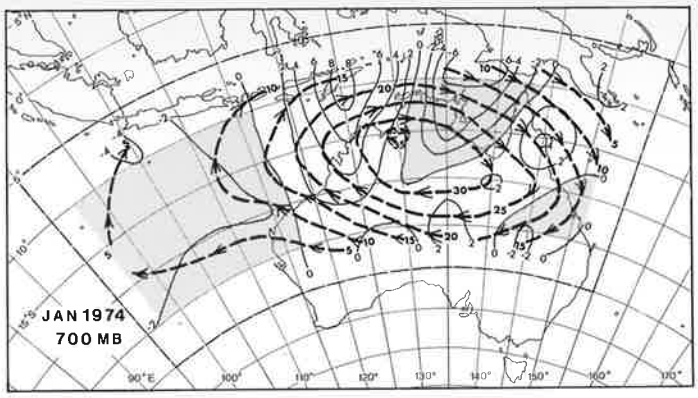
JAN 1974
700 MB

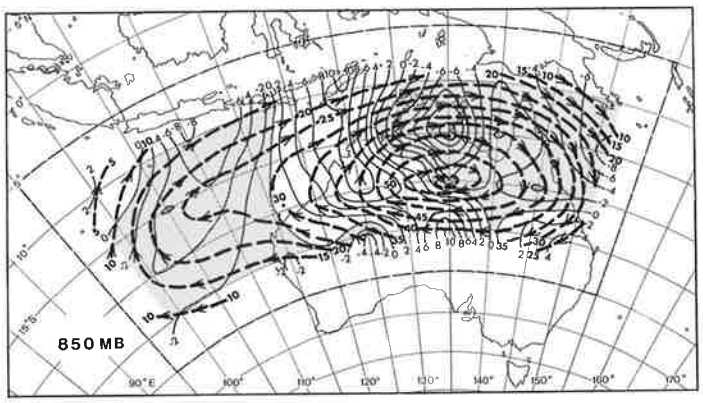
850 MB

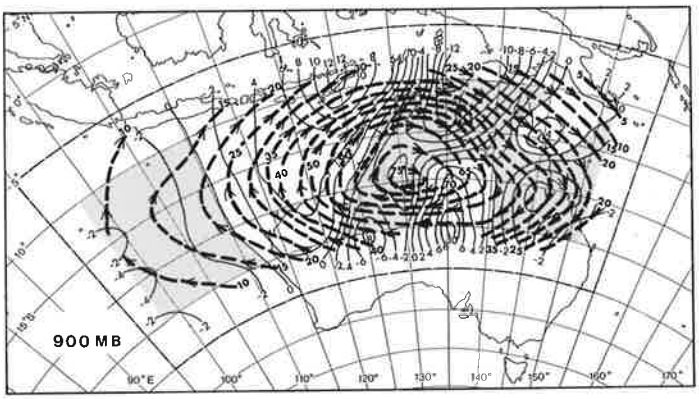
900 MB

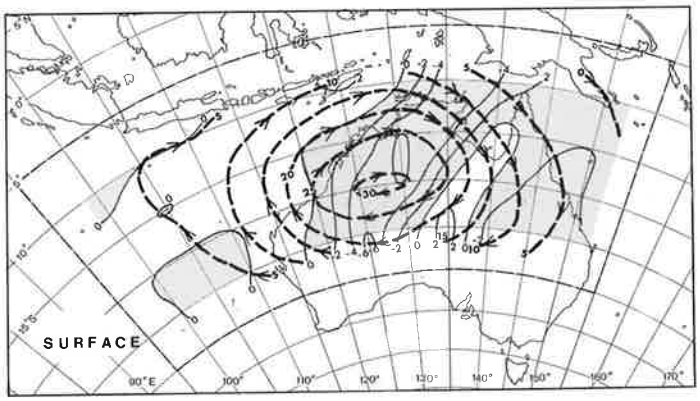
SURFACE

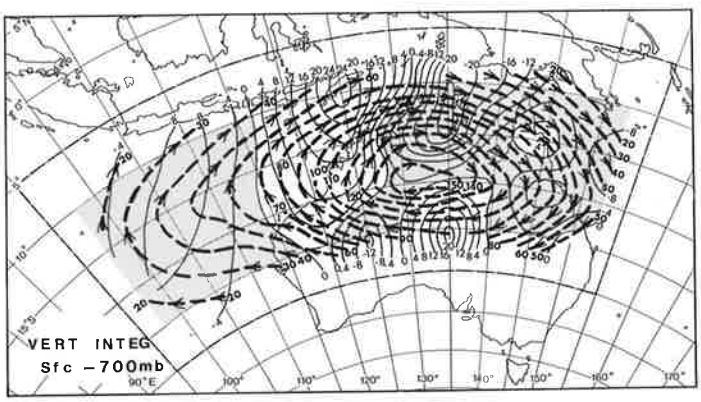
VERT INTEG
Sfc – 700mb

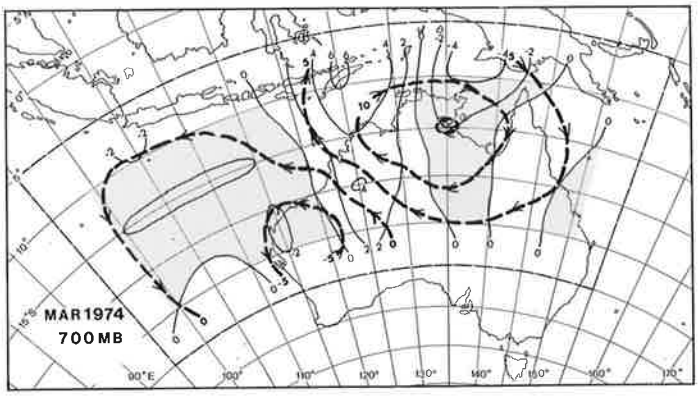
MAR 1974
700MB

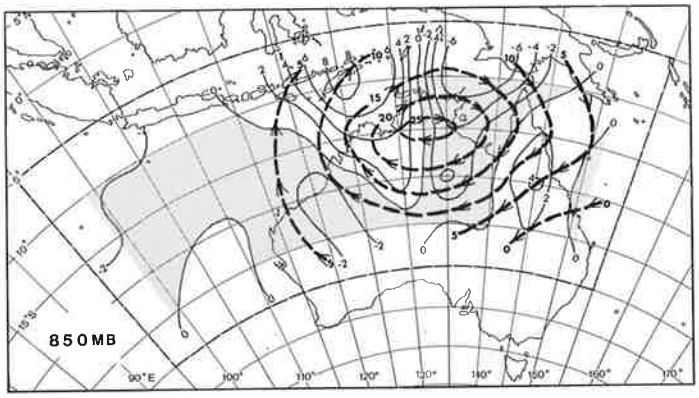
850MB

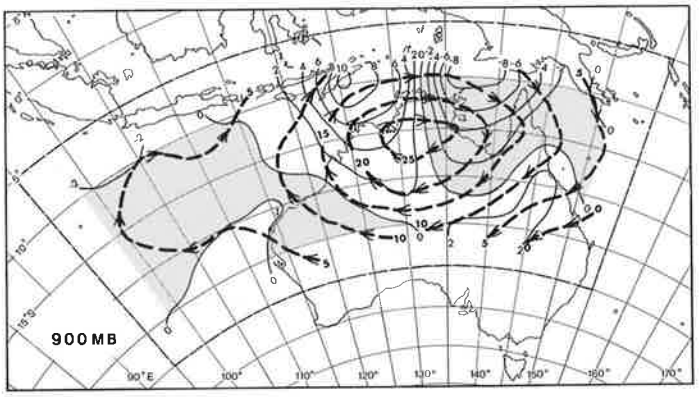
900MB

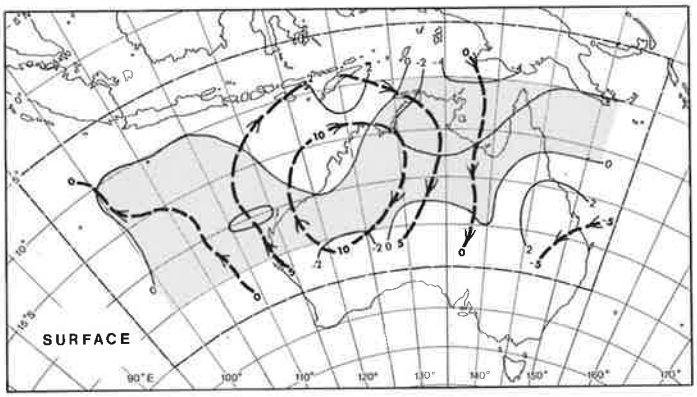
SURFACE

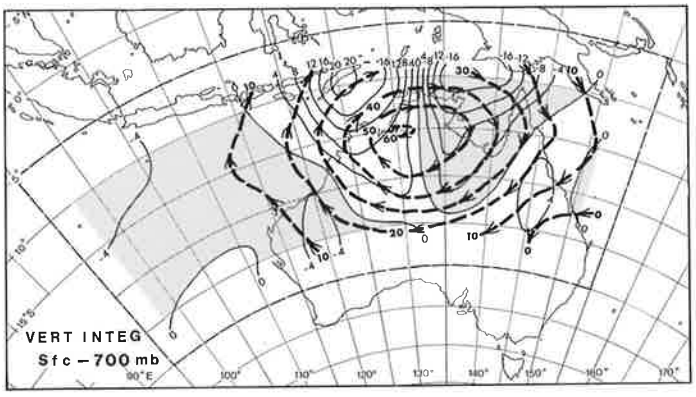
VERT INTEG
Sfc – 700 mb

convergence are dominant at all levels in Figure 52, with the system possessing little vertical tilting but well organized convective elements. Marked gradients in circulation and advective moisture fluxes result in the potential for rapid overturnings of mass and moisture. A brief comparison between the January 1974 sequence (Fig.52) and others in the period highlights the magnitude and extent of monsoonal processes in this month.

By February 1974 (Fig.53) the monsoon is still strong, although not as dominant as in January 1974. Cyclonic circulation is still predominant throughout the low levels, but a more distinct southwest-northeast vertical tilt in the closed centres is apparent. The NET_{SH} again shows a 900 mb maximum in circulation, although 850 mb flow approaches these values with deepest advective moisture convergence occupying the north-northeastern region of the continent.

March 1974 (Fig.54) completes a season of vigorous monsoon activity with circulation and advective moisture convergence being very much above the 1957-75 average. Cyclonic circulation and advective moisture convergence remain deep and, although there is some anticyclonicity by 700 mb, the NET_{SH} is still evident.

If the 1974 summer marks the peak of monsoonal activity in the 1973-77 period, then the 1975 summer marks a distinctly low ebb. January 1975 (Fig.55) presents a picture of the Australian continent under the influence of weak and shallow monsoon conditions. Organized cyclonic circulation is only fully evident up to 900 mb and the marked southwest-northeast tilt between this level and the remnant of the NET_{SH} at 850 mb suggests a pronounced weakening of cyclonic circulation. Anticyclonicity at 700 mb is amongst the strongest observed in any month during the 1973-77 period, with the vertically integrated field showing very poor cyclonic circulation conditions. The shallow nature of the cyclonic flow in this month may be reflected in the generally shallower advective moisture convergence maximum in the near-equatorial zone of the vertical cross sections of velocity potential (Fig.30). If this is true, it may imply that convective conditions over a large part of

Figure 55 Monthly mean advective water vapour flux divergence (light lines, convergence shaded) and the streamfunction of the advective water vapour flux (heavy dashed lines) at surface, 900, 850 and 700 mb levels over the local domain in January 1975. Advective water vapour flux divergence is in units of 10^{-6} gm cm^{-2} mb^{-1} s^{-1} at intervals of 2 units and the streamfunction of the advective water vapour flux is in units of 10^{5} gm mb^{-1} s^{-1} at intervals of 5 units. Vertically integrated (surface - 700 mb) advective water vapour flux divergence is in units of 10^{-4} gm cm^{-2} s^{-1} at intervals of 4 units and the vertically integrated streamfunction of the advective water vapour flux is in units of 10^{7} gm cm^{-1} mb^{-1} s^{-1} at intervals of 10 units.

Figure 56 Monthly mean advective water vapour flux divergence (light lines, convergence shaded) and the streamfunction of the advective water vapour flux (heavy dashed lines) at surface, 900, 850 and 700 mb levels over the local domain in February 1975. Advective water vapour flux divergence is in units of 10^{-6} gm cm^{-2} mb^{-1} s^{-1} at intervals of 2 units and the streamfunction of the advective water vapour flux is in units of 10^{5} gm mb^{-1} s^{-1} at intervals of 5 units. Vertically integrated (surface - 700 mb) advective water vapour flux divergence is in units of 10^{-4} gm cm^{-2} s^{-1} at intervals of 4 units and the vertically integrated streamfunction of the advective water vapour flux is in units of 10^{7} gm cm^{-1} mb^{-1} s^{-1} at intervals of 10 units.

Figure 57 Monthly mean advective water vapour flux divergence (light lines, convergence shaded) and the streamfunction of the advective water vapour flux (heavy dashed lines) at surface, 900, 850 and 700 mb levels over the local domain in March 1975. Advective water vapour flux divergence is in units of 10^{-6} gm cm^{-2} mb^{-1} s^{-1} at intervals of 2 units and the streamfunction of the advective water vapour flux is in units of 10^{5} gm mb^{-1} s^{-1} at intervals of 5 units. Vertically integrated (surface - 700 mb) advective water vapour flux divergence is in units of 10^{-4} gm cm^{-2} s^{-1} at intervals of 4 units and the vertically integrated streamfunction of the advective water vapour flux is in units of 10^{7} gm cm^{-1} mb^{-1} s^{-1} at intervals of 10 units.

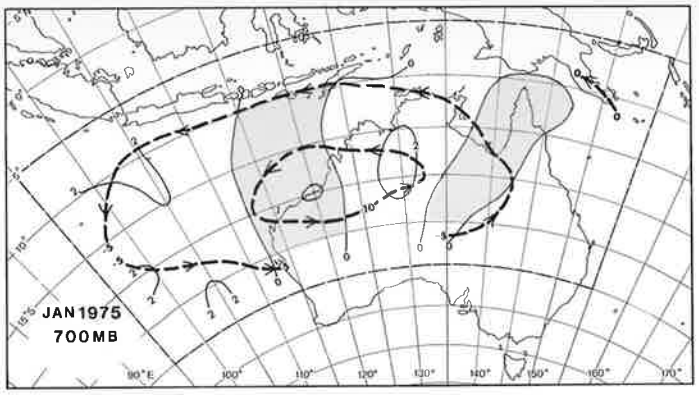
JAN 1975
700MB

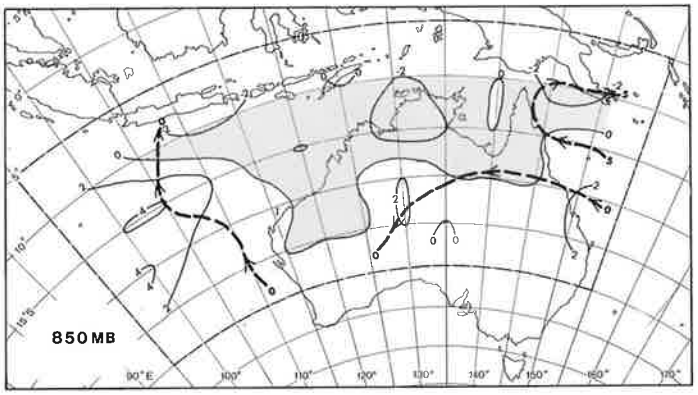
850MB

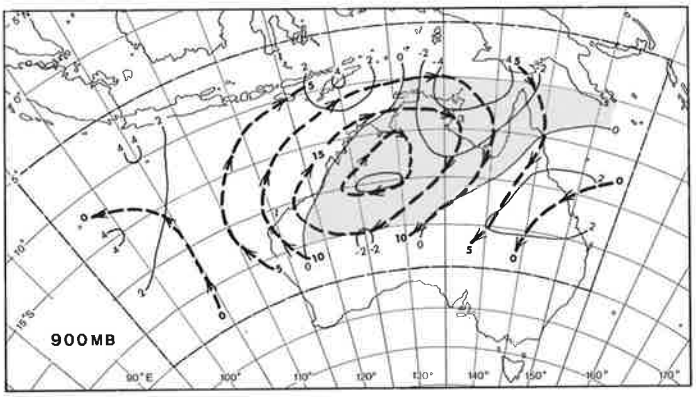
900MB

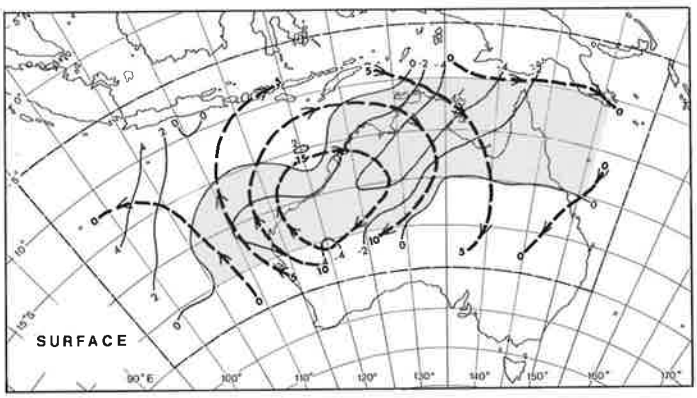
SURFACE

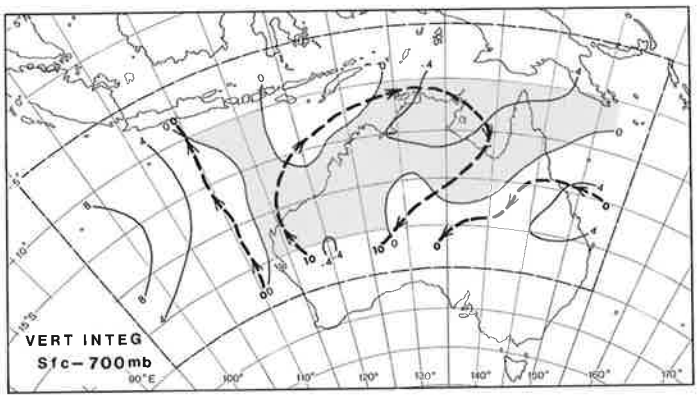
VERT INTEG
Sfc–700mb

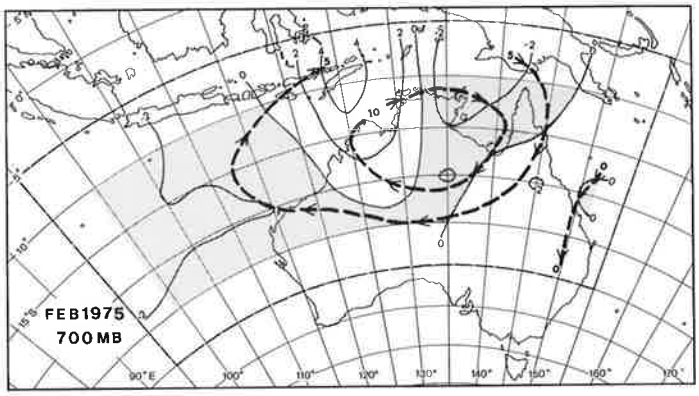
FEB1975
700MB
90°E
100°
110°
120°
130°
140°
150°
160°
170°

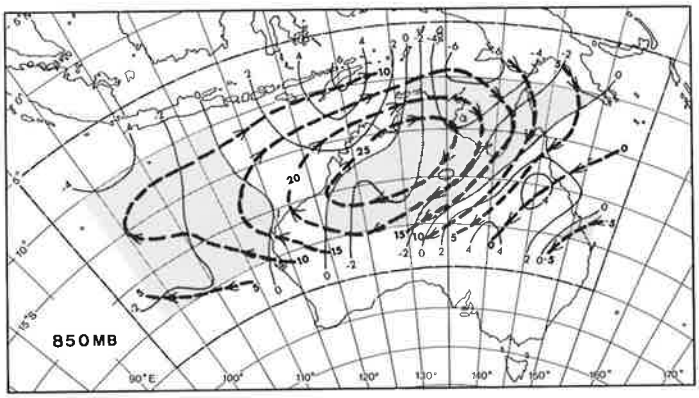
850MB
90°E
100°
110°
120°
130°
140°
150°
160°
170°

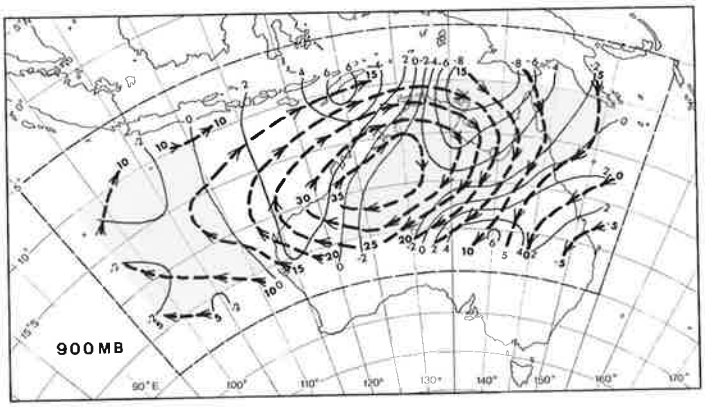
900MB
90°E
100°
110°
120°
130°
140°
150°
160°
170°

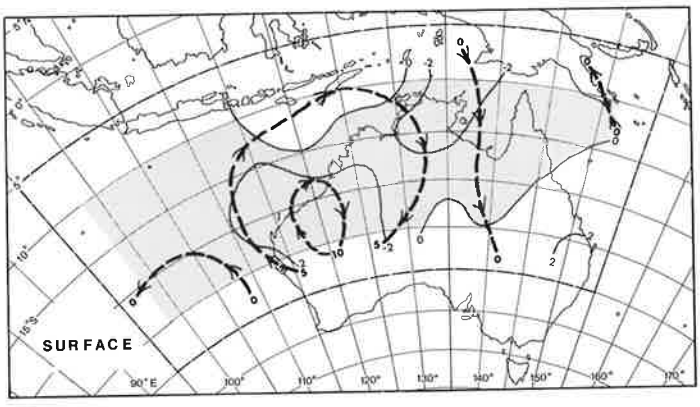
SURFACE
90°E
100°
110°
120°
130°
140°
150°
160°
170°

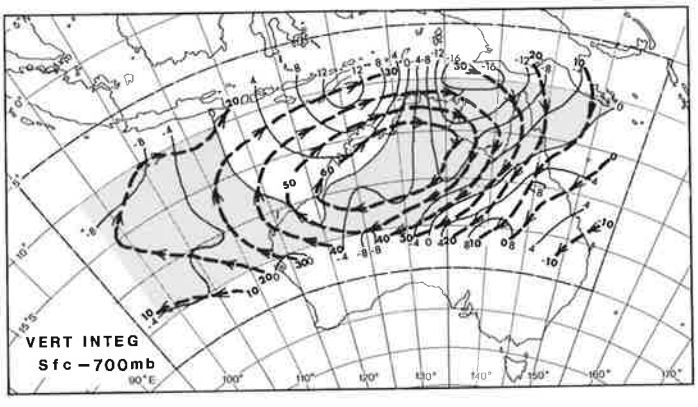
VERT INTEG
Sfc – 700mb
90°E
100°
110°
120°
130°
140°
150°
160°
170°

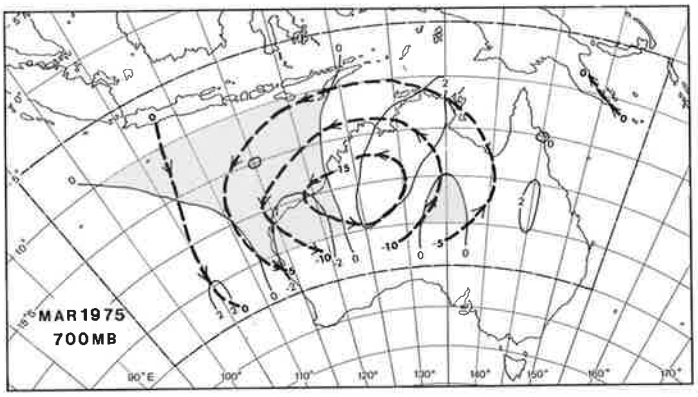
MAR1975
700MB
90°E
100°
110°
120°
130°
140°
150°
160°
170°

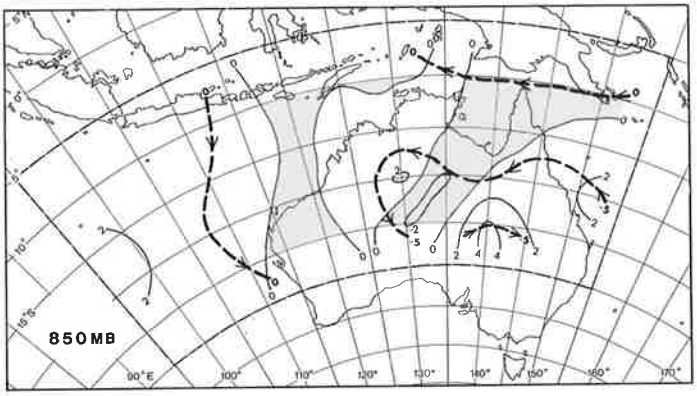
850MB
90°E
100°
110°
120°
130°
140°
150°
160°
170°

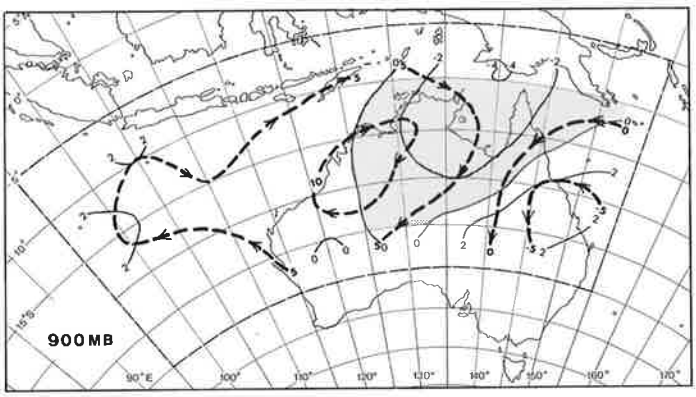
900MB
90°E
100°
110°
120°
130°
140°
150°
160°
170°

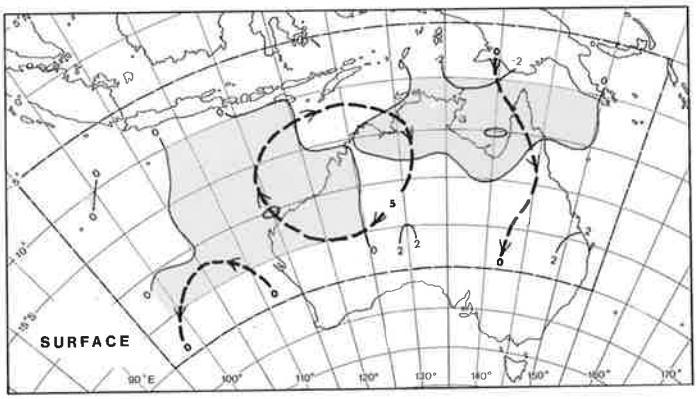
SURFACE
90°E
100°
110°
120°
130°
140°
150°
160°
170°

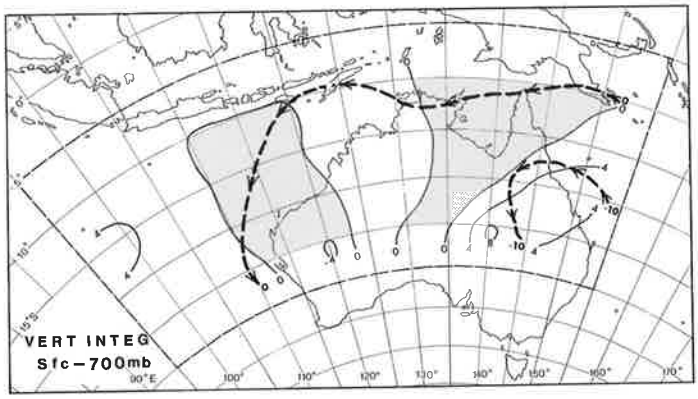
VERT INTEG
Sfc–700mb
90°E
100°
110°
120°
130°
140°
150°
160°
170°

the monsoon region were affected. Certainly, advective moisture convergence over the Australian continent is significantly weakened, particularly in the convective region over north-northeastern Australia.

As can be seen by a comparison of Figures 55 and 56, February 1975 marks the restoration of more pronounced monsoon activity. Cyclonic circulation is still evident at 700 mb, although it is interesting to note that cyclonic circulation at the surface is stronger and more organized in January than February 1975. However, at both the 850 mb and 900 mb levels, intense cyclonic circulation signifies more complete monsoonal processes in February 1975. Once again, a notable tilt is found in the centres of cyclonic circulation in the vertical plane and strong divergent and convergent maxima are distributed about the NET_{SH}.

By March 1975 (Fig.57) the monsoon has become very weak with circulation and advective moisture convergence being shallow and with strong anti-cyclonicity prevailing at 700 mb. This month represents the weakest monsoonal activity in the five year period and concludes a summer of marked intra-seasonal variability. Interestingly, as the 1957-75 averages suggest, February appears to be the month in which the most dominant monsoonal activity can be expected. By March, monsoonal conditions have generally deteriorated as the system 'withdraws' further north.

The 1976 season shows the second peak in monsoonal activity over the 1973-77 period, with strong cyclonic circulation and advective moisture convergence dominant in all three months. In January 1976 (Fig.58) a deep NET_{SH} with a marked southwest-northeast vertical tilt influences the continent. Pronounced convective activity, approaching February 1974 magnitudes, is once again evident over north-northeastern Australia and is also reflected in the strength of the vertically integrated circulation and advective moisture convergence in Figure 58.

Yet, February 1976 (Fig.59) represents the peak in the 1976 monsoon season, with cyclonic circulation only second to the January 1974 values. In fact, absolute values of advective moisture convergence at most levels are

Figure 58 Monthly mean advective water vapour flux divergence (light lines, convergence shaded) and the streamfunction of the advective water vapour flux (heavy dashed lines) at surface, 900, 850 and 700 mb levels over the local domain in January 1976. Advective water vapour flux divergence is in units of 10^{-6} gm cm^{-2} mb^{-1} s^{-1} at intervals of 2 units and the streamfunction of the advective water vapour flux is in units of 10^{5} gm mb^{-1} s^{-1} at intervals of 5 units. Vertically integrated (surface - 700 mb) advective water vapour flux divergence is in units of 10^{-4} gm cm^{-2} s^{-1} at intervals of 4 units and the vertically integrated streamfunction of the advective water vapour flux is in units of 10^{7} gm cm^{-1} mb^{-1} s^{-1} at intervals of 10 units.

Figure 59 Monthly mean advective water vapour flux divergence (light lines, convergence shaded) and the streamfunction of the advective water vapour flux (heavy dashed lines) at surface, 900, 850 and 700 mb levels over the local domain in February 1976. Advective water vapour flux divergence is in units of 10^{-6} gm cm^{-2} mb^{-1} s^{-1} at intervals of 2 units and the streamfunction of the advective water vapour flux is in units of 10^{5} gm mb^{-1} s^{-1} at intervals of 5 units. Vertically integrated (surface - 700 mb) advective water vapour flux divergence is in units of 10^{-4} gm cm^{-2} s^{-1} at intervals of 4 units and the vertically integrated streamfunction of the advective water vapour flux is in units of 10^{7} gm cm^{-1} mb^{-1} s^{-1} at intervals of 10 units.

Figure 60 Monthly mean advective water vapour flux divergence (light lines, convergence shaded) and the streamfunction of the advective water vapour flux (heavy dashed lines) at surface, 900, 850 and 700 mb levels over the local domain in March, 1976. Advective water vapour flux divergence is in units of 10^{-6} gm cm^{-2} mb^{-1} s^{-1} at intervals of 2 units and the streamfunction of the advective water vapour flux is in units of 10^{5} gm mb^{-1} s^{-1} at intervals of 5 units. Vertically integrated (surface - 700 mb) advective water vapour flux divergence is in units of 10^{-4} gm cm^{-2} s^{-1} at intervals of 4 units and the vertically integrated streamfunction of the advective water vapour flux is in units of 10^{7} gm cm^{-1} mb^{-1} s^{-1} at intervals of 10 units.

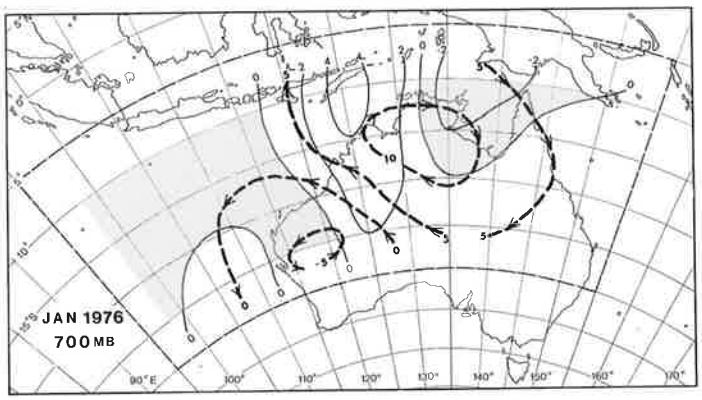
JAN 1976
700MB

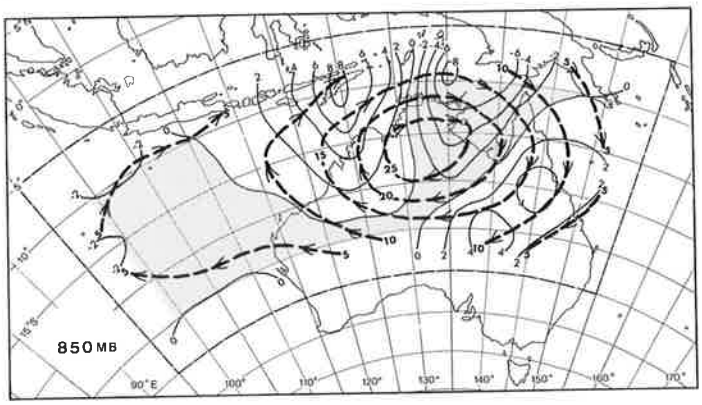
850MB

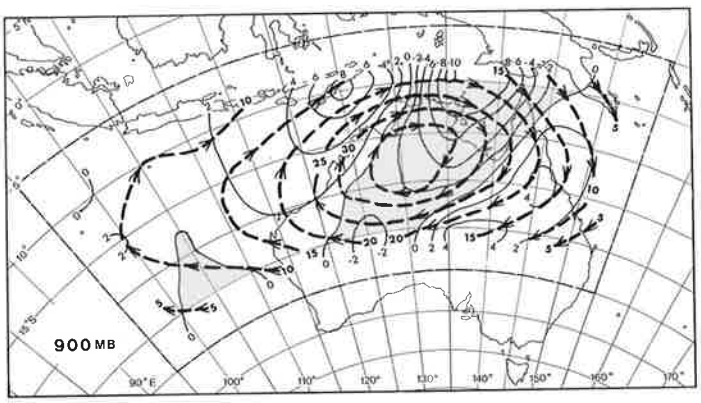
900MB

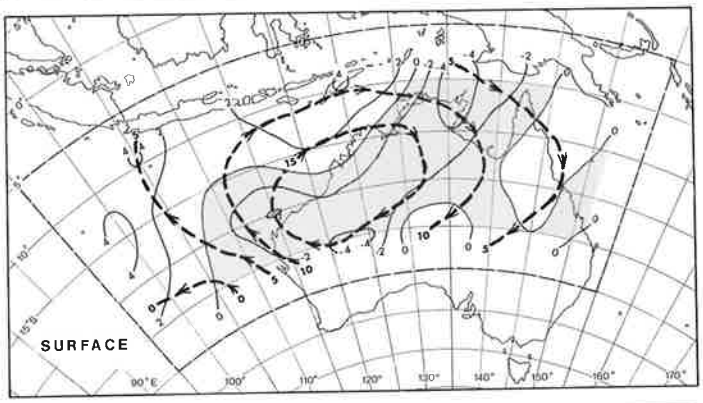
SURFACE

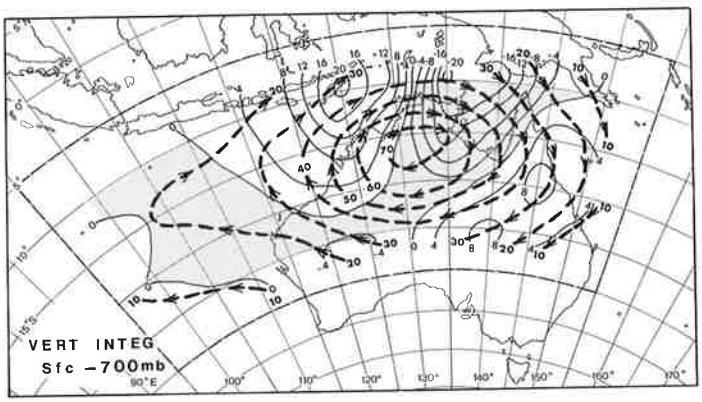
VERT INTEG
Sfc –700mb

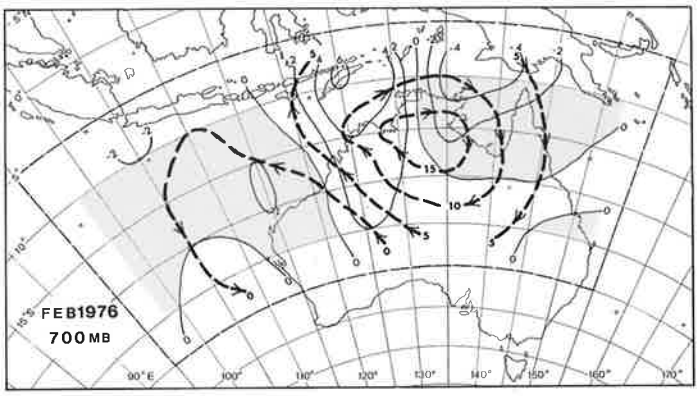
FEB1976
700MB

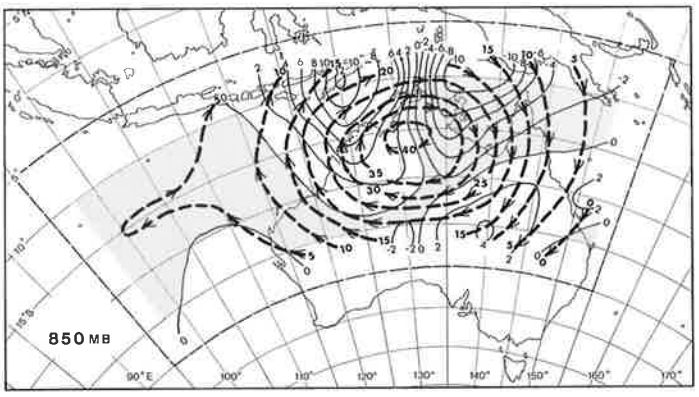
850MB

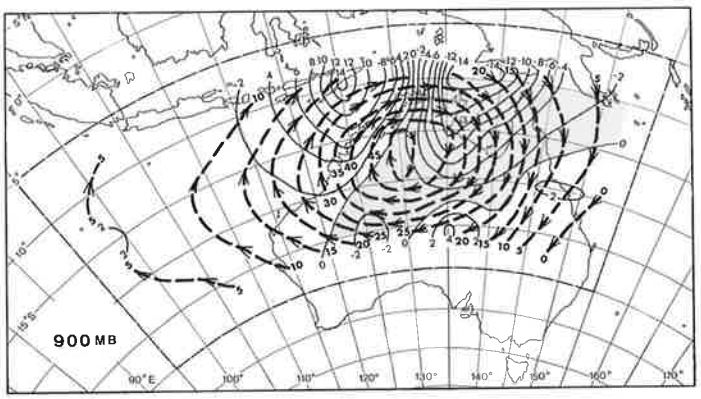
900MB

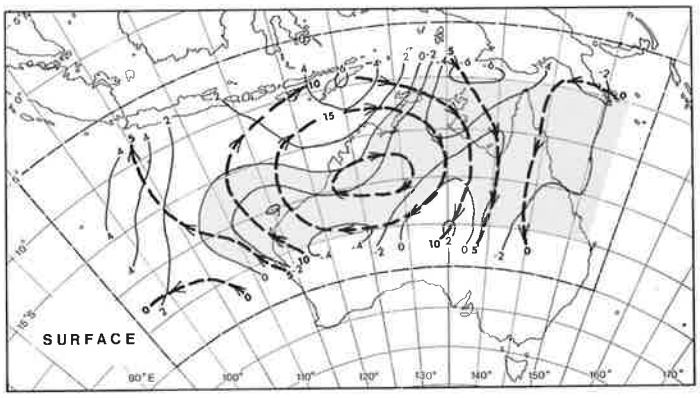
SURFACE

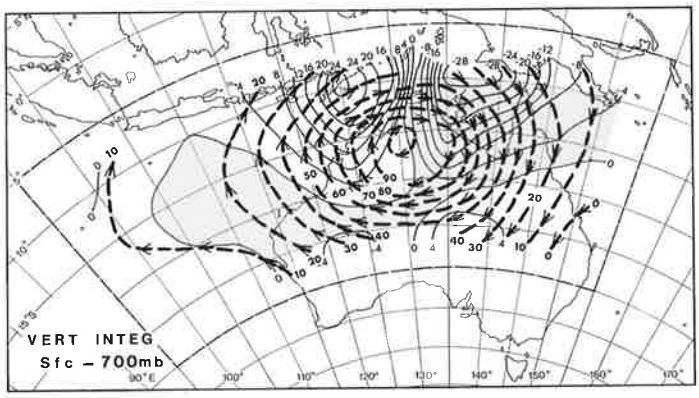
VERT INTEG
Sfc – 700mb

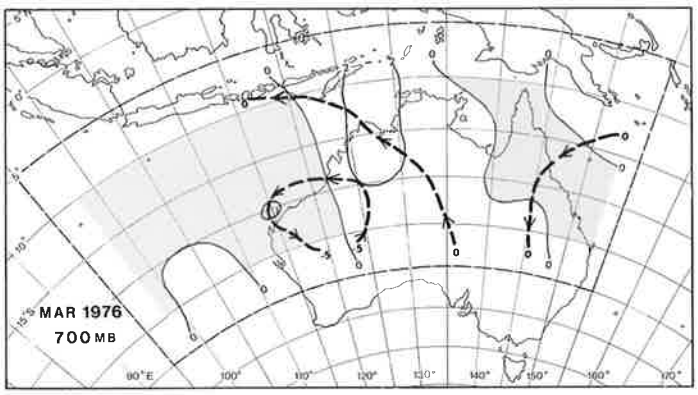
MAR 1976
700 MB
90°E
100°
110°
120°
130°
140°
150°
160°
170°

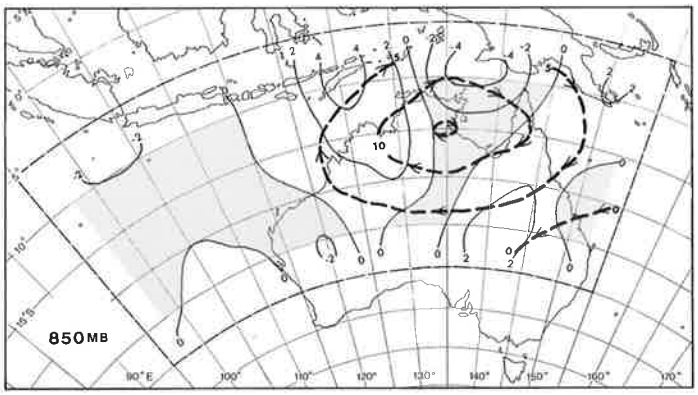
850 MB
90°E
100°
110°
120°
130°
140°
150°
160°
170°

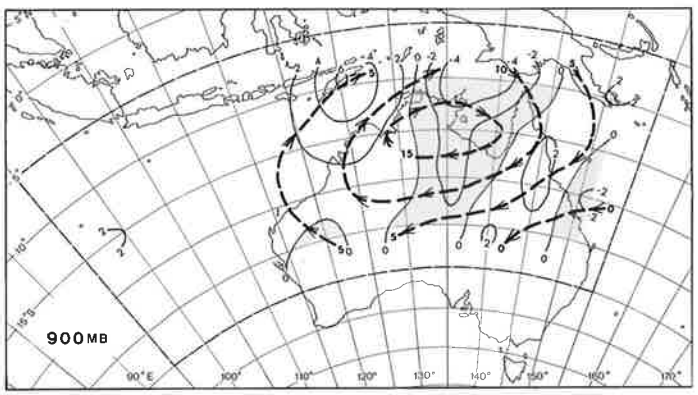
900 MB
90°E
100°
110°
120°
130°
140°
150°
160°
170°

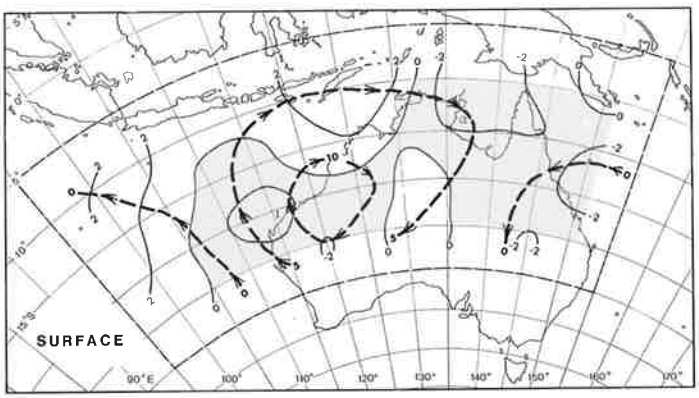
SURFACE
90°E
100°
110°
120°
130°
140°
150°
160°
170°

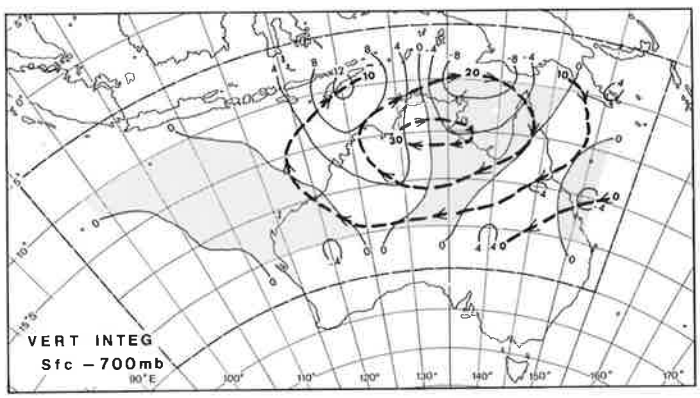
VERT INTEG
Sfc – 700mb
90°E
100°
110°
120°
130°
140°
150°
160°
170°

marginally greater in February 1976 than in January 1974. However, the overall organization of convective activity in January 1974 is greater than that in either January 1976 or February 1976. The southwest-northeast tilt in the trough is again prevalent and, as in other 'wetter' summers, cyclonic circulation extends to 700 mb.

March 1976 (Fig.60) concludes a dominant monsoonal season with moderate circulation and advective moisture convergence patterns. Cyclonic circulation is all but gone from the continent by 700 mb and reaches magnitudes a little above average at the other levels.

The 1977 season ends the five year sequence with moderate monsoonal conditions. January 1977 (Fig.61) experiences slightly above average monsoon circulation, with features similar to the other months in the period. Distinct anticyclonicity by 700 mb indicates that the cyclonic circulation, despite significant advective moisture convergence values at the levels below 700 mb, is not on the same scale as in the peak months of 1974 and 1976. It is evident that the southwest-northeast vertical tilt of cyclonic circulation centres, the orientation of advective moisture convergence fields, 900 mb cyclonic circulation and advective moisture convergence maxima, and the 700 mb change to anticyclonic conditions are important features of Australian monsoon seasons.

February 1977 (Fig.62) follows the tendency of a February maximum in monsoonal circulation over the continent of Australia. Intensities in the latter month closely approximate those in the 1973 and 1975 Februarys, although advective moisture convergence is somewhat less at the 900 mb and 850 mb levels.

By March 1977 (Fig.63) the monsoon has again weakened, with well developed 700 mb anticyclonicity above moderately strong 900 mb and 850 mb cyclonic circulation. Although not as strong as in March 1974, monsoon activity in March 1977 is on a par with that in March 1976.

Figures 64 and 65 are included to summarize the extent of intraseasonal and interannual variability of cyclonic circulation and advective moisture

Figure 61 Monthly mean advective water vapour flux divergence (light lines, convergence shaded) and the streamfunction of the advective water vapour flux (heavy dashed lines) at surface, 900, 850 and 700 mb levels over the local domain in January 1977. Advective water vapour flux divergence is in units of 10^{-6} gm cm^{-2} mb^{-1} s^{-1} at intervals of 2 units and the streamfunction of the advective water vapour flux is in units of 10^{5} gm mb^{-1} s^{-1} at intervals of 5 units. Vertically integrated (surface - 700 mb) advective water vapour flux divergence is in units of 10^{-4} gm cm^{-2} s^{-1} at intervals of 4 units and the vertically integrated streamfunction of the advective water vapour flux is in units of 10^{7} gm cm^{-1} mb^{-1} s^{-1} at intervals of 10 units.

Figure 62 Monthly mean advective water vapour flux divergence (light lines, convergence shaded) and the streamfunction of the advective water vapour flux (heavy dashed lines) at surface, 900, 850 and 700 mb levels over the local domain in February 1977. Advective water vapour flux divergence is in units of 10^{-6} gm cm^{-2} mb^{-1} s^{-1} at intervals of 2 units and the streamfunction of the advective water vapour flux is in units of 10^{5} gm mb^{-1} s^{-1} at intervals of 5 units. Vertically integrated (surface - 700 mb) advective water vapour flux divergence is in units of 10^{-4} gm cm^{-2} s^{-1} at intervals of 4 units and the vertically integrated streamfunction of the advective water vapour flux is in units of 10^{7} gm cm^{-1} mb^{-1} s^{-1} at intervals of 10 units.

Figure 63 Monthly mean advective water vapour flux divergence (light lines, convergence shaded) and the streamfunction of the advective water vapour flux (heavy dashed lines) at surface, 900, 850 and 700 mb levels over the local domain in March 1977. Advective water vapour flux divergence is in units of 10^{-6} gm cm^{-2} mb^{-1} s^{-1} at intervals of 2 units and the streamfunction of the advective water vapour flux is in units of 10^{5} gm mb^{-1} s^{-1} at intervals of 5 units. Vertically integrated (surface - 700 mb) advective water vapour flux divergence is in units of 10^{-4} gm cm^{-2} s^{-1} at intervals of 4 units and the vertically integrated streamfunction of the advective water vapour flux is in units of 10^{7} gm cm^{-1} mb^{-1} s^{-1} at intervals of 10 units.

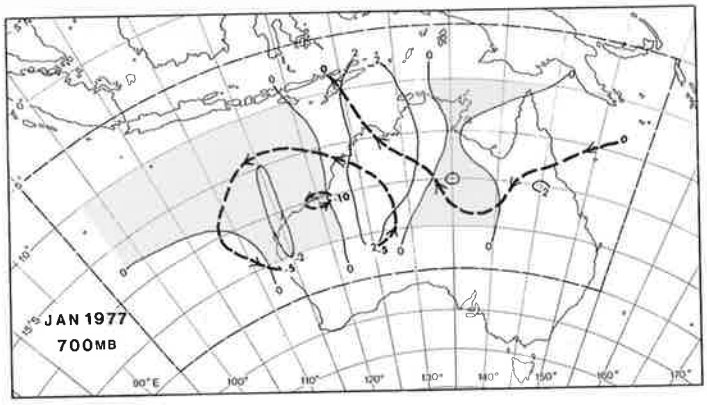
JAN 1977
700MB

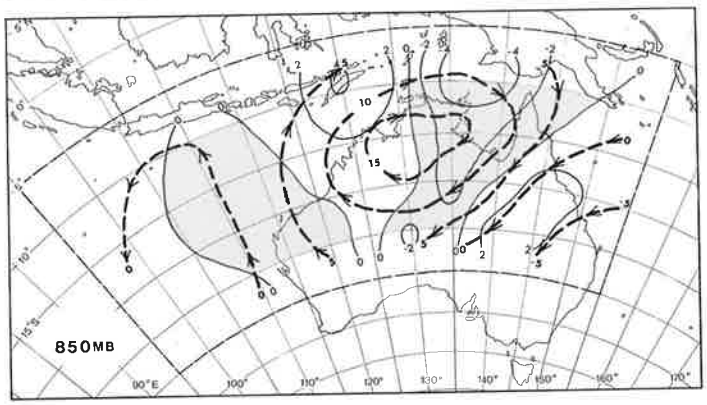
850MB

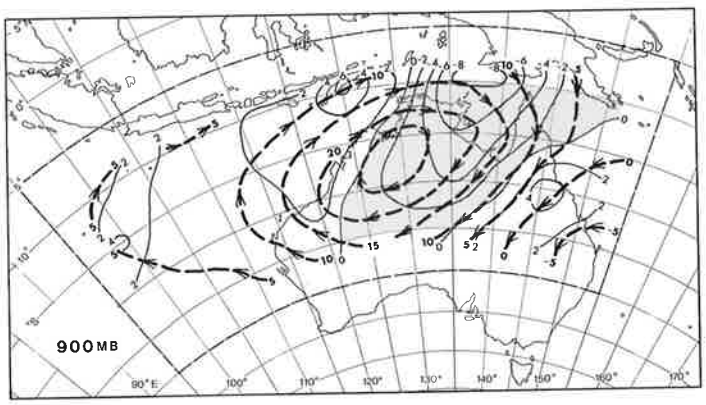
900MB

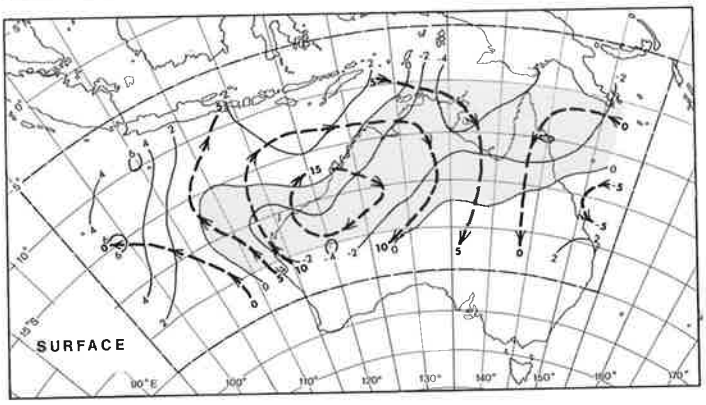
SURFACE

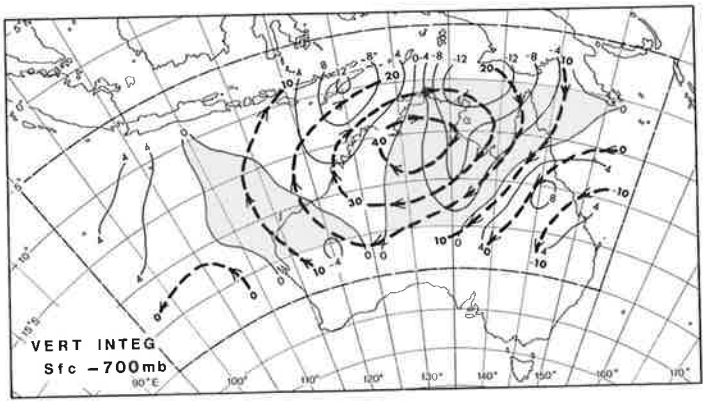
VERT INTEG
Sfc – 700mb

convergence conditions between the surface and 700 mb levels. In particular, it is important to note the contrast between individual months during 1973-77 and the 1957-75 monthly averages. Whether comparing individual months or seasons, it is apparent that cyclonic circulation magnitudes in the 1973-77 period are generally above the 19 year (1957-75) averages (Fig.64). Only in the months of January and March of 1975 do cyclonic circulation distributions fall below 1957-75 results. As noted in Section 3.1.1, the 1975 season marks a distinctly poor monsoonal episode.

As observed previously, the 1974 and 1976 summers over northern Australia are influenced by intense monsoonal circulations. Peak cyclonic circulation, as reflected in positive values of the vertically integrated streamfunction of the advective water vapour flux, is present in January 1974 and, to a lesser degree, in February 1976 (Fig.64). During these months, values are respectively five and two-and-a-half-times the 1957-75 January and February averages. In both of the above months, cyclonic circulation is still dominant at 700 mb. In fact, in the 1974 and 1976 seasons, only March 1976 is notable for a distinct change from closed cyclonic to anti-cyclonic conditions. However, these changes in circulation are prominent during each January and March in the 1973, 1975 and 1977 summers. As previously noted, such alternations are absent from the Februarys of any of the 1973-77 seasons.

At individual pressure levels, circulation patterns in the majority of months show the tendency for a 900 mb maximum, with 850 mb magnitudes often only marginally weaker (Fig.64). The 1957-75 magnitudes reflect this trend, with an indication that very similar vertical structures of cyclonic circulation occur in January and February. At the surface, the 19 year average traces suggest that January magnitudes are slightly above those in February or March. This may be related to the strength of the low-level heat low over northwestern Australia, although the only supporting evidence for this is found in the slightly higher January mean surface temperatures at Port Hedland, Broome and Giles (Maher and Lee, 1977).

Figure 64 Monthly mean streamfunction of the advective water vapour flux in cyclonic/NET_{SH} centres over Australia for January, February and March in the period 1957-75 and in the individual years from 1973-77. Vertical traces are in units of 10^5 gm mb^{-1} s^{-1} at the surface, 900, 850 and 700 mb levels. Dashed lines indicate abrupt changes from cyclonic to anticyclonic circulation and VI and AVI designate vertically integrated and average vertically integrated values respectively. The latter are in units of 10^7 gm cm^{-1} mb^{-1} s^{-1}.

Figure 65 Monthly mean advective water vapour flux convergence over north-northeastern (heavy lines) and west-southwestern (light lines) Australia for January, February and March in the period 1957-75 and in individual years from 1973-77. Both vertical traces are in units of 10^{-6} gm cm^{-2} mb^{-1} s^{-1} at the surface, 900, 850 and 700 mb levels.

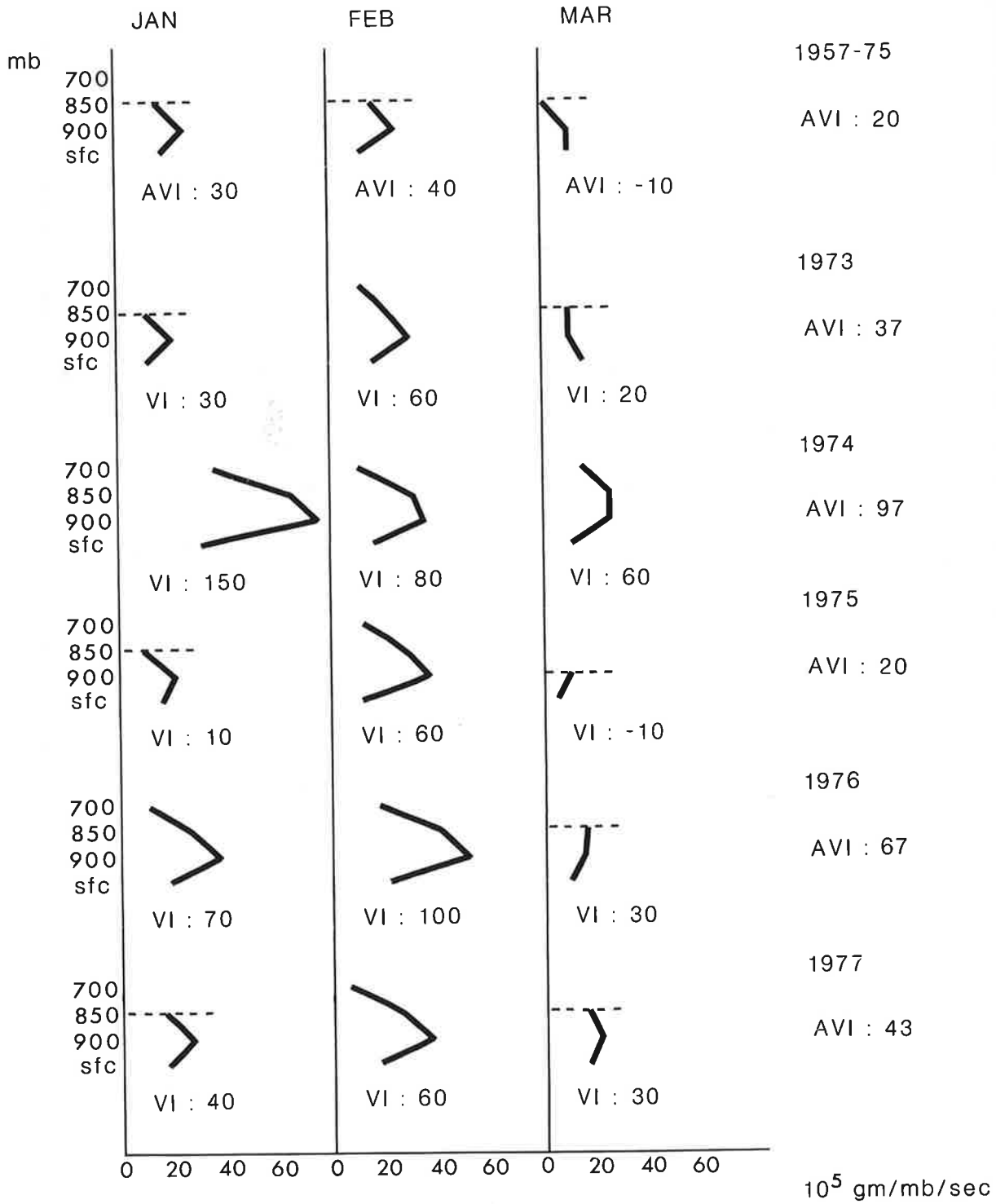
JAN
FEB
MAR
mb
700
850
900
sfc
AVI : 30
AVI : 40
AVI : -10
1957-75
AVI : 20
VI : 30
VI : 60
VI : 20
1973
AVI : 37
VI : 150
VI : 80
VI : 60
1974
AVI : 97
VI : 10
VI : 60
VI : -10
1975
AVI : 20
VI : 70
VI : 100
VI : 30
1976
AVI : 67
VI : 40
VI : 60
VI : 30
1977
AVI : 43
0 20 40 60
10^5 gm/mb/sec

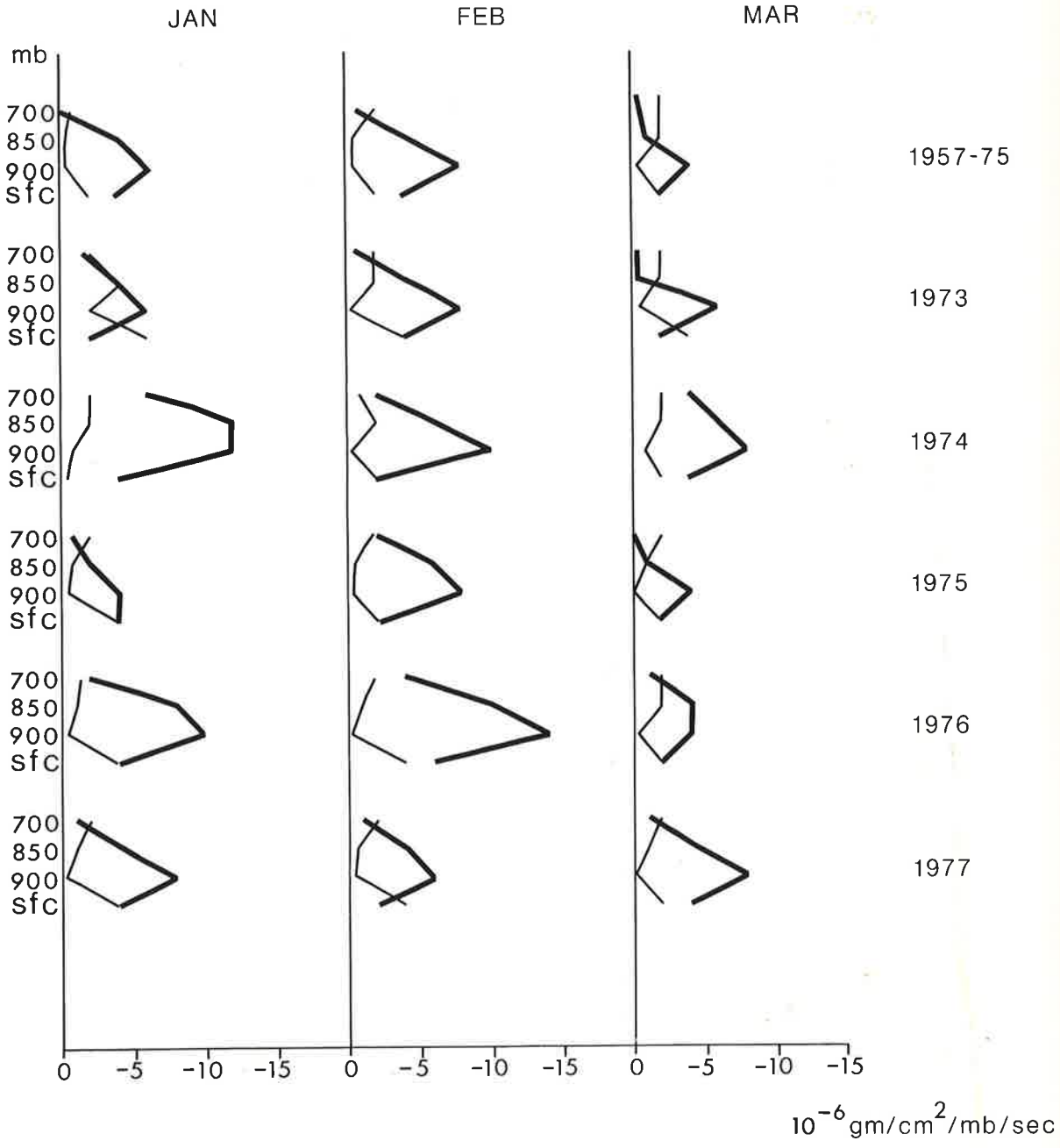
JAN
FEB
MAR
mb
700
850
900
sfc
1957-75
1973
1974
1975
1976
1977
0
-5
-10
-15
10^{-6} gm/cm^2/mb/sec

Between 850 mb and 700 mb levels, all of the 1957-75 monthly averages show a marked change from cyclonic to anticyclonic flow patterns. Surprisingly, the 1973-77 February traces all show deep cyclonic circulation up to 700 mb and tend to suggest that, during the 1973-77 period, there was above average persistence in monsoonal activity during February (see discussion in Section 3.1.1).

Figure 65 provides a similar summary of advective moisture convergence variability over north-northeastern and west-southwestern Australia. In particular, the figure illustrates that advective moisture convergence over the former region is usually much more pronounced than in the latter. This is perhaps to be expected as there is a tendency for atmospheric moisture to be high over north-northeastern Australia during summer (Maher and Lee, 1977) and, coupled with any strong northeast monsoon flow, for the most intense convergence to develop in this region. However, it should be noted that the local orography of the southwestern region would appear to be a factor influencing moist processes, with the Hamersley Ranges containing peaks of between 600 to 1200 metres (Fig.44).

It is apparent, when comparing Figures 64 and 65, that cyclonic circulation magnitudes correspond best with advective moisture convergence traces over north-northeastern Australia. Both figures show a tendency for strong cyclonicity and north-northeastern advective moisture convergence during the 1974 and 1976 seasons, with the reverse occurring in 1975. In January 1973 (Fig.65), when the NET_{SH} has an apparently anomalous southeast-northwest tilt and a major El Niño episode is drawing to a close, advective moisture convergence magnitudes in the two regions are comparable. Lesser variants of the above are found in the March 1957-75, 1973, 1975, 1976 and January 1975 traces. A marked discontinuity is evident in the vertical structure of the traces in the north-northeastern and west-southwestern regions of the continent. Traces in the north-northeastern sector show evidence of a further relation to cyclonic circulation magnitudes, with the most pronounced advective moisture convergence occurring at 900 mb followed

by a general weakening up to 700 mb. Yet, in the west-southwestern region, almost all traces weaken rapidly, from often high surface values to very low 900 mb values. In fact, the strongest coherence between advective moisture convergence values in both regions exists at the surface.

As is the case with cyclonic circulation diagrams, intraseasonal variability is most prominent in the north-northeastern region in 1975, with a slight suggestion of similar changes in 1973. Apart from this, there is a distinct seasonal signal in many summers with indications of the withdrawal of the monsoon in March. The latter is most pronounced in the 19 year averages, although 1973, 1975 and 1976 summers reflect similar trends.

Over the west-southwestern sector of the continent the above trends are hardly evident. Thus it would seem that advective moisture convergence over northeastern Australia is more prominent in summers of above average monsoonal activity and, together with cyclonic circulation, this provides an insight into aspects of moisture processes over northern Australia. Yet, most importantly, there is also a suggestion that the depth of cyclonic circulation (NET_{SH}) and advective moisture convergence vary considerably between monsoonal extremes.

A summary of the atmospheric moisture content at various Australian radiosonde stations during 1973-77 is provided in Figure 66. Basically, it illustrates broad trends in precipitable water content over northern Australia.

As expected, January 1974 stands out as the month in which there is the most marked increase in atmospheric moisture content at Australian stations. Other smaller station conjunctions occur in the Februarys of 1973, 1975, 1976 and 1977 and these probably give further credence to the suggestion of a February peak in monsoonal activity. These are interspersed with four periods of poor moisture characteristics in March 1973, January 1975, March 1975 and January 1977. However, the secondary monsoon incursion in the 1976 summer is not marked by the pronounced moisture increases observed in January 1974.

Figure 66 Monthly mean total precipitable water content at various Australian radiosonde stations for January (J), February (F) and March (M) 1973-77. Total precipitable water content is in units of gm cm^{-2} . Stations used are D (Darwin, large dots), B (Broome, small dots), P (Port Hedland, dashed line), C/M (Cloncurry/Mount Isa, solid line), T (Townsville, smallest dotted line), CI (Cocos Island, open circles), WI (Willis Island, solid diamonds), A (Alice Springs, open diamonds) and CA (Carnarvon, solid squares).

TOTAL PRECIPITABLE WATER CONTENT (gm/cm^2)

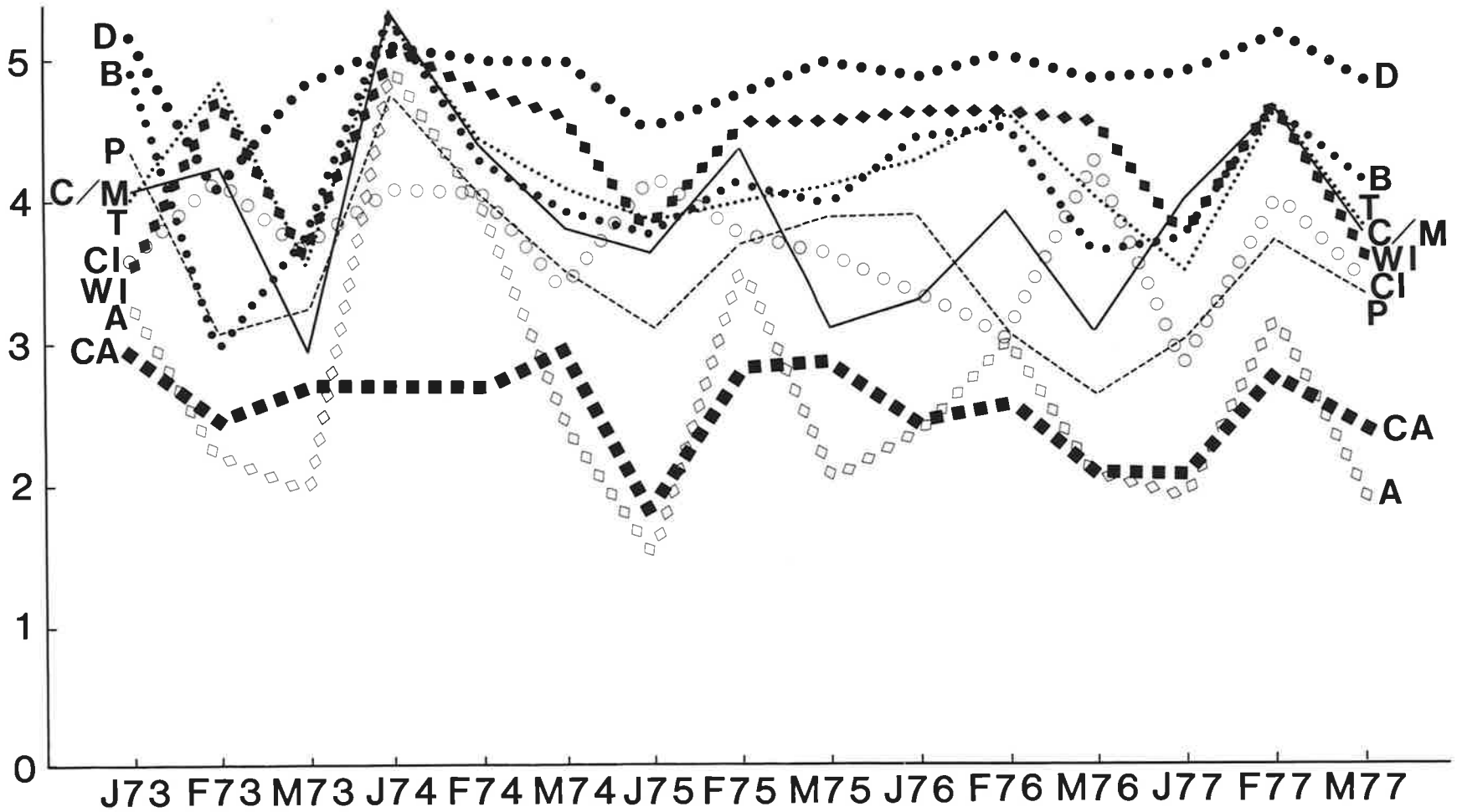

In Figure 66 it can be seen that there are often as many stations showing an increase in moisture content as there are stations showing a decrease. Thus it is obvious that monsoonal influence is spatially variable, with only strong monsoonal extremes providing any similar tendency in moisture characteristics. Further compounding the situation is the observation that low latitude stations show less variability than their sub-tropical continental counterparts. This was alluded to earlier in this discussion (Fig.48) and is best seen in Figure 66 when the traces for Darwin and Alice Springs are compared. On the other hand, zonal differences in stations are exemplified by oceanic and coastal continental stations such as Cocos Island, Carnarvon and Townsville. At these locations the responses not only differ in magnitude but also in phase. Thus moisture responses in the local domain form a complicated amalgam that is at its most coherent during major extremes in monsoonal activity.

Figure 67 concludes this discussion because it shows aspects of wind direction steadiness at the 850 mb level. Steadiness is given as the ratio of the speed of the monthly mean vector wind to the speed of the monthly mean scalar wind, expressed as a percentage. Thus high(low) percentages indicate a low(high) degree of wind direction fluctuations within a month.

Station averages at the base of the 1973-77 sequence in Figure 67 tend to provide further support for the concept that near-equatorial locations possess more variations in their wind regimes than do sub-tropical locations (e.g. 45 per cent at Darwin and Cocos Island as against 72 per cent and 76 per cent at Alice Springs and Giles). On the other hand, the monthly averages on the right-hand side of Figure 67 indicate that steadiness over Australia is high(low) during periods of high(low) monsoonal activity. This is most evident in the months of January 1974 (75 per cent) and 1975 (45 per cent) when markedly contrasting monsoonal conditions influence the continent. The monsoon incursion during 1976 is most evident in February when monthly average steadiness reaches 65 per cent.

As the percentage steadiness at stations across the centre of the

Figure 67 Monthly mean 850 mb wind steadiness at various Australian upper wind stations. Wind steadiness values are given as a per cent and are the ratio of the speed of the monthly mean vector wind to the monthly mean scalar wind. Stations used are D (Darwin), CI (Cocos Island), T (Townsville), WI (Willis Island), P (Port Hedland), G (Giles), A (Alice Springs), C/M (Cloncurry/Mount Isa), CA (Carnarvon), CV (Charleville) and E (Eagle Farm).

850 MB WIND STEADINESS %

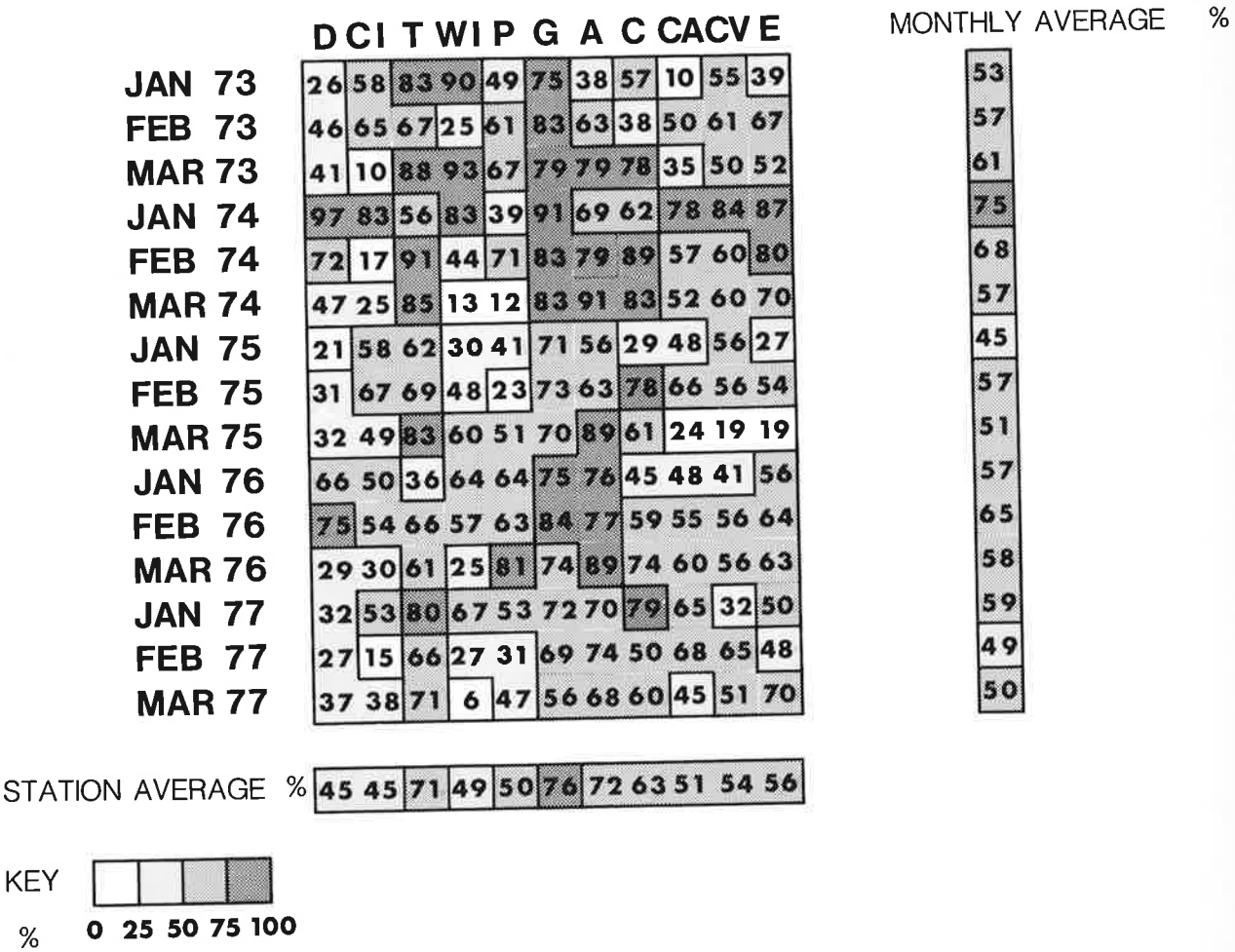

continent is rarely low (being greater than or equal to 75 per cent during at least half of the entire 1973-77 summer period), it is apparent that any pronounced fluctuation in average Australian steadiness must be the result of major changes in steadiness at near-equatorial stations. Figure 67 indicates that periods of strong(weak) monsoonal activity are marked by improved(poor) wind direction steadiness at near-equatorial stations. The latter would tend to give credence to the suggestion that more enhanced and persistent flow conditions tend to predominate during monsoon incursions.

(ii) Monthly Mean 850 mb Transient Eddy Moisture Characteristics

This discussion analyses several aspects of moisture processes in fields of monthly mean 850 mb transient eddy water vapour flux divergence and the streamfunction of the transient eddy water vapour flux (Figs.68-72). The aim of this analysis is to evaluate transient eddy moisture characteristics for comparison with the advective moisture characteristics discussed in Section 3.2.1 *(i)*. As Hutchings (1961:628) notes :

> These fluctuations [transient eddies] have a clear physical significance in that they are directly related to the cyclones, anticyclones, troughs, ridges and other synoptic features....

However, this does not imply that individual eddies will be detected and that transient systems such as tropical cyclones or rain depressions are resolvable, but rather that monthly averages of all transient eddy fluctuations will be deduced. Finally, the importance of each component of the flow (Appendix 6.1) is then examined in Figures 73-77 where total, advective and transient eddy water vapour fluxes at 850 mb are presented.

Figure 68, showing the transient eddy fluctuations in 1973, indicates that January 1973 stands out as a month in which pronounced transient eddies occurred. If compared with the monthly mean 850 mb advective fields (Fig.49), it is apparent that there is almost a complete alternation or reversal in the circulation and in the moisture divergence distributions.

Figure 68 Monthly mean 850 mb transient eddy water vapour flux divergence (light lines, convergence shaded) and the streamfunction of the transient eddy water vapour flux (heavy dashed lines) over the local domain in January, February and March 1973. Transient eddy water vapour flux divergence is in units of 10^{-6} gm cm^{-2} mb^{-1} s^{-1} at intervals of 2 units and the streamfunction of the transient eddy water vapour flux is in units of 10^{5} gm mb^{-1} s^{-1} at intervals of 5 units.

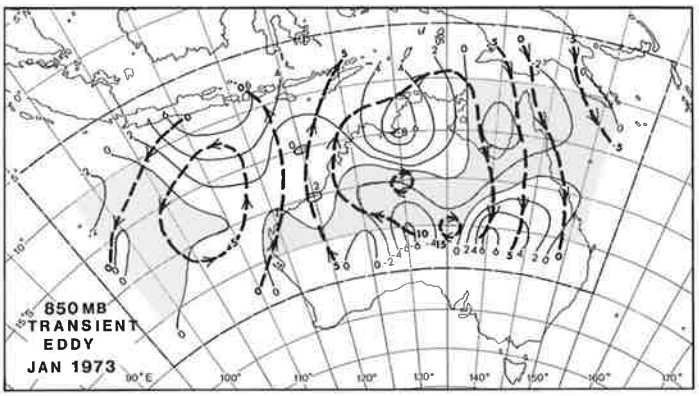
850MB
TRANSIENT
EDDY
JAN 1973
90°E
100°
110°
120°
130°
140°
150°
160°
170°

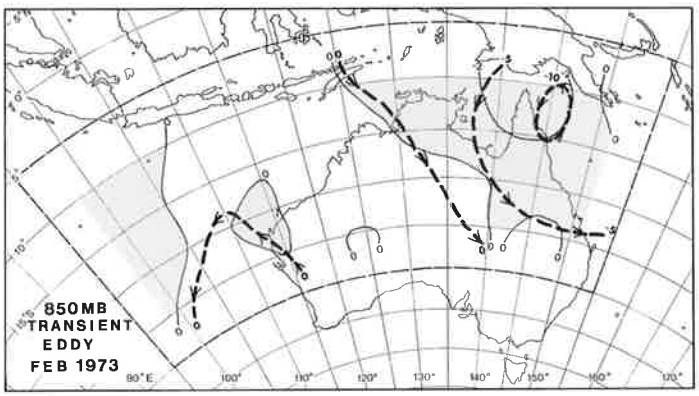
850MB
TRANSIENT
EDDY
FEB 1973
90°E
100°
110°
120°
130°
140°
150°
160°
170°

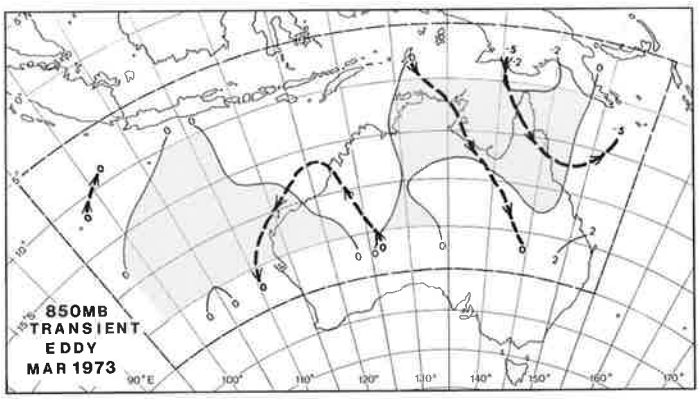
850MB
TRANSIENT
EDDY
MAR 1973
90°E
100°
110°
120°
130°
140°
150°
160°
170°

Figure 69 Monthly mean 850 mb transient eddy water vapour flux divergence (light lines, convergence shaded) and the streamfunction of the transient eddy water vapour flux (heavy dashed lines) over the local domain in January, February and March 1974. Transient eddy water vapour flux divergence is in units of 10^{-6} gm cm^{-2} mb^{-1} s^{-1} at intervals of 2 units and the streamfunction of the transient eddy water vapour flux is in units of 10^{5} gm mb^{-1} s^{-1} at intervals of 5 units.

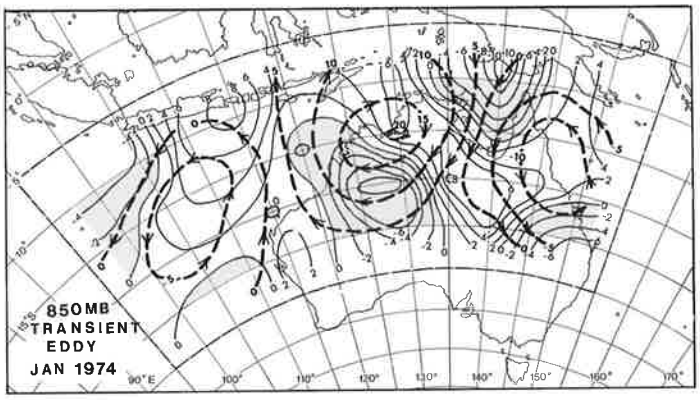
850MB
TRANSIENT
EDDY
JAN 1974

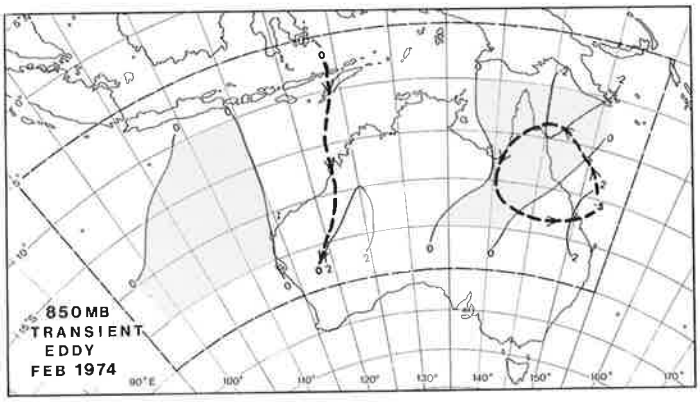
850MB
TRANSIENT
EDDY
FEB 1974

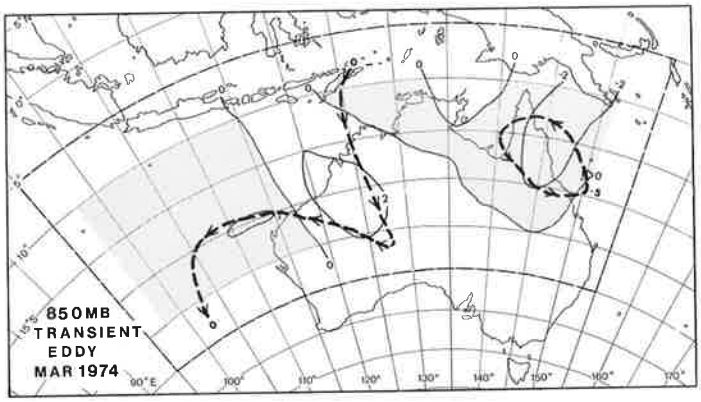
850MB
TRANSIENT
EDDY
MAR 1974

is again prominent over eastern Australia. However, similar to the February 1973 situation, advective fields (Fig.53) dominate and no distinct alternations are evident. Certainly, there are no pronounced alternations of the moisture convergence and divergence patterns.

March 1974 shows transient eddy and advective fields (Figs.69 and 54) with very similar characteristics to February 1974 distributions. There are no widespread alternations in circulation or moisture convergence distributions, only a weak tendency for the moisture convergence pattern to shift from being over most of the 'top end' of the Northern Territory and the Gulf of Carpentaria in the advective fields, to over Cape York in the eddy fields. A slight alternation of moisture convergence and divergence is possibly detected over Western Australia.

Transient eddy fluctuations are weak throughout 1975 (Fig.70), being marginally stronger in January than in the other two months. In January 1975, transient eddy fluctuations are equal to, if not slightly stronger than the advective fields (Fig.55). Alternations in circulation and moisture convergence are prevalent, even if the fields in question are weak. Advective cyclonic circulation to the northeast of Australia is replaced by anticyclonic circulation in the transient eddy pattern. The amorphous circulation over the continent in the advective fields is replaced by more cyclonic circulation in the transient eddy fields, while moisture convergence and divergence patterns alternate to the west and northwest of Australia, over the 'top end' and over central Australia.

By February 1975 the circulation and moisture convergence patterns in the advective fields are strong, while transient eddy fields show weaker activity (Figs.56 and 70). As in Februarys 1973 and 1974, alternations are poorly defined and total flow is dominated by advective terms. In fact, the February 1975 regime fails to achieve the type of circulation and moisture convergence magnitudes in Februarys 1973 and 1974.

In March 1975 both advective and eddy fields are of poor magnitude (Figs.57 and 70), with cyclonic eddies over the Australian continent alternating

Figure 70 Monthly mean 850 mb transient eddy water vapour flux divergence (light lines, convergence shaded) and the streamfunction of the transient eddy water vapour flux (heavy dashed lines) over the local domain in January, February and March 1975. Transient eddy water vapour flux divergence is in units of 10^{-6} gm cm^{-2} mb^{-1} s^{-1} at intervals of 2 units and the streamfunction of the transient eddy water vapour flux is in units of 10^{5} gm mb^{-1} s^{-1} at intervals of 5 units.

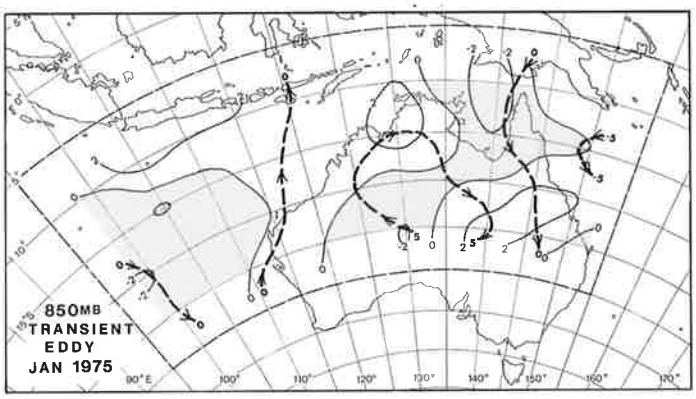
850MB
TRANSIENT
EDDY
JAN 1975
90°E
100°
110°
120°
130°
140°
150°
160°
170°

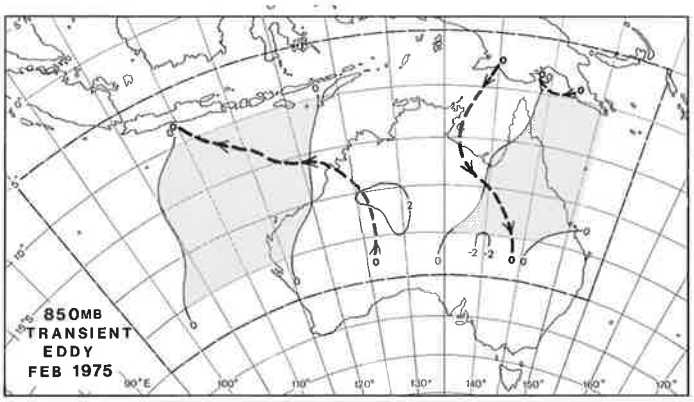
850MB
TRANSIENT
EDDY
FEB 1975
90°E
100°
110°
120°
130°
140°
150°
160°
170°

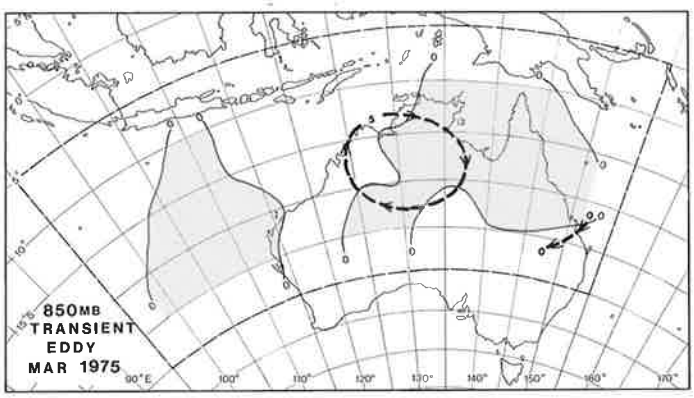
850MB
TRANSIENT
EDDY
MAR 1975
90°E
100°
110°
120°
130°
140°
150°
160°
170°

with anticyclonicity in the advective fields. However, moisture convergence alternations are once again ill-defined and the month completes a season of indifferent transient eddy patterns.

The 1976 season (Fig.71) is similar to 1975, in that poorly defined transient eddy conditions prevail throughout. January 1976 fails to show definite alternations of circulation or moisture convergence, with circulation dominated by a strong NET_{SH} over the continent in advective fields (Fig.58) and transient eddy patterns showing matching, although weaker, cyclonic circulation (Fig.71). Only the eastward displacement of the moisture convergence over north-northeastern Australia between advective fields (Fig.58) and transient eddy fields (Fig.71) is notable in the moisture convergence patterns.

February 1976, with stronger advective NET_{SH} conditions than January 1976, is influenced by weak transient eddy cyclonic circulation over north-eastern Australia. A weak alternation in circulation is evident over the remainder of the continent, with the strong advective NET_{SH} giving way to weak anticyclonic flow. Similarly, the only alternation in moisture convergence and divergence fields occurs over northwestern Australia where strong advective moisture divergence (Fig.59) is replaced by weak transient eddy moisture convergence (Fig.71).

By March 1976, weaker circulation and moisture convergence is observed in both advective and transient eddy fields. The NET_{SH} activity over the continent in the advective fields (Fig.60) alternates with weak transient eddy anticyclonicity (Fig.71). However, moisture convergence fields do not display any distinctly complementary fluctuations.

To complete the 1973-77 period, the 1977 season (Fig.72) is also dominated by weak transient eddy fields. As in March 1976, there is a slight alternation in circulation during January 1977, from moderately strong advective NET_{SH} (Fig.61) to amorphous transient eddy anticyclonic conditions (Fig.72). Slight moisture convergence and divergence alternations are evident over northwestern, central and eastern Australia.

Figure 71 Monthly mean 850 mb transient eddy water vapour flux divergence (light lines, convergence shaded) and the streamfunction of the transient eddy water vapour flux (heavy dashed lines) over the local domain in January, February and March 1976. Transient eddy water vapour flux divergence is in units of 10^{-6} gm cm^{-2} mb^{-1} s^{-1} at intervals of 2 units and the streamfunction of the transient eddy water vapour flux is in units of 10^{5} gm mb^{-1} s^{-1} at intervals of 5 units.

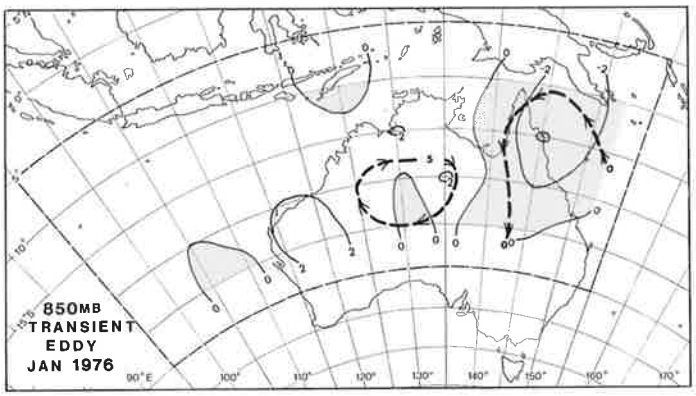
850MB
TRANSIENT
EDDY
JAN 1976
90°E
100°
110°
120°
130°
140°
150°
160°
170°

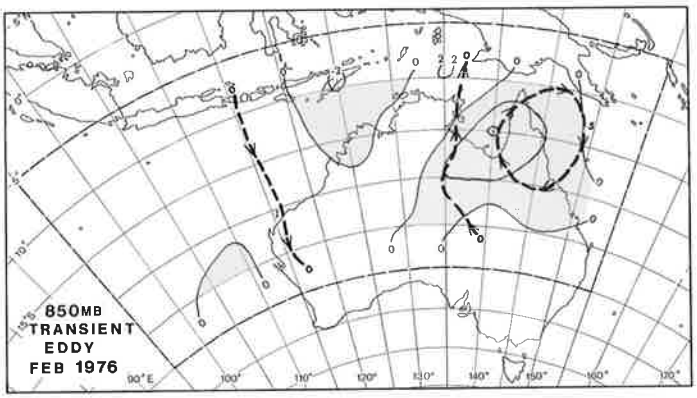
850MB
TRANSIENT
EDDY
FEB 1976
90°E
100°
110°
120°
130°
140°
150°
160°
170°

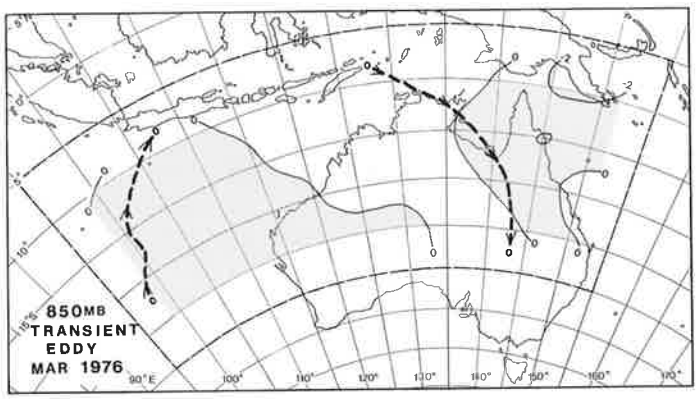
850MB
TRANSIENT
EDDY
MAR 1976
90°E
100°
110°
120°
130°
140°
150°
160°
170°

In February 1977, cyclonic circulation reaches the peak for the 1977 season in the advective fields (Fig.62) and alternates with transient eddy anticyclonicity over the continent (Fig.72). However, moisture convergence/divergence alternations are poorly defined and restricted to eastern Australia. In the Cape York region, marked transient eddy moisture convergence magnitudes are allied with the anticyclonic cell centred over the 'top end'.

Finally, March 1977 sees a weakening in advective NET_{SH} (Fig.63) activity as the monsoon retreats and very weak transient eddy anticyclonicity influences the northwest of the continent (Fig.72). Although poorly defined, moisture convergence/divergence alternations are not restricted to eastern Australia but also occur over the west-northwest of the continent.

So far, it has not been possible to discern much more about the composition of transient eddies, other than whether they are cyclonic or anticyclonic and if they contribute significantly to moisture characteristics. Perhaps the most complete way to illustrate the nature of the flow regime during the 1973-77 period is to examine total, advective and transient eddy fields. An analysis of total, advective and transient eddy water vapour fluxes, in both zonal and meridional planes (Appendix 6.1), highlights further aspects of these features (Figs.73-77).

Most prominent are the causes of fluctuations and alternations in the circulation and convergence/divergence fields. Essentially, they develop from situations in which total and advective zonal and/or meridional water vapour flux components are strong in magnitude but opposite in direction. Fluctuations develop in cases where the total water vapour flux is most pronounced; alternations occur when advective conditions prevail. Areas in the domain, where either of the above situations predominate, exhibit marked transient eddy characteristics. The opposite occurs when total and advective zonal and/or meridional water vapour flux components are closely aligned in magnitude and direction. In such circumstances, transient eddy water vapour fluxes are quite weak.

Figure 72 Monthly mean 850 mb transient eddy water vapour flux divergence (light lines, convergence shaded) and the streamfunction of the transient eddy water vapour flux (heavy dashed lines) over the local domain in January, February and March 1977. Transient eddy water vapour flux divergence is in units of 10^{-6} gm cm^{-2} mb^{-1} s^{-1} at intervals of 2 units and the streamfunction of the transient eddy water vapour flux is in units of 10^{5} gm mb^{-1} s^{-1} at intervals of 5 units.

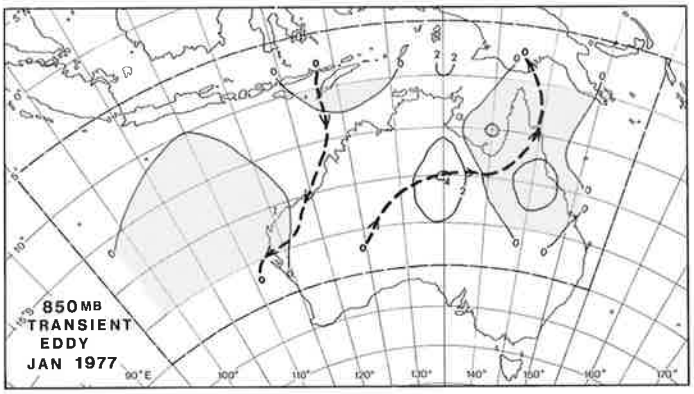
850MB
TRANSIENT
EDDY
JAN 1977
90°E
100°
110°
120°
130°
140°
150°
160°
170°

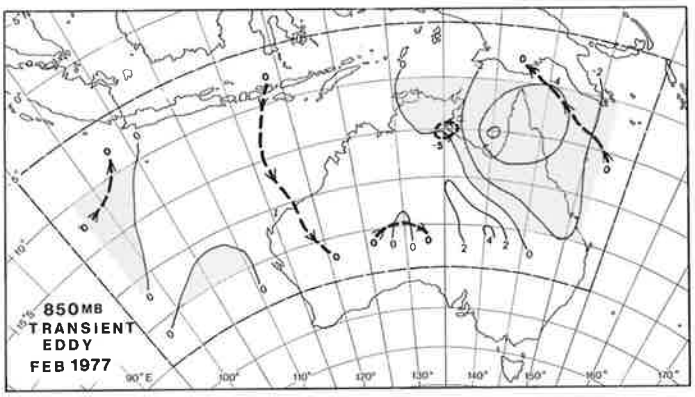
850MB
TRANSIENT
EDDY
FEB 1977
90°E
100°
110°
120°
130°
140°
150°
160°
170°

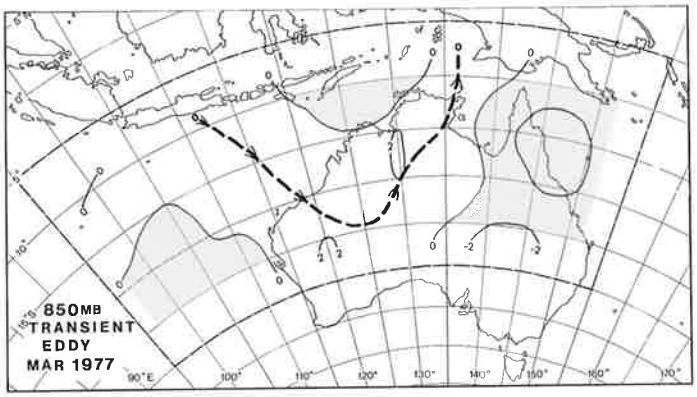
850MB
TRANSIENT
EDDY
MAR 1977
90°E
100°
110°
120°
130°
140°
150°
160°
170°

One important consideration is that the transient eddy water vapour flux component in the meridional plane tends to be of a similar magnitude to both total and advective meridional water vapour flux components (Figs.73-77). This is not evident in the zonal plane, where total and advective water vapour flux components tend to dominate. Moreover, this gives credence to some of the findings of Hutchings (1961). Hence, over the five summers from 1973-77, total and advective water vapour fluxes are usually the strongest elements in the flow regime. However, this does not imply that a combination of total and advective water vapour fluxes will necessarily ensure that the transient eddy water vapour flux component in the zonal plane is stronger than its meridional counterpart. In fact, similar transient eddy zonal and meridional water vapour flux components can develop when both weak total and advective meridional, and strong total and advective zonal water vapour flux components occur. Finer aspects of the above interactions are evident in the 1973-77 summers.

Despite the fact that the months of January 1973 and 1974 both display strong transient eddy zonal and meridional water vapour flux components (Figs.73 and 74), they differ in many respects. In January 1973, both transient eddy zonal and meridional water vapour flux components occur in regions where total and advective water vapour fluxes are of similar magnitude but opposite in direction. This differs from January 1974 where total and advective zonal water vapour flux components are stronger than their meridional counterparts. A closer examination of circulation regimes during the above months suggests that low-level flow over Australasia was not only stronger but distinctly more zonal in January 1974. The net result is that, although January 1973 and January 1974 display similar transient eddy water vapour flux characteristics, these develop from different combinations of total and advective water vapour fluxes.

A further aspect of the nature of the transient eddy water vapour fluxes is found in February and March 1973. In these months the transient eddy zonal water vapour flux components only noticeably outweigh their meridional

Figure 73 Monthly mean 850 mb total, advective and transient eddy water vapour fluxes in the meridional (Q_v) and zonal (Q_u) planes over the local domain in January, February and March 1973. Water vapour fluxes are in units of gm cm^{-1} mb^{-1} s^{-1} at intervals of 5 units (arrows schematically denote the direction of the flow).

Figure 74 Monthly mean 850 mb total, advective and transient eddy water vapour fluxes in the meridional (Q_v) and zonal (Q_u) planes over the local domain in January, February and March 1974. Water vapour fluxes are in units of gm cm^{-1} mb^{-1} s^{-1} at intervals of 5 units (arrows schematically denote the direction of the flow).

Figure 75 Monthly mean 850 mb total, advective and transient eddy water vapour fluxes in the meridional (Q_v) and zonal (Q_u) planes over the local domain in January, February and March 1975. Water vapour fluxes are in units of gm cm^{-1} mb^{-1} s^{-1} at intervals of 5 units (arrows schematically denote the direction of the flow).

Figure 76 Monthly mean 850 mb total, advective and transient eddy water vapour fluxes in the meridional (Q_v) and zonal (Q_u) planes over the local domain in January, February and March 1976. Water vapour fluxes are in units of gm cm^{-1} mb^{-1} s^{-1} at intervals of 5 units (arrows schematically denote the direction of the flow).

Figure 77 Monthly mean 850 mb total, advective and transient eddy water vapour fluxes in the meridional (Q_v) and zonal (Q_u) planes over the local domain in January, February and March 1977. Water vapour fluxes are in units of gm cm^{-1} mb^{-1} s^{-1} at intervals of 5 units (arrows schematically denote the direction of the flow).

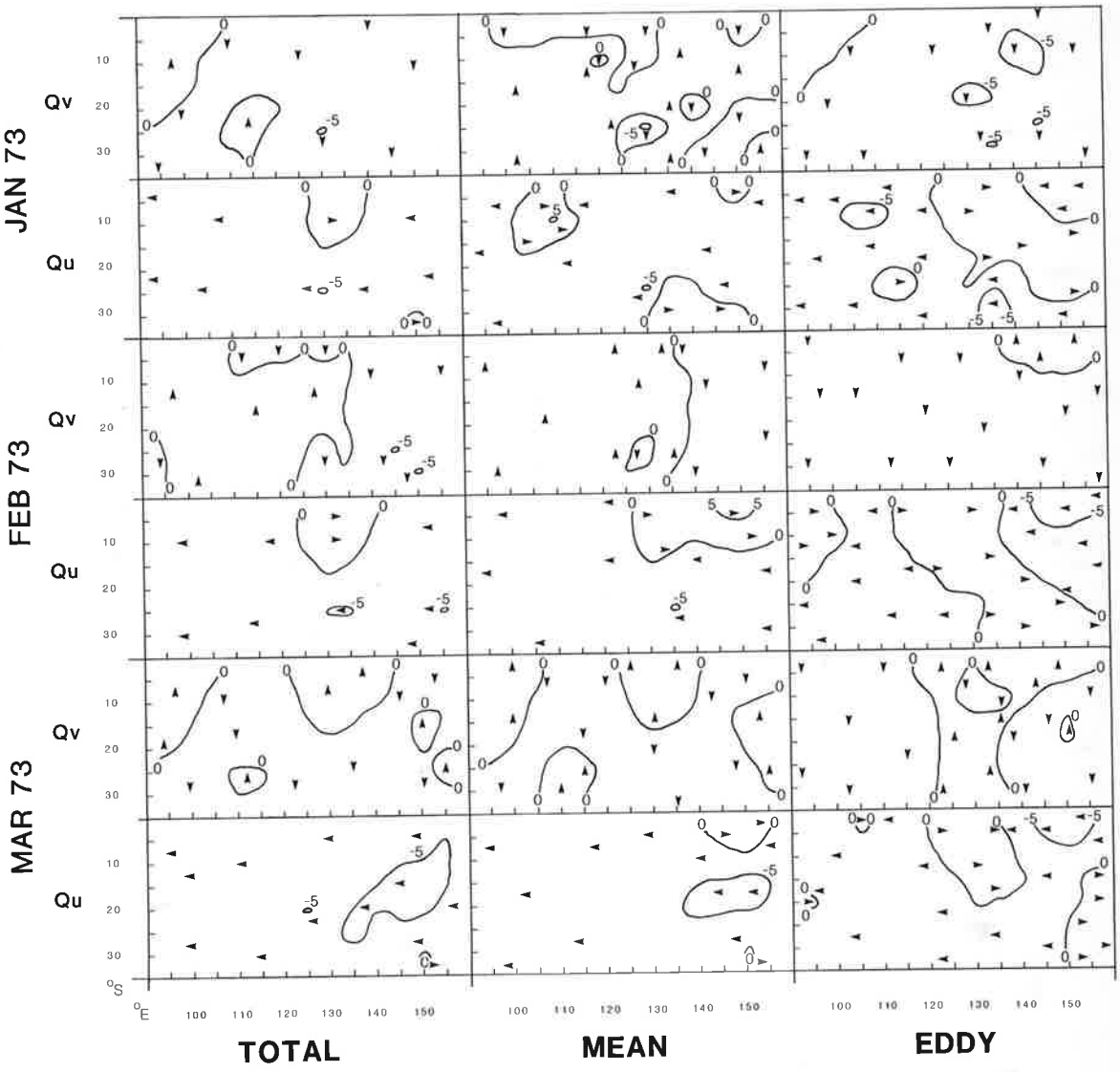
JAN 73
FEB 73
MAR 73
Qv
Qu
TOTAL
MEAN
EDDY
°S
°E
100
110
120
130
140
150

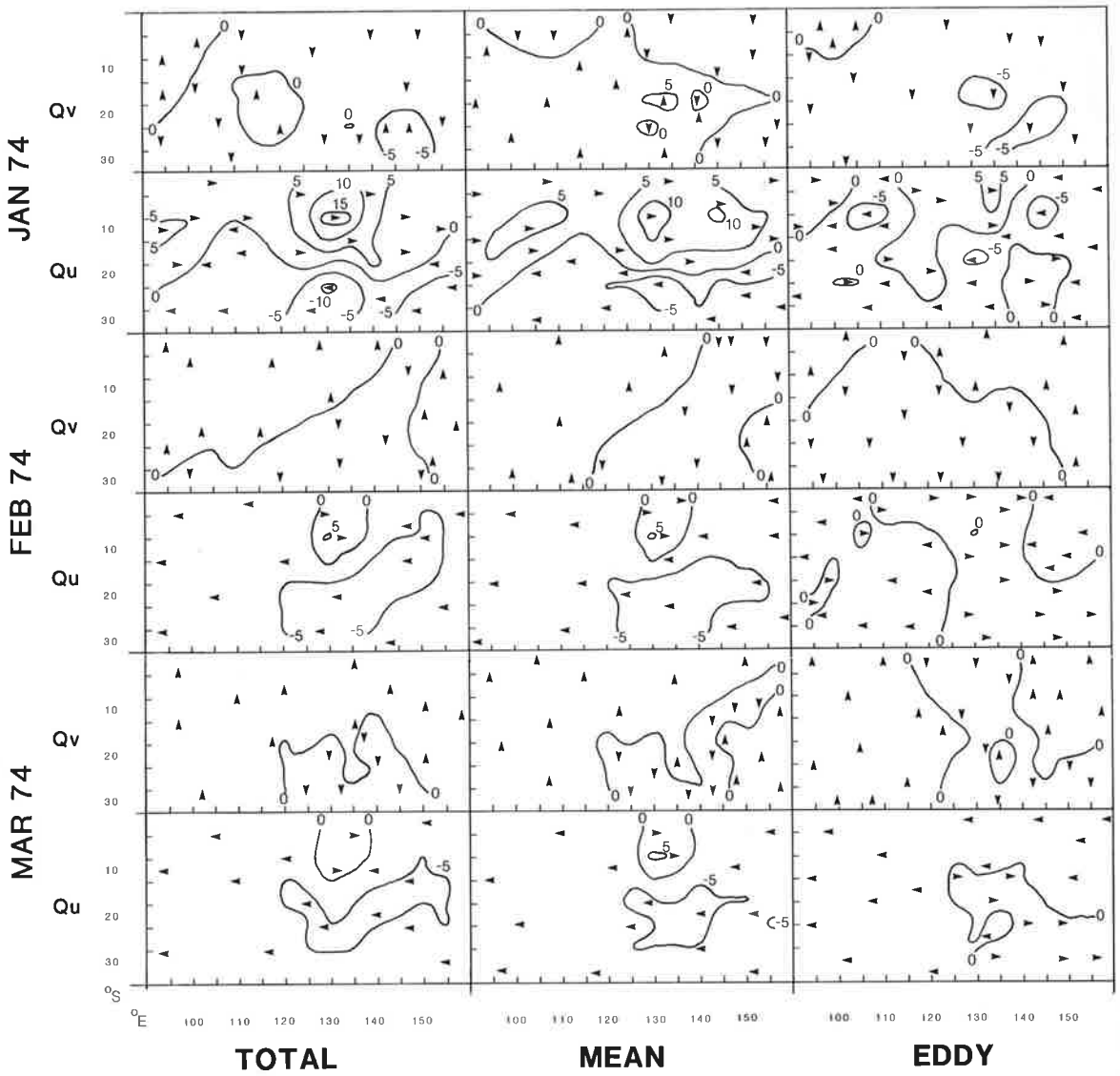
JAN 74
FEB 74
MAR 74
Qv
Qu
Qv
Qu
Qv
Qu
TOTAL
MEAN
EDDY
°S
°E
100
110
120
130
140
150

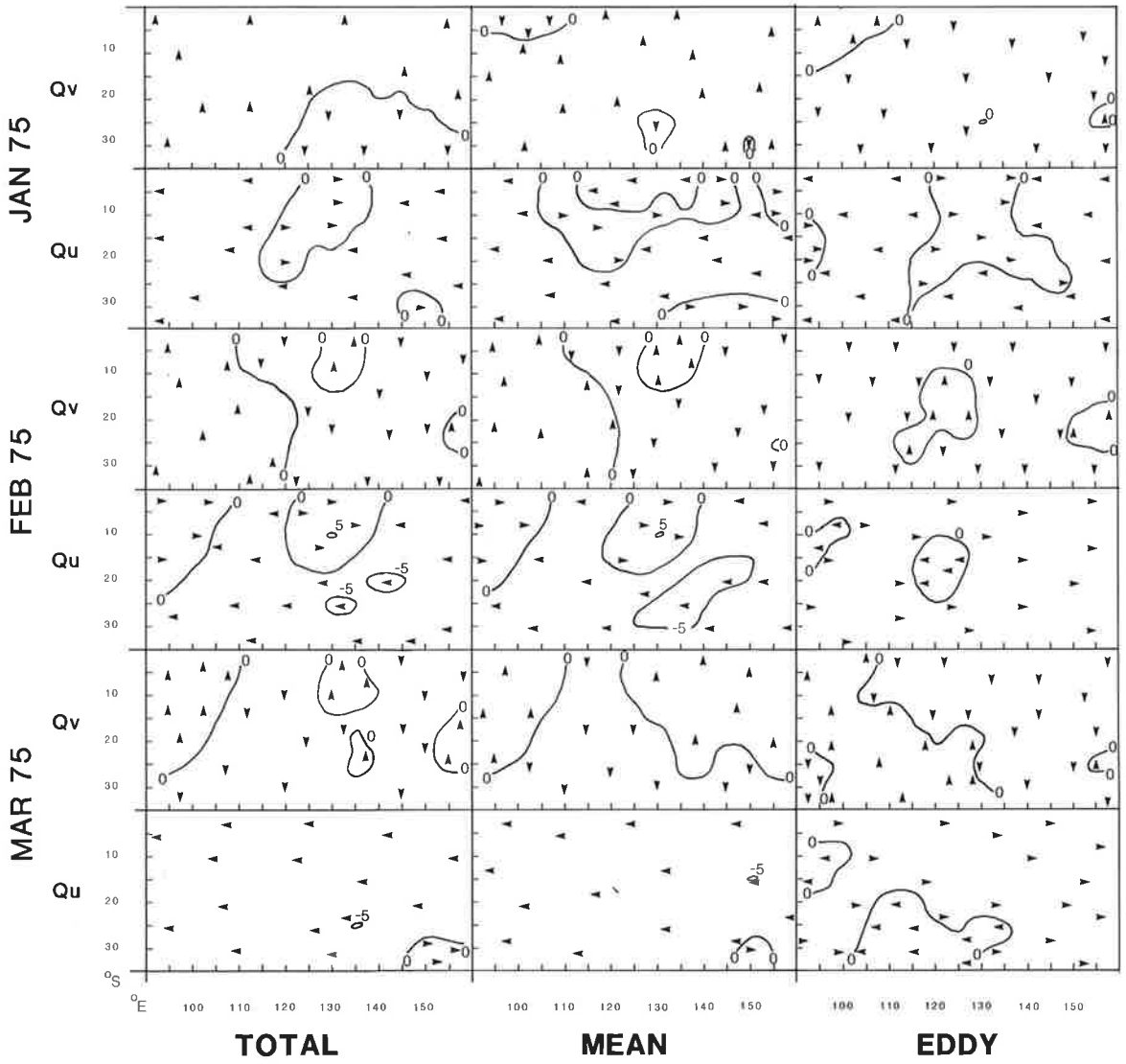
JAN 75
FEB 75
MAR 75
Qv
Qu
Qv
Qu
Qv
Qu
10
20
30
°S
°E
100
110
120
130
140
150
TOTAL
MEAN
EDDY

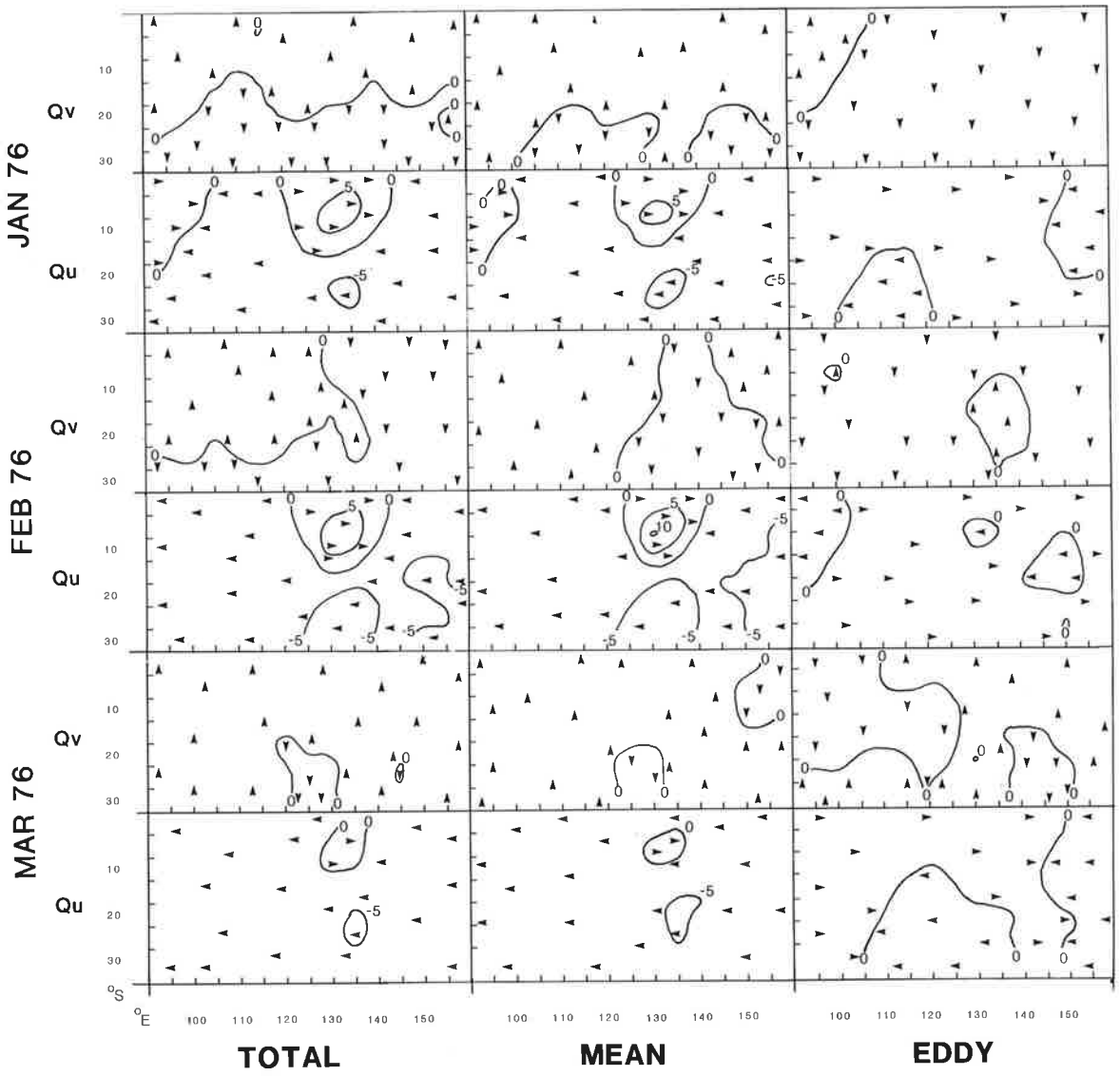
JAN 76
FEB 76
MAR 76
Qv
Qu
Qv
Qu
Qv
Qu
10
20
30
°S
°E
100
110
120
130
140
150
TOTAL
MEAN
EDDY

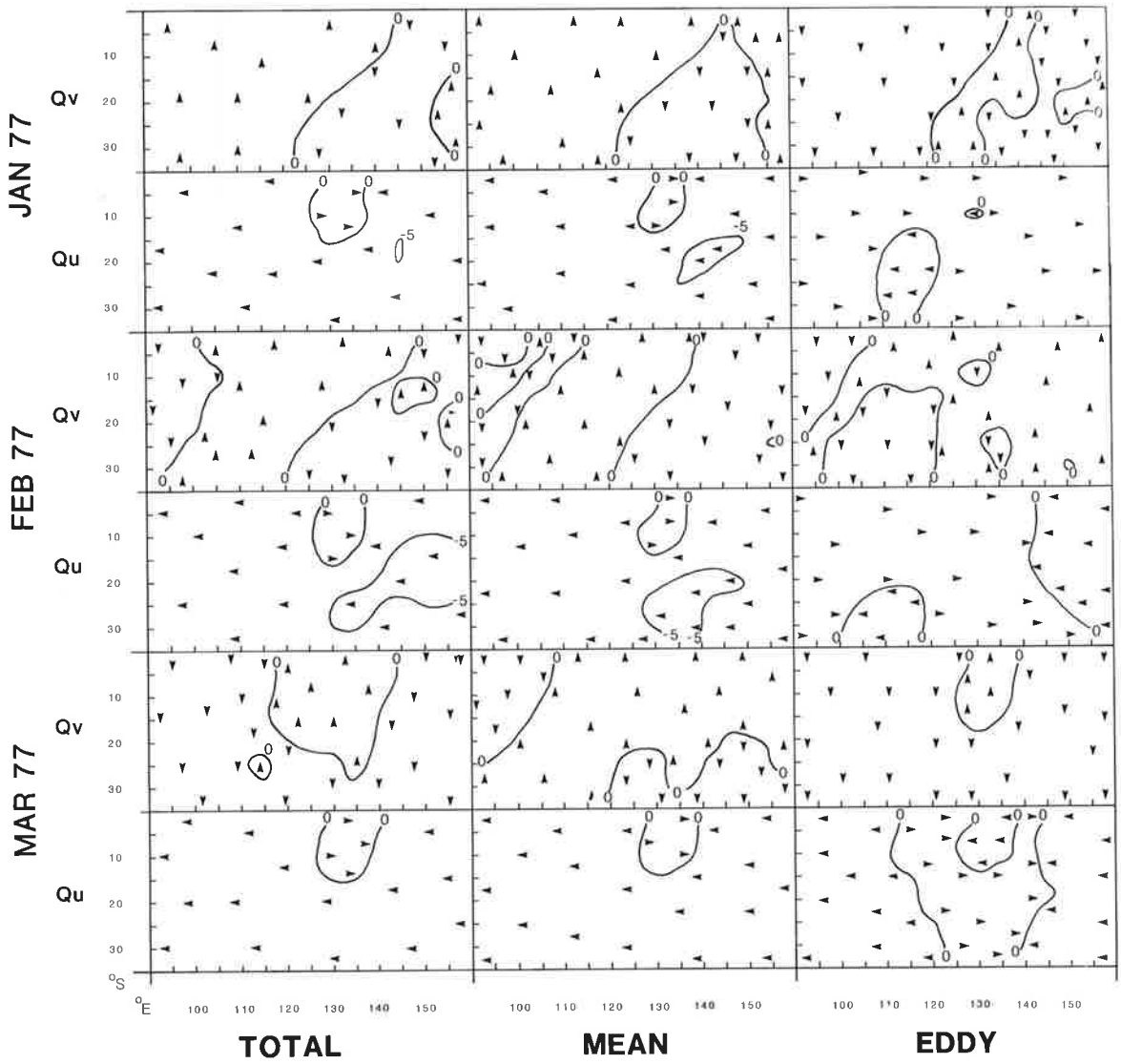
JAN 77
FEB 77
MAR 77
Qv
Qu
Qv
Qu
Qv
Qu
10
20
30
°S
°E
100
110
120
130
140
150
TOTAL
MEAN
EDDY

counterparts in a portion of the near-equatorial latitudes of the diagrams (Fig.73). This suggests that transient eddy water vapour fluxes may not only develop through large-scale field responses but can be more localized.

The 1975 and 1977 sequences (Figs.75 and 77) illustrate that zonal and meridional water vapour flux components can be depressed. This is most evident in January 1975 and March 1977 with no areas above five gm cm^{-1} mb^{-1} s^{-1} in either the total, advective or transient eddy water vapour fluxes over the domain. As the streamfunction fields in Section 3.1.1 indicate that Australasian circulation in January 1975 was particularly weak, it is suggested that a poor wind field may have been the cause of the low water vapour fluxes. In the remaining summer months, total and advective water vapour flux components in the zonal direction are marginally stronger than those in the meridional plane.

During 1976 (Fig.76), the total and advective zonal water vapour flux components are again stronger than those in the meridional plane. Yet, being of similar magnitude and direction, they produce only weak transient eddy water vapour fluxes. It can be seen that the advective zonal water vapour flux component slightly dominates over the total zonal water vapour flux component in isolated regions of this sequence.

A consequence of this discussion is that substantial transient eddy fluctuations are more often part of an alternation with advective conditions. This would seem to indicate the response of the northern Australian monsoonal regime to large-scale circulation changes on synoptic time scales. Only in January 1974 is there overwhelming evidence that time average fields respond to a major monsoon incursion.

(iii) Vertical Cross Sections (Surface - 700 mb) of Monthly Mean Advective Water Vapour Flux Divergence over Australia along 20°S during Monsoon Extremes : A Comparison between Major Period and 19 year Average Fields

To aid in constructing a more complete picture of the vertical structure of moisture characteristics over northern Australia during monsoon seasons,

this discussion focuses on vertical cross sections of monthly mean advective water vapour flux divergence along 20°S (Figs.78-80). The cross sections are made at this latitude in an effort to bisect the heat low complex that dominates low-level circulation in the Australian summer. The 19 year average fields are included to provide an analog of longer-term conditions against which the vertical structure and variability during selected months in the 1973-77 period can be contrasted. Furthermore, these cross sections show an aspect of the vertical, as opposed to the horizontal, dimension of northern Australian relief detailed in Figure 44.

Figure 78 provides a comparison between January 1957-75 and January 1973, 1974 and 1975 situations. As noted in previous discussion, advective moisture convergence and divergence fields in January 1973 and 1974 are very much stronger than the 1957-75 averages. However, the vertical distributions in Figure 78 show that not only is the magnitude of advective moisture convergence and divergence high, but that significant changes in the depth and structure of these fields occur.

In January 1973, marked advective moisture convergence occurs between approximately 110°E and 125°E off the Western Australian coast. As observed in Figures 26 and 49, this region constitutes a major convective source influencing the Australian continent at this time. In the 20°S cross section, this convective area is by far the strongest, deepest and most organized. In fact, the presence of an upper-level divergent maxima to the north-northwest of Australia (Fig.21) and the rainfall regime (Fig.10 top) strongly support the importance of this convective region. Over central Australia, the low-level convective field is weaker, shallower and topped by strong advective moisture divergence by about 850 mb. Advective moisture fluxes are weaker over the arid continental interior, with the structure of the vertical advective moisture convergence and divergence fields seeming to result from the dynamics of heat low or NET_{SH} conditions. Certainly, the indifferent upper-level fields over this region (Figs.21 and 26) would tend to prevent the type of deep convective activity seen further to the west. Over eastern

Figure 78 Vertical cross sections (surface - 700 mb) of monthly mean advective water vapour flux divergence over Australia along 20°S for January 1957-75 and in the individual January of 1973, 1974 and 1975. Advective water vapour flux divergence is in units of 10^{-6} gm cm^{-2} mb^{-1} s^{-1} at intervals of 2 units (convergence shaded).

CROSS–SECTION ALONG 20°S

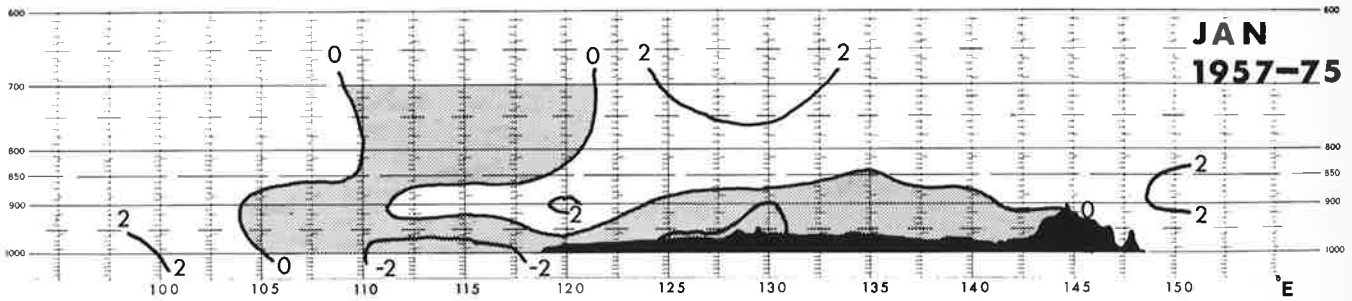

CROSS–SECTION ALONG 20°S

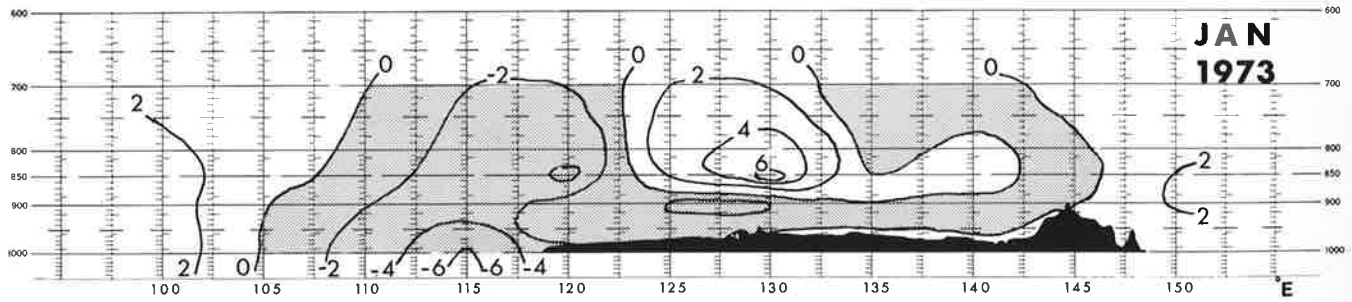

CROSS–SECTION ALONG 20°S

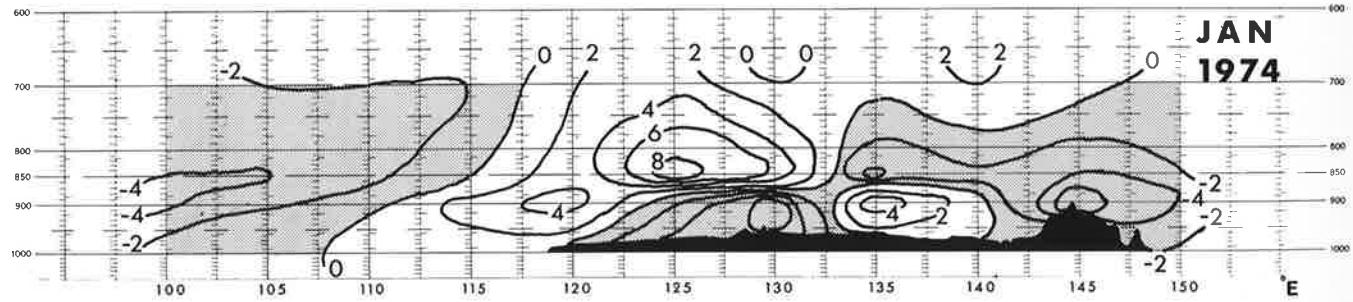

CROSS–SECTION ALONG 20°S

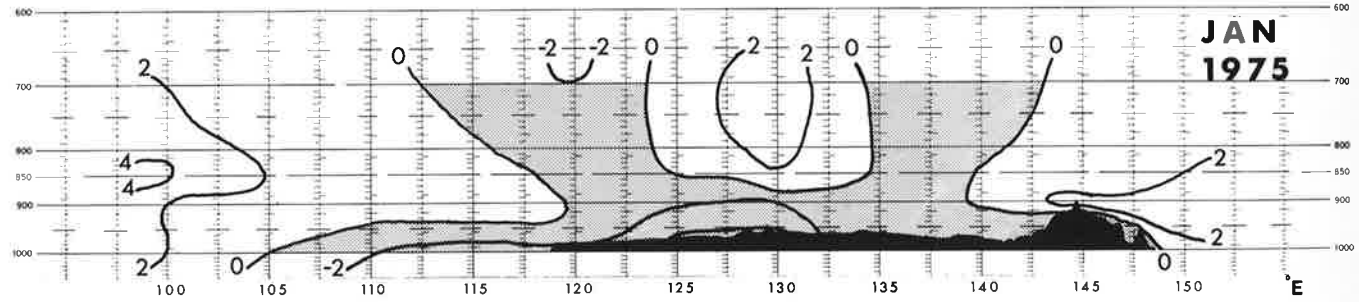

Australia, little organization is evident with subsidence being the prime atmospheric state.

January 1974 distributions again reflect the massive NET_{SH} activity occurring at this time. During such a monsoonal incursion, all of the prime factors influencing convection appear to be acting, i.e. fields reflect increased magnitude, extent, depth and organization of convective elements. At the extreme western edge of the cross section (100°-110°E), deep advective moisture convergence with more of a lower middle-level (around 900-850 mb) convective focus than in January 1973 in prominent. With strong and widespread upper-level divergence evident over this region in Figure 21, enhanced convection would be expected.

Over the more western to central regions of the continent a similar vertical distribution to that in January 1973 appears to be evident, while further west marked advective moisture divergence and subsidence, extending to the surface between approximately 110°-120°E, becomes established. With strong low-level advective moisture convergence in the more west-central regions, some shallow overturnings could occur. Certainly, the widespread upper-level divergence field over the above area is at its weakest (Fig.21). By about 135°E the sequence reverses, with a distinct low-level (sfc-900 mb) pocket of advective moisture divergence overlain by middle-level advective moisture convergence and upper-level divergence. Such a distribution is likely to result in a moderately effective convective system with middle-level moisture sources predominating. However, it is to the east that a more organized convective entity exists, with the added orographic potential of the Great Dividing Range and still useful upper-level divergent influence. Yet, it would appear from Figure 28 that the centre of most pronounced convection is in more northern latitudes.

Although displaying similar vertical advective moisture characteristics, the January 1973 and 1974 distributions also show important differences. Most evident is the degree of vertical complexity displayed by the January 1974 field, especially over the Australian continent proper. Not only does

the middle-level subsidence over the west-central region suggest another variant of the 1957-75, 1973 and 1975 patterns, but it testifies to the magnitude and steep gradients of advective divergence and convergence fields induced by massive NET_{SH} activity. The deep convection over eastern Australia in January 1974 is only a small southward extension of the expanded advective moisture convergence field over north-northeastern Australia. This extension is not evident in January 1973, as the north-northeastern advective moisture convergence zone is smaller, weaker and more localized than in January 1974. To the west of the continent there is almost a complete reversal of advective moisture convergence and divergence maxima, although the expected convective activity associated with the January 1974 situation over Australia is not really evident in the global oceanic rainfall rates (Fig.24 centre).

The January 1975 field (Fig.78) most closely resembles the 19 year average distribution and lends further support to the findings in Section 3.1. With weak NET_{SH} activity in the lower layers, the advective moisture convergence and divergence fields are subsequently reduced and convective processes diminished. In the westernmost longitudes, pronounced low-level advective moisture divergence is evident and, despite strong upper-level divergence (Fig.21), convective activity is poor. Near the Western Australian coast, middle-level advective moisture convergence is supported by weaker upper-level divergence (Fig.21), with the result that convective processes are still not well organized. Over the west-central interior (near 130°E) the configuration suggests heat low conditions with shallow advective moisture convergence overlain by advective moisture divergence to 700 mb and weak upper-level divergence. Between about 135°-140°E, a column of advective moisture convergence extends up to 700 mb, but it is not strong and convective processes do not appear to be overly enhanced by the marked improvement in divergence magnitudes aloft. In the east, subsidence dominates with advective moisture divergence prominent in low levels and strong divergence existing at upper levels.

In general, the January 1975 situation indicates that deep and organized convective processes are absent from the Australian continent at 20°S. Certainly, the type of advective moisture convergence and divergence structures evident in January 1973 and January 1974 are only poorly represented in January 1975, the latter probably being a direct result of the marked shallowness of the NET_{SH} over the Australian continent at this time.

In Figure 79 the February 1957-75 averages are compared with February 1975, 1976 and 1977 distributions. The February 1957-75 cross section is little different from that noted in January 1957-75 (Fig.78). Only the presence of middle-level advective moisture convergence in the vicinity of 105°E and an expanded 'dome' centred on 900 mb between 130°-140°E are notable. When under the influence of favourable upper-level divergence patterns, the latter region could contribute to stronger convective processes. This seems to be supported by the more persistent cyclonic activity that is observed in the February $\bar{\psi}_{850}$ and February streamfunction of the advective water vapour flux diagrams (Figs.8 and 46).

As would be expected with the intraseasonal changes in streamfunction patterns and intensities noted in Section 3.1.1, February 1975 provides a sharp contrast with January 1975. To the west of Australia and out over the Indian Ocean, moderate advective moisture convergence extends from the near-surface to 700 mb levels. With upper-level divergence extending from Indonesian longitudes, convective activity would be expected. However, the oceanic rainfall rates (Fig.25 bottom) seem to indicate that rainfall producing mechanisms are more prominent further to the north where a core of organized uplift is located (see Fig.31). In the vicinity of the Western Australian coast a lobe of advective moisture divergence, centred on 900 mb, is once again probably related to the dynamics of heat low or NET_{SH} activity. Further east, in the centre of the continent, indifferent advective moisture convergence (extending to 800 mb) is overlain by advective moisture divergence which, in turn, gives way to deeper and more organized advective moisture

Figure 79 Vertical cross sections (surface - 700 mb) of monthly mean advective water vapour flux divergence over Australia along 20°S for February 1957-75 and in the individual February of 1975, 1976 and 1977. Advective water vapour flux divergence is in units of 10^{-6} gm cm^{-2} mb^{-1} s^{-1} at intervals of 2 units (convergence shaded).

CROSS–SECTION ALONG 20°S

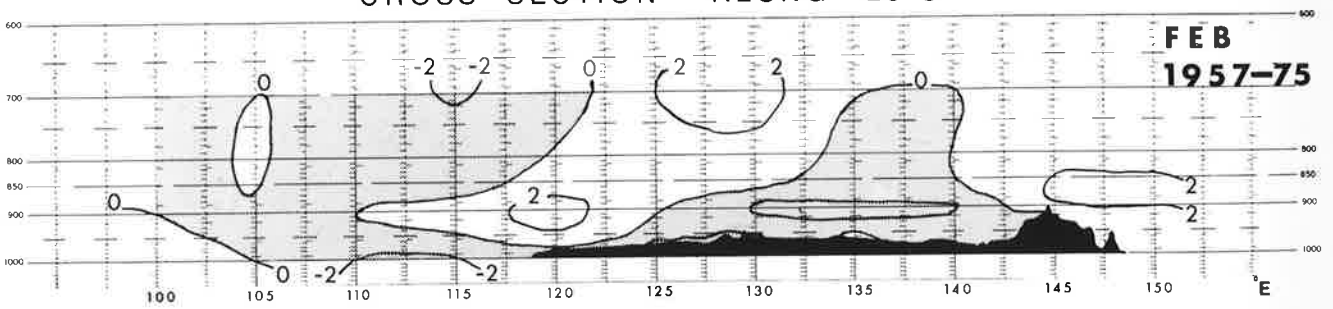

CROSS–SECTION ALONG 20°S

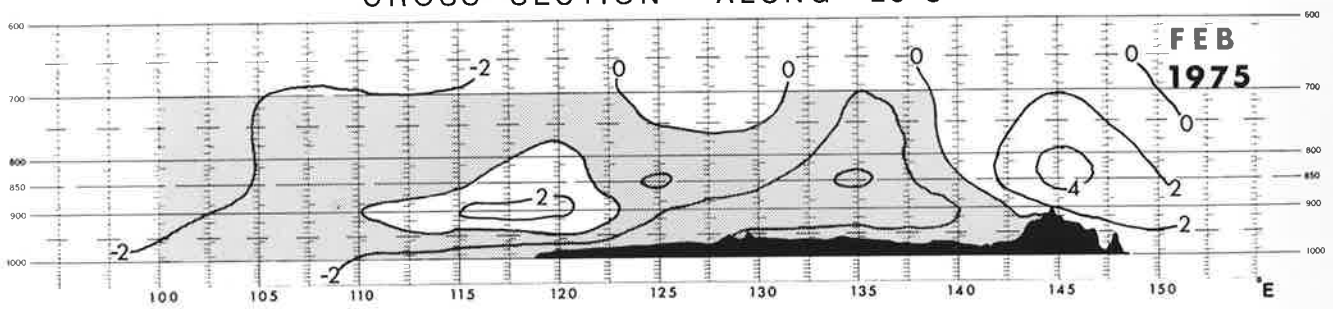

CROSS–SECTION ALONG 20°S

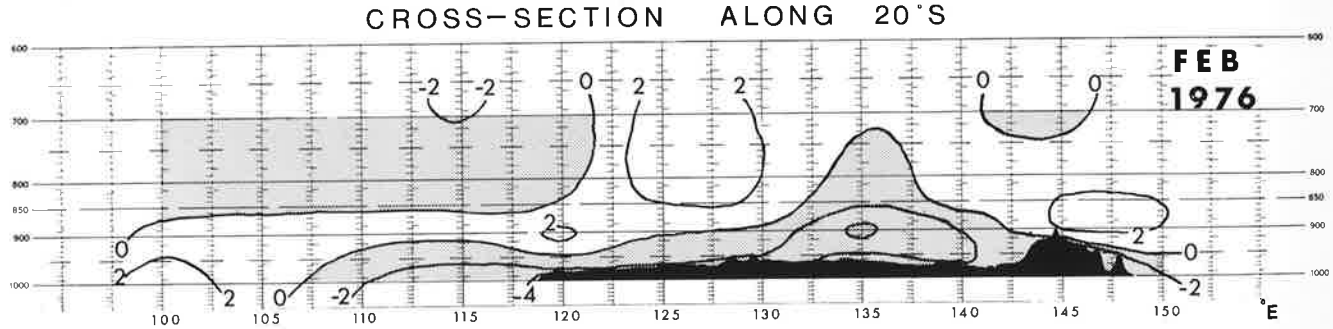

CROSS–SECTION ALONG 20°S

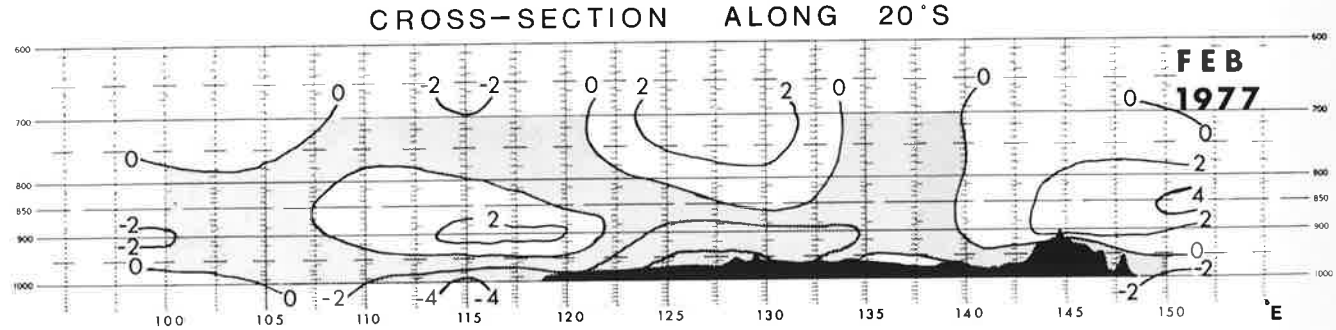

convergence and, by 135°E, strong upper-level divergence (Fig.22). Certainly, there is strong support for heavy rainfall in this region in the February 1975 decile rainfall pattern (Fig.12 centre). However, eastern Australia is once again under the influence of subsidence, with marked low-level advective moisture divergence below moderate upper-level divergence.

February 1976 experiences a similar distribution to February 1975 with the major differences occurring to the east and west of the continent. Over the Indian Ocean, the field grades from middle-level advective moisture convergence overlaying low-level advective moisture divergence (in the extreme west), to middle-level advective moisture convergence above a shallow band of advective moisture divergence and a low-level layer of advective moisture convergence off the Western Australian coast. In the west-central area, the near-persistent configuration of a deep advective moisture divergence layer overlaying shallow low-level advective moisture convergence is again evident. The presence of this feature during a period of deep cyclonic circulation over the continent (Fig.59) suggests that it develops mainly as a consequence of NET_{SH} rather than shallow heat low activity. Over the eastern half of Australia, a small area of middle-level advective moisture convergence, centred around 140°-145°E, is found in the presence of moderate advective moisture divergence. In the far east of the section, convective activity is shallow as convergence of moisture is confined to a thin band near the surface.

The sequence is completed by the February 1977 distribution in which the arrangement of convergent and divergent maxima shows both similarities and differences with February 1975 and February 1976 situations. Western areas of the cross section display a degree of complexity in the vertical structure of the moisture fields. Between 100°-105°E a pronounced band of low-level advective moisture convergence is bounded by advective moisture divergence both below and above it. Distinctly strong upper-level divergence in the latter region may then provide the trigger for some convective activity. In the west-central area, the sequence of low-level advective moisture

convergence with middle- and upper-level divergence continues, the low-level component being stronger than in either February 1975 or February 1976 and perhaps partly contributing to the rainfall maximum centred around Alice Springs in central Australia (Fig.14 centre). Certainly, the deeper, although weaker, advective moisture convergence column around 135°-140°E may have also been involved. However, the distribution and magnitude of the rainfall event (Fig.14 centre) suggests that it is more likely to have been produced by synoptic-scale influence in the form of a rain depression, NET_{SH} excursion or cut-off low (Bureau of Meteorology, 1977). More information on the vertical temperature structure is also necessary in order to know whether inversion conditions (associated with the northwestern Australian heat low and usually aiding in the suppression of convection) are prominent. Over eastern Australia, advective moisture divergence influences all but a very shallow, near-surface layer of advective moisture convergence. Subsidence dominates in this region with a magnitude similar to February 1975.

The final set of cross sections in Figure 80 provide a comparison between March 1957-75 and March 1974, 1975 and 1977 fields. The 19 year average distributions for March display similar characteristics to those in January and February. Over the far western area of the cross section, advective moisture divergence is much the same as in January 1957-75, while a region of lower middle-level moisture convergence, between about 110°-120°E, is common to all three monthly averages. Similarly, the arrangement of lower middle-level moisture divergence overlaying shallow, low-level moisture convergence in west-central to central localities is common to all months. The presence of an advective moisture convergence 'dome' between 135°-140°E follows the February 1957-75 pattern. The 'dome' is probably just the southern extension of the vigorous convective region further to the north-northeast. Yet, its absence in January 1957-75 averages (Fig.78) may be indicative of the slight tendency for February to be the most dominant monsoonal month, with perhaps some late season carryover into March. As in the other monthly averages, the easternmost region of the cross section is dominated

Figure 80 Vertical cross sections (surface - 700 mb) of monthly mean advective water vapour flux divergence over Australia along 20°S for March 1957-75 and in the individual March of 1974, 1975 and 1977. Advective water vapour flux divergence is in units of 10^{-6} gm cm^{-2} mb^{-1} s^{-1} at intervals of 2 units (convergence shaded).

CROSS–SECTION ALONG 20°S

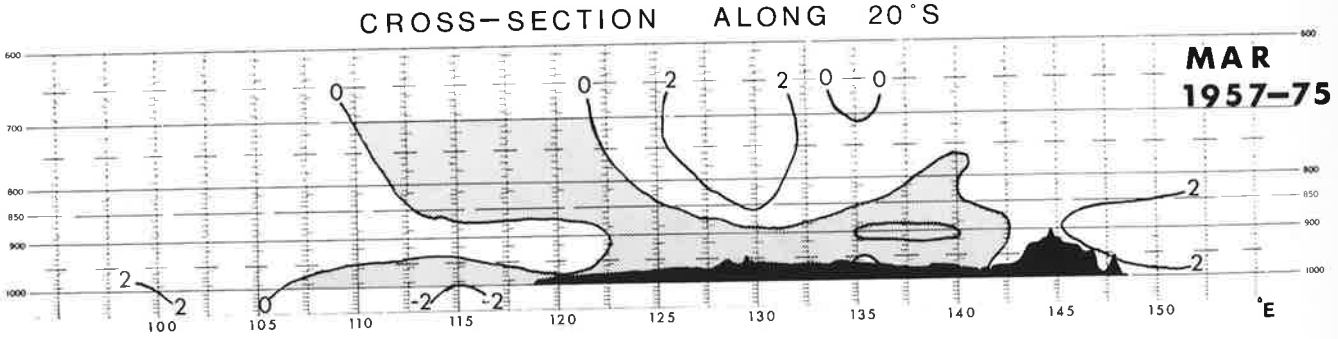

CROSS–SECTION ALONG 20°S

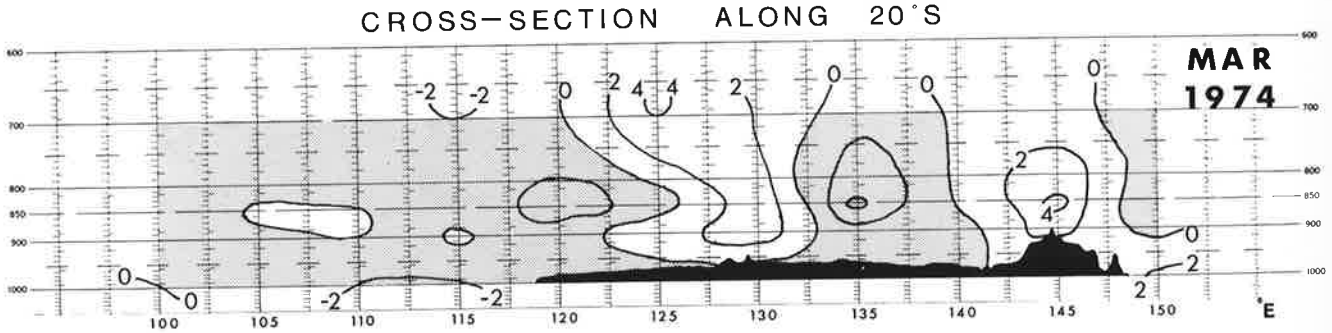

CROSS–SECTION ALONG 20°S

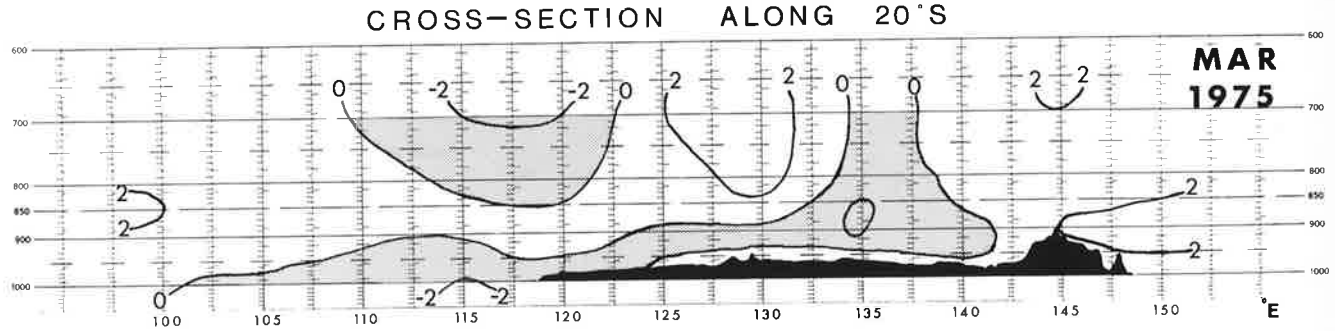

CROSS–SECTION ALONG 20°S

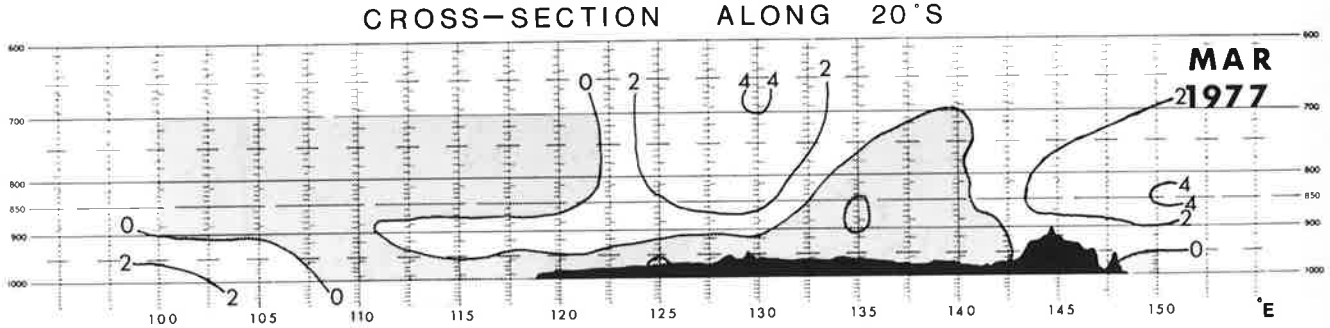

by advective moisture divergence and thus probably strong subsidence.

In Figure 80, the March 1974 cross section is dominated by areas of deep advective moisture convergence. Over the western and near-central regions (between about 100°E and 125°E), distinct advective moisture convergence maxima are imbedded in a deep and broad advective moisture convergence band. With upper-level divergence being particularly strong over the greater part of this region (Fig.23), some convective activity would be expected. Over west-central areas, advective moisture divergence is prominent throughout most of the vertical column up to 700 mb, and subsident motion acts to suppress convective activity. By 135°E advective moisture convergence takes over, with marked convective activity being the result of the coupling between the latter and a divergence maxima aloft (Fig.23). Once again, subsidence becomes prominent in eastern longitudes, with a distinct advective moisture divergence maximum centred around 145°E. However, in the far east (150°E), the latter distribution is abruptly terminated by an area of weak advective moisture convergence, although there is no evidence in the rainfall deciles (Fig.11 bottom) to suggest that such a change has any marked effect on rainfall distributions.

As noted in previous discussion, March 1975 completes a season of generally poor monsoonal activity. Unlike March 1974, the organization of strong and deep convective elements is absent from this cross section. The far west of the March 1975 distribution is more closely related to the 19 year average pattern, with a deep advective moisture divergence layer being gradually undercut by low-level advective moisture convergence to 110°E. Between about 110°E and 120°E, middle-level advective moisture convergence develops, so that by 115°E advective moisture divergence has shrunk to a thin layer between two advective moisture convergence maxima. In the presence of a weakening divergence gradient aloft (Fig.23), convective organization is probably not sufficient to produce any pronounced rainfall maximum. Although weaker, the distinct advective moisture divergence maximum over the west-central region is no doubt a quasi-permanent feature of all cross sections.

Coupled with a shallow layer of near-surface advective moisture divergence, convection is once again absent. However, by 135°E, an advective moisture convergence 'column' dominates the cross section. The rainfall deciles (Fig.12 bottom) would suggest that pronounced convection occurs within this month, even though only weak to moderate divergence is aloft (Fig.23). Nevertheless, such a conclusion needs to be qualified with respect to the influence of synoptic-scale phenomena. Further east, subsidence associated with advective moisture divergence throughout the cross section predominates. Although such an atmospheric structure is a feature of the majority of cross sections, it is not on the same scale as in other months.

The final cross section of March 1977 reveals similar vertical structures to many of the other distributions in the sequence. Once again, advective moisture convergence is prominent at middle levels between 100°E and 120°E, with a small area of low-level advective moisture divergence in the far west. Shallow, low-level advective moisture convergence develops by 110°E and extends into west-central regions where it is overlain by the deep advective moisture convergence zone associated with cyclonic circulation over the continent. In more central longitudes, around 135°E, an advective moisture convergence 'column' or 'dome' extends to the 700 mb level but, with poorly defined divergence aloft (Fig.23), little convective organization is evident. Certainly, the rainfall deciles (Fig.14 bottom) tend to support the above observation. By 145°E, subsidence is again established as advective moisture divergence dominates the section in these longitudes.

Thus the most persistent characteristics of these cross sections are the middle-level advective moisture divergence zone in the west-central region (between 125°-130°E), the advective moisture convergence 'column' or 'dome' in more central areas and the subsidence to the east. The first two features would appear to result from the atmospheric dynamics associated with circulation over the continent. However, there is no certainty that this includes more elusive elements such as the quasi-permanent continental heat lows. Yet, the influence of the Australian continent cannot be overlooked,

as it is an important heat source in summer. The heat low complex is a consequence of this action and, at the very least, provides an anchoring for the NET_{SH}. Even Figure 5 indicates that, on average, the monsoonal pressure trough dips some 5°-10°S over Australia in January. To the west of Australia, the cross sections do not show quite the same persistence of vertical structures. Although lower middle-level advective moisture convergence is evident in some of the cross sections, it is probably a dynamic result of anticyclonic conditions that tend to develop by 700 mb in many months. Nevertheless, the focus of anticyclonic activity at 700 mb is centred on the continent of Australia rather than the oceanic regions around it. Hence, Australia makes a major contribution to monsoon structure, not through any overwhelming orographic influence, but as a large land mass in an otherwise oceanic and 'maritime continental' environment.

As far as the prospect of distinct changes in the depth of advective moisture convergence during monsoon extremes is concerned, the cross sections tend to suggest that variations in such an element cannot be divorced from those of convective organization. Thus the weak monsoonal month of January 1975 exhibits weaker convective features than in, say, January 1974. The overall appearance is then one of expansion(contraction) of advective moisture convergence and divergence features and a tightening(relaxation) of their gradients during periods of strong(weak) monsoonal activity. This action has distinct spatial characteristics, but it is very different from the concept of a changing depth of advective moisture convergence or divergence features caused solely by the raising or lowering of the monsoonal layer during extremes.

It would seem that the most distinct feature modulating the Australian continent's monsoonal moisture characteristics is the heat low/NET_{SH} complex. However, the existing array of data recording stations does not fully resolve the heat low/NET_{SH} complex. As Figures 37-42 indicate, there are usually two thermal low pressure centres over the continent in summer, but the streamfunction fields only concur with the more dominant northwestern focus

of the low. Thus the following discussion aims to present data from the northwestern sector of the continent where pressure, geopotential height and streamfunction fields all resolve a quasi-permanent cyclonic centre that appears to represent the major heat low/NET_{SH} dichotomy.

(iv) Aerological Traces and Precipitable Water Content over Australia during Monsoon Extremes

A more complete understanding of continental low pressure influence on monsoonal processes over Australia can be obtained by an analysis of aerological (dew point and dry bulb temperature) traces and precipitable water content. As the monthly streamfunction fields (Figs.7, 8, 9 and 36) tend to resolve only the larger-scale aspects of the northwestern heat low, the above parameters are deduced at selected stations surrounding the average position of this feature. Figures 81-83 show this information for the radiosonde stations at Darwin (94120), Broome (94203), Port Hedland (94312), Carnarvon (94300), Giles (94461), Alice Springs (94326) and Cloncurry (94335) or, after 1975, Mount Isa (94332). In these figures, the months of January 1973, 1974 and 1975, February 1975, 1976 and 1977 and March 1974, 1975 and 1977 are used, the aim being to add to the information accumulated in the previous discussion by focusing on a slightly finer spatial scale.

Figure 81 shows the January 1973, 1974 and 1975 traces over northwestern Australia. Precipitable water values for three standard 100 mb intervals, to 700 mb, complement the difference between dry bulb and dew point temperature traces. Generally, they show that precipitable water content in all three layers tends to be larger at coastal, rather than at continental interior, stations. This is the expected dominant spatial characteristic, especially if longer-term average values are considered. However, there is still a substantial measure of variability in the moisture and temperature patterns during these months.

In January 1973 (Fig.81 top), the traces at Darwin, Broome and Port Hedland reflect the high moisture content over this part of the continent.

Figure 81 Monthly mean aerological traces and precipitable water content over northern Australia in January 1973, 1974 and 1975. Dashed traces indicate dew point temperatures (in °C) and solid traces indicate dry bulb temperatures (in °C). Precipitable water values are indicated for three 100 mb layers (1000-900, 900-800 and 800-700 mb) in units of gm cm^{-2}.

JAN 1973

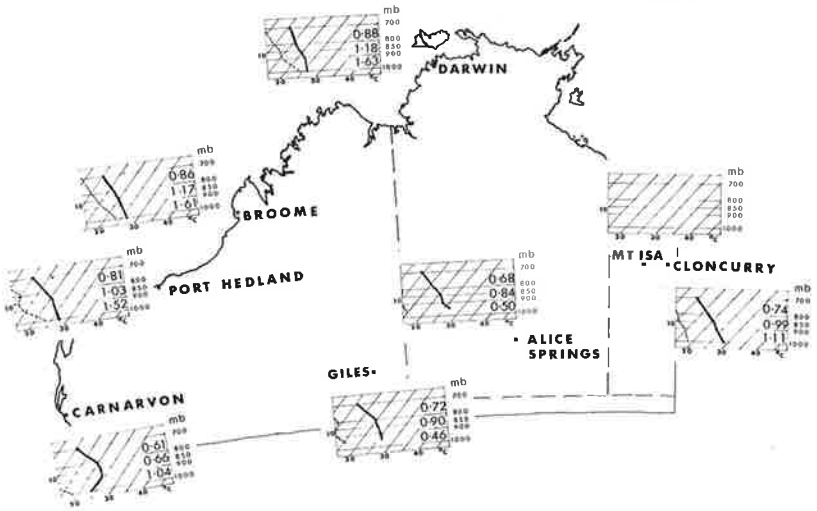

JAN 1974

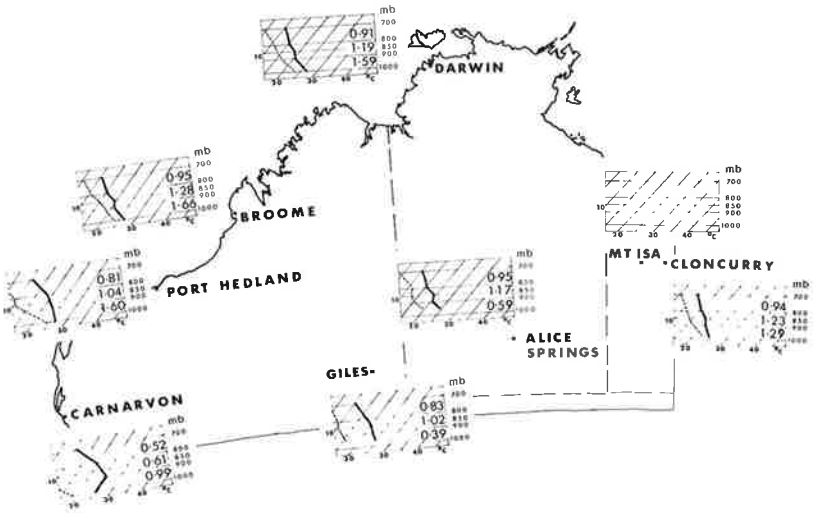

JAN 1975

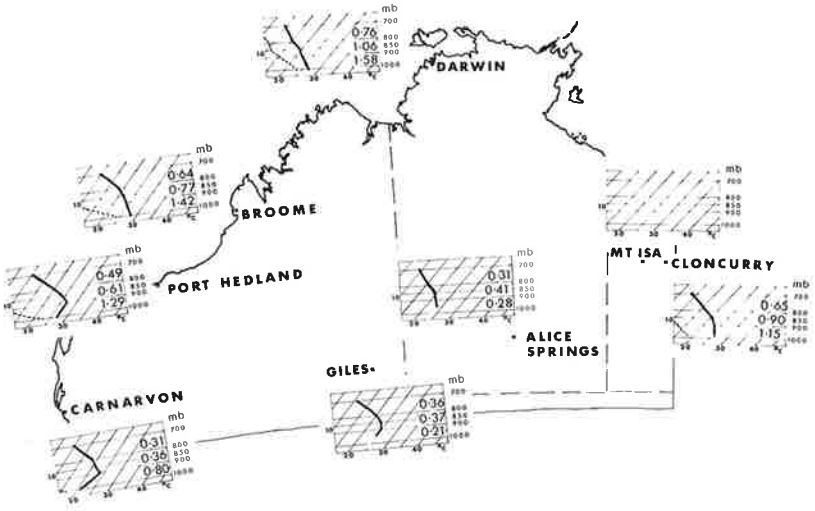

Values above one gm cm^{-2} predominate in the surface-900 mb and 900-800 mb intervals, indicating that moisture is of substantial magnitude and influences a considerable atmospheric depth (about two kilometres) along the northwestern coast. Lapse rates in this area are not overly large and weaken as one moves south-southwest down the coast. At Carnarvon (24°53'S, 113°39'E), distinct inversion conditions are evident and precipitable water values above one gm cm^{-2} occupy only the lowest kilometre of the troposphere. The traces further inland at Giles (25°2'S, 128°18'E) are similar to those on the northwestern coast, although moisture content is markedly reduced. Moisture content reduction is also observed at Alice Springs (23°48'S, 133°53'E) where precipitable water values also fail to reach one gm cm^{-2} in any layer. Of particular interest is the tendency for moisture content to be highest in the 900-800 mb interval, with lowest values in the surface-900 mb band. This may imply that moist flow from more tropical sources penetrated furthest inland at lower middle levels in January 1973. At lower levels, any moist onshore flow of oceanic origin would soon lose most of its moisture content, especially with the long overland trajectories evident in Figures 7 and 36. Interestingly, the dry bulb temperature trace at Alice Springs probably displays the steepest lapse rate of any of the stations analysed in January 1973. However, with no high moisture content in this area, marked convective activity would not be expected. An examination of raw mixing ratio or specific humidity data and rawinsonde observations in this region shows that the lower middle levels of the atmosphere are the most conducive to a peak in water vapour flux values. This occurs because the moisture component is often only marginally less than that at the surface and low-level wind fields are at their strongest.

At the easternmost station of Cloncurry (20°40'S, 140°30'E) a more promising moisture regime is evident. Precipitable water content exceeds one gm cm^{-2} in the surface-900 mb layer and is close to one gm cm^{-2} in the 900-800 mb interval. Importantly, the source regions from which this moisture is derived are influenced by a mix of cyclonic and anticyclonic

systems. It must be noted that Cloncurry is closer to oceanic moisture sources than either Giles or Alice Springs.

It would be optimistic to claim that one could discern any definite evidence of heat low activity from the sole inversion trace at Carnarvon. Such a claim needs the support of similar traces at several of the other inland stations. This is not evident in January 1973.

In January 1974 (Fig.81 centre), moisture content at the coastal stations of Darwin, Broome and Port Hedland is similar to that in January 1973. However, there is considerable evidence of marked penetration of moisture into the inland in the precipitable water magnitudes at Alice Springs and Giles. At the coastal stations, aerological traces suggest that rainfall producing mechanisms are more prominent during January 1974. Certainly, conditional instability in January 1974 is evident in the traces, even into the interior of the continent. Moisture content values exceed one gm cm^{-2} in both the surface-900 mb and 900-800 mb intervals at Darwin, Broome, Port Hedland and Cloncurry, and in the 900-800 mb layer at Alice Springs and Giles. Only at Carnarvon, where inversion conditions persist, does the moisture content in either of the above layers fail to reach one gm cm^{-2}. As in January 1973, moisture content is lowest in the surface-900 mb interval at Alice Springs and Giles, and highest in the layer immediately above it (900-800 mb). Once again, this may be the result of long overland trajectories which tend to produce a large modification of near-surface wind fields. This suggestion gains more credence with the observation that the surface-900 mb precipitable water content at Giles and Carnarvon is marginally lower in January 1974 than in January 1973 (Fig.81 top and centre). Both stations are subject to stronger east-northeast winds, with long continental trajectories, in January 1974.

The January 1975 (Fig.81 bottom) regime is different from either January 1973 or January 1974 in that both the aerological traces and precipitable water contents indicate that generally drier conditions prevail. This is most apparent at continental interior stations where precipitable water values

are two or three times less than January 1973 or January 1974 values. At the northernmost coastal station, the surface-900 mb moisture characteristics show a tendency to be of similar magnitude to January 1973 and 1974 values (Fig.81 top and centre), but precipitable water content falls off rapidly with height. This is most noticeable as one follows the coast south to Port Hedland or Carnarvon. At these stations even the lower-level moisture content begins to lag markedly behind January 1973 and 1974 magnitudes. Seeming to accompany these trends is the presence of marked inversion conditions at Port Hedland, Carnarvon and Giles. More stable conditions are also detected at Alice Springs, Broome and Cloncurry. Such evidence supports the earlier assertions that heat low type conditions in January 1975 seem to have outweighed NET_{SH} activity, even on monthly mean scales. In fact, not only are inversion conditions present, but moisture content and convergent motion (Figs.66 and 78) are poorly defined in the lower layers over central and west-central Australia. As in January 1973 and 1974, inland stations experience a peak in precipitable water content in the 900-800 mb layer.

However, it is important to note that the low 900-800 mb layer precipitable water content may be an indirect result of drier conditions in the continental interior. This is most evident if one examines the mixing ratio values at standard pressure levels for either Alice Springs or Giles. Generally, they show a tendency to be consistently low between the surface and 700 mb levels, with the smallest difference in values often in the 900-800 mb interval (this is most evident in the 19 year average values in Maher and Lee, 1977). As Appendix 6.6 illustrates, precipitable water content is entirely a function of the mean layer mixing ratio when pressure intervals are of homogeneous depth.

In Figure 82, the traces and water content magnitudes for Februarys 1975, 1976 and 1977 reflect most of the characteristics noted in the January sequence (Fig.81). Yet, none of these months experience the moisture extremes represented by the January 1974 and 1975 situations.

Figure 82 Monthly mean aerological traces and precipitable water content over northern Australia in February 1975, 1976 and 1977. Dashed traces indicate dew point temperatures (in °C) and solid traces indicate dry bulb temperatures (in °C). Precipitable water values are indicated for three 100 mb layers (1000-900, 900-800 and 800-700 mb) in units of gm cm^{-2}.

FEB 1975

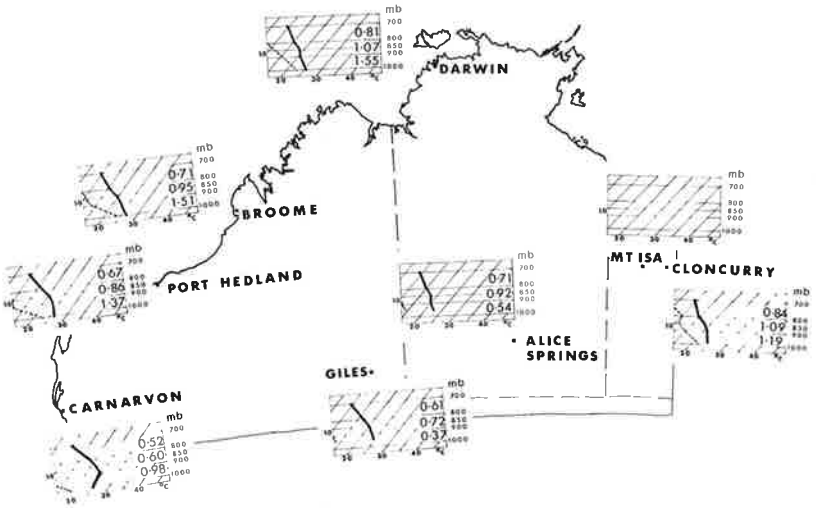

FEB 1976

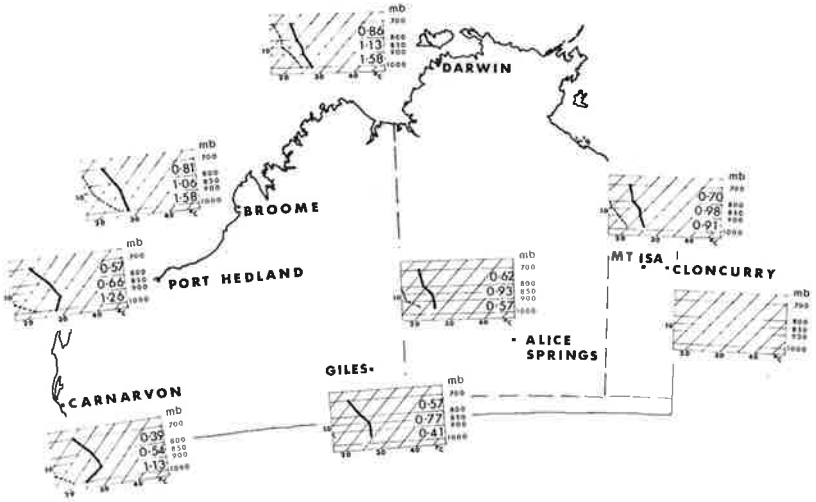

FEB 1977

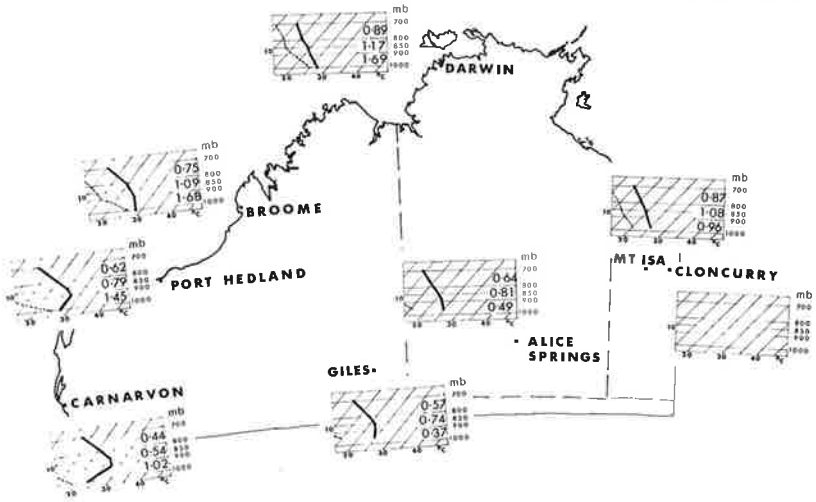

February 1975 (Fig.82 top) provides some interesting contrasts with January 1975 (Fig.81 bottom). Perhaps most noticeable is the general recovery of moisture characteristics, especially in the continental interior. The widespread inversion conditions in the west-central region during January 1975 are reduced and mainly confined to the Carnarvon area. Improvements in moisture conditions are evident at the more northwestern coastal stations, although precipitable water values do not nearly approach those in January 1974 (Fig.81 centre). Water content values above one gm cm^{-2} only occur in both the surface-900 mb and 900-800 mb layers at Darwin and Cloncurry. This suggests that the most moist conditions are in the north-northeast of the region. The more southern of the northwestern coastal stations have surface-900 mb interval water content magnitudes above one gm cm^{-2} as a result of moist, low-level onshore flow.

In February 1976 (Fig.82 centre), moisture characteristics at most stations are marginally higher than in February 1975 (Fig.82 top). This is mirrored by a slight steepening of lapse rates in the north, although more widespread and pronounced inversion conditions occur in the west-central region. Precipitable water magnitudes above one gm cm^{-2} in the surface-900 mb and 900-800 mb intervals are now located in the vicinity of the northernmost coastal stations of Darwin and Broome. As in other months, moisture values decrease towards the interior of the continent, although there is some suggestion that this trend is not nearly as marked in February 1976. However, it does not approach the January 1974 (Fig.81 centre) situation when a most pronounced moisture incursion occurred. Yet, the extent of dry bulb and dew point temperature traces at Alice Springs suggests that a weaker monsoon incursion did penetrate some way inland in February 1976. At the same time, it must be remembered that synoptic-scale disturbances, in the form of rain depressions (Loursenz, 1981), played an important role by affecting central to eastern areas of the continent in both January and February 1976. As in January 1974, and to a much lesser degree in February 1975, the greatest instability occurs in the smaller 850-800 mb layer at

Darwin, Cloncurry, Alice Springs and Giles. However, it is difficult to relate this directly to the advective moisture convergence patterns in Section 3.2.1 *(i)*.

February 1977 (Fig.82 bottom) presents a situation in which the most prominent moisture conditions again focus on the north-northwestern coast. In the surface-900 mb and 900-800 mb layers, precipitable water values again only exceed one gm cm^{-2} at Darwin and Broome. This is to be expected, as 850 mb streamfunction fields ($\bar{\psi}_{850}$) in Figure 8 suggest that moist onshore flow is weak along most parts of the northern coast. Over the central regions of the continent, moisture values are slightly down on those in February 1976 (Fig.82 centre), while in the west-central area strong inversion conditions persist. However, despite similar spatial distributions of moisture characteristics in both February 1976 and 1977, aerological traces suggest that atmospheric stability is more prominent in February 1977. This is reflected in the spatial extent of rainfall (Figs.13 and 14 centre).

The final map sequence is for the months of March 1974, 1975 and 1977 (Fig.83). As this month generally showed indications of monsoon weakening and withdrawal in Section 3.1, it is interesting to observe that moisture characteristics do not reveal any markedly homogeneous changes indicative of seasonal retreat.

During March 1974 (Fig.83 top), moisture fields display features similar to those in the January and February sequences, with the 900-800 mb layer precipitable water content maximum at inland stations and the generally coastal to continental interior moisture gradient being evident. Only at Darwin and Cloncurry are precipitable water content magnitudes above one gm cm^{-2} in the surface-900 mb and 900-800 mb intervals. This is indicative of persistent moisture over the north-northwestern segment of the continent following the large January to February 1974 monsoon incursion and the moist onshore flow influencing both stations in Figure 54. Despite the extent of inversion conditions at Port Hedland, Carnarvon and Giles, aerological traces at Darwin and Cloncurry suggest that more unstable

Figure 83 Monthly mean aerological traces and precipitable water content over northern Australia in March 1974, 1975 and 1977. Dashed traces indicate dew point temperatures (in °C) and solid traces indicate dry bulb temperatures (in °C). Precipitable water values are indicated for three 100 mb layers (1000-900, 900-800 and 800-700 mb) in units of gm cm^{-2}.

MAR 1974

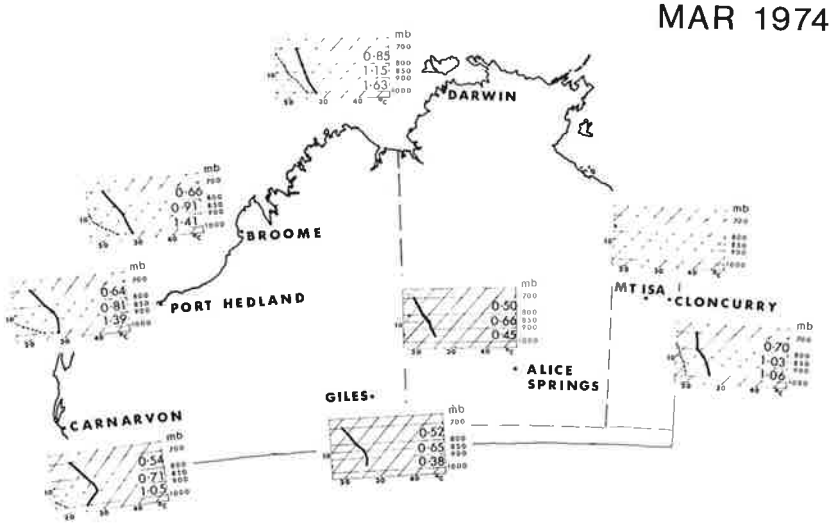

MAR 1975

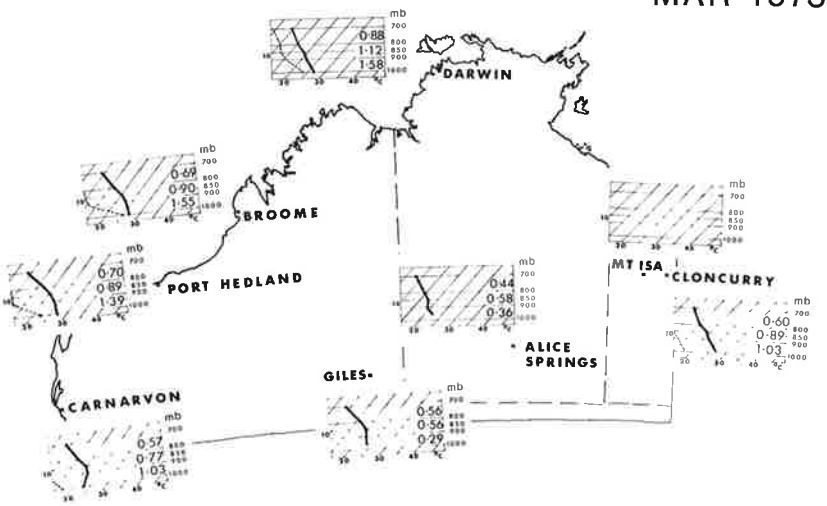

MAR 1977

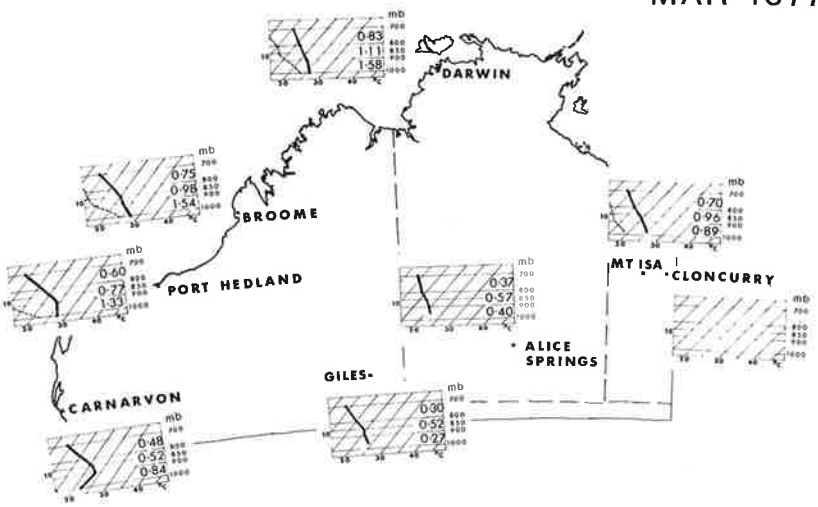

characteristics accompany the deeper moist layers in this region. Once again, the distribution of rainfall deciles (Fig.11 bottom) go some way to substantiate this assertion. Over the continental interior, precipitable water magnitudes fail to reflect the large incursion values of January 1974 and, with moisture and vertical motion reduced over the west-central region, rainfall producing mechanisms are weak.

The March 1975 (Fig.83 centre) diagram highlights a month in which moisture conditions over the continental interior reflect slightly poorer monsoon penetration. Yet, heavy rainfall centred on the Alice Springs area (Fig.12 bottom) did occur in March 1975 but was probably a result of synoptic-scale rain depression activity (Loursenz, 1981). Certainly, the rainfall distribution is not as indicative of the action of widespread rainfall mechanisms as in other seasons in the sequence. As the cyclonic circulation and advective moisture flux convergence diagrams (Fig.57) in Section 3.2.1 indicate, March 1975 is a month of poorly defined monsoonal influence. Inversion conditions continue to be favoured in the west-central region, while Darwin is the only station to register water content values above one gm cm^{-2} in both the surface-900 mb and 900-800 mb intervals. Precipitable water content magnitudes at the other coastal stations and aerological traces at almost all stations remain close to March 1974 values.

In the final diagram (Fig.83 bottom), the March 1977 situation highlights conditions very similar to March 1974 and 1975, although steeper aerological traces at most stations suggest greater atmospheric stability. Moisture content values are also reduced, especially in parts of central Australia, with the most noticeable changes in the west-central margins of the continent. As Figure 9 (Section 3.1.1) shows, the monthly mean circulation at 850 mb is dominated by strong anticyclonicity over the centre of the continent and flow with a markedly overland trajectory. This is further exemplified by the extent of inversion conditions at Carnarvon and the magnitude of dew point temperature traces at most continental interior stations. Consequently, as in both March 1974 and 1975 (Fig.83 top and bottom), Darwin is the only

station to record precipitable water content values above one gm cm^{-2} in the surface-900 mb and 900-800 mb layers.

One feature of the February and March sequences which is of passing interest is that pre-1976 precipitable water content magnitudes at Cloncurry have a different structure to post-1976 values when the station was moved to Mount Isa. In the case of Cloncurry, precipitable water values tend to decrease with height in successive layers. However, at Mount Isa, values show a tendency to develop a 900-800 mb layer maximum much like the stations in the continental interior. Such differences in stations in relatively close proximity may either be a quirk of the periods sampled or reflect local influences.

In summary, precipitable water content and aerological traces illustrate the broad coastal to inland moisture gradient over Australia. Most penetration of moisture into the inland occurs in the 900-800 mb layer, with January 1974 and, to a lesser extent, February 1976 being months when pronounced monsoon incursions develop. The opposite extreme is evident in January 1975 when the weak monsoonal activity observed in Sections 3.1 and 3.2.1 *(i)* and *(ii)* is reflected by the poor moisture content over the continent. With moisture values low and inversion conditions predominant over the northwest of Australia, there is further support for the contention that heat low, rather than NET_{SH}, characteristics are prominent in January 1975.

Intraseasonal variability is reflected in the improvement in moisture conditions from January to February 1975. This observation closely follows the pattern of upper air dynamics noted in Section 3.1. Persistence of moisture conditions also generally follows the conclusions of earlier sections, with a tendency for the 1974 summer to be influenced by high atmospheric moisture content from January to March. However, the March sequence (Fig.83) indicates that there are no distinct changes in moisture content indicative of monsoon withdrawal. This is contrary to the evidence for monsoon 'retreat' in the upper air dynamics and moisture characteristics

in Sections 3.1 and 3.2.1 *(i)* and *(ii)*.

3.2.2 Sub-Period : Cold Surges - January 1973-75

So far, this discussion has examined aspects of monthly mean total, advective and transient eddy moisture characteristics. In the course of this examination it has been suggested that transient eddy fluctuations represent changing synoptic-scale patterns. One feature of the Asian monsoon regime (summer and winter) that is bound up with such variations is the cold surge.

Thus it is useful to attempt to examine the preponderance, evolution and equatorial penetration of Northern Hemisphere winter cold surges during the January 1973-75 period. This is particularly important in view of earlier discussions of monthly mean low-level flow and interhemispheric interactions (Sections 3.1 and 3.2.1) and recent indications that the Asian teleconnection extensions may be enhanced by cold surge activity (Chang *et. al.*, 1979; Chang and Lau, 1980, 1982; Lau, 1982). In fact, as Keen (1982) suggests, single synoptic events may even play a vital role in the outcome of subsequent large-scale teleconnection anomalies. Nevertheless, it should be noted that no analysis of the vertical structure of surges is attempted due to the absence of comprehensive data from Indonesian stations prior to 1975-76.

The following discussion of cold surges is divided into three parts : *(i) Development, (ii) Evolution and Equatorial Penetration* and *(iii) Influence on Northern Australia*. The Januarys of 1973, 1974 and 1975 are examined because they represent three months of markedly different monsoonal characteristics (Sections 3.1 and 3.2.1). In the first part of the discussion, seven major cold surges are detected in a Hong Kong cold surge index (using temperature differences) and surface pressure data. However, following the discussion in Lau (1982), it was also decided to include the surface wind field in a cold surge cross section (through Hong Kong - Ishigakijima - Naha) of daily observations in each of the three months

(Figs.84-86). This cross section is chosen to register the outbreak of cold surges from Asia, following collapses of the Siberian anticyclone. The second part of the discussion examines the evolution and possible cross-equatorial penetration of these surges in a spatio-temporal framework. To these ends, a series of surface streamline charts obtained from the Bureau of Meteorology are used to show four day sequences, commencing with the day of the surge (as determined by the Hong Kong cold surge index) for six of the seven major cold surge events (Figs.87-92). Charts for the seventh event in 1975 were not available from the Bureau of Meteorology's Darwin Office due to the damage to facilities caused by Cyclone Tracy in late December 1974. Finally, Figure 93 is included to show the daily distribution of water vapour fluxes over northwestern Australia and their possible relationship to cross-equatorial surges.

(i) Development

In the cold surge cross sections, the seven major surges are divided as follows : three in January 1973, three in January 1974 and one in January 1975 (Figs.84-86). It is apparent that the sections contain more surges than those dictated by temperature increments alone. However, it was decided to focus primarily on the seven major cold surges and sequences when pronounced pressure and wind changes occurred. The most obvious difference between the three months is found in the overall pressure and wind field distributions. In particular, strong South China Sea surges would seem to be favoured by a rapid pressure fall and southwesterly progressing wind speed maxima.

During January 1973 (Fig.84), the above conditions are most evident over the later part of the month, with the most complete surges occurring on the 17th and 24th (the absence of wind data for Naha does not negate the fact that the surge on the 1st is followed by poor development of the wind). In both periods, pressures below 1015-1010 mb on the Naha (N) side of the section are followed by the rapid progression of a wind speed maximum through

Figure 84 Cold surges as dictated by surface pressure and wind data in the cross section from Hong Kong through Ishigakijima to Naha in January 1973. Surge passages are indicated by the schematic arrow marker on the left-hand side of the diagram.

Figure 85 Cold surges as dictated by surface pressure and wind data in the cross section from Hong Kong through Ishigakijima to Naha in January 1974. Surge passages are indicated by the schematic arrow marker on the left-hand side of the diagram.

Figure 86 Cold surges as dictated by surface pressure and wind data in the cross section from Hong Kong through Ishigakijima to Naha in January 1975. Surge passages are indicated by the schematic arrow marker on the left-hand side of the diagram.

COLD SURGE CROSS SECTION

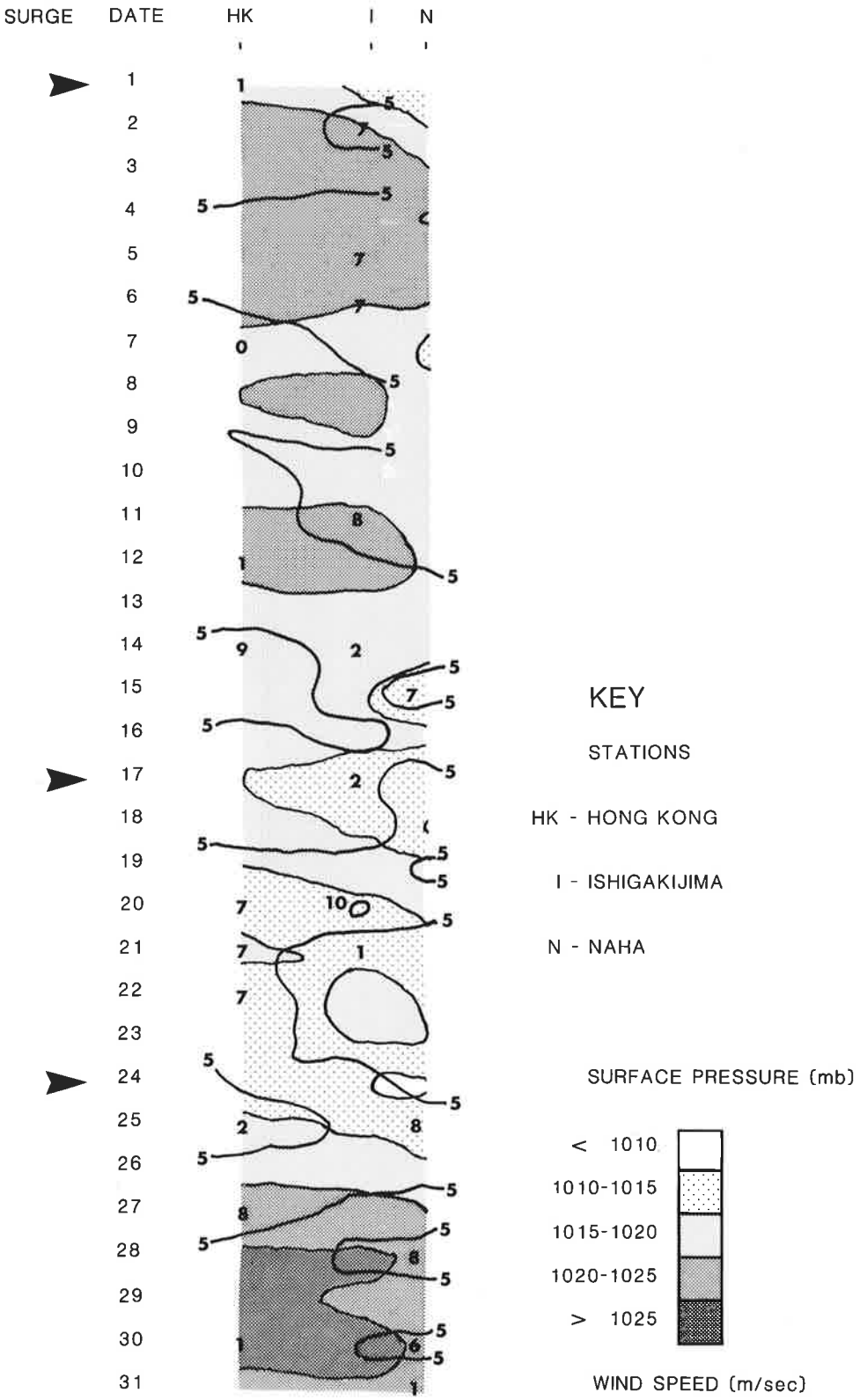

JAN 1973

COLD SURGE CROSS SECTION

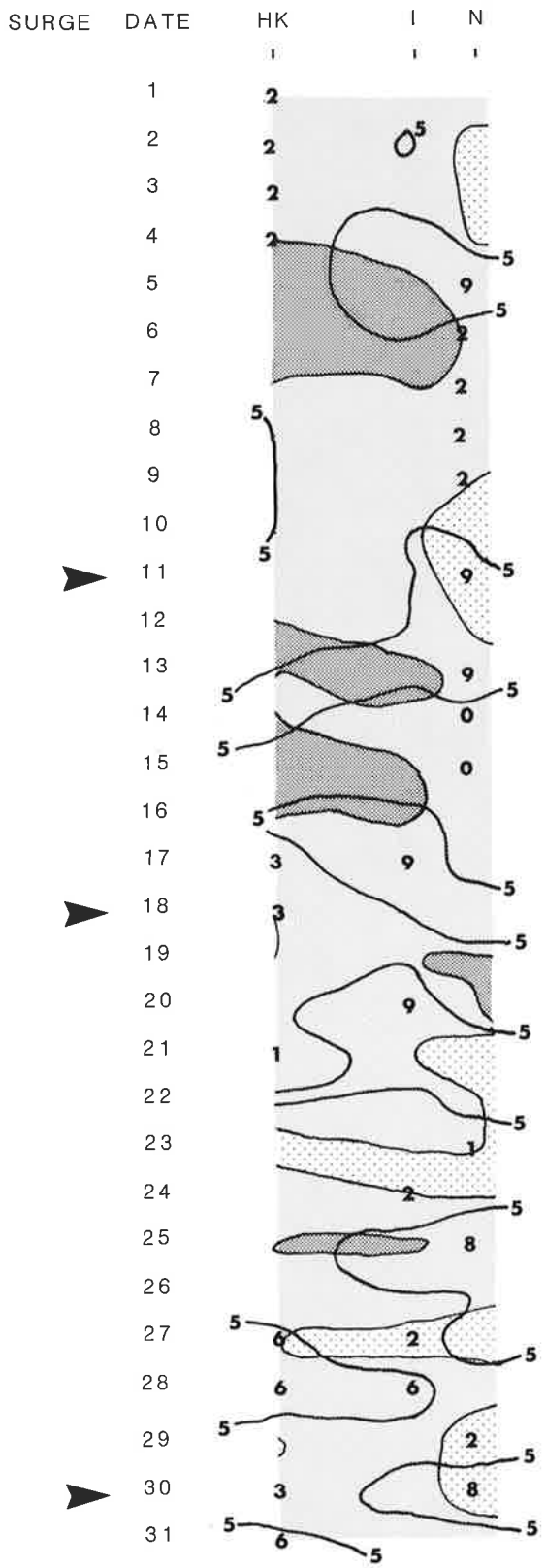

KEY

STATIONS

HK - HONG KONG

I - ISHIGAKIJIMA

N - NAHA

SURFACE PRESSURE (mb)

< 1010

1010-1015

1015-1020

1020-1025

> 1025

WIND SPEED (m/sec)

JAN 1974

COLD SURGE CROSS SECTION

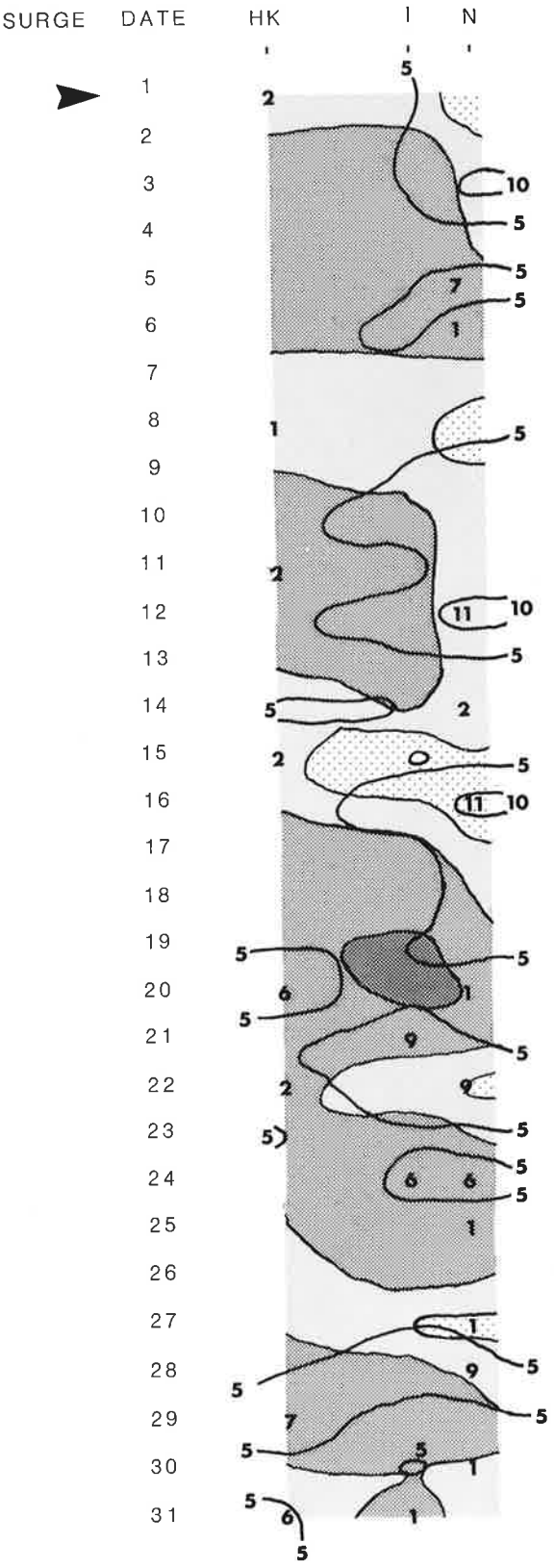

JAN 1975

KEY

STATIONS

HK - HONG KONG

I - ISHIGAKIJIMA

N - NAHA

SURFACE PRESSURE (mb)

< 1010

1010-1015

1015-1020

1020-1025

> 1025

WIND SPEED (m/sec)

Ishigakijima (I) and Hong Kong (HK). Although other periods display wind maxima in the cross section they are not extensive and/or fail to accompany any marked pressure changes. Thus one would expect the surges on the 17th and 24th of January to be more likely to influence convective conditions further to the south.

In January 1974 (Fig.85), the pressure distribution is much weaker and less variable than in January 1973. Although the same number of surges occur in both months, only the surge on the 11th follows the pattern of pressure and wind field evolution that is suggestive of a strong and potentially penetrative South China Sea surge. The other surges, on the 18th and 30th, are not well defined in terms of the above scenario. In particular, the surge on the 18th is unusual in that pressure and wind conditions would appear to be more conducive to a surge on the 21st or 23rd of the month.

Basically, January 1975 (Fig.86) displays the most pronounced wind speed maxima and periodic pressure tendency of the three months. In particular, wind speed maxima (and to a lesser extent the pressure minima) are more restricted to the Naha side of the diagram. However, there are three periods, centred around the 15th, 22nd and 27th, when one would have thought that surges could have resulted. Certainly, pressure and wind distributions suggest that some type of surge would have occurred on or about the above dates. Unfortunately, the absence of streamline data in January 1975 restricts any further analysis of surges in this month.

(ii) Evolution and Equatorial Penetration

The subsequent evolution and possible equatorial penetration of the surges observed in Figures 84-86 are examined in a time sequence of synoptic charts, commencing on the day of the surge. Each of the sequences are of four days' duration and, although less than the period used in Lau (1982), detail the major consequences of the surges.

During January 1973, three surge sequences occur between the 1st-4th,

17th-20th and 24th-27th days of the month (Figs.87-89). If the day of the surge as indicated by the Hong Kong surge index is deemed to be Day 0, then surges appear to be concentrated around Days 2 and 3 in South East Asian near-equatorial regions. As Lau (1982:1307) remarks :

> ...a feature that appears to be common to all surges is the rather abrupt increase in surface northerly wind over a large part of the South China Sea within one to two days after the surge onset.

In fact, Southern Hemisphere systems seem to be most markedly influenced by Asian surges on the 3rd, 4th, 26th and 27th (Days 2 and 3 of the 1st-4th and 24th-27th day sequences). Only on Days 0 and 1 of the 1st-4th surge sequence (Fig.87) is there any indication of the enhancement of Asian near-equatorial circulation, and possibly convection, following initial or pre-surge activity (as noted in other sequences by Chang and Lau, 1982; Lau, 1982).

Over the northwestern Pacific Ocean, cold surges associated with the northeast trades are often prevalent throughout Days 0 to 3 but, although outnumbering their South China Sea counterparts, they do not appear to contribute substantially to the development of Southern Hemisphere systems. Certainly, cross-equatorial flow associated with the eastern section of the NET_{NH} and anticyclonicity over eastern Australia are predominant throughout the sequences, with the former being a notable element in the monthly mean surface streamfunctions (Fig.36). However, the western sections of the NET_{NH} and NET_{SH} probably interact more closely, with the strength and development of the latter being at least partly a consequence of the influence of cold surges from the South China Sea. Yet, it would appear that the only distinct cold surge penetration into the Southern Hemisphere occurs on the 27th, following the lowest pressure fall on the Naha side of the 1973 cross section (less than 1010 mb on the 24th) (Fig.84). Interestingly, it is possible that the deep convective region in the vicinity of Java in January 1973 may owe much to the cold surges of the 1st and 24th (Figs.87 and 89). The weekly mean oceanic rainfall rates for January 1973 (Rao *et. al.*, 1976) indicate that the highest rainfall rates in the Javan region

Figure 87 Daily streamline charts in the near tropical portion of the regional domain (20°N-20°S; 90°E-175°E) for the January 1973 surge period of 1st-4th (Days 0 to 3). Heavy dashed lines indicate wind isotachs, with areas of 15 knots and above shaded (redrawn from the Bureau of Meteorology's Darwin Regional Office charts).

Figure 88 Daily streamline charts in the near tropical portion of the regional domain (20°N-20°S; 90°E-175°E) for the January 1973 surge period of 17th-20th (Days 0 to 3). Heavy dashed lines indicate wind isotachs, with areas of 15 knots and above shaded (redrawn from the Bureau of Meteorology's Darwin Regional Office charts).

Figure 89 Daily streamline charts in the near tropical portion of the regional domain (20°N-20°S; 90°E-175°E) for the January 1973 surge period of 24th-27th (Days 0 to 3). Heavy dashed lines indicate wind isotachs, with areas of 15 knots and above shaded (redrawn from the Bureau of Meteorology's Darwin Regional Office charts).

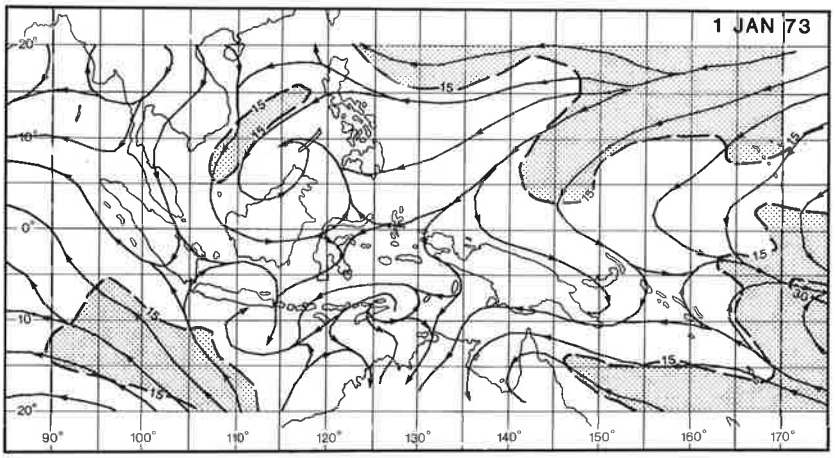
1 JAN 73
20°
10°
0°
10°
20°
90°
100°
110°
120°
130°
140°
150°
160°
170°
15
30

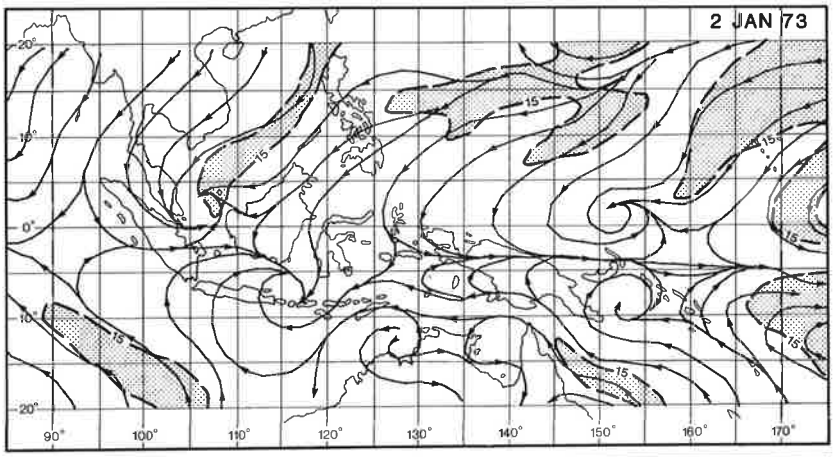
2 JAN 73
20°
10°
0°
10°
20°
90°
100°
110°
120°
130°
140°
150°
160°
170°
15

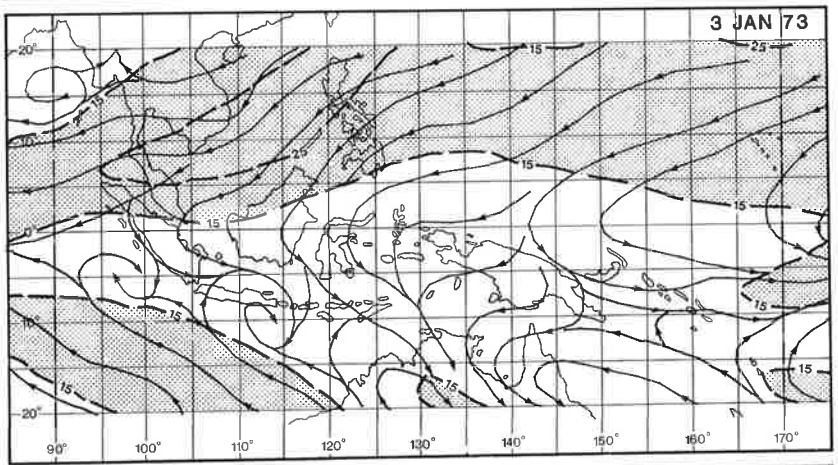
3 JAN 73
20°
10°
0°
10°
20°
90°
100°
110°
120°
130°
140°
150°
160°
170°
15
25

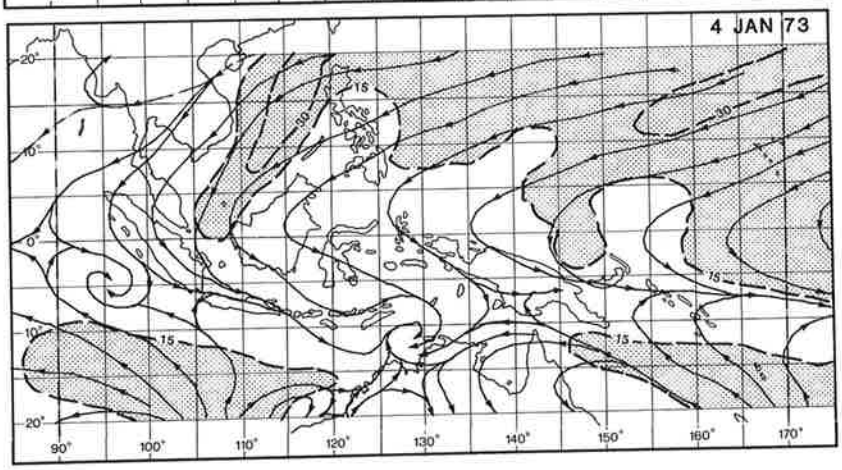
4 JAN 73
20°
10°
0°
10°
20°
90°
100°
110°
120°
130°
140°
150°
160°
170°
15
30

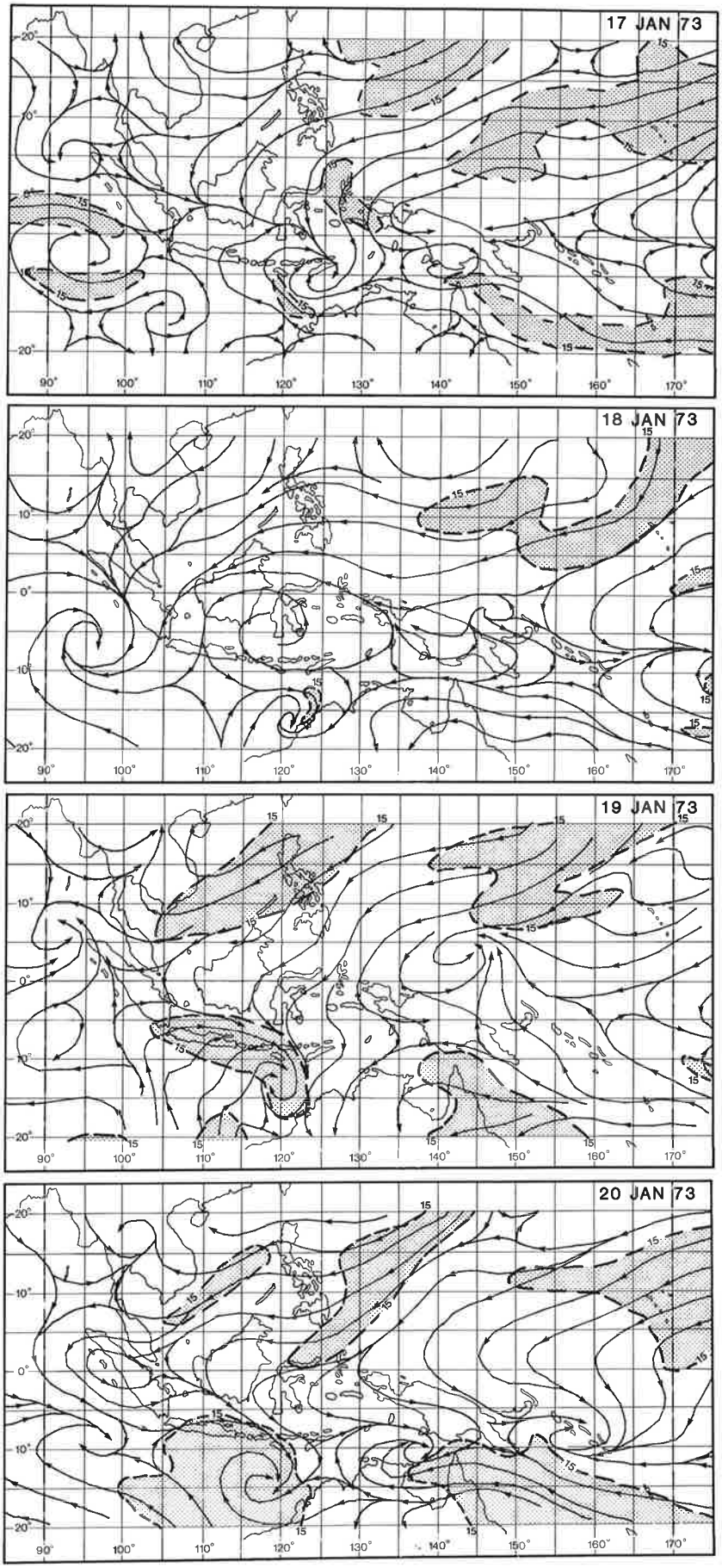
17 JAN 73
18 JAN 73
19 JAN 73
20 JAN 73
20°
10°
0°
10°
20°
90°
100°
110°
120°
130°
140°
150°
160°
170°
15

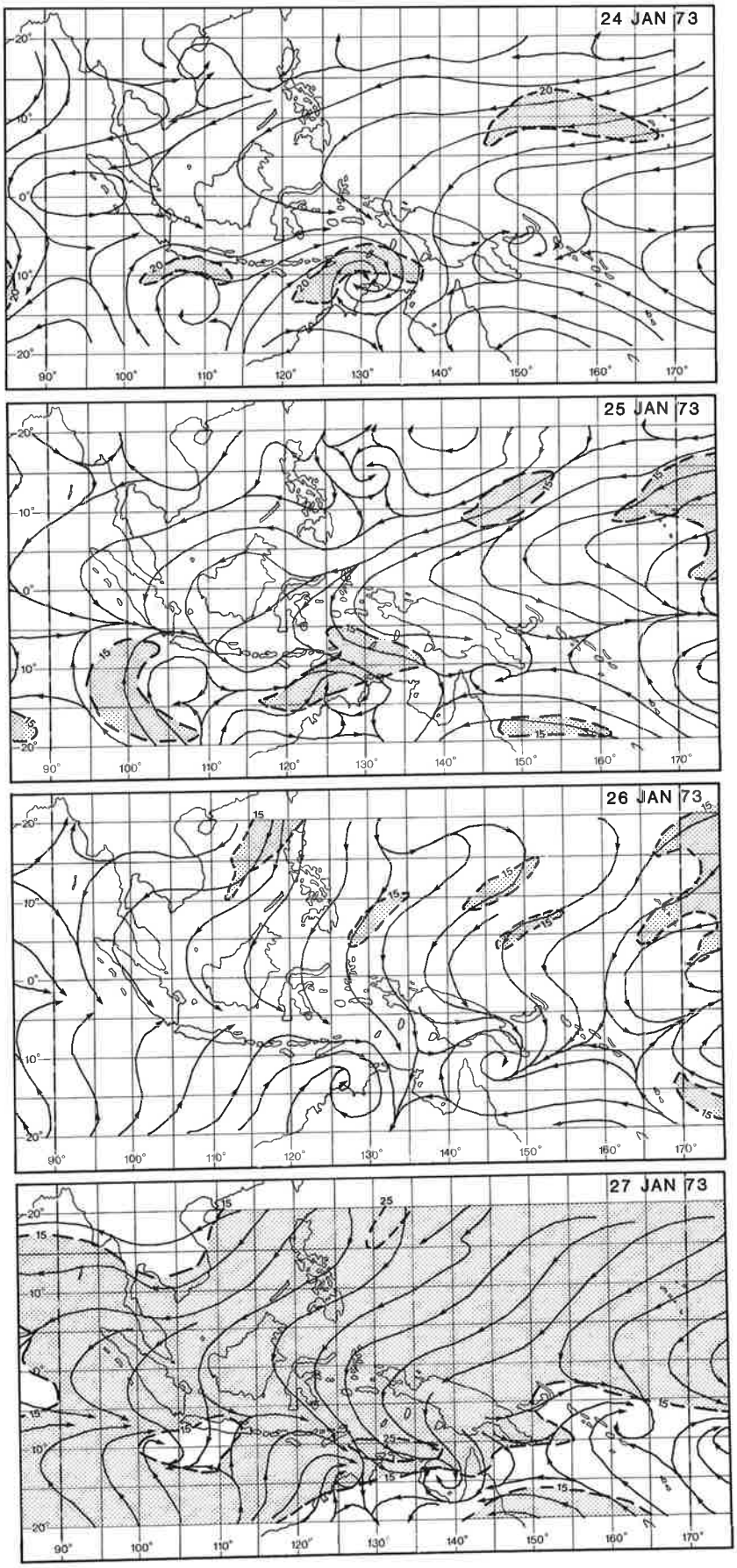
24 JAN 73
25 JAN 73
26 JAN 73
27 JAN 73
90°
100°
110°
120°
130°
140°
150°
160°
170°
20°
10°
0°
10°
20°

occurred between the 8th-14th (1.7 mm hr^{-1}), the 15th-21st (1.2 mm hr^{-1}) and the 29th-31st (2.0 mm hr^{-1}). Convective activity in the western Pacific Ocean (NET_{NH} eastern section), in Figure 26, seems to be restricted to shallower trade wind influences.

The January 1974 cold surge sequences occur during the 11th-14th, 18th-21st and 30th-2nd February (Figs.90-92). However, the timing of these cold surges differs from those in January 1973 in that isotach maxima generally appear earlier over the South China Sea and northern Pacific (on Days 2 and 3) following the surge. Furthermore, most South China Sea and North Pacific cold surges seem to be more spatially allied and perhaps result from related mid to higher latitude forcings. In fact, there would appear to be a higher number of surges in the region of Asia than in the northern Pacific in January 1974.

The penetration of surges into near-equatorial regions in January 1974 is centred more on Asia than the northwestern Pacific. Yet, it would seem that cross-equatorial penetration into the Southern Hemisphere is complicated by the fact that the NET_{SH} is extremely strong and displaced to the south. As a result of this feature and the persistent cyclonic centres across the northwestern Pacific, pronounced cross-equatorial flow follows longer and more zonal trajectories, often only penetrating the equator in westernmost longitudes (Indian Ocean). Nevertheless, there are some exceptions to this pattern on the 19th, 20th and 30th (Figs.91 and 92) when cross-equatorial flow, and possibly cold surges (30th), are prevalent over the more eastern longitudes. It should also be noted that wind speeds are above 15 knots in northern Australian regions throughout the three sequences, probably as a result of the strong NET_{SH}, the more pronounced western portion of the NET_{NH} and persistent Asian cold surges into the Indonesian region. The presence of cross-equatorial flow in the western, rather than the eastern, section of the NET_{NH} is promoted by the cyclonic circulation that persists over the northwestern Pacific. Further to the west, the displacement of the NPA (as seen in the monthly mean fields in Figure 7) tends to impede

Figure 90 Daily streamline charts in the near tropical portion of the regional domain (20°N-20°S; 90°E-175°E) for the January 1974 surge period of 11th-14th (Days 0 to 3). Heavy dashed lines indicate wind isotachs, with areas of 15 knots and above shaded (redrawn from the Bureau of Meteorology's Darwin Regional Office charts).

Figure 91 Daily streamline charts in the near tropical portion of the regional domain (20°N-20°S; 90°E-175°E) for the January 1974 surge period of 18th-21st (Days 0 to 3). Heavy dashed lines indicate wind isotachs, with areas of 15 knots and above shaded (redrawn from the Bureau of Meteorology's Darwin Regional Office charts).

Figure 92 Daily streamline charts in the near tropical portion of the regional domain (20°N-20°S; 90°E-175°E) for the surge period from 30th January to 2nd February 1974 (Days 0 to 3). Heavy dashed lines indicate wind isotachs, with areas of 15 knots and above shaded (redrawn from the Bureau of Meteorology's Darwin Regional Office charts).

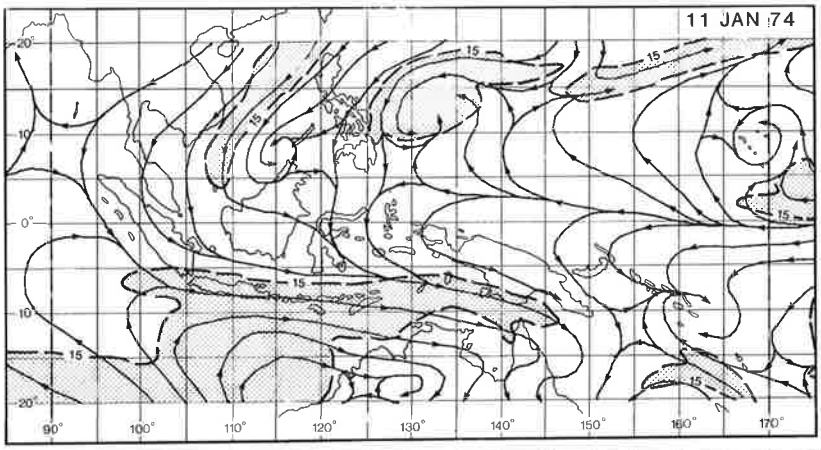
11 JAN 74
20°
10°
0°
10°
20°
90°
100°
110°
120°
130°
140°
150°
160°
170°
15

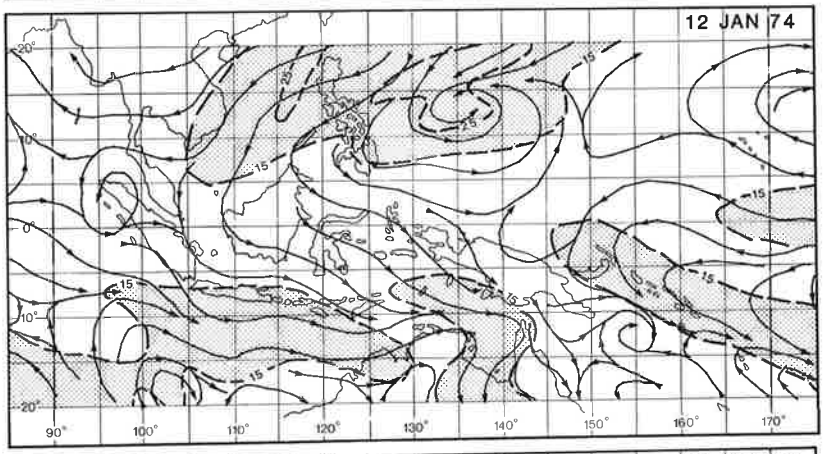
12 JAN 74
20°
10°
0°
10°
20°
90°
100°
110°
120°
130°
140°
150°
160°
170°
15

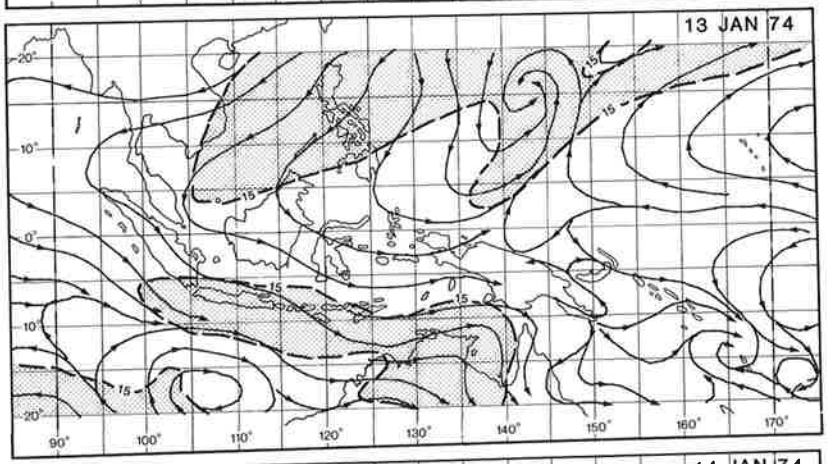
13 JAN 74
20°
10°
0°
10°
20°
90°
100°
110°
120°
130°
140°
150°
160°
170°
15

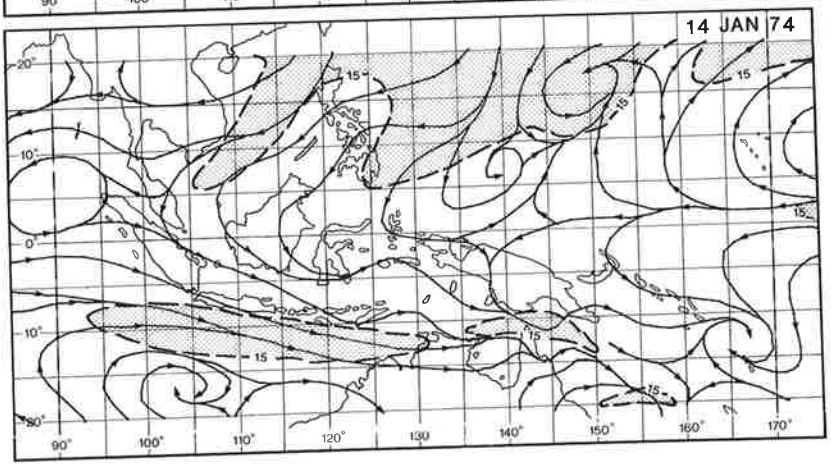
14 JAN 74
20°
10°
0°
10°
20°
90°
100°
110°
120°
130°
140°
150°
160°
170°
15

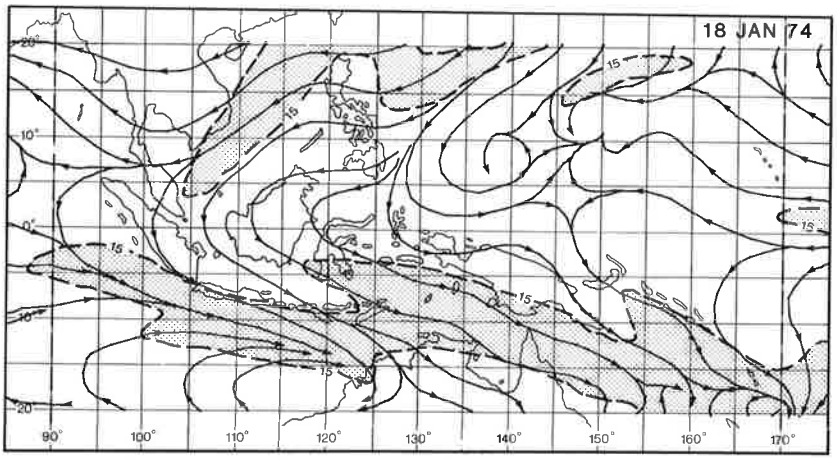
18 JAN 74
20°
10°
0°
10°
20°
90°
100°
110°
120°
130°
140°
150°
160°
170°
15
30

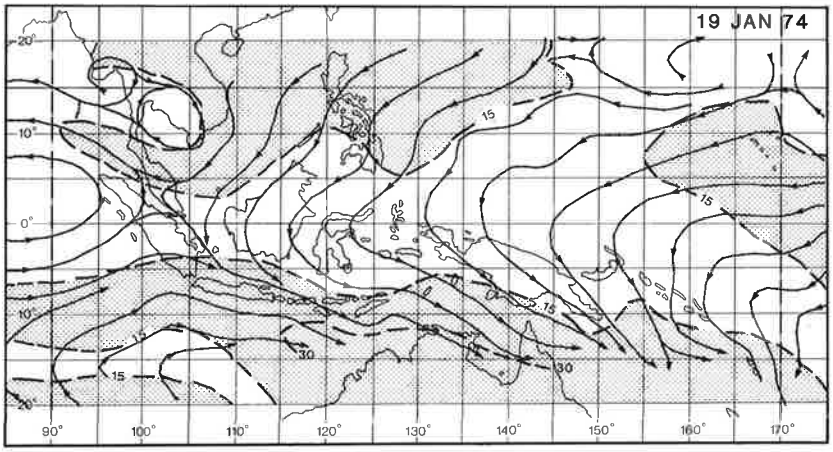
19 JAN 74
20°
10°
0°
10°
20°
90°
100°
110°
120°
130°
140°
150°
160°
170°
15
30

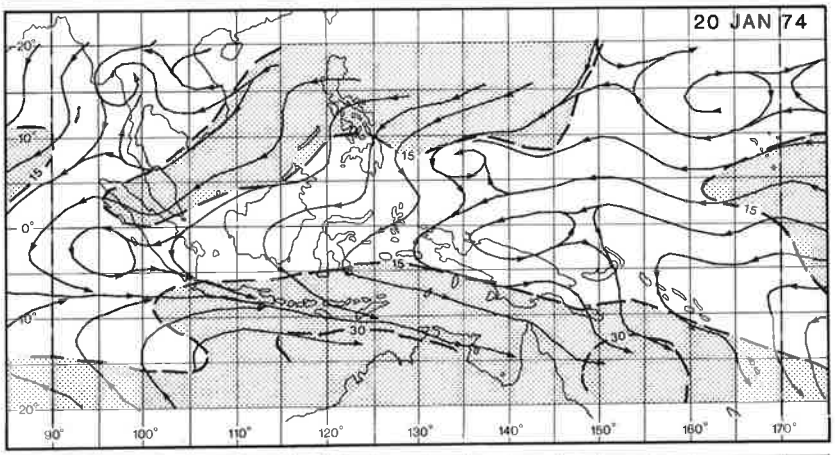
20 JAN 74
20°
10°
0°
10°
20°
90°
100°
110°
120°
130°
140°
150°
160°
170°
15
30

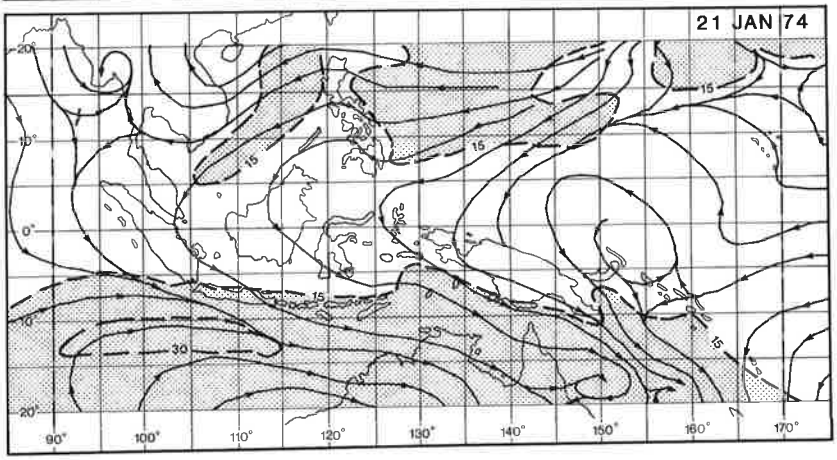
21 JAN 74
20°
10°
0°
10°
20°
90°
100°
110°
120°
130°
140°
150°
160°
170°
15
30

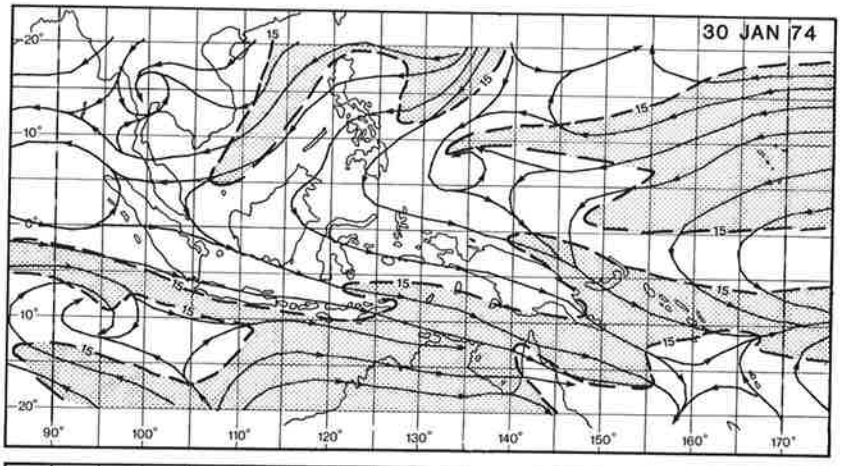
30 JAN 74
20°
10°
0°
10°
20°
90°
100°
110°
120°
130°
140°
150°
160°
170°

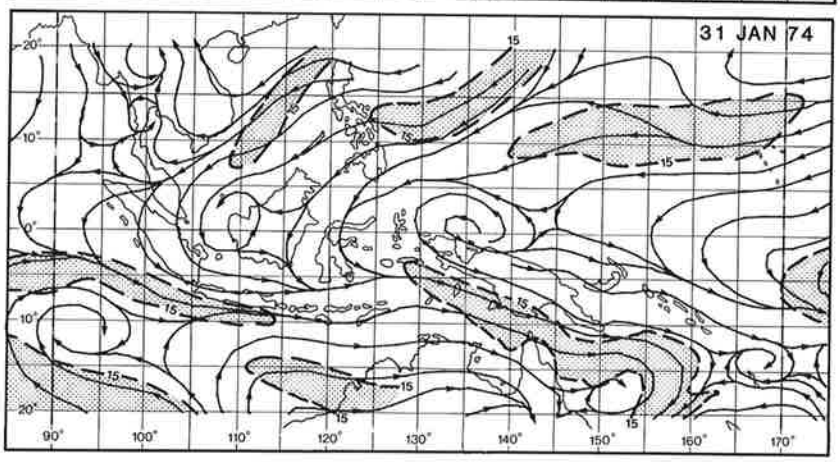
31 JAN 74
20°
10°
0°
10°
20°
90°
100°
110°
120°
130°
140°
150°
160°
170°

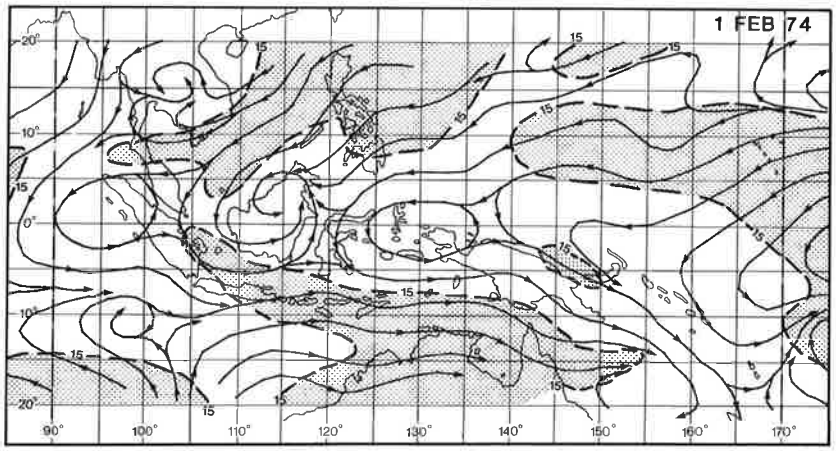
1 FEB 74
20°
10°
0°
10°
20°
90°
100°
110°
120°
130°
140°
150°
160°
170°

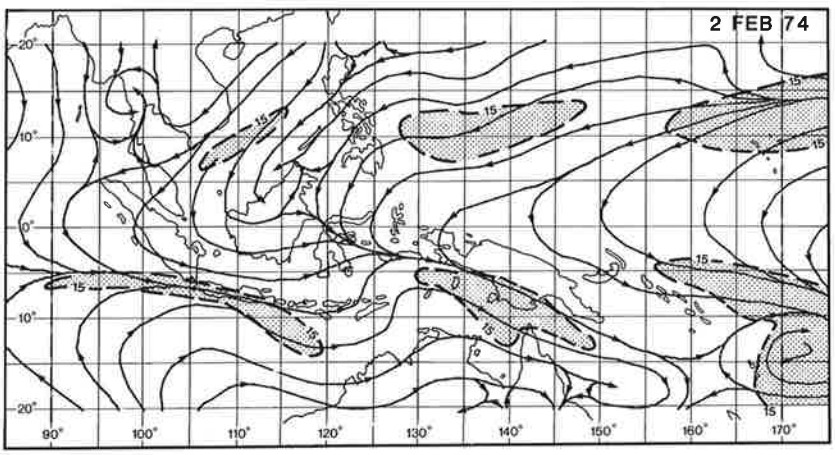
2 FEB 74
20°
10°
0°
10°
20°
90°
100°
110°
120°
130°
140°
150°
160°
170°

trade wind flow towards the equator, with the result that the NET_{NH} (eastern section) is weaker than in January 1973. However, there does appear to be one distinct indication of Northern Hemisphere near-equatorial circulation being influenced by an Asian cold surge. This occurs in the 30th-2nd February cold surge sequence (Fig.92) when a cyclonic system develops over Borneo on Day 1.

(iii) Influence on Northern Australia

It would seem that any influence of cross-equatorial cold surges on Australian circulation and convective systems is more likely to be discernible in January 1973 than January 1974. This is borne out by the daily water vapour flux roses in Figure 93. In fact, only the cold surge penetration on the 26th-27th of January 1973 (Fig.89) (and perhaps for a few days later) is readily evident in the Darwin flux roses. However, there is some suggestion in the Giles and Alice Springs roses that this cold surge, or synoptic features that were enhanced by it, penetrated further inland on the 27th-29th. With the advective surface circulation field in Figure 49 indicating that the NET_{SH} has a tendency towards an elongated centre located over the northwest to northeast of the continent in January 1973, the daily distribution of water vapour fluxes over northwestern Australia shows a very variable pattern. Apart from the persistent south to southeasterly flow at Carnarvon, other stations register little consistency in water vapour fluxes, with stations on the northern coasts experiencing a high number of calm days (Darwin 19, Port Hedland 19 and Broome 18). It is also possible that the strong eddy fields in January 1973 (Fig.68) are a reflection of this type of pattern.

By January 1974 (Fig.93 centre) the situation is radically reversed. In fact, the dominant monthly mean cyclonic circulation over the continent is markedly evident in the pattern of daily water vapour fluxes over the northwestern Australian sector. As a result of the high NET_{SH} activity in January 1974 (Fig.52), the number of calm days at stations along the northern

Figure 93 Daily water vapour flux roses for Darwin, Broome, Port Hedland, Carnarvon, Giles, Alice Springs and Cloncurry in January 1973, 1974 and 1975. Water vapour fluxes are in units of gm cm^{-1} mb^{-1} s^{-1} with small arrows denoting water vapour flux in the range of 0-5 gm cm^{-1} mb^{-1} s^{-1}, medium arrows denoting water vapour flux in the range 5-10 gm cm^{-1} mb^{-1} s^{-1} and large arrows denoting water vapour flux in the range of greater than 10 gm cm^{-1} mb^{-1} s^{-1}.

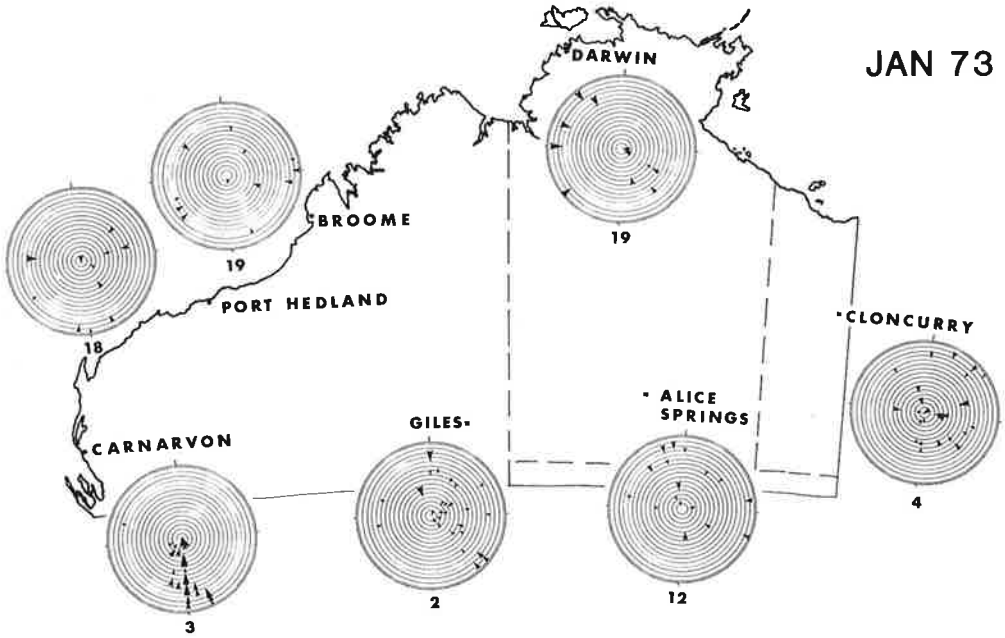
JAN 73
DARWIN
19
BROOME
19
PORT HEDLAND
18
CLONCURRY
4
ALICE SPRINGS
12
GILES
2
CARNARVON
3

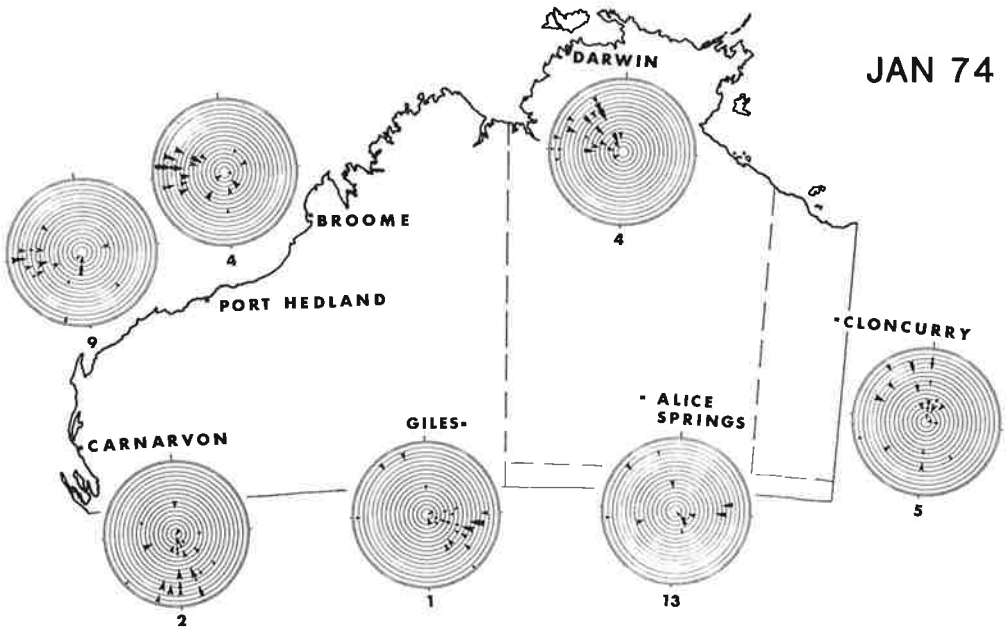
JAN 74
DARWIN
4
BROOME
4
PORT HEDLAND
9
CLONCURRY
5
ALICE SPRINGS
13
GILES
1
CARNARVON
2

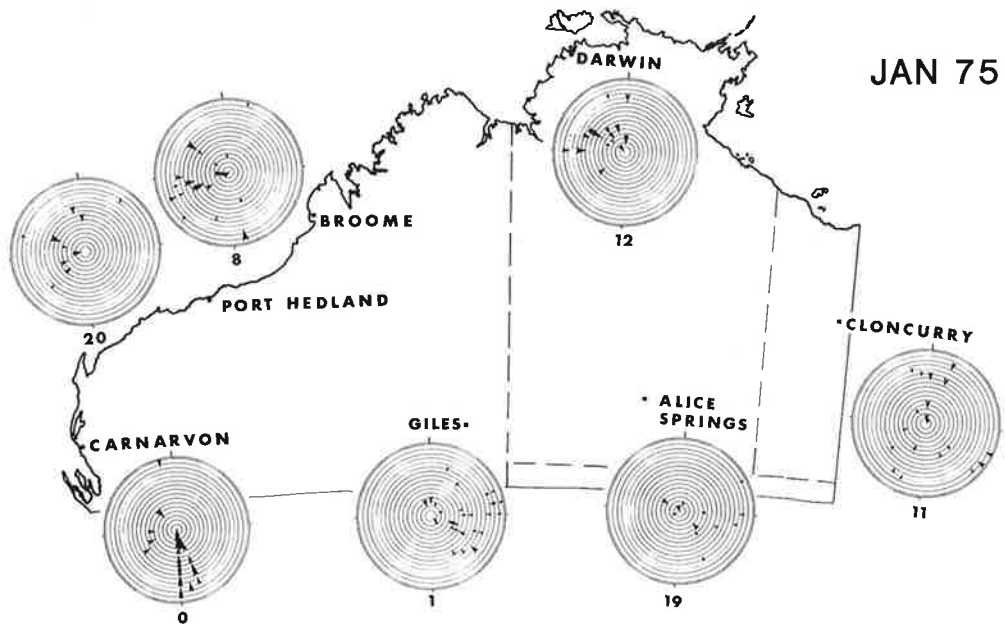
JAN 75
DARWIN
12
BROOME
8
PORT HEDLAND
20
CLONCURRY
11
ALICE SPRINGS
19
GILES
1
CARNARVON
0

coasts is also reduced. Consequently, detection of cold surge influences is made all the more difficult, with high wind speeds associated with the northern flank of the strong NET_{SH} being a persistent feature throughout the month. However, it is possible that the slight increase in the magnitude of west to northwesterly water vapour fluxes at Darwin, Broome and Port Hedland in the latter half of January 1974 may be influenced by the 18th-21st and 30th-2nd February cold surge sequences (Figs.91 and 92). With a more stringent criteria for defining cold surge and break periods, Chang and Lau (1982) only detected two strong cold surge cases for the whole period from November 1973 to February 1974.

Although no streamline analysis was available for January 1975 surges, the daily distribution of water vapour fluxes is still included (Fig.93 bottom). As in January 1974, aspects of monthly mean circulation are reflected in the pattern of daily water vapour fluxes at northwestern Australian stations. Weak cyclonic circulation is centred on the above region, with a return to the January 1973 situation (Fig.93 top) of a large number of calms at stations on the north to northwestern coast. As in the other two months examined, Carnarvon continues to be dominated by strong southerly flow. The work of Chang and Lau (1982) indicates that cold surge activity could have occurred at this time (they detailed four strong cold surges in the period from November 1974 to February 1975), but the poor definition of cold surges in the January 1975 cross section (Fig.86) indicates that synoptic data are required to fully evaluate such suggestions.

Essentially, only two months of contrasting monsoonal activity have been examined in this sub-period. Nevertheless, there are indications that cold surge activity differs in the sub-period, with January 1973 displaying more cold surge influence than January 1974. This is evident over northern Asia in the cold surge cross sections, sub-tropical and near-equatorial regions in the streamline charts and northern Australia in the water vapour flux roses. In general, variations in cold surge activity, timing, spatial extent and structure, and penetration into the Southern Hemisphere occur during the

January 1973-75 sub-period.

Given the remarks about pronounced changes in cross-equatorial flow between early (November - mid January) and late (late January - February) monsoon periods in Lim and Quah (1978), it would have been useful to have compared cold surge sequences in January and February. However, the constraints of long-term data availability and spatial coverage, which have also plagued more ambitious projects (Chang and Lau, 1980), have precluded such analysis.

3.3 LONG-TERM INTERANNUAL AND INTRASEASONAL VARIABILITY - MONSOON AND SOUTHERN OSCILLATION/WALKER CIRCULATION DYNAMICS, INDICES AND CORRELATIONS OVER THE INDO-PACIFIC (35°N-35°S; 30°E-60°W) AND REGIONAL (35°N-35°S; 85°E-175°E) DOMAINS

The preceding discussions examined upper air dynamics and moisture characteristics over the Australasian region during the Southern Hemisphere summer monsoon seasons of 1973-77. These investigations have several implications for monsoonal and teleconnection structure and variability. In the following discussion an attempt is made to determine whether dynamic features in the area and period examined are representative of wider spatial conditions and longer temporal sequences. Implicit in such an evaluation is the need to use the maximum extent of upper air data in tandum with longer records of surface pressure indices. This poses the question of whether indices and correlations of monsoon and teleconnection phenomena are supported by upper air dynamics.

An Indo-Pacific domain (35°N-35°S; 30°E-60°W) is used in conjunction with a longer-term sequence in the regional domain (35°N-35°S; 85°E-175°E) and over the Australian continent to present :

a) the wider spatial pattern of upper air dynamics during two months (January 1973 and January 1974) and two composites ($-15 \leq SOI \geq +15$; 1957-81) of contrasting monsoonal and SO/WC activity (Section 3.3.1)

b) the temporal variability and vertical structure of upper air patterns over 14 Januarys (1965-78) and their relationship to Australian rainfall regimes (Section 3.3.2)

c) long-term aspects of the interpretation of correlations and indices of the SOI, SO/WC and Australasian monsoon phenomenon. and physical manifestations of their interactions (Section 3.3.3)

3.3.1 Indo-Pacific Circulation and Teleconnection Variability

In this section, gridded wind vectors and horizontal divergence are calculated at 850 mb and 200 mb levels over an Indo-Pacific domain

(35°N-35°S; 30°E-60°W) in order to examine broader upper air patterns during SOI extremes. This analysis contrasts : a) the extremes of January 1973 and January 1974 and b) composites of + SOI and - SOI extremes (+ SOIs are Januarys 1962, 1967 and 1974 and Februarys 1971 and 1974; - SOIs are Januarys 1958 and 1959 and Februarys 1959, 1970, 1973 and 1978).

The distribution of data stations used to evaluate fields of divergence and gridded wind vectors in the Indo-Pacific domain (35°N-35°S; 30°E-60°W) is shown in Figure 94. It can be seen that there are some large gaps in this array, particularly over the east to southeastern Pacific and southern Indian Ocean. Originally, the processing of data was intended to evaluate streamfunctions and velocity potentials. Unfortunately, it was found that some of the final fields were seriously affected in the above regions. This was most marked at 200 mb, where the strong winter jetstream across the Northern Hemisphere totally biased the final fields over the data-sparse Southern Hemisphere oceans. Therefore, it was decided to reduce this error by presenting fields in the least possible processed form. This was achieved by the use of gridded wind vectors and divergence which provide a much better resolution of the data.

(i) Monthly Mean 850 mb and 200 mb Divergence and Wind Vectors : January 1973 El Niño and January 1974 anti-El Niño Periods

Despite the fact that wind vector and divergence fields are 'noisier' than streamfunctions and velocity potentials, they reiterate the major findings in Section 3.1. However, variations in circulation and teleconnection features over the regional domain (35°N-35°S; 85°E-175°E) (Fig.6) are not the only upper air changes occurring in January 1973 and January 1974. Synonymous with these months of weak negative and strong positive Southern Oscillation Indices (SOIs) are interrelated developments to the east and west of this segment of the Indo-Pacific domain (Fig.94).

In the section of the Indo-Pacific domain to the west of 90°E there are marked variations in circulation and divergence fields at both 850 mb and 200 mb levels. As with the observations in the regional domain, they

Figure 94 Distribution of upper air and upper wind stations in the Indo-Pacific Domain.

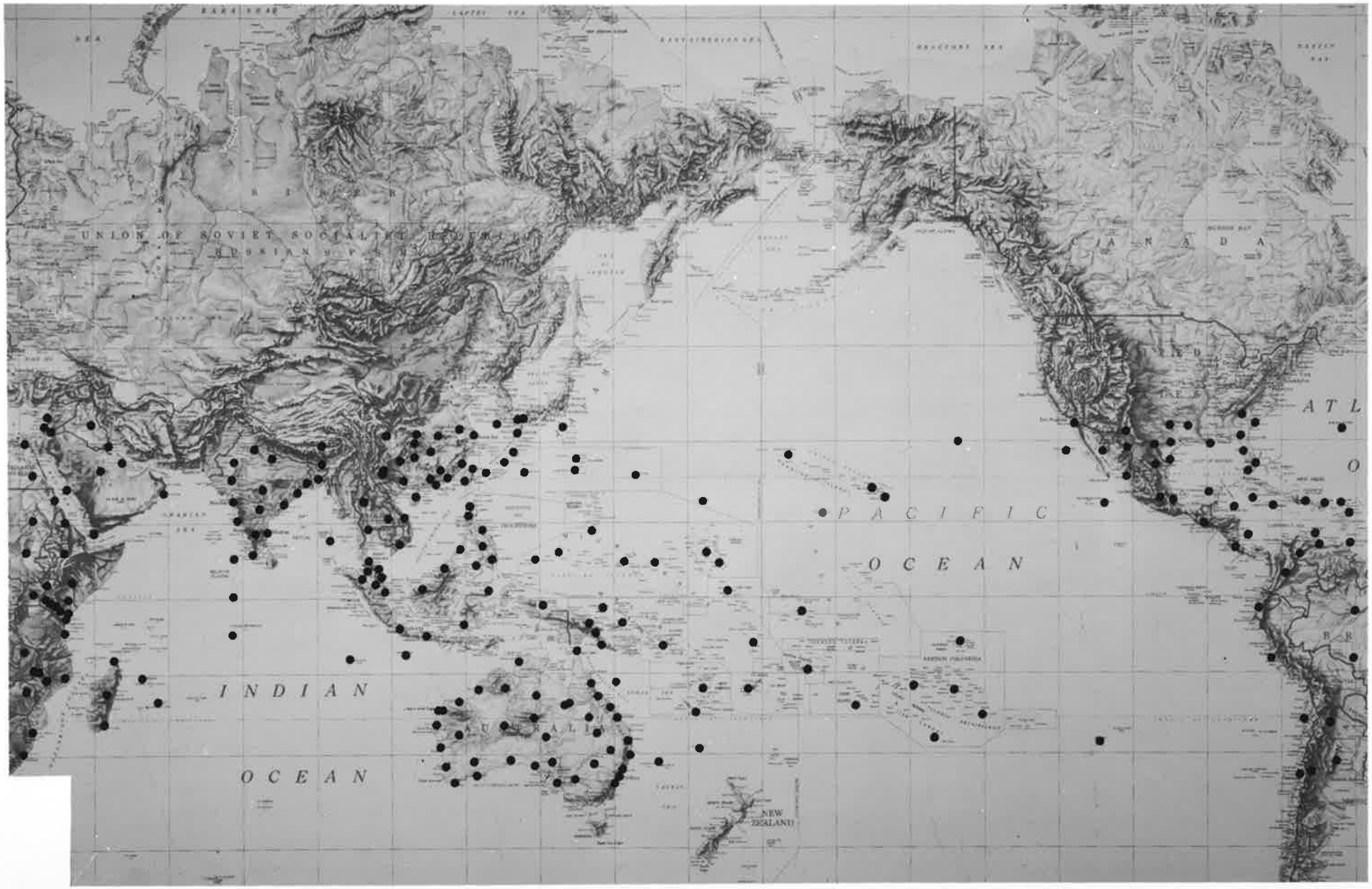
UNION OF SOVIET SOCIALIST REPUBLICS
RUSSIAN S.F.S.R.
C A N A D A
P A C I F I C
O C E A N
I N D I A N
O C E A N
A T L
O
NEW ZEALAND

are found to be strongly supported by the remotely-sensed rainfall and upper cloud distributions of Rao *et. al.* (1976) and Barton (1983). These results are evident in the following comparison of 850 mb and 200 mb level circulation and divergence during January 1973 and January 1974 (Figs.95 and 96).

At the 850 mb level, wind vectors in January 1974 are somewhat stronger and more organized than in January 1973. This is most evident with regard to circulation about the anticyclonic vortices over India and the southern Indian Ocean off the Malagasy Republic, and the low latitude cyclonic flow in a westward extension of the NET_{NH} (the dashed line in the Northern Hemisphere in Figure 96). As a consequence, the divergence and convergence fields in this part of the hemisphere are also enhanced. In particular, the regions of convergence covering southern Africa and the Malagasy Republic, and the equatorial area across southern India and immediately south of Sri Lanka are noticeably stronger. Further south, in the middle latitudes of the Indian Ocean, divergence is more prominent in January 1974.

The 200 mb pattern suggests that the type of upper air variations noted in the regional domain also apply to this section of the Indo-Pacific domain. Most prominent in this regard are the anticyclonic elements across the Northern Hemisphere subtropics and in the Southern Hemisphere midlatitudes. Both of these features are more strongly defined in January 1973 (Fig.95) than January 1974 (Fig.96), although the western edge of the equatorial easterly flow maximum associated with a jet-like area in Indonesian longitudes is zonally stronger in January 1974. Over the southern Indian Ocean, anticyclonicity is apparently influenced by the same northward displacement in the sub-tropical jetstream that was noted in Australian longitudes in January 1973.

The distribution and intensity of 200 mb divergence and convergence fields reflect many of the above changes. Of particular importance to the concept of teleconnection variability are the enhancement of the divergence regions over the East African coast and to the southeast of the Indian

Figure 95 Monthly mean 850 and 200 mb wind vectors and divergence (convergence shaded) over the Indo-Pacific domain in the January 1973 - SOI phase. Wind vectors are in units of m s^{-1} with vectors of 1 cm length equal to 37 m s^{-1} and dashed lines in the 850 mb diagrams indicating the position of the (NET_{NH} and NET_{SH}). Divergence fields are in units of 10^{-6} s^{-1} at intervals of 5 units. Grey areas on the land masses at 850 mb indicate the distribution of relief.

Figure 96 Monthly mean 850 and 200 mb wind vectors and divergence (convergence shaded) over the Indo-Pacific domain in the January 1974 + SOI phase. Wind vectors are in units of m s^{-1} with vectors of 1 cm length equal to 37 m s^{-1} and dashed lines in the 850 mb diagrams indicating the position of the (NET_{NH} and NET_{SH}). Divergence fields are in units of 10^{-6} s^{-1} at intervals of 5 units. Grey areas on the land masses at 850 mb indicate the distribution of relief.

JAN 73 - SOI

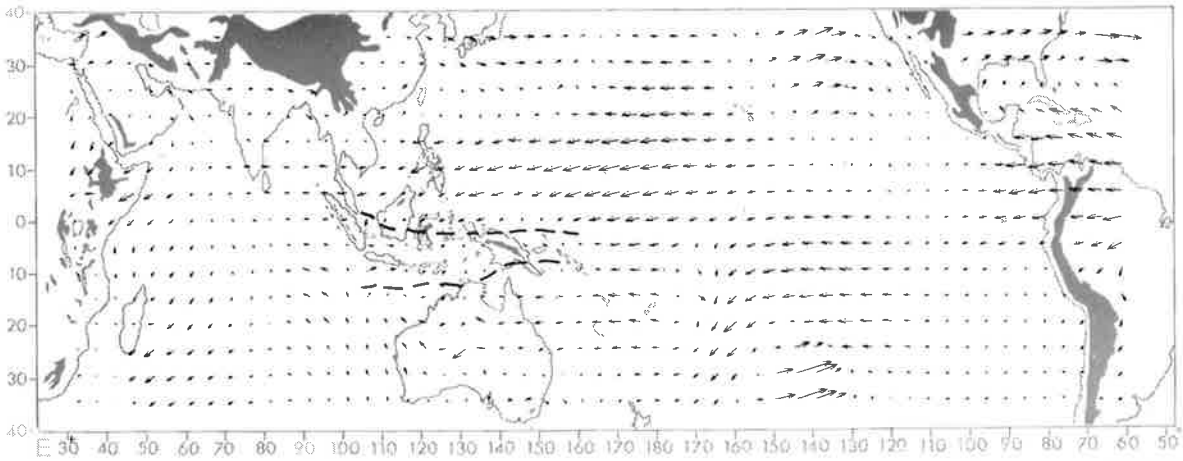

V 850

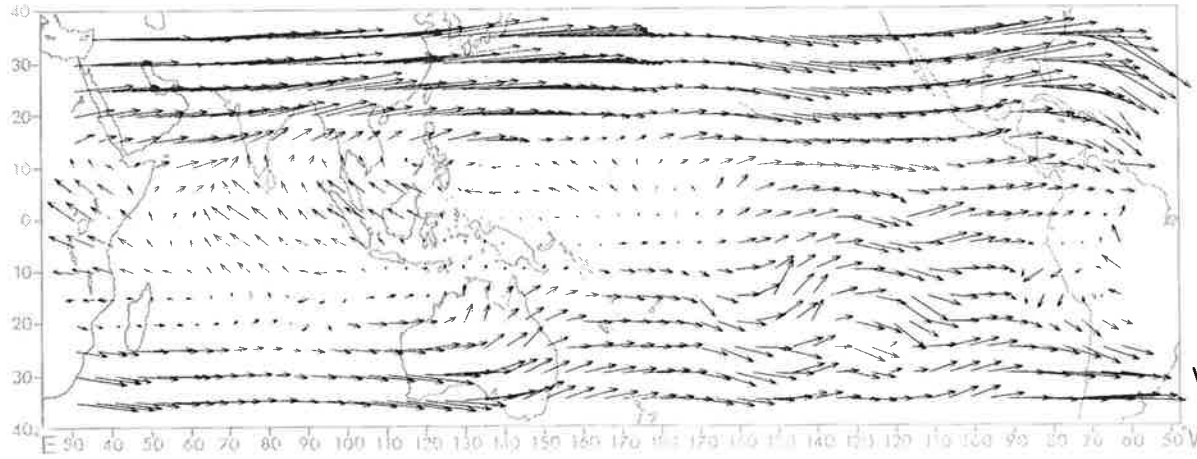

V 200

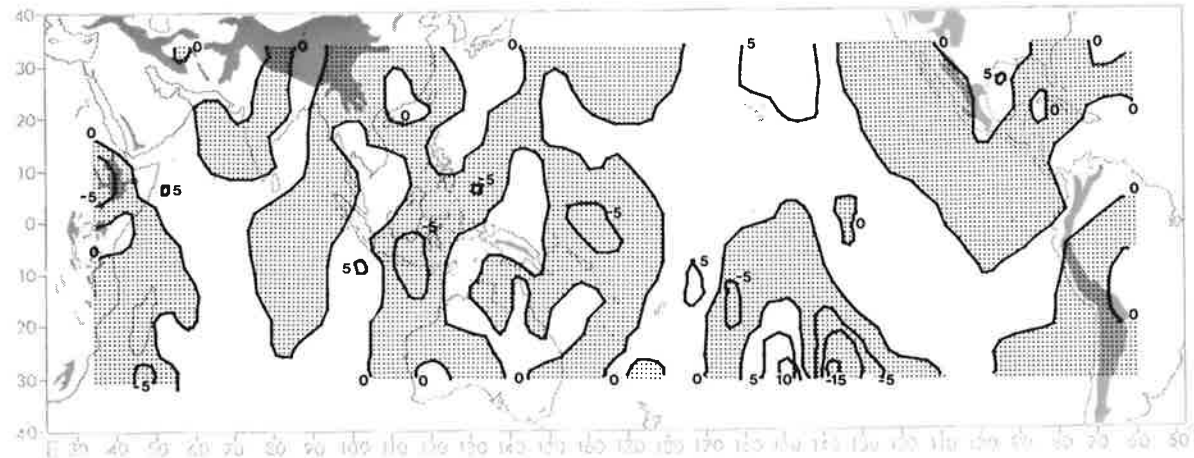

DIV 850

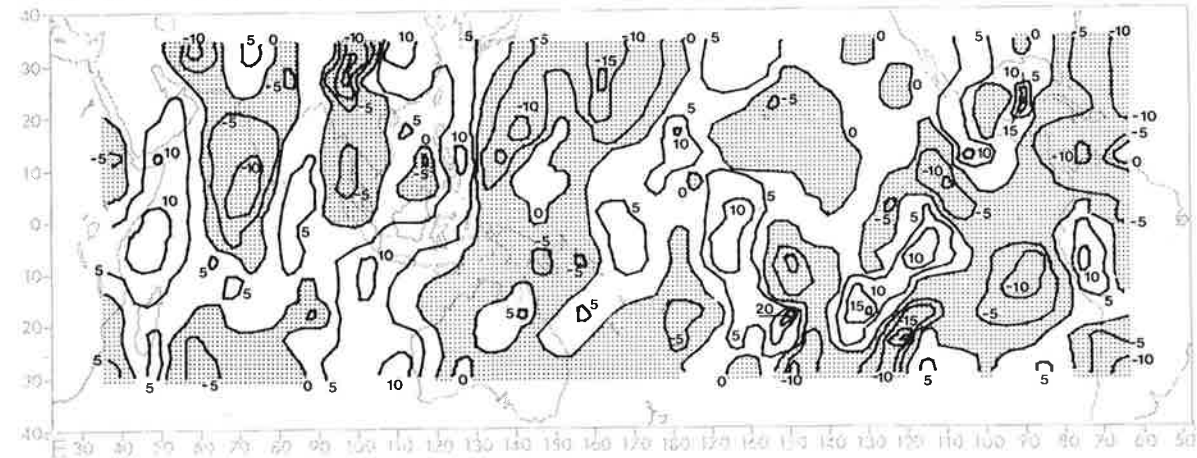

DIV 200

JAN 74 + SOI

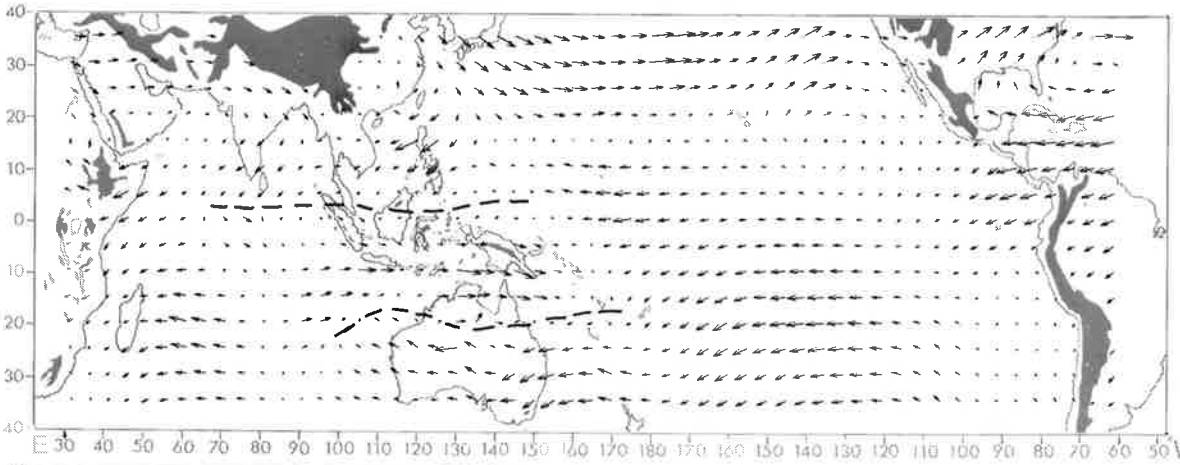

V 850

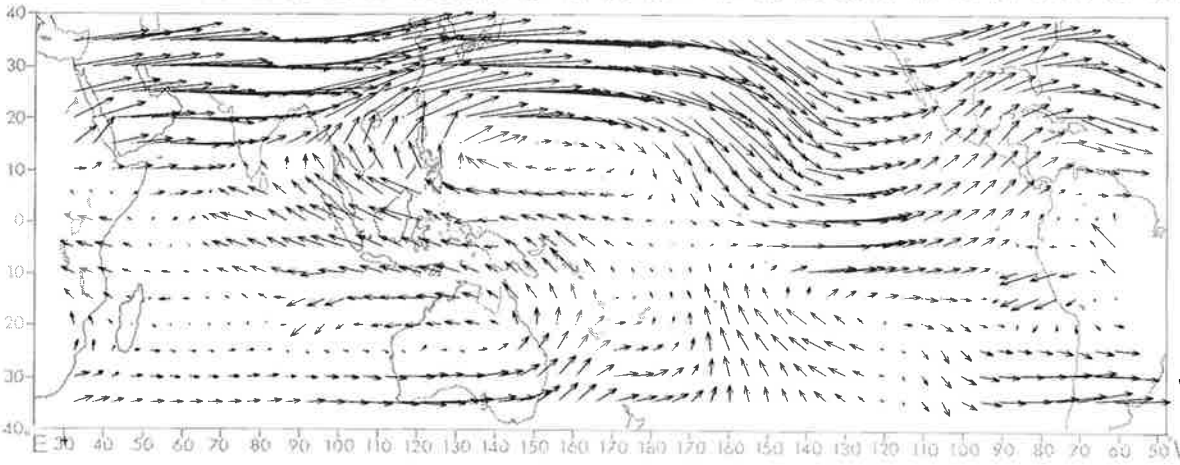

V 200

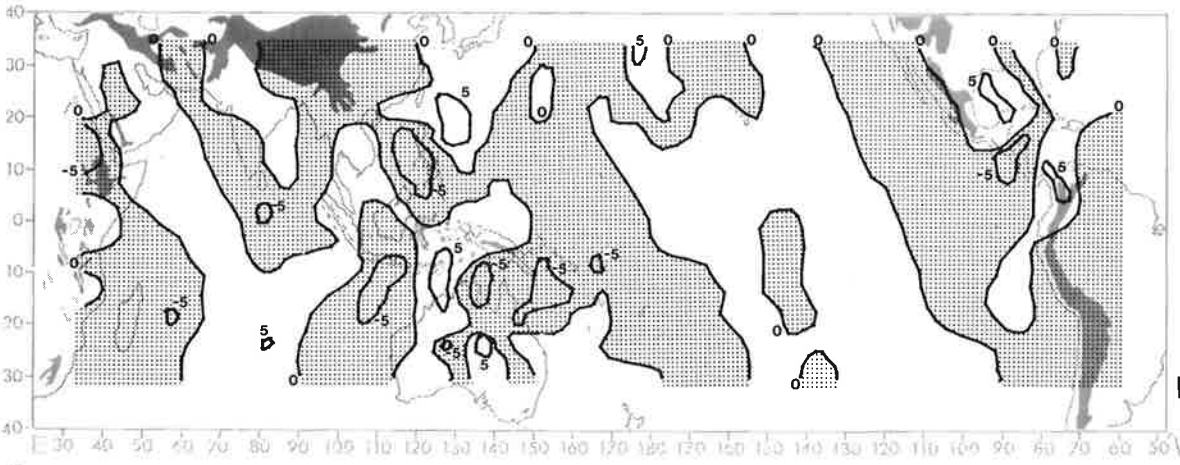

DIV 850

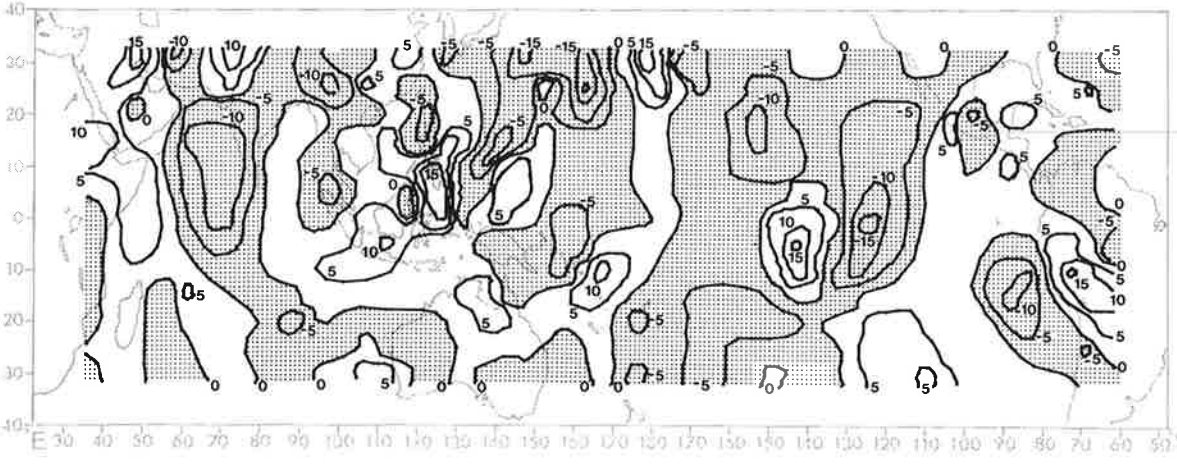

DIV 200

subcontinent in January 1973 (Fig.95). Coupled with 850 mb convergence, these areas seem to be the source of teleconnection extensions (Hobbs, 1975) that probably were responsible for the rainfall outbreaks across the Indian Ocean at this time (Rao *et. al.*, 1976). Certainly, they are related geographically to these extensive rainfall zones. Further south, the strong Southern Hemisphere jetstream in January 1973 seems to have promoted the expansion of an area of upper-level convergence that covers much of the midlatitude Indian Ocean.

To the east of the dateline and the regional domain, variations in circulation and divergence fields also indicate that large-scale changes in atmospheric features occur in January 1973 and January 1974. As in the western section, they share a close relationship with the findings in Rao *et. al.* (1976) and Barton (1983). Furthermore, they confirm that the tendency towards many localized teleconnection overturnings in January 1973 is a large-scale response.

At the 850 mb level, several pronounced circulation changes mark the January 1973 and January 1974 fields (Figs.95 and 96). Most evident is the development of a strong and distinctive anticyclonic cell over the Southern Hemisphere midlatitude Pacific in January 1973. Further north, strong flow in the Panama zone in January 1974 is allied with a similar increase in North American wind speeds and results in a strengthening of the anti-cyclone over the Gulf of Mexico. Increased westerly flow at Northern Hemisphere midlatitudes is notable across the entire eastern section of the hemisphere in January 1974. These changes would seem to reflect the recent attention by American researchers to the development of atmospheric anomalies over the United States during SOI extremes (Angell, 1981; Horel and Wallace, 1981).

During January 1974 (Fig.96), major changes in the 850 mb divergence fields revolve around the intensification of divergence over the Gulf of Mexico and Colombian region, and convergence in the intervening Panama zone. The intensification of marked convergence and divergence fields in the

Southern Hemisphere midlatitude Pacific follows the establishment of strong anticyclonicity in January 1973 (Fig.95). A major alternation in divergence/convergence conditions is found in the Northern Hemisphere mid-latitudes of the Pacific Ocean, with strong divergence in January 1973 giving way to convergence in January 1974 following the increased westerly regime in the latter month. Otherwise, the region is dominated by persistent convergence off the west coast of Mexico and over the western portion of South America, and divergence further to the west in both hemispheres.

By 200 mb, the circulation displays mid Pacific anomalies that conform to the findings of Arkin (1982). These anomalies are characterized by the presence of strong cyclonic flow associated with a pair of mid Pacific troughs in January 1974 (Fig.96) (a period of strong positive SOI). During January 1973 (weak negative SOI) (Fig.95) the troughs are only weakly defined. Obviously related to the above phenomenon is the variation in Northern Hemisphere winter jetstream intensity over the United States. Zonal isotachs (not shown) indicate that the jet contains maxima with wind speeds greater than 50 m s^{-1} in January 1973 but only in the order of 30 m s^{-1} in January 1974. The distinct Pacific troughing in the latter month is accompanied by a strong easterly jet maximum over the central equatorial Pacific. Anticyclonicity over South America is much the same in both months, although an increase in the strength of the Southern Hemisphere jetstream in January 1973 is in line with similar observations over the entire Indo-Pacific domain.

Upper-level divergence patterns are strongly influenced by the above circulation changes, to the extent that broad-scale convergence in January 1974 (Fig.96) replaces the localized divergence and convergence centres that mark the January 1973 situation (Fig.95). Certainly, the divergence distribution in the latter month again emphasizes the nature of negative SOI rainfall outbreaks over the PDZ. Further east, in the Americas, rainfall regimes in January 1974 are particularly enhanced by increased divergence

over central South America (Barton, 1983).

As a consequence of the above discussion, it would appear that teleconnection changes during SO/WC extremes both directly and indirectly involve large-scale atmospheric responses. To fully evaluate the strength of this assertion, it is necessary to examine the nature of circulation features over the Indo-Pacific domain during a number of SO/WC episodes. The following discussion attempts such an investigation, using SOI's (Troup, 1981; personal communication) to delineate SO/WC extremes. However, as will be evident in later discussions, this assumes that positive and negative SOI values (whether constructed from normalized area averages or two station differences in surface pressure or upper-level GPHs) provide an adequate measure of what has been seen to be a highly variable spatial-temporal phenomenon. In fact, as Rasmusson and Carpenter (1982) stress, the SO/WC cannot be adequately resolved in terms of standing fluctuations.

(ii) Monthly Mean 850 mb and 200 mb Divergence and Wind Vectors : Composites of January and February Southern Oscillation Index Extremes from 1957-81

An examination of Troup's abbreviated Southern Oscillation Index (Troup, 1981; personal communication) reveals that there were a number of large positive and negative index values during the peak of the Australian summers (January and February) from 1932-81. In attempting to analyse the pattern of upper air dynamics during summer months which experienced high and low SOI extremes, the above period had to be shortened to allow for the fact that the number of upper air and upper wind stations capable of recording data above approximately 600-700 mb was minimal prior to 1957. Therefore, it was decided to construct only composites of summer months with positive and negative SOI's during the period from 1957-81.

Rather subjective SOI cut-off levels of + and - 15 are used to delineate strong and weak SO/WC episodes, mainly on the grounds that SOI values of + and - 10 are too low as limits for strong and weak SO/WC phases when values of + 23 and - 32 occur during the period (Pazan and Meyers, 1982,

used other SOI values of + and - 2, while Arkin, 1982 used + and - 0.65). There are five peak summer months with SOI greater than or equal to + 15 (Januarys 1962, 1967 and 1974 and Februarys 1971 and 1974) and six peak summer months with SOI greater than or equal to - 15 (Januarys 1958 and 1959 and Februarys 1959, 1970, 1973 and 1978).

As in the previous discussion, fields of 850 mb and 200 mb divergence and circulation (wind vectors) are evaluated over the Indo-Pacific domain. These display the six months of weak SOI phase and the five months of strong SOI phase as negative (- SOI) and positive (+ SOI) composites (Figs.97 and 98).

At 850 mb, circulation in the Indo-Pacific domain is generally more intense in the + SOI composite (Fig.98). However, a more accurate appraisal of the two extremes can be found by an investigation of localized variations in circulation intensity and displacement (as noted by Van Loon and Madden, 1981, for surface pressure patterns during SO/WC extremes). The majority of these changes involve anticyclonic circulation at higher latitudes in both hemispheres. In the Northern Hemisphere, this contrast is manifest by increases in anticyclonicity over the Gulf of Mexico, India and Arabia between negative and positive composites. Overall variations in the NPA tend to be less obvious, although observed displacements in the wind field probably give rise to changes in the structure of this feature. Across the Southern Hemisphere the above tendencies are not as distinct. Although midlatitude South Pacific anticyclonic circulation increases in intensity during + SOI phases (Fig.98), this is not as definite in the midlatitude Indian Ocean, while, over Australia the opposite occurs, with anticyclonicity being stronger in - SOI periods (Fig.97). Major increases in atmospheric flow occur in the central-western equatorial Pacific (Pazan and Meyers, 1982) and Panama zone. In fact, as noted in Egger *et. al.* (1981), although northeast trade wind flow over the former area is generally stronger in the positive composite, it is still strong but directed equatorward over the western Pacific in the negative composite. This would seem to support the

Figure 97 Monthly mean 850 and 200 mb wind vectors and divergence (convergence shaded) over the Indo-Pacific domain in the - SOI composite (January 1958 and 1959 and February 1959, 1970, 1973 and 1978). Wind vectors are in units of m s^{-1} with vectors of 1 cm length equal to 37 m s^{-1} and dashed lines in the 850 mb diagrams indicating the position of the (NET_{NH} and NET_{SH}). Divergence fields are in units of 10^{-6} s^{-1} at intervals of 5 units. Grey areas on the land masses at 850 mb indicate the distribution of relief.

Figure 98 Monthly mean 850 and 200 mb wind vectors and divergence (convergence shaded) over the Indo-Pacific domain in the + SOI composite (January 1962, 1967 and 1974 and February 1971 and 1974). Wind vectors are in units of m s^{-1} with vectors of 1 cm length equal to 37 m s^{-1} and dashed lines in the 850 mb diagrams indicating the position of the (NET_{NH} and NET_{SH}). Divergence fields are in units of 10^{-6} s^{-1} at intervals of 5 units. Grey areas on the land masses at 850 mb indicate the distribution of relief.

COMPOSITE - SOI

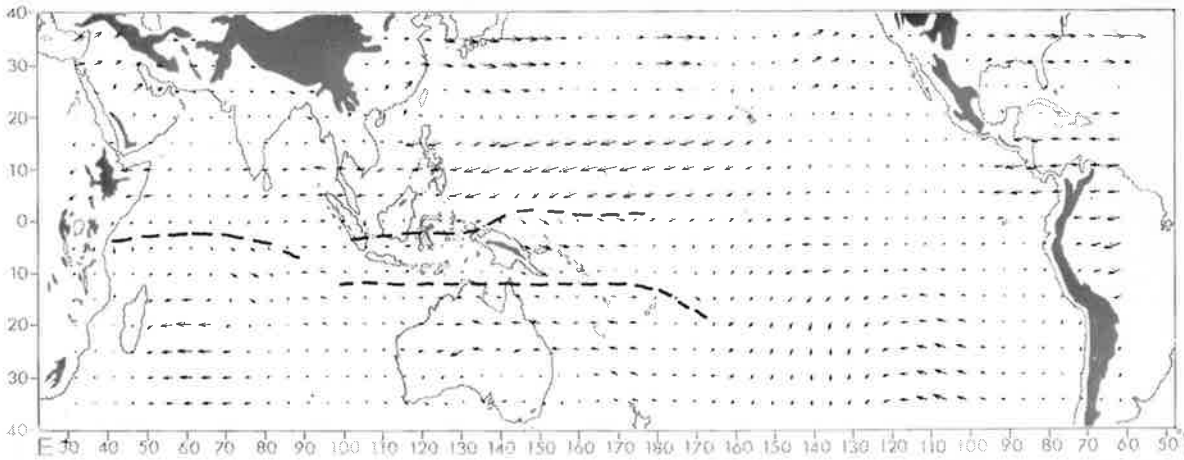

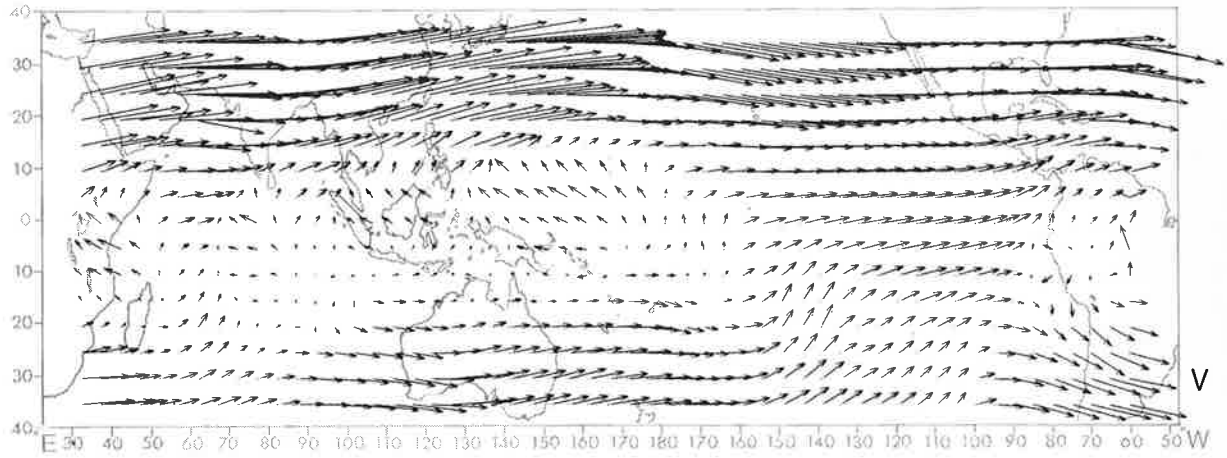

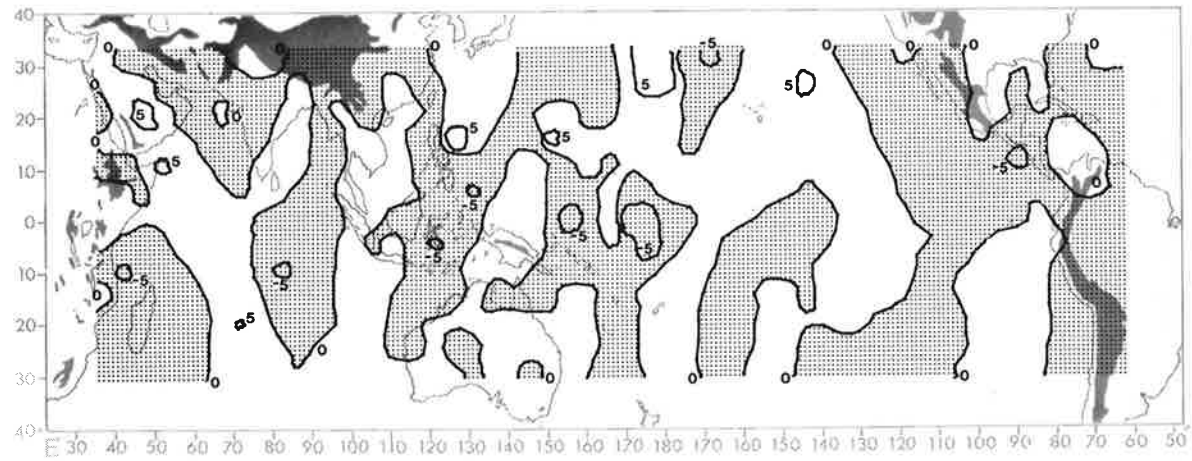

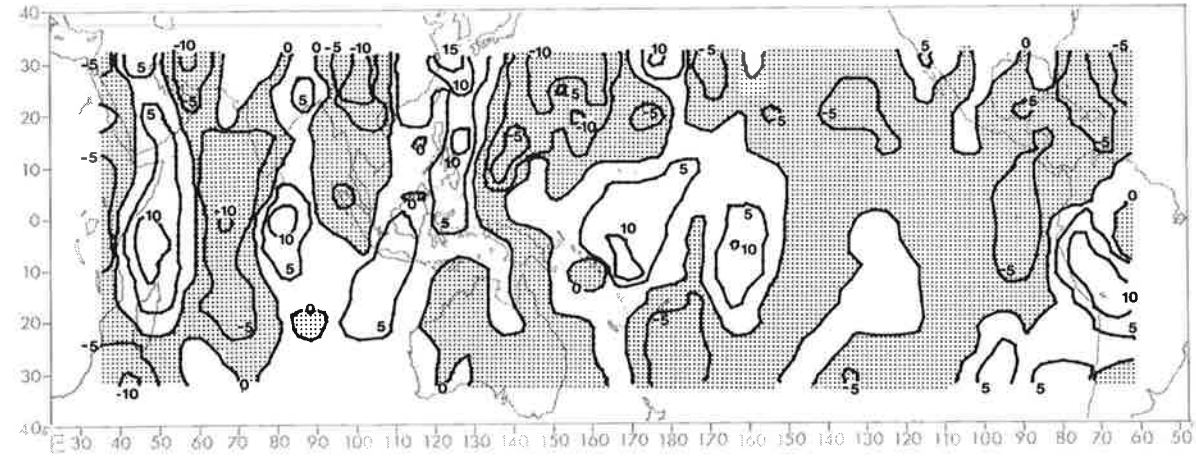

observation that the NET_{NH} (eastern section) is most intense during the latter period. The Panama zone would appear to be influenced by slightly stronger flow in + SOI extremes.

Cyclonic changes revolve around displacements and intensity changes in the NETs (NET_{NH} and NET_{SH}). As in January 1974 (Fig.96), the positive composite (Fig.98) is marked by a southward displacement in the NET_{SH}, there being some 5° latitude difference between its location in + and - SOI extremes. This feature is somewhat stronger in the positive composite, but it does not extend out into the southwestern Pacific as it does in - SOI periods (perhaps being related to the SPCZ and cyclone pairs observed in Keen, 1982). The NET_{NH} is only minimally displaced over Asia between negative and positive composites. However, to the east and west of the 'maritime continent' there are notable changes. In the east, as noted above, the NET_{NH} (eastern) is most pronounced in - SOI periods (Fig.97) when the northeast trades direct rapid flow towards the equator (also observed in Egger *et. al.*, 1981 and Pazan and Meyers, 1982). West of the Indonesian longitudes the NET_{NH} extends into the western Indian Ocean in the positive composite, with a weak and disjointed NET appearing in Southern Hemisphere near-equatorial longitudes in the negative composite. As in the January 1974 situation (Fig.96), the NET_{NH} is strongest in its western section during + SOI extremes. No doubt this feature owes much to increased Indian anticyclonicity and marginally stronger cross-equatorial flow over Asia at 850 mb during the above extreme.

At the 200 mb level there are major changes in circulation features. Most notable is the marked increase in the intensity of the NPA in + SOI phases (Fig.98). This is associated with a sharp increase in the speed of the easterlies over the 'maritime continent' and the eastern Indian Ocean. However, there do not appear to be major changes in the speed of the winter jetstream across Asia. As in January 1974, a pronounced variation in mid Pacific troughing occurs in both hemispheres. The swing from pronounced cyclonic vortices straddling the equator during + SOI extremes to far weaker cyclonic tendencies in - SOI episodes follows the anomaly sequence noted

in Arkin (1982). Over Australia the anticyclonic cell is displaced some 5°-10° further south in the positive composite (Fig.98) but still occupies a westerly location with respect to the Australian continent. Nevertheless, the cell is notably displaced to the northwest of Australia during - SOI phases (Fig.97). Coincidental with this is the observation of anticyclonic flow in the central western Pacific near the dateline. Such a feature is not evident in the positive composite, which suggests that it may play an integral part in the development of upper-level divergence and thus provide an impetus for PDZ rainfall producing mechanisms.

Variations in Southern Hemisphere anticyclonicity over Africa and South America are not as pronounced, although there is an indication of increased sub-tropical jetstream intensity in the former region during - SOI phases. Interestingly, there is not the definite increase in Southern Hemisphere jetstream speed that was observed between the months of January 1973 and January 1974 (Figs.95 and 96), although easterly flow is certainly displaced 5°-10° further north over much of the hemisphere in the negative composite. Rogers and Van Loon (1982) suggest that associations at higher latitudes are only prominent during SOI extremes. It is also possible that some of this difference could be attributed to the fact that the sampling of composite data from January and February tends to lessen the influence of changes in the January location of the jetstream due to monsoon onset characteristics. Arkin (1982) shows a correlation of + 0.2 between 200 mb zonal anomalies and a Tahiti-Darwin SOI. Other features that occur in the January 1973/74 comparison and in the composites, are the stronger zonal flow over the United States in - SOI phases and the equatorial mid Pacific westerly wind maximum in + SOI phases.

The divergence fields at 850 mb and 200 mb in January 1973 and 1974 (Figs.95 and 96) provide direct evidence of teleconnection changes on broad spatial scales. This is also true in the negative and positive composites (Figs.97 and 98). The most marked variation in 850 mb and 200 mb couplings occurs across the PDZ where pronounced vertical ascent in the central western

region in the positive composite is noticeably weakened in the negative composite. Certainly, there is a complete reversal in coupling, and thus teleconnection fields, in the central Pacific from - to + SOI phases.

Over the 'maritime continent' there is evidence of marginally stronger vertical ascent (especially since convergence at the 850 mb level is more intense across Indonesia) in + SOI episodes. However, vertical ascent in both composites is primarily located in areas to the west (Indonesia) and east (central western Pacific) of New Guinea. Perhaps this again testifies to the observations of Tsuchiya (1970), Nicholls (1973), Musk (1976), Barry (1978) and Fleer (1981) who suggest that New Guinea is generally in a transitional zone with respect to the SO/WC. One other interesting aspect of the South East Asian region is the persistence of subsidence, extending from Vietnam to Malaysia and Sumatra, and weak vertical ascent in the vicinity of Taiwan and the South China Sea, during both composites.

The Australian region is also little changed from - to + SOI episodes (Figs.97 and 98). There is marginally stronger upper-level divergence across the 'top end', Gulf of Carpentaria and Cape York in the positive composite, but this is only coupled with a small area of weak 850 mb convergence. In fact, evidence of an upper-level 'breakdown' in the SO/WC is strongest in the negative composites (with convergence enveloping much of Australia), and continues to be quite dominant in + SOI episodes. Certainly, there is not the marked development of a major vertical overturning across northern Australia as there is in the January 1974 + SOI extreme (Fig.96).

To the west of the regional domain, major teleconnection changes occur in the vicinity of the Malagasy Republic and east coast of Africa, and in the equatorial Indian Ocean. In the former region, enhanced upper-level divergence and lower-level convergence suggest that vertical ascent is promoted in this area during - SOI phases. In the positive composite, the above teleconnection source region is still observed but it is noticeably weaker. Further to the northeast, in the central equatorial Indian Ocean, vertical ascent follows a similar pattern to that noted over East Africa.

Here, stronger upper-level divergence in the negative composite is coupled with persistent 850 mb convergence (perhaps slightly more extensive in the positive composite) to promote an enhanced teleconnection source. From the above it would seem that - SOI episodes (Fig.97) are marked by rainfall outbreaks in the Indian Ocean. However, they are not as marked nor as dramatic as those in the PDZ where large-scale subsidence and ascent alternate with SOI extremes.

In the region of the Americas, the most notable changes in teleconnection sources and sinks occur in the Panama zone and over Colombia and central South America. The two former regions show contrasting divergence and convergence couplings during the positive composite, with the Panama zone experiencing localized vertical ascent and Colombia being under the influence of strong subsidence. In the negative composite, only weak subsidence is seen to persist over Colombia. Central South America shows the least change of any of the three regions, with strong upper-level divergence and weak lower-level convergence in both composites.

From Figures 97 and 98 it would seem that strong + and - SOI events are most marked by teleconnection changes in the central to western Pacific (Egger *et. al.*, 1981; Arkin, 1982; Pazan and Meyers, 1982). Some enhancement of the regions of vertical ascent occurs across the Indian Ocean as far as Africa in - SOI phases, but most other variations in the Indo-Pacific domain are weaker. Over Australia, the situation is particularly interesting because divergence and convergence couplings suggest that there is little change in teleconnection fields during SO/WC extremes. This is contrary to the evidence presented in the 1973-77 period (Section 3.1) and in the January 1973 and 1974 Indo-Pacific fields (Figs.95 and 96) and supports the inference by Arkin (1982) that anomalies outside of the equatorial Pacific are often probably seasonally dependent. The following discussion attempts to explore this discrepancy and to examine the whole question of SOI's and SO/WC dynamics.

3.3.2 Upper Air Data over Australia : January 1965-78

This section examines the longer-term association between circulation features, SOI's and the SO/WC during Southern Hemisphere summer monsoon seasons. In particular, it provides the basis for an evaluation of circulation elements (dynamic signatures) that appear to be indicative of SO/WC extremes during the 1973-77 Australian summers (Sections 3.1 and 3.2). Inherent in such an evaluation, and especially pertinent to the previous discussion, is the closer examination of SOI's and upper air dynamics, and thus the choice of months used in the positive and negative composites (Figs.97 and 98).

Fields of monthly mean streamfunction and velocity potential are calculated at 850, 700 and 200 mb levels over the regional domain and are presented as spatio-temporal and vertically overlain (paired with remotely-sensed total cloud cover sets) sequences respectively (Figs.99 and 100). However, the above analysis only focuses on the period from 1965-78 due to the fact that :

a) Australian upper air and upper wind stations lack observations from high tropospheric levels prior to the mid 1950's (Streten, 1982)

b) the distribution of tropical and sub-tropical data stations in the regional domain is poor before the early 1960's

c) consistent information on cloud cover from meteorological satellites was not achieved until the mid to late 1960's

d) the most complete cloud cover set (a combination of Sadler *et. al.*, 1976 and Shideler and Sadler, 1979) provided no information beyond 1978

Due to time limitations, this analysis is restricted to the compilation of only one month's data sequence. The month of January was chosen because it contain the most variability in circulation and SO/WC features during the discussion of events in 1973-77 (Section 3.1).

However, a consequence of the above is that it was not possible to

delineate the finer details of vertical motion over Australia. In an effort to overcome this problem, a sequence of monthly mean divergence overlays (850, 700 and 200 mb) is meshed with continental isohyets (Fig.101). This permits an easy appraisal of the relationship between rainfall patterns and more localized, time-average teleconnection fields. Unfortunately, the sequence is cut short at 1976 due to the termination of Bureau of Meteorology charts showing monthly mean isohyets over Australia. It should also be noted that the grading from streamfunctions and velocity potentials to divergence fields includes a shrinkage of scale from regional to local conditions. This in itself illustrates some of the complexities and interactions of scale involved in teleconnection patterns.

(i) Monthly Mean Streamfunction and Velocity Potential Sequences (850, 700 and 200 mb) : January 1965-78

In Sections 3.1 and 3.2, aspects of several Australasian circulation features during the 1973-77 Southern Hemisphere summers are cited as possible dynamic signatures of SO/WC extremes. Basically, they revolve around the location, intensity and vertical depth of the NETs (NET_{NH} and NET_{SH}), the NPA, anticyclonicity in the Australian region (particularly at upper levels) and the 'breakdown' of the upper-level divergence arm across eastern Australian and New Guinean longitudes. The following discussion is intended to provide a more comprehensive evaluation of the signature value of the above features, the nature of circulation and teleconnection patterns and their relationship to Troup's SOI (Troup, 1981; personal communication) over 14 Januarys (1965-78) (Figs.99 and 100).

NET_{NH} and NET_{SH} activity at 850 mb and 700 mb levels is quite variable during the 1965-78 period (Fig.99). In the Northern Hemisphere the NET has an easterly focus that persists for about 86 per cent of the period. Only in Januarys 1971, 1974 and 1976 is there any evidence of a pronounced westerly centre, with both Januarys of 1971 and 1976 displaying dual east and west centres. In fact, the westerly centre is dominant only in Januarys of

Figure 99 Monthly mean streamfunction fields at 850, 700 and 200 mb in January 1965-78. Fields are in units of 10^5 m^2 s^{-1} (850 and 700 mb) at intervals of 1 unit and in units of 10^6 m^2 s^{-1} (200 mb) at intervals of 5 units. Dashed lines at 850 and 700 mb levels indicate the position of the (NET_{NH} and NET_{SH}) and the SOI values on the right-hand side of the diagram are those of Troup.

850 mb	700 mb	200 mb	SOI
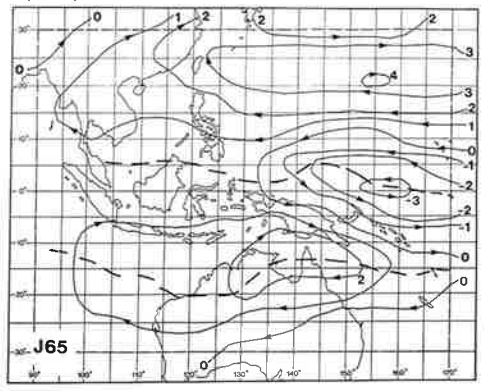 J65	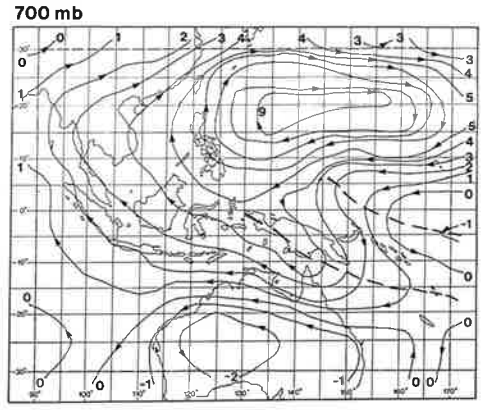	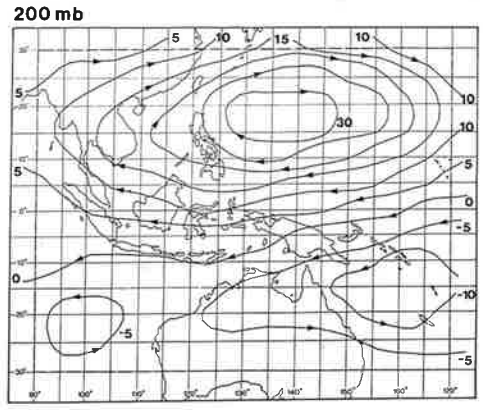	-5
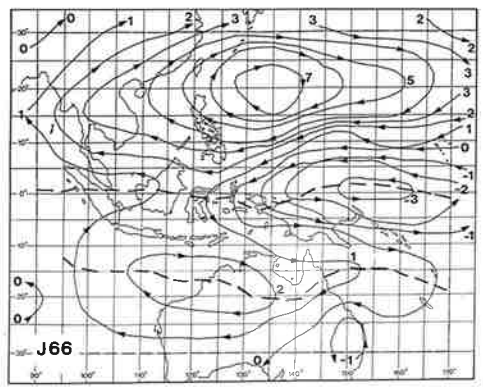 J66	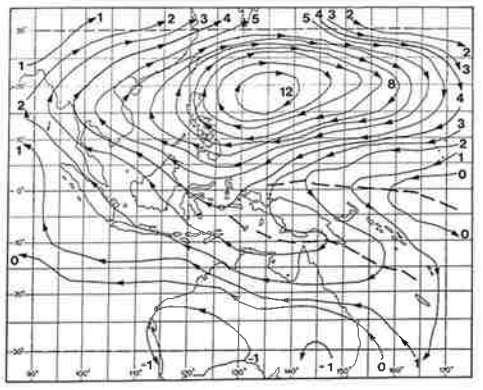	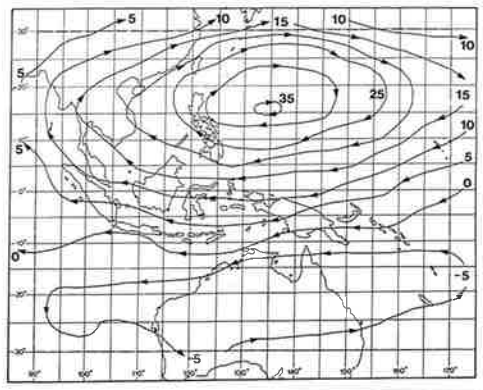	-13
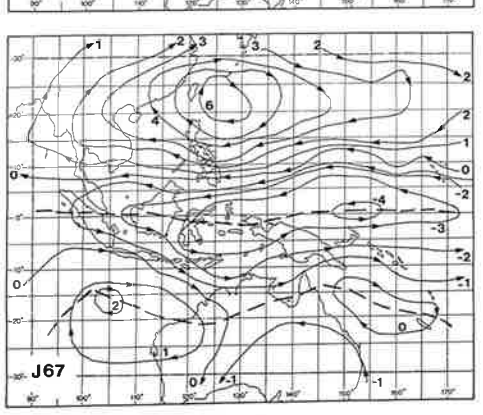 J67	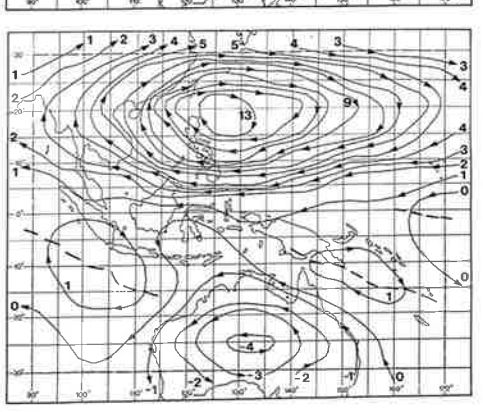	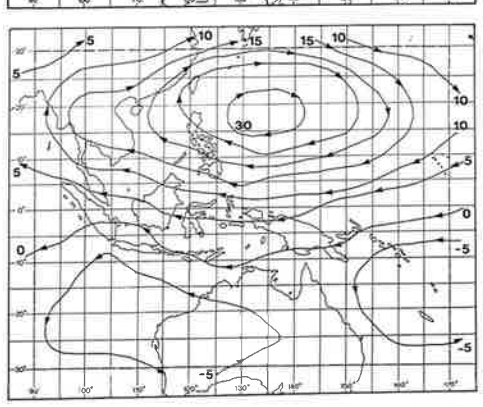	+15
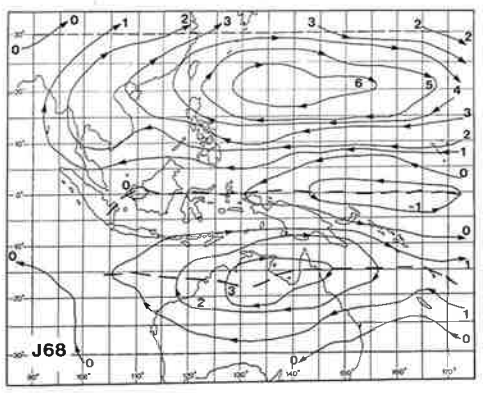 J68	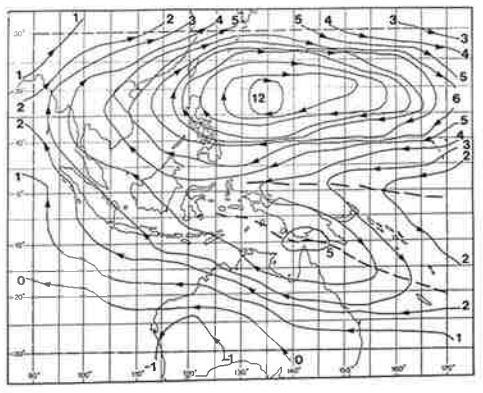	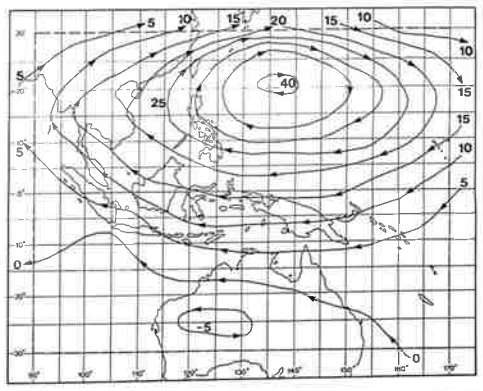	+4
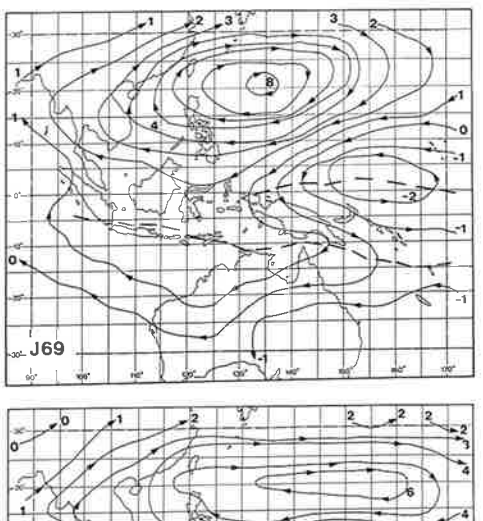 J69	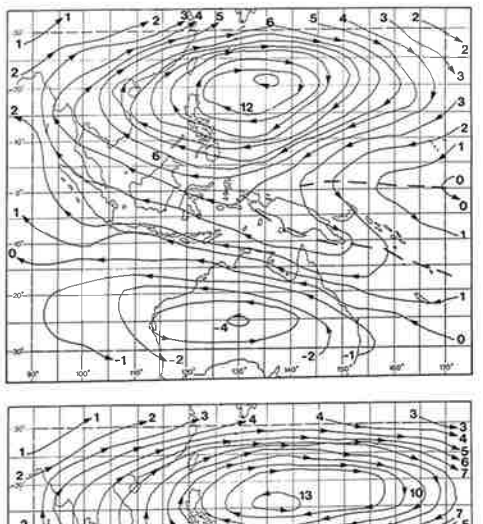	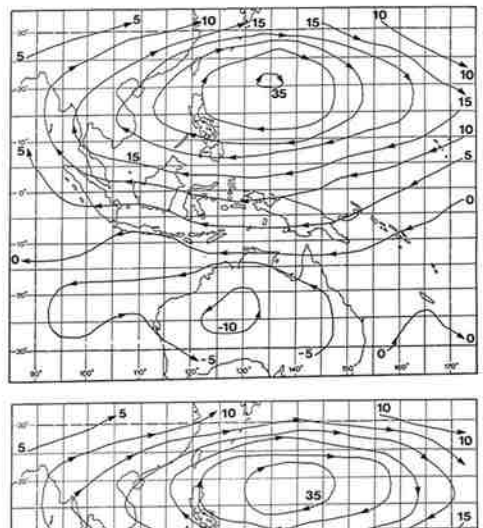	-15
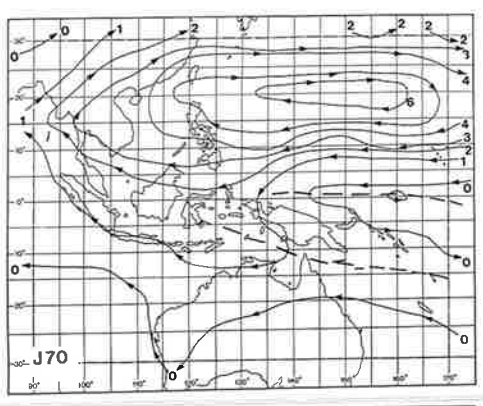 J70	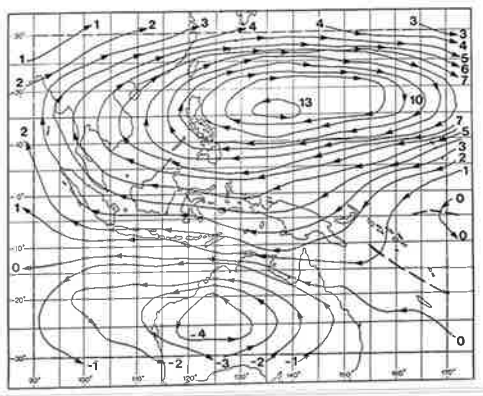	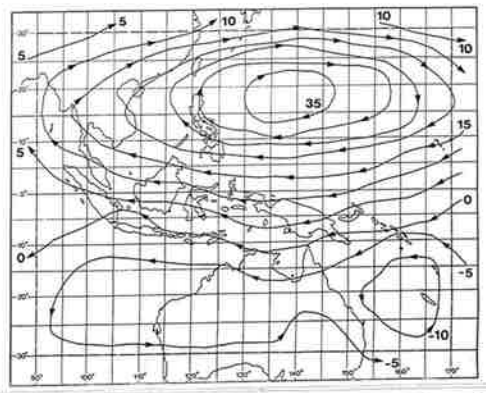	-12
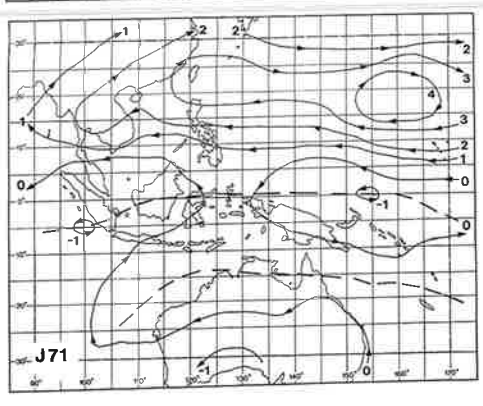 J71	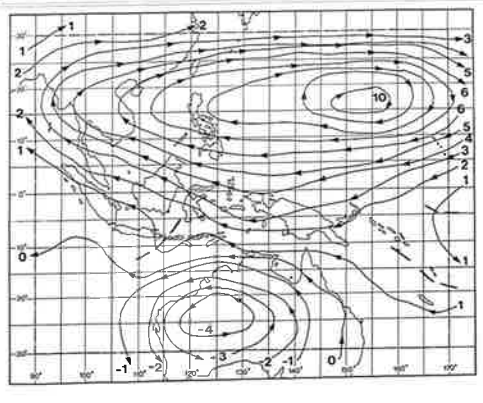	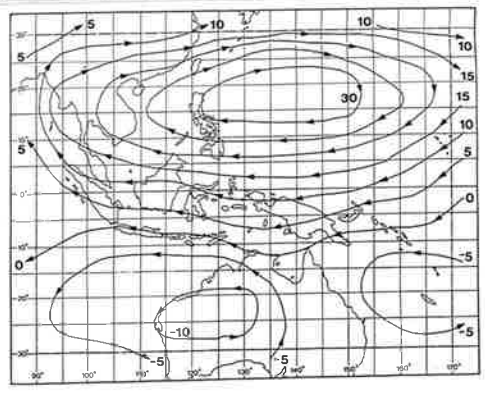	+2

	850 mb	700 mb	200 mb	SOI
J72	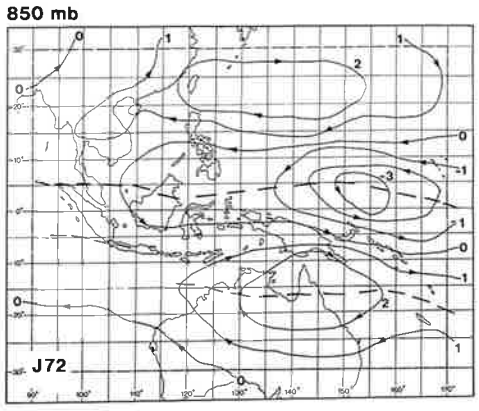	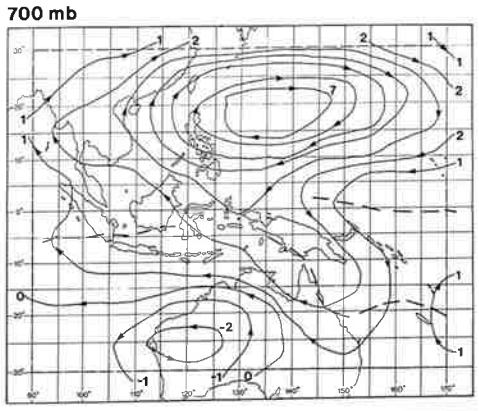	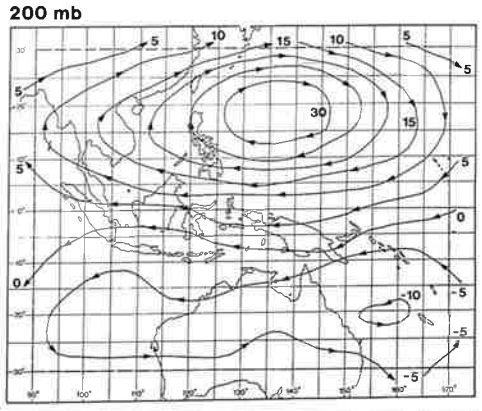	+3
J73	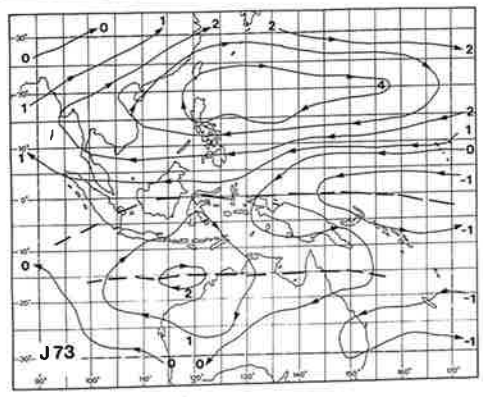	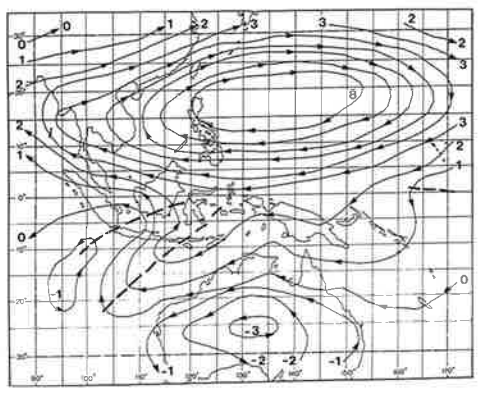	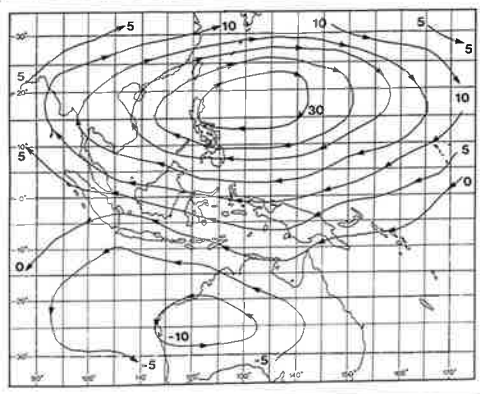	-4
J74	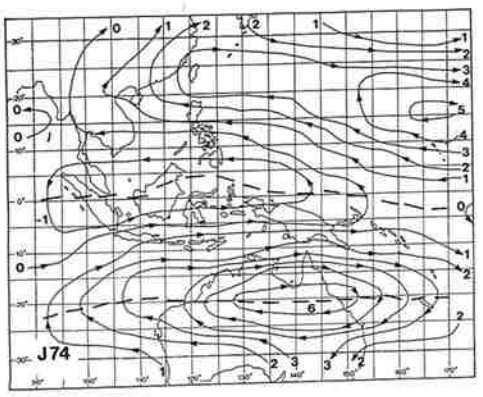	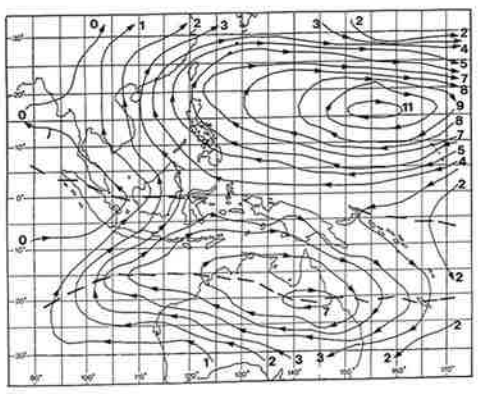	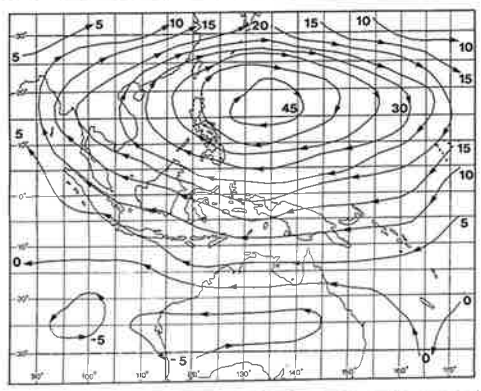	+23
J75	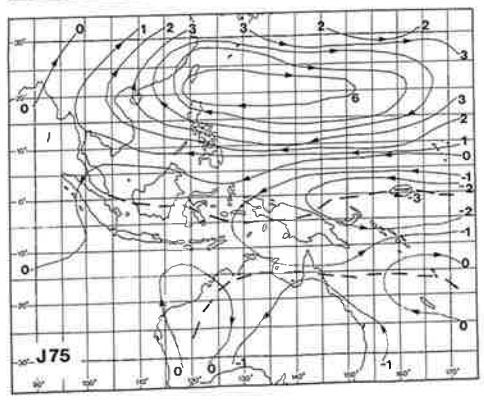	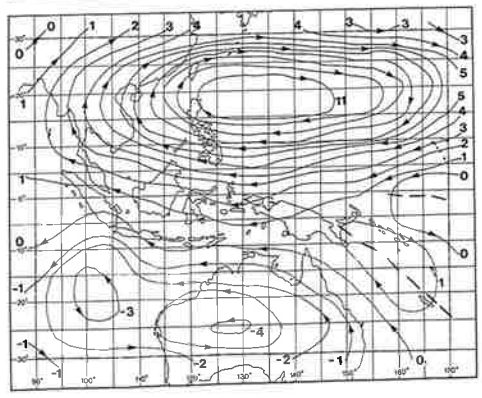	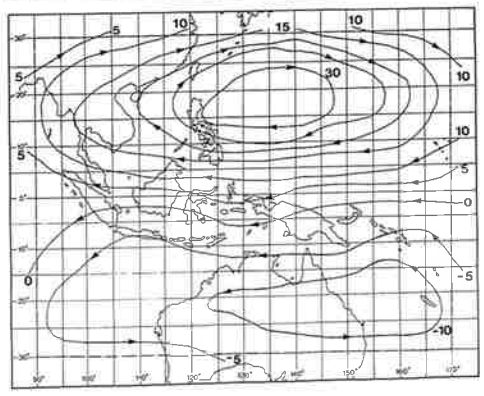	-8
J76	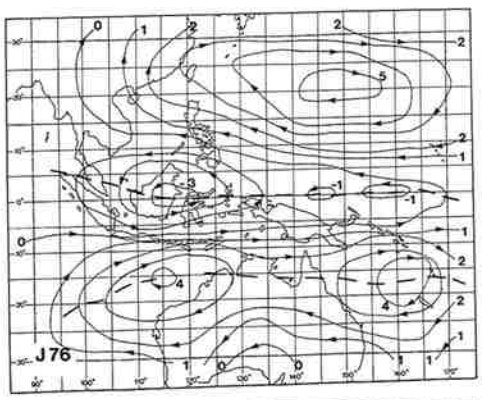	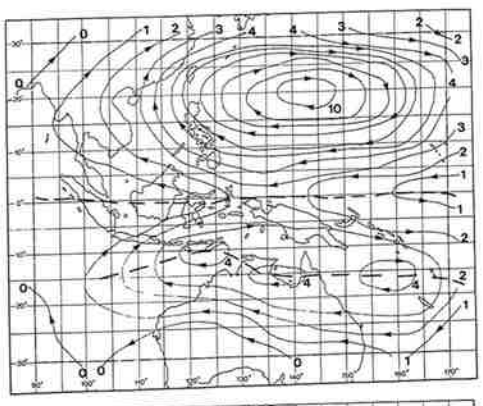	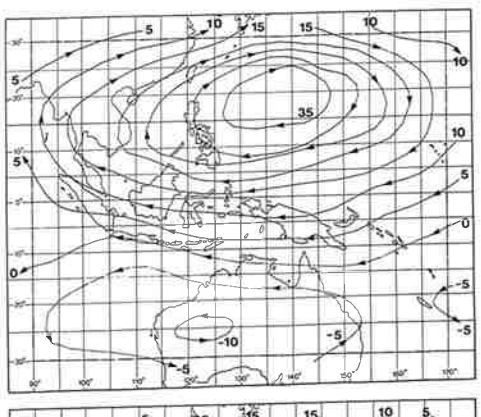	+12
J77	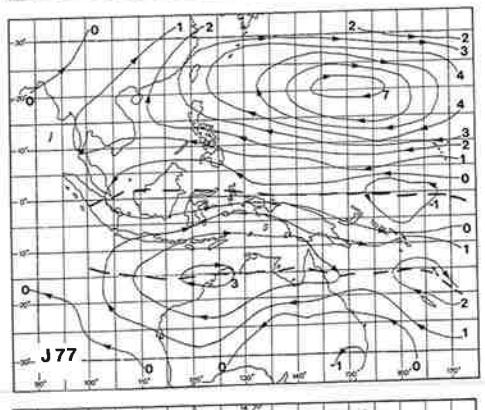	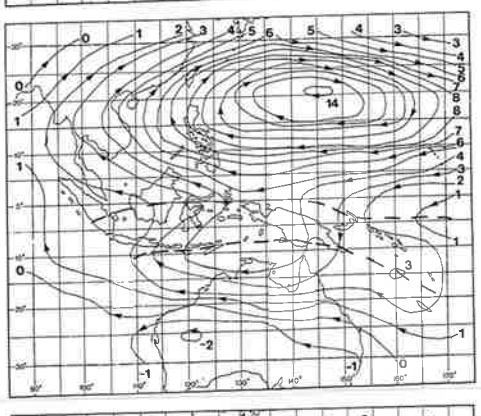	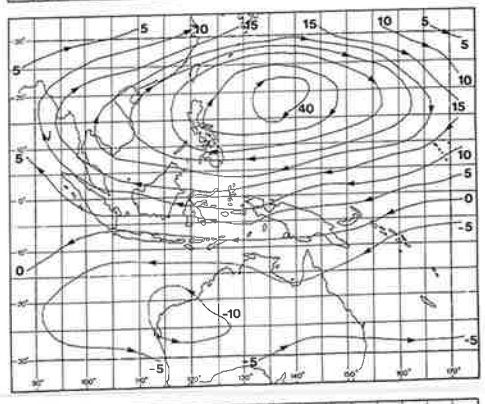	-5
J78	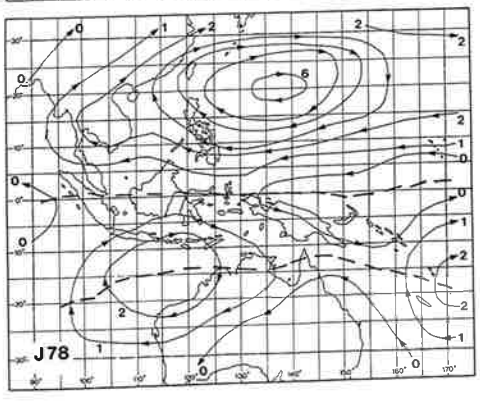	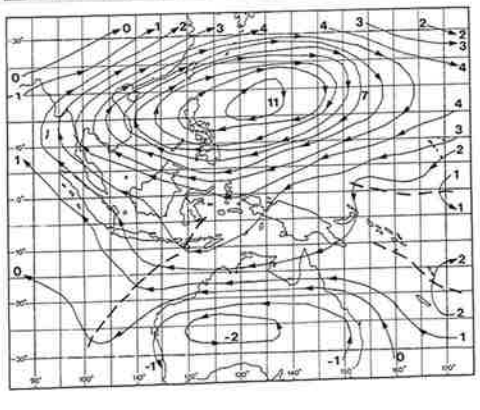	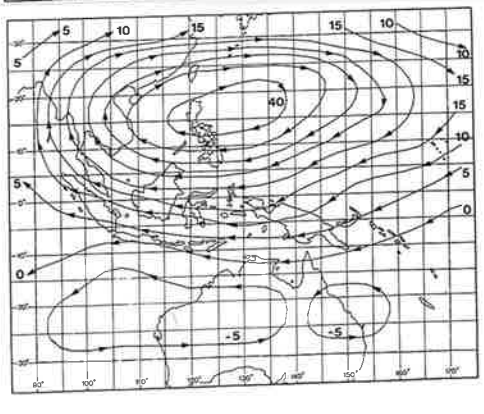	-4

1974 and 1976, the two months of strong monsoon activity over northern Australia. Throughout the period, the most intense circulation in the NET_{NH} (eastern section) is confined to the 850 mb level with particularly active phases prominent in Januarys 1965, 1966, 1967, 1972 and 1975. Interestingly, there is little latitudinal displacement of the NET_{NH} at the 850 mb level and insufficient spatial extent to judge this at 700 mb.

Over the Southern Hemisphere, the NET displays greater variability than its Northern Hemisphere counterpart. Only in regard to its vertical depth is it seen to be particularly persistent, with 70-85 per cent of the period being marked by closed cyclonic circulation at 850 mb giving way to anticyclonic flow at 700 mb. In fact, only in the 'wetter' Australian monsoon months of Januarys 1968, 1974 and 1976 is the NET_{SH} still strong at 700 mb across the continent. However, the NET_{SH} is highly variable in its location although periods of both strong circulation and southerly displacement of the NET_{SH} are rare. In the opposite sense, marked northerly displacement of a weak NET_{SH} is only observed in Januarys 1969 and 1970. On the whole, moderately developed NET_{SH}s over the continent at 850 mb are generally tilted equatorward in the vertical plane. By 700 mb the NET_{SH} is usually in the form of a weak trough line, oriented northwest to southeast and located parallel to, and immediately south of, the New Guinea coast. Januarys 1967, 1971, 1972, 1973 and 1978 display a 700 mb NET_{SH} to the northwest of the continent. In most cases the trough is oriented northeast to southwest across Indonesian longitudes, with both northwest and northeast NET_{SH} locations at 700 mb in Januarys 1967, 1971, 1972 and 1978. The January 1967 case is perhaps slightly different in that the 700 mb NET_{SH} is still associated with a cyclonic cell over the Indian Ocean and south of Indonesia.

Anticyclonicity at all three levels is a particularly prominent feature in both hemispheres during the Januarys from 1965-78 (Fig.99). At 850 mb it is a persistent element over the North Pacific, showing a tendency to vary most noticeably in a longitudinal sense. In Januarys 1965, 1971, 1974, 1976 and 1977, the NPA is distinctly displaced into more easterly longitudes,

when compared to its westerly position in other years. However, there does not appear to be any noticeable change in intensity of circulation associated with such variations. By 700 mb, such longitudinal displacements seem to be restricted to January 1971 and January 1974. It is of interest to note that both of these years display westerly NET_{NH} centres (January 1974 being the stronger), but are totally different in terms of NET_{SH} activity. This would appear to quash any suggestion that marked easterly displacements of the NPA are directly associated with increased NET_{SH} activity and monsoonal processes over northern Australia. As is the case with 850 mb there are apparently no distinct intensity changes related to NPA locations.

The 200 mb situation presents a pattern that is little better in terms of signatures. In all cases, the NPA is centred between 120°E and 150°E but varies far less in latitude. There are four Januarys (1968, 1974, 1977 and 1978) when it is particularly strong, although these do not relate decisively to sequences of either SO/WC, SOI or northern Australian monsoon extremes.

In the Southern Hemisphere the pattern of anticyclonicity in the Australian region would appear to be more promising. Yet, as in the Northern Hemisphere, this is not quite true of the lower levels of the atmosphere. Certainly, it would seem that the converse of a deep NET_{SH} (cyclonic to 700 mb) is the type of deep Australian anticyclone which occurs in Januarys 1967, 1969, 1970, 1971 and 1975. However, this does not present a concise pattern with regard to SOI or SO/WC situations.

At 200 mb, there is evidence that anticyclonic patterns may be more distinct. The Januarys of 1966, 1969, 1973 and 1977 are coincident with the four most prominent El Niño phases noted in Quinn *et. al.* (1978), while January 1978 would qualify according to Troup's SOI. Of these five periods, Januarys 1969, 1973 and 1977, and to a lesser degree 1978, show that the Australian anticyclone is strong and has a focus over the west-central region of the continent. Therefore, it would seem that the above feature may have an affinity with weak SO/WC phases, if not always distinct - SOIs.

Nevertheless, the circulations in January 1971 and January 1976 alone would cast some doubt on the west to northwest displacement concept. What seems more reasonable is that Januarys 1969, 1973 and 1977 are the only months in the period when the Australian upper anticyclonic pattern has one distinctly intense centre that is displaced to the west-northwest of the continent.

At the other extreme are weak southerly-displaced Australian anticylonic cells. However, this observation also needs qualification because it applies particularly to the Januarys of 1967, 1968 and 1974. Of these months, only January 1967 and January 1974 are associated with high + SOI's and, as such, are included in the positive composite (Fig.98). Furthermore, January 1976 is somewhat of an enigma, in that Australian monsoonal activity is high and the upper anticyclone is strong and displaced to the west at 25°S. It would seem that this signature is also incompatible with SOI extremes, despite its prevalence in the positive composite.

As a consequence of the above discussion, it would appear that circulation signatures and SOI associations are limited. There is a better association with SO/WC phases but the latter are, by nature, broader and less specific. At best, it can be said that in the months of + SOI $\geqq$ + 10 (Januarys 1967, 1974 and 1976) the NET_{SH} is still evident at 700 mb and upper-level Australian anticyclonicity has a tendency to be weak and southerly displaced (at least in the two former months). During - SOI phases $\leqq$ - 10, the NET_{SH} circulation is restricted to the lower levels (less than 700 mb) with anticyclonicity dominating the circulation over Australia at 700 mb and above. However, the dilemma of associations between SOI's and dynamic features is exemplified in the January 1967 situation. If there is a tendency for a lowering of pressure in the Indonesian region and a rising of pressure in the southeastern Pacific during strong SO/WC episodes, or + SOI phases, then a single numerical value given by the SOI cannot indicate where this lower pressure region is precisely located in space. Certainly, it is not always located at, or near, the pressure recording stations used

in the Indonesian region (in most cases Darwin). In fact, it can be located, as the January 1967 circulation suggests, in the Indian Ocean south of Indonesia proper. Likewise, cyclonic circulation in January 1974 and January 1976 is found across the north of Australia. This simple observation begins to highlight the problem of expecting SOI's and dynamic signatures to coincide spatially. However, as only one month is examined, it is not possible to evaluate the temporal links and lags involved. In fact, if Chen (1982 a) and Rasmusson and Carpenter (1982) are considered, even a wide range of SOIs cannot resolve more than fragments of a phenomenon that is definitely not a standing fluctuation. In Australian longitudes this would appear to be made more difficult because teleconnection sources generally seem to develop to the northwest (Indonesia) and northeast (PDZ) (as observed in negative and positive composites) of the continent.

To examine this further and, in turn, to look at the extent and timing of upper-level 'breakdowns' over Australia, velocity potential fields at 850, 700 and 200 mb are overlain and paired with total cloud cover sets (Sadler *et. al.*, 1976; Shideler and Sadler, 1979) for the Januarys from 1965-78 (Fig.100). Remotely-sensed cloud cover is missing for January 1965 and patchy in January 1966, due to the lack and insufficient coverage of satellite scanning respectively. A combination of coloured isolines of velocity potentials at each of three levels and symbols for their net vertical motion effect (ascent or subsident) are displayed on the right-hand side of the figures. Regions of strongest ascending motion are deduced somewhat subjectively, to be those areas where 850 mb and 700 mb velocity potentials are greater than or equal to + 2 x 10^6 m^2 s^{-1}, and 200 mb velocity potential are less than or equal to - 2 x 10^6 m^2 s^{-1}.

From Figure 100, it can be seen that some degree of vertical ascent is located across the 'maritime continent' for most of the January 1965-78 period. In fact, strong and extensive ascending motion occurs in the above region for about half the sequence (Januarys 1965, 1967, 1973, 1974, 1975, 1976, 1977 and 1978). Further east, in the central western equatorial

Figure 100 Monthly mean velocity potential overlays (850, 700 and 200 mb) in January 1965-78 and total cloud cover distributions over the Pacific region (Sadler *et. al.*, 1976 and Shidler and Sadler, 1979) in the same period (January 1965 unavailable). Velocity potential overlay features are explained by the symbols and colours on the diagram, while total cloud cover regions of 5 octa and above are shaded blue. Velocity potential fields are in units of 10^6 m^2 s^{-1} at intervals of 2 units.

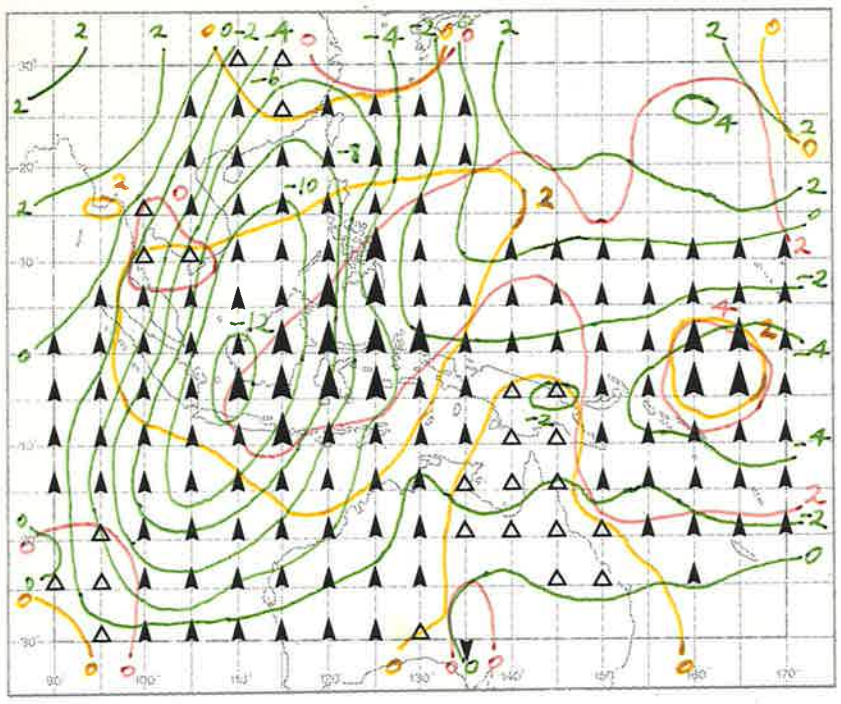

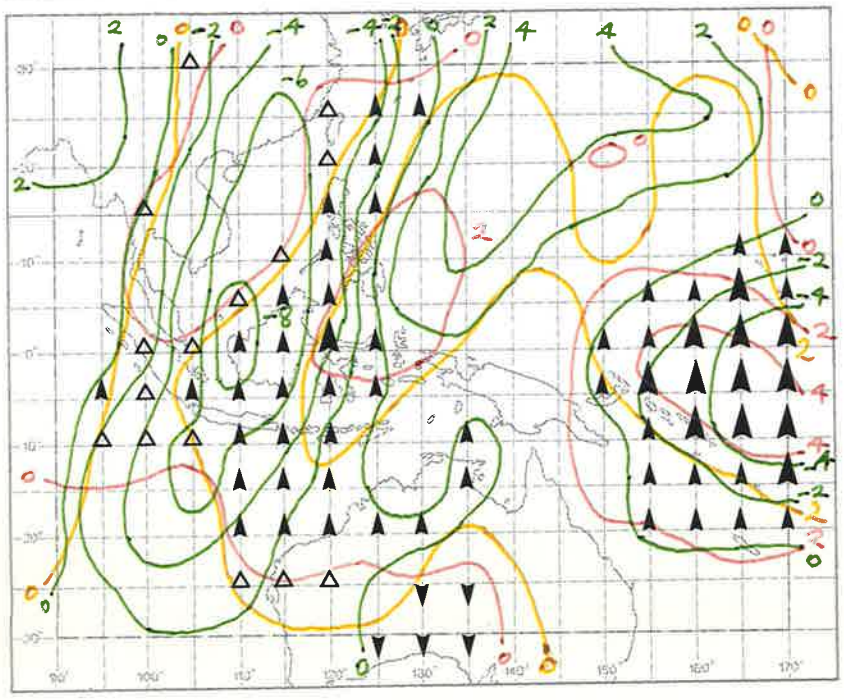

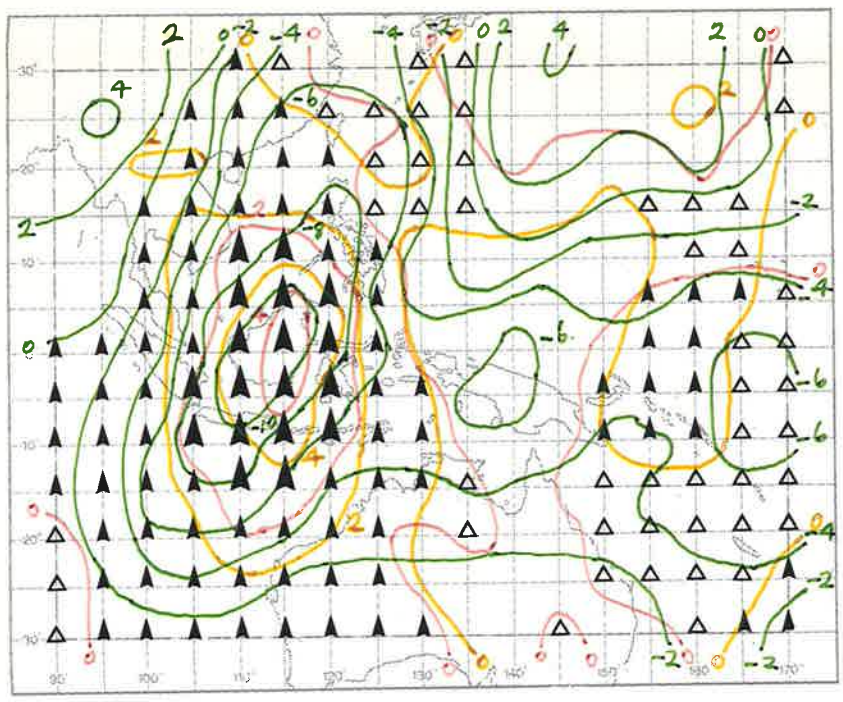

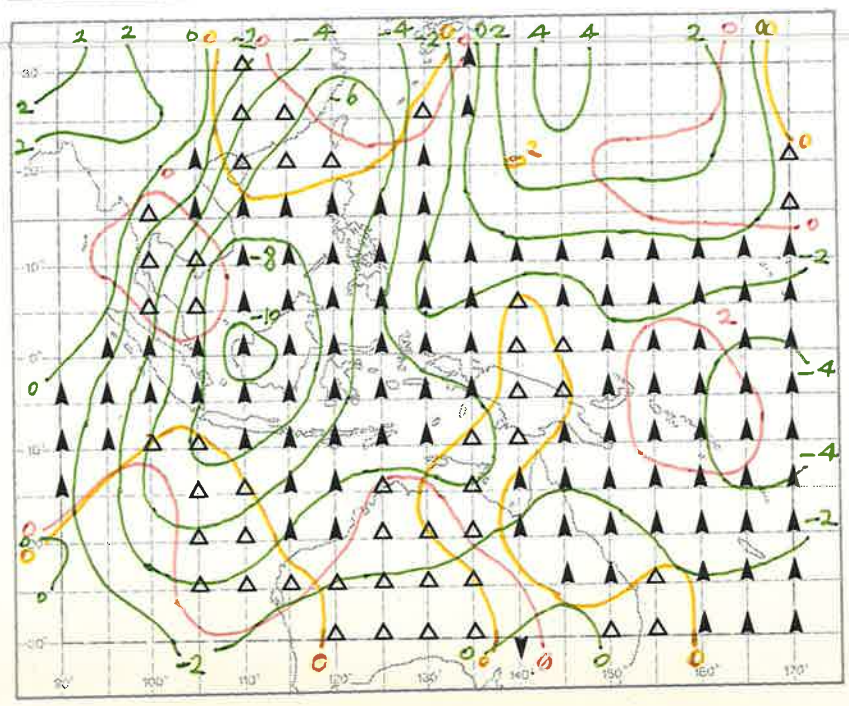

Symbols

▲ 850 & 700 mb CONV 200 mb DIV

▲ 850 & 700 mb CONV $>2 \times 10^6 m^2/sec$

200 mb DIV $<-2 \times 10^6 m^2/sec$

△ 850 or 700 mb CONV 200 mb DIV

▼ 850 & 700 mb DIV 200 mb CONV

Colours

850 mb 700 mb 200 mb

JAN 65

JAN 66

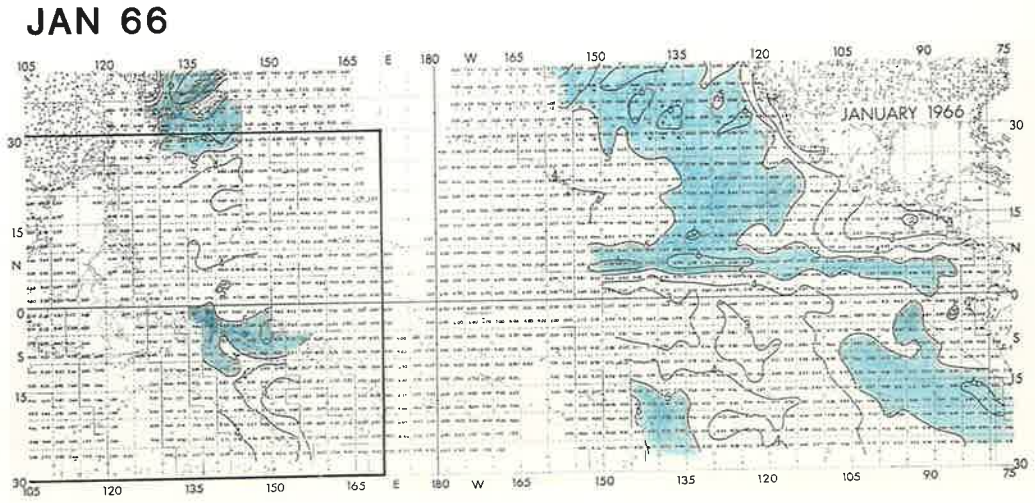

JAN 67

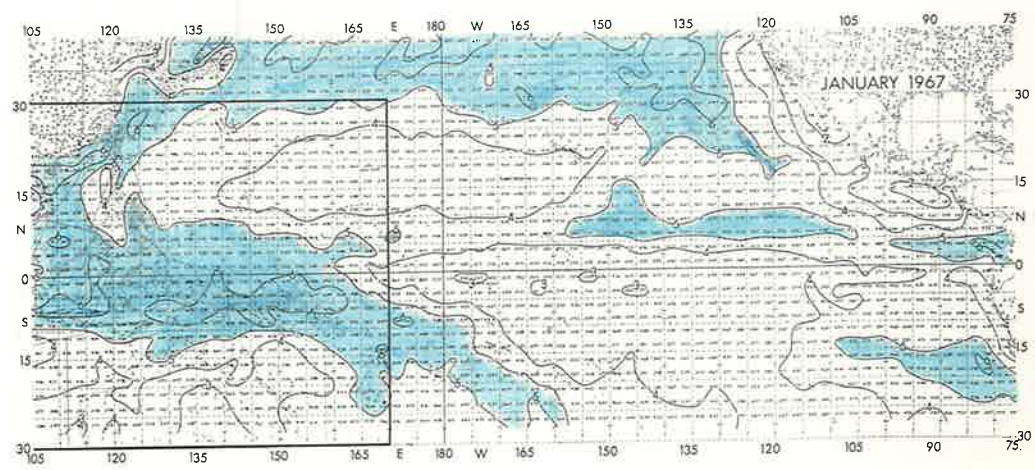

JAN 68

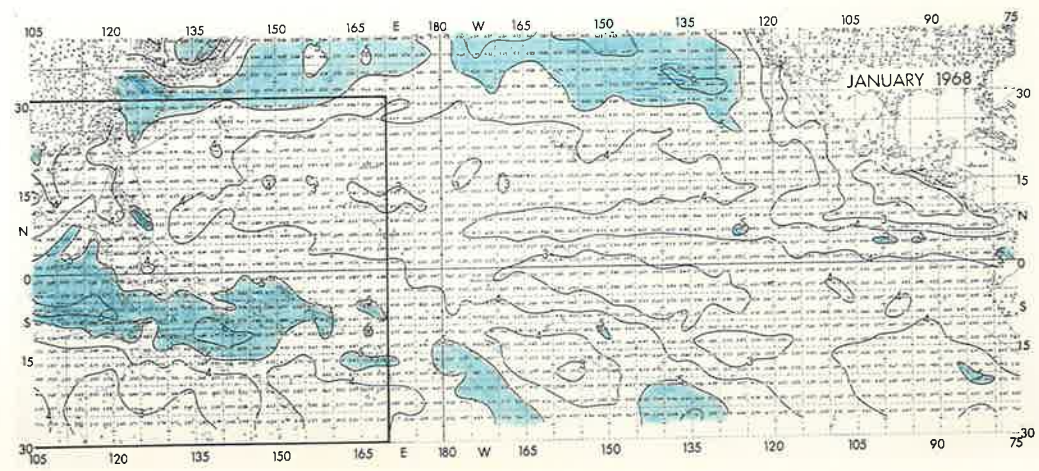

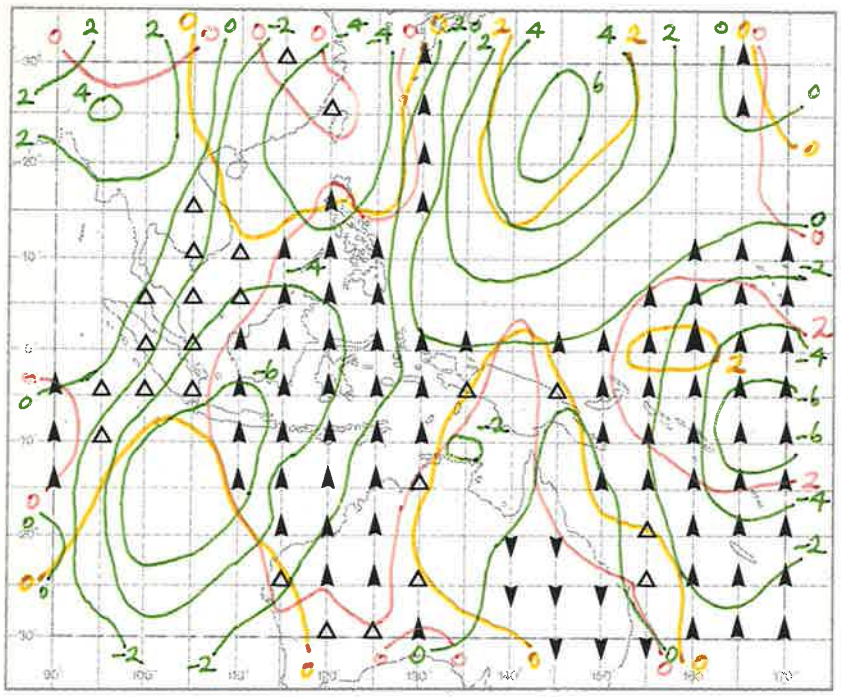

JAN 69

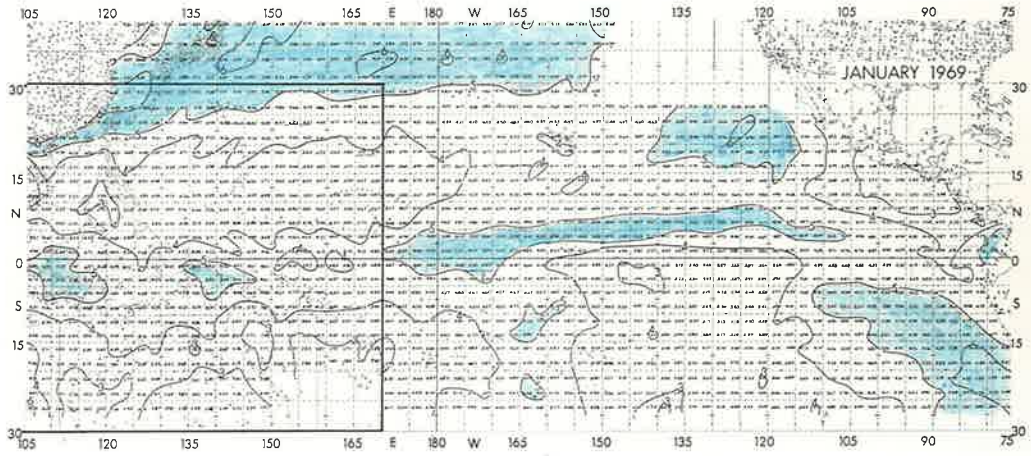

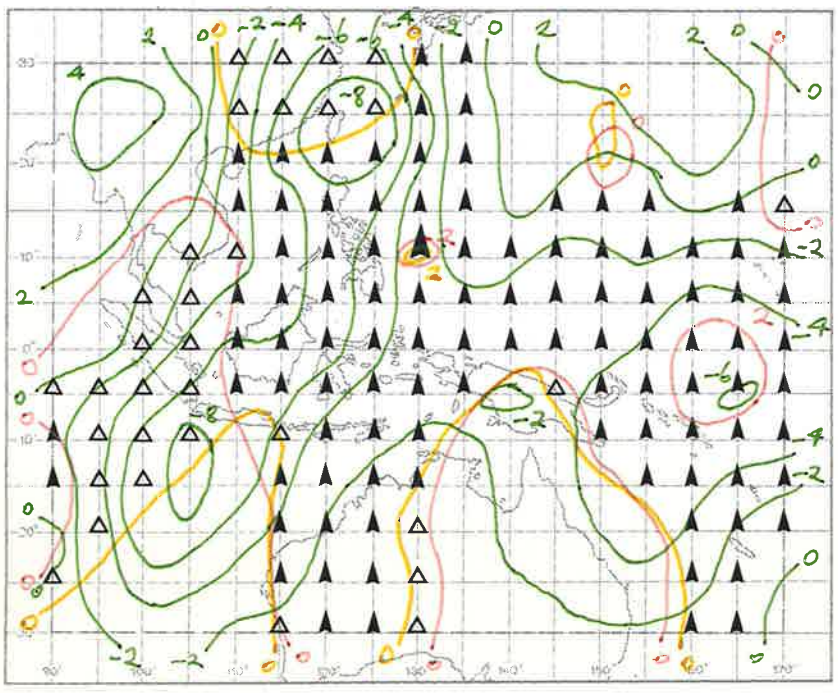

JAN 70

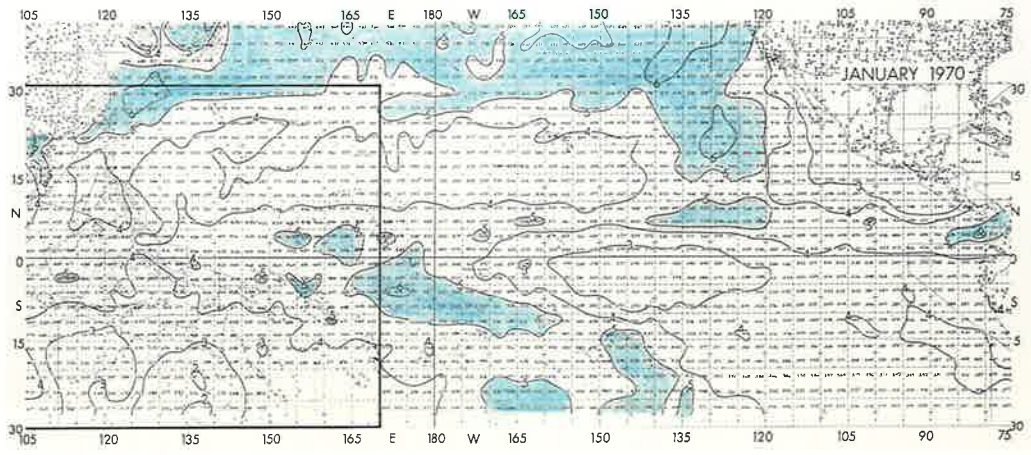

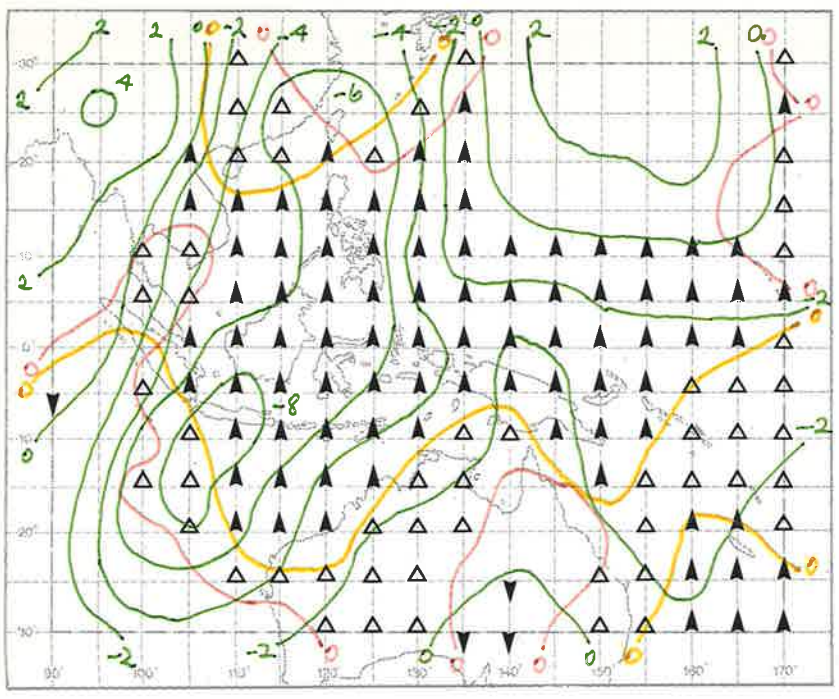

JAN 71

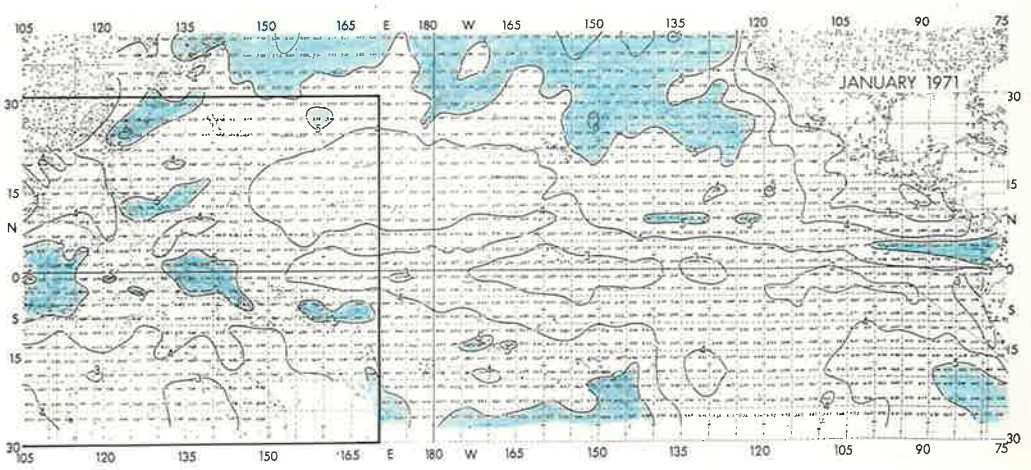

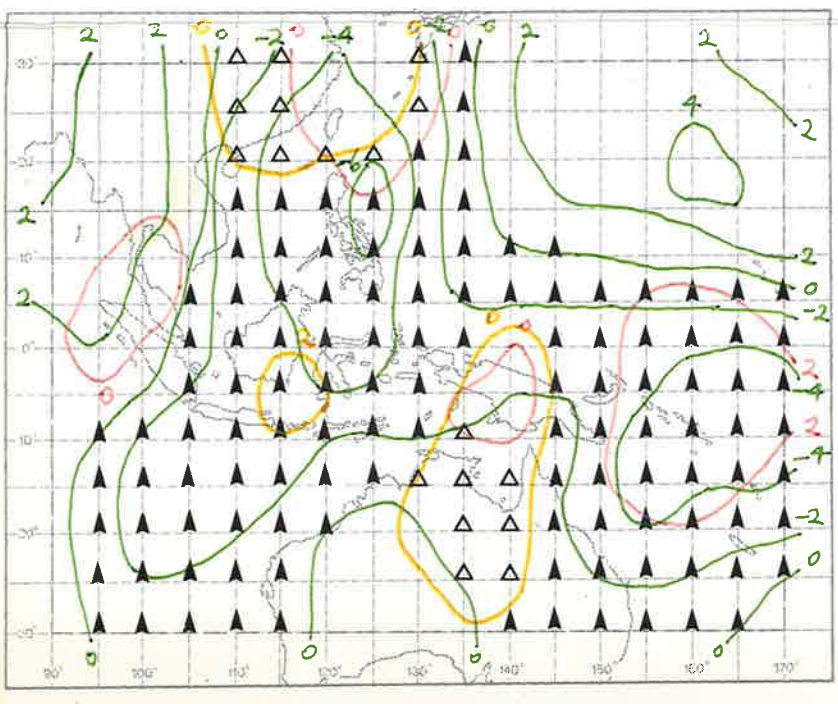

JAN 72

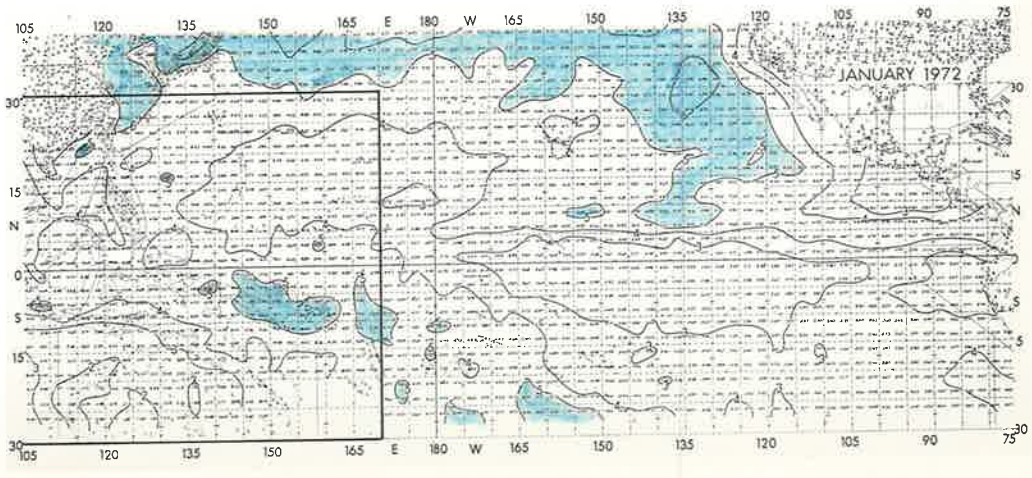

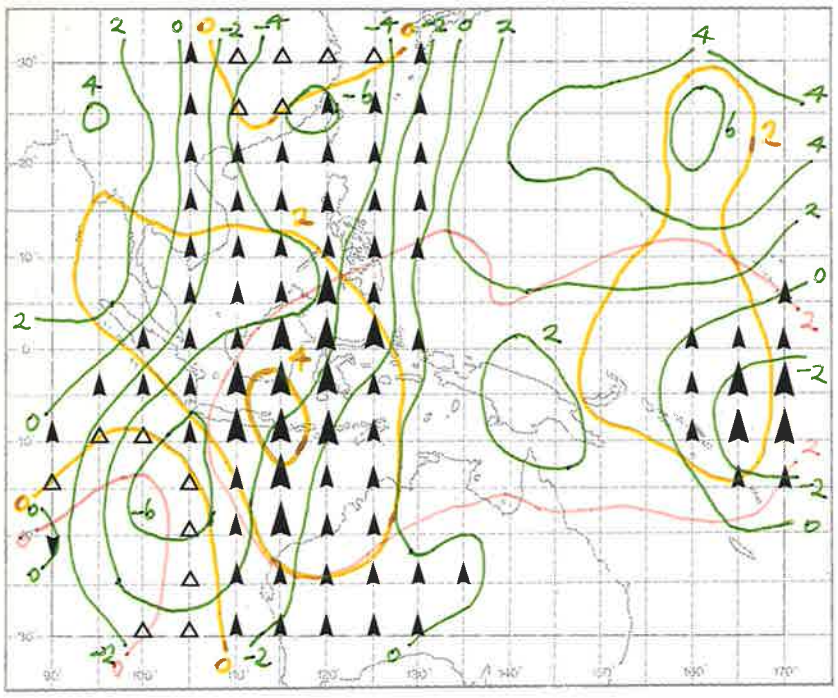

JAN 73

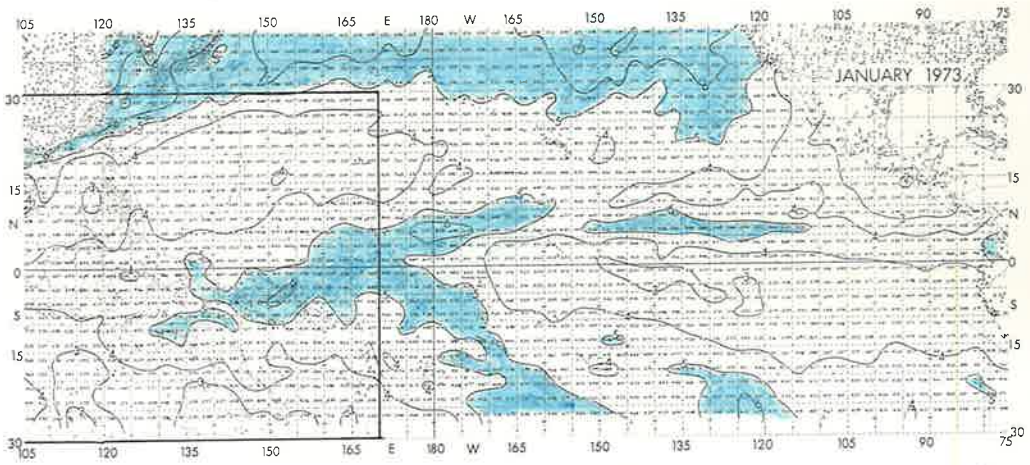

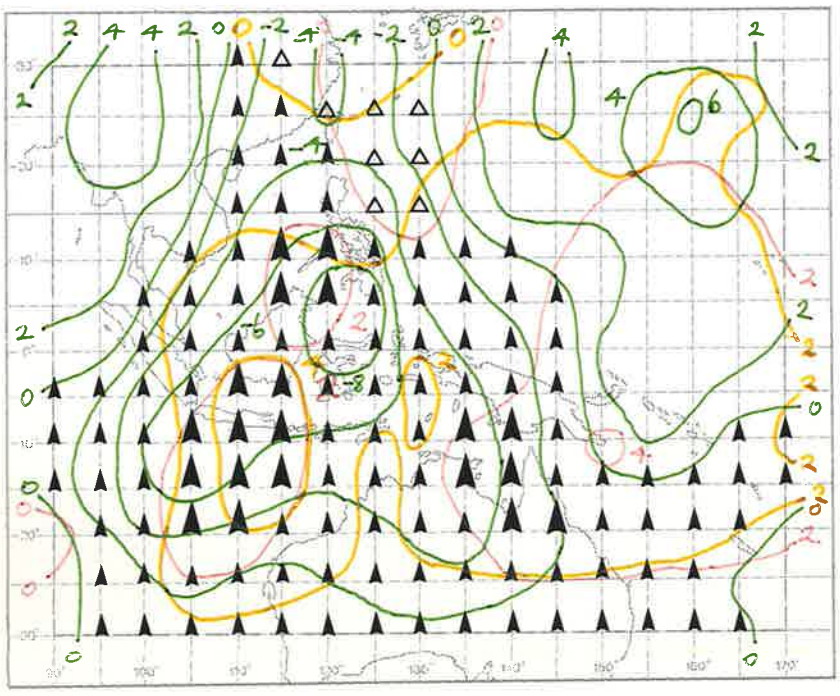

JAN 74

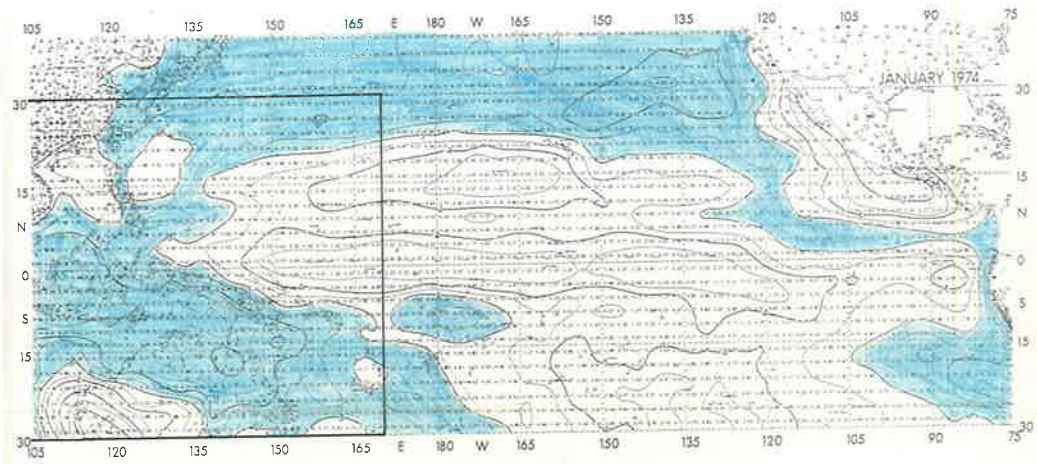

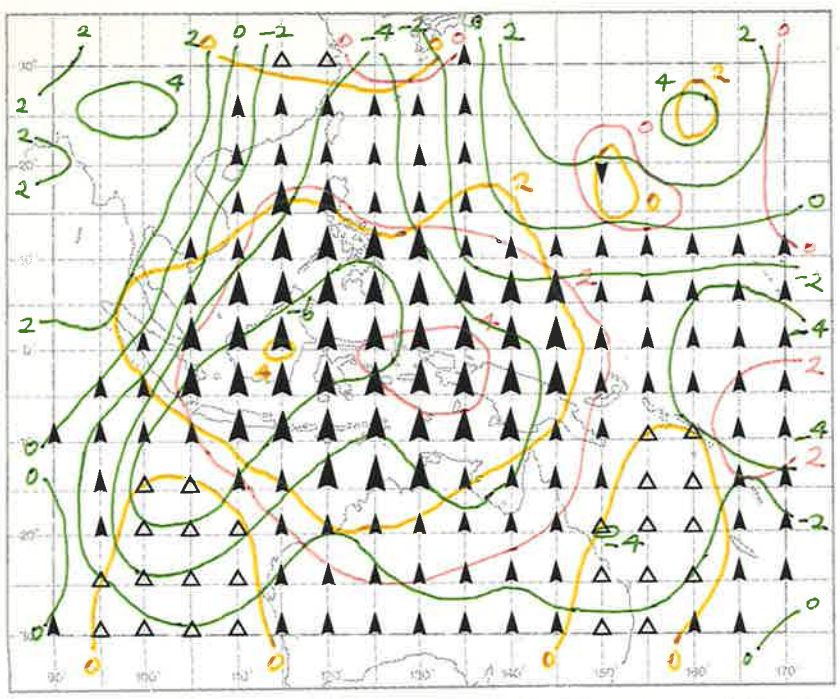

JAN 75

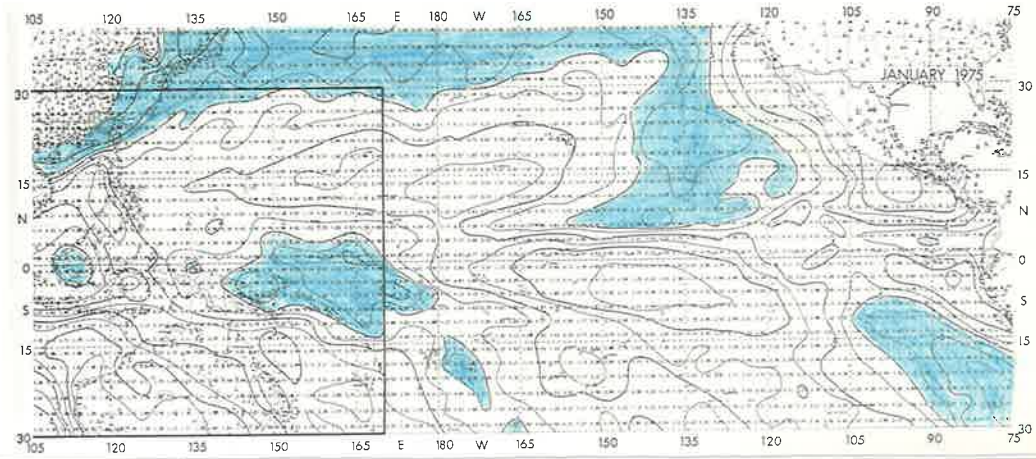

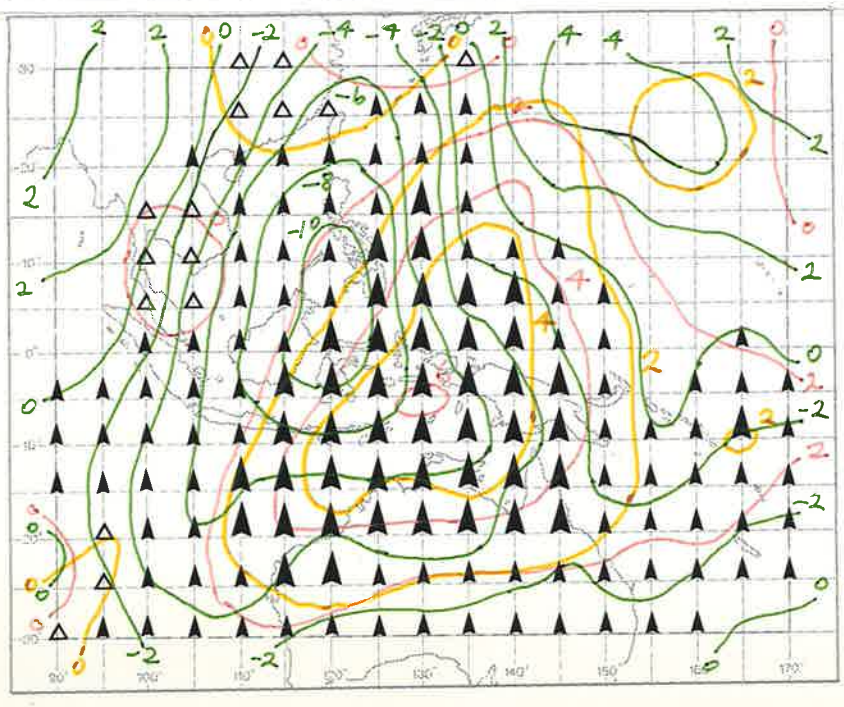

JAN 76

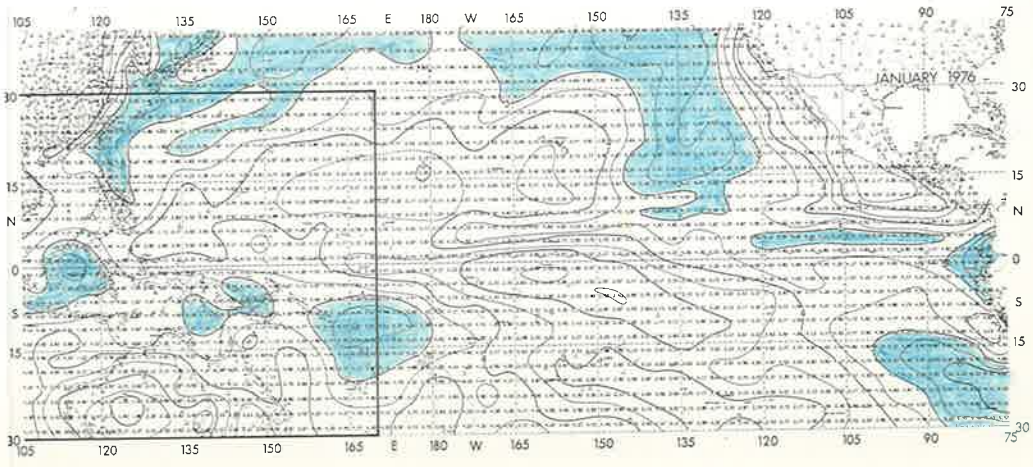

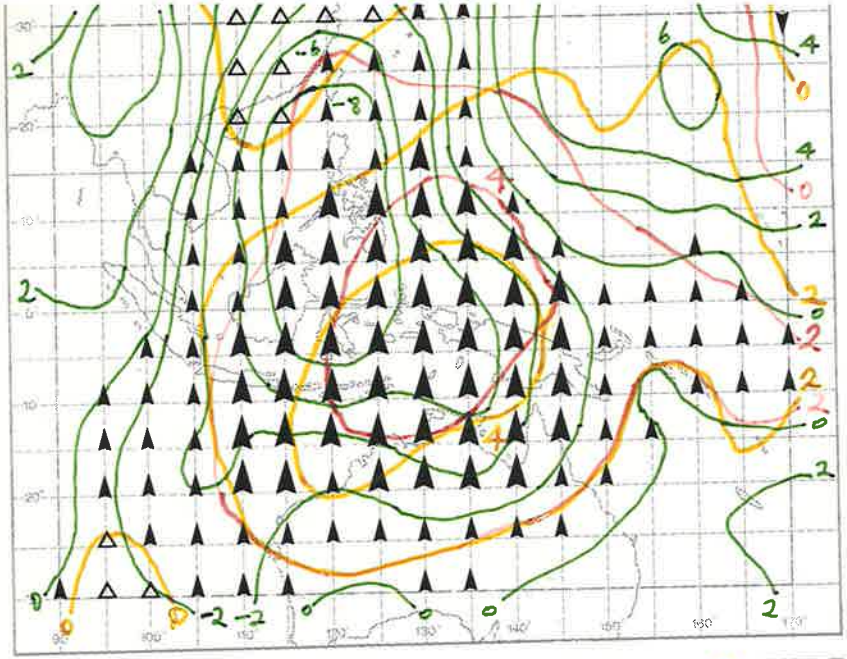

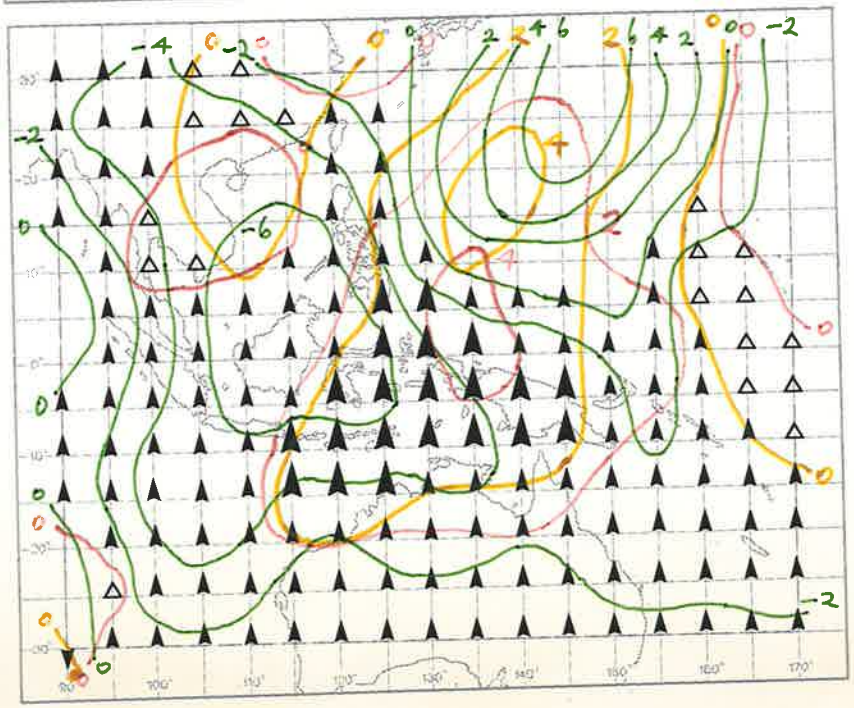

JAN 77

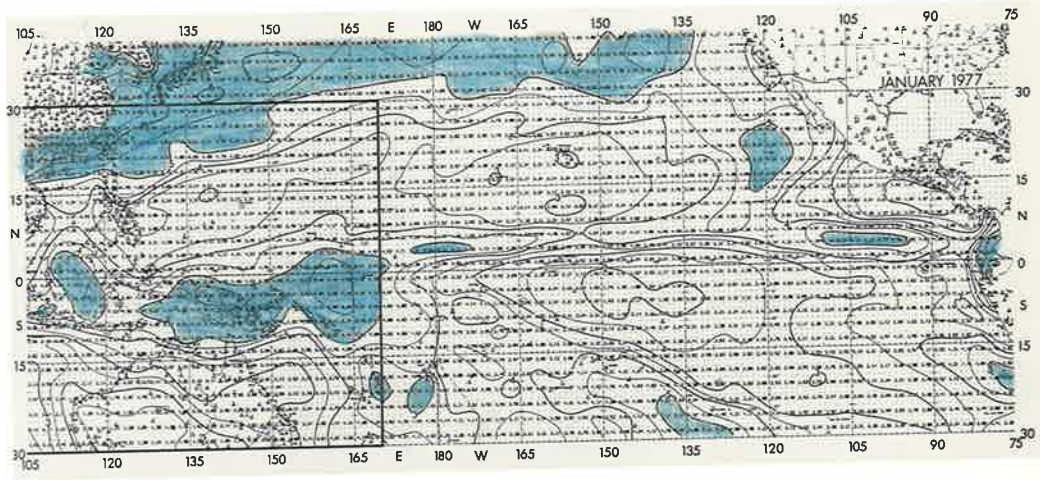

JAN 78

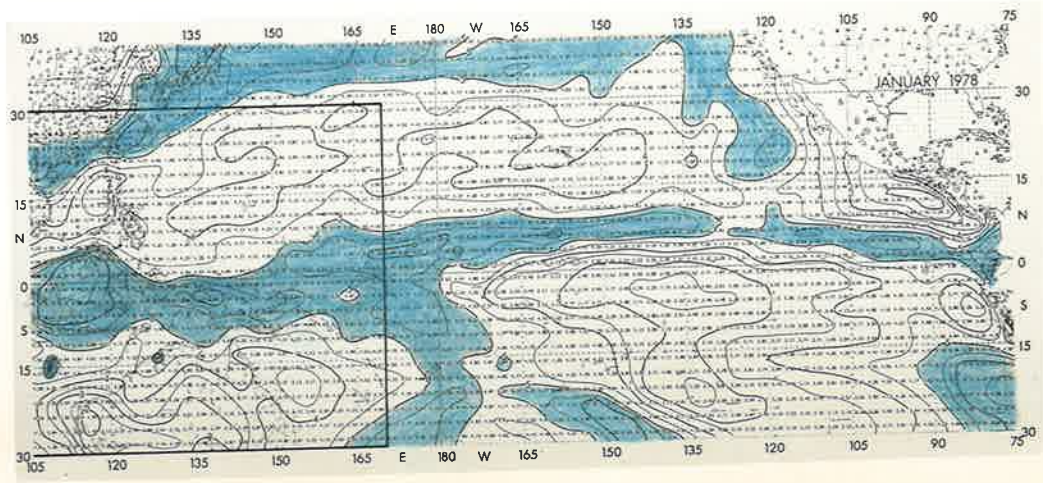

Pacific (westernmost extent of the PDZ), ascending motion occurs in about half the months in the period, but is most extensive and pronounced in Januarys 1965, 1966 and 1973. Strong, but less extensive, vertical ascent in the PDZ is evident in January 1969 and January 1976. Although the above periods do not consistently coincide with the - SOI's in Figure 99, they are related to the El Niño phases noted in Quinn *et. al.* (1978). Of these periods, Januarys 1965 and 1973 display dual centres of ascending motion with ascent over the 'maritime continent' and the PDZ. Only in January 1966 and, to a lesser degree, January 1969 are there some indications of the suppression or reduction of vertical ascent over the 'maritime continent' in the face of enhancement in the central western Pacific.

One interesting aspect of the ascending motion in the above regions is the vertical depth and location of the lower-level convergence maxima. Over the 'maritime continent', periods of intense ascending motion are, at times, marked by convergence with a distinctly 700 mb focus (i.e. January 1973 and January 1974). In fact, nearly half the periods of strong low-level convergence display 700 mb velocity potential values above + 4 x 10^6 m^2 s^{-1}. In the central western Pacific, low-level convergence is often weaker and shallower than that over the 'maritime continent'. Consequently, there are no periods when 700 mb velocity potentials reach values of + 4 x 10^6 m^2 s^{-1}. Hence, strong convergence is noticeably restricted to 850 mb in Januarys 1968, 1970, 1972 and 1975, while only Januarys 1965 and 1966 experience 850 mb velocity potential values greater than + 4 x 10^6 m^2 s^{-1}. Complicating this picture even further are the observations of moderate, low-level convergence in the PDZ region in January 1974 and January 1977 (in the absence of marked 200 mb divergence) and strong upper-level divergence in January 1967 (with poorly defined low-level convergence).

Therefore, it would seem that the poor definition of the NET_{NH} (eastern section) above 850 mb (Fig.99) results in weak convergence above this level. As northeast trade wind changes have been related to PDZ rainfall outbreaks and El Niños (Wyrtki, 1975, 1977, 1979; Reiter, 1978, 1979), it would seem

that the convergence they induce is an important low-level (up to 850 mb) component in the phenomenon. The persistence of some measure of deep ascending motion over the 'maritime continent' suggests that this broad region is a quasi-permanent teleconnection source. With probably a particularly deep monsoonal layer extending up to 700 mb in these tropical latitudes, deep vertical ascending motion can be expected. Furthermore, strong NET_{SH} (western) sections at 700 mb in Januarys 1967, 1973, 1974, 1976, 1977 and 1978 dictate that strong convergence is especially favoured over parts of the 'maritime continent' at such times. A distinct PDZ location for satellite-derived cloudiness in the Southern Hemisphere summer of 1978 would appear to be the result of a dominant negative SOI in February.

Over northern Australia, vertical ascent is not as dominant as it is in more tropical latitudes. Pronounced convergence through 850 mb and 700 mb levels occurs in about half of the months shown in the sequence (Fig.100). However, in many cases, it is confined to small portions of the north and northwestern coasts. Only in Januarys 1974, 1975, 1976 and 1977 does it penetrate well inland. However, to trigger deep convective activity and rainfall, the situation demands strong upper-level divergence and high atmospheric moisture content. Coincidences of low-level convergence and intense 200 mb divergence (velocity potentials of the order of -4×10^6 m^2 s^{-1} and larger) occur in Januarys 1967, 1973, 1974, 1975, 1976, 1977 and 1978. Of these, the January 1967, 1973 and 1978 associations involve very small spatial regions, while January 1975 and January 1977 situations experience poor moisture conditions (Fig.66). Only during the monsoonal incursions of January 1974 and January 1976 are teleconnection couplings and moisture conditions pronounced.

Already, it would appear that a similar situation to that encountered with circulation signatures occurs with velocity potential overlays; that is, dynamic signatures do not relate consistently to SOI extremes, although they can be seen to equate with broad SO/WC phases. The only other aspect that remains to be examined is the concept of upper-level 'breakdowns' in

the divergence pattern over Australia.

An examination of 200 mb velocity potential fields indicates that areas of pronounced convergence occur over eastern Australian and New Guinean longitudes in January 1966, 1969 (not quite complete) and 1973. Of these periods, January 1966 and January 1969 are also associated with marked subsidence over Australia and thus coincide with two out of the three months with - SOI's $\leq$ - 10. On the other hand, they are again consistent with the major SO/WC phases noted in Quinn *et. al.* (1978). What makes their timing all the more significant is that they appear to be distinguishable from other periods when low-level divergence is prominent over eastern Australia (i.e. Januarys 1967, 1970, 1971 and 1972). Therefore, it would seem that markedly weak SO/WC phases (El Niño) and, to a lesser degree, - SOI extremes are closely associated with upper-level 'breakdowns' over eastern Australian and New Guinean longitudes.

The relationship between signatures, SO/WC episodes, SOI's and total cloud distributions is particularly complex. A comparison of vertical ascending regions and cloud octa maxima (shaded in Fig.100) suggests that associations are, at best, only moderately strong. This is supported by the observation that equatorial and near-equatorial cloud bands are often extensive and imbedded with a number of particularly strong foci, some of which are clearly related to vertical ascending zones, while others show poor or no association. In general, these relationships are strongest in the PDZ, moderate in Indonesian regions, but poor over New Guinea and northern Australia.

This range of associations could perhaps be blamed exclusively on the station distributions in the latter regions if it were not for the fact that SOI extremes are no better related to cloud fields. What must also be taken into account is that there are a number of factors that complicate the above relationships. For instance, the cloud distributions are for total cover and thus do not give an indication of cloud heights. As has been noted in Section 3.1.2 *(i)* there are some poor associations between the total cloud

cover sequences and the upper cloud information in Barton (1983). In particular, the convective areas over Indonesia and the PDZ in January 1973 (Fig.100) are more closely related to the Barton (1983) distribution than to the Sadler *et. al.* (1976) and Shideler and Sadler (1979) total cloud fields. To a lesser degree this can also be said of the configurations in January 1975. Considering the investigations of Webster and Stephens (1980) and Lyons (1981), the extent of upper tropospheric extended clouds and lower-level stratus clouds is not discernible in these fields and could account for the above differences. Certainly, incidences of strong 200 mb divergence and poor low-level convergence are associated with cloud maxima in Januarys 1967 (New Guinea), 1969 (Indonesia), 1971 (Indonesia), 1975 (PDZ) and 1978 (Indonesia). Another factor that cannot be derived from the 850 mb and 700 mb velocity potential fields in Figure 100 is that strong (probably moist) onshore flow can be orographically lifted to produce the type of persistent lower-level cloud decks that would appear as a maxima in total cloud fields. This is most noticeable in regard to the New Guinea highlands and potentially strong onshore flows in Januarys 1969, 1971 and 1973 (Fig.99). Finally, the smoothing effects of successive data processing steps lead to the velocity potential fields being more suited to large-scale resolutions. As a result, finer scale processes can become 'lost' because the final fields are too coarse. In regard to the Australian situation, an attempt is made in the following discussion to lessen this effect by using divergence, rather than velocity potential, overlays. This seems to be particularly important in view of the comments made earlier in this discussion with regard to the location of Australia and the most persistently active convective regions.

(ii) Divergence Overlays (850, 700 and 200 mb) and Rainfall over Australia : January 1965-76

Australia tends to be influenced by relatively weaker vertical ascending regions than those occurring immediately to the west and east of the continent.

As a consequence, it was found to be more useful to examine the Australian situation by divergence overlays than by velocity potentials. This approach has the added advantage of using fields a stage prior to, and less effectively smoothed than, the final velocity potential fields.

The January 1965-76 sequence of shaded and unshaded patterns in Figure 101 shows the summation of monthly mean divergence/convergence for 850, 700 and 200 mb levels overlaying isohyets of monthly mean rainfall of 0, 200, 400 and 800 mm magnitudes. The final shading patterns, created by the divergence/convergence component of this overlay, give some approximation of the likely extent of organized vertical motion. Schematic diagrams in the key to Figure 101 show the nature of vertical motion likely to be produced by the shading patterns. The numbers at various grid points in Figure 101 detail the magnitude of divergence (+) and convergence (-) at 200 mb (top number) and 850 mb (bottom number) levels.

It has already been suggested by analysis of velocity potential and streamfunction fields (Figs.99 and 100) that some major extremes in monsoonal patterns occurred over Australasia during the Januarys 1965-78. Basically, these extremes are related to large-scale circulation variability which is manifested in the Australian region by latitudinal and longitudinal changes in upper-level anticyclonicity and low-level NET_{SH} activity. The divergence/convergence fields in Figure 101 support this conjecture and suggest that coupling of upper- and lower-level divergent/convergent maxima, although not as pronounced as in the more tropical areas to the northwest and northeast of the continent, is an important component of rainfall mechanisms.

The largest areas of strong vertical ascent occur in Januarys 1974 and 1976. The ascent covers most of northeastern Australia in January 1974 and the 'top end' in January 1976. Low-level patterns and magnitudes (bottom grid point numbers) suggest that deep convergence occurs during these months (one - 11 x 10^{-6} s^{-1} maximum at 850 mb in January 1974 and several - 9 x 10^{-6} s^{-1} maxima at 850 mb in January 1976). When coupled with the large divergence values at 200 mb (11-12 x 10^{-6} s^{-1} in January 1974

Figure 101 Monthly mean divergence overlays (850, 700 and 200 mb) over the Australian continent in January 1965-76. Shading relationships and underlying isohet patterns are shown in the accompanying key. The numbers at some grid point intersections indicate 200 mb divergence/convergence (top) and 850 mb divergence/convergence (bottom) values of significant magnitude. Divergence is in units of 10^{-6} s^{-1}.

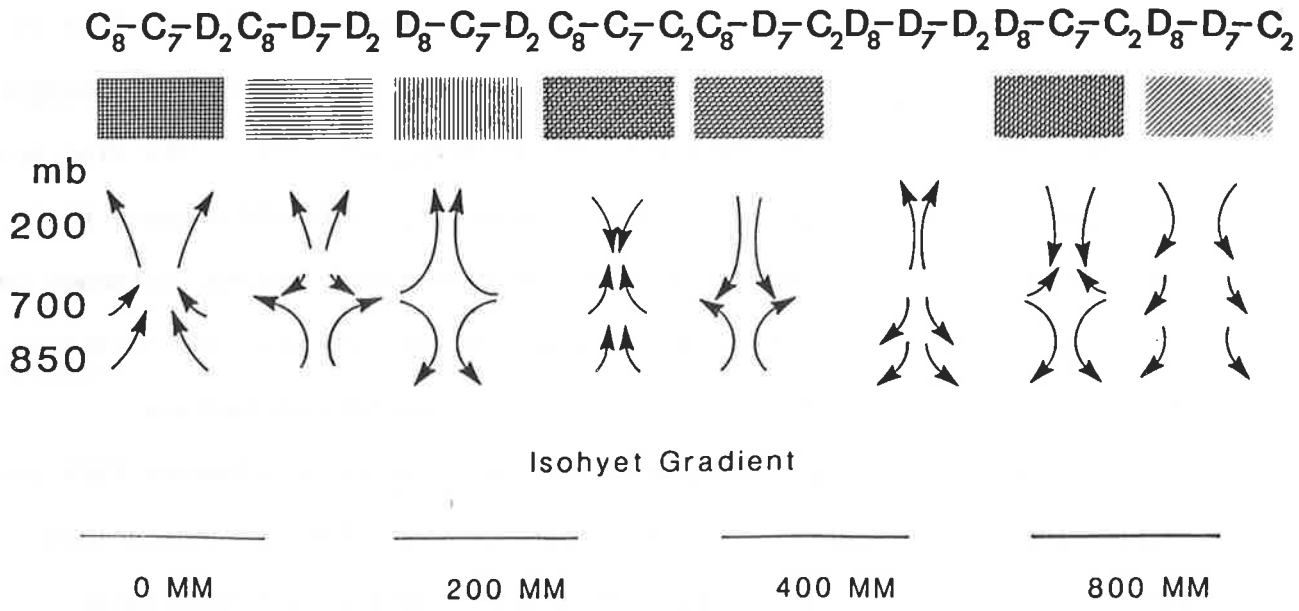

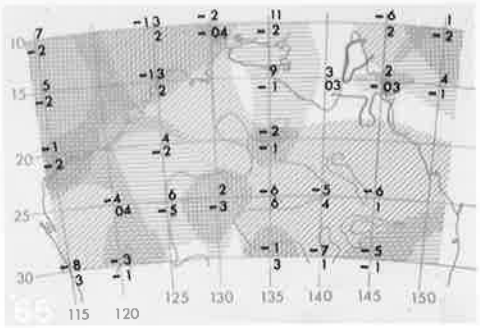
10
15
20
25
30
115
120
125
130
135
140
145
150

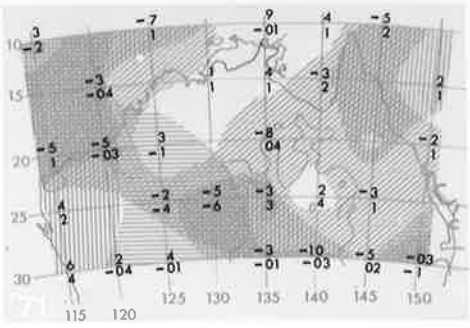
10
15
20
25
30
115
120
125
130
135
140
145
150

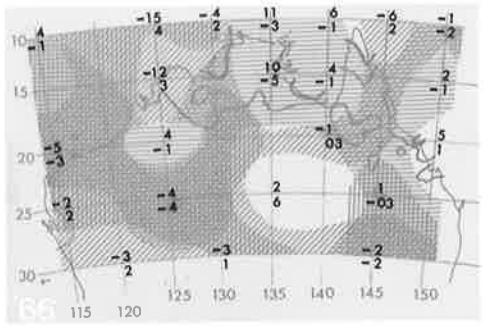
10
15
20
25
30
115
120
125
130
135
140
145
150

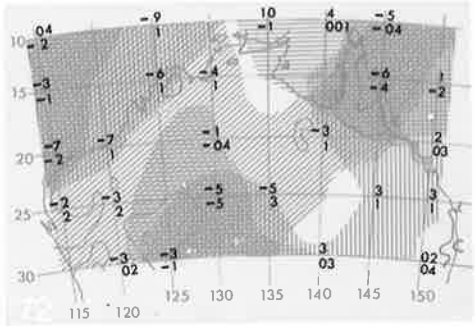
10
15
20
25
30
115
120
125
130
135
140
145
150

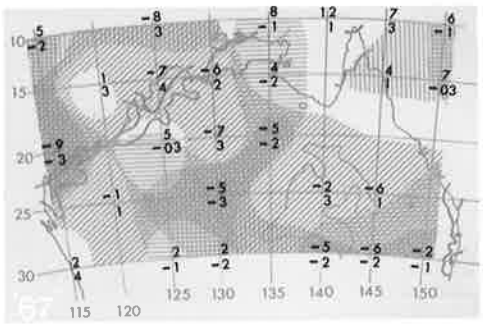
10
15
20
25
30
115
120
125
130
135
140
145
150

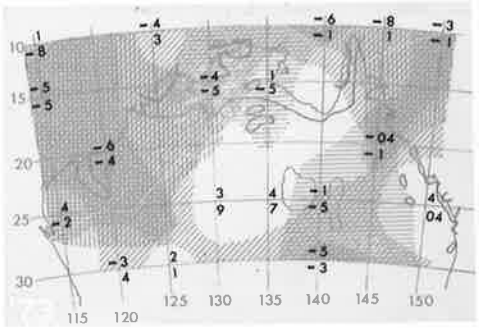
10
15
20
25
30
115
120
125
130
135
140
145
150

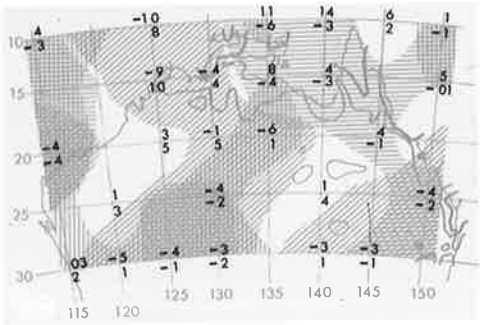
10
15
20
25
30
115
120
125
130
135
140
145
150

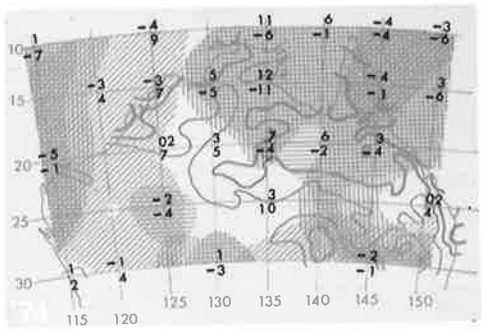
10
15
20
25
30
115
120
125
130
135
140
145
150

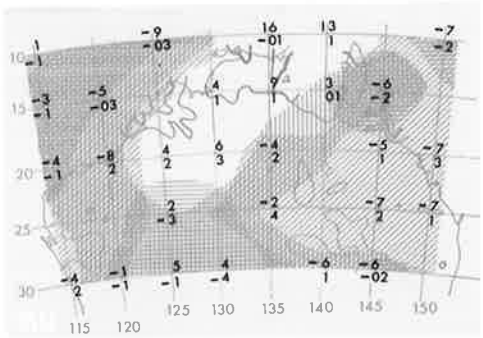
10
15
20
25
30
115
120
125
130
135
140
145
150

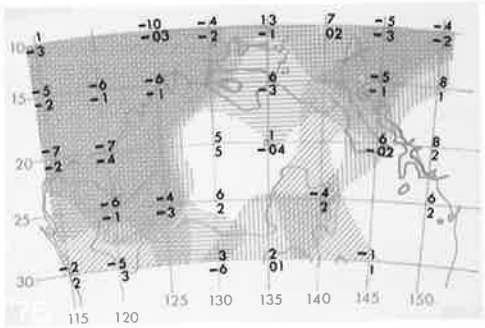
10
15
20
25
30
115
120
125
130
135
140
145
150

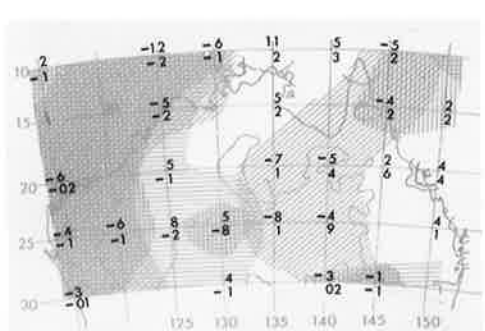
10
15
20
25
30
115
120
125
130
135
140
145
150

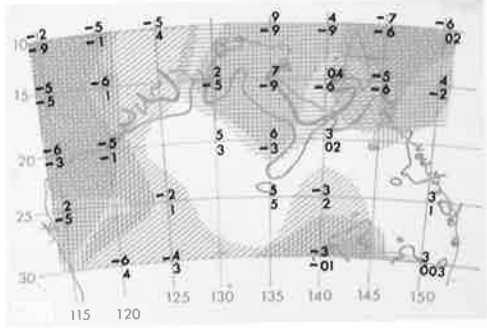
10
15
20
25
30
115
120
125
130
135
140
145
150

and 7-9 x 10^{-6} s^{-1} in January 1976), vigorous ascending motions could be expected over these parts of the continent. This scenario is supported by the isohyets, with many of the areas receiving over 800 mm per month in the vicinity of the ascending regions.

Areas of organized, but less intense, vertical ascending motion occur in the Januarys of 1966, 1968 and 1975 over the northern and northeastern areas of the continent. As in the previous situations, these areas are often flanked by the edges of the strong ascending motion (indicated by the velocity potential analysis) to the northwest and northeast of Australia. Once again there is a good correlation between ascending regions and rainfall areas, but the amount and extent of moisture available to the convective processes is not directly evident. Some measure of the magnitude of the moisture parameter can be inferred from the intensity and direction of the lower-level flow in Figure 99. For example, the massive cyclonic circulation about the NET_{SH} in January 1974 seems to draw in moisture from tropical and Indian Ocean regions. Flow in January 1976 is not as strong but still shows a tendency for infeed and advection of air across warm tropical seas.

In January 1975, however, the NET_{SH} is weak over Australia and any moisture infeed from the tropics is shallow, being mainly concentrated in near-surface levels (i.e. January 1975 $\bar{\psi}_{sfc}$ in Fig.36). Thus despite the moderately well organized ascent over Australia at this time, the amount and depth of moisture to be uplifted by the vertical motions could be expected to be considerably less than in Januarys 1974 or 1976. In fact, it would seem that more moisture is available in Januarys 1966 and 1968.

A combination of monthly mean divergent/convergent patterns, lower-level flow (Fig.99) and disturbance tracks (Loursenz, 1981) can be used to explain most of the rainfall isohyet patterns in the entire January 1965-76 sequence. Even in drier Januarys, such as 1969-71, this approach is successful. Considering that strong lower-level flow coming across the Australian coasts from oceanic regions (Fig.99) is likely to be quite moist, many of the rainfall patterns not overlain by vertical ascending regions can be explained

by orographic lifting (Fig.44) of moist onshore winds (i.e. the small rainfall maxima over the 'top end' in January 1969 and the slow, 850 mb tropical onshore flow in Fig.99). Most of the remaining heavy rainfall areas are aligned with the passage of tropical disturbances (i.e. Kimberley coast rainfall in January 1974 and a tropical cyclone track passing across the coast).

At the other extreme, areas of major subsident motion relate well to regions of little or no rainfall over Australia. Low rainfall areas are most pronounced over parts of central Australia in Januarys 1965, 1967, 1969, 1970, 1971, 1972 and 1975, and are aligned with subsident motion in Januarys 1967, 1969, 1971 and 1972 and, to a lesser degree, Januarys 1965, 1970 and 1975. In the latter situations, strong to moderately organized ascent would appear to be evident around 25°S, 130°E in inland Australia over portions of the very low rainfall regions. It would seem that these ascending patterns do not relate well to the rainfall regime because of the dichotomy between the NET_{SH} and the quasi-permanent shallow heat lows of Western Australia and Queensland. Even the 850 mb flow does not really provide a complete picture of the heat lows which are more easily detected in near-surface streamfunction or pressure fields (Figs.37-42). Yet, several of the documented features of the heat lows can be partly deduced and used to show factors suppressing the development of deep and/or moist vertically ascending motion.

Heat lows are usually quite markedly 'capped' by an inversion above the shallow near-surface layers of ascending motion. When established, such an inversion is associated with a change in circulation from cyclonic at low levels to anticyclonic into the greater part of the troposphere (Ramage, 1971). In Januarys 1965, 1969 and 1970, in particular, convective activity appears to be so strongly organized around 25°S, 130°E that no inversion layer (at least up to 700 mb) is present. Yet, the rainfall pattern associated with this situation is poor. A possible explanation for this is that moisture is generally very low in these inland areas.

Evidence for this can be found by analysing a humidity parameter, such as mixing ratio, from the nearby meteorological station at Giles (25° 2'S, 128° 13'E). During the 13 year period, monthly mean mixing ratios at Giles (Maher and Lee, 1977), for both the surface and 850 mb levels, reach distinctly low values in Januarys 1965, 1970-72, 1975 and 1977 and relatively higher values for the remainder of the period. It would seem that, in almost all cases, areas of little or no rainfall in inland Australia are related to periods of strongly subsident vertical motion in the near-surface layers (Januarys 1967, 1969, 1971 and 1972), or to combinations of subsidence with the capping inversion of heat low conditions, very low moisture characteristics and upper-level convergent motion (Januarys 1965, 1970 and 1975).

Thus a combination of velocity potential and streamfunction fields on a broad scale and more localized divergence/convergence analysis can provide a useful insight into teleconnection and monsoonal patterns over Australasia. Certainly, in the short term, this type of appraisal is more productive than the use of SOIs.

3.3.3 Longer-Term Monsoon and Teleconnection Variability

In Sections 3.1, 3.2, 3.3.1 and 3.3.2, several of the basic aspects of the SO/WC phenomenon and its relationship to the Asian monsoon system were described. This description, together with the following discussion, indicates that the SO/WC is a complex feature which can have direct and indirect influences on a wide range of atmospheric elements.

One particular parameter which has been consistently used in order to gauge the strength and phase of this fluctuation is the Southern Oscillation Index (SOI). Unfortunately, there would appear to be some basic problems and major drawbacks in relating moderate to weak SOI values with dynamic features. As has been shown, broad SO/WC extremes are most strongly related to events in the PDZ and, to a lesser degree, the 'maritime continent'. In the Australian region such associations appear to be inconsistent,

although the coincidence of SO/WC phases and upper-level 'breakdowns' gives the impression that the eastern Australian-New Guinean area is in something of a transitional zone (Tsuchiya, 1970; Fleer, 1981; see also OLR distributions in Heddinghause and Krueger, 1981). A consequence of this is that physical manifestations of SO/WC episodes are more readily apparent in the Pacific Basin (i.e. El Niño and PDZ rainfall outbreaks). Over the 'maritime continent', such manifestations are mainly in the form of protracted droughts (Quinn *et. al.*, 1978), while further south in Australia little attempt to identify manifestations has been made.

The following discussion is intended to present a summation of longer-term SO/WC and Australasian monsoon correlations, indices and relationships, together with evidence of physical manifestations in Australia. Several indices of the SO/WC (SOIs) are compared and contrasted, with the emphasis on examining the longest data sets available. Furthermore, associations and correlations between SOIs and indices of Australasian monsoon intensity are deduced in order to demonstrate aspects of the spatial extent of SOI influence over this region. Finally, evidence from Lake Eyre floodings and Australian rainfall patterns is used to examine the suggestion that associations with very strong SO/WC phases could have long-term signature value.

i) Southern Oscillation Indices (SOIs) and the Southern Hemisphere Summer Monsoon

Over the years since Sir Gilbert Walker and his co-workers developed the concept of the SO/WC from research into numerous atmospheric correlations in the Indo-Pacific region, a number of these correlations have been used as indices of this phenomenon (see Julian and Chervin, 1978 and Rasmusson and Carpenter, 1982 for reviews of this and earlier SO/WC research). Following renewed interest in the SO/WC over the last 15 to 20 years, the number of indices has increased dramatically. Table 1 outlines the nature of some of the more widely reported long-term SOIs, and highlights their strong bias

TABLE 1

List of Recent Southern Oscillation Indices (SOIs)

Researcher(s)	Parameter	Level	Record	Period	Stations
Quinn (1974);	pressure	surface	1861-1881	monthly	Santiago-Bombay
Quinn and Burt	"	"	1882-1976	"	Santiago-Darwin
(1972);	"	"	1942-1976	"	Easter Is.-Darwin
Quinn *et. al.*	"	"	1948-1976	"	J Fernandez-Darwin
(1978)	"	"	1952-1976	"	Totegegie-Darwin
	"	"	1951-1976	"	Rapa-Darwin
	"	"	1948-1976	"	Tahiti-Darwin
Troup (1981; personal communication)	"	"	1932-1981	"	Tahiti-Darwin
Wright (1977);					
Lamb (1977);	"	"	1860-1975	seasonal	Area Average
Wright (1981; personal communication);	"	"	1941-1978	"	" "
Pazan and Myers (1982)	"	"	1941-1978	"	" "
Tanaka (1981)	"	"	1961-1980	"	Tahiti-Cocos Is.
Horel and Wallace (1981)	GPH	200 mb	1951-1978	"	Area Average
Van Loon and Madden (1981);	pressure	surface	1953-1978	"	Tahiti-Cocos Is.
Van Loon and Rogers (1981)	"	"	1899-1979	"	Station Composites

towards the use of sea level pressure data.

As can be seen from Table 1, the majority of SOIs have either been derived from two station differences or area average considerations (often using principle components). Moreover, they almost exclusively use one parameter at one atmospheric level (surface) to produce a single monthly or seasonal mean SOI value. Obviously, the historical background to SO/WC research and the long temporal length of surface pressure records has played a major part in shaping such SOI developments. Nevertheless, individual SOIs cannot resolve the spatial or vertical structure of the SO/WC phenomenon. Furthermore, despite the growing upper air record (Streten, 1982, estimates around 25 to 30 years in the Australasian region), to the author's knowledge the Horel and Wallace (1981) SOI is the only one to have been formulated from upper-level data. What this suggests, and the previous discussion in this thesis supports, is the need to identify the nature of SO/WC fluctuations in a spatio-temporal framework and from a wide range of atmospheric variables. In fact, it is only recently that researchers have focused their attention on correlations and associations between the SO/WC, SOIs and upper-level dynamics, particularly in the Northern Hemisphere (e.g. Parthasarathy and Mooley, 1978; Khandekar, 1979, 1982; Bhalme and Mooley, 1980; Angell, 1981) and the Pacific to North American sector (e.g. White and Walker, 1973; Angell, 1981; Horel and Wallace, 1981; Van Loon and Rogers, 1981; Arkin, 1982; Chen, 1982 b; Harnack *et. al.*, 1982; Keshavamurty, 1982). Yet, it is important to examine what SOIs alone indicate about the SO/WC, especially in the Australasian region.

The first step in this direction would appear to be an analysis of the interactions and responses of the various SOIs to SO/WC events. This seems to have occurred, with Chen (1982 a) and Rasmusson and Carpenter (1982) indicating just how detailed the phenomenon is in a spatio-temporal sense and how much of such information individual SOIs are able to project. As one would expect, the largest SO/WC extremes and - and + SOI values (lagged and unlagged) seem to closely reflect broad-scale atmospheric responses.

Figure 102 Matching of three surface pressure derived SOIs (Wright's 'old' and 'new', and Troup's) with a 200 mb geopotential height (GPH) SOI (Horel and Wallace, 1981) for the Southern Hemisphere summers (December - February) from 1951-78. Stippled areas in the diagram indicate strong, - SOI phases and horizontal shadings indicate strong, + SOI phases when both surface and 200 mb SOIs concur.

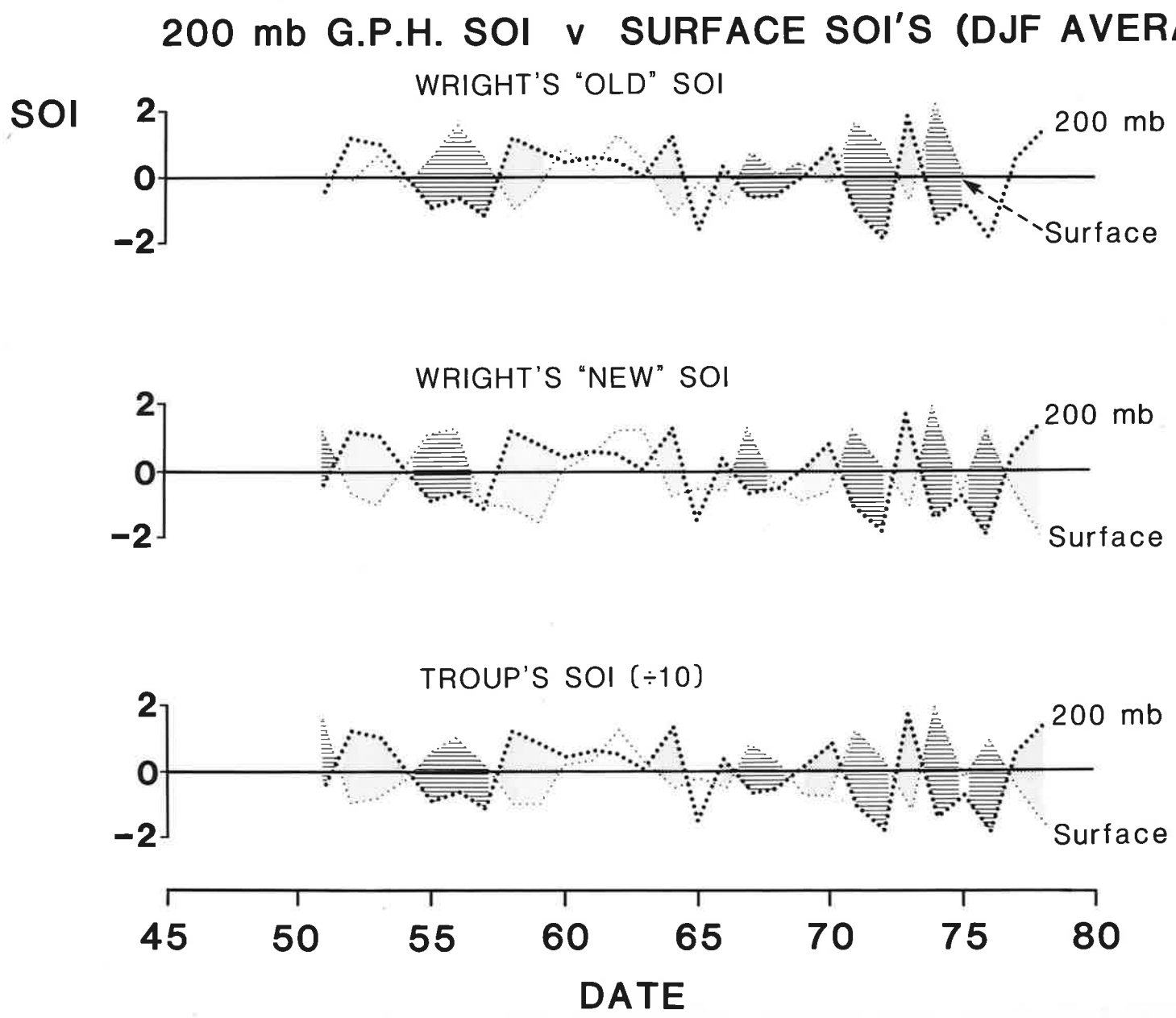
200 mb G.P.H. SOI v SURFACE SOI'S (DJF AVERAGE)
WRIGHT'S "OLD" SOI
SOI
2
0
-2
200 mb
Surface
WRIGHT'S "NEW" SOI
2
0
-2
200 mb
Surface
TROUP'S SOI (÷10)
2
0
-2
200 mb
Surface
45
50
55
60
65
70
75
80
DATE

This can be seen in Figure 102 where three surface SOIs are matched against Horel and Wallace's 200 mb SOI for the Southern Hemisphere summers (December-February) from 1951 to 1978. The earlier (1951-60) and later (1971-78) periods of Figure 102 distinctly coincide with the most pronounced SO/WC extremes noted in Van Loon and Madden (1981), with the later period including the five years examined in this study. However, there are sufficient anomalies in this comparison to suggest that care should be taken even when using large SOI extremes. For instance, the poor matching of the SOIs in the early 1960's in all three diagrams seems to be synonymous with a major change or disruption of SO/WC trends.

Bearing all this in mind, it is useful to investigate some of the ramifications of the links between the Southern Hemisphere summer monsoon and SOI intensities noted in Tanaka (1981). In Figure 103, the top diagram shows the relationship and correlation (r = + 0.94) between an SOI (Tahiti-Cocos Island) and Tanaka's indice (150 mb zonal wind speed at Singapore) of the Asian monsoon during the Southern Hemisphere summers from 1961-80. Given the findings of the composites in Section 3.3.1 *(ii)*, a strong correlation is expected, as + and - SOI phases are usually associated with pronounced increases and decreases in the zonal upper wind speed over the Indonesian longitudes respectively. However, to make this analysis more comparable with the evidence presented in Section 3.3.2, it was necessary to relate individual peak summer monthly mean wind speeds and SOIs (Fig.103 centre and bottom). Despite the fact that it relates Tahiti-Darwin differences, the Troup SOI was used as it provides a monthly mean record of surface pressure tendencies.

From the middle diagram in Figure 103, it can be seen that the above SOI/monsoon intensity relationship has a finer structure than the top diagram would suggest, indicating that some monsoon seasons can show strong SOI and monsoon index correlations which are primarily the contribution of one month's activity (i.e. 1962, 1971, 1975 and 1978). This is also reflected in a decrease in the correlation coefficients from + 0.94 (Fig.103 top) to

Figure 103 Relationships between the Southern Hemisphere summer monsoon of Australasia and SOI intensities. The top diagram from Tanaka (1981) shows the matching and correlation (+ 0.94) between an index of the Asian monsoon (150 mb zonal wind speed at Singapore) and an SOI or Walker Circulation Index (surface pressure difference between Tahiti and Cocos Island) in the Southern Hemisphere summers from 1961-80. The two remaining diagrams illustrate a similar relationship between Troup's SOI and Singapore 150 mb zonal wind speed and Troup's SOI and Darwin 150 mb zonal wind speed in the Southern Hemisphere summer months of January and February from 1961-81. The correlations for the latter are + 0.76 and + 0.50 respectively. In the top diagram, numbers on the right-hand side are of zonal wind speed in m s^{-1} while those on the left-hand side are those of the Walker Circulation Index.

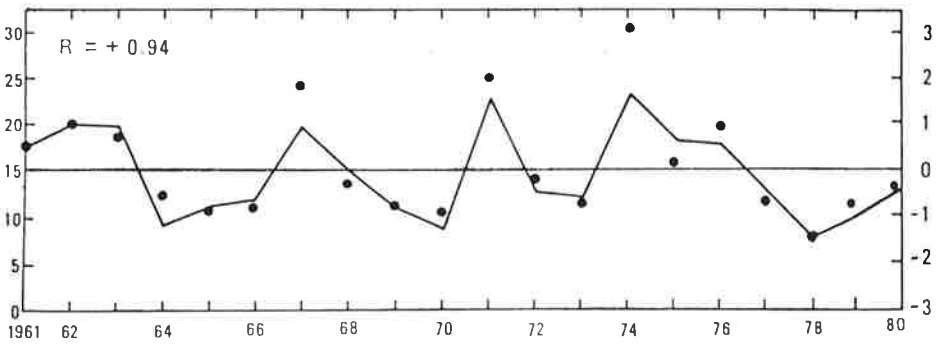

TROUP'S SOI v SINGAPORE 150 mb WIND SPEED

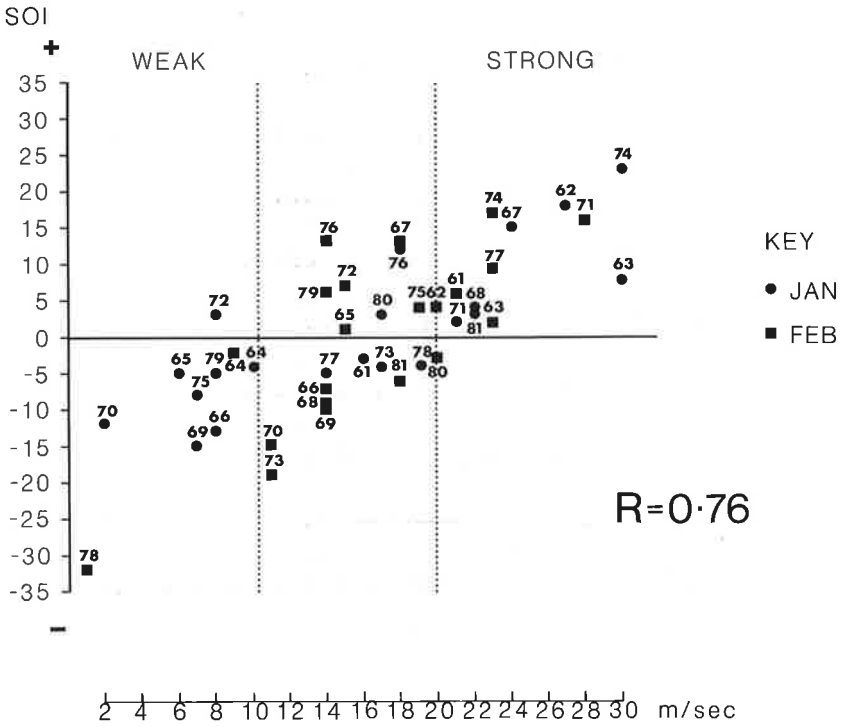

TROUP'S SOI v DARWIN 150 mb WIND SPEED

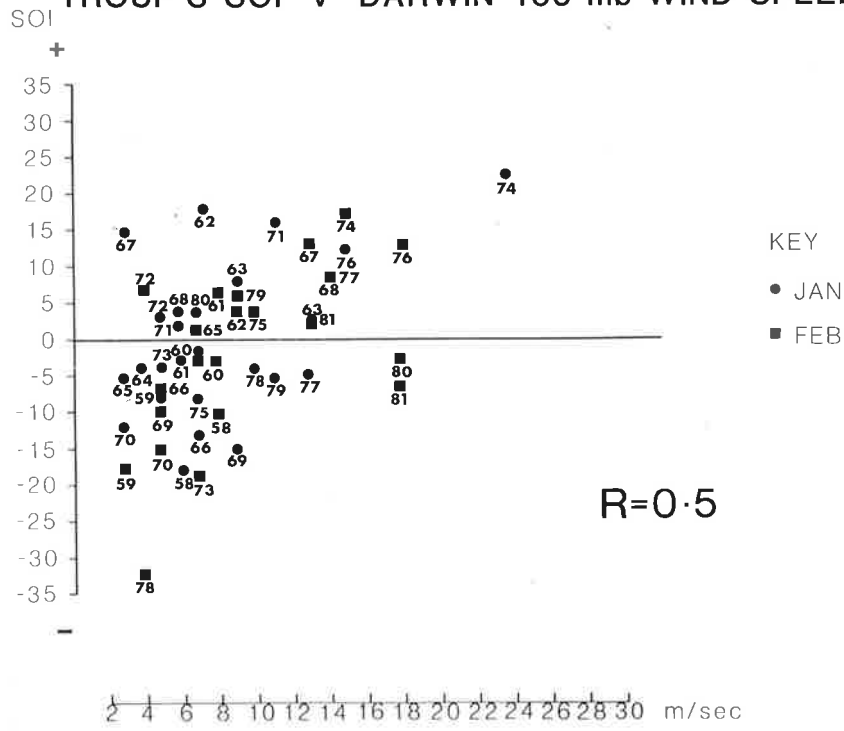

+ 0.76 (Fig.103 centre) and in the only incidences of associations with pronounced ascending motion over the Indonesian region in Januarys 1967 and 1974. Therefore, it seems that correlations between the SOI, ascending vertical motion and summer monsoon intensity over the western extent of the 'maritime continent' are, at best, only moderately strong. This is supported by instances where ascent is strong in the face of poor SOI/monsoon index correlations. Nevertheless, the latter may only reflect the bias of SOIs towards the monsoon index used.

If the situation over the 'maritime continent' shows some expected associations, then the poorer correlation (+ 0.50) at Darwin (Fig.103 bottom) testifies to the spasmodic nature of large monsoonal incursions over Australia. In this regard, January 1974 is prominent, with a lesser signature in February 1976. Moreover, the heavy bunching of values at low wind speeds and spanning weak to moderate SOI's again indicates that northern Australian longitudes do not present much hope for consistent associations with strong SOI's. This may be exacerbated by the evidence of a non-stationary time scale associated with the SO/WC (Wright, 1977; Van Loon and Madden, 1981) and thus the tendency for some periods in the temporal record to be better correlated with atmospheric variables and physical manifestations than others.

Overall, the fact still remains that a single SOI value does little more than indicate a pressure tendency and is by no means a certain indicator of ascending motion. As noted earlier in this discussion, manifestations of strong SO/WC phases in the wind circulation field over Australasia can be located anywhere in the Indonesian/Malesian sector. Added to this is the indication in Section 3.1.2 *(iii)* that poor geostrophic relationships occur in equatorial and near-equatorial regions, indicating that direct pressure/circulation comparisons can be misleading.

Therefore, the above discussion presents something of a paradox, in that it indicates that the potential of upper air data used in Section 3.3.2 is of short temporal duration, making it useless for longer period analyses

of SO/WC tendencies. Yet, what it has shown is that if long-term surface pressure-derived SOI records are the only indicator available, then one should only place confidence in extremely strong values. As a consequence, extended temporal analyses, which can provide important climatic information, must inevitably fall back on SOIs, hopefully taking into account what has been demonstrated concerning their relationship to dynamic features.

(ii) The Southern Oscillation, Australian Rainfall and Lake Eyre Floodings

In this section, aspects of SOI, SO/WC relationships with physical manifestations over Australia are examined through rainfall/SOI correlations, historical SOI/Lake Eyre flooding/PDZ rainfall associations and inferences from palaeo-environmental evidence. In this regard, the SOIs of Troup and Wright ('old' - Lamb, 1977 and 'new' - Wright, 1981; personal communication), SOI/rainfall correlations of Pittock (1975), Nicholls and McBride (1981; personal communication) and McBride and Nicholls (1983), Lake Eyre flooding data (Bonython and Mason, 1953; Mason, 1955; Bonython, 1960, 1963; Tetzlaff, unpublished; Graetz, 1980), PDZ rainfall data (Quinn and Burt, 1970; Reiter, 1978, 1979) and Lake Frome pollen analysis (Singh, 1981) are presented.

It has been suggested that strong SO/WC phases can play an important role in Australian summer rainfall mechanisms. Despite this, the SO/WC teleconnection has not been previously equated with any physical manifestations over the Australian continent, except for some early suggestions of rainfall forecasting signatures in the Darwin pressure records (Quayle, 1918, 1929), rainfall associations with Walker's original Southern Oscillation Index (Rimmer and Hossack, 1939) and recent reappraisals of this evidence (Priestley, 1962; Coughlan, 1975; Pittock, 1975; Nicholls, 1979 b; Angell, 1981; Nicholls and Woodcock, 1981; Nicholls *et. al.*, 1982; McBride and Nicholls, 1983). However, during the 1974 flooding/filling of the Lake Eyre salt pan in northern South Australia (Douglas and Hobbs, 1974; Vickery, 1974; Serventy, 1975; Dulhunty, 1979), this teleconnection

appeared to play a vital role (in conjunction with the Australasian monsoon) in generating deep convective processes.

In terms of area, the Lake Eyre Basin (Fig.104) is one of the major drainage systems of the Australian continent. However, its flow is non-perennial and, according to Mawson (1950), Bonython and Mason (1953), Mason (1955) and Graetz (1980), only carries consistently large volumes of water when heavy, summer monsoonal rainfall occurs in the Queensland section of the Basin. Included in this part of the catchment area are the central-western extremities of the Great Dividing Range and the central Queensland tablelands, which together provide additional orographic influence (see Fig.44).

Nevertheless, as noted previously, correlations and associations between the SO/WC and monsoonal activity over Australia should be made with care. This is also borne out by the spatial correlations presented in Pittock (1975) and Nicholls and McBride (1981; personal communication). In Pittock (1975) (Fig.105), two diagrams show the pattern of equal correlation coefficients between an annual mean Southern Oscillation Index (Troup's SOI) and district mean annual rainfall, and between the annual mean latitude of the surface high pressure belt over eastern Australia and district mean annual rainfall. Of these patterns, the one related to the SOI provides the best correlation with high rainfall totals over northern Australia. From a brief appraisal, it could be said that of the diagrams in Figure 105, the right-hand diagram appears to reflect a dominant 'summer-like' (SOI) distribution (similar to the pattern over Australia in Stoeckenius, 1981). However, such an examination of annual patterns does not discern the true seasonal composition of such correlations and, as Figure 106 shows, can be totally misleading.

Using the 'old' SOI (developed by Wright, 1977) Nicholls and McBride (1981; personal communication) analysed the seasonal pattern of SOI/rainfall correlations over Australia during 1933-74 (Fig.106). As can be seen, the association is most spatially extensive in March-May (autumn), June-August (winter) and September-November (spring), while correlations are weakest in

Figure 104 Lake Eyre drainage system from Department of National Resources Australian Water Resources Council, 1976.

Figure 105 Pattern of equal correlation coefficients between an annual mean Southern Oscillation Index (Troup's SOI) and district mean annual rainfall (left-hand diagram) and between the annual mean latitude of the surface high pressure belt over eastern Australia and district mean annual rainfall (right-hand diagram) from 1941-70 (from Pittock, 1975).

Figure 106 Pattern of equal correlation coefficients between a seasonal mean Southern Oscillation Index (Wright's 'old' SOI) and district mean seasonal rainfall from 1933-74. Seasons are defined as summer (December - February), autumn (March - May), winter (June - August) and spring (September - November) (from Nicholls and McBride, 1981 personal communication).

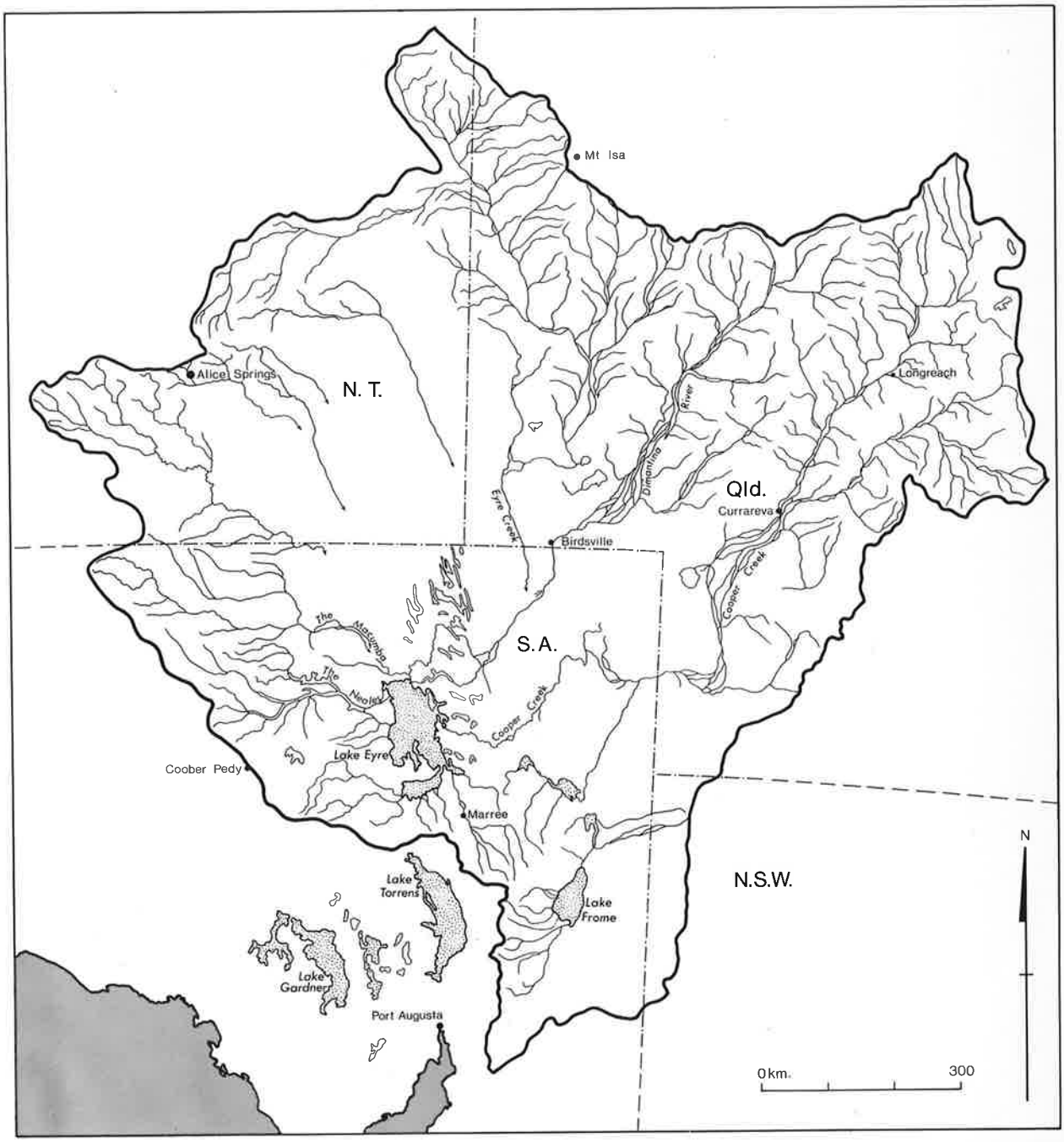
Mt Isa
Alice Springs
N. T.
Longreach
Diamantina River
Qld.
Currareva
Eyre Creek
Birdsville
Cooper Creek
The Macumba
The Neales
S.A.
Cooper Creek
Lake Eyre
Coober Pedy
Marree
Lake Torrens
Lake Frome
N.S.W.
Lake Gardner
Port Augusta
N
0km.
300

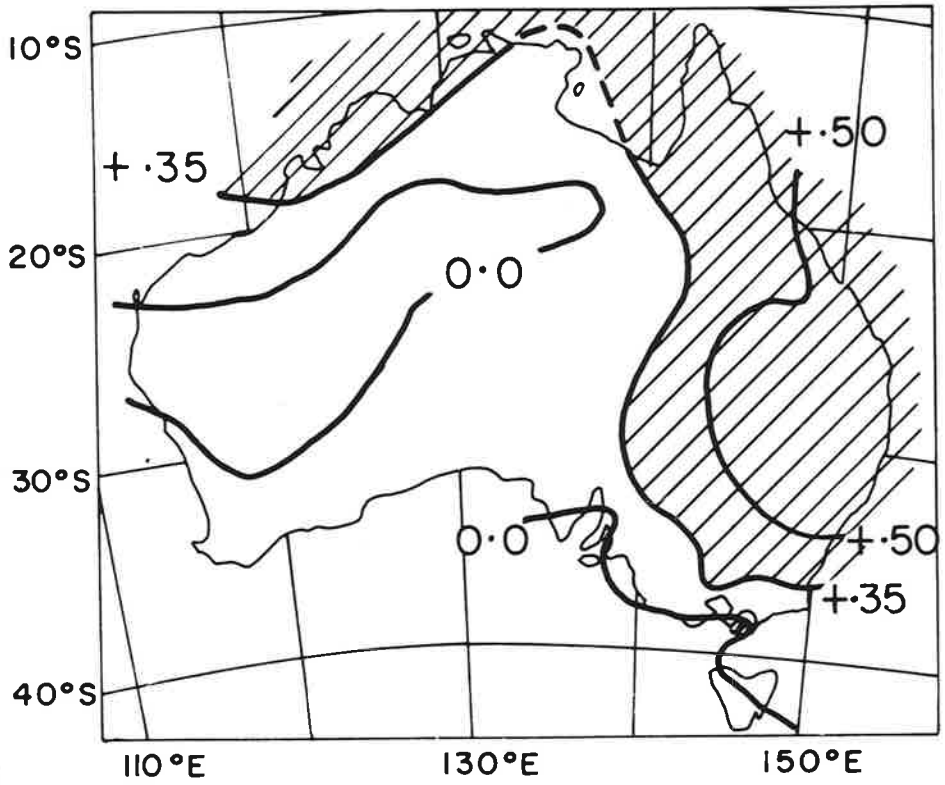
10°S
20°S
30°S
40°S
110°E
130°E
150°E
+·35
0·0
+·50
0·0
+·50
+·35

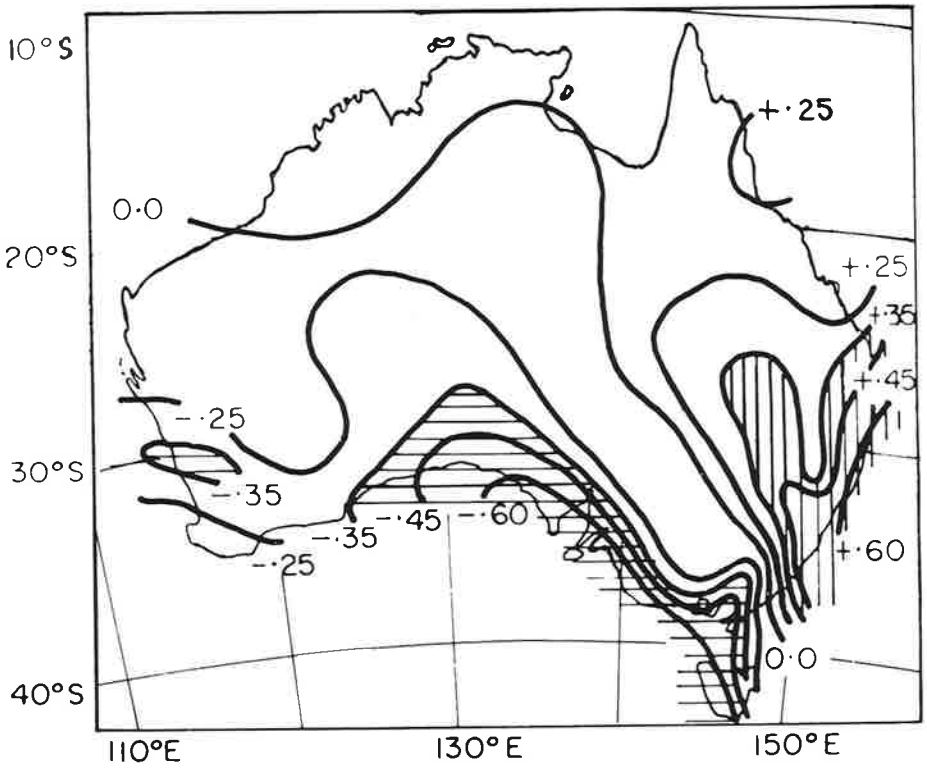
10°S
20°S
30°S
40°S
110°E
130°E
150°E
+·25
0·0
+·25
+·35
+·45
+·60
0·0
−·25
−·35
−·45
−·60
−·35
−·25

WRIGHT'S "OLD" SOI v AUSTRALIAN RAINFALL IN THE SAME SEASON 1933-74

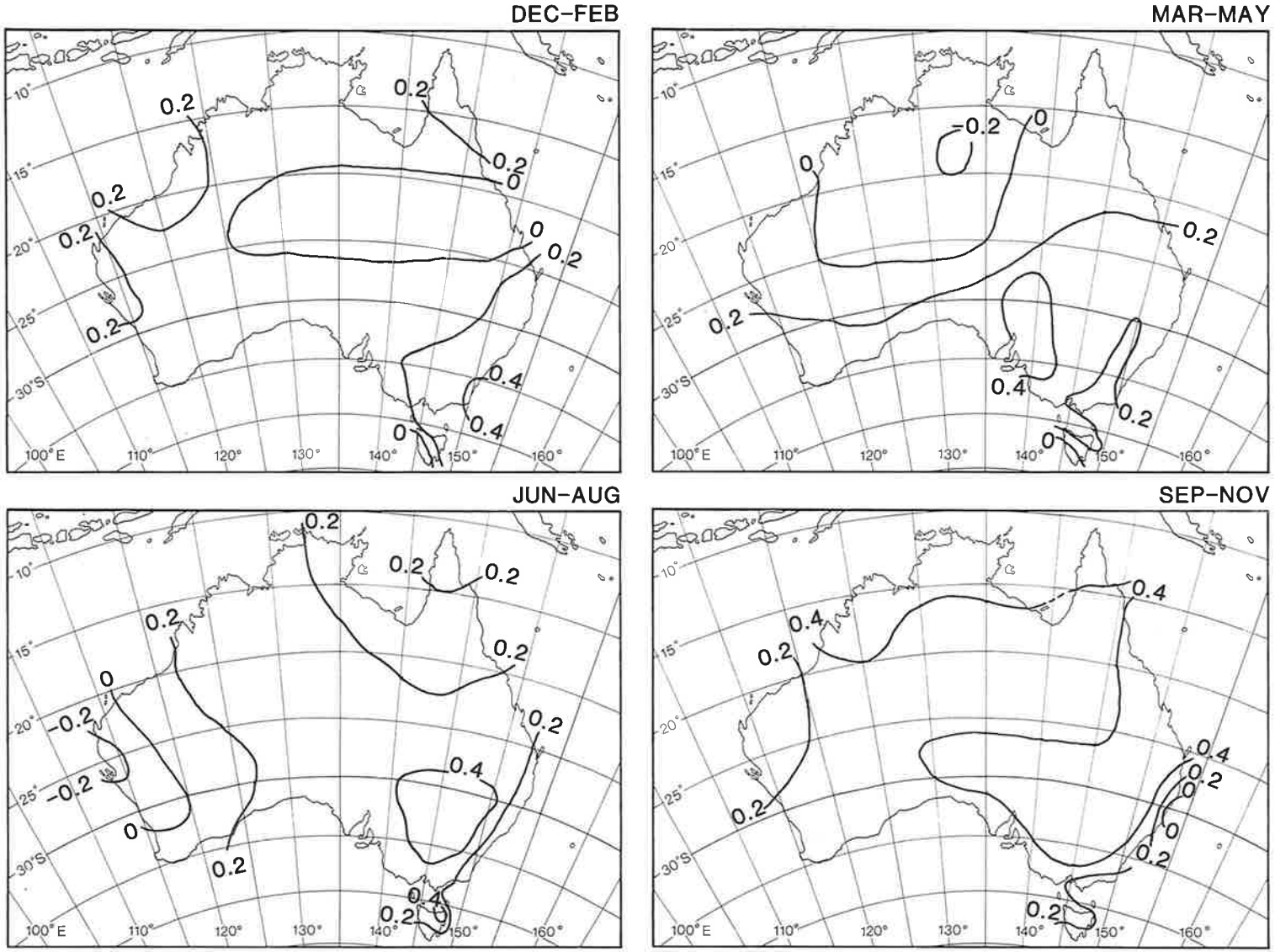

the Southern Hemisphere summer (December-February). Moreover, similar relationships were identified for Troup's SOI (McBride and Nicholls, 1983). Interestingly (according to Pazan and Meyers, 1982), Wright's (1981; personal communication) 'new' SOI shows the largest standard deviation and pronounced bimodality of values in December-February during the period from 1947-73 (Table 2). However, using Wright's 'old' SOI (Table 3), the situation becomes very untenable, with none of the aspects of the Pazan and Meyers (1982) (Table 2) evaluation being evident.

The major difference in the above SOIs appears to be in the number and distribution of stations used in their construction. In the 'old' SOI, Wright (Lamb, 1977) used up to eight stations, including Adelaide, Apia, Bombay, Cape Town, Darwin, Santiago, Batavia (Jakarta) and Honolulu, while the 'new' SOI relied on only five stations (Wright, 1981; personal communication). According to Pazan and Meyers (1982), these were Bombay, Darwin, Apia, Tahiti and Easter Island. Obviously, the 'old' SOI is more of an Indo-Pacific average, while the 'new' SOI has a distinctly Australasian to Pacific bias. Therefore, it is perhaps no surprise that the latter is more responsive to the nature of persistence in the Australian region (Priestley, 1962; Troup, 1965) and Pacific region (Wright, 1979 a). It would be interesting to be able to compare the 1947-73 SOI histogram with those in other periods in order to gauge the extent of the non-stationary temporal element in such distributions. Despite its faults, the 'old' SOI has the necessary temporal coverage and, like the four 32 year power spectra diagrams (Fig.3; Section 1.1.2), shows a degree of variation that is, in this case, most prominent in the earliest (1851-1882) and latest (1941-1972) periods.

Following the research of McBride and Nicholls (1983), it is obvious that correlations between various SOIs and Australian summer rainfall are generally poor. However, as noted above and in Pittock (1981), the non-stationary temporal element dictates that such correlations can be markedly variable through time (see also Pittock, 1975; Russell, 1981; Streten, 1982).

TABLE 2

Histogram of Wright's 'new' SOI values by Season 1947-73

	SOI value					
Season	- 2.5	- 1.5	- 0.5	0.5	1.5	2.5
DJF	1	10	6	9	0	
MAM	1	6	13	4	2	
JJA	2	5	11	7	1	
SON	2	8	10	5	1	

TABLE 3

Histogram of Wright's 'old' SOI values by Season 1947-73

	SOI value					
Season	- 2.5	- 1.5	- 0.5	0.5	1.5	2.5
DJF		4	14	8	1	
MAM		1	14	9	3	
JJA	2	1	10	12	2	
SON		6	6	11	4	

Nevertheless, there is evidence in the raw SOI data of periods of extensive persistence of + SOI phases (see Pittock, 1981) from autumn/winter into the following summer. Using Troup's SOI, this is most evident in 1938-39, 1950-51, 1955-56, 1962-63, 1970-72, 1973-74 and 1975-76, with all periods containing intense + SOI elements. As has already been noted in the present study, the 1973-74 and 1975-76 situations coincide with strong Asian monsoonal activity and incursions into Australia. Therefore, if the phenomenon of Lake Eyre flooding/filling is to be considered as a physical manifestation of strong + SOI episodes or high SO/WC activity, its relation to the above periods is critical.

Several researchers, using some of the earliest reports and rainfall records, have suggested that there is evidence of past floodings of Lake Eyre. Yet, prior to 1950, there was much contention as to whether the lake did and/or could actually flood. Much of the confirmation of flooding/filling phases in the lake was due to expeditions and subsequent research by members of the Royal Geographical Society of Australasia, South Australian Branch (general reports are found in Mawson, 1950; Bonython, 1951, 1959). In their study of the 1949-1950 filling, Bonython and Mason (1953) indicated that earlier Lake Eyre fillings may have occurred in 1890-91, 1906-7, 1916-18 and 1920-21. In a later report, Mason (1955) suggested that 1869, 1885, 1887, 1894, 1903, 1939 and 1941 might be included as years when the lake was partly flooded. Bonython (1960, 1963) added the more recent dates of 1951, 1953, 1956, 1957, 1958, 1959 and 1963, while Tetzlaff (unpublished) attempted to order the sequence into a set of flooding extremes. The Lake Eyre flooding index in Figure 107 is a combination of these authors' major and minor flooding dates and is primarily based on rainfall figures for the Queensland section of the drainage basin. Index values from 1963 to 1975 are deduced from Graetz's (1980) criteria for the size of floods at Currareeva on the Cooper Creek (1939-1976) and at Birdsville on the Diamantina River (1949-1977) (see Fig.105 for place location).

The 'old' SOI compiled by Wright (in Lamb, 1977) for the period from

Figure 107 Relationship between Wright's 'old' SOI, extensive or isolated outbreaks of equatorial PDZ rainfall and major or minor floodings of Lake Eyre in South Australia over the period 1860-1975. PDZ data from a combination of material in Quinn and Burt (1970) and Reiter (1978, 1979) and Lake Eyre flooding data from a combination of material in Bonython and Mason (1953), Mason (1955), Bonython (1960, 1963), Tetzlaff (unpublished) and Graetz (1980).

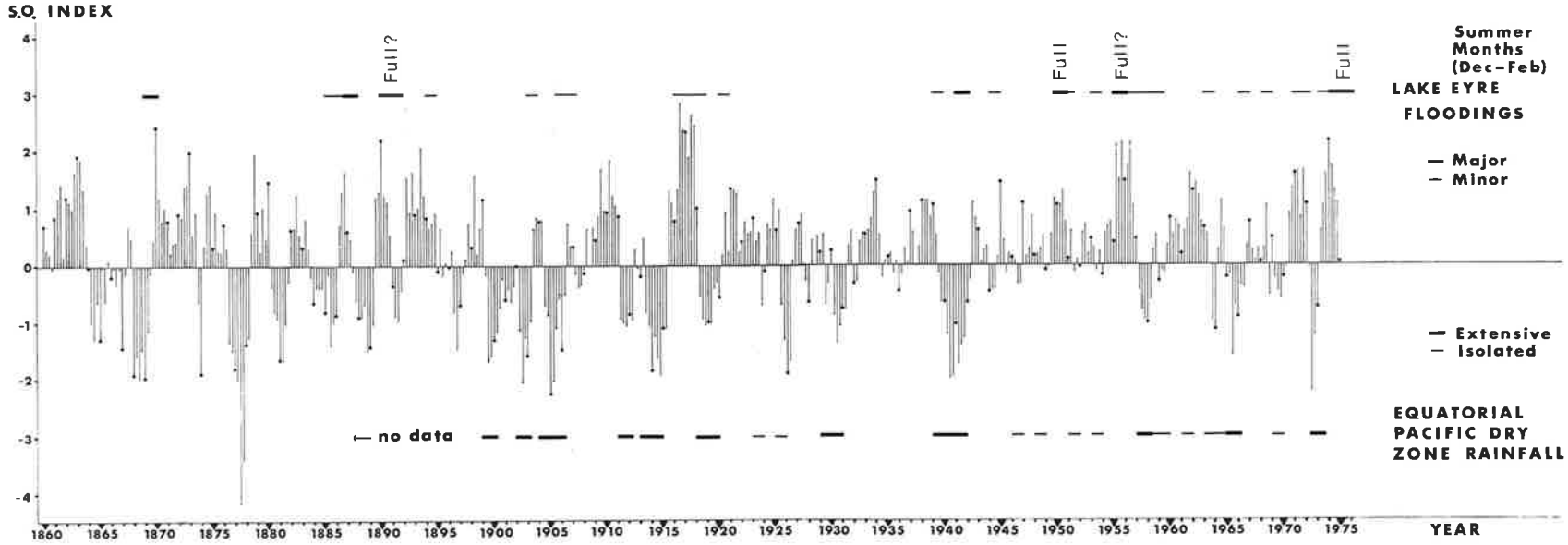
S.O. INDEX
4
3
2
1
0
-1
-2
-3
-4
Full?
Full
Full?
Full
Summer Months (Dec-Feb)
LAKE EYRE FLOODINGS
Major
Minor
Extensive
Isolated
no data
EQUATORIAL PACIFIC DRY ZONE RAINFALL
1860
1865
1870
1875
1880
1885
1890
1895
1900
1905
1910
1915
1920
1925
1930
1935
1940
1945
1950
1955
1960
1965
1970
1975
YEAR

1860 to 1975 is presented in Figure 107 as a series of seasonal values Each year is divided into summer (December-February), autumn (March-May), winter (June-August) and spring (September-November). The summer periods are specifically marked (by a dot at the end of the index departure increment) to investigate possible associations with periods of extreme summer monsoon rainfall and extensive floodings. Dates of precipitation extensiveness in the equatorial PDZ are obtained from Quinn and Burt (1970) and cover the period from 1890 to 1966. Subsequent data have been inferred from Reiter's (1978, 1979) precipitation index for the Line Islands.

Figure 107 indicates that major floodings are generally related to strong positive peaks in the SOI. The most significant exception is the 1941 case which is only designated as a major flooding by Tetzlaff (unpublished). Dates which all the authors recognize as probable major flooding/filling periods are 1890-91, 1949-50, 1955 and 1974-76. These times are directly related to positive peaks in at least the summer SOI. In fact, above average winter and spring rainfall, followed by an intense summer extreme, appears to be necessary to ensure a major flooding, if not filling, episode. Further situations may be inferred if prolonged peaks in the SOI can be interpreted as wetter periods over Australia.

Several periods of high positive SOI coincide with either minor or no recognized flooding of the lake. Such periods may reflect times when the spatial distribution of rainfall did not favour the drainage basin/ catchment region. A lack of major rainfall in the Queensland section of the catchment appears to preclude a major Lake Eyre flooding (Bonython and Mason, 1953; Mason, 1955). The final decision of the authors to describe a period of past flooding as major or minor was often based on comparisons with known rainfall figures and river levels during more recent floodings. Thus years such as 1916-18 may not have been regarded as major flooding periods by some authors because of the criteria used to rank floods. Alternatively, this could reflect a lack of direct observational evidence at the time (coinciding with World War I). This is possibly true for other

similar periods in the record. In fact, the amount of detailed information available peaked in the decade following the first definitely recorded filling in 1949-50. Co-ordinated analysis of satellite imagery could now provide a more satisfactory monitoring base.

One of the most interesting applications for confirmed associations between marked monsoon activity, a strong SO/WC and major Lake Eyre floodings could be in providing possible evidence of Quaternary climatic patterns and the potential for future climatic scenarios over Australia. Recent research on Quaternary changes in Australasian environments would suggest that marked climatic variability has affected this region (i.e. Vestappen, 1975, 1980; Williams, 1975; Bowler *et. al.*, 1976; Rognon and Williams, 1977; Pittock *et. al.*, 1978; Webster and Streten, 1978; Bowler and Jones, 1979; Henderson and Stephenson, 1980; Pittock, 1980; Prell *et. al.*, 1980; Singh, 1981; Singh *et. al.*, 1981; Thom and Watson, 1982). Such claims have been largely derived from geomorphological evidence. As direct glacial effects are confined to New Guinea, Tasmania and the Australian Alps, information about the Quaternary in mainland Australia has come primarily from studies of dunes and lakes.

While palynological examination of lake bed sediments has taken place in eastern and southeastern Australia (i.e. Lake George, Lynch's Crater, Lashmars Lagoon, Wyrie Swamp, Lake Leake, Lake Keilambete, Lake Colongulac, Lake Corangamite and the Willandra Lakes) and southwestern Western Australia (i.e. Scott River, Boggy Lake, Weld Swamp and Myalup) (Thom and Watson, 1982), little has been done in the playa lakes of the arid interior (Bowler, 1981; Fig.108). Only at Lake Frome in South Australia (to the author's knowledge) has a pollen record been fully reported (Singh, 1981). Singh (1981) suggests not only that high pollen levels could be related to high rainfall periods but also that the floral nature of the pollen may give some insight into the seasonality of the rainfall. Thus incidences of high grass pollen in 1973-77 have been related to periods of heavy summer rainfall and, indeed, monsoon incursions into the continent in 1974 and 1976. The consequent

Figure 108 Distribution of playa lakes over the Australian continent (from Bowler, 1981).

Figure 109 Lake Frome pollen diagram over the last 10,000 years. Pollen catch A is the modern annual pollen influx (grains cm^2 yr^{-1}) and charcoal particle influx (numbers greater than 10 μ cm^2 yr^{-1} x 5) from 13th November 1973 to 13th November 1977. Fossil pollen record B shows percentages of total land plant pollen and the charcoal influx record (numbers greater than 10 μ cm^3 yr^{-1}) from the sediments of the lake (from Singh, 1981).

L. Woods
L. Gregory
L. Buchanan
L. Galilee
L. Eyre
L. Frome
L. Torrens
L. Gairdner
L. Tyrrell
L. George
L. Keilambete
L. Gnotuk

RADIOCARBON YEARS BP BEFORE PRESENT
STRATIGRAPHY
POLLEN ZONE
SAMPLE INTERVAL
POLLEN CATCH
TREES
TALL SHRUBS
LOW SHRUBS AND HERBS
MODERN POLLEN RAIN
FOSSIL POLLEN SEQUENCE
EUCALYPTUS
CASUARINA
MYRTACEOUS SHRUBS
ACACIA
DODONAEA
LODOICEA
CHENOPODIACEAE
POACEAE
CYPERACEAE
PLANTAGO
TUBULIFLORAE
TOTAL POLLEN INFLUX PER CM3 x 10
NUMBER OF CHARCOAL PARTICLES >10 µ PER CM2 PER YEAR x 5
POLLEN SUM
CHARCOAL INFLUX
N S W 9300 ↑ 600
N S W 4270 : 230
N S W 4180 : 590
Diatomaceous clay with small gypsum crystals
Diatomite
Laminated clay with small gypsum crystals
< 1%

analysis of the lake core's fossil (Holocene) pollen assemblage was then made with the above in mind (Fig.109). It produced evidence of a 9500-8000 years BP rainfall maximum (warmest Holocene period in the Southern Hemisphere) with a secondary peak in the 7000-4200 years BP period.

It would seem that if similar palynological, plus sedimentological and stratigraphical, analyses could be made of cores taken from Lake Eyre, then some sequence of long-term monsoon variability could be attempted. An analysis of wave built shingle terraces by Dulhunty (1975) suggests that there is evidence of major Lake Eyre fillings some 2.8, 1.6 and 0.7 metres above 1974 levels. These are tentatively dated at 5000-1000, 1000 and 500 years BP respectively. From considerations of both the extent of modern Lake Eyre and Lake Frome floods and the nature of the Lake Eyre drainage basin's stream system (which can be seen to include Lake Frome in Fig.104), it would seem that Lake Eyre pollen and sediment assemblages should give a better indication of monsoon incursions than any taken from Lake Frome (although logistical and poor data problems could be paramount - Bowler, 1982; personal communication). No doubt, a cross correlation with cores taken from several of the other playa lakes would be useful in evaluating the spatial sensitivity of the basin to major hydrological variations. This is especially important when one considers that most of the inflow into the basin comes via the Cooper Creek and the Diamantina River which ultimately discharge directly into Lake Eyre.

Thus, as shown earlier, periods of lake flooding, if not filling, tend to occur when monsoon rainfall markedly affects the Queensland section of the basin. These are most likely to be recorded by analysis of sediments alone, although only periods reflecting major changes in, or incursions of, the monsoon system are likely to result in the type of precipitation event that would inundate the inland and thus influence vegetation and pollen counts.

It would seem that evidence from modern meteorological data and historical records are a useful starting point for a reconstruction of Quaternary monsoon

regimes over Australia. If, as suggested, pollen type can be related to the seasonality of rainfall and cross correlated with sedimentological evidence in the Lake Eyre Basin, then inferences about long-term monsoon, and perhaps SO/WC, variability can possibly be made.

CHAPTER IV - CONCLUSION

This thesis has endeavoured to provide an appraisal of the spatio-temporal patterns of Southern Hemisphere summer monsoon seasons and related teleconnection fields over Australasia. Overall results would appear to suggest that the Australian continent is in a peripheral region of the Asian monsoon system and a transitional zone of the Southern Oscillaion/Walker Circulation (SO/WC) phenomenon. Nevertheless, large-scale monsoon and teleconnection extremes are evident over Australia in contemporary analyses, historical records and Holocene sequences (proxy data).

On the scale of the Indo-Pacific (35°N-35°S; 30°E-60°W) and regional (35°N-35°S; 85°E-175°E) domains, summer mean convective activity is generally centred on the 'maritime continent'. However, the most pronounced variability in atmospheric features (i.e. vertical ascending motion, rainfall, trade winds) occurs over the equatorial Pacific and, in particular, the Pacific Dry Zone (PDZ). During extremes of the SO/WC, convective activity is seen to fluctuate between the above locations. Yet, there is only scant evidence of a distinct shift in the entire convective focus from Asia to the PDZ during weak SO/WC episodes.

Over the 'maritime continent', low-level convergence often has a pronounced 700 mb maximum, while in the region of the PDZ it is only centred as high as 850 mb in the most extreme rainfall outbreaks. The latter is seen to follow the pattern of NET_{NH} enhancements and thus changes in the depth of the northeast trade wind field accompanying weak phases of the SO/WC. Moreover, 200 mb velocity potential fields indicate that upper-level divergence predominates over the 'maritime continent' in almost all cases, with PDZ rainfall outbreaks being accompanied by a separate or secondary upper divergence region.

Thus, on average, large-scale convective sources tend to occur to the north-northeast and north-northwest of Australia, with only occasional monsoon incursions penetrating into the inland. During the latter episodes, the

continent is influenced by strong upper-level divergence, an intense and deep NET_{SH}, spatially enhanced moisture characteristics and greater vertical organisation of convective elements. In fact, incursions seem to reflect a marked increase in the SO/WC overturning, while most other seasons display amorphous monsoon and teleconnection patterns. However, there are periods which are accompanied by a distinct 'breakdown' in the upper-level divergence field, weak or poorly defined NET_{SH} activity capped by anticyclonicity at 850 or 700 mb levels and poor moisture characteristics. These are seen to develop during very weak SO/WC phases, PDZ rainfall outbreaks and El Niño episodes.

The above observations strongly support the concept that Australia lies in a transitional zone of the SO/WC. Only during the more rare occasions of pronounced SO/WC extremes is the continent influenced by either the expanded convective 'maritime continent' source or the marked subsidence between localized 'maritime continent' and enhanced PDZ sources. Perhaps even rarer are the situations when PDZ convection is the dominant low latitude source, and subsidence over eastern Australia reaches a maximum.

Such evaluations become particularly complicated when considering the nature of cross-equatorial flow, surges and transient features in the Australasian and northern Australian regions. There is substantial evidence of the influence of cross-equatorial interaction across the low latitude 'maritime continent' region (e.g. Chang *et. al.*, 1979; Chang and Lau, 1980; Webster, 1981 a) but little of its penetration into Australia (Williams, 1979). The short period of observation in this thesis suggests that there are marked variations in cross-equatorial flow between the surface and 850 mb levels. In fact, there are indications that the NET_{NH} (western section) at 850 mb is enhanced during strong SO/WC phases but that its surface counterpart is poorly defined. During weak SO/WC phases the opposite appears to occur. The relationship between these events and the northern Australian heat low complex still requires elucidation, as the above implies greater heat low activity in drier periods and less heat low activity, but greater NET_{SH}

intensity, during wetter phases. Cold surge penetration into the Southern Hemisphere as far south as Australia is also difficult to evaluate from a limited data sequence. Nevertheless, such action is observed in this study and may be more prevalent during particularly anomalous circulation modes or SO/WC extremes. Finally, transient eddy fields illustrate the nature of time-average features and testify to the progression and alternation of systems across Australia.

A more detailed analysis of circulation features and convective systems over northern Australia is revealed in the local domain (5°S-30°S; 95°E-155°E). The months of January and February are seen to represent the peak period of monsoonal activity, with March frequently marking the beginning of its cessation and withdrawal. Of the standard levels analysed, 900 mb is generally the level where circulation and convective elements are at a maximum. No doubt, this would apply to regions just above the planetary boundary layer, where surface frictional effects diminish. In most NET_{SH} situations, the trough shows a tendency to weaken as it tilts equatorward (from south to north) in the vertical plane. This is probably a result of the loss of the anchor for the trough provided by the near-surface heat low complex, although this effect is not evident in very intense NET_{SH} systems. Perhaps more importantly, an analysis of long-term average zonal and meridional wind and mixing ratio distributions indicates that the wind (in particular the zonal component) is more variable in tropical latitudes, while the mixing ratio is high but varies much less. In sub-tropical latitudes the reverse appears to be the case. Thus monsoon incursions would seem to be a major source of large-scale moisture penetration into the inland.

From the above discussions, it is obvious that monsoon and SO/WC actions over Australia are often elusive. Historically, this teleconnection's phase and intensity have been deduced from various indices of surface pressure tendency (SOIs). In regard to PDZ events and, to a lesser degree, those over the 'maritime continent', this index has been a useful indicator. However, in the Australian region it has been found to be somewhat inconclusive

(McBride and Nicholls, 1983). In fact, as SOIs are generally constructed from one parameter at one level in the atmosphere and appear as discrete positive and negative numerical values, it is not surprising that their ability to resolve fully the SO/WC teleconnection is questionable. This is particularly emphasized by Van Loon and Madden (1981), Chen (1982 a) and Rasmusson and Carpenter (1982) when they indicate that the SO/WC phenomenon is a non-stationary spatio-temporal fluctuation that produces varied responses in atmospheric and oceanic features. Furthermore, the analysis of stream-function and GPH fields shows a strong ageostrophic component in low latitude flow and thus the limited potential of SOIs deduced from one parameter alone.

As a consequence, moderate to weak SOIs are poor indicators of SO/WC phases, especially over Australia. In an attempt to overcome some of this problem, both the core period (1973-77) and longer-term data sequence (1958-81) in the thesis focuses on Australasian monsoon and teleconnection dynamics. In the 1973-77 period, a number of dynamic signatures appear to be evident in the Australian region. Yet, an appraisal of longer-term data indicates that there are probably only a handful of these signatures that are still valid. Basically, it would seem that the most useful dynamic manifestations of SO/WC extremes are : 1) the depth and position of the NET_{SH} over Australia; 2) the nature of 200 mb anticyclonicity in the Southern Hemisphere; and 3) indications of an SO/WC 'breakdown' by the presence of upper-level convergence over eastern Australian/Papua New Guinean longitudes.

When compared with the more spectacular examples of SO/WC action in the Pacific basin, the Australasian region appears to have little to offer in the way of physical manifestations. This has been further compounded by poor correlations between SOIs and Australian summer rainfall patterns (McBride and Nicholls, 1983). In this thesis, it has been suggested that very strong SO/WC phases coincide with pronounced floodings and fillings of the Lake Eyre salt pan in South Australia. From contemporary data and historical records, this association would appear to be the culmination of extensive periods of deep convective organisation over northern Australia.

As such events seem to mirror the general pattern of persistence in the Australian region, it is suggested that they may involve a reinforcing and/or locking of the circulation in an enhanced SO/WC mode. Yet, the question of SO/WC phases and Lake Eyre floodings/fillings is complicated by the often poor relationship between SOIs and upper air dynamics. This is particularly evident when considering the possibility of long-term associations between the SO/WC and physical manifestations over Australia. Although palaeo-environmental sampling and analysis is still to be done at Lake Eyre, further research will be necessary to resolve many of the above problems.

Thus this thesis indicates that the major aspects of Australasian monsoon and SO/WC structure and timing would appear to be evident in upper air and upper wind fields, OLR, oceanic rainfall rates, cloud distributions, moisture characteristics and rainfall patterns. Unfortunately, the study has been restricted to the analysis of peak summer months and thus does not have the capacity to evaluate the seasonal distribution and evolution of teleconnection patterns over Australasia. Moreover, the genesis and cessation of monsoon extremes probably owe much to events during the rest of the year. Such factors have recently been exemplified by the wide-ranging 1982-83 drought in Australasia and severe El Niño in the Pacific (Climate Analysis Center, 1982). Similar to the strong SO/WC and Lake Eyre flooding events, the present anomaly would appear to involve a persistently weak SO/WC mode and major re-distributions of circulation systems and convective patterns. In fact, the possible range of SO/WC interactions on a global scale is given by the growing number of papers which suggest direct and indirect links with features such as carbon dioxide and ozone distributions, atmospheric angular momentum changes and stratospheric responses (i.e. Bacastow, 1976; Bacastow *et. al.*, 1980; Sadler *et. al.*, 1982; Stefanick, 1982; Van Loon *et. al.*, 1982; Zerefos *et. al.*, 1982). Such material now puts the SO/WC phenomenon firmly into consideration in theories of longer-term climatic variability and change.

Overall, it would appear that investigations of links between the SO/WC and the Asian monsoon system need to be conducted over a number of years. Similar to the MONEX sub-programme (Murakami, 1979), they must involve international support for a detailed appraisal of data at all levels of scale and continued efforts to upgrade existing observational networks. Over Australia, the need for increased SO/WC and monsoon research is paramount, with the continuing hope that some of the observed statistical and dynamic signatures may prove useful as forecasting tools. However, the non-stationary spatio-temporal nature of the SO/WC, together with Australia's location with respect to the major convective sources, makes the task most difficult.

APPENDIX 1

Upper Air and Upper Wind Stations; Regional Domain

Station	Station Number	Latitude	Longitude
American Trust Territories (North Pacific Islands)			
Wake Island	(91245)	19° 17'N	166° 39'E
Guam, Taguac, Mariana Islands	(91217)	13° 33'N	144° 50'E
Yap, Caroline Islands	(91413)	9° 29'N	138° 5'E
Kwajalein, Marshall Islands	(91366)	8° 43'N	167° 44'E
Truk, Caroline Islands	(91334)	7° 28'N	151° 51'E
Koror, Palau Islands	(91408)	7° 20'N	134° 29'E
Majuro, Marshall Islands	(91376)	7° 5'N	171° 23'E
Ponape, Caroline Islands	(91348)	6° 58'N	158° 13'E
Tarawa, Gilbert Islands	(91610)	1° 21'N	172° 55'E
Midway Island	(91066)	28° 13'N	177° 22'W
Australia			
Cocos Island	(96996)	12° 11'S	96° 50'E
Broome	(94203)	17° 57'S	122° 13'E
Port Hedland	(94312)	20° 23'S	118° 37'E
North West Cape	(94301)	21° 49'S	114° 10'E
Carnarvon	(94300)	24° 53'S	113° 39'E
Geraldton	(94403)	28° 48'S	114° 42'E
Perth Airport	(94610)	31° 56'S	115° 58'E
Albany	(94802)	34° 57'S	117° 48'E
Esperance	(94638)	33° 49'S	121° 53'E
Halls Creek	(94212)	18° 14'S	127° 40'E
Giles	(94461)	25° 2'S	128° 18'E
Meekatharra	(94430)	26° 35'S	118° 30'E
Kalgoorlie	(94637)	30° 46'S	121° 27'E
Forrest	(94646)	30° 50'S	128° 6'E
Willis Island	(94299)	16° 18'S	149° 59'E
Thursday Island	(94175)	10° 35'S	142° 13'E
Darwin Airport	(94120)	12° 26'S	130° 52'E
Tennant Creek	(94238)	19° 33'S	134° 11'E
Alice Springs	(94326)	23° 48'S	133° 53'E
Mount Isa	(94332)	20° 40'S	139° 29'E
Cloncurry	(94335)	20° 40'S	140° 30'E
Onslow	(94305)	21° 40'S	115° 7'E
Longreach	(94346)	23° 26'S	144° 15'E
Charleville	(94510)	26° 25'S	146° 17'E
Cairns	(94287)	16° 55'S	145° 44'E
Townsville	(94294)	19° 16'S	146° 46'E
Mackay	(94367)	21° 7'S	149° 10'E
Gladstone	(94380)	23° 51'S	151° 16'E
Brisbane/Eagle Farm	(94578)	27° 26'S	153° 5'E
Oodnadatta	(94476)	27° 33'S	135° 27'E
Woomera	(94659)	31° 9'S	136° 48'E
Moree	(94527)	29° 28'S	149° 51'E
Coffs Harbour	(94791)	30° 18'S	153° 8'E
Nowra	(94750)	34° 57'S	150° 32'E
Cobar	(94711)	31° 29'S	145° 50'E
Mildura	(94693)	34° 14'S	142° 5'E

Station	Station Number	Latitude	Longitude
Adelaide Airport	(94672)	34° 57'S	138° 32'E
Williamtown	(94776)	32° 49'S	151° 50'E
Ceduna	(94653)	32° 8'S	133° 42'E
Mascot (Sydney Airport)	(94767)	33° 57'S	151° 11'E
Honiara	(91517)	9° 25'S	159° 58'E
Norfolk Island	(94996)	29° 3'S	167° 56'E
Lord Howe Island	(94995)	31° 32'S	159° 4'E
Christmas Island	(96994)	10° 25'S	105° 43'E
China (Peoples Republic) (except for Januarys 1973 and 1974 at 200 mb, after 1977)			
Changsha	(57679)	28° 12'N	112° 48'E
Lhasa	(55591)	29° 42'N	91° 8'E
Hankow/Wuhan	(57494)	30° 24'N	114° 18'E
Chengsien	(57972)	25° 48'N	113° 0'E
Zhijiang	(57745)	27° 27'N	109° 38'E
Haikou	(59758)	20° 2'N	110° 21'E
Kantze	(56146)	31° 36'N	100° 1'E
Guiyang	(57816)	26° 36'N	106° 42'E
Nanjing	(58238)	32° 6'N	118° 48'E
Hokow	(56989)	24° 24'N	103° 54'E
Shantou	(59316)	23° 24'N	116° 42'E
Yichang	(57461)	30° 42'N	111° 5'E
Chengdu	(56294)	30° 40'N	104° 1'E
Fuzhou	(58847)	26° 6'N	119° 18'E
Nanning	(59431)	22° 49'N	108° 21'E
Guangzhou	(59287)	23° 8'N	113° 19'E
Kunming	(56778)	25° 1'N	102° 41'E
Shanghai	(58367)	31° 10'N	121° 26'E
East Pakistan (Bangladesh) (January 1965 only)			
Dacca/Tezgaon	(41917)	23° 46'N	90° 23'E
Fiji			
Nandi	(91680)	17° 45'S	177° 27'E
Hong Kong			
King's Park	(45004)	22° 19'N	114° 10'E
India			
Gauhati	(42410)	26° 6'N	91° 35'E
Calcutta/Dum Dum	(42809)	22° 39'N	88° 27'E
Bhubaneswar	(42971)	20° 13'N	85° 50'E
Port Blair	(43333)	11° 40'N	92° 43'E
Indonesia (data only available for analysis in the final section)			
Djakarta/Kemayoran	(96743)	6° 9'S	106° 51'E
Surabaya/Perak	(96933)	7° 13'S	112° 43'E
Biak/Mokmer	(97560)	1° 11'S	136° 7'E
Ujung Pandang/Hasanuddin	(97180)	5° 4'S	119° 33'E
Manado/Dr Sam Ratulangi	(97014)	1° 32'N	124° 55'E
Medan/Polonia	(96035)	3° 34'N	98° 41'E

Station	Station Number	Latitude	Longitude
Japan			
Fukuoka	(47807)	33° 35'N	130° 23'E
Naze/Funchatoge	(47909)	28° 23'N	129° 33'E
Naha/Kagamizu	(47936)	26° 12'N	127° 40'E
Kagoshima/Yoshino	(47827)	31° 38'N	130° 36'E
Ishigakijima	(47918)	24° 20'N	124° 10'E
Shionomisaki	(47778)	33° 27'N	135° 46'E
Minamidaitojima	(47945)	25° 50'N	131° 14'E
Hachijojima/Omure	(47678)	33° 7'N	139° 47'E
Chichijima	(47971)	27° 5'N	142° 11'E
Minamitorishima/Marcus Island	(47991)	24° 18'N	153° 58'E
Iwo Jima	(91115)	24° 47'N	141° 19'E
Malaysia			
Penang/Bayan Lepas	(48601)	5° 18'N	100° 16'E
Kota Kinabalu	(96471)	5° 57'N	116° 3'E
Kuantan	(48657)	3° 47'N	103° 13'E
Kuching	(96413)	1° 29'N	110° 20'E
Kota Bharu	(48615)	6° 10'N	102° 17'E
Kuala Lumpur/Subang	(48647)	3° 6'N	101° 39'E
New Caledonia			
Noumea	(91592)	22° 16'S	166° 27'E
New Hebrides (Vanuatu)			
Vila	(91558)	17° 44'S	168° 19'E
New Zealand (United Kingdom Trust Territory)			
Funafuti	(91643)	8° 31'S	179° 13'E
Papua New Guinea			
Lae	(94027)	6° 43'S	147° 0'E
Port Moresby Airport	(94035)	9° 26'S	147° 13'E
Momote	(94044)	2° 4'S	147° 26'E
Rabaul	(94085)	4° 13'S	152° 11'E
Madang	(94014)	5° 13'S	145° 48'E
Philippines (data only available for analysis in the final section, except Clark)			
Clark Air Force Base	(98327)	15° 10'N	120° 34'E
Zamboanga	(98836)	6° 54'N	122° 4'E
Legaspi City	(98444)	13° 8'N	123° 44'E
Laoag City	(98223)	18° 4'N	120° 32'E
Puerto Princessa City	(98618)	9° 45'N	118° 44'E
Davao City	(98754)	7° 4'N	125° 36'E
Cebu/Mactan	(98646)	10° 19'N	123° 59'E

Station	Station Number	Latitude	Longitude
Singapore			
Singapore Airport	(48694)	1° 22'N	103° 55'E
South Korea			
Mosulpo	(47187)	33° 11'N	126° 13'E
Taiwan			
Taipei/Pan Chiao	(46692)	25° 0'N	121° 26'E
Tungkong	(46747)	22° 30'N	120° 24'E
Thailand			
Bangkok	(48455)	13° 44'N	100° 30'E
Songkhla	(48568)	7° 11'N	100° 37'E
Ubon Ratchathani	(48407)	15° 15'N	104° 53'E
Chiangmai	(48327)	18° 47'N	98° 59'E
Vietnam			
Saigon/Ho Chi Min City	(48900)	10° 49'N	106° 40'E
Danang/Tansonnhut	(48855)	16° 4'N	108° 13'E

Upper Air/Radiosonde Stations; Local Domain

Station	Station Number	Latitude	Longitude
Australia			
Cocos Island	(96996)	12° 11'S	96° 50'E
Broome	(94203)	17° 57'S	122° 13'E
Port Hedland	(94312)	20° 23'S	118° 37'E
Carnarvon	(94300)	24° 53'S	113° 39'E
Giles	(94461)	25° 2'S	128° 18'E
Alice Springs	(94326)	23° 48'S	133° 53'E
Darwin	(94120)	12° 26'S	130° 52'E
Cloncurry	(94335)	20° 40'S	140° 30'E
Mount Isa	(94332)	20° 40'S	139° 29'E
Willis Island	(94299)	16° 18'S	149° 59'E
Townsville	(94294)	19° 16'S	146° 46'E
Charleville	(94510)	26° 25'S	146° 17'E
Moree	(94527)	29° 28'S	149° 51'E
Brisbane/Eagle Farm	(94578)	27° 26'S	153° 5'E
Gladstone	(94380)	23° 51'S	151° 16'E
Papua New Guinea (1973 only)			
Lae	(94027)	6° 43'S	147° 0'E

Upper Air and Upper Wind Stations; Indo-Pacific Domain (includes only those stations additional to the Regional Domain)

Station	Station Number	Latitude	Longitude
American Samoa			
Pago Pago	(91765)	14° 20'S	170° 43'W
Argentina			
Salta Aero	(87047)	24° 51'S	65° 29'W
Mendoza Aero	(87418)	32° 51'S	68° 47'W
Cordoba Aero	(87344)	31° 19'S	64° 13'W
Bahrain			
Bahrain/Muharraq	(40427)	26° 16'N	50° 37'E
Bermuda			
Kindley Field	(78016)	32° 24'N	64° 42'W
Brazil			
Manaus Aero Ponta Pelada	(82332)	3° 9'S	59° 59'W
Vilhena Aeroporto	(83208)	12° 44'S	60° 8'W
British Protectorate of Aden (now Democratic Yemen)			
Aden/Khormaksar	(40597)	12° 48'N	45° 0'E
British West Indies			
Grand Cayman, Cayman Islands	(78383)	19° 15'N	81° 25'W
Canton Island			
Canton Island, Phoenix Islands	(91700)	2° 48'S	171° 42'W
Chile			
Antofagasta/Cerro Moreno	(85442)	23° 28'S	70° 26'W
Quintero	(85543)	32° 47'S	71° 32'W
Isla de Pascua/Mataveri	(85469)	27° 10'S	109° 26'W
Colombia			
Bogota/Eldorado	(80222)	4° 42'N	74° 8'W
San Andres	(80001)	12° 35'N	81° 42'W

Station	Station Number	Latitude	Longitude
Costa Rica			
San Jose/Juan Santamaria	(78762)	10° 0'N	83° 3'W
Dominican Republic			
Santo Domingo	(78486)	18° 28'N	69° 53'W
Egypt			
Helwan	(62378)	29° 52'N	31° 20'E
Asswan	(62414)	23° 58'N	32° 47'E
Equador			
Guayaquil/Simon Bolivar	(84129)	2° 9'S	79° 53'W
Ethiopia			
Asmara	(63021)	15° 17'N	38° 55'E
Addis Ababa	(63450)	8° 59'N	38° 48'E
French Polynesia			
Tahiti, Society Islands	(91938)	17° 33'S	149° 37'W
Atuona, Marquesas Islands	(91925)	9° 48'S	139° 2'W
Hao, Tuamotu Islands	(91944)	18° 4'S	140° 57'W
Totegegie, Gambier Islands	(91948)	23° 6'S	134° 52'W
Rapa, Austral Islands	(91958)	27° 37'S	144° 20'W
Guadeloupe			
Raizet	(78897)	16° 16'N	61° 31'W
Guatemala			
Guatemala City/La Aurora Airport	(78641)	14° 35'N	90° 31'W
Hawaiian Islands			
Lihue, Kauai	(91165)	21° 59'N	159° 21'W
Hilo/General Lyman	(91285)	19° 43'N	155° 4'W
India			
New Delhi/Safdarjung	(42182)	28° 35'N	77° 12'E
Jodhpur	(42339)	26° 18'N	73° 1'E
Lucknow/Amausi	(42369)	26° 45'N	80° 53'E
Ahmadabad	(42647)	23° 4'N	72° 38'E
Nagpur/Sonegaon	(42867)	21° 6'N	79° 3'E

Station	Station Number	Latitude	Longitude
Bombay/Santacruz	(43003)	19° 7'N	72° 51'E
Hyderabad Airport	(43128)	17° 27'N	78° 28'E
Vishakhapatnam	(43149)	17° 43'N	83° 14'E
Goa/Panjim	(43192)	15° 29'N	73° 49'E
Madras/Minambakkam	(43279)	13° 0'N	80° 11'E
Bangalore	(43295)	12° 58'N	77° 35'E
Panambur	(43285)	12° 57'N	74° 50'E
Minicoy	(43369)	8° 18'N	73° 0'E
Trivandrum	(43371)	8° 29'N	76° 57'E
Gan, Maldive Islands	(41350)	0° 41'S	73° 9'E
Iraq			
Baghdad	(40650)	33° 20'N	44° 24'E
Israel			
Bet Dagan	(40179)	32° 0'N	34° 49'E
Jamaica			
Norman Manley International Airport (formerly Kingston/Palisadoes)	(78397)	17° 54'N	76° 48'W
Johnston Island			
Johnston Island	(91275)	16° 44'N	169° 31'W
Jordan			
Mafraq	(40265)	32° 22'N	36° 16'E
Kenya			
Nairobi/Dagoretti	(63741)	1° 19'S	36° 55'E
Kisumu	( )	0° 6'S	34° 45'E
Malindi	( )	3° 14'S	40° 6'E
Mombasa	( )	4° 2'S	39° 37'E
Lodwar	( )	3° 7'N	35° 37'E
Makindu	( )	2° 17'S	37° 50'E
Garissa	( )	0° 28'S	39° 38'E
Mandera	( )	3° 56'N	41° 52'E
Kericho	( )	0° 22'S	35° 21'E
Kuwait			
Kuwait International Airport	(40372)	29° 13'N	47° 59'E
Lebanon			
Beyrouth/Khaldeh	(40100)	33° 49'N	35° 29'E

Station	Station Number	Latitude	Longitude
Malagasy Republic (formerly Madagascar)			
Diego Suarez	(67009)	12° 21'S	49° 18'E
Tananarive/Ivato	(67083)	18° 48'S	47° 29'E
Fort Dauphin	(67197)	25° 0'S	47° 0'E
Malawi			
Chileka	( )	15° 41'S	34° 58'E
Lilongwe	(67587)	13° 58'S	33° 42'E
Mauritius			
Vacoas	(61995)	20° 18'S	57° 30'E
Diego Garcia	(61967)	7° 12'S	72° 24'E
Mexico			
Isla Guadalupe, B.C.	(76151)	29° 10'N	118° 19'W
Chihuahua University	(76225)	28° 36'N	106° 6'W
Empalme	(76256)	27° 57'N	110° 48'W
Monterrey International Airport	(76394)	25° 52'N	100° 14'W
Mazatlan Carrasco	(76458)	23° 12'N	106° 24'W
Merida International Airport	(76644)	20° 57'N	89° 40'W
Mexico City International Airport	(76679)	19° 26'N	99° 4'W
Vera Cruz, Ylang Ylang	(76692)	19° 9'N	96° 7'W
Socorro Island	(76723)	18° 14'N	111° 3'W
Mozambique			
Nampula	(67237)	15° 6'S	39° 17'E
Lourenco Marques (Maputo)	(67341)	25° 55'S	32° 34'E
Netherlands Antilles			
Curacao/ Dr A Plesman Airport	(78988)	12° 12'N	68° 58'W
Saint Maarten/Juliana Airport	(78866)	18° 3'N	63° 7'W
New Zealand			
Rarotonga, Cook Islands	(91843)	21° 12'S	159° 49'W
Oman			
Masirah Island/U.K.	(40564)	20° 41'N	58° 54'E
Peru			
Lima - Callao	(84628)	12° 0'S	77° 7'W
Puerto Rica			
San Juan International Airport	(78526)	18° 26'N	66° 0'W

Station	Station Number	Latitude	Longitude
Reunion			
Tromelin Island	(61976)	15° 53'S	54° 31'E
Rhodesia (Zimbabwe)			
Salisbury/Belvedere	(67774)	17° 50'S	31° 1'E
Saudi Arabia			
Riyadh	(40438)	24° 42'N	46° 44'E
Jeddah	(40477)	21° 30'N	39° 12'E
South Africa			
Durban/Louis Botha	(68588)	29° 58'S	30° 57'E
Sudan			
Port Sudan	(62641)	19° 35'N	37° 13'E
Khartoum	(62721)	15° 36'N	32° 33'E
Malakal	(62840)	9° 33'N	31° 39'E
Tanzania			
Dar es Salaam Airport	(63894)	6° 53'S	39° 12'E
Trinidad			
Piarco International Airport	(78970)	10° 36'N	61° 22'W
Uganda			
Entebbe Airport	(63705)	0° 43'N	32° 37'E
United States of America			
Miami	(72202)	25° 48'N	80° 16'W
Key West	(72201)	24° 34'N	81° 48'W
Boothville	(72232)	29° 20'N	89° 24'W
Charleston	(72208)	32° 54'N	80° 2'W
Brownsville	(72250)	25° 54'N	97° 26'W
Victoria	(72255)	28° 51'N	96° 55'W
El Paso	(72270)	31° 48'N	106° 24'W
San Diego	(72290)	32° 44'N	117° 10'W
Shreveport	(72248)	32° 30'N	93° 48'W
Swan Island (Isle del Cisne)	(78501)	17° 35'N	84° 0'W
Athens	(72311)	33° 57'N	83° 24'W
Del Rio	(72261)	29° 23'N	100° 56'W
Fort Worth	(72259)	32° 45'N	97° 20'W
Tampa	(72211)	27° 58'N	82° 38'W
Waycross	(72213)	31° 15'N	82° 24'W

Station	Station Number	Latitude	Longitude
Venezuela			
Maracay - B.A. Sucre	(80413)	10° 15'N	67° 39'W
San Antonio Del Tachira	(80447)	7° 51'N	72° 27'W
Weather Ships			
N (Nectar)	(99014)	30° 0'N	140° 0'W
Zambia			
Kasama	(67475)	10° 13'S	31° 8'E
Chipata	(67581)	13° 33'S	32° 35'E

APPENDIX 2

Theory of Time, Space, and Space-Time Component Decomposition

Component decomposition in this study is derived from equations given in Lorenz (1955) and Oort (1964), where three types of mean and eddy component form are examined.

Of the three approaches, only the first two are used to develop mean and eddy fields of kinetic energy, flux divergence and water vapour fluxes. The third approach is included to illustrate that when comparing results with other studies decomposition forms may vary the configuration of the resultant fields.

2.1 Time Domain

Any quantity can be expressed as the sum of its time mean and transient eddy (instantaneous departure from time mean) terms;

$$(\vec{V}) = (\bar{\vec{V}}) + (\vec{V}') \qquad \ldots(1)$$

where $(\vec{V})$ is, for example, a resultant wind vector, with $(\bar{\vec{V}})$ = time mean and $(\vec{V}')$ = transient eddy terms.

Similarly, the components of this wind vector u and v can be decomposed to;

$$(u) = (\bar{u}) + (u') \qquad \ldots(2a)$$

$$(v) = (\bar{v}) + (v') \qquad \ldots(2b)$$

The designation $(\bar{\ })$ for the mean of a quantity is expressed as;

$$(\bar{\ }) = \frac{1}{\tau}\int_{o}^{\tau} (\ )\, dt \cong \frac{1}{N} \sum_{i=1}^{i=N} (\ ) \qquad \ldots(3)$$

where dt and τ = time increment and time, and N = number of observations of ( ) in the time period t.

Thus only ( ) need be known, with $(\bar{\ })$ derived from the known (from 3) for (') to be determined via a simple rearrangement of (2a and 2b).

2.2 Space Domain

A quantity measured in a defined physical space is able to be represented

by the sum of its space mean and space (standing) eddy components i.e.;

$$\vec{V} = [\vec{V}] + [\vec{V}^*] \qquad \ldots(4)$$

where $[\vec{\ }]$ = space mean, $[\vec{\ }^*]$ = space eddy (deviation from the space mean). As with (2a) and (2b), the u and v components of $\vec{V}$ in space mean and eddy forms are;

$$u = [u] + [u^*] \text{ (zonal)} \qquad \ldots(5a)$$

$$v = [v] + [v^*] \text{ (meridional)} \qquad \ldots(5b)$$

where $[\ ] = \frac{1}{A} \int (\ ) dA$, (A = domain area) or, in a more applicable form,

$$[\ ] \cong \frac{1}{N} \sum_{i=1}^{i=N} (\ ) \qquad \ldots(6)$$

where N = number of observations of ( ) in the domain area or A.

2.3 Space-Time Domain

A quantity can also be decomposed into space-time components, i.e. for u and v wind components;

$$u = [\bar{u}] + [u]' + \bar{u}^* + u'^* \qquad \ldots(7a)$$

$$v = [\bar{v}] + [v]' + \bar{v}^* + v'^* \qquad \ldots(7b)$$

where [ ] = space mean, * = space eddy, $\bar{\ }$ = time mean, and ' = transient eddy terms.

APPENDIX 3

Determination of Divergence and Relative Vorticity via Finite Difference Approximation

According to Panofsky (1946), relative vorticity and divergence in curvilinear co-ordinates are defined by;

$$\zeta_r = \frac{\partial v}{\partial x} - \frac{\partial u}{\partial y} + \frac{u}{r}\tan\theta \qquad \ldots(8a)\ (s^{-1})$$

$$\vec{\nabla}.\vec{V} = \frac{\partial u}{\partial x} + \frac{\partial v}{\partial y} - \frac{v}{r}\tan\theta \qquad \ldots(8b)\ (s^{-1})$$

and can be evaluated by finite difference approximations, i.e. where r = radius of the earth, θ = latitude and the last terms on the far right-hand side of the above equations take account of the convergence of meridians, $\vec{\nabla}$ = the horizontal gradient operator (del operator) = $\vec{i}\frac{\partial}{\partial x} + \vec{j}\frac{\partial}{\partial y}$, $\vec{V}$ = a resultant wind vector, u and v = zonal and meridional wind components, $\zeta_r = \vec{k}.\vec{\nabla} \times \vec{V}$ = relative vorticity.

Applying a centred differencing approach, (8a) and (8b) become;

$$\zeta_{r_0} = \frac{(v_3 - v_1) - (u_4 - u_2)}{2d} \qquad \ldots(9a)\ (s^{-1})$$

$$\vec{\nabla}.\vec{V}_0 = \frac{(u_3 - u_1) + (v_4 - v_2)}{2d} \qquad \ldots(9b)\ (s^{-1})$$

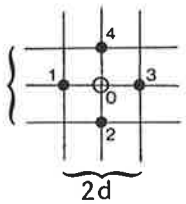

where u_1, u_2, u_3, u_4, v_1, v_2, v_3, v_4 are the wind components at the grid points $_{1,2,3,4}$, ζ_{r_0} and $\vec{\nabla}.\vec{V}_0$ are the relative vorticity and divergence values required at grid point o ; and 2d = twice the grid length d.

N.B. d for a 5°/5° grid ≅ 482,804 metres while with an original 15 x 19 grid, step (iv) in Chapter II, 2.2.1 reduces the total size to a 13 x 17 grid simply by virtue of the finite difference approximation when applied to the boundary points.

APPENDIX 4

Theory of Velocity Potential and Streamfunction Evaluation

From Helmholtz's theorem in fluid mechanics, a horizontal wind vector $\vec{V}$ can be decomposed into the sum of its irrotational and rotational components. In a cartesian co-ordinate system;

$$\vec{V} = \vec{\nabla}\chi + \vec{k} \times \vec{\nabla}\psi \qquad \ldots(10)$$

where χ = velocity potential, ψ = stream function, $\vec{k}$ = a unit vector in the z direction of a right-hand cartesian co-ordinate system and $\vec{\nabla}$ is the horizontal gradient operator (del operator) = $\vec{i}\,\frac{\partial}{\partial x} + \vec{j}\,\frac{\partial}{\partial y}$.

These components, when defined separately, become;

$$\vec{V}_\chi = \vec{\nabla}\chi \qquad \ldots(11a)$$

$$\vec{V}_\psi = \vec{k} \times \vec{\nabla}\psi \qquad \ldots(11b)$$

Thus velocity potential χ, as defined by (11a), is a function whose gradient is equal to the irrotational component of the velocity field, while streamfunction ψ, as defined by (11b), is a function whose curl is equal to the rotational component of the velocity field.

Examining (11a) and (11b) further it can be seen that;

$$\vec{k} \times \vec{\nabla}\psi = \vec{k} \times \left(\vec{i}\,\frac{\partial\psi}{\partial x} + \vec{j}\,\frac{\partial\psi}{\partial y}\right)$$

and as $\vec{k} \times \vec{i} = \vec{j}$ and $\vec{k} \times \vec{j} = -\vec{i}$

therefore $\vec{k} \times \vec{\nabla}\psi = -\vec{i}\,\frac{\partial\psi}{\partial y} + \vec{j}\,\frac{\partial\psi}{\partial x}$

as $\vec{V} = \vec{i}u + \vec{j}v$ or $\vec{V}_\psi = \vec{i}u_r + \vec{j}v_r$

therefore $u_r = -\frac{\partial\psi}{\partial y}$ and $v_r = \frac{\partial\psi}{\partial x}$ (rotational terms)

while $\vec{\nabla}\chi = \vec{i}\,\frac{\partial\chi}{\partial x} + \vec{j}\,\frac{\partial\chi}{\partial y}$

as $\vec{V}_\chi = \vec{i}u_{ir} + \vec{j}v_{ir}$

therefore $u_{ir} = \frac{\partial\chi}{\partial x}$ and $v_{ir} = \frac{\partial\chi}{\partial y}$ (irrotational terms)

The total u and v components for an original wind vector can be reformed from the sum of the rotational and irrotational terms;

$$u = u_r + u_{ir} = -\frac{\partial \psi}{\partial y} + \frac{\partial \chi}{\partial x}$$

$$v = v_r + v_{ir} = \frac{\partial \psi}{\partial x} + \frac{\partial \chi}{\partial y}$$

Taking the vertical component of the curl of the left-hand side of (11b) and the dot product of the left-hand side of (11a) produces equations of the Poisson type;

$$\vec{\nabla}.\vec{V} = \nabla^2 \chi \qquad \ldots(12a)$$

$$\zeta_r = \vec{k}.\vec{\nabla} \times \vec{V} = \nabla^2 \psi \qquad \ldots(12b)$$

where $\vec{\nabla}.\vec{V}$ = horizontal divergence, $\zeta_r = \vec{k}.\vec{\nabla} \times \vec{V}$ = relative vorticity, ∇^2 = Laplacian operator = $\frac{\partial^2}{\partial x^2} + \frac{\partial^2}{\partial y^2}$

Velocity potential and streamfunction can be found by solutions to (12a) and (12b) subject to the specification of boundary conditions and knowledge of the fields of divergence and relative vorticity within a bounded domain.

APPENDIX 5

Iteration Procedure for Streamfunction and Velocity Potential Determination

1. χ and ψ at all interior points are evaluated by a rearrangement of (12a) and (12b) containing a finite difference approximation to the second order partial derivatives of the Laplacian operator, while at all boundary points χ and ψ are made equal to zero in the initial solutions.

2. The finite difference approximation is a five point centred difference form (Hess, 1959) i.e.;

$$\nabla^2 \chi = \frac{\chi_1 + \chi_2 + \chi_3 + \chi_4 - 4\chi_0}{d^2} \qquad \ldots(13a)$$

$$\nabla^2 \psi = \frac{\psi_1 + \psi_2 + \psi_3 + \psi_4 - 4\psi_0}{d^2} \qquad \ldots(13b)$$

where $\chi_0, \chi_1, \chi_2, \chi_3, \chi_4, \psi_0, \psi_1, \psi_2, \psi_3, \psi_4$ are the velocity potential and streamfunction values at the grid points 0, 1, 2, 3, 4 and d is the grid length.

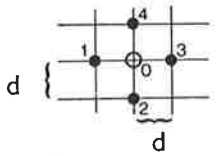

3. Substituting the above approximations into (12a) and (12b) gives;

$$\vec{\nabla}.\vec{V}_0 = \frac{\chi_1 + \chi_2 + \chi_3 + \chi_4 - 4\chi_0}{d^2} \qquad \ldots(14a)$$

$$\vec{k}.\vec{\nabla} \times \vec{V} = \zeta_{r_0} = \frac{\psi_1 + \psi_2 + \psi_3 + \psi_4 - 4\psi_0}{d^2} \qquad \ldots(14b)$$

4. It can be seen that an iterative solution of (14a) and (14b) requires some initial guessed field for the unknown χ and ψ values at all the surrounding grid points. Previously, as in 1., the boundary point values for χ and ψ had been set to zero. If this value is used as an initial guess for the remaining interior grid points a residual error will result in each calculation from (14a) and (14b); i.e. rearranging these equations;

$$\frac{\chi_1 + \chi_2 + \chi_3 + \chi_4}{4} - \chi_o - \frac{d^2(\vec{\nabla}.\vec{V}_o)}{4} = E_o \quad \ldots(15a)$$

$$\frac{\psi_1 + \psi_2 + \psi_3 + \psi_4}{4} - \psi_o - \frac{d^2(\zeta r_o)}{4} = F_o \quad \ldots(15b)$$

where E_o and F_o are the residual errors at grid point o.

5. The aim of the iterative technique is thus to reduce these residual errors to a negligible amount (approaching close to zero). To achieve this a new guess for the χ and ψ values at all interior grid points for each successive iteration through the grid is required.

6. If the resulting residual error from each iteration is added to the previous guessed value of χ and ψ a new guess value for each interior grid point is developed, i.e.;

$$\chi_{o\alpha} + E_{o\alpha+1} = \chi_{o\alpha+1} \quad \ldots(16a)$$

$$\psi_{o\alpha} + F_{o\alpha+1} = \psi_{o\alpha+1} \quad \ldots(16b)$$

where α refers to N number of iterations (1 to N).

7. This method is said to converge if, after a number of iterations, the residual errors have everywhere been reduced to near zero when the technique is applied to each point in the field.

5.1 Boundary Correction Technique

The initial assumption that χ and ψ are equal to zero along the boundaries causes poor resolution of the fields at and in from the boundary points. Shukla and Saha (1974) detail a method for correcting boundary problems which they imply is superior to other approaches and is an extension of Sangster's (1960) method.

This method is to relax alternately the finite difference approximation for the Laplacian of one field to obtain values in the domain, then use this field to evaluate the other field's boundary values. These boundary values

are determined by a step-wise integration of the boundary conditions in terms of χ and ψ given by;

$$\vec{n}.\vec{V} = V_n = -\frac{\partial\psi}{\partial s} + \frac{\partial\chi}{\partial n} \qquad \ldots(17a)$$

$$\vec{s}.\vec{V} = V_s = \frac{\partial\psi}{\partial n} + \frac{\partial\chi}{\partial s} \qquad \ldots(17b)$$

where $\vec{n}$ = the unit vector normal to the boundary, $\vec{s}$ = the unit vector along the boundary (positive anticlockwise), V_n = the velocity component normal to the boundary and V_s = velocity component along the boundary. This approach was found to give the best results if initially the χ field was determined and then used as the basis for an integration and iteration re-evaluation sequence; i.e.

1. initial $\chi_n \rightarrow \psi_b$ by integration of $\frac{\partial\psi}{\partial s} = -V_n + \frac{\partial\chi}{\partial n}$
2. $\psi_b \rightarrow \psi_n$ by relaxation of (12b) knowing ψ_b values from 1.
3. $\psi_n \rightarrow \chi_b$ by integration of $\frac{\partial\chi}{\partial s} = V_s - \frac{\partial\chi}{\partial n}$
4. $\chi_b \rightarrow \chi_{n+1}$ by relaxation of (12a) knowing χ_b values from 3.

where n = repeat number of sequence 1 to 4 included in total iteration procedure, and b = field at the boundary.

At the boundaries of the domain the correction method requires the determination of $-V_n$, $\frac{\partial\chi}{\partial n}$, V_s and $-\frac{\partial\psi}{\partial n}$ in the rearranged forms of (17a) and (17b);

$$\frac{\partial\chi}{\partial s} = \chi_{i+1} - \chi_{i-1} = V_s - \frac{\partial\psi}{\partial n} \qquad \ldots(18a)$$

$$\frac{\partial\psi}{\partial s} = \psi_{i+1} - \psi_{i-1} = -V_n + \frac{\partial\chi}{\partial n} \qquad \ldots(18b)$$

As the boundary of the grid is rectangular, V_n on each of the four sides are;

north v component
east u component
south - v component
west - u component

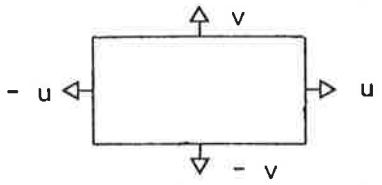

V_s on each of the four sides are (positive anticlockwise);

north - u component
east v component
south u component
west - v component

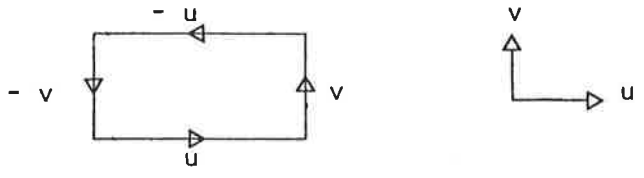

Similarly, $\frac{\partial \chi}{\partial n}$ and $\frac{\partial \psi}{\partial n}$ can also be determined by methods that Shukla and Saha (1974) have developed from Sangster (1960) and Hawkins and Rosenthal (1965) where;

$$\left(\frac{\partial \chi}{\partial n}\right)_o = 2\left(\frac{\partial \chi}{\partial n}\right)_1 - \left(\frac{\partial \chi}{\partial n}\right)_2 \qquad \ldots(19)$$

with; $\left(\frac{\partial \chi}{\partial n}\right)_1 = \frac{\chi_o - \chi_2}{2d}$; $\left(\frac{\partial \chi}{\partial n}\right)_2 = \frac{\chi_1 - \chi_3}{2d}$

Subscripts o,1,2 and 3 refer to the boundary points and points one, two and three grid lengths in from the boundary respectively and d = grid length.

Similarly, for ψ;

$$\left(\frac{\partial \psi}{\partial n}\right)_o = 2\left(\frac{\partial \psi}{\partial n}\right)_1 - \left(\frac{\partial \psi}{\partial n}\right)_2 \qquad \ldots(20)$$

where; $\left(\frac{\partial \psi}{\partial n}\right)_1 = \frac{\psi_o - \psi_2}{2d}$; $\left(\frac{\partial \psi}{\partial n}\right)_2 = \frac{\psi_1 - \psi_3}{2d}$

Several points on the boundary present problems in obtaining a complete solution to the boundary problem. The four corner points do not have solutions for $\frac{\partial \chi}{\partial n}$ or $\frac{\partial \psi}{\partial n}$ because, as the following diagram shows, the concept of a normal to a corner point is not plausible.

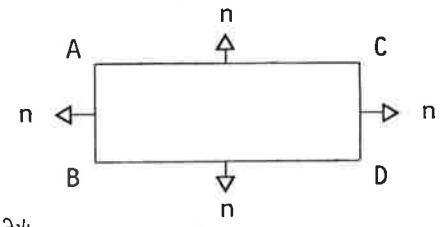

Hence, $\frac{\partial \chi}{\partial n}$, $\frac{\partial \psi}{\partial n}$, V_n and V_s can be found for all points between AC, AB, BD, DC but not directly at A, B, C or D.

The method used to overcome this problem is to simply leave the corner points with their original zero value and evaluate the equations along each of the individual lengths i.e. all points between AC, AB, BD and DC but not at A, B, C or D. This approach does not contradict Sangster (1960), where a cycle anticlockwise around the whole boundary surface was employed. Rather, it does each side in correct sequence and direction to achieve the same result.

Values of χ_b and ψ_b (the final solution rather than components) at A, B, C and D need then only to be determined by averaging the adjacent boundary

point values to each corner point; i.e.

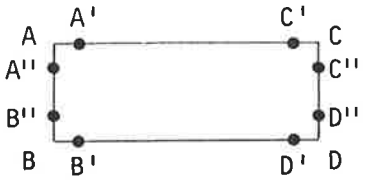

where $A = \frac{A'' - A'}{2}$, $B = \frac{B'' - B'}{2}$, $C = \frac{C'' - C'}{2}$ and $D = \frac{D'' - D'}{2}$.

Any residuals produced by the process, as strictly defined by Sangster's (1960) actual cyclic evaluation are thus distributed at the corner points and not around the entire boundary. Hence, no arbitrary point value for a corner need be used as an initial starting point and the residuals caused by such an approach are reduced.

5.2 Matrix Method of Velocity Potential and Streamfunction Determination

Although the matrix solution to χ and ψ fields is much quicker in obtaining a resultant field and is not as dictated by boundary conditions, it is governed by grid size restrictions far greater than the iterative approach.

As with the iterative approach, the same steps which develop (13a) and (13b) are employed for use in a sparse matrix. However, even with a moderately sized grid system, initially of size 15 x 19 and thus 285 individual points, the approach is overcome simply by the size of the matrix generated during domain solution.

The following description of the steps required highlights the constraints imposed by large matrix size. The entire method is based on simple matrix inversion laws where one initially has forms;

$$\underset{\text{known}}{(A)} \quad \underset{\text{unknown}}{(\chi)} = \underset{\text{known}}{\{(\vec{\nabla}.\vec{V})d^2\}} \qquad \ldots(21a)$$

$$\underset{\text{known}}{(A)} \quad \underset{\text{unknown}}{(\psi)} = \underset{\text{known}}{\{(\zeta_r)d^2\}} \qquad \ldots(21b)$$

where (A) is the matrix form of the five point Laplacian finite difference scheme, which can be illustrated for a very simple 4 x 4 matrix as;

$$\begin{pmatrix} -4 & 1 & 1 & 0 \\ 1 & -4 & 0 & 1 \\ 1 & 0 & -4 & 1 \\ 0 & 1 & 1 & -4 \end{pmatrix}$$

Thus to solve the column vectors (χ) or (ψ) in (21a) and (21b), one can take the inverse of $(A) = (A)^{-1}$ which, for (A) matrix, will give the identity matrix I if it is pre- or post-multiplied by the initial matrix (A);

$$(A)\ (A)^{-1} = I$$

This means that the solutions to (21a) and (21b) above become;

$$(\chi) = (A)^{-1} \left\{(\vec{\nabla}.\vec{V})d^2\right\} \qquad \ldots(22a)$$

$$(\psi) = (A)^{-1} \left\{(\zeta_r)d^2\right\} \qquad \ldots(22b)$$

where the unknowns (χ) and (ψ) for a 15 x 19 matrix are 285 value column vectors, $(A)^{-1}$ is an inverse of the five point Laplacian of matrix size 285 x 285 and $\left\{(\vec{\nabla}.\vec{V})d^2\right\}$ and $\left\{(\zeta_r)d^2\right\}$ are 285 value column vectors containing the products of the knowns at each grid point; i.e.

$$\begin{Bmatrix} \chi_1 \\ \downarrow \\ \downarrow \\ \chi_{285} \end{Bmatrix} = \begin{Bmatrix} A \rightarrow \rightarrow \rightarrow 285^{-1} \\ \downarrow \\ \downarrow \\ 285 \end{Bmatrix} \begin{Bmatrix} (\vec{\nabla}.\vec{V})d_1^2 \\ \downarrow \\ \downarrow \\ (\vec{\nabla}.\vec{V})d_{285}^2 \end{Bmatrix}$$

$$\begin{Bmatrix} \psi_1 \\ \downarrow \\ \downarrow \\ \psi_{285} \end{Bmatrix} = \begin{Bmatrix} A \rightarrow \rightarrow \rightarrow 285^{-1} \\ \downarrow \\ \downarrow \\ 285 \end{Bmatrix} \begin{Bmatrix} (\zeta_r)d_1^2 \\ \downarrow \\ \downarrow \\ (\zeta_r)d_{285}^2 \end{Bmatrix}$$

Any boundary problems, as in the iterative approach, can be lessened for this matrix by taking the domain size as larger than required. This is done at the first steps from which u and v components are deduced so when solving (12a) and (12b) to find ζ_r and $\vec{\nabla}.\vec{V}$ one is still analysing an area larger than is required in the final solutions for χ and ψ. Therefore, in setting up the matrices as in (21a) and (21b), one has the first χ or ψ corner point 2 grid lengths in from the known u and v outer boundary and one grid length in from the deduced ζ_r or $\vec{\nabla}.\vec{V}$ outer boundary; i.e.

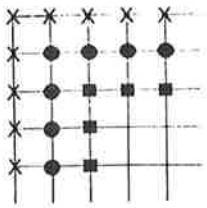

outer boundary x

outer boundary ●

outer boundary ■

where x are grid points to which u and v are evaluated, ● are grid points to which ζ_r or $\vec{\nabla}.\vec{V}$ are evaluated and ■ are grid points to which χ or ψ are evaluated.

The very need to make the area in question initially larger than the final region again highlights the size factor so critical to the matrix method. Attempts at inversion of the smallest sized region, under the study requirements 13 x 17 or 221 x 221 in the matrix working, have been unsuccessful because of the limitations of computer matrix inversion sub-routines. Therefore, the large size factor of the area alone makes the matrix method unworkable and the iterative approach more practical.

APPENDIX 6

Theory of Moisture Characteristics

6.1 Water Vapour Flux Derivation

The flux or transfer of water vapour, by definition the amount of water vapour crossing a unit area per unit time for a point at a particular level in the atmosphere, is given by;

$$\vec{Q} = \rho_w \vec{V} \qquad \ldots(23) \ (\text{gm cm}^{-2} \text{ s}^{-1})$$

where $\vec{Q}$ = water vapour transfer or flux, ρ_w = density of water vapour and $\vec{V}$ = resultant wind vector.

Equation (23) can be rearranged slightly to express the right-hand side in terms of specific humidity q. This quantity relates the mass of water vapour to the unit mass of total air; i.e.

$$\frac{\rho_w}{\rho} = q \qquad \ldots(24)$$

where ρ = density of air.

Thus (23) is rewritten as;

$$\vec{Q} = q\rho\vec{V} \qquad \ldots(25)$$

The rate of transfer or flux of water vapour through an area 1 cm wide and 1 mb in height is given by;

$$\vec{Q} = q\rho\vec{V}\, dz \qquad \ldots(26)$$

where dz = thickness of a 1 mb slab.

Using the hydrostatic equation;

$$\rho g = -\frac{\partial p}{\partial z} \qquad \ldots(27)$$

and solving it for ∂z; i.e.

$$\partial z = -\frac{\partial p}{\rho g} \qquad \ldots(28)$$

Equation (26), assuming ∂p = 1 mb, becomes;

$$\vec{Q} = \frac{1}{g} q\vec{V} \qquad \ldots(29) \ (\text{gm cm}^{-1} \text{ mb}^{-1} \text{s}^{-1})$$

(Units in (29) are as indicated, provided q is entered in gm kgm^{-1}.)

Decomposing $\vec{V}$ into its u and v components, under time-averaging conditions, (29) becomes;

$$(Q_u) = \frac{1}{g}(\overline{qu}) \qquad \ldots(30a)$$

$$(Q_v) = \frac{1}{g}(\overline{qv}) \qquad \ldots(30b)$$

where (Q_u) and (Q_v) = the total zonal and meridional fluxes of water vapour. According to Starr and Peixoto (1964) the covariances $(\overline{qu})$ and $(\overline{qv})$ can be expanded to;

$$(\overline{qu}) = (\overline{q})(\overline{u}) + (\overline{q'u'}) \qquad \ldots(31a)$$

$$(\overline{qv}) = (\overline{q})(\overline{v}) + (\overline{q'v'}) \qquad \ldots(31b)$$

where $(\overline{q'u'})$ and $(\overline{q'v'})$ are instantaneous covariances of the deviations from the time mean and are defined as transient eddy covariance terms.

Expanding the time domain terms in (30a) and (30b) under the definition given by (3) in Appendix 2.1;

$$(Q_u) = \frac{1}{gN}\sum_{i=1}^{i=N} q_i u_i \qquad \ldots(32a)$$

$$(Q_v) = \frac{1}{gN}\sum_{i=1}^{i=N} q_i v_i \qquad \ldots(32b)$$

} total

$$(\overline{Q_u}) = \frac{1}{g}\left(\frac{1}{N}\sum_{i=1}^{i=N} q_i\right)\left(\frac{1}{N}\sum_{i=1}^{i=N} u_i\right) \qquad \ldots(32c)$$

$$(\overline{Q_v}) = \frac{1}{g}\left(\frac{1}{N}\sum_{i=1}^{i=N} q_i\right)\left(\frac{1}{N}\sum_{i=1}^{i=N} v_i\right) \qquad \ldots(32d)$$

} advective

$$(Q_u') = \frac{1}{g}\overline{q'u'} \qquad \ldots(32e)$$

$$(Q_v') = \frac{1}{g}\overline{q'v'} \qquad \ldots(32f)$$

} transient eddy

where $(Q_u') = (Q_u) - (\overline{Q_u})$ and $(Q_v') = (Q_v) - (\overline{Q_v})$.

6.2 Water Vapour Flux Divergence Formulation

As horizontal divergence is defined by the dot product $\vec{\nabla}.\vec{V}_h$; horizontal moisture divergence is defined by the dot product $\vec{\nabla}.\vec{Q}$. Thus taking the dot product of each of the time domain terms of water vapour transfer;

$$\vec{\nabla}.(\vec{Q}) = \frac{\partial(Q_u)}{\partial x} + \frac{\partial(Q_v)}{\partial y} - \frac{(Q_v)}{r} \tan\theta \quad \ldots(33a)$$

$$\vec{\nabla}.(\vec{\overline{Q}}) = \frac{\partial(\overline{Q_u})}{\partial x} + \frac{\partial(\overline{Q_v})}{\partial y} - \frac{(\overline{Q_v})}{r} \tan\theta \quad \ldots(33b)$$

$$\vec{\nabla}.(\vec{Q}') = \frac{\partial(Q_u')}{\partial x} + \frac{\partial(Q_v')}{\partial y} - \frac{(Q_v')}{r} \tan\theta \quad \ldots(33c)$$

$(gm\ cm^{-2}\ mb^{-1}\ s^{-1})$

Therefore, (33a), (33b) and (33c) are total, advective and transient eddy water vapour flux divergence terms respectively.

6.3 Streamfunction of the Water Vapour Flux Formulation

To obtain the streamfunction of the water vapour flux it is necessary to follow the same steps as in streamfunction derivation (Appendices 3,4 and 5) except using the total, advective and transient eddy water vapour flux components (Appendix 6.1) rather than wind components. The total, advective and transient eddy forms become;

$$\text{total} \quad \nabla^2(\psi_w) = \frac{\partial(Q_v)}{\partial x} - \frac{\partial(Q_u)}{\partial y} + \frac{(Q_u)}{r} \tan\theta \ldots(34a)$$

$$\text{advective} \quad \nabla^2(\overline{\psi_w}) = \frac{\partial(\overline{Q_v})}{\partial x} - \frac{\partial(\overline{Q_u})}{\partial y} + \frac{(\overline{Q_u})}{r} \tan\theta \ldots(34b)$$

$$\text{eddy} \quad \nabla^2(\psi_w') = \frac{\partial(Q_v')}{\partial x} - \frac{\partial(Q_u')}{\partial y} + \frac{(Q_u')}{r} \tan\theta \ldots(34c)$$

$(gm\ mb^{-1}s^{-1})$

Evaluation of ψ_w, $\overline{\psi_w}$ and ψ_w' follow from the use of the iterative technique used in Appendix 5.

6.4 Vertical Integration of Water Vapour Flux Divergence

The water vapour flux divergence is vertically integrated in the following manner;

1. Taking water vapour flux in the general form of (29); i.e.

$$\vec{Q} = \frac{1}{g} q\vec{V}$$

vertically integrate between the levels required (in this case 1000 to 700 mb); i.e.

$$\vec{Q}_{\int} = \frac{1}{g} \int_{p_{10}}^{p_7} q\vec{V}\, dp \quad \ldots(35)\ (gm\ cm^{-1}s^{-1})$$

where p_{10} = 1000 mb and p_7 = 700 mb in this case.

2. Vertically integrate the decomposed total, advective and eddy terms in (32a - f) and substitute them into the required forms of water vapour flux divergence to obtain the vertically integrated water vapour flux divergence forms.

total $$\vec{\nabla}.(\vec{Q})_{\int} = \frac{\partial (Q_u)}{\partial x}^{\int} + \frac{\partial (Q_v)}{\partial y}^{\int} - \frac{(Q_v)}{r}^{\int} \tan\theta \quad \ldots(36a)$$

advective $$\vec{\nabla}.(\vec{\bar{Q}})_{\int} = \frac{\partial (\overline{Q_u})}{\partial x}^{\int} + \frac{\partial (\overline{Q_v})}{\partial y}^{\int} - \frac{(\overline{Q_v})}{r}^{\int} \tan\theta \quad \ldots(36b)$$

eddy $$\vec{\nabla}.(\vec{Q}')_{\int} = \frac{\partial (Q_u')}{\partial x}^{\int} + \frac{\partial (Q_v')}{\partial y}^{\int} - \frac{(Q_v')}{r}^{\int} \tan\theta \quad \ldots(36c)$$

(gm cm^{-2} s^{-1})

where $(Q_u)_{\int}$, $(Q_v)_{\int}$, $(\overline{Q_u})_{\int}$, $(\overline{Q_v})_{\int}$, $(Q_u')_{\int}$ and $(Q_v')_{\int}$ are the u and v vertically integrated total, advective and eddy water vapour flux components.

6.5 Vertical Integration of the Streamfunction of the Water Vapour Flux

Vertical integration of the streamfunction of the water vapour flux follows a similar pattern to step 2. in Appendix 6.4.

1. Using the total, advective and eddy forms of (34a), (34b) and (34c), replace the water vapour flux components with their vertically integrated forms as used in (36a), (36b) and (36c) above;

total $$\nabla^2 (\psi_w)_{\int} = \frac{\partial (Q_v)}{\partial x}^{\int} - \frac{\partial (Q_u)}{\partial y}^{\int} + \frac{(Q_u)}{r}^{\int} \tan\theta \quad \ldots(37a)$$

advective $$\nabla^2 (\overline{\psi_w})_{\int} = \frac{\partial (\overline{Q_v})}{\partial x}^{\int} - \frac{\partial (\overline{Q_u})}{\partial y}^{\int} + \frac{(\overline{Q_u})}{r}^{\int} \tan\theta \quad \ldots(37b)$$

eddy $$\nabla^2 (\psi_w')_{\int} = \frac{\partial (Q_v')}{\partial x}^{\int} - \frac{\partial (Q_u')}{\partial y}^{\int} + \frac{(Q_u')}{r}^{\int} \tan\theta \quad \ldots(37c)$$

(gm cm^{-1} mb^{-1} s^{-1})

Evaluation of $(\psi_w)_{\int}$, $(\overline{\psi_w})_{\int}$ and $(\psi_w')_{\int}$ follow from the use of the iterative technique used in Appendix 5.

6.6 Precipitable Water Derivation

Precipitable water is defined as '... the mass of water vapour contained in a vertical column of air, of unit cross-section, between any two levels ....' (McIntosh and Thom, 1973:68).

It can be derived in the following manner: As the density of water vapour is related to its mass and volume, for an element of moist air with unit cross-sectional area, the density can be defined as;

$$\rho_w = \frac{dm}{dz} \qquad \ldots(38)$$

where dm = mass of water vapour in the element of moist air, dz = vertical depth or thickness of the moist air, and ρ_w = density of water vapour.

A vertical thickness of any quantity has both upper and lower bounds, in this case z_1 to z_2, and consequently pressure bounds of p_1 and p_2.

Therefore, (38) rearranges to;

$$m = \int_{z_1}^{z_2} \rho_w \, dz \qquad \ldots(39)$$

Recalling the hydrostatic equation and rearranging it for dz ($dz = -\frac{dp}{\rho g}$).

Equation (39) now becomes;

$$m = -\int_{p_1}^{p_2} \frac{\rho_w dp}{\rho g} \qquad \ldots(40)$$

As (24) indicates, $\frac{\rho_w}{\rho} = q$, the more useful forms of (39) are;

$$m = \frac{1}{g} \int_{p_1}^{p_2} q \, dp \qquad \ldots(41a)$$

or more completely via the mean-value theorem;

$$m = \frac{\bar{q} \, (p_1 - p_2)}{g} \qquad \ldots(41b) \ (\text{gm cm}^{-2})$$

where $\bar{q}$ = mean specific humidity for the layer p_1 to p_2.

Equation (41b) is the final form of the water vapour content or precipitable water quantity.

Precipitable water in this analysis has been calculated for 100 mb thicknesses from 1000 to 700 mb; the set of thicknesses are 1000-900 mb, 900-800 mb, 800-700mb. Thus for the total precipitable water content between 1000 and 700 mb, it is just a matter of summing the values for the three 100 mb thicknesses; i.e. m(1000-900 mb) + m(900-800 mb) + m(800-700 mb) = m(1000-700 mb).

APPENDIX 7

Determination of Kinetic Energy Generation Parameter

In the equations used to define the energy balance of atmoshperic systems in Kung (1966), McInnis and Kung (1972), Smith (1973), Pearce (1974), Kung and Baker (1975), Kung and Tsui (1975), and Kung and Burgdorf (1978), the ageostrophic generation of kinetic energy due to cross isobaric motion is given by;

$$\frac{dk}{dt} = - \vec{V}.\vec{\nabla}\phi = - \left(u \frac{\partial \phi}{\partial x} + v \frac{\partial \phi}{\partial y}\right) \qquad \ldots(42)$$

where $\frac{dk}{dt}$ = time rate of change of kinetic energy, $\vec{V}$ = a resultant wind vector, $\vec{\nabla}$ = the del operator, $\phi = gz$ (geopotential height), u and v = zonal and meridional wind components in the x and y planes.

As in Appendix 3, (42) can be defined by a finite difference approximation;

$$\frac{dk}{dt} = - \vec{V}.\vec{\nabla}\phi_o = - \left(\frac{u_o g (z_3 - z_1) + v_o g (z_4 - z_2)}{2d} \right) \qquad \ldots(43)$$

$(W\ gm^{-1})$

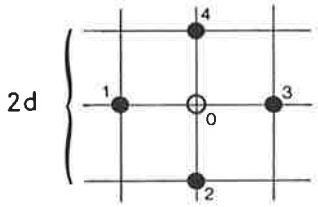

where $- \vec{V}.\vec{\nabla}\phi_o$ = kinetic energy generation at grid point o; z_1, z_2, z_3, z_4 are the heights of the pressure surface at grid points 1, 2, 3 and 4; u_o and v_o = the zonal and meridional wind components at grid point o; and 2d = twice the grid length d (Appendix 3).

APPENDIX 8

Determination and Interpretation of Velocity Potential Cross Sections

Vertical cross sections were determined by a normalization procedure. Monthly mean velocity potential values at seven standard pressure levels, from the surface to 100 mb, were vertically integrated and then averaged for the whole column;

$$\bar{\chi}_I = \frac{1}{900}\int_{100}^{1000} \bar{\chi}_L \, dP \qquad \ldots(44)$$

where $\bar{\chi}_I$ = column averaged monthly mean velocity potential, $\bar{\chi}_L$ = monthly mean velocity potential averaged for each pressure layer and dP = pressure increment.

The normalized velocity potential (χ_N) was then evaluated by subtracting the column averaged value ($\bar{\chi}_I$) from each standard pressure level value ($\bar{\chi}_L$);

$$\chi_N = \bar{\chi}_L - \bar{\chi}_I \qquad \ldots(45)$$

Finally, cross sections were drawn from the surface to 200 mb. At 100 mb a lid was placed on the troposphere and velocity potential initially assumed to be zero.

In interpreting the velocity potential cross sections (Figs.26-31), the gradient of velocity potential in the vertical plane ($\frac{\partial \chi}{\partial z}$) is obviously not *per se* meaningful. Mathematically, the velocity potential fields at each pressure level are only defined to within an arbitrary constant which varies with height in this case.

Thus if $\chi_o(x,z)$ represents the velocity potential fields at standard atmospheric levels, then;

$$\chi(x,z) = \chi_o(x,z) + A(z) \qquad \ldots(46)$$

where A(z) is an arbitrary function of height and is an equally valid velocity potential for the flow field under discussion.

Since it can be shown that;

$$\frac{\partial \chi(x,z)}{\partial z} = \frac{\partial \chi_o(x,z)}{\partial z} + \frac{dA(z)}{dz} \qquad \ldots(47)$$

It is obvious that $\frac{\partial \chi_o}{\partial z}$ is also only defined to within an arbitrary function of height $\frac{dA}{dz}$. However, because;

$$\nabla\left(\frac{\partial \chi}{\partial z}\right) = \nabla\left(\frac{\partial \chi_o}{\partial z}\right) \qquad \ldots(48)$$

$$\text{and} \quad \nabla^2\left(\frac{\partial \chi}{\partial z}\right) = \nabla^2\left(\frac{\partial \chi_o}{\partial z}\right) \qquad \ldots(49)$$

the latter derivatives and equivalent derivatives $\frac{\partial}{\partial z}(\nabla \chi_o)$ and $\frac{\partial}{\partial z}(\nabla^2 \chi_o)$ are defined uniquely, i.e. independently of the datum level chosen for the labelling of the $\chi_o(x,z)$ field.

APPENDIX 9

Monthly Weather Review article on aspects of Section 3.1

Monsoon and Teleconnection Variability over Australasia During the Southern Hemisphere Summers of 1973–77

ROBERT J. ALLAN

Department of Geography, University of Adelaide, Adelaide, South Australia 5001

(Manuscript received 22 June 1981, in final form 4 October 1982)

ABSTRACT

Interactions between monsoon and teleconnection circulations over the greater Australasian region 35°N–35°S, 85°E–175°E, are observed in 850 and 200 mb monthly mean velocity potential ($\bar{\chi}$) and streamfunction ($\bar{\psi}$) fields during the peak of the Southern Hemisphere summers (January and February 1973–77) prior to the Winter Monsoon Experiment (WMONEX). Aspects of the spatial and temporal structure of the Australasian monsoon and teleconnection systems are presented through a closer examination of the January 1973–75 sub-period, using vertical cross sections of monthly mean divergence and monthly mean surface streamfunction ($\bar{\psi}_{sfc}$) fields.

Most importantly, this study suggests that large-scale Southern Oscillation/Walker Circulation (SO/WC) teleconnection patterns are associated with variations in components of the Asian monsoon system. Interannual and intraseasonal fluctuations in the Near Equatorial Troughs of the Northern (NET_{NH}) and Southern (NET_{SH}) Hemispheres appear to be related to large-scale atmospheric circulation changes. Over Australia, the southward displacement of a strong section of the NET_{SH} is observed during the "wet" summers of 1974 and 1976. It is suggested that, at least in the lower levels, the Australian monsoon circulation in 1974 was almost entirely contained and maintained within the Southern Hemisphere. In the equatorial western Pacific, fluctuations in the NET_{NH} broadly coincide with northeast trade wind variability and possibly the El Niño cycles of 1972–73, 1975 and 1976.

At 200 mb, circulation patterns suggest that changes in anticyclonic maxima ($\bar{\psi}$ minima) in the Australian region are associated with teleconnection overturnings. In the 1973 summer, 200 mb velocity potential fields appear to be synonymous with a SO/WC "breakdown" and the development of a strong El Niño phenomenon.

The variable structure of the SO/WC overturning, which would accompany some of the above events, is observed in a series of vertical cross sections of monthly mean divergence between the surface and 200 mb levels during January 1973–75. Evidence is presented to show that the concept of the SO/WC as a simple large-scale vertical cell which fluctuates in magnitude and direction may be something of a simplification.

In January 1973–75, $\bar{\psi}_{sfc}$ fields suggest that NET_{NH} activity in the Asian sector is not homogeneous between the surface and 850 mb levels. The extent of cross-equatorial flow into Australia seems to be related to the coupling between the NET_{NH} and the cyclonic activity over the northwest of the continent. In fact, variability in this flow may result from either a low-level, quasi-permanent heat low or deeper and more structured NET_{SH} conditions being dominant in this region. Rainfall and monsoonal activity in Australia appear to be related to extremes in this phenomenon.

1. Introduction

During the past decade, research in tropical meteorology has increasingly focused on teleconnections between the monsoon systems and other components of the planetary-scale circulation. Such relationships have been demonstrated by Bjerknes (1969, 1972), examined in papers such as Flöhn (1973) and Flöhn and Fleer (1975), and investigated on a seasonal basis by Krishnamurti (1971), Krishnamurti *et al.* (1973) and Kanamitsu and Krishnamurti (1978). As a result, teleconnections have been identified with the interacting zonal and meridional exchanges that serve atmospheric mass and energy balance processes.

Within the near-tropical latitudes, three major equatorial source regions for these teleconnections have been associated with convective maxima over South America, Africa and South East Asia/Malesia (Barry, 1978). Both Krishnamurti *et al.* (1973) and Murakami and Unninayar (1977) have shown that the most active region for divergent mass outflow at 200 mb during the Southern Hemisphere summer is located in the vicinity of the low-latitude convective region in South East Asia/Malesia. On a planetary scale, the dominance of this maximum and its winter counterpart has been stressed by Krishnamurti (1971), Ramage (1971) and Webster *et al.* (1977).

The most documented of the near-zonal teleconnections is the Southern Oscillation (SO) or Walker Circulation (WC) phenomenon (Bjerknes, 1969), which is rooted in the South East Asian/Malesian convective maximum and extends out into a subsi-

© 1983 American Meteorological Society

dence zone over the equatorial to the subtropical South Pacific Ocean. Although physical evidence for this standing fluctuation has been found in the Pacific Basin (*viz.*, the El Niño current off the coast of South America and the occasionally extreme rainfall in the Pacific Dry Zone), much remains to be understood concerning the Australasian region where monsoon features are often elusive (Troup, 1961).

Since the works of Berson and Troup (1961), Berson (1961) and Troup (1961), monsoon dynamics in the region of northern Australia have not been analyzed as extensively as in Asian, Indian or West African systems. However, some of the research in the Asian region has important ramifications for monsoon processes over Australia. In particular, Chang *et al.* (1979), Chang and Lau (1980), Cheang (1977), Murakami (1977), Nicholls (1977), Paegle *et al.* (1979), Tanaka (1981), Williams (1979) and Webster (1981a) have demonstrated various spatial and temporal aspects of teleconnection and cross-equatorial interactions (flow and/or periodic surges) across the Australasian and Asian sector in both summer and winter. Distributions of tropical cloudiness have been used by Krueger and Winston (1974, 1975), Murakami (1975, 1980a,b), Webster and Stephens (1980) and Barton (1983) to infer circulation, convection and teleconnection changes and to examine radiation balances, particularly in the South East Asian/Malesian convective region. Some studies now point to links at a similar longitude between upper-level Hadley Circulation and subtropical jet stream maxima in the winter hemisphere, where a sinking arm of this cell is located. It has also been suggested (Murakami and Unninayar, 1977) that a similar, but weaker, interaction occurs in the summer hemisphere.

In response to the expanded use of satellite data and the various monsoon sub-programs of the Global Atmospheric Research Programme (GARP), interest in all scales of monsoon and teleconnection dynamics has increased. Yet, it has only been since the availability of data collected during the Winter Monsoon Experiment (WMONEX, 1 December 1978–5 March 1979) that a formalized program of tropical meteorological research has been initiated in Australia (Webster, 1981, personal communication).

This study investigates variations in Australasian tropical circulation, monsoon activity and the Southern Oscillation/Walker Circulation (SO/WC) teleconnection during the months of January and February 1973–77. To compare results with existing satellite-derived oceanic rainfall data, upper-cloud and nephanalysis distributions, a sub-period, consisting of the Januarys of 1973, 1974 and 1975, is also used. Monthly mean fields of velocity potential and streamfunction are calculated at the 850 and 200 mb levels over the domain 35°N–35°S, 85°E–175°E to examine and compare the variability of the major components of circulation with the location, intensity and significance of the Hadley cell and east–west sources and sinks. Satellite-derived oceanic rainfall rates (Rao *et al.*, 1976), references to upper-cloud patterns (Barton, 1983), and nephanalyses (Sadler *et al.*, 1976; Shideler and Sadler, 1979) for January 1973, 1974 and 1975 are used in conjunction with vertical cross sections of monthly mean divergence, for all standard levels up to 200 mb, to investigate the nature of convective processes that generate extensive precipitation zones. During this sub-period, a more precise picture of low-level flow over Australia is also sought by analyzing monthly mean surface streamfunction fields.

2. Theory and computational procedures

From Helmholtz's theorem, a horizontal wind vector V, can be decomposed into the sum of its divergent and rotational components (Holton, 1979, pp. 305–306). In a Cartesian coordinate system, this decomposition is given by the relationship

$$\mathbf{V} = \nabla\chi + \mathbf{k} \times \nabla\psi, \tag{1}$$

where χ is the velocity potential, ψ the streamfunction, $\mathbf{k}$ a unit vector in the vertical plane of a right-hand Cartesian coordinate system, and ∇ is the horizontal gradient or del operator.

These components are defined separately, via two equations of Poisson type, by the vertical component of the curl of the rotational field and the dot product of the divergent field:

$$\mathbf{k} \cdot \nabla \times \mathbf{V} = \nabla^2\psi, \tag{2}$$

$$\nabla \cdot \mathbf{V} = \nabla^2\chi, \tag{3}$$

where $\nabla \cdot \mathbf{V}$ is the horizontal divergence, $\mathbf{k} \cdot \nabla \times \mathbf{V}$ the relative vorticity and ∇^2 the Laplacian operator.

Using a regular 5° latitude by 5° longitude grid of the domain, monthly mean zonal (u) and meridional (v) components of wind observations were gridded by an objective analysis procedure (Yanai, 1964). From these gridded components monthly mean divergence and relative vorticity fields were then evaluated by a five-point centered difference approximation. An iterative solution to (2) and (3), in this case in terms of monthly mean velocity potential ($\bar{\chi}$) and streamfunction ($\bar{\psi}$), then depends on a knowledge of boundary conditions and a centered difference approximation for the Laplacian operator. Initially, both boundary and internal grid point values of $\bar{\chi}$ were set to zero with the use of a boundary correcting algorithm (Shukla and Saha, 1974), after each iteration, to produce successive improvements in both the $\bar{\chi}$ and $\bar{\psi}$ fields.

From a rearrangement of (3), the divergent part of the wind ($\mathbf{V}_\chi$) can be expressed in the form

$$\mathbf{V}_\chi = \nabla\chi, \tag{4}$$

where $\nabla\chi = \mathbf{i}\partial\chi/\partial x + \mathbf{j}\partial\chi/\partial y$ and $\mathbf{V}_\chi = \mathbf{i}u_d + \mathbf{j}v_d$ (u_d and v_d are the divergent zonal and meridional components and **i** and **j** are unit vectors in the x and y planes).

It is now possible to express (4) in terms of divergent zonal and meridional terms, i.e.,

$$u_d = \frac{\partial\chi}{\partial x}, \tag{5}$$

$$v_d = \frac{\partial\chi}{\partial y}. \tag{6}$$

Using a centered difference approximation to (5) and (6), the divergent part of the wind, in Cartesian coordinates, can be shown by the ticks, the symbol (/), emanating from each grid point in the monthly mean velocity potential diagrams (Figs. 5–6 and 9–10).

Vertical cross sections were determined by a normalization procedure. Monthly mean divergence values at seven standard pressure levels, from the surface to 100 mb, were vertically integrated and then averaged for the whole column, i.e.,

$$\bar{D}_I = \frac{1}{900}\int_{100}^{1000} \bar{D}_L dP, \tag{7}$$

where $\bar{D}_I$ is the column averaged monthly mean divergence, $\bar{D}_L$ is the monthly mean divergence averaged for each pressure layer and dP is the pressure increment.

The normalized divergence (D_N) was then evaluated by subtracting the column averaged value ($\bar{D}_I$) from each standard pressure level value ($\bar{D}_L$):

$$D_N = \bar{D}_L - \bar{D}_I. \tag{8}$$

Finally, cross sections were drawn from the surface to 200 mb. At 100 mb a lid was placed on the troposphere and divergence initially assumed to be zero.

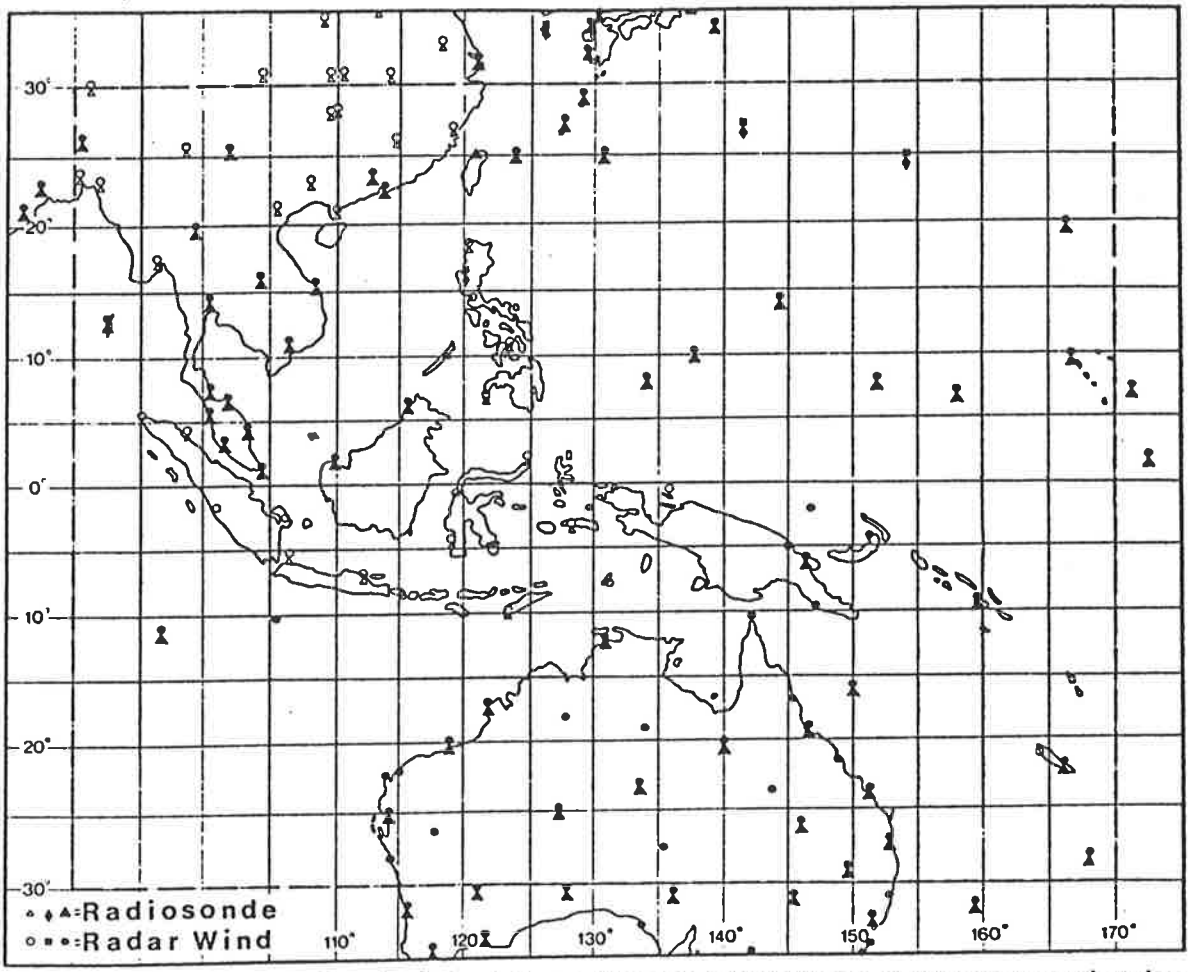

FIG. 1. Distribution of upper air stations in the study area. Solid symbols (circle/triangle, circle) denote upper air stations from which data were available for this study. Stations known to have been operating during all or part of the major study period, but from which no data were available, are designated by corresponding open symbols, while a combination solid symbol (square/diamond) indicates upper air stations from which data were only available to supplement the data set for monthly mean divergence cross sections and surface streamfunction fields.

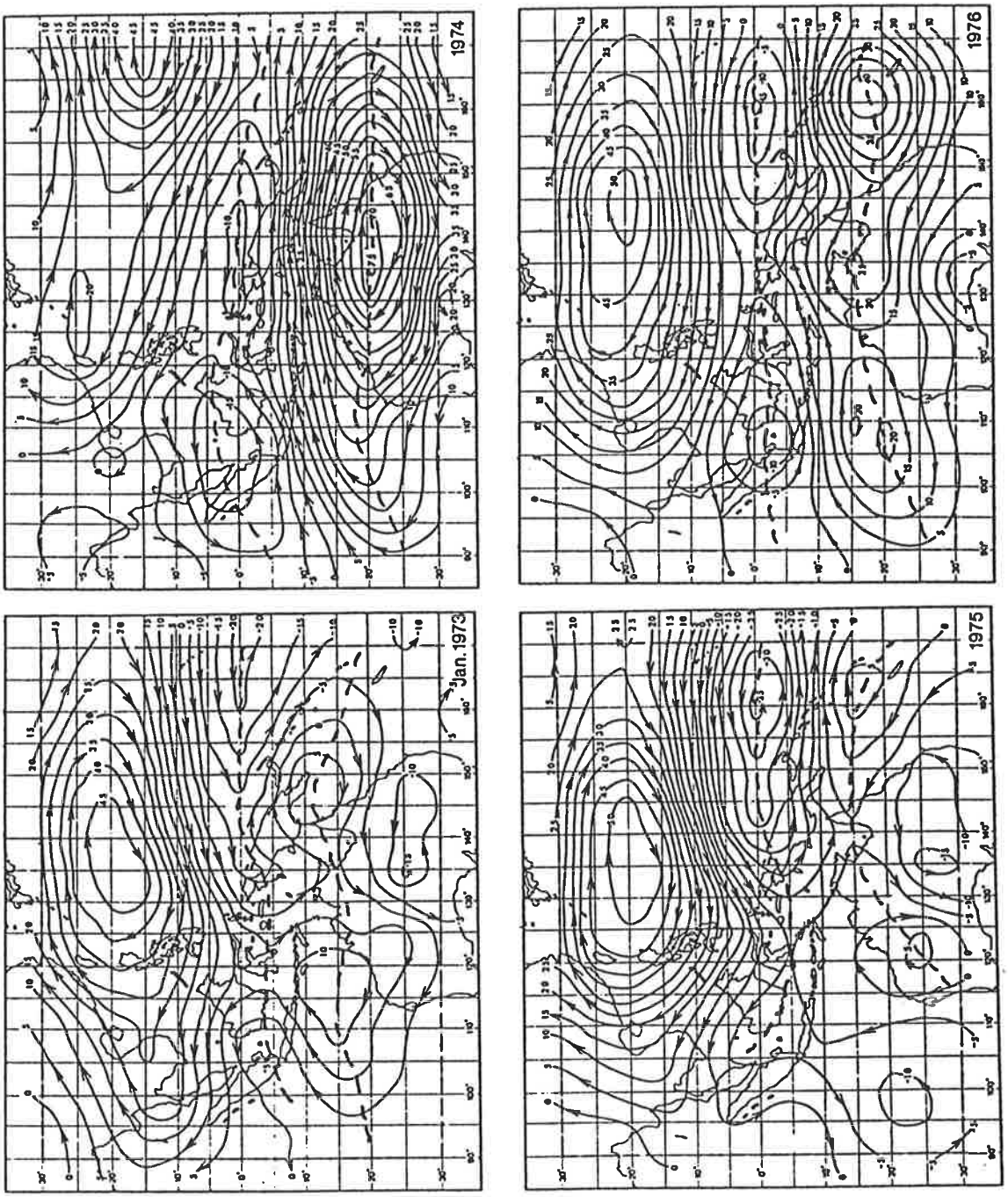

FIG. 2. Monthly mean 850 mb streamfunction fields (10^5 m^2 s^{-1}) at intervals of 5 units over the study area during the Januarys from 1973 to 1977. Heavy dashed lines indicate the positions of NET_{NH} and NET_{SH} referred to in the text.

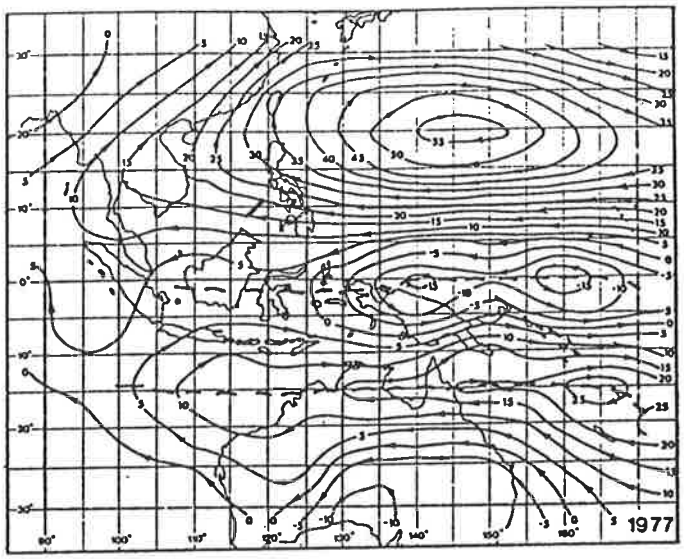

FIG. 2. (*Continued*)

3. Data sources

Individual monthly resultant wind vectors for standard isobaric levels were obtained from *Monthly Climatic Data for the World* (National Climatic Center) and supplemented by monthly records from the Australian Bureau of Meteorology, *U.S. Climatological Data—National Summary* (National Climatic Center), Malaysian Meteorological Service, Service de la Meteorologie en Nouvelle-Caledonie and the Thai Meteorological Department. Additional upper air data obtained from the publication *Aerological Data for Japan* (Japanese Meteorology Agency) were used to supplement the data set in both cross sections and surface streamfunction fields. A complete distribution of all upper air stations used is shown in Fig. 1.

In generating any field within a bounded domain, the distribution of data stations is crucial to the degree of resolution. As Fig. 1 shows, there are some areas in the domain where data distribution is very sparse. The lack of data from Indonesia, mainland China (prior to 1977), the Philippines and from the easternmost Japanese island stations generates some weaknesses in the major data set. The 200 mb fields (Figs. 7 and 8) showing monthly mean streamfunction and zonal wind component isotachs, most clearly illustrate resolution errors generated in data-sparse areas during the initial gridding of the wind field and carried over into the final fields. Resolution errors are also evident when monthly mean velocity potential fields generated with the additional Japanese Meteorology Agency data (not shown) are compared with those presented in this study. The most notable change is in the 200 mb $\bar{\chi}$ fields, where the large positive values in the North Pacific (top right-hand portion) section of Figs. 9 and 10 are reduced. Generally, field patterns are not unduly affected by the absence of subsequently-obtained data.

4. Results and discussion

Fields of streamfunction and velocity potential, computed as described from monthly mean zonal and meridional wind components at 850 and 200 mb levels, are shown in Figs. 2–3 and 5–10. During this 1973–77 period, the discussion focuses on circulations in the tropical domain from 35°N–35°S and 85°E–175°E. The sub-period of January 1973–75 analyses relationships between the vertical structure of teleconnection circulations (Figs. 12–14), oceanic rainfall rates (Fig. 11), upper-cloud distributions and nephanalyses along four fixed latitudinal (equator, 5°S, 10°S and 15°S) and four variable longitudinal (between 85 and 180°E) cross sections. This sub-period also includes an investigation of monthly mean surface streamfunction fields (Fig. 15).

a. 850 mb monthly mean streamfunction ($\bar{\psi}_{850}$) and velocity potential ($\bar{\chi}_{850}$); 1973–77

The 850 mb level is chosen for the initial broad-scale analysis of low-level monsoon flow because it is usually below the "average" trade wind inversion layer (Riehl, 1979). It is an intermediate zone between lower levels, which experience progressively larger frictional effects in the planetary boundary layer, and higher levels, where anticyclonic patterns tend to persist.

Variability of circulation is evident in the map sequences of Figs. 2 and 3, both in an interannual and intraseasonal sense. Over Australia, the summers of 1974 and 1975 differ radically from each other in

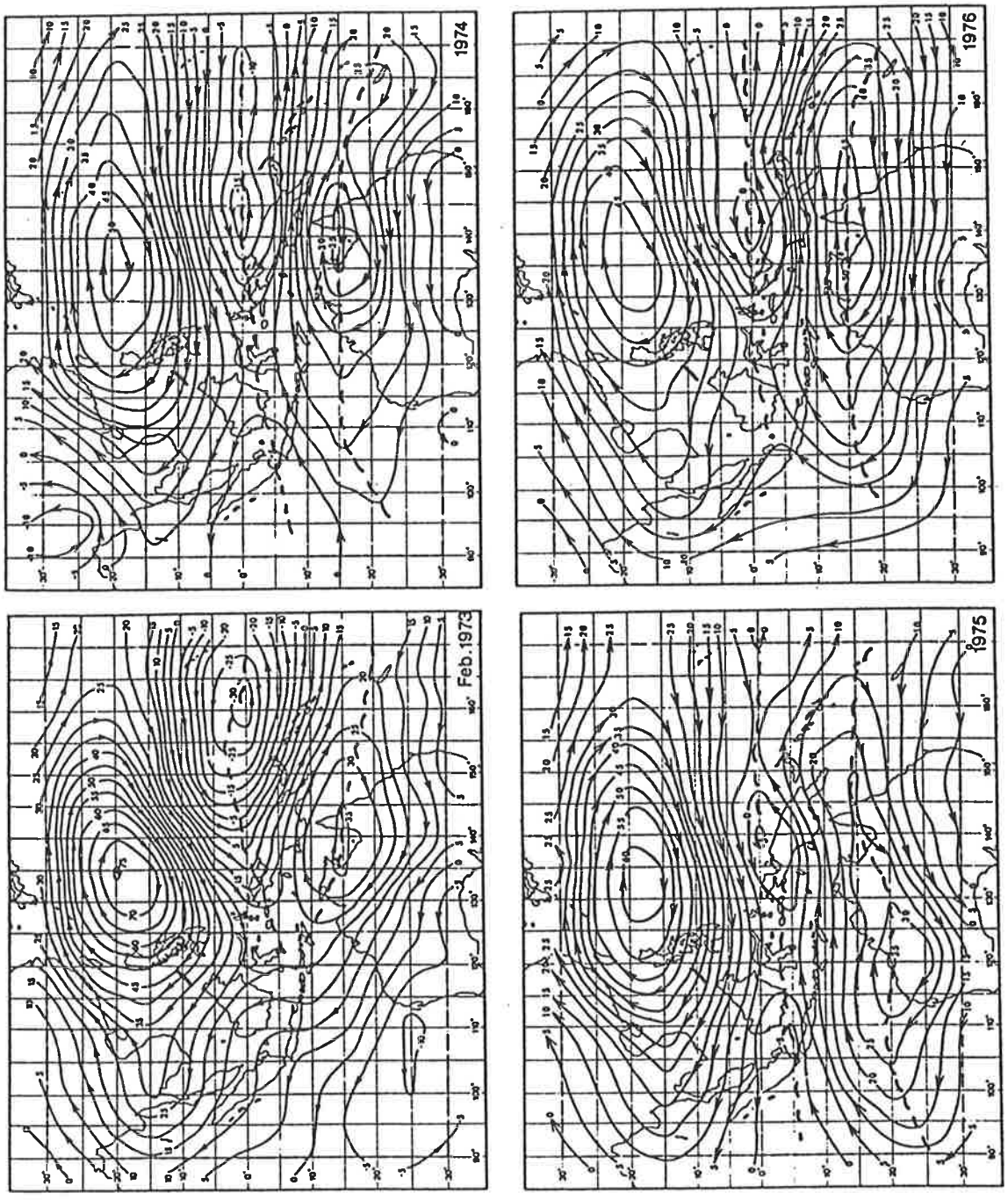

FIG. 3. As in Fig. 2, except during the Februarys from 1973 to 1977.

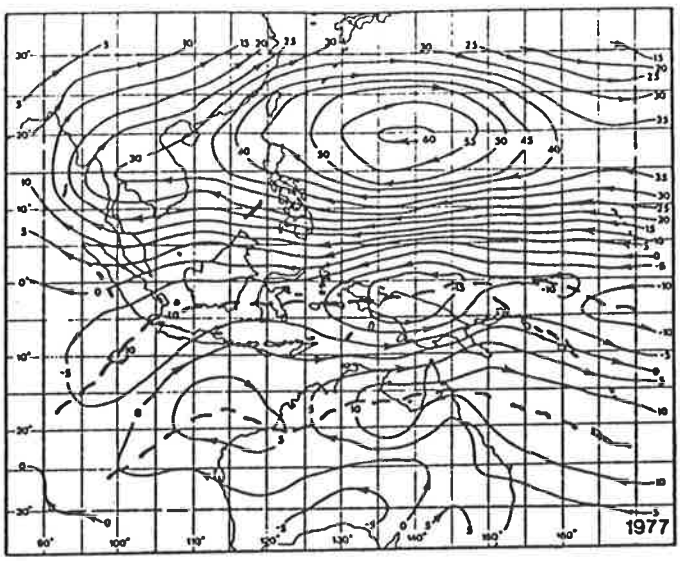

FIG. 3. (*Continued*)

terms of cyclonic circulation. In particular, the month of January during these two years shows strongly contrasting monsoonal activity and flow patterns. During the period of above-average monsoon rainfall in January 1974 (Fig. 2), the Southern Hemisphere Near Equatorial Trough (NET_{SH}) was extremely strong, displaced to 20°S and centered over the continent. However, in January 1975, a very weak cyclonic circulation over the western portion of the continent is more in character with summer heat low conditions (Ramage, 1971, p. 15).

Marked summer rainfall variability is evident within this five-year period (Fig. 4). However, only the alternation of monsoon activity by the Januarys of odd (drier) and even (wetter) years suggests any regular quasibiennial pattern. Although it could possibly be argued that such variability is a reflection of the monsoon onset characteristics noted by Troup (1961) and examined in greater detail by McAvaney *et al.* (1981) and Davidson *et al.* (1981). In fact, over the five-year period, February (Fig. 3) exhibits the strongest interannual persistence and organization of monsoonal activity and is responsible for the major rainfall contributions in the summers of 1973 and 1975 (Fig. 4). This may imply that in very wet summers (i.e., 1974) monsoon flow tends to become established earlier in the season, perhaps around early to mid-December, and is carried over into March (map sequence not shown). Yet, even when established, the monsoon regime experiences distinctive "break-like" periods (Troup, 1961; Webster *et al.*, 1977; McBride, 1981; Webster, 1981b).

The data suggest that extremes in the Australian monsoon are linked with broad, hemispheric circulation changes and interhemispheric interactions. The position and intensity of the quasi-permanent North Pacific anticyclone and the more variable Northern Hemisphere Near Equatorial Trough (NET_{NH}) appear to have some influence on Southern Hemisphere systems. This is particularly true of the NET_{NH} which, in response to the equatorially-converging Northern Hemisphere northeast trade winds of Figs. 2 and 3, exhibits greater vigour in the eastern section to the northwest of Papua New Guinea. Once recurving into near-equatorial Southern Hemisphere regions, this flow is then westerly and probably contributes to the convergence field under changing Coriolis deflection. In the wet summer periods (especially in the Januarys of 1974 and 1976), circulation in the western portion of the NET_{NH} (west of 115°E) intensifies, matching that in its eastern extremity. This action, at least at 850 mb, probably promotes slow cross-equatorial flow from more Asian sources into the Australian region. In contrast, during the drier January of 1975 and the moderately wet (at least on the Australian east coast) February of 1973 (Fig. 4), there is stronger circulation in the eastern section of the NET_{NH}, the latter being responsible for cross-equatorial flow across Papua New Guinea and areas to the north-northwest of Australia. Yet, there are some grounds to suggest that during certain periods of strong northeast monsoon activity, Australian monsoon circulation is maintained by processes almost entirely within the Southern Hemisphere. Thus, despite the relatively stronger western portion of the NET_{NH} in January 1974 and 1976, the massive cyclonic circulation over Australia draws much of its mass and moisture from Southern Hemisphere sources.

The influence of the North Pacific anticyclone is harder to interpret. However, the extremely anomalous flow pattern in January 1974 indicates that this

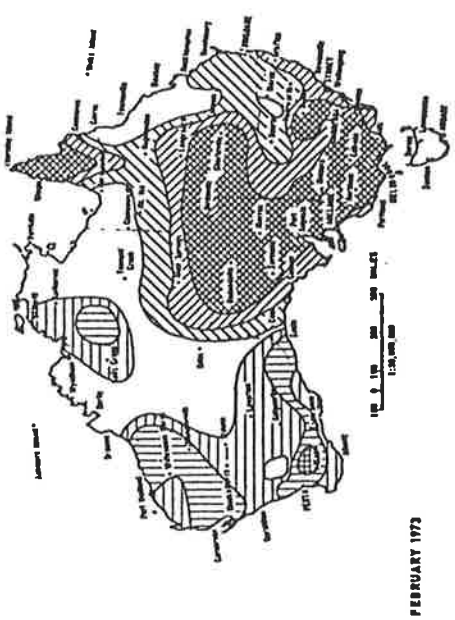

FEBRUARY 1973

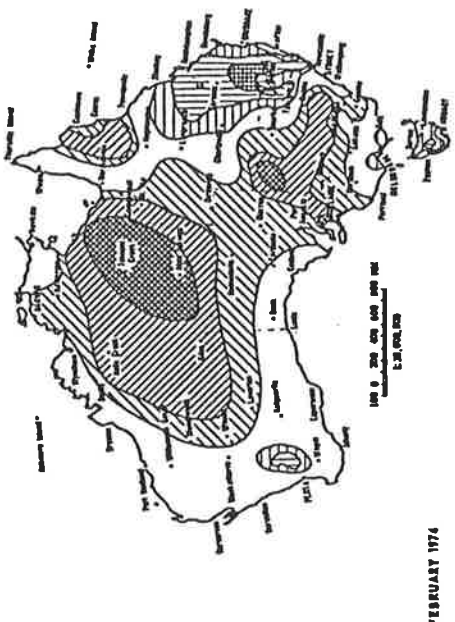

FEBRUARY 1974

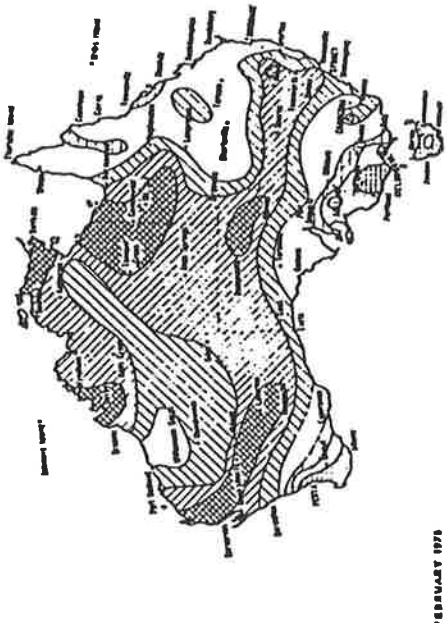

FEBRUARY 1975

JANUARY 1973

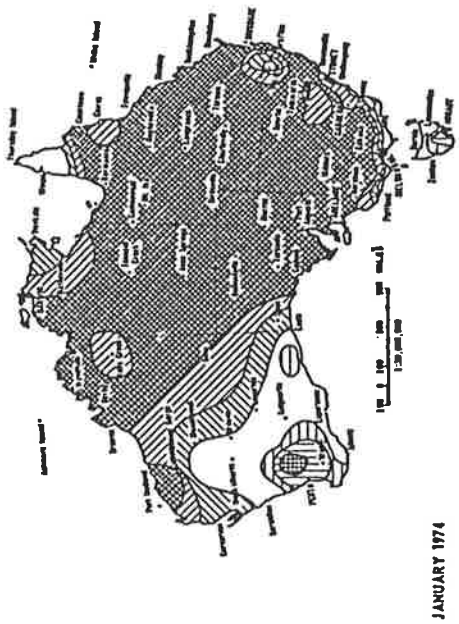

JANUARY 1974

JANUARY 1975

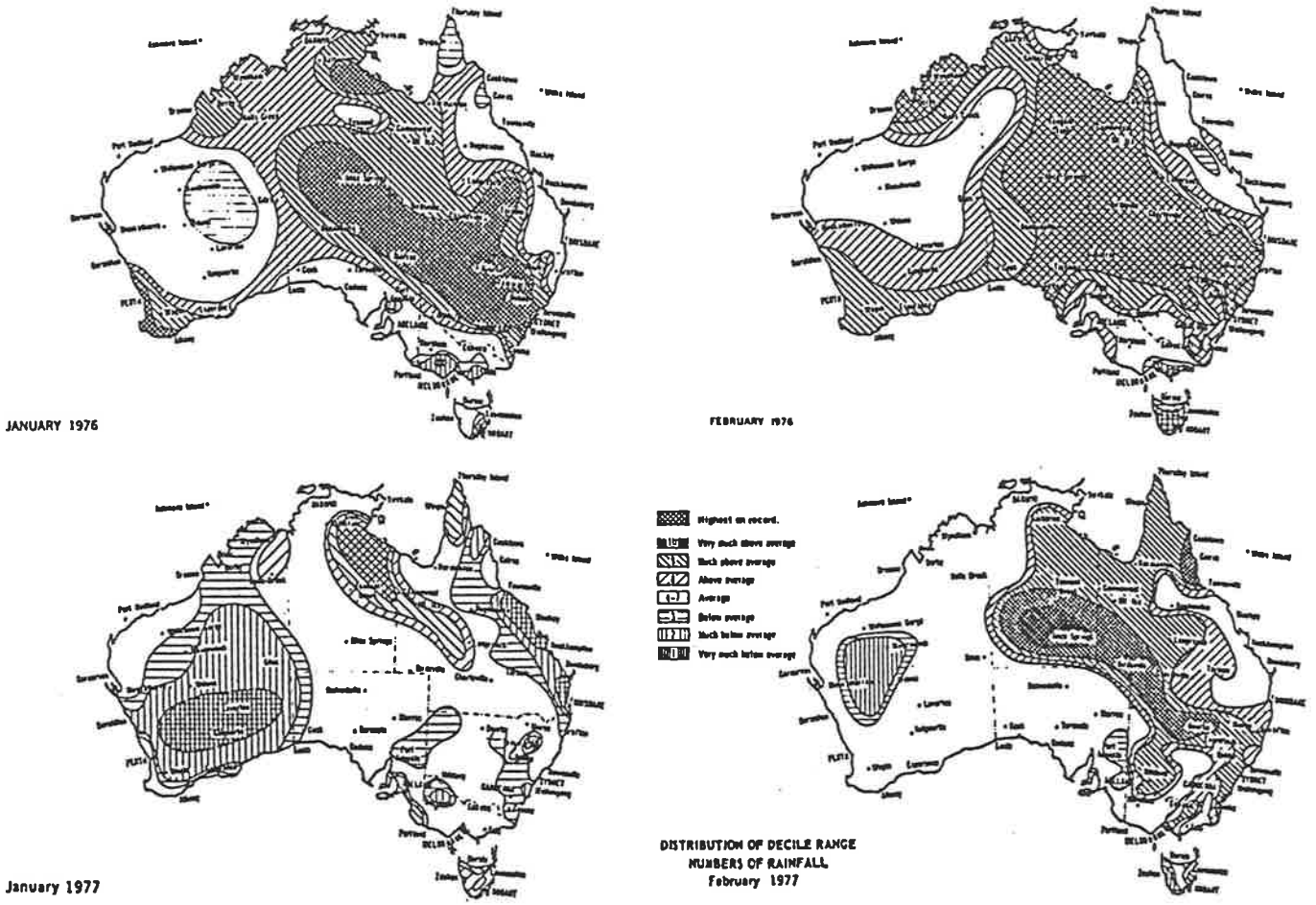

FIG. 4. Decile rainfall distributions over Australia: January and February 1973–77.

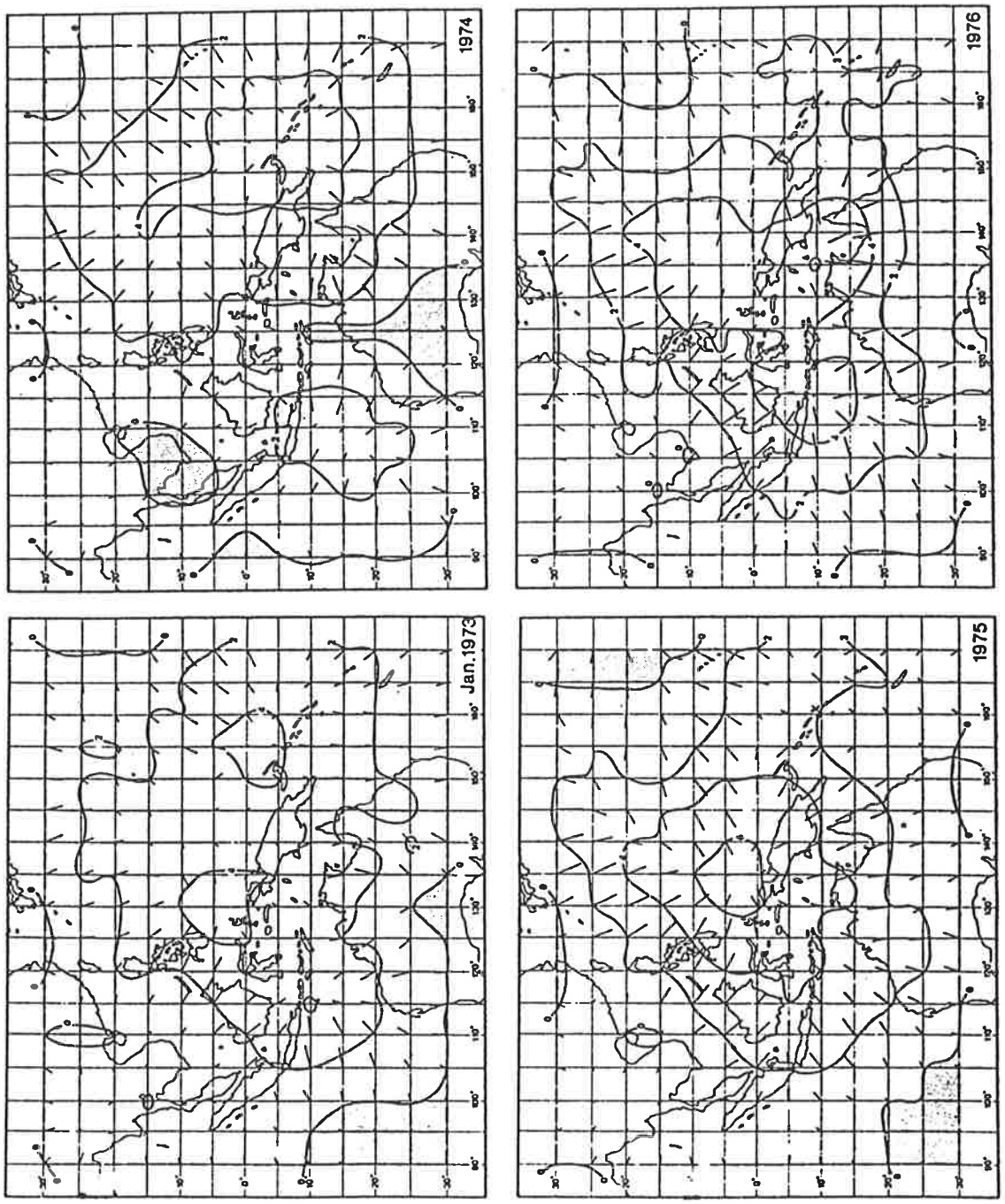

FIG. 5. As in Fig. 2, except for velocity potential fields (10^6 m^2 s^{-1}) at intervals of 2 units. The symbols / indicate the direction and magnitude of the divergent part of the wind, where a length of one grid interval equals 9.5 m s^{-1}.

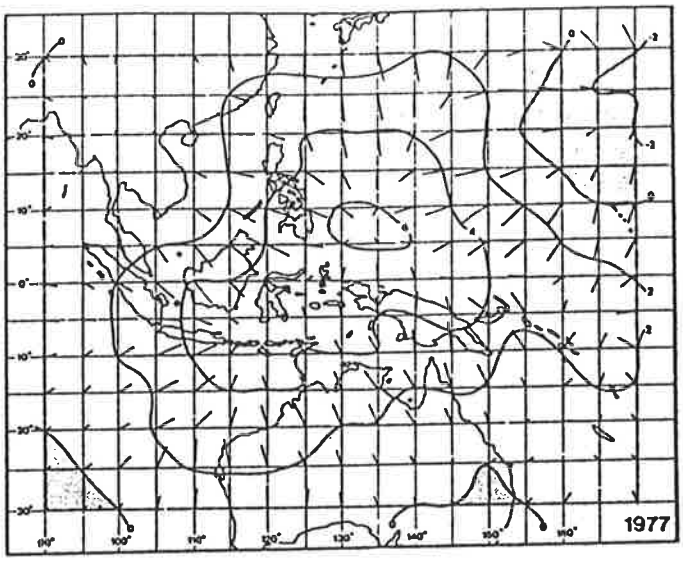

FIG. 5. (*Continued*)

anticyclone may respond to broad-scale interactions. Such interactions are manifest by Hadley cell and east-west teleconnections, which form from vertical cells originating in the monsoon foci of South East Asia/Malesia. Oceanographical and meteorological research (Flöhn, 1973; Flöhn and Fleer, 1975; Julian and Chervin, 1978; Quinn, 1974; Quinn and Burt, 1970; Quinn, 1972; Quinn *et al.*, 1978; Ramage, 1975; Ramage *et al.*, 1980; Ramage and Hori, 1981; Reiter, 1978, 1979; Wyrtki, 1975, 1977, 1979) indicates that variations in the strength of the Pacific trade wind system may be a response to, and/or initiate changes in, the SO/WC.

It would seem that the El Niño cycles of 1972–73, 1975 and 1976 are reflected in the strength of circulation in the eastern extremity of the NET_{NH}. Wyrtki (1975, 1977) indicates that the termination of the 1972–73 El Niño was heralded by an increase in equatorial Pacific trade wind activity. This activity also appears to coincide with the very strong eastern section of the NET_{NH} in February 1973. Ramage (1975) states that this El Niño terminated in March 1973. Evidence of trade wind and NET_{NH} changes, which may have occurred at either the beginning or end of the very weak El Niño of early 1975, are harder to find. Wyrtki *et al.* (1976) note that cruise observations found evidence for El Niño development in February and March and cessation by April and May of 1975. In the former period, the eastern section of the NET_{NH} shows a marked weakening in February (Fig. 3), followed by recovery in March (not shown). A moderate El Niño in mid-1976 was heralded by weakening equatorial trade winds in late 1975 and early 1976, while its termination coincided with strengthening trade winds in early 1977 (Wyrtki, 1979). Again the best evidence for trade wind weakening comes from the February $\bar{\psi}_{850}$ fields, with February 1976 showing a marked drop in NET_{NH} strength from January values (Figs. 2 and 3). This cycle was apparently completed by an increase in trade wind strength in the entire 1977 sequence of Southern Hemisphere summer months (Figs. 2 and 3).

Although being a dynamically-induced component of horizontal circulation systems, divergent or convergent motions are usually an order of magnitude less than the circulations that induce them (Haltiner, 1971, p. 57). As shown by Eq. (3), the velocity potential fields used in this study are determined from divergence distributions. Although not entirely coincident, positive velocity potential maxima approximate regions of convergence while negative velocity potential maxima approximate regions of divergence (Krishnamurti *et al.*, 1973).

In Figs. 5 and 6, the major $\bar{\chi}_{850}$ maxima tend to occur in the near-equatorial zone, extending on occasions to about 10°N and 10°S latitude. Like the circulation regimes that induce them, they would seem to exhibit a degree of variability which is directly related to large-scale teleconnection fluctuations. These centers of action are the broad-scale, low-level moisture and latent heat sources which, when coupled with upper-level divergent maxima ($\bar{\chi}_{200}$ minima) (Figs. 9 and 10), fuel the teleconnection extensions. It would seem that these $\bar{\chi}_{850}$ maxima are analogous with the regions of time-averaged moisture convergence, and thus condensational heating sources, which are seen by Cornejo-Garrido and Stone (1977) as the prime driving force for the Walker Circulation.

During the 1973 summer, low-level $\bar{\chi}_{850}$ maxima appear in the near-equatorial region around 160°E. These centers seem to result from convergence in-

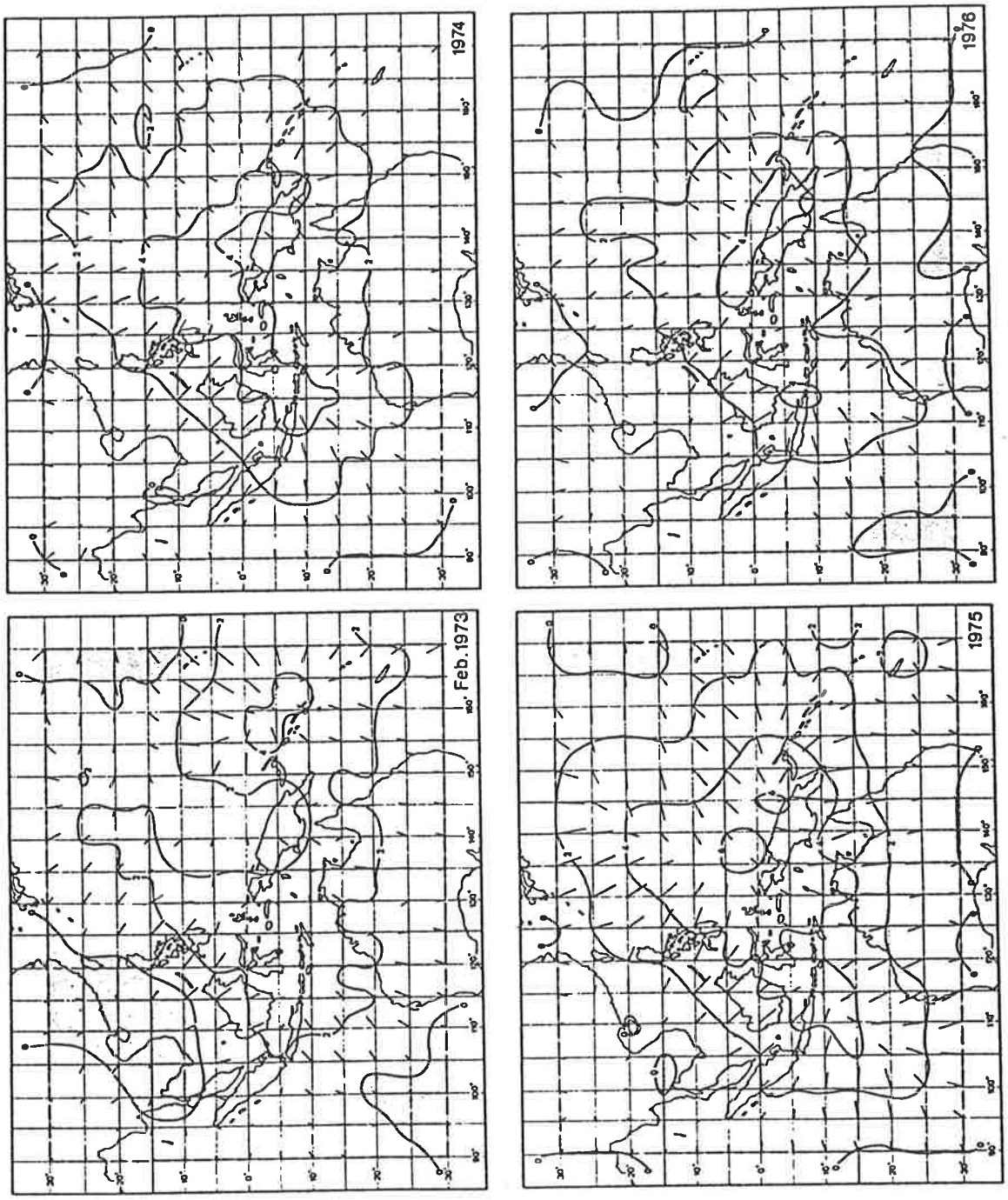

FIG. 6. As in Fig. 5, except during the Februarys from 1973 to 1977.

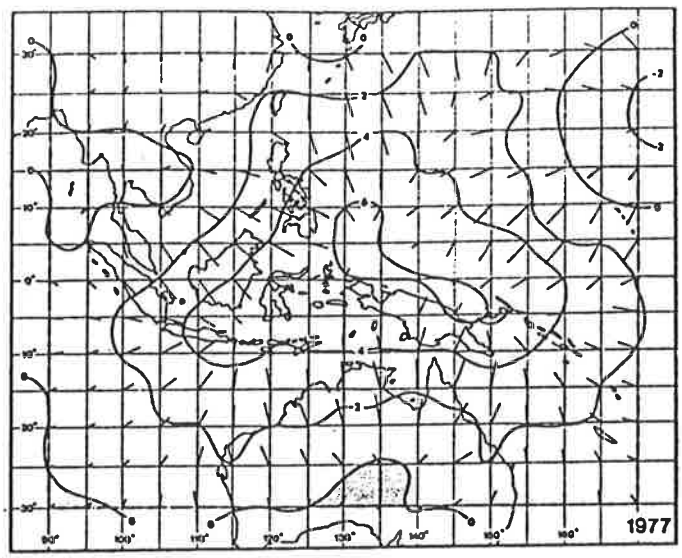

FIG. 6. (*Continued*)

duced by the strong circulation ($-\bar{\psi}_{850}$) in the eastern section of the NET_{NH} and consequently, from a peak in the Pacific northeast trade wind regime.

In very wet summer periods (e.g., 1974 and 1976) low-level velocity potential maxima with strong convective motion intrude into the Australian continent. In January 1974, there are two strong $\bar{\chi}_{850}$ maxima of opposite sign affecting the Australian continent. Some of the low-level impetus for the extreme rainfall at this time comes from convergence in that section of the $\bar{\chi}_{850}$ maxima (shown by the size and orientation of the symbol (/) in January 1974) encompassing much of Queensland and the Northern Territory. The summer of 1973–74 is notable for above-average rainfall across northern Australia (Fig. 4) and subsequently, for the most documented flooding of the Lake Eyre salt pan (centered around 28°30′S, 137°15′E).

Although broad-scale convergence over northern Australia is strongest in January 1976 (Fig. 5), rainfall in most districts did not exceed the January 1974 totals (Fig. 4). This apparent anomaly can be explained by the fact that the vertical extent (between the surface and 700 mb levels) of low-level convergence (in diagrams not shown) and its coupling with upper-level divergent maxima was stronger, deeper and more organized in 1974. In addition, inland areas of eastern Australia were influenced by tropical cyclone remnants (strong rain depressions) in January and February 1976.

In the relatively drier summers of 1975 and 1977, $\bar{\chi}_{850}$ maxima appear to be strong and displaced somewhat to the north of the equator. This pattern would indicate that the NET_{NH} is enhanced and systems in general are displaced into the Northern Hemisphere. Tanaka (1980, 1981) suggests that periods of strong monsoonal activity are characterized by two low-level Inter-Tropical Convergence Zones (ITCZs), while in weaker periods only one ITCZ forms. Although the notion of two ITCZs is disputed by Gruber (1972) and Hubert *et al.* (1969), it would appear that major segments of the NET_{SH} weaken in a relatively dry Australian summer month, such as January 1975 (Fig. 2), while the converse may be true for some sections of the NET_{NH} in wet Australian summer months (Januarys 1974 and 1976).

The northwest–southeast oriented convergence band dipping out of the diagrams around 160–170°E and 5–15°S in January 1975, 1976 and 1977 in Fig. 5, and the closely aligned NET_{SH} in Fig. 2, may be more related to the South Pacific Convergence Zone (SPCZ) examined by Streten (1970, 1973), Trenberth (1976) and Musk (1976).

b. 200 mb monthly mean streamfunction ($\bar{\psi}_{200}$) and velocity potential ($\bar{\chi}_{200}$); 1973–77

The 200 mb level is analysed because it highlights the position and magnitude of upper-level features set up under the influence of large-scale planetary flow.

Figs. 7 and 8 show the presence of some distinct anticyclonic systems in the regions of Australia and the northwest Pacific. The zonal wind component isotachs illustrate jet stream locations in Southern Hemisphere summer and Northern Hemisphere winter situations. Strong jet maxima off Japan are a feature of the entire map sequence. However, subtropical jet maxima over southern Australia are more variable, and being evident only in January 1973 and 1975, may reflect changes in upper-level flow characteristic of monsoon onset (Troup, 1961; McBride,

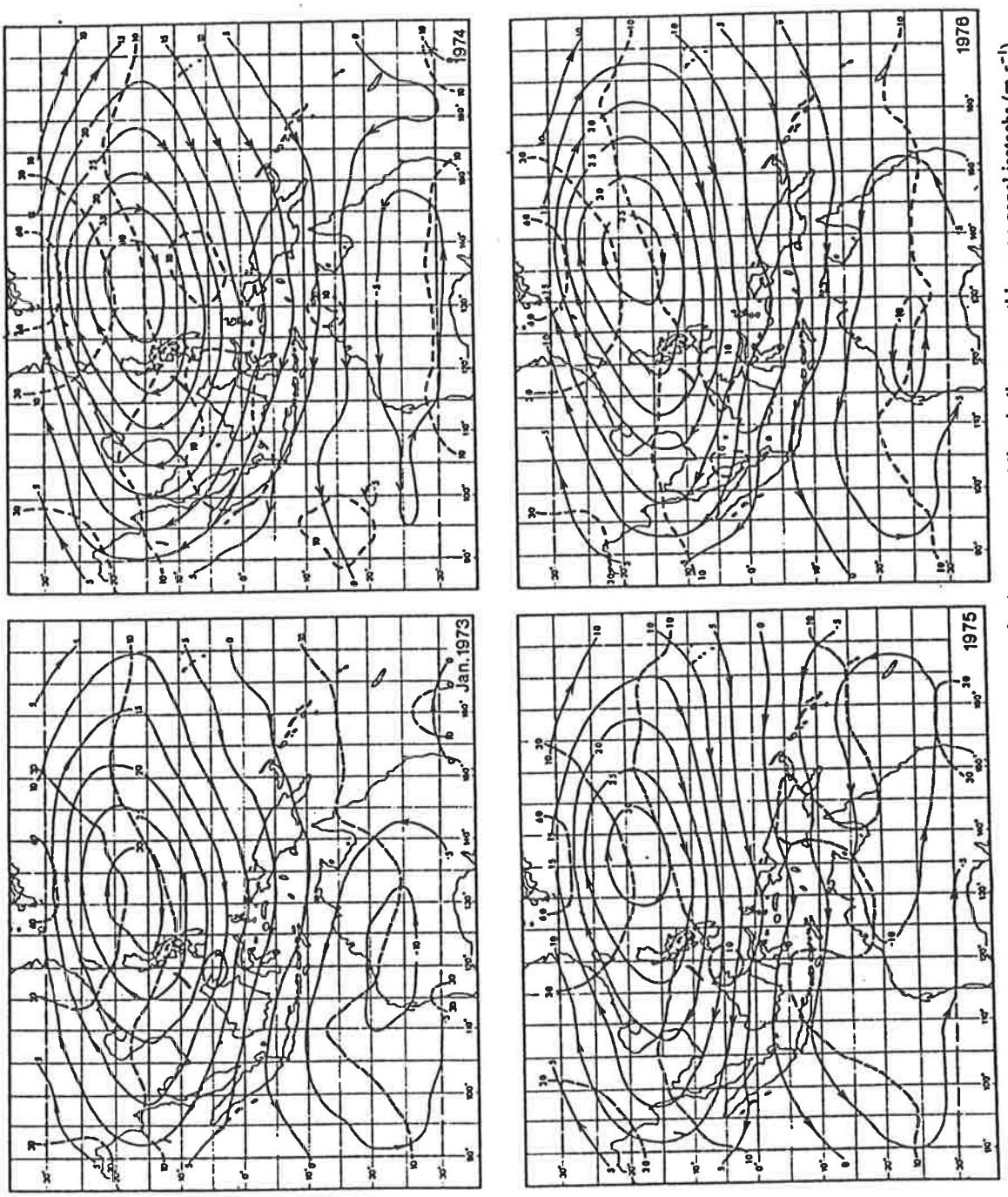

FIG. 7 As in Fig. 2, except for 200 mb and in units of 10^6 m^2 s^{-1}. Heavy dashed lines indicate monthly mean zonal isotachs (m s^{-1}).

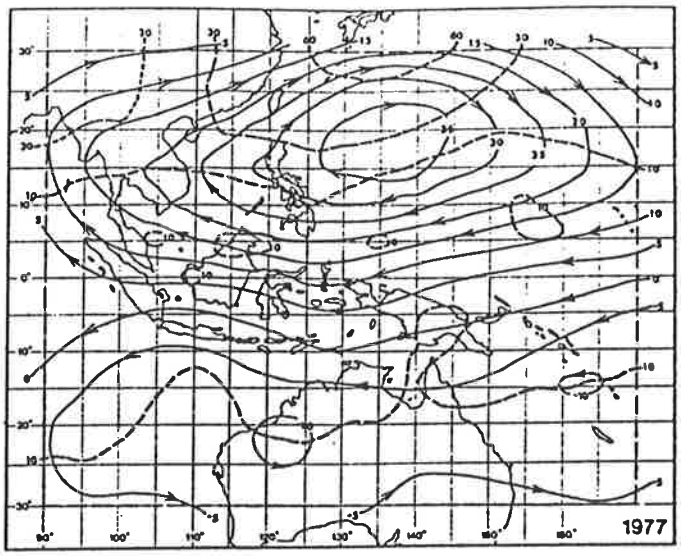

FIG. 7. (*Continued*)

1981). Yet, the major feature of this map sequence is the periodic change in the intensity and pattern of Australian upper-level anticyclonic flow. In summer, upper-level anticyclonic maxima appear to be directly caused by the sensible and latent heat released into the upper atmosphere by strong continental heating and monsoonal convective activity (Ramage, 1971). Although not possessing any elevated heat source to anchor and develop strong quasi-permanent upper anticyclonic features, the Australian continent seems to produce a distinctive, although more variable, upper anticyclonic pattern.

In 1973, the anticyclonic pattern shows a strong, distinctly cellular focus over the western portion of the Australian continent. January 1973 also exhibits the northern edge of a subtropical jet maximum in this western area (peak at 30°S, 115°E). The month of January 1974, coinciding with the extreme Australian summer flooding period, is the most anomalous shown. Australian anticyclonicity is weak, with a cellular arrangement spread out over the broad expanse of the continent. In the 1974 summer months, the isotach field shows no subtropical jet stream maxima, while the major jet-like flow has an easterly maximum in the region of Darwin during January. January 1975 provides another situation where the cell is very strong and broad but displaced to the eastern areas of Australia. This summer period also shows a major intraseasonal swing in the location and strength of the cell, from its strong easterly position in January to a weaker westerly location in February. Such variability suggests that changes in continental heat, radiation or convective processes may influence the atmosphere on relatively short time scales.

Although displaced slightly to the west in 1976, the anticyclonic cell still covers much of the continent. However, anticyclonicity is somewhat greater than in the other major wet season of 1974. Yet, during the extremely wet months of 1974 and 1976, the anticyclonic pattern is one of relatively weaker, more southerly displaced centers over the continent than in the other drier months in the period. On the other hand, the relatively dry January of 1977 is dominated by a broad belt of anticyclonicity across the entire domain south of 10°S and anticyclonic ($-\bar{\psi}_{200}$) maxima over the northwest of the continent and out to the northeast over the New Hebrides. There is little change in this pattern through February 1977, with only an eastward shift in $-\bar{\psi}_{200}$ maxima over Australia.

It could be argued that large amounts of latent heat, released into the upper atmosphere by the deep convection in 1974 and 1976, would have contributed to strong anticyclonicity. However, this is not evident in the anticyclonic circulation regime during the 1974 summer. One possible conclusion is that horizontal processes aloft were acting to vigorously remove this liberated heat. Ramage (1971, p. 234) suggests that mechanisms such as strong vertical teleconnection circulations could act to rapidly remove latent heat in these circumstances. Such a process would allow lapse rates to remain steep and keep convective processes strong throughout a considerable depth of the atmosphere. It is suggested that teleconnections, particularly the strong SO/WC in 1974, performed this function. Interestingly, the 200 mb temperature field over inland Australia (not shown) was 2–3°C warmer than average in January 1974 but had returned to near average values by February 1974.

It would seem that the position and strength of upper-level anticyclonic features have an important bearing on atmospheric flow, jet stream location and

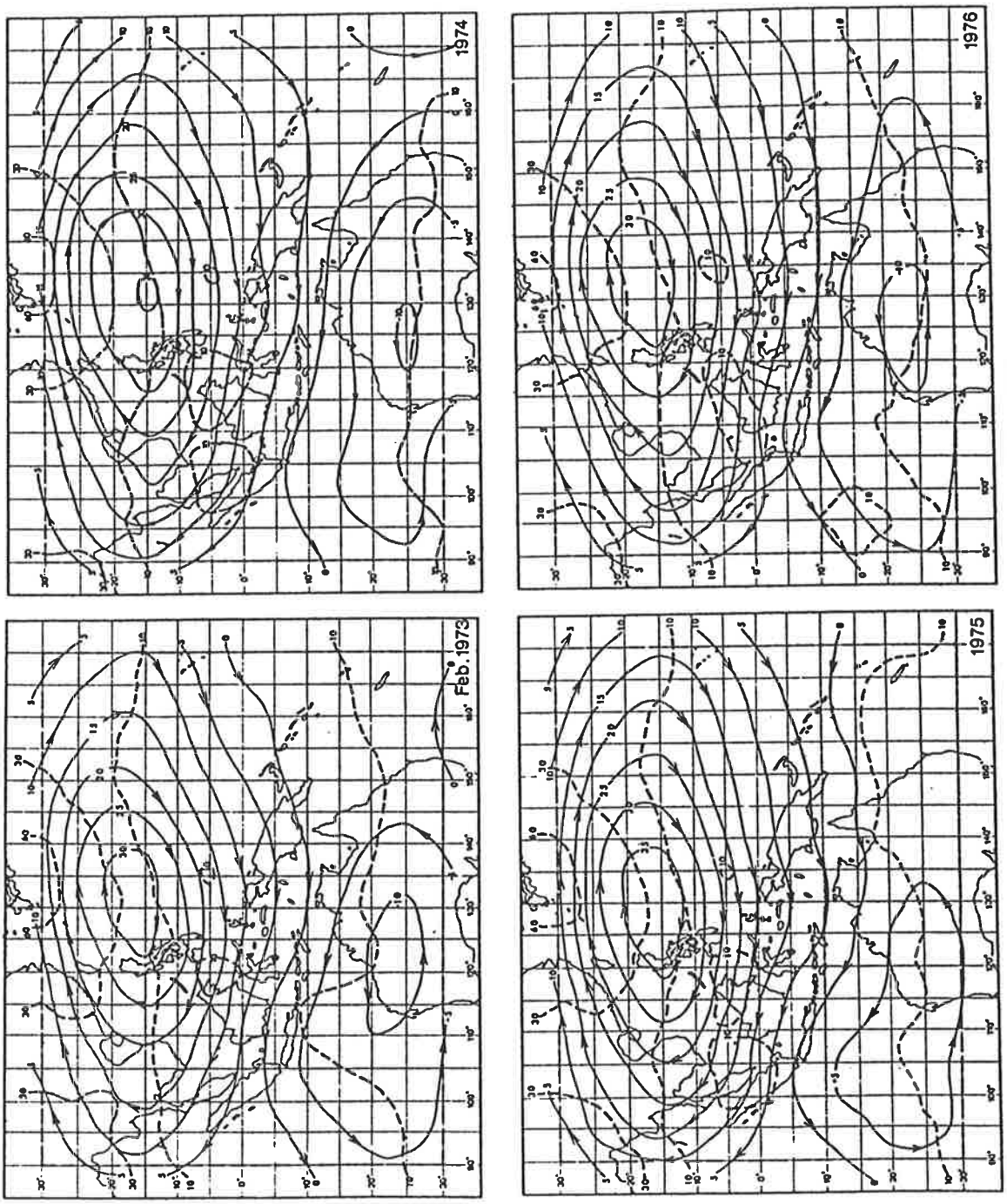

FIG. 8. As in Fig. 7, except during the Februarys from 1973 to 1977.

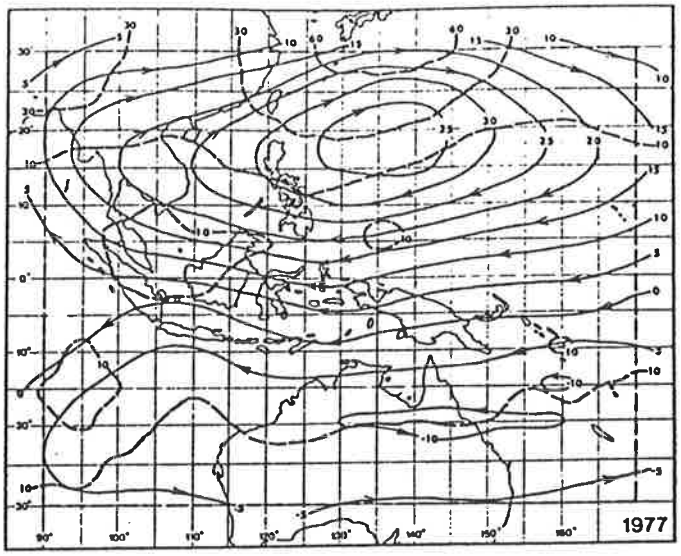

FIG. 8. (*Continued*)

convective processes. The Northern Hemisphere upper anticyclone would seem to be involved in such interactions and probably has a direct effect on the nature of upper-level divergence fields. In the wetter months, this anticyclonic cell appears to expand and strengthen (as in January 1974) at the expense of its Southern Hemisphere counterpart. Such a process tends to coincide with the previous observation of a weaker, southerly displaced anticyclonic circulation over Australia in the wet summer months.

The 200 mb velocity potential fields in Figs. 9 and 10 provide further evidence of the variability of upper-level circulation. Negative velocity potential predominates over the South East Asian/Indonesian sector, and illustrates the strong, divergent mass outflow associated with the vigorous convection during the northeast monsoon regime. The symbols (/) in Figs. 9 and 10 testify to the strength, direction and extent of the divergent motion spilling out from this region.

The locations of coupled 200 mb divergent and 850 mb convergent maxima during the summers of 1975–77 closely coincide with regions of remotely-sensed Outgoing Longwave Radiation (OLR) minima (Winston *et al.*, 1979) and nephanalysis cloud octa maxima (Shideler and Sadler, 1979). Around the convective maxima, parts of the upper-level divergent outflow may also be related to the large areas of tropical upper tropospheric extended cloud noted by Webster and Stephens (1980) and upper-level cloud distributions of Barton (1983).

Predominant elongations of divergent maxima, extending in approximately meridional (Hadley) and zonal (east–west and SO/WC) directions, illustrate the preferred modes or teleconnections powered by the monsoon foci of South East Asia. However, as Krishnamurti (1971) and Krishnamurti *et al.* (1973) suggest, and Figs. 9 and 10 show, these divergent arms form a set of radial rather than distinctly orthogonal overturnings.

One feature of most diagrams in Figs. 9 and 10 is a divergent lobe or arm which extends across the northeastern section of Australia and out into the South Pacific. Variations in anticyclonic flow in both hemispheres would appear to cause this arm to oscillate in strength and extent. The previously noted extreme of a westerly displaced cell with increased anticyclonicity, should result in stronger divergent and convergent maxima about the system. Such a pattern occurs during the 1973 circulations. In fact, coinciding with an SO/WC "breakdown" in January 1973 (Flöhn, 1973; Flöhn and Fleer, 1975; Quinn *et al.*, 1978; Ramage, 1975; Ramage and Hori, 1981; Rao and Theon, 1977), the divergent arm disappears and is replaced by weak convergent motion over the eastern half of the continent. This trend is a feature of the entire 1973 Southern Hemisphere summer and extends late into the season (showing signs of the return of divergent motion by March).

Periods when strong anticyclonic cells are displaced to the east of Australia provide further evidence of major changes in $\bar{\chi}_{200}$ fields. January 1975 is such a case. This month shows a strong divergent arm across Australia, with local divergent maxima along its whole length and in the near-equatorial region east of 160°E. The $-\bar{\chi}_{200}$ centers in the latter regions strongly coincide with the lower-level convergent maxima (Figs. 5 and 6) in the summer of 1973 and to a lesser degree in the Januarys of 1975, 1976 and 1977. They apparently represent circulation patterns which constitute a part of SO/WC anomalies. In fact, the $\bar{\chi}_{200}$ pattern in the Southern Hemisphere summers of 1975–77 highlights a range of

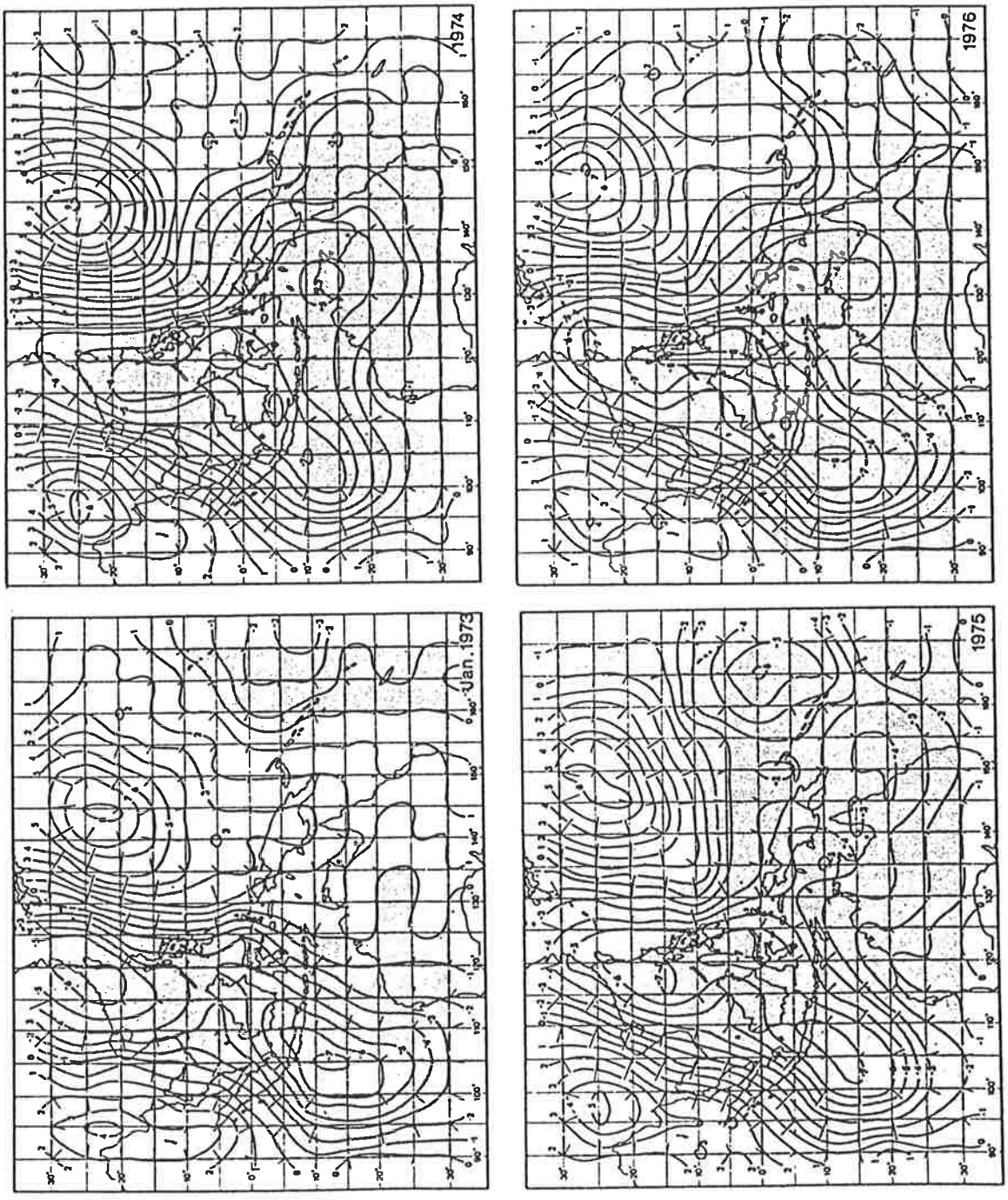

FIG. 9. As in Fig. 5, except for 200 mb and at intervals of 1 unit.

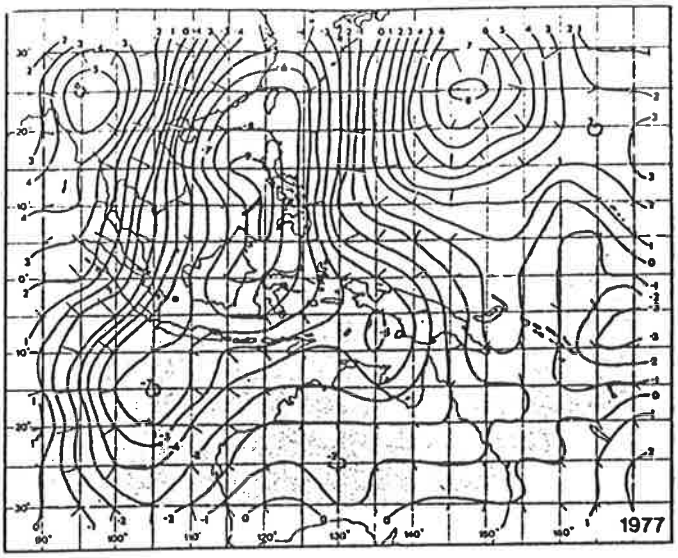

FIG. 9. (*Continued*)

breakdowns in the divergent arm across northern Australia. The abortive El Niño of early 1975 is perhaps reflected in the weakening of the divergent arm from January to February of that year (Figs. 9 and 10). However, definite evidence of such a direct interrelationship is difficult to find in the other two summer sequences. Only the formation of a $-\bar{\chi}_{200}$ maximum in the east, around 160–170°E during the early months of 1976, seems to be related to a pending breakdown of the SO/WC. The 1977 summer pattern fails to support a strengthening of trade winds and the SO/WC.

Strong SO/WC phases in both January 1974 and 1976 (Troup, 1982, personal communication) are manifest by a pronounced divergent arm across northern Australia and a local divergent maximum over Darwin (Fig. 9). Similar, although less well defined, features are prevalent in the Februarys of 1974–76. In the abnormally wet summers of 1974 and 1976 there would appear to be strong coupling between $-\bar{\chi}_{200}$ and $+\bar{\chi}_{850}$, with January 1974 standing out as a month in which Australian upper-level anticyclonicity was weak, the Northern Hemisphere upper anticyclone and the South East Asian/Malesian divergence field expanded, a northern Australian easterly jet maximum was set up and the SO/WC divergent arm was enhanced.

c. *Vertical cross sections (surface to 200 mb) of monthly mean divergence: January 1973–75*

The analysis of $\bar{\chi}_{850}$ and $\bar{\chi}_{200}$ fields alone does not provide a clear picture of the vertical coupling and structure of teleconnection patterns. Variations in Australasian and western Pacific oceanic rainfall patterns (Rao *et al.*, 1976) in Fig. 11, upper cloud distributions (Barton, 1983) and nephanalyses (Sadler *et al.*, 1976; Shideler and Sadler, 1979) are closely related to the vertical circulations shown in the latitudinal and longitudinal cross sections of monthly mean divergence (Figs. 12–14). However, it must be remembered that the nephanalyses refer to total cloud cover and do not resolve the various heights of clouds.

Coinciding with the final stages of the severe El Niño conditions of 1972–73 the rainfall regime in January 1973 (Fig. 11 top) shows an area of extensive precipitation in the western to central equatorial region of the Pacific Dry Zone (PDZ).[1] A second rainfall maximum exists in the Indonesia/Timor Sea region. Both areas are closely aligned with the distribution of upward vertical motion in the latitudinal cross sections of Fig. 12 and the upper-level cloud maxima noted by Barton (1983), although the latter center is not as distinct in Sadler *et al.* (1976). A third, but smaller, rainfall maximum around Taiwan and mainland China is also associated with ascending motion in the 115 and 125°E longitudinal cross sections. Vertical motion appears to be organized along 5°S with strong, low-level convergent and upper-level divergent maxima over Indonesia and, to a lesser degree, over the western Pacific (schematic arrows in Fig. 12). Interestingly, the convergent maxima in the 5 and 10°S cross sections occur at about 700 mb, indicating a deep convective zone near the equator.

[1] Following Quinn and Burt (1970, p. 25) the Pacific Dry Zone is described as ". . . a rather extensive feature of the middle and lower latitude eastern South Pacific which slims down to a narrow tongue as it extends westward through the central equatorial Pacific into the western equatorial Pacific."

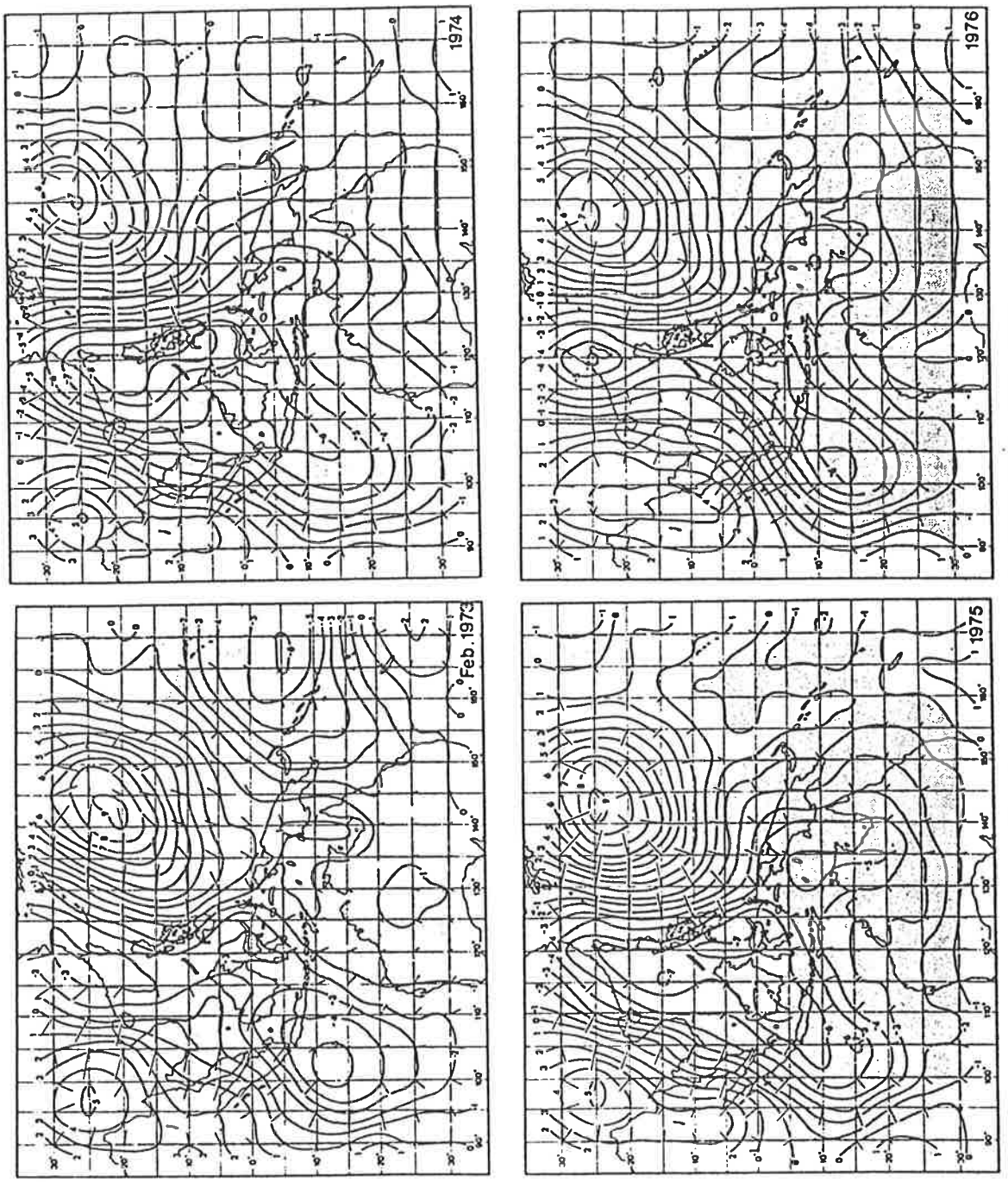

FIG. 10. As in Fig. 9, except during the Februarys from 1973 to 1977.

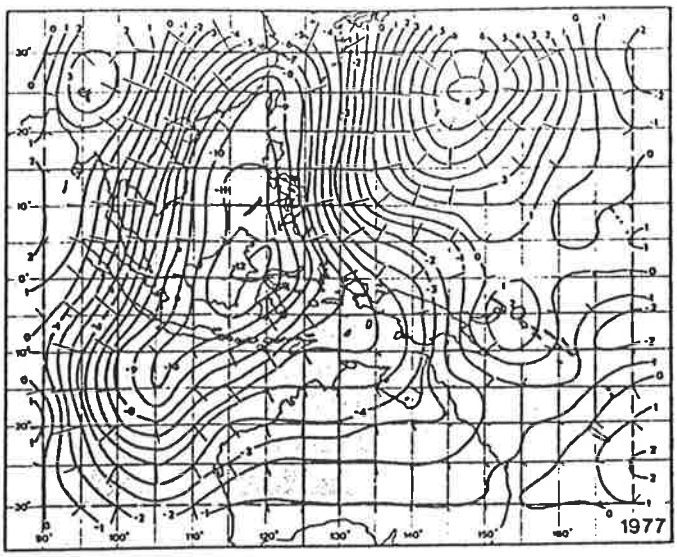

FIG. 10. (*Continued*)

All four latitudinal cross sections show a distinctly bi-cellular mode of zonal circulation. This arrangement agrees well with the previously observed major breakdown in the SO/WC overturning in 1973 ($\bar{\chi}_{200}$ fields in Figs. 9 and 10). As Ramage (1975) suggests, such periods are most likely characterized by "localized" convective maxima over the PDZ with sinking motion to the east (South America) and the west (Australia). The latter circulation arm is certainly evident in January 1973. However, suppression of convective activity over the Indonesian region by the type of large-scale SO/WC reversal often attributed to Bjerknes (1969) is not observed. On the contrary, broad-scale precipitation is very high over parts of Indonesia in January 1973, with mass removed by both the Hadley Circulation and a reduced SO/WC arm (latitudinal cross sections in Fig. 12).

Contributions to meridional, Hadley-type Circulation are most evident in the winter hemisphere between 115–125°E and at 175°E in the January 1973 longitudinal cross sections. Although not on the same scale as the Asian system in the west, the 175°E cell represents a significant anomaly in the meridional field at this longitude. Such enhanced Hadley Cell activity in this region (especially in the Northern Hemisphere branch) has been suggested by Bjerknes (1966, 1969, 1972) for the El Niño's of 1957–58, 1963–64 and 1965–66.

In January 1974, the major oceanic rainfall maxima in the Australian region (Fig. 11 center), upper-level cloud maxima (Barton, 1983) and cloud octa maxima (Shideler and Sadler, 1979) coincide with a large-scale vertical motion field which is suggestive of a large, strong SO/WC overturning (Fig. 13). Such an extensively organized near-zonal circulation seems to be a hallmark of strong SO/WC periods. Regions of subsidence are evident in the extreme east and west of all latitudinal cross sections. As Musk (1976) speculates, the eastern regions are either allied with, or a consequence of, processes normally suppressing PDZ rainfall.

Latitudinal cross sections in January 1974 show aspects of the major rainfall features in Fig. 11 center. In particular, they suggest that vertical motion in the Malesian/Australasian region was generally more organized than in January 1973. The extent of such changes over northern Australia is chiefly observed in a comparison of the 10 and 15°S cross sections in Figs. 12 and 13. Another important feature of the January 1974 distribution is that there is no indication of the type of secondary cell in the PDZ vicinity that occurred in January 1973. However, the inherent "noiseness" of the divergence cross sections appears to limit the extent to which they can be used in conjunction with the broader scale upper-cloud distributions of Barton (1983).

The January 1974 longitudinal cross sections suggest that important changes have also occurred in meridional circulation. Within the northwestern Pacific bounds of Fig. 13, the moderate to heavy precipitation in the vicinity of the Philippines (Fig. 11 center) is consistent with a strong vertical motion maximum centered on 10°N in the 120°E cross section. Abrupt vertical motion changes in this region are suggested by the divergence distributions in the 130°E diagram. The most noticeable facet of the cross sections in regards to the Australian rainfall maximum, is the presence of convective centers around 15°S at 130 and 155°E. Of particular interest in the final longitudinal cross section, at 180°E, is the absence of the type of meridional anomaly occurring in January 1973. In its place is a meridional circu-

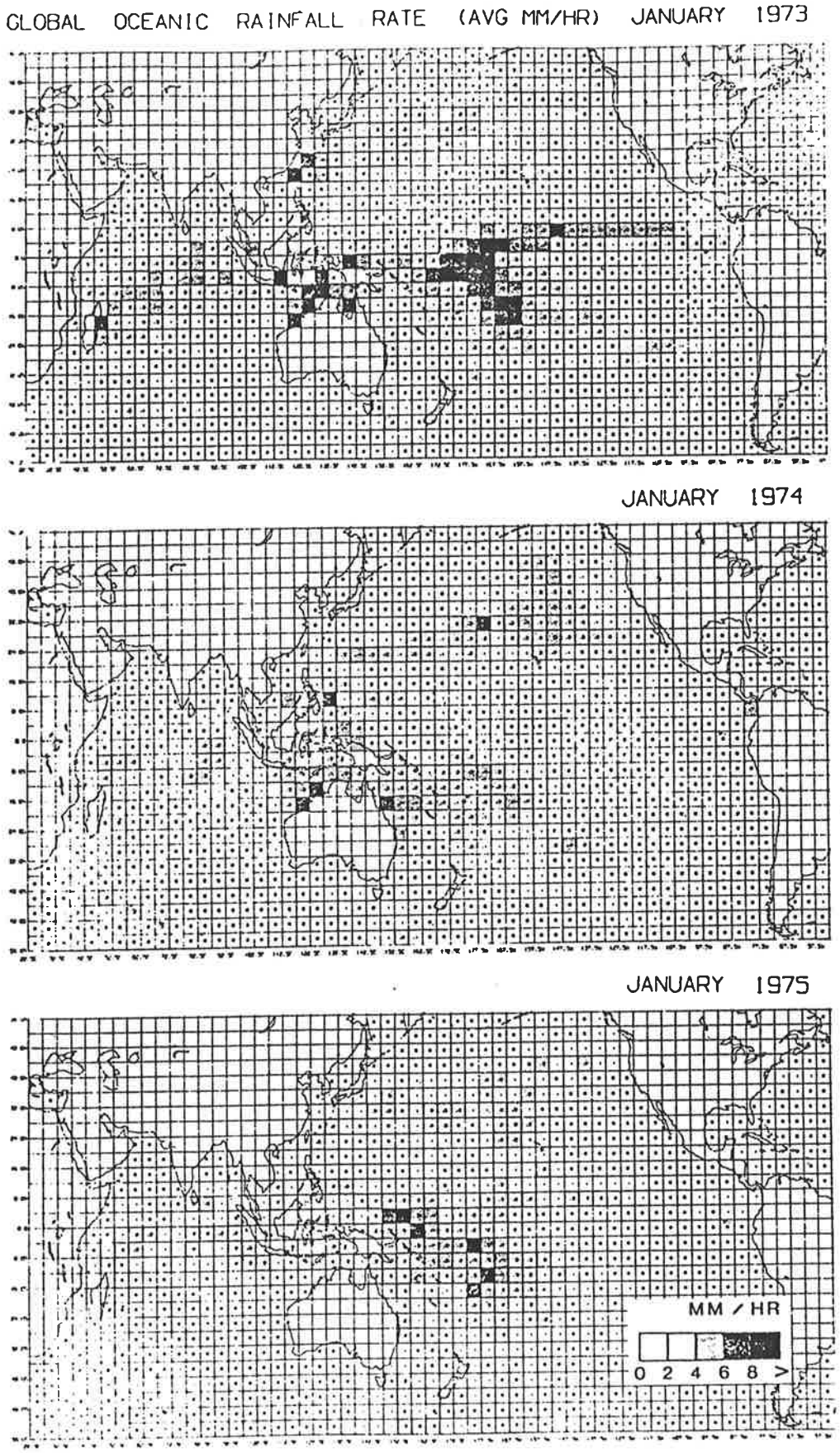

FIG. 11. Satellite-derived oceanic rainfall rates (mm h^{-1}) during the Januarys from 1973 to 1975 (Rao *et al.*, 1976).

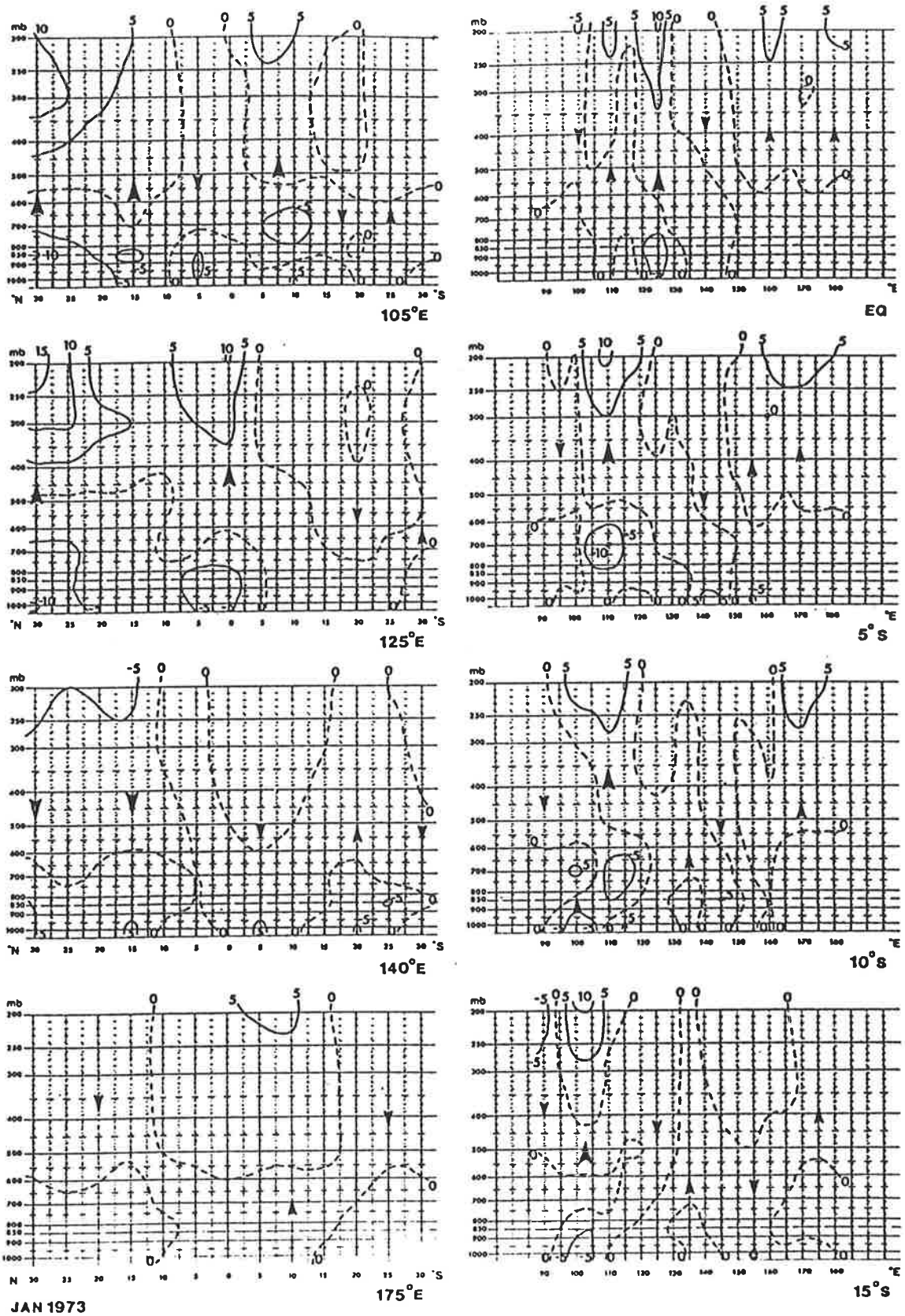

FIG. 12. Latitude and longitude cross sections of monthly mean divergence (10^6 m^2 s^{-1}) at intervals of 2 units for January 1973. Schematic arrows show strong and weak vertical motions, using large and small solid arrows, respectively.

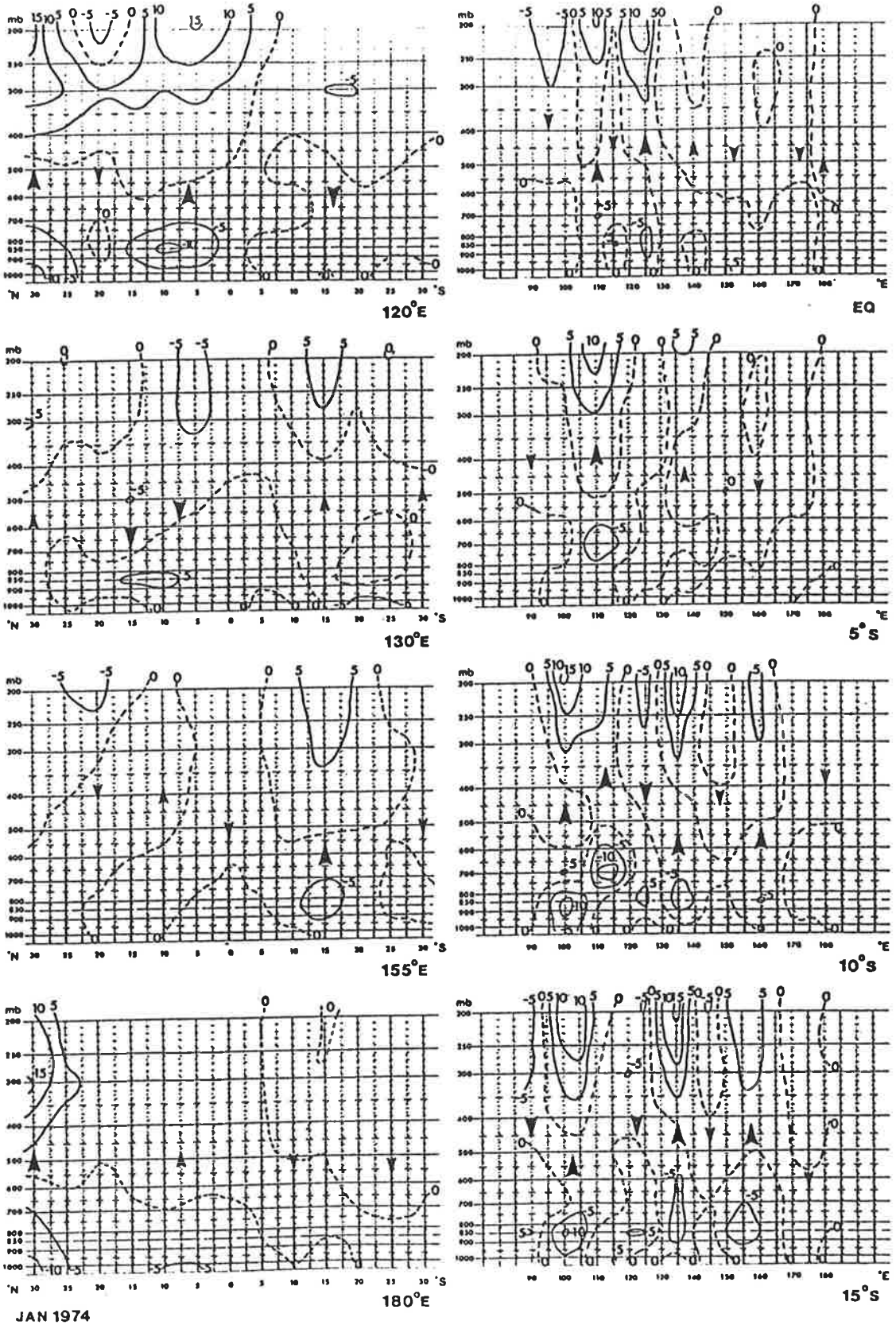

FIG. 13. As in Fig. 12, except for January 1974.

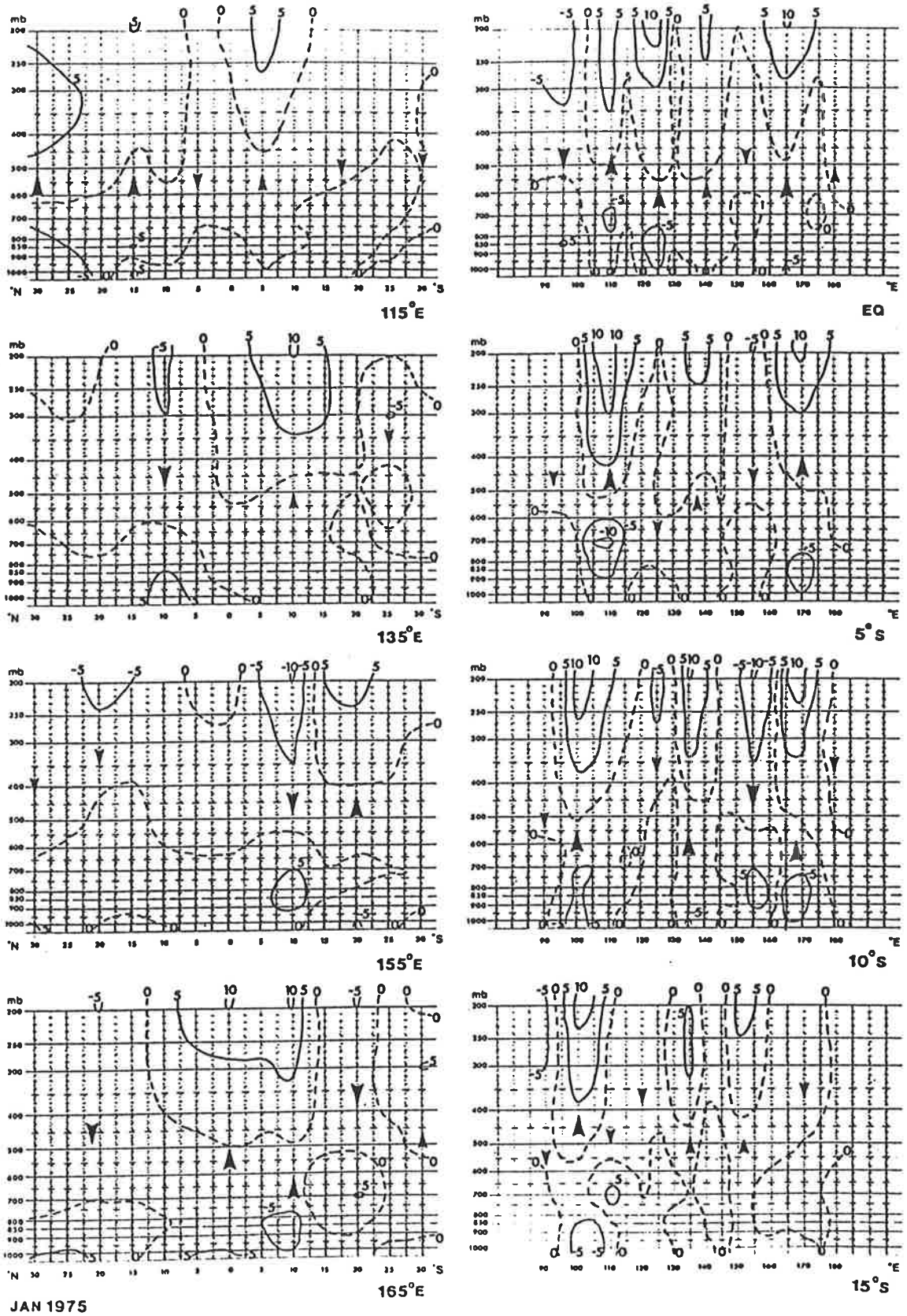

FIG. 14. As in Fig. 12, except for January 1975.

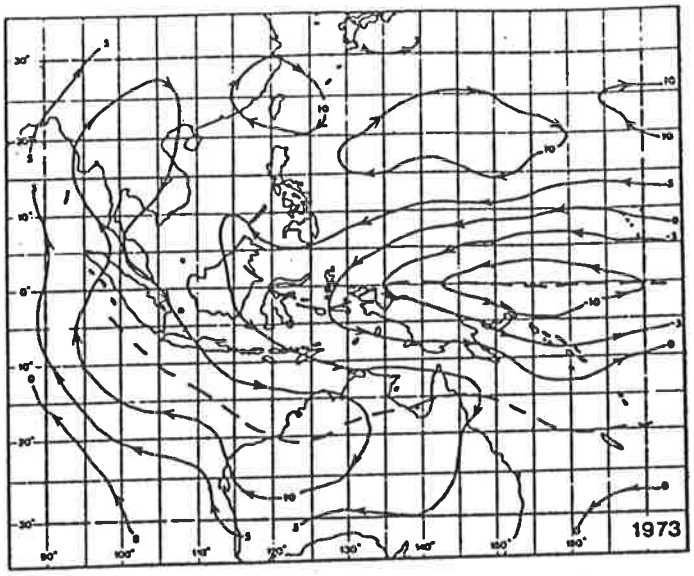
1973

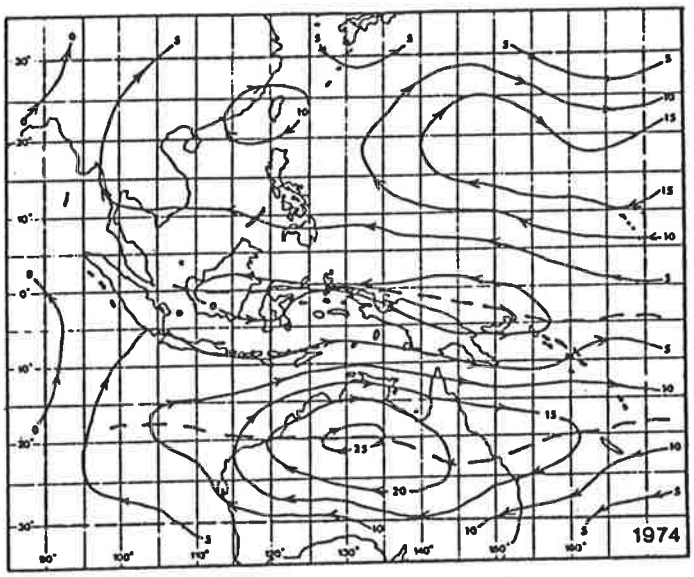
1974

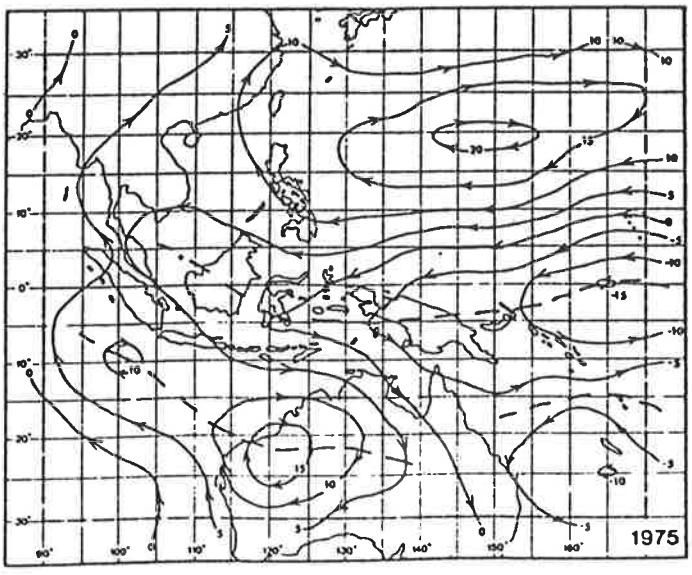
1975

lation dominated by strong vertical motion near 30°N, the latter region being coincident with an area of high oceanic rainfall rates in the mid North Pacific.

In the January 1975 situation, the major concentration of high oceanic rainfall rates (Fig. 11 bottom) is in the equatorial and near-equatorial region between about 150°E and the dateline. This distribution is closely aligned with the location of the upper-cloud maximum in Barton (1983) and an area of high cloud octa magnitudes in Shideler and Sadler (1979). However, the latter source also locates an area of marked cloudiness in the region of Borneo, which could be related to the vertical motion area observed in the equatorial and 5°S latitudinal cross sections (Fig. 14).

Latitudinal cross sections in January 1975 (Fig. 14) tend to show some semblence of bi-cellular, if not multi-cellular, overturnings. However, this mode seems to differ from that in January 1973, as there is relatively well organized vertical ascent to 145–150°E, with a small subsident area (especially in the 10°S cross section) around 155–160°E and a second ascending region near 165–170°E. In fact, the breakdown in January 1975 is centered on 155–160°E, while that in January 1973 occurred further to the west, near 135–140°E. This arrangement is evident in the first three latitudinal cross sections and may be related to the occurrence of an abortive El Niño at this time. On the other hand, the sequence does not have the degree of organization of vertical motion that was observed at 10 and 15°S in January 1974. Even the magnitude of convective motion at 15°S in Figs. 13 and 14 is noticeably different. Further north, the amount of precipitation over Indonesia (Fig. 11) and the extent of upper-level cloud (Barton, 1983) are below the January 1973 and 1974 values, although there is some support for the presence of the latter center in the nephanalysis of Shideler and Sadler (1979).

Pronounced meridional overturnings are evident in most of the longitudinal cross sections, with a major change in the pattern occurring around 155°E near the subsident area in the zonal teleconnections. Although the Hadley Circulation is strong in the winter hemisphere branch between 115–130°E, the local contribution provided by the convective activity near 165°E cannot be neglected. However, it is difficult to judge from this analysis whether the latter provides as distinct a mass and momentum source as does the Asian focus to the winter jet stream near Japan (Murakami and Unninayar, 1977; Webster, 1981a). Certainly, there would appear to be evidence of relationships between Australian subtropical jet stream locations in January 1973 (displaced to the north near 115°E) and January 1975 (displaced to the north near 150–160°E) and the Southern Hemisphere Hadley branch.

The overall pattern in all of the latitudinal cross sections is one of marked variability in the extent, intensity and organization of the SO/WC phenomenon. It appears that strong SO/WC periods can be partially characterized by the type of large-scale near-zonal overturning that many researchers envisage, although in itself this is a product of the coalescence of a number of smaller overturnings. However, other SO/WC periods reflect a tendency for the overturning to breakdown into a series of less organized and more isolated local cells. This variability in SO/WC structure may explain some of the inconsistancies in statistical methods aimed at relating Australian and Papua New Guinean rainfall to Southern Oscillation indices. As Barry (1978), Nicholls (1973) and Musk (1976) note, SO/WC variations form a highly complex spatial and temporal pattern, which cannot be explained by simple correlations alone.

d. Surface monthly mean streamfunction ($\bar{\chi}_{sfc}$): January 1973–75

The pattern of cross-equatorial flow into northern Australia in the monthly mean surface streamfunction ($\bar{\chi}_{sfc}$) fields of January 1973–75 (Fig. 15) is somewhat at variance with that observed at 850 mb. At the surface, cross-equatorial flow is most evident in the Januarys of 1973 and 1975, while in the wet Australian January of 1974 (Fig. 4) this flow is minimal. As was previously suggested, the extreme wetness in this month appears to be a consequence of a southerly displaced Australian monsoon system which, at least at low levels, was probably maintained primarily by Southern Hemisphere derived mass, energy and momentum sources.

It is evident that in January 1973 and 1975 the eastern section of the NET_{NH} is strong at both the surface and 850 mb levels and directs northeast trade wind flow across the equator into the New Guinean sector. Only in these two months does the western section of the NET_{NH} interact with the northwest Australian heat low or trough to initiate pronounced inflow from across Indonesia into this part of the Southern Hemisphere. As Murakami (1980a,b) suggests, the Indonesian longitudes are a preferred area for cross-equatorial flows and surges from Asia.

As a quasi-permanent feature of the low-level Australian summer circulation, the northwest heat low appears to act as an anchoring mechanism for the NET_{SH}. A second continental heat low, centered near Cloncurry (20°42′S, 140°30′E) in Queensland, is only evident in pressure and geopotential fields (Leslie,

FIG. 15. Monthly mean surface streamfunction fields (10^5 m^2 s^{-1}) at intervals of 5 units over the study area during the Januarys from 1973 to 1975. Heavy dashed lines indicate the positions of NET_{NH} and NET_{SH} referred to in the text.

1980). Its function in Australian summer rainfall mechanisms is not discernible in this study.

There is a suggestion that on shorter time scales, the northwestern heat low and the NET_{SH} may become synonymous with the heat low's capping inversion being destabilized by periods of strong tropical and near-tropical moisture input into the low (Webster, 1981b, p. 77–80). In fact, during the month of January 1974, the NET_{SH} totally dominates the Australian circulation pattern. At this time, Australian rainfall was not only high, but widespread (Fig. 4), and appears to have been associated with a pronounced monsoon incursion rather than transient features. Such periods reflect the organizing effect which a strong NET_{SH} exerts on low-level circulation over Australia and the Indo-Pacific region as a whole. However, they appear to be distinctly different from periods when low-level flow in the Australian region is marked by the shallow, cyclonic circulation of the heat lows and monsoon activity is weak. In the latter situations, the northwest heat low seems to draw in more cross-equatorial flow from Asian sources. The resolution of this type of dichotomy requires the additional analysis of daily flows and surges before any firm conclusions can be made.

5. Conclusion

During the Southern Hemisphere summers of 1973–77, fields of monthly mean velocity potential, streamfunction and divergence were used as the basis for an investigation of large-scale monsoon variability and teleconnection patterns. Particular emphasis was placed on examining evidence from the Australasian region.

Although areas of sparse data were encountered in the study domain, overall results compare favorably with WMONEX findings, especially in view of the comparisons in Sumi and Murakami (1981) and Tanaka (1981). This study suggests the following:

1) Monsoon fluctuations, shown in the 850 mb fields of monthly mean velocity potential ($\bar{\chi}_{850}$) and streamfunction ($\bar{\psi}_{850}$), were prevalent during the 1973–77 Australasian summers. A strong, southerly-displaced NET_{SH} over Australia in 1974, with low-level monsoonal circulation predominantly contained within the Southern Hemisphere, appears to have organized the deep convective activity which affected the continent at this time. A similar, but weaker, effect was observed in 1976. Marked intraseasonal monsoon variability is suggested by the increase in NET_{SH} intensity and organization between January and February 1975. There are also indications that the El Niño cycles of 1972–73, 1975 and 1976 were related to the changing strength of the eastern section of the NET_{NH} and northeast trade wind activity in the equatorial Pacific.

2) At 200 mb, monthly mean velocity potential ($\bar{\chi}_{200}$) and streamfunction ($\bar{\psi}_{200}$) fields reveal aspects of the major variation of the SO/WC in 1972–73. Monthly mean velocity potential ($\bar{\chi}_{200}$) fields show a breakdown in the upper-level divergent arm across northern Australia/Papua New Guinea during the Southern Hemisphere summer of 1973. Monthly mean streamfunction ($\bar{\psi}_{200}$) fields indicate an upper-level pattern dominated by anticyclonic circulations in both hemispheres. The marked variability of the Australian upper-level anticyclone seems to be related to SO/WC breakdowns. Periods when this cell is displaced to the west of the Australian continent appear to coincide with a breakdown in the SO/WC. During the wet Januarys of 1974 and 1976, the SO/WC is strong, with the upper anticyclonic cell being weak and displaced south over inland Australia. Major vertical overturnings seem to be favored in regions of strong vertical coupling between the upper and lower level velocity potential fields.

3) Cross sections of monthly mean divergence, in the January 1973–75 sub-period, provide further evidence for the structure of teleconnection fields over the study domain. The concept of the SO/WC as a simple, large-scale vertical cell which reverses in direction during anomalous periods is found to be something of an over-simplification. While strong SO/WC periods do seem to partly suggest the influence of a large-scale overturning, other SO/WC events in this study are characterized by the formation of more distinct local overturnings. During the SO/WC mode of January (and possibly February and March) 1973, there were at least two major overturning cells in the study domain, with the breakdown occurring in a more western location than during January 1975. In the longitudinal cross sections, there is evidence of important variations in the Hadley Circulation and some support for the concept that the higher latitude jet streams in the winter and summer hemispheres are strengthened by mass injected from the upper-level branches of the Hadley overturnings.

4) The January 1973–75 monthly mean surface streamfunction ($\bar{\chi}_{sfc}$) fields indicate that cross-equatorial flow into northern Australia is at a maximum in the relatively drier Januarys of 1973 and 1975, and at a minimum in the wetter January of 1974. This fact tends to be at odds with the type of evidence from the 850 mb monthly mean streamfunction ($\bar{\psi}_{850}$) fields during this period. It suggests that some of the vagaries of Australian monsoonal rainfall may be related to variations in the consistency, magnitude and depth of the low-level flow into the Australian heat low complex from across Indonesia. As in January 1974, other periods may be subject to the strong, dominant NET_{SH} of intense cyclonic circulations located well over the continent. No doubt, the dichotomy between heat low and NET_{SH} could only be re-

solved by thorough studies of shorter time-period variations in Australasian monsoon circulation.

Acknowledgments. I would like to thank Mr. Adrian Gordon, Dr. R. A. D. Byron-Scott, Dr. Peter Webster and Dr. Peter Lamb for helpful comments, encouragement and discussions of the manuscript. The author also appreciates the cartographic assistance of Mr. Max Foale, Ms. Debbie Oakley and Mrs. Chris Crothers and the Commonwealth Bureau of Meteorology for permission to reproduce the monthly rainfall deciles.

REFERENCES

Barry, R., 1978: Aspects of the precipitation characteristics of the New Guinea mountains. *J. Trop. Geogr.*, 47, 13–30.

Barton, I., 1983: Upper level cloud climatology from an orbiting satellite. *J. Atmos. Sci.*, 40 (in press).

Berson, F. A., 1961: Circulation and energy balance in a tropical monsoon. *Tellus*, 13, 472–485.

——, and A. J. Troup, 1961: On the angular momentum balance in the equatorial trough zone of the eastern hemisphere. *Tellus*, 13, 66–78.

Bjerknes, J., 1966: A possible response of the atmospheric Hadley circulation to equatorial anomalies of ocean temperature. *Tellus*, 18, 820–829.

——, 1969: Atmospheric teleconnections from the equatorial Pacific. *Mon. Wea. Rev.*, 97, 163–172.

——, 1972: Large-scale atmospheric response to the 1964–65 Pacific equatorial warming. *J. Phys. Oceanogr.*, 2, 212–217.

Chang, C.-P., J. E. Erickson and K. M. Lau, 1979: Northeasterly cold surges and near-equatorial disturbances over the Winter MONEX area during December 1974. Part I: Synoptic aspects. *Mon. Wea. Rev.*, 107, 812–829.

——, and K. M. Lau, 1980: Northeasterly cold surges and near-equatorial disturbances over the Winter MONEX area during December 1974. Part II: Planetary-scale aspects. *Mon. Wea. Rev.*, 108, 298–312.

Cheang, B. K., 1977: Synoptic features and structures of some equatorial vortices over the South China Sea in the Malaysian region during the winter monsoon, December 1973. *Pure. Appl. Geophys.*, 115, 1303–1334.

Cornejo-Garrido, A. G., and P. H. Stone, 1977: On the heat balance of the Walker Circulation. *J. Atmos. Sci.*, 34, 1155–1162.

Davidson, N. E., J. L. McBride and B. J. McAvaney, 1981: The onset of the Australian monsoon during Winter MONEX. Extended abstract for paper presented at the International Conference on the Scientific Results of the Monsoon Experiment, Denpasar, Bali, Indonesia 26-30 October.*

Flöhn, H., 1973: Remarks on climatic intransitivity and the 1972 Pacific anomaly. *Atmosphere.*, 11, 134–140.

——, and H. Fleer, 1975: Climatic teleconnections with the equatorial Pacific and the role of ocean/atmosphere coupling. *Atmosphere.*, 13, 96–109.

Gruber, A., 1972: Fluctuations in the position of the ITCZ in the Atlantic and Pacific Oceans. *J. Atmos. Sci.*, 29, 193–197.

Haltiner, G. J., 1971: *Numerical Weather Prediction.* Wiley, 317 pp.

Holton, J. R., 1979: *An Introduction to Dynamic Meteorology*, 2nd ed. Academic Press, 391 pp.

Hubert, L. F., A. F. Krueger and J. S. Winston, 1969: The double intertropical convergence zone—Fact or fiction? *J. Atmos. Sci.*, 26, 771–773.

Julian, P. R., and R. M. Chervin, 1978: A study of the Southern Oscillation and Walker Circulation phenomena. *Mon. Wea. Rev.*, 106, 1433–1451.

Kanamitsu, M., and T. N. Krishnamurti, 1978: Northern summer tropical circulations during drought and normal rainfall months. *Mon. Wea. Rev.*, 106, 331–347.

Krishnamurti, T. N., 1971: Tropical east-west circulations during the northern summer. *J. Atmos. Sci.*, 28, 1342–1347.

——, M. Kanamitsu, W. J. Koss and J. D. Lee, 1973: Tropical east-west circulations during the northern winter. *J. Atmos. Sci.*, 30, 780–787.

Krueger, A. F., and J. S. Winston, 1974: A comparison of the flow over the tropics during two contrasting circulation regimes. *J. Atmos. Sci.*, 31, 358–370.

——, and ——, 1975: Large-scale circulation anomalies over the tropics during 1971–72. *Mon. Wea. Rev.*, 103, 465–473.

Leslie, L. M., 1980: Numerical modelling of the summer heat low over Australia. *J. Appl. Meteor.*, 19, 381–387.

McAvaney, B. J., N. E. Davidson and J. L. McBride, 1981: The onset of the Australian northwest monsoon during Winter MONEX: Broadscale flow revealed by an objective analysis scheme. Paper presented at the International Conference on Early Results of FGGE and Large-scale aspects of its Monsoon Experiments. Tallahessee, 12–17 January.*

McBride, J. L., 1981: Characteristic space and time scales of the Australian northwest monsoon. Extended abstract for paper presented at the International Conference on the Scientific Results of the Monsoon Experiment. Denpasar, Bali, Indonesia 26–30 October.*

Murakami, T., 1975: Interannual cloudiness changes. *Mon. Wea. Rev.*, 103, 465–473.

——, 1977: Changes in regional energetics over the North Pacific, South China Sea and the Indonesian Seas during winter. *Mon. Wea. Rev.*, 105, 1508–1520.

——, 1980a: Temporal variations of satellite-observed outgoing longwave radiation over the winter monsoon region. Part I: Long-period (15–30 day) oscillations. *Mon. Wea. Rev.*, 108, 408–426.

——, 1980b: Temporal variations of satellite-observed outgoing longwave radiation over the winter monsoon region. Part II: Short-period (4–6 day) oscillations. *Mon. Wea. Rev.*, 108, 427–444.

——, and M. S. Unninayar, 1977: Atmospheric circulation during December 1970 through February 1971. *Mon. Wea. Rev.*, 105, 1024–1038.

Musk, L. F., 1976: Rainfall variability and the Walker Cell in the equatorial Pacific Ocean. *Weather*, 31, 34–46.

Nicholls, N., 1973: The Walker Circulation and Papua New Guinea rainfall. Tech. Rep. No. 6, 40/169, Bureau of Meteorology, Australia, 13 pp.

——, 1977: Tropical-extratropical interactions in the Australian region. *Mon. Wea. Rev.*, 105, 826–832.

Paegle, J., J. E. Paegle, F. P. Lewis and A. J. McGlasson, 1979: Description and interpretation of planetary flow structure of the winter 1976 DST data. *Mon. Wea. Rev.*, 107, 1506–1514.

Quinn, W. H., 1972: Use of the Southern Oscillation in weather prediction. *J. Appl. Meteor.*, 11, 616–628.

——, 1974: Monitoring and predicting El Niño invasions. *J. Appl. Meteor.*, 13, 825–830.

——, and W. V. Burt, 1970: Prediction of abnormally heavy precipitation over the equatorial Pacific dry zone. *J. Appl. Meteor.*, 9, 20–28.

——, D. O. Zopf, K. S. Short and R. T. W. Kuo Yang, 1978: Historical trends and statistics of the Southern Oscillation, El Niño, and Indonesian droughts. *Fish. Bull.*, 76, 663–678.

Ramage, C. S., 1971: *Monsoon Meteorology.* Academic Press, 296 pp.

——, 1975: Preliminary discussion of the meteorology of the 1972–73 El Niño. *Bull. Amer. Meteor. Soc.*, 56, 234–242.

——, C. W. Adams, A. M. Hori, B. J. Kilonsky and J. C. Sadler, 1980: *Meteorological Atlas of the 1972–73 El Niño.* UHMET 80-03, Dept. of Meteorology, University of Hawaii at Manoa, 101 pp.

——, and A. M. Hori, 1981: Meteorological aspects of El Niño. *Mon. Wea. Rev.*, 109, 1827–1835.

Rao, M. S. V., W. V. Abbott III and J. S. Theon, 1976: *Satellite-derived Global Oceanic Rainfall Atlas (1973 and 1974)*, NASA SP-410., Goddard Spaceflight Center, Washington, DC, 31 pp.

——, and J. S. Theon, 1977: New features of global climatology revealed by satellite-derived oceanic rainfall maps. *Bull. Amer. Meteor. Soc.*, 58, 1285–1288.

Reiter, E. R., 1978: Long-term wind variability in the tropical Pacific, its possible causes and effects. *Mon. Wea. Rev.*, 106, 324–330.

——, 1979: Trade-wind variability, Southern Oscillation and Quasi-Biennial Oscillation. *Arch. Meteor. Geophys. Bioklim.*, A28, 113–126.

Riehl, H., 1979: *Climate and Weather in the Tropics*. Academic Press, 611 pp.

Sadler, J. C., L. Oda and B. J. Kilonsky, 1976: *Pacific Ocean Cloudiness from Satellite Observations*. UHMET 76-01, Dept. of Meteorology, University of Hawaii at Manoa, 137 pp.

Shideler, D. H., and J. C. Sadler, 1979: *Pacific Ocean Cloudiness from Satellite Observations Part II*. UHMET 79-13, Dept. of Meteorology, University of Hawaii at Manoa, 56 pp.

Shukla, J., and K. R. Saha, 1974: Computation of non-divergent streamfunction and irrotational velocity potential from the observed winds. *Mon. Wea. Rev.*, 102, 419–425.

Streten, N. A., 1970: A note on the climatology of the satellite observed zone of high cloudiness in the central south Pacific. *Aust. Meteor. Mag.*, 18, 31–38.

——, 1973: Some characteristics of satellite observed bands of persistent cloudiness over the Southern Hemisphere. *Mon. Wea. Rev.*, 101, 486–495.

Sumi, A., and T. Murakami, 1981: Large-scale aspects of the 1978–79 winter circulation over the greater WMONEX region. Part I: Monthly and season mean fields. *J. Meteor. Soc. Japan*, 59, 625–645.

Tanaka, M., 1980: Role of the circulation at the 150 mb level in the winter and summer monsoon in the Asian and Australian regions. Climatol. Note No. 26, Occas. Pap. No 2., Institute of Geoscience, The University of Tsukuba, Ibaroki Pref. 305, Japan, 134 pp.

——, 1981: Interannual fluctuations of the tropical monsoon circulation over the greater WMONEX area. *J. Meteor. Soc. Japan.*, 59, 825–831.

Trenberth, K. E., 1976: Spatial and temporal variations of the Southern Oscillations. *Quart. J. Roy. Meteor. Soc.*, 102, 639–653.

Troup, A. J., 1961: Variations in upper tropospheric flow associated with the onset of the Australian summer monsoon. *Indian. J. Meteor. Geophys.*, 12, 217–229.

Webster, P. J., 1981a: Mechanisms determining the mean and transient structure of the large-scale winter monsoon: Cold surges. Paper presented at the International Conference on Early Results of FGGE and Large-scale aspects of its Monsoon Experiments, Tallahessee, 12–17 January.*

——, 1981b: Monsoons. *Sci. Amer.*, 245, No. 2, 70–80.

——, L. Chou and K. M. W. Lau, 1977: Mechanisms effecting the state, evolution and transition of the planetary scale monsoon. *Pure. Appl. Geophys.*, 115, 1463–1491.

——, and G. L. Stephens, 1980: Tropical upper-tropospheric extended clouds: Inferences from Winter MONEX. *J. Atmos. Sci.*, 37, 1521–1541.

Williams, M., 1979: Interhemispheric interaction during Winter MONEX. *Preprints Australia-New Zealand GARP Symposium*, Melbourne, Australia.*

Winston, J. S., A. Gruber, T. I. Gray Jr., M. S. Varnadore, C. L. Earnest and L. P. Mannello, 1979: Earth-atmosphere radiation budget analyses derived from NOAA satellite data June 1974–February 1978, Vol. I. NOAA, NESS, 8 pp.

Wyrtki, K., 1975: El Niño—The dynamic response of the equatorial Pacific Ocean to atmospheric forcing. *J. Phys. Oceanogr.*, 5, 572–584.

——, 1977: Sea level during the 1972 El Niño. *J. Phys. Oceanogr.*, 7, 779–787.

——, 1979: The response of sea surface topography to the 1976 El Niño. *J. Phys. Oceanogr.*, 9, 1223–1231.

——, E. Stroup, W. Patzert, R. Williams and W. Quinn, 1976: Predicting and observing El Niño. *Science.*, 191, 343–346.

Yanai, M., 1964: An experimental objective analysis in the tropics. Tech. Pap. No. 62., Dept. Atmos. Sci., Colorado State University, 23 pp.

---

* Available from Joint Planning Staff for GARP and WCRP, World Meteorological Organization, C.P. No. 5, CH-1211, Geneva 20, Switzerland.

BIBLIOGRAPHY

Allison, L.J., E.R. Kreins, F.A. Godshall and G. Warnecke, 1969: Examples of the usefulness of satellite data in general atmospheric circulation research Part I - Monthly global atmospheric circulation characteristics as reflected in Tiros VII radiometric measurements. *NASA Technical Note TN D-5630*, Washington, D.C., 75 pp.

Angell, J.K., 1981: Comparison of variations in atmospheric quantities with sea-surface temperature variations in the equatorial eastern Pacific. *Mon. Wea. Rev., 109*, 230-243.

Arakawa, H. (Ed), 1969: *Climates of Northern and Eastern Asia, World Survey of Climatology Volume 8.* Elsevier Publishing Company, Amsterdam, 248 pp.

Arkin, P.A., 1982: The relationship between interannual variability in the 200 mb tropical wind field and the Southern Oscillation. *Mon. Wea. Rev., 110*, 1393-1404.

Ashford, O.M., 1982: The launching of GARP. *Weather, 37, 9*, 265-272.

Atkinson, G.D., and J.C. Sadler, 1970: *Mean-cloudiness and gradient-level wind charts over the tropics: Vol.I, Data.* Tech. Rep. 215, U.S. Air Weather Service, 48 pp.

————————, and ————————, 1970: *Mean-cloudiness and gradient-level wind charts over the tropics: Vol.II, Charts.* Tech. Rep. 215, U.S. Air Weather Service.

Bacastow, R.B., 1976: Modulation of atmospheric carbon dioxide by the Southern Oscillation. *Nature, 261*, 116-118.

————————, J.A. Adams, C.D. Keeling, D.J. Moss, T.P. Whorf and C.S. Wong, 1980: Atmospheric carbon dioxide, the Southern Oscillation, and the weak 1975 El Niño. *Science, 210*, 66-68.

Barnett, T., 1977 a: The principal time and space scales of the Pacific trade wind fields. *J. Atmos. Sci., 34*, 221-236.

————————, 1977 b: An attempt to verify some theories of El Niño. *J. Phys. Oceanogr., 7*, 633-647.

————————, 1981: Statistical relations between ocean/atmosphere fluctuations in the tropical Pacific. *J. Phys. Oceanogr., 11*, 1043-1058.

Barry, R., 1975: Climate models in paleoclimatic reconstruction. *Palaeogeogr., Palaeoclimatol., Palaeoecol., 17*, 123-137.

————————, 1978: Aspects of the precipitation characteristics of the New Guinea mountains. *J. Trop. Geogr., 47*, 13-30.

————————, 1979: Recent advances in climate theory based on simple climate models. *Prog. Phys. Geogr., 3*, 119-131.

————————, and R.J. Chorley, 1976: *Atmosphere, Weather and Climate.* Methuen, UK, 3rd Ed. 432 pp.

Barton, I.J., 1983: Upper level cloud climatology from an orbiting satellite. *J. Atmos. Sci., 40,* 435-447.

Bé, A.W.H., and J-C. Duplessy, 1976: Subtropical convergence fluctuations and Quaternary climates in middle latitudes of the Indian Ocean. *Science, 194,* 419-422.

Berson, F.A., 1961: Circulation and energy balance in a tropical monsoon. *Tellus., 13,* 472-485.

————————, and A.J. Troup, 1961: On the angular momentum balance in the equatorial trough zone of the eastern Hemisphere. *Tellus., 13,* 66-78.

Bhalme, H.N., and D.A. Mooley, 1980: Large-scale droughts/floods and monsoon circulation. *Mon. Wea. Rev., 108,* 1197-1211.

Bjerknes, J., 1966: A possible response of the atmospheric Hadley circulation to equatorial anomalies of ocean temperature. *Tellus., 18,* 820-829.

————————, 1969: Atmospheric teleconnections from the equatorial Pacific. *Mon. Wea. Rev., 97,* 163-172.

————————, 1972: Large-scale atmospheric response to the 1964-65 Pacific equatorial warming. *J. Phys. Oceanogr., 2,* 212-217.

————————, L.J. Allison, E.R. Kreins, F.A. Godshall and G. Warnecke, 1969: Satellite mapping of the Pacific tropical cloudiness. *Bull. Amer. Meteor. Soc., 50,* 313-322.

Bonython, C.W., 1951: The evaporating waters of Lake Eyre. *Weather, 6,* 310-314.

————————, 1959: The Lake Eyre Depression. *Proc. Roy. Geogr. Soc. Austr. S.Aust. Branch., 60,* 1-16.

————————, 1960: A decade of watching for water in Lake Eyre. *Proc. Roy. Geogr. Soc. Austr. S.Aust. Branch, 61,* 2-8.

————————, 1963: Further light on river floods reaching Lake Eyre. *Proc. Roy. Geogr. Soc. Austr. S.Aust. Branch, 64,* 9-22.

————————, and B. Mason, 1953: The filling and drying of Lake Eyre. *Geogr. J., 119,* 321-330.

Boucher, K., 1975: *Global Climate.* English Universities Press, UK, 326 pp.

Bowen, D.Q., 1979: Geographical perspective on the Quaternary. *Prog. Phys. Geogr., 3,* 167-186.

Bowler, J.M., 1981: Australian salt lakes. *Hydrobiol., 82,* 431-444.

————————, and R. Jones, 1979: Australia was a land of lakes. *Geogr. Mag., 51,* 679-685.

————————, G.S. Hope, J.N. Jennings, G. Singh and D. Walker, 1976: Late Quaternary climates of Australia and New Guinea. *Quat. Res., 6,* 359-394.

Brookfield, H.C. and D. Hart, 1966: *Rainfall in the Tropical South-West Pacific.* Research School of Pacific Studies, Department of Geography Publication G/3, ANU, Canberra, 25 pp.

Bryan, K., S. Manabe and R. Pacanowski, 1975: A global ocean-atmosphere climate model, Part II, the oceanic circulation. *J. Phys. Oceanogr., 5,* 30-46.

Bryson, R.A., 1968: All other factors being constant... *Weatherwise, 21,* 56-61.

————————, 1973: Drought in Sahelia : Who or what is to blame? *Ecologist, 3,* 366-371.

————————, 1974: A perspective on climatic change. *Science, 184,* 753-760.

————————, 1975: The lessons of climatic history. *Environmental Conservation, 2,* 163-170.

Bureau of Meteorology, 1960-81: *Annual Rainfall Review - Australia, 1960-81.* Melbourne, Australia.

————————————, 1973-77: *Monthly Rainfall Review - Australia, 1973-77.* Department of Science, Melbourne, Australia

————————————, 1977: *Monthly Weather Review - South Australia, February 1977.* Department of Science, Melbourne, Australia, 13 pp.

Caviedes, C.N., 1973: Secas and El Niño : Two simultaneous climatical hazards in South America. *Proc. Assoc. Amer. Geogr., 5,* 44-49.

————————————, 1982: Natural hazards in South America : In search of a method and theory. *GeoJournal, 6,* 101-109.

Chang, C-P., 1977: Some theoretical problems of the planetary scale monsoons. *Pure. Appl. Geophys., 115,* 1089-1109.

————————, and K.M. Lau, 1980: Northeasterly cold surges and near-equatorial disturbances over the Winter MONEX area during December 1974. Part II : Planetary-scale aspects. *Mon. Wea. Rev., 108,* 298-312.

————————, and ————————, 1982: Short-term planetary-scale interactions over the tropics and midlatitudes during northern winter. Part I : Contrasts between active and inactive periods. *Mon. Wea. Rev., 110,* 933-946.

————————, J.E. Erickson and K.M. Lau, 1979: Northeasterly cold surges and near-equatorial disturbances over the Winter MONEX area during December 1974. Part I : Synoptic aspects. *Mon. Wea. Rev., 107,* 812-829.

Cheang, B.K., 1977 a: Synoptic features and structures of some equatorial vortices over the South China Sea in the Malaysian region during the winter monsoon, December 1973. *Pure. Appl. Geophys., 115,* 1303-1333.

————————, 1977 b: Equatorial easterlies and rainfall in peninsular Malaysia during March and April 1974. *J. Trop. Geogr., 44,* 1-11.

Chen, W.Y., 1982 a: Assessment of Southern Oscillation sea-level pressure indices. *Mon. Wea. Rev., 110,* 800-807.

Chen, W.Y., 1982 b: Fluctuations in Northern Hemisphere 700 mb height field associated with the Southern Oscillation. *Mon. Wea. Rev., 110,* 808-823.

CLIMANZ Conference Abstracts, 1981: *Quaternary climatic history of Australia, New Zealand and Antarctica and surrounding seas.* Australian Academy of Science and the Royal Society of New Zealand, Howmans Gap, 18-23 February, 96 pp.

CLIMAP Project Members, 1976: The surface of the Ice-Age Earth. *Science, 191,* 1131-1136.

Climate Analysis Center, 1982: *The global climate fluctuation of June - August 1982.* Special Climate Diagnostics Bulletin, Diagnostics Branch of the Climate Analysis Center, NMC, NWS, NOAA, 3 pp.

Colton, D.E., 1973: Barotropic scale interactions in the tropical upper troposphere during the northern summer. *J. Atmos. Sci., 30,* 1287-1302.

Cornejo-Garrido, A.G. and P.H. Stone, 1977: On the heat balance of the Walker Circulation. *J. Atmos. Sci., 34,* 1155-1162.

Coughlan, M., 1975: The evidence for climatic change in some Australian meteorological data. Paper prepared for presentation at the *Australian Conference on Climate and Climatic Change,* Monash University, Victoria, Australia, 11 pp.

Davidson, N.E., J.L. McBride and B.J. McAvaney, 1981: The onset of the Australian monsoon during Winter MONEX. Extended abstract for paper presented at the *International Conference on the Scientific Results of the Monsoon Experiment,* Denpasar, Bali, Indonesia 26-30 October, 5-17 to 5-20.

Department of Minerals and Energy, 1973: *Atlas of Australian Resources - Second Series : Landforms.* Canberra, Australia.

Department of National Resources Australian Water Resources Council, 1976: *Review of Australian Water Sources.* Australian Government Publishing Service, Canberra, Australia, 170 pp.

Donguy, J.R. and C. Henin, 1980: Climatic teleconnections in the western South Pacific with El Niño phenomenon. *J. Phys. Oceanogr., 10,* 1952-1955.

Douglas, I. and J. Hobbs, 1974: Deluge in Australia. *Geogr. Mag., 46,* 465-471.

Dulhunty, J.A., 1975: Shoreline shingle terraces and prehistoric fillings of Lake Eyre. *Trans. R. Soc. S.Aust., 99,* 183-188.

Dulhunty, R., 1979: *When the Dead Heart Beats Lake Eyre Lives.* Lowden Publishing, Kilmore, Victoria, Australia, 271 pp.

Duplessy, J-C., 1982: Glacial to interglacial contrasts in the northern Indian Ocean. *Nature, 295,* 494-498.

Dyer, T.G.J., 1979: Rainfall along the east coast of southern Africa, the Southern Oscillation, and the latitude of the subtropical high pressure belt. *Quart. J. Roy. Meteor. Soc., 105,* 445-451.

Egger, J., G. Meyers and P.B. Wright, 1981: Pressure, wind and cloudiness in the tropical Pacific related to the Southern Oscillation. *Mon. Wea. Rev., 109,* 1139-1149.

Enfield, D.B., 1981: Annual and nonseasonal variability of monthly low-level wind fields over the southeastern tropical Pacific. *Mon. Wea. Rev., 109,* 2177-2190.

ESSA, 1966-70: *Monthly Climatic Data for the World 1966-70.* Asheville, N.C.

Falls, R., 1970: Some synoptic models - North Australia. In *Proceedings of the Symposium on Tropical Meteorology,* American Meteorological Society and WMO, Honolulu, Hawaii, 2-11 June, EV - 1-8.

Fleer, H.E., 1981: Teleconnections of rainfall anomalies in the tropics and subtropics. Chapter 1 in *Monsoon Dynamics.* Lighthill, J. and R.P. Pearce (Ed.), Cambridge University Press, UK, 5-18.

Fletcher, R.D., 1945: The general circulation of the tropical and equatorial atmosphere. *J. Meteor., 2,* 167-174.

Flöhn, H., 1955: *Tropical Circulation Patterns.* WMO Technical Note 9, 12 pp.

————, 1973: Remarks on climatic intransitivity and the 1972 Pacific anomaly. *Atmosphere, 11,* 134-140.

————, and H. Fleer, 1975: Climatic teleconnections with the equatorial Pacific and the role of ocean/atmosphere coupling. *Atmosphere, 13,* 96-109.

————, and S. Nicholson, 1980: Climate fluctuations in the arid belt of the 'Old World' since the last glacial maximum; possible causes and future implications. *Palaeoecology of Africa, 12,* 3-21.

Forecasting Section, Divisional Office, Perth, 1959: Tropical depressions in the north western Australian region during the 1957-1958, 1958-1959 seasons. *Aust. Meteor. Mag., 26,* 18-49.

————————————————————, Brisbane, 1959: Occurrence of tropical depressions and cyclones in the north eastern Australian region during the season 1958-1959. *Aust. Meteor. Mag., 26,* 50-76.

————————————————————, Perth, 1961: Tropical depressions and cyclones in the north western Australian region during the 1959-60 season. *Aust. Meteor. Mag., 32,* 26-40.

Garbell, M.A., 1947: *Tropical and Equatorial Meteorology.* Pitman and Sons, London, UK, 237 pp.

Gates, W.L., 1976 a: Modelling the Ice Age Climate. *Science, 191,* 1138-1144.

————, 1976 b: The numerical simulation of Ice Age climate with a global general circulation model. *J. Atmos. Sci., 33,* 1844-1873.

Geisler, J.E., 1981: A linear model of the Walker Circulation. *J. Atmos. Sci., 38,* 1390-1400.

Gentilli, J., 1958: *A Geography of Climate.* University of Western Australia Press, Australia, 172 pp.

Gentilli, J., 1961: Quaternary climates of the Australian region, *Annals of the New York Academy of Science, 95,* 465-501.

————————(Ed), 1971: *Climates of Australia and New Zealand, World Survey of Climatology Volume 13.* Elsevier Publishing Company, Amsterdam, 405 pp.

————————, 1972: *Australian Climate Patterns.* Nelson, Australia, 285 pp.

————————, 1977: Climate. Chapter 1 in *Australia - A Geography.* Jeans, D.N. (Ed), Sydney University Press, Australia, 571 pp.

Gill, A.E., 1980: Some simple solutions for heat-induced tropical circulation. *Quart. J. Roy. Meteor. Soc., 106,* 447-462.

Glenn, A.H., 1947: Circulation and convergence in the equatorial zone between 95°E and 160°E : December to February. *Bull. Amer. Meteor. Soc., 28,* 453-463.

Godshall, F.A., L.J. Allison, E.R. Kreins and G. Warnecke, 1969: Examples of the usefulness of satellite data in general atmospheric circulation research Part II - An atlas of average cloud cover over the tropical Pacific Ocean. *NASA Technical Note TN D-5631,* Washington. D.C., 41 pp.

Graetz, R.D., 1980: The potential application of LANDSAT imagery to land resource management in the channel country. *Technical Memorandum 80/2.* CSIRO Division of Land Resources Management, Perth, 26 pp.

Gruber, A., 1972: Fluctuations in the position of the ITCZ in the Atlantic and Pacific Oceans. *J. Atmos. Sci., 29,* 193-197.

Haltiner, G.J., 1971: *Numerical Weather Prediction.* Wiley, New York, 317 pp.

Hahn, D.G. and S. Manabe, 1975: The role of mountains in the south Asian monsoon circulation. *J. Atmos. Sci., 32,* 1515-1541.

Hare, F.K., 1977: Man gets his deserts. *Geogr. Mag., 49,* 705-708.

Harnack, R.P., J.R. Lanzante and J. Harnack, 1982: Associations among the tropical Pacific wind and sea surface termperature fields and higher latitude circulation. *J. Climatol., 2,* 267-290.

Hastenrath, S. and P.J. Lamb, 1977: *Climatic Atlas of the Tropical Atlantic and Eastern Pacific Oceans.* University of Wisconsin Press, 105 pp.

————————, and ————————, 1978: *Heat Budget Atlas of the Tropical Atlantic and Eastern Pacific Oceans.* University of Wisconsin Press, 104 pp.

————————, and ————————, 1979 a: *Climatic Atlas of the Indian Ocean - Part 1. Surface Circulation and Climate.* University of Wisconsin Press, 109 pp.

————————, and ————————, 1979 b: *Climatic Atlas of the Indian Ocean - Part 2. The Oceanic Heat Budget.* University of Wisconsin Press, 104 pp.

————————, and E.B. Kaczmarczyk, 1981: On spectra and coherence of tropical climate anomalies. *Tellus, 33,* 453-462.

Hawkins, H.F. and S.L. Rosenthal, 1965: On the computation of stream functions from the wind field. *Mon. Wea. Rev., 93,* 245-252.

Heathcote, R.L. and B.G. Thom (Ed), 1979: *Natural Hazards in Australia.* Proceedings of a symposium sponsored by The Australian Academy of Science, Institute of Australian Geographers, Academy of the Social Sciences in Australia, Canberra, Australia, 531 pp.

Hecht, A.D. and J. Imbrie, 1979: Toward a comprehensive theory of climatic change. *Quat. Res., 12,* 2-5.

Heddinghaus, T.R. and A.F. Krueger, 1981: Annual and interannual variations in outgoing longwave radiation over the tropics. *Mon. Wea. Rev., 109,* 1208-1218.

Henderson, R.A. and P.J. Stephenson (Ed), 1980: *The Geology and Geophysics of North Eastern Australia.* Geological Society of Australia, Queensland Division, 468 pp.

Hess, S.L., 1959: *Introduction to Theoretical Meteorology.* Holt and Company, New York, 362 pp.

Hickey, B., 1975: The relationship between fluctuations in sea-level, wind stress and sea surface temperature in the equatorial Pacific. *J. Phys. Oceanogr., 5,* 460-475.

Hobbs, J.E., 1975: Low latitude westerlies over the Indian Ocean. *Austr. Geogr., 13,* 41-51.

Horel, J.D. and J.M. Wallace, 1981: Planetary-scale atmospheric phenomena associated with the Southern Oscillation. *Mon. Wea. Rev., 109,* 813-829.

Houze, R.A., S.G. Geotis, F.D. Marks and A.K. West, 1981: Winter monsoon convection in the vicinity of North Borneo. Part 1 : Structure of the clouds and precipitation. *Mon. Wea. Rev., 109,* 1595-1614.

Hubert, L.F., A.F. Krueger and J.S. Winston, 1969: The double intertropical convergence zone - Fact or fiction? *J. Atmos. Sci., 26,* 771-773.

Hunt, H.A., G. Taylor and E.T. Quayle, 1913: *The Climate and Weather of Australia.* Commonwealth Bureau of Meteorology, Melbourne, 93 pp.

Hurlburt, H.E., J.C. Kindle and J.J. O'Brien, 1976: A numerical simulation of the onset of El Niño. *J. Phys. Oceanogr., 6,* 621-631.

Hutchings, J.W., 1961: Water vapour transfer over the Australian continent. *J. Atmos. Sci., 18,* 615-634.

Japanese Meteorology Agency, 1973-77: *Aerological Data for Japan - 1973-77.* Tokyo, Japan.

———————————, 1958-72: *Aerological Data for Japan - 1958-72.* Tokyo, Japan.

Johnson, R.H. and D.L. Priegnitz, 1981: Winter monsoon convection in the vicinity of North Borneo. Part 11 : Effects of large-scale fields. *Mon. Wea. Rev., 109,* 1615-1628.

Julian, P.R. and R.M. Chervin, 1978: A study of the Southern Oscillation and Walker Circulation phenomenon. *Mon. Wea. Rev., 106,* 1433-1451.

Kanamitsu, M., T.N. Krishnamurti and C. Depradine, 1972: On scale interaction in the tropics during northern summer. *J. Atmos. Sci., 29,* 698-706.

Kanamitsu, M., and T.N. Krishnamurti, 1978: Northern summer tropical circulations during drought and normal rainfall months. *Mon. Wea. Rev., 106,* 331-347.

Keen, R.A., 1982: The role of cross-equatorial tropical cyclone pairs in the Southern Oscillation. *Mon. Wea. Rev., 110,* 1405-1416.

Keshavamurty, R.N., 1982: Response of the atmosphere to sea surface temperature anomalies over the equatorial Pacific and the teleconnections of the Southern Oscillation. *J. Atmos. Sci., 39,* 1241-1259.

Khandekar, M.L., 1979: Climatic teleconnections from the equatorial Pacific to the Indian monsoon-analysis and implications. *Arch. Meteor. Geophys. Bioklim., A28,* 159-168.

————————, 1982: Comments on "Planetary-scale atmospheric phenomena associated with the Southern Oscillation". *Mon. Wea. Rev., 110,* 1495-1496.

Kidson, E., 1925: Some periods in Australian weather. *Bulletin No.17,* Bureau of Meteorology, Melbourne, 5-33.

Kidson, J.W., 1975: Tropical eigenvector analysis and the Southern Oscillation. *Mon. Wea. Rev., 103,* 187-196.

————————, D.G. Vincent and R.E. Newell, 1969: Observational studies of the general circulation of the tropics : Long term mean values. *Quart. J. Roy. Meteor. Soc., 95,* 258-287.

Kreins, E.R. and L.J. Allison, 1969: An atlas of Tiros VII monthly maps of emitted radiation in the 8-12 micron atmospheric window over the Indian Ocean area. *NASA Technical Note TN D-5101,* Washington, D.C., 25 pp.

Krishnamurti, T.N., 1971 a: Tropical east-west circulation during the northern summer. *J. Atmos. Sci., 28,* 1342-1347.

————————, 1971 b: Observational study of the tropical upper tropospheric motion field during the Northern Hemisphere summer. *J. Appl. Meteor., 10,* 1066-1096.

————————, and H.N. Bhalme, 1976: Oscillations of a monsoon system. Part 1 Observational aspects. *J. Atmos. Sci., 33,* 1937-1954.

————————, M. Kanamitsu, W.J. Koss and J.D. Lee, 1973: Tropical east-west circulations during the northern winter. *J. Atmos. Sci., 30,* 780-787.

Krueger, A.F., and J.S. Winston, 1974: A comparison of the flow over the tropics during two contrasting circulation regimes. *J. Atmos. Sci., 31,* 358-370.

————————, and ————————, 1975: Large-scale circulation anomalies over the tropics during 1971-72. *Mon. Wea. Rev., 103,* 465-473.

Kung, E.C., 1966: Kinetic energy generation and dissipation in the large-scale atmospheric circulation. *Mon. Wea. Rev., 94,* 67-82.

————————, and W.E. Baker, 1975: Energy transformations in middle-latitude disturbances. *Quart. J. Roy. Meteor. Soc., 101,* 793-815.

Kung, E.C. and Tsui, T.L., 1975: Subsynoptic-scale kinetic energy balance in the storm area. *J. Atmos. Sci., 32,* 729-740.

————, and H.A. Burgdorf, 1978: Maintenance of kinetic energy in large-scale tropical disturbances over the eastern Atlantic. *Quart. J. Roy. Meteor. Soc., 104,* 393-412.

Kutzbach, J.E., 1981: Monsoon climate of the early Holocene : climatic experiment using the Earth's orbital parameters for 9000 years ago. *Science, 214,* 59-61.

————————, and B.L. Otto-Bliesner, 1982: The sensitivity of the African-Asian monsoonal climate to orbital parameter changes for 9000 years BP in a low-resolution general circulation model. *J. Atmos. Sci., 39,* 1177-1188.

Lamb, H.H., 1977: *Climate : Present, Past and Future. Volume 2 Climatic History and the Future.* Methuen, London, 835 pp.

Lamb, P.J., 1979: Some perspectives on climate and climate dynamics. *Prog. Phys. Geogr., 3,* 215-235.

————, 1981: An attempt to address the question, 'Are weather patterns changing?' for a nonspecialist audience. *Bull. Amer. Meteor. Soc., 62,* 376-380.

Lau, K.M.W., 1978: Experiment with a simple ocean-atmosphere climate model - the role of the ocean in the global climate. *J. Atmos. Sci., 35,* 1144-1163.

————, 1979: A numerical study of tropical large-scale air-sea interaction. *J. Atmos. Sci., 36,* 1467-1489.

————, 1981: Oscillations in a simple equatorial climate system. *J. Atmos. Sci., 38,* 248-261.

————, 1982: Equatorial response to northeasterly cold surges as inferred from satellite cloud imagery. *Mon. Wea. Rev., 110,* 1306-1313.

————, and H. Lim, 1982: Thermally driven motions in an equatorial β-plane : Hadley and Walker Circulations during the winter monsoon. *Mon. Wea. Rev., 110,* 336-353.

Leslie, L.M., 1980: Numerical modelling of the summer heat low over Australia. *J. Appl. Meteor., 19,* 381-387.

Liebmann, B. and D.L. Hartmann, 1982: Interannual variations of outgoing IR associated with tropical circulation changes during 1974-78. *J. Atmos. Sci., 39,* 1153-1162.

Lighthill, J. and R.P. Pearce (Ed), 1981: *Monsoon Dynamics.* Cambridge University Press, UK, 735 pp.

Lim, J.T., 1976: Rainfall minimum in peninsular Malaysia during the northeast monsoon. *Mon. Wea. Rev., 104,* 96-99.

————, and L.C. Quah, 1978: Cross-equatorial flow over South East Asia during the northeast monsoon. *Indian J. Met. Hydrol. Geophys., 29,* 5-15.

Linacre, E.T. and J.E. Hobbs, 1977: *The Australian Climate Environment.* Wiley, Brisbane, Australia, 354 pp.

Lockwood, J.G., 1974: *World Climatology - An Environmental Approach.* Edward Arnold, UK, 330 pp.

Lorenz, E.N., 1955: Available potential energy and the maintenance of the general circulation. *Tellus, 7,* 157-167.

————————, 1968: Climatic determinism. *Meteor. Monogr., 8,* 1-3.

————————, 1970: Climatic change as a mathematical problem. *J. Appl. Meteor., 9,* 325-329.

————————, 1976: Nondeterministic theories of climatic change. *Quat. Res., 6,* 495-506.

————————, 1979: Forced and free variations of weather and climate. *J. Atmos. Sci., 36,* 1367-1376.

Lourensz, R.S., 1977: Tropical cyclones in the Australian region July, 1909 to June 1975. *Meteorological Summary,* Bureau of Meteorology, Government Publishing Service, Canberra, 111 pp.

————————, 1981: Tropical cyclones in the Australian region July, 1909 to June 1980. *Meteorological Summary,* Bureau of Meteorology, Government Publishing Service, Canberra, 94 pp.

Lyons, S.W., 1981: Planetary-scale aspects of outgoing longwave radiation and vorticity over the global tropics during winter. *Mon. Wea. Rev., 109,* 1773-1787.

Madden, R.A. and P.R. Julian, 1971: Detection of a 40-50 day oscillation in the zonal wind in the tropical Pacific. *J. Atmos. Sci., 28,* 702-708.

————————, and ————————, 1972: Description of global-scale circulation cells in the tropics with a 40-50 day period. *J. Atmos. Sci., 29,* 1109-1123.

Maher, J.V. and D.M. Lee, 1977: Upper air statistics Australia - Surface to 5 mb 1957 to 1975. *Meteorological Summary,* Bureau of Meteorology, Government Publishing Service, Canberra, 202 pp.

Maley, J., 1982: Dust, clouds, rain types, and climatic variations in tropical North Africa. *Quat. Res., 18,* 1-16.

Manabe, S. and D.G. Hahn, 1977: Simulation of the tropical climate of an Ice Age. *J. Geophys. Res., 82,* 3889-3911.

————————, J.L. Holloway, Jr., and H.M. Stone, 1970: Tropical circulation in a time integration of a global model of the atmosphere. *J. Atmos. Sci., 27,* 580-613.

————————, D.G. Hahn and J.L. Holloway, Jr., 1974: The seasonal variation of the tropical circulation as simulated by a global model of the atmosphere. *J. Atmos. Sci., 31,* 43-72.

————————, K. Bryan and M.J. Spelman, 1975: A global ocean-atmospheric climate model. Part I. The atmospheric circulation. *J. Phys. Oceanogr.,5,* 3-29.

Mangunredjo, I., 1964: Synoptic weather analysis in Indonesia. In *Proceedings of the Symposium on Tropical Meteorology*. Hutchings, J.W. (Ed), NZ Meteorological Service, Wellington, 347-351.

Mason, B., 1955: Rainfall in the Lake Eyre catchment. In *Lake Eyre, South Australia - The Great Flooding of 1949-50*. Royal Geographical Society of Australasia, South Australian Branch, 11-26.

Mawson, D., 1950: Occurrence of water in Lake Eyre, South Australia. *Nature, 166*, 667-668.

McAlpine, J.R., G. Keig and K. Short, 1975: Climatic tables for Papua New Guinea. *Technical Paper No.37*, CSIRO Division of Land Use Research, 177 pp.

———————— and R. Falls, 1983: *Climate of Papua New Guinea*. Australian National University Press, Canberra (in press).

McAvaney, B.J., N.E. Davidson and J.L. McBride, 1981: The onset of the Australian northwest monsoon during Winter MONEX : Broadscale flow revealed by an objective analysis scheme. Paper presented at the *International Conference on Early Results of FGGE and Large-scale aspects of its Monsoon Experiments*. Tallahesse, Florida, 12-17 January, 10-7 to 10-11.

————————, 1983: Tests of the ANMRC tropical analysis scheme using analytic data. Extended abstract in *Australian Conference on Tropical Meteorology*, Bureau of Meteorology and Royal Meteorological Society (Australian Branch), Melbourne, 24-25 March, 33-34.

McBoyle, G.R., 1971: Climatic classification of Australia by computer. *Austr. Geogr. S., 9*, 1-14.

McBride, J.L., 1981: Characteristic space and time scales of the Australian northwest monsoon. Extended abstract for paper presented at the *International Conference on the Scientific Results of the Monsoon Experiment*. Denpasar, Bali, Indonesia 26-30 October, 5-50 to 5-53.

————————, and N. Nicholls, 1983: Seasonal relationships between Australian rainfall and the Southern Oscillation. (Submitted to *Mon. Wea. Rev.*).

McCreary, J., 1976: Eastern tropical ocean response to changing wind systems : With application to El Niño. *J. Phys. Oceanogr., 6*, 632-645.

McInnis, D.H. and E.C. Kung, 1972: A study of sub-synoptic scale energy transformations. *Mon. Wea. Rev., 100*, 126-132.

McIntosh, D.H. and A.S. Thom, 1973: *Essentials of Meteorology*. Wykeham Science Series No.3, Wykeham Publications, UK, 240 pp.

McWilliams, J.C. and P.R. Gent, 1978: A coupled air-sea model for the tropical Pacific. *J. Atmos. Sci., 35*, 962-989.

Miller, D., 1971: *Global Atlas of Relative Cloud Cover 1967-70 Based on Data from Meteorological Satellites*. US Department of Commerce/NOAA/NESS and US Airforce/Air Weather Service, Washington, D.C., 66 pp.

Mitchell, J.M., Jr., 1961: Recent secular changes of global temperature. *Annals of the New York Academy of Sciences, 95*, 235-250.

Moore, T.C., Jr., L.H. Burckle, K. Geitzenauer, B. Luz, A. Molina-Cruz, J.H. Robertson, H. Sachs, C. Sancetta, J. Thiede, P. Thompson and C. Wenkam, 1980: The reconstruction of sea surface temperatures in the Pacific Ocean of 18000 BP. *Mar. Micropaleontol., 5,* 215-247.

Murakami, T., 1973: On the interaction between the zonal mean flow and equatorial waves excited by diabatic heat sources at 20° latitude. *J. Atmos. Sci., 30,* 984-996.

————, 1974: Steady and transient waves excited by diabatic heat sources during the summer monsoon. *J. Atmos. Sci., 31,* 340-357.

————, 1975: Interannual cloudiness changes. *Mon. Wea. Rev., 103,* 996-1006.

————, 1977 a: Regional energetics over the North Pacific, South China Sea and the Indonesian Seas during winter. *Pure. Appl. Geophys., 115,* 1283-1301.

————, 1977 b: Changes in regional energetics over the North Pacific, South China Sea and the Indonesian Seas during winter. *Mon. Wea. Rev., 105,* 1508-1520.

————, 1978: Regional energetics of the 200 mb summer circulations. *Mon. Wea. Rev., 106,* 614-628.

————, 1979: Scientific objectives of the Monsoon Experiment (MONEX). *GeoJournal, 3,* 117-136.

————, 1980 a: Temporal variations of satellite-observed outgoing longwave radiation over the winter monsoon region. Part I : Long-period (15-30 day) oscillations. *Mon. Wea. Rev., 108,* 408-426.

————, 1980 b: Temporal variation of satellite-observed outgoing longwave radiation over the winter monsoon region. Part II : Short period (4-6 day) oscillations. *Mon. Wea. Rev., 108,* 427-444.

————, and M.S. Unninayar, 1977: Atmospheric circulation during December 1970 through February 1971. *Mon. Wea. Rev., 105,* 1024-1038.

————, and ————, 1978: Fluctuations in the Northern Hemisphere winter circulations. *Indian. J. Met. Hydrol. Geophys., 29,* 187-197.

————, and A. Sumi, 1981: Large-scale aspects of the 1978-79 winter circulation over the greater WMONEX region. Part II : Long-period perturbations. *J. Meteor. Soc. Japan, 59,* 646-671.

Musk, L.F., 1976: Rainfall variability and the Walker Cell in the equatorial Pacific Ocean. *Weather, 31,* 34-46.

Namias, J., 1972: Influence of Northern Hemisphere general circulation on drought in northeast Brazil. *Tellus, 24,* 336-343.

Newell, R., J. Kidson, D. Vincent and G. Boer, 1972: *The General Circulation of the Tropical Atmosphere,* Vol.1, MIT Press, 258 pp.

————, ————, ———— and ————, 1974: *The General Circulation of the Tropical Atmosphere,* Vol.2, MIT Press, 371 pp.

Newman, B.W. and A.T. Bath, 1959: Occurrence of tropical depressions and cyclones in the northeastern Australian region during the season 1957-1958. *Aust. Meteor. Mag., 24,* 35-64.

————, A.R. Martin and W.R. Wilkie, 1956: Occurrence of tropical depressions and cyclones in the Australian region during the summer of 1955-56. *Proceedings of the Tropical Cyclone Symposium,* Brisbane, Australia, 25-55.

Newton, C.W., 1972: *Meteorology of the Southern Hemisphere. Meteor. Monogr., No. 35,* American Meteorological Society, 263 pp.

Nicholls, N., 1973: The Walker Circulation and Papua New Guinea rainfall. *Technical Report No. 6, 40/169,* Bureau of Meteorology, Australia, 13 pp.

————, 1977: Tropical-extratropical interactions in the Australian region. *Mon. Wea. Rev., 105,* 826-832.

————, 1978: Air-sea interaction and the quasi-biennial oscillation. *Mon. Wea. Rev., 106,* 1505-1508.

————, 1979 a: A simple air-sea interaction model. *Quart. J. Roy. Meteor. Soc., 105,* 93-105.

————, 1979 b: A possible method for predicting seasonal tropical cyclone activity in the Australian region. *Mon. Wea. Rev., 107,* 1221-1224.

————, and F. Woodcock, 1981: Verification of an empirical long-range weather forecasting technique. *Quart. J. Roy. Meteor. Soc., 107,* 973-976.

————, J.L. McBride and R.J. Ormerod, 1982: On predicting the onset of the Australian wet-season at Darwin. *Mon. Wea. Rev., 110,* 14-17.

Nieuwolt, S., 1968: Uniformity and variation in an equatorial climate. *J. Trop. Geogr., 27,* 23-39.

————, 1977: *Tropical Climatology - An Introduction to the Climates of the Low Latitudes.* Wiley, UK, 207 pp.

NOAA, 1971-72: *Monthly Climatic Data for the World 1971-72.* Asheville, N.C.

——, 1973-77 a: *Monthly Climatic Data for the World 1973-77.* Asheville, N.C.

——, 1973-77 b: *US Climatological Data - National Summary 1973-77.* Asheville, N.C.

——, 1978-81: *Monthly Climatic Data for the World 1978-81.* Asheville, N.C.

Oliver, J.E., 1974: Tropical cyclones as natural hazards : An evaluation of Queensland experience in its meteorological context. *Aust. Meteor. Mag., 22,* 49-52.

————, 1975: The geographers concern with natural hazard studies. *Geographical Education, 2,* 339-348.

————, (Ed), 1979: *Response to Disaster.* Collected papers and discussion from the Seminar 'Response to Disaster' held at James Cook University of North Queensland, Centre for Disaster Studies, 16-18 July, 355 pp.

O'Mahony, G., 1961: Time series analysis of some Australian rainfall data. *Meteorological Studies No. 14*, Bureau of Meteorology, Australia, 65 pp.

Oort, A.H., 1964: On estimates of the atmospheric energy cycle. *Mon. Wea. Rev., 92*, 483-493.

Paegle, J., J.E. Paegle, F.P. Lewis and A.J. McGlasson, 1979: Description and interpretation of planetary flow structure of the winter 1976 DST data. *Mon. Wea. Rev., 107*, 1506-1514.

Paltridge, G. and S. Woodruff, 1981: Changes in global surface temperature from 1880 to 1977 derived from historical records of sea surface temperature. *Mon. Wea. Rev., 109*, 2427-2434.

Panofsky, H.A., 1946: Methods of computing vertical motion in the atmosphere. *J. Meteor., 3*, 45-49.

Parthasarathy, B. and D.A. Mooley, 1978: Some features of a long homogeneous series of Indian summer monsoon rainfall. *Mon. Wea. Rev., 106*, 771-781.

Patzert, W.C., T.J. Cowles and C.S. Ramage, 1978: *El Niño Watch Atlas*. Scripps Institution of Oceanography, La Jolla, 24 pp.

Pazan, S. and G. Meyers, 1982: Interannual fluctuations of the tropical Pacific wind field and the Southern Oscillation. *Mon. Wea. Rev., 110*, 587-600.

Pearce, R.P., 1974: The design and interpretation of diagnostic studies of synoptic-scale atmospheric systems. *Quart. J. Roy. Meteor. Soc., 100*, 265-285.

Philander, S.G.H., 1981: The response of equatorial oceans to a relaxation of the trade winds. *J. Phys. Oceanogr., 11*, 176-189.

———————, 1983: El Niño Southern Oscillation phenomena. *Nature, 302*, 295-301.

Pickup, G. (Ed), 1979: *Natural Hazards Management in North Australia*. Proceedings of and Papers arising out of a Seminar held by the North Australia Research Unit of the Australian National University, Darwin, 11-14 September, 493 pp.

Pike, A.C., 1971: Intertropical convergence zone studied with an interacting atmosphere and ocean model. *Mon. Wea. Rev., 99*, 469-477.

Pittock, A.B., 1973: Global meridional interactions in stratosphere and troposphere. *Quart. J. Roy. Meteor. Soc., 99*, 424-437.

————————, 1974: Global interactions in stratosphere and troposphere. *Proceedings of the International Conference on Structure, Composition and General Circulation of the Upper and Lower Atmospheres and possible Anthropogenic Perturbations. Vol.II*, 14-25 January, University of Melbourne, Australia, 716-726.

————————, 1975: Climatic change and the patterns of variation in Australian rainfall. *Search, 6*, 498-504.

————————, 1980: Towards a warm earth scenario for Australia. In *Carbon Dioxide and Climate : Australian Research*. Pearman, G.I. (Ed), Australian Acadamy of Science, Canberra, 197-209.

Pittock, A.B., 1981: Long term climatic trends in eastern Australia. In *Cropping at the Margins*. Proceedings of a Seminar, Australian Institute of Agricultural Science and Water Research Foundation of Australia, Dubbo, 11 August, 23-39.

————————, and M.J. Salinger, 1982: Towards regional scenarios for a CO_2-warmed earth. *Climatic Change, 4,* 23-40.

————————, L.A. Frakes, D. Jenssen, J.A. Peterson and J.W. Zillman (Ed), 1978: *Climatic Change and Variability - A Southern Perspective*. Cambridge University Press, Melbourne, 455 pp.

Prell, W.L. and W.H. Hutson, 1979: Zonal temperature-anomaly maps of Indian Ocean surface waters : Modern and Ice-Age patterns. *Science, 206,* 454-456.

————————, W.H. Hutson, D.F. Williams, A.W.H. Bé, K. Geitzenauer and B. Molfino, 1980: Surface circulation of the Indian Ocean during the last glacial maximum, approximately 18000 year BP. *Quat. Res., 14,* 309-336.

Priestley, C.H.B., 1962: Some lag associations in Darwin pressure and rainfall. *Aust. Meteor. Mag., 38,* 32-42.

Quayle, E.T., 1918: Tropical control of Australian rainfall. *Bulletin No.15,* Bureau of Meteorology, Melbourne, 24 pp.

————————, 1929: Long range rainfall forecasting from tropical (Darwin) air pressures. *Proc. R. Soc., Victoria, 41,* 160-164.

Quinn, W.H., 1974: Monitoring and predicting El Niño invasions. *J. Appl. Meteor., 13,* 825-830.

————————, and W.V. Burt, 1970: Prediction of abnormally heavy precipitation over the equatorial Pacific dry zone. *J. Appl. Meteor., 9,* 20-28.

————————, and ————————, 1972: Use of the Southern Oscillation in weather prediction. *J. Appl. Meteor., 11,* 616-628.

————————, D.O. Zopf, K.S. Short and R.K. Yang, 1978: Historical trends and statistics of the Southern Oscillation, El Niño, and Indonesian droughts. *Fish. Bull., 76,* 663-678.

Ramage, C.S., 1964: Diurnal variation of summer rainfall of Malaya. *J. Trop. Geogr., 19,* 62-68.

————————, 1968: Role of a tropical "maritime continent" in the atmospheric circulation. *Mon. Wea. Rev., 96,* 365-370.

————————, 1971: *Monsoon Meteorology*. Academic Press, New York, 296 pp.

————————, 1975: Preliminary discussion of the meteorology of the 1972-73 El Niño. *Bull. Amer. Meteor. Soc., 56,* 234-242.

————————, and A.M. Hori, 1981: Meteorological aspects of El Niño. *Mon. Wea. Rev., 109,* 1827-1835.

Rao, M.S.V. and J. Theon, 1977: New features of global climatology revealed by satellite-derived oceanic rainfall maps. *Bull. Amer. Meteor. Soc., 58,* 1285-1288.

Rao, M.S.V., W.V. Abbott III and J.S. Theon, 1976: *Satellite-derived Global Oceanic Rainfall Atlas (1973 and 1974).* NASA SP-410, Goddard Spaceflight Center, Washington, D.C., 31 pp.

Raschke, E. and W.R. Bandeen, 1967: A quasi-global analysis of tropospheric water vapour content from Tiros IV radiation data. *J. Appl. Meteor., 6,* 468-481.

Rasmusson, E.M. and T.H. Carpenter, 1982: Variations in tropical sea surface wind fields associated with the Southern Oscillation/El Niño. *Mon. Wea. Rev., 110,* 354-384.

Reiter, E.R., 1978: Long-term wind variability in the tropical Pacific, its possible causes and effects. *Mon. Wea. Rev., 106,* 324-330.

————————, 1979: Trade-wind variability, Southern Oscillation and Quasi-Biennial Oscillation. *Arch. Meteor. Geophys. Bioklim., A28,* 113-126.

Riehl, H., 1967: Some problems of research and education in Australian Meteorology. Unpublished paper, 12 pp.

————————, 1969: On the role of the tropics in the general circulation of the atmosphere. *Weather, 24,* 288-308.

————————, 1979: *Climate and Weather in the Tropics.* Academic Press, New York, 611 pp.

Rimmer, T. and A.W.W. Hossack, 1939: Foreshadowing summer rain in Queensland. *University of Queensland Papers, Department of Physics, 1,* 15 pp.

Rogers, J.C. and H. Van Loon, 1982: Spatial variability of sea level pressure and 500 mb height anomalies over the Southern Hemisphere. *Mon. Wea. Rev., 110,* 1375-1392.

Rognon, P. and M.A.J. Williams, 1977: Late Quaternary climatic changes in Australia and North Africa : A preliminary interpretation. *Palaeogeogr., Palaeoclimatol., Palaeoecol., 21,* 285-327.

Romanov, Yu. A. and N.A. Romanova, 1976: Some results of the surface wind and atmospheric pressure fields analysis near the equator. *Tellus, 28,* 524-532.

Rossignol-Strick, M., W. Nesteroff, P. Olive and C. Vergnaud-Grazzini, 1982: After the deluge : Mediterranean stagnation and sapropel formation. *Nature, 295,* 105-110.

Rowntree, P.R., 1972: The influence of tropical east Pacific Ocean temperatures on the atmosphere. *Quart. J. Roy. Meteor. Soc., 98,* 290-321.

————————, 1976: Tropical forcing of atmospheric motions in a numerical model. *Quart. J. Roy. Meteor. Soc., 102,* 583-605.

Russell, J.S., 1981: Geographic variation in seasonal rainfall in Australia - An analysis of the 80 year period 1895-1974. *Austr. J. Agric. Res., 47,* 59-66.

Sadler, J.C., 1969: Average cloudiness in the tropics from satellite observations. *International Indian Ocean Expedition Meteor., Monogr., 2,* East-West Center Press, Honolulu, Hawaii, 22 pp.

Sadler, J., L. Oda and B. Kilonsky, 1976: *Pacific Ocean cloudiness from satellite observations.* UHMET 76-01, Dept. of Meteorology, University of Hawaii, 137 pp.

————, C.S. Ramage and A.M. Hori, 1982: Carbon dioxide variability and atmospheric circulation. *J. Appl. Meteor., 21,* 793-805.

Salinger, M.J. and J.M. Gunn, 1975: Recent climatic warming around New Zealand. *Nature, 256,* 396-398.

Sangster, W.E., 1960: A method of representing the horizontal pressure force without reduction of pressures to sea level. *J. Meteor., 17,* 166-176.

Sarnthein, M., G. Tetzlaff, B. Koopmann, K. Wolter and U. Pflaumann, 1981: Glacial and inter glacial wind regimes over the eastern subtropical Atlantic and north-west Africa. *Nature, 293,* 193-196.

Sasamori, T., 1982: Stability of the Walker Circulation. *J. Atmos., Sci., 39,* 518-527.

Serventy, V., 1975: The lake that is that wasn't. *Hemisphere, 19,* 2-6.

Service de la Meteorologie en Nouvelle-Calédonie, 1973-77: *Nouvelle-Calédonie et Dependances : Observations Climatologiques Mensuelles Mesures en Altitudes 1973-77.* Rue Vincent Auriol, Noumea.

Seymour J, 1981: Australia's monsoon. *ECOS, 27,* 18-21.

Shideler, D.H. and J.C. Sadler, 1979: *Pacific Ocean cloudiness from satellite observations Part II.* UHMET 79-13, Dept. of Meteorology, University of Hawaii, 56 pp.

Shukla, J. and K.R. Saha, 1974: Computation of non-divergent streamfunction and irrotational velocity potential from the observed winds. *Mon. Wea. Rev., 102,* 419-425.

Singh, G., 1981: Late Quaternary pollen records and seasonal palaeoclimates of Lake Frome, South Australia. *Hydrobiol., 82,* 419-430.

————, A.P. Kershaw and R. Clark, 1981: Quaternary vegetation and fire history in Australia. Chapter 2 in *Fire and the Australian Biota.* Gill, A.M., R.H. Groves and I.R. Noble (Ed), Australian Academy of Science, Canberra, 23-54.

Skinner, T.C.L. and L.M. Leslie, 1982: Predictability experiments with the Australian west coast summer trough. *Aust. Meteor. Mag., 30,* 241-249.

Smith, P.J., 1973: Midlatitude synoptic scale systems : Their kinetic energy budgets and role in the general circulation. *Mon. Wea. Rev., 101,* 757-762.

Southern, R.L., 1964: Application of satellite data in the northern Australian tropical region during the summer monsoon. In *Proceedings of the Symposium on Tropical Meteorology,* American Meteorological Society and WMO, Honolulu, Hawaii, 2-11 June, 572-580.

————————, W.R. Kininmonth and N.R. Pescod, 1970: Derivation of convective forecasting models for northern Australia from a climatology of lightning discharges. In *Proceedings of the Conference on the Summer Monsoon of South East Asia.* Ramage, C.S. (Ed), Naval Weather Research Facility, Norfolk, Virginia, 239-254.

Staff Members, 1972: Drought in the Papua New Guinea Highlands during the period June to September 1972. *Working Paper No. 161, 40/169*, Bureau of Meteorology, Australia, 31 pp.

Staff of Divisional Office, Brisbane, 1961: Tropical cyclones in the northeastern Australian region - 1960-61 season. *Aust. Meteor. Mag., 35*, 43-60.

———————————————, 1962 a: Tropical cyclones in the northeastern Australian region - 1961-62 season. *Aust. Meteor. Mag., 38*, 15-47.

———————————————, Perth, 1962 b: Tropical cyclones in the northwestern Australian region during the 1960-61 season. *Aust. Meteor. Mag., 37*, 35-46.

———————————————, 1962 c: Tropical cyclones in the northwestern Australian region during the 1961-62 season. *Aust. Meteor. Mag., 39*, 49-62.

———————————————, Brisbane and Perth, 1965: Tropical cyclones in the northeastern and northwestern Australian regions for 1962-63 season. *Meteorological Summary*, Bureau of Meteorology, Melbourne, 83 pp.

Staffs of Regional Offices, Brisbane and Perth, 1966: Tropical cyclones in the northeastern and northwestern Australian regions for 1963-64 season. *Meteorological Summary*, Bureau of Meteorology, Melbourne, 84 pp.

———————————————, Darwin, Brisbane and Perth, 1968 a: Tropical cyclones in the northern Australian regions for the 1964-65 season. *Meteorological Summary*, Bureau of Meteorology, Melbourne, 88 pp.

———————————————————————————————, 1968 b: Tropical cyclones in the northern Australian regions, 1965-66 season. *Meteorological Summary*, Bureau of Meteorology, Melbourne, 60 pp.

———————————————————————————————, 1969: Tropical cyclones in the northern Australian regions, 1966-67 season. *Meteorological Summary*, Bureau of Meteorology, Melbourne, 77 pp.

———————————————————————————————, 1970: Tropical cyclones in the northern Australian regions, 1967-68 season. *Meteorological Summary*, Bureau of Meteorology, Melbourne, 50 pp.

———————————————————————————————, 1971: Tropical cyclones in the northern Australian regions, 1968-69 season. *Meteorological Summary*, Bureau of Meteorology, Melbourne, 76 pp.

———————————————————————————————, 1973 a: Tropical cyclones in the northern Australian regions, 1969-70 season. *Meteorological Summary*, Bureau of Meteorology, Melbourne, 110 pp.

———————————————————————————————, 1973 b: Tropical cyclones in the northern Australian regions, 1970-71 season. *Meteorological Summary*, Bureau of Meteorology, Melbourne, 95 pp.

———————————————————————————————, 1975: Tropical cyclones in the northern Australian regions, 1971-72 season. *Meteorological Summary*, Bureau of Meteorology, Melbourne, 119 pp.

Starr, V.P. and M.P. Peixoto, 1964: The hemispheric eddy flux of water vapour and its implications for the mechanics of the general circulation. *Arch. Meteor. Geophys. Bioklim., A14,* 111-130.

Stefanick, M., 1982: Interannual atmospheric angular momentum variability 1963-1973 and the Southern Oscillation. *J. Geophys. Res., 87,* 428-432.

Stephens, J.J. and K.W. Johnson, 1978: Rotational and divergent wind potentials. *Mon. Wea. Rev., 106,* 1452-1457.

Stoeckenius, T., 1981: Interannual variations of tropical precipitation patterns. *Mon. Wea. Rev., 109,* 1233-1247.

Street, F.A., 1981: Tropical palaeoenvironments. *Prog. Phys. Geogr., 5,* 157-185.

————————, and A.T. Grove, 1979: Global maps of lake-level fluctuations since 30000 yr BP. *Quat. Res., 12,* 83-118.

Streten, N.A., 1970: A note on the climatology of the satellite-observed zone of high cloudiness in the central South Pacific. *Aust. Meteor. Mag., 18,* 31-38.

————————, 1973: Some characteristics of satellite-observed bands of persistent cloudiness over the Southern Hemisphere. *Mon. Wea. Rev., 101,* 486-495.

————————, 1975: Satellite derived inferences to some characteristics of the South Pacific atmospheric circulation associated with the Niño event of 1972-73. *Mon. Wea. Rev., 103,* 989-995.

————————, 1982: Exploring Southern Hemisphere climates. *Aust. Meteor. Mag., 30,* 143-153.

Sumi, A. and T. Murakami, 1981: Large-scale aspects of the 1978-79 winter circulation over the greater WMONEX region. Part 1 : Monthly and season mean fields. *J. Meteor. Soc., Japan, 59,* 625-645.

Sutrisno, C., 1964: The effect of tropical cyclones in the western North Pacific and the Bay of Bengal on the weather in the southwestern part of Indonesia. In *Proceedings of the Symposium on Tropical Meteorology.* Hutchings, J.W. (Ed), NZ Meteorological Service, Wellington, 201-206.

Taljaard, J.J., H. Van Loon, H.L. Crutcher and R.L. Jenne, 1969: Temperatures, dew points, and heights at selected pressure levels. *Climate of the Upper Air : Southern Hemisphere, Vol. 1,* NAVAIR 50-1C-55, Chief of Naval Operations, Washington, D.C., 135 pp.

Tanaka, M., 1980: Role of the circulation at the 150 mb level in the winter and summer monsoon in the Asian and Australian regions. *Climatol. Note No. 26, Occas. Pap. No.2.,* Institute of Geoscience, The University of Tsukuba, Ibaroki Pref. 305, Japan, 134 pp.

————————, 1981: Interannual fluctuations of the tropical monsoon circulation over the greater WMONEX area. *J. Meteor. Soc., Japan, 59.,* 825-831.

Taylor, G., 1918: The Australian environment. *Advisory Council of Science and Industry Memoir No.1,* Melbourne, 188 pp.

Taylor, G., 1920: *Australian Meteorology.* Oxford at the Clarendon Press, UK, 312 pp.

Taylor, V.R. and J.S. Winston, 1968: Monthly and seasonal global charts of brightness from ESSA 3 and ESSA 5 digitized pictures, February 1967 - February 1968. *ESSA Tech. Rept. NESC-46,* Washington D.C., 9 pp.

Tetzlaff, G., (unpublished): The precipitation patterns around and including flooded Lake Eyre, 12 pp.

Thiede, J., 1979: Wind regimes over the late Quaternary southwest Pacific Ocean. *Geology, 7,* 259-262.

Thom, B.G. and R. Wasson (Ed)., 1982: Holocene research in Australia 1978-1982. *Occasional Paper No. 33,* Department of Geography, Faculty of Military Studies, University of NSW, Royal Military College, Duntroon, ACT, 134 pp.

Thom, R., 1975: *Structural Stability and Morphogenesis : An Outline of the General Theory of Models.* Translation from the French edition, as updated by the Author, by Fowler, D.H., W.A. Benjamin Inc., Reading, Massachusetts, USA, 348 pp.

Treloar, H.M., 1934: Foreshadowing monsoonal rains in northern Australia. *Bulletin No.18,* Bureau of Meteorology, Melbourne, 29 pp.

————————, and A.M. Grant, 1953: Some correlation studies of Australian rainfall. *Austr. J. Agric. Res., 4,* 424-429.

Trenberth, K.E., 1975: A quasi-biennial standing wave in the Southern Hemisphere and interrelations with sea-surface temperature. *Quart. J. Roy. Meteor. Soc., 101,* 55-74.

————————, 1976 a: Fluctuations and trends in indices of the Southern Hemispheric circulation. *Quart. J. Roy. Meteor. Soc., 102,* 65-76.

————————, 1976 b: Spatial and temporal variations of the Southern Oscillation. *Quart. J. Roy. Meteor. Soc., 102,* 639-653.

Trewartha, G.T., 1954: *An Introduction to Climate.* McGraw-Hill, New York, 402 pp.

Troup, A.J., 1961: Variations in upper tropospheric flow associated with the onset of the Australian summer monsoon. *Indian. J. Meteor. Geophys., 12,* 217-229.

————————, 1965: The Southern Oscillation. *Quart. J. Roy. Meteor. Soc., 91,* 490-506.

————————, 1967: Opposition of anomalies of upper tropospheric winds at Singapore and Canton Island. *Aust. Meteor. Mag., 15,* 32-37.

————————, 1974: The mean flow at the boundary of the Australian continent. *Aust. Meteor. Mag., 22,* 61-66.

Tsuchiya, I., 1970: Year to year variations of rainfall over the India-Equatorial Pacific region and of low and middle latitude circulations in the Southern Hemisphere. *Pap. Meteor. Geophys., 21,* 73-87.

Tucker, G.B., 1975: Climate : Is Australia's changing?. *Search, 6,* 323-328.

US Weather Bureau, 1958-65: *Monthly Climatic Data for the World 1958-65.* Asheville, N.C.

Van Campo, E., J.C. Duplessy and M. Rossignol-Strick, 1982: Climatic conditions deduced from a 150-kyr oxygen isotope - pollen record from the Arabian Sea. *Nature, 296,* 56-59.

Van Loon, H. and R.L. Jenne, 1969: The half-yearly oscillations in the tropics of the Southern Hemisphere. *J. Atmos. Sci., 26,* 218-232.

————, and ————, 1970: On the half-yearly oscillations in the tropics. *Tellus, 22,* 391-398.

————, and R.A. Madden, 1981: The Southern Oscillation : Part I : Global associations with pressure and temperature in northern winter. *Mon. Wea. Rev., 109,* 1150-1162.

————, and J. Rogers, 1981: The Southern Oscillation : Part II : Associations with changes in the middle troposphere in the northern winter. *Mon. Wea. Rev., 109,* 1163-1168.

————, C.S. Zerefos and C.C. Repapis, 1982: The Southern Oscillation in the stratosphere. *Mon. Wea. Rev., 110,* 225-229.

————, J.J. Taljaard, T. Sasamori, J. London, D.V. Hoyt, K. Latitzke, and C.W. Newton, 1972: Meteorology of the Southern Hemisphere. *Meteor. Monogr., Vol. 13 No. 35,* American Meteorological Society, Boston, 263 pp.

Verstappen, H. Th., 1975: On palaeo climates and landform development in Malesia. *Modern Quaternary Research in South East Asia, 1,* Balkema, A.A., Rotterdam, 3-35.

————————, 1980: Quaternary climatic changes and natural environment in S.E. Asia. *GeoJournal, 4,* 45-53.

Vickery, J., 1974: The greater flooding of the Lake Eyre basin - 1974. *Proc. Roy. Geogr. Soc. Austr. S.Aust. Branch, 75,* 23-36.

Vis, J.C.C., 1966: Some aspects of analysis and climatology in the tropics. *Meteorological Note No.3,* Bureau of Meteorology, Melbourne, 6 pp.

Walker, D. (Ed), 1972: *Bridge and Barrier : The Natural and Cultural History of Torres Strait.* Research School of Pacific Studies, Department of Biogeography and Geomorphology, Publication BG/3, ANU, Canberra, 437 pp.

Walker, G.T., 1923: Correlation in seasonal variations of weather, VIII : A preliminary study of world weather. *Mem. Indian Meteor. Dep., 24,* 75-131.

————————, 1924: Correlation in seasonal variations of weather, IX : A further study of world weather. *Mem. Indian Meteor. Dep., 24,* 275-332.

————————, 1928: World Weather III. *Mem. Roy. Meteor. Soc., 2,* 97-106.

————————, and E.W. Bliss, 1930: World Weather IV. *Mem. Roy. Meteor. Soc., 3,* 81-95.

————————, and ————————, 1932: World Weather V. *Mem. Roy. Meteor. Soc., 4,* 53-84.

————————, and ————————, 1937: World Weather VI. *Mem. Roy. Meteor. Soc., 4,* 119-139.

Wallace, J.M. and P.V. Hobbs, 1977: *Atmospheric Science an Introductory Survey*. Academic Press, New York, 467 pp.

Washington, W.M. and R.M. Chervin, 1980: Response time of an atmospheric general circulation model to changes in ocean surface temperature : Implications for interactive large-scale atmosphere and ocean models. *Tellus, 32,* 119-123.

Webster, P.J., 1972: Response of the tropical atmosphere to local, steady forcing. *Mon. Wea. Rev., 100,* 518-541.

————, 1973 a: Remote forcing of the time-independent tropical atmosphere. *Mon. Wea. Rev., 101,* 58-68.

————, 1973 b: Temporal variation of low-latitude zonal circulation. *Mon. Wea. Rev., 101,* 803-816.

————, 1978: Lateral effects on monsoon systems. *Indian J. Met. Hydrol. Geophys., 29,* 235-244.

————, 1981 a: Mechanisms determining the mean and transient structure of the large-scale winter monsoon : Cold surges. Paper presented at the *International Conference on Early Results of FGGE and Large-scale aspects of its Monsoon Experiments*. Tallahessee, Florida, 12-17 January, 4-20 to 4-29.

————, 1981 b: Mechanisms determing the atmospheric response to sea surface temperature anomalies. *J. Atmos. Sci., 38,* 554-571.

————, 1981 c: Monsoons. *Sci. Amer., 245,* 70-80.

————, 1982: Seasonality in the local and remote atmospheric response to sea surface temperature anomalies. *J. Atmos. Sci., 39,* 41-52.

————, and N.A. Streten, 1972: Aspects of late Quaternary climate in tropical Australasia. In *Bridge and Barrier : The Natural and Cultural History of Torres Strait*. Walker, D. (Ed). Research School of Pacific Studies, Department of Biogeography and Geomorphology, Publication BG/3, ANU, Canberra, 39-60.

————, and K.M.W. Lau, 1977: A simple ocean-atmosphere climate model : Basic model and a simple experiment. *J. Atmos. Sci., 34,* 1063-1084.

————, and ————, 1978: Simulation of the global monsoon sequence by a simple ocean-atmosphere interaction model. *Indian J. Met. Hydrol. Geophys., 29,* 314-326.

————, and N.A. Streten, 1978: Late Quaternary Ice Age climates of tropical Australasia : Interpretations and reconstructions. *Quat. Res., 10,* 279-309.

————, and G.L. Stephens, 1980: Tropical upper-tropospheric extended clouds : Inferences from Winter MONEX. *J. Atmos. Sci., 37,* 1521-1541.

————, and J.R. Holton, 1982: Cross-equatorial response to middle-latitude forcing in a zonally varying basic state. *J. Atmos. Sci., 39,* 722-733.

Webster, P.J., L. Chou and K.M.W. Lau, 1977: Mechanisms effecting the state, evolution and transition of the planetary scale monsoon. *Pure. Appl. Geophys., 115,* 1463-1491.

Wells, N.C., 1979: A coupled ocean-atmosphere experiment : The ocean response. *Quart. J. Roy. Meteor. Soc., 105,* 355-370.

————, 1982: Ocean-atmosphere interaction - A current perspective. *Weather, 39,* 162-164.

White, W.B. and A.E. Walker, 1973: Meridional atmospheric teleconnections over the North Pacific from 1950 to 1972. *Mon. Wea. Rev., 101,* 817-822.

Whittingham, H.E., 1960: Tropical cyclones in the northeastern Australian region - 1959-60 season. *Aust. Meteor. Mag., 30,* 1-38.

Willett, H.C. and F.T. Bodurtha, Jr., 1952: An abbreviated Southern Oscillation. *Bull. Amer. Meteor. Soc., 33,* 429-430.

Williams, J., 1978: A brief comparison of model simulations of glacial period maximum atmospheric circulation. *Palaeogeogr., Palaeoclimatol., Palaeoecol., 25,* 191-198.

————, R.G. Barry and W.M. Washington, 1974: Simulation of the atmospheric circulation using the NCAR global circulation model with Ice Age boundary conditions. *J. Appl. Meteor., 13,* 305-317.

Williams, M.A.J., 1975: Late Pleistocene tropical aridity synchronous in both hemispheres? *Nature, 253,* 617-618.

Williams, M., 1979: Interhemispheric interaction during winter MONEX. *GARP Special Report No.34.* Report on the Sixth Planning Meeting for the Monsoon Experiment, WMO, 16 pp.

Winstanley, D., 1973 a: Recent rainfall trends in Africa, the Middle East and India. *Nature, 243,* 464-465.

————, 1973 b: Rainfall patterns and the general atmospheric circulation. *Nature, 245,* 190-194.

Winston, J., A. Gruber, T. Gray, M. Varnadore, C. Earnest and J. Manello, 1979: *Earth-Atmosphere Radiation Budget Analyses Derived from NOAA Satellite Data, June 1974 - February 1978, Vols. 1,2.* Meteorological Satellite Laboratory, NOAA/NESS, Washington, D.C., 8 pp.

Wittwer, E.L., 1971: *Wet Season Climatology of North West Australia.* Unpublished M.A. Thesis, Department of Geography, University of Adelaide, 90 pp.

————, 1973: Seasonal changes in wind regimes of the north Australian and adjoining intertropical area. *Austr. Geogr., 12,* 340-362.

Wright, P.B., 1977: The Southern Oscillation - patterns and mechanisms of the teleconnections and the persistence. *Hawaii Inst. Geophys. Rep. HIG-77-13,* 107 pp.

————, 1978: The Southern Oscillation. In *Climatic Change and Variability - A Southern Perspective.* Pittock, A.B., L.A. Frakes, D. Jenssen, J.A. Peterson and J.W. Zillman (Ed). Cambridge University Press, Melbourne, 180-185.

Wright, P.B., 1979 a: Persistence of rainfall anomalies in the central Pacific. *Nature, 277,* 371-374.

————————, 1979 b: A simple model for simulating regional short-term climatic changes. *Mon. Wea. Rev., 107,* 1567-1580.

Wyrtki, K., 1975: El Niño - the dynamic response of the equatorial Pacific Ocean to atmospheric forcing. *J. Phys. Oceanogr., 5,* 572-584.

————————, 1977: Sea level during the 1972 El Niño. *J. Phys. Oceanogr., 7,* 779-787.

————————, 1979: The response of sea surface topography to the 1976 El Niño. *J. Phys. Oceanogr., 9,* 1223-1231.

————————, and G. Meyers, 1976: The trade wind field over the Pacific Ocean. *J. Appl. Meteor., 15,* 698-704.

————————, E. Stroup, W. Patzert, R. Williams and W. Quinn, 1976: Predicting and observing El Niño. *Science, 191,* 343-346.

Wyrwoll, K-H., 1979: Late Quaternary climates of Western Australia : Evidence and mechanisms. *J. Roy. Soc., West. Aust., 62,* 129-142.

Yanai, M., 1964: An experimental objective analysis in the tropics. *Tech. Pap. No.62,* Dept. Atmos. Sci., Colorado State University, 23 pp.

Yi-Hui, D. and E.R. Reiter, 1981: Some conditions influencing the variability of typhoon formation over the west Pacific Ocean. *Arch. Meteor. Geophys. Bioklim., A30,* 327-342.

Yoshino, M.M., 1971: *Water Balance of Monsoon Asia.* University of Tokyo Press, 308 pp.

Zebiak, S.E., 1982: A simple atmospheric model of relevance to El Niño. *J. Atmos. Sci., 39,* 2017-2027.

Zerefos, C.S., H. Van Loon and C.C. Repapis, 1982: Possible evidence of the Southern Oscillation in total ozone at Arosa. *Arch. Meteor. Geophys. Bioklim., A31,* 231-235.

Zuta, S., D. Enfield, J. Valdivia, P. Lagos and C. Blandin, 1980: Physical aspects of the 1972-73 'El Niño' phenomenon. In *Proceedings of the Workshop on the Phenomenon known as 'El Niño'*, Guayaquil, Ecuador, 4-12 December, UNESCO, Belgium, 11-62.